

Talanta

The International Journal of Pure and Applied Analytical Chemistry

Aims & Scope

Talanta provides a forum for the publication of original research papers, preliminary communications, and reviews in all branches of pure and applied analytical chemistry. Analytical data should be submitted only if they are clearly related to new analytical measurements. Original research papers on fundamental studies and novel sensor and instrumentation development are especially encouraged. Novel or improved applications in areas such as clinical chemistry, environmental analysis, geochemistry, and materials science and engineering are welcome. Methods should be validated by comparison with a standard method or analysis of a certified reference material, and relevant literature should be cited. Since classical spectrophotometric measurements and applications, solvent extraction, titrimetry, chemometrics, etc. are well established, studies in such areas should demonstrate a unique and substantial advantage over presently known systems. New reagents or systems should demonstrate clear advantage, and their presentation should be comprehensive rather than generating a series of similar papers for several analytes. Modifications of reagents should demonstrate significant improvements. Solvent extraction methods in particular, but others as well, should focus on the use of non-hazardous material substitutes and the minimization of waste generation. But obvious application of known chemistries or methods to established techniques are discouraged. Application of classical analytical approaches to relatively sample matrices having no major interferences, such as pharmaceutical preparations or reconstituted samples, are discouraged unless considerable improvements over other methods in the literature are demonstrated. Papers dealing with analytical data such as stability constants, pK_a values, etc. should be published in more specific journals, unless novel analytical methodology is demonstrated, or important analytical data are provided which could be useful in the development of analytical procedures.

Editors-in-Chief

Professor G.D. Christian, University of Washington, Department of Chemistry, 36 Bagely Hall, P.O. Box 351700, Seattle, WA 98195-1700, U.S.A.

Professor J.-M. Kauffmann, Université Libre de Bruxelles, Institut de Pharmacie, Campus de la Plaine, C.P. 205/6, Boulevard du Triomphe, B-1050 Bruxelles, Belgium

Associate Editors

Professor J.-H. Wang, Research Center for Analytical Sciences, Northeastern University, Box 332, Shenyang 110004, China

Professor J.L. Burguera, Los Andes University, IVAQUIM, Faculty of Sciences, P.O. Box 542, 5101-A Mérida, Venezuela.

Assistant Editors

Dr R.E. Synovec, Department of Chemistry, University of Washington, Box 351700, Seattle, WA 98195-1700, U.S.A.

Professor J.-C. Vire, Université Libre de Bruxelles, Institut de Pharmacie, Campus de la Plaine, C.P. 205/6, Boulevard du Triomphe, B-1050 Bruxelles, Belgium

Talanta

R. Apak (Istanbul, Turkey)
E. Bakker (Auburn, AL, U.S.A.)
D. Barceló (Barcelona, Spain)
B. Birch (Luton, UK)
K. S. Booksh (Tempe, AZ, U.S.A.)
J.-L. Capelo-Martinez (Caparica, Portugal)
Z. Cai (Kowloon, Hong Kong)
O. Chailapakul (Thailand)
S. Cosnier (Grenoble, France)
D. Diamond (Dublin, Ireland)
W. Frenzel (Berlin, Germany)
A.G. Gonzales (Seville, Spain)
P. de B. Harrington (OH, U.S.A.)

A. Ho (Hsin-chu, Taiwan)
P. Hubert (Liège, Belgium)
J. Kalivas (Pocatella, ID, U.S.A.)
B. Karlberg (Stockholm, Sweden)
J.-M. Lin (Beijing, China)
Y. Lin (Richland, WA, U.S.A.)
M.D. Luque de Caastro (Cordoba, Spain)
I.D. McKelvie (Victoria, Australia)
S. Motomizu (Okayama, Japan)
J.-M. Pingarron (Madrid, Spain)
E. Pretsch (Zürich, Switzerland)
W. Schuhmann (Bochum, Germany)
M. Shamsipur (Kermanshah, Iran)

M. Silva (Porto Alegre, Brazil)
P. Solich (Hradec Králové, Czech Republic)
K. Suzuki (Yokohama, Japan)
D.G. Themelis (Thessaloniki, Greece)
D.L. Tsalev (Sofia, Bulgaria)
B. Walzac (Katowice, Poland)
J. Wang (Tempe, AZ, U.S.A.)
J.D. Winefordner (Gainesville, U.S.A.)
Xiu-Ping Yan (Tianjin, China)
E.A.G. Zagatto (Piracicaba, SP, Brazil)
X. Zhang (China)



Application of Chemcatcher passive sampler for monitoring levels of mercury in contaminated river water

Rocío Aguilar-Martínez^a, M. Milagros Gómez-Gómez^{a,*}, Richard Greenwood^b,
Graham A. Mills^c, Branislav Vrana^b, María A. Palacios-Corvillo^d

^a Department of Analytical Chemistry, Faculty of Chemistry, University Complutense of Madrid, Ciudad Universitaria, 28040 Madrid, Spain

^b School of Biological Sciences, University of Portsmouth, King Henry I Street, Portsmouth PO1 2DY, United Kingdom

^c School of Pharmacy and Biomedical Sciences, University of Portsmouth, White Swan Road, Portsmouth PO1 2DT, United Kingdom

ARTICLE INFO

Article history:

Received 9 June 2008

Received in revised form 5 September 2008

Accepted 21 September 2008

Available online 30 September 2008

Keywords:

Mercury

Chemcatcher passive sampler

River water

Contamination monitoring

ABSTRACT

A passive sampler (Chemcatcher) consisting of a 47 mm Empore™ chelating disk (CHE) with iminodiacetic groups as the receiving phase overlaid with a diffusion membrane was developed and calibrated for the monitoring of Hg in water. Three different diffusion membranes including cellulose acetate (CA), polyethersulphone (PS) and cellulose dialysis membrane (D) were tested. The best performance was obtained with the CHE-PS tandem. The effective sampling rate of the device (R_s , L day⁻¹) is defined as the equivalent volume of water extracted per unit time, and is analyte specific and can be determined experimentally in a flow-through tank. Effects of water temperature and turbulence on the uptake rate of Hg were assessed under controlled laboratory conditions. Sampling rates were in the range of 0.029–0.091 L day⁻¹. An increase in sampling rate with turbulence was demonstrated. The detection limit of the sampler obtained in flowing waters ranged between 2.2 and 2.9 ng L⁻¹ Hg. The performance of Chemcatcher was tested alongside spot water sampling in a 14-day field deployment at two locations on the Valdeazogues River, Almadén, Spain. In general, the Hg concentration estimated by the Chemcatcher was lower than that found in spot water samples collected over the same period. This may be explained by the behaviour of this sampler that measures only the labile fraction of Hg in water, and this will exclude some species. However, Chemcatcher preconcentrates Hg allowing its determination in some places where its concentration is below the detection limit of spot sampling.

© 2008 Elsevier B.V. All rights reserved.

1. Introduction

Mercury (Hg) metal and its organometallic compounds are defined as priority pollutants by the European Union [1] and by a number of other countries throughout the world. The United States Environmental Protection Agency (EPA) has set the maximum allowed concentration of Hg as 2.4 µg L⁻¹ for river water [2], and the World Health Organization has suggested maximum allowable concentration of 1.0 µg L⁻¹ total Hg (average monthly) for inland surface waters [3]. Recently the European Union, within the context of the Water Framework Directive (WFD) [1], has set the environmental quality standards (EQS) for Hg in surface waters between 0.05 and 0.07 µg L⁻¹, and the chosen analytical methods should be able to detect down to 30% of this value (i.e., 15–21 ng L⁻¹ Hg). Gold and Hg mining activities [4,5] and waste Hg

discharges [6] can contaminate the aquatic environment leading to levels of Hg higher than those allowed by legislation.

The concentration of Hg in surface and coastal waters is usually measured in bottle (spot) samples of water followed by laboratory analysis. This approach gives only a snapshot of the level of pollution at the time of sampling. Where levels fluctuate (e.g., due to tides, and effluent discharges), it is desirable to monitor over longer time periods to be able to determine the time-weighted average (TWA) water concentration. A number of different methods can be used to calculate TWA concentrations including continuous monitoring [7], sediment analysis with back calculation to the water concentration [8], bio-monitoring [9,10] and passive sampling [11,12], the latter being an emerging methodology. Most designs of passive sampler consist of a receiving phase with a high affinity for the pollutants of interest separated from the external aquatic environment by a thin diffusion membrane. In most cases, uptake of analytes is controlled by Fickian diffusion [12]. Passive samplers have several advantages over conventional water monitoring methods: (i) they enable the estimation of the TWA water

* Corresponding author. Tel.: +34 91394 5146; fax: +34 91394 4329.

E-mail address: mmgomez@quim.ucm.es (M.M. Gómez-Gómez).

concentration of a compound over the deployment period, (ii) in some cases the amount of a chemical accumulated by the device reflects the concentration of the freely dissolved and labile fraction that is assumed to be the most readily bioavailable; compounds bound to suspended matter or dissolved organic carbon (DOC) are generally not accumulated [12], (iii) they can both preconcentrate and stabilise the sampled species until analysis and (iv) the analytes are effectively separated from the bulk water phase and matrix interferences are therefore minimised [13].

There is a number of different passive sampling systems available for monitoring pollutants in water, with most being suited for non-polar ($\log K_{ow}$ greater than 4) compounds, and to a lesser extent heavy metals [14,15]. Some passive sampling devices for monitoring Hg in air and water have been described. The passive integrative Hg sampler (PIMS) measures Hg^0 vapour in air and consists of a polyethylene tube filled with a HNO_3 /gold reagent combination as the receiving phase [16]. The diffusive gradient in thin films (DGT) device was developed for monitoring a variety of heavy metals [17]. The variant for Hg has two configurations: a special Chelex-100 resin with iminodiacetic groups or a Spheron-Thiol gel as receiving phases; and an agarose-gel as the diffusive medium layer for both. The sampler has been used to measure labile Hg in river water [18,19]. The use of both receiving phases with different capture efficiencies to Hg could be used to distinguish between Hg complexes in water. The high Hg affinity of Spheron-thiol resin allowed the accumulation of Hg bonded in very strong complexes, meanwhile Chelex-100 measured only ionic Hg and weak complexes.

Kingston et al. [20] and Persson et al. [21] developed a passive sampler, known as Chemcatcher, for the measurement of TWA concentrations of a range of organic compounds and metals in different aquatic environments. The system is based on diffusion of target compounds through a specific membrane and their subsequent accumulation in an appropriate receiving phase consisting of a solid adsorbent material. Several designs of the Chemcatcher suitable for sampling both polar and non-polar organic contaminants have been calibrated in the laboratory using flow-through tanks and trialled in a range of aquatic environments [20–22]. For heavy metals (i.e. Cd, Cu, Ni, Pb, Zn) a 3 M Empore iminodiacetic Chelating disk was used as the receiving phase and a cellulose acetate disk as membrane.

A new configuration of Chemcatcher for monitoring Hg and organotin compounds in water was described in an earlier paper [23]. In this work the sorption of Hg in different diffusion membranes and its effect on accumulation into receiving phase was investigated. The new version of Chemcatcher comprises an iminodiacetic Chelating disk (CHE) as receiving phase and a polyethersulphone membrane (PS) as diffusion membrane. The performance of the CHE-PS sampler has been tested under controlled conditions of temperature and turbulence to assess the effect of these parameters on the uptake kinetics. The sampler was tested in the Valdeazogues River (Almadén, Spain) in an area near the world's largest Hg mine (not operational since May 2002). The range of TWA water concentrations of Hg measured using the sampler was compared with that measured in spot water samples taken during the trial in order to assess the utility of the device.

2. Materials and methods

2.1. Chemicals and reagents

Reagents were analytical grade or better purity. Ultrapure Milli-Q water (Millipore, Ohio, USA) was used throughout. A standard stock solution (1.0 g L^{-1} as Hg) of $HgCl_2$ (Alfa Aesar, Karlsruhe,

Germany) was prepared by dissolving appropriate amounts in 1% HNO_3 (65%, w/v Merck, Darmstadt, Germany). A stock solution (10 mg L^{-1}) was prepared in 1% HNO_3 and stored in amber glass bottles at 4°C in the dark. Working solutions were prepared daily by appropriate dilution of the stock solution. A distilled HCl (37%, w/v, Scharlau, Barcelona, Spain) solution (0.24 mol L^{-1}) was used as the carrier for the inductively coupled plasma mass spectrometry (ICP-MS) analysis.

2.2. Materials of construction and sampler design

2.2.1. Receiving phase

Iminodiacetic Chelating Empore™ disks (47 mm diameter, 0.5 mm thickness) containing iminodiacetic groups (CHE) were from 3 M (Bioanalytical Europe, Neuss, Germany). The disks were washed with HCl (6 mol L^{-1} , 20 mL) for 30 min in an ultrasonic bath to remove any traces of Hg contamination. The disks were then placed in a vacuum manifold and washed with water (50 mL), followed by HCl (3 mol L^{-1} , 20 mL) and then rinsed with water ($50\text{ mL} \times 2$). Finally ammonium acetate buffer (pH 5.3, 0.1 mol L^{-1}) was added (50 mL) and followed by water washes ($20\text{ mL} \times 3$). Disks were stored in a Petri dish and kept damp until use.

2.2.2. Diffusion membranes

All membranes were of 47 mm diameter. Polyethersulphone (PS) (Z-Bind™ 0.2 μm pore size, 152 μm thickness) and cellulose acetate (CA) (0.45 μm pore size, 152 μm thickness) were purchased from Pall Europe (Portsmouth, UK). Cellulose dialysis membrane (D) (3500 molecular mass cut-off) was from Spectra/Por™ (Spectrum Europe V, Breda, The Netherlands). Membranes were shown to be free of Hg contamination and did not require a pre-conditioning step before use.

2.2.3. Chemcatcher™ sampler

The Chemcatcher™ design has been showed elsewhere [20,23,24]. Sampler bodies that retain both the receiving phase and diffusion membrane were made of PTFE. For all configurations tested, the diffusion membrane (47 mm diameter) was placed on the top of the conditioned CHE receiving phase disk avoiding formation of air bubbles between the two layers. Once the sampler was assembled, the cavity in front of the diffusion membrane was filled with water and then sealed until use by a PTFE cap and locking ring. The PTFE was shown to be free of contamination by Hg.

2.3. Flow-through exposure tank experiments

The flow-through exposure tank was similar to that described by Vrana et al. [24]. It comprised a glass tank ($31.5\text{ cm} \times 38\text{ cm} \times 40\text{ cm}$) with an overflow to waste. For the uptake experiments low saline content tap water was fed (30 mL min^{-1}) into the tank using a peristaltic pump (Watson Marlow Model 323 E, Falmouth, UK) together with a separate solution of Hg fed (0.3 mL min^{-1}) using second peristaltic pump (Minipuls Gilson, Villiers-le-Bel, France). A constant nominal concentration (0.2 or $0.4\text{ }\mu\text{g L}^{-1}$ as Hg) of $HgCl_2$ was maintained throughout. In order to keep homogeneous conditions the water was gently stirred (RZ1 overhead stirrer, Heidolph Instruments GmbH & Co. KG, Schwabach, Germany). The system was operated for a minimum of 48 h before sampler deployment to stabilise the analyte concentration. A refrigeration unit (FRIGEDOR 3001214, P Selecta, Barcelona, Spain) was used to control the water temperature in the tank. Pre-cleaned PTFE tubing (i.d. 0.6 mm), Tygon tubing (i.d. 0.6 and 1.6 mm) and Omnifit connectors were used to connect the different components of the system.

A PTFE carousel (made at University of Portsmouth, Portsmouth, UK) similar to that described previously [23,24] was used to hold

Table 1

Conditions used in the flow-through tank calibration experiments for the calculation of uptake rates of Hg.

Calibration experiment no.	1	2	3	4	5
Water temperature (°C)	4	4	11	11	11
Carousel rotation speed (min ⁻¹)	40	70	0	40	70
Estimated linear velocity ^a (cm s ⁻¹)	40	70	0	40	70

^a Linear velocity was calculated as $2\pi rf$, where r is the radius between the centre of the calibration carousel and the centre of the sampler and f is the rotation speed.

the samplers. The carousel comprised two horizontal turntables and a supporting rod that was connected to an overhead stirrer. Each turntable held 7 samplers, and therefore 14 samplers could be exposed simultaneously. Two different temperatures (4 and 11 °C) and three different levels of water turbulence were simulated in the uptake studies. Stirring level 1 (SL1), corresponding to the samplers placed at the bottom of the tank facing upwards, and the overhead stirrer working as indicated above; SL2 with the samplers loaded in the carousel rotating at 40 rpm and SL3 with the carousel rotating at 70 rpm.

In order to determine the accumulation rate of Hg by the receiving disk under the different temperature and turbulence conditions, 14 samplers were placed in the flow-through tank with or without the carousel for up to 14 days. Two or three replicates were retrieved after 2, 5, 8, 11 and 14 days of exposure and the amount of Hg accumulated in the receiving disks determined. Two samplers were used as fabrication blanks. Duplicate water samples were taken daily from the outlet of the tank to measure the concentration of Hg during the exposure study. Water samples were analysed directly by ICP-MS. The exposure conditions are summarized in Table 1.

2.4. Extraction of Hg from the diffusion and receiving phase and instrumental conditions

The Hg was extracted (10 min) from membranes and the receiving phases with two aliquots (10 mL) of HCl (12 mol L⁻¹) in an ultrasonic bath. Hg was measured by FI-ICP-MS (Model HP 4500, Agilent Technologies, Bracknell, UK) equipped with a Babington type nebulizer, a Fassel torch and a double-pass Scott-type spray chamber cooled by a Peltier system. The ICP-MS was operated at a power of 1300 W with a carrier gas flow of 1.01 L min⁻¹. The sampling loop was 500 µL. Data were collected by monitoring specific Hg ions at $m/z=200$ and $m/z=202$ with a 0.1 s integration time per isotope.

2.5. Field trial location and analysis of water samples and extracts

Two sampling sites were selected near to a known Hg contaminated site. The first station was close to the end of the Entredicho Hg mine, in a section of the Valdeazogues river and the La Serena dam (location 1). The second site was about 15 km downstream of the first site where Hg contamination was expected to be lower (location 2). Further information on the field locations is available [25,26]. Sampling was performed from 25th February to 11th March 2006. Six samplers were deployed at each sampling site. A nylon line was used to suspend the samplers in a horizontal position, 30–40 cm below the water surface, with the diffusion membrane facing downwards to minimize the settlement of silt and algae colonisation. After 14 days, the samplers were retrieved, filled with water from the sampling site (to avoid the receiving phase drying out), sealed and kept refrigerated during transport to the laboratory. The samplers were dismantled and the receiving phase stored at –18 °C until analysis. Two samplers were prepared as control blanks

to assess Hg contamination from the sampler components, laboratory storage, processing and analytical procedures. Two samplers were prepared to act as field blanks to assess Hg contamination during transport (to and from the field) and during deployment and retrieval of the devices.

Three replicate spot water samples (1 L) were collected from both sites at the beginning (day 0), at day 7 and the end (day 14) of the trial. Water samples were collected into pre-washed amber glass bottles and 1 mL of concentrated HNO₃ per litre of water added for stabilization of Hg. Samples were refrigerated during transport to the laboratory and stored at 4 °C until analysis. Water pH was measured *in situ* by a portable pH meter (Crison 507, Net Interlab, Madrid, Spain). Samples were analysed directly by FI-ICP-MS without filtration. Fig. 1 presents an overview of the analytical protocol for calibration and field trial studies.

3. Results and discussion

3.1. Stability studies

The adsorption of Hg to glassware and into other materials is a documented phenomena [19,27]. Exhaustive cleaning procedures and low affinity materials are necessary to minimize adsorption and memory effects. In this study these were reduced during the analysis by using a flow injection ICP-MS system (FI-ICP-MS) instead of continuous nebulization. All tubing connections and ICP-MS glassware were cleaned between samples or standards by injection of 3 mol L⁻¹ HCl as a wash solution.

A check was made for the sorption of Hg on the PTFE sampler body. Fourteen Chemcatcher bodies (without diffusion membranes or receiving phases) were placed at the bottom of the tank and exposed for 24 and 48 h to 20 L of water with a fixed concentration (250 ng L⁻¹) of Hg. The solution was stirred at 40 rpm by the overhead stirrer. The concentration of Hg in water was periodically checked, and the sorption of Hg on PTFE sampler bodies was also assessed by their extraction with concentrated HCl acid in an ultrasonic bath. After 24 h a 23% decrease in the Hg concentration in the water was observed. After 48 h losses of Hg from the tank were similar, and the sorption of Hg on the PTFE bodies was equivalent to 0.9% of the original nominal water concentration per sampler. Therefore, it is necessary to use an equilibration period of at least 48 h before each calibration experiment.

The stability of Hg in water samples stabilised with HNO₃ (1 mL per L of water), and stored at 4 °C in glass bottles was also checked. No significant losses of Hg were observed after up to 14 days of storage.

3.2. Diffusion membrane materials selection

The diffusion membrane acts as a semipermeable barrier between the receiving phase and the aqueous medium [28]. Since it is known that Hg has strong sorption properties, and could adsorb to the diffusion membrane material before reaching the receiving phase, the degree of Hg binding to the different candidate membrane materials was evaluated. This was taken into account in the selection of the definitive sampler configuration for Hg. Three different commercially available membranes, cellulose acetate, polyethersulphone and acetate dialysis, were tested in combination with a chelating receiving phase. Three replicates of each sampler configuration (CHE-diffusion membrane) were exposed for 48 h at a fixed concentration of Hg (2 µg L⁻¹), and at 11 °C and turbulence level SL1. After exposure, the Hg was extracted from both the receiving phase and the diffusion membrane. The relative accumulation factor (AF) in both the diffusion membrane

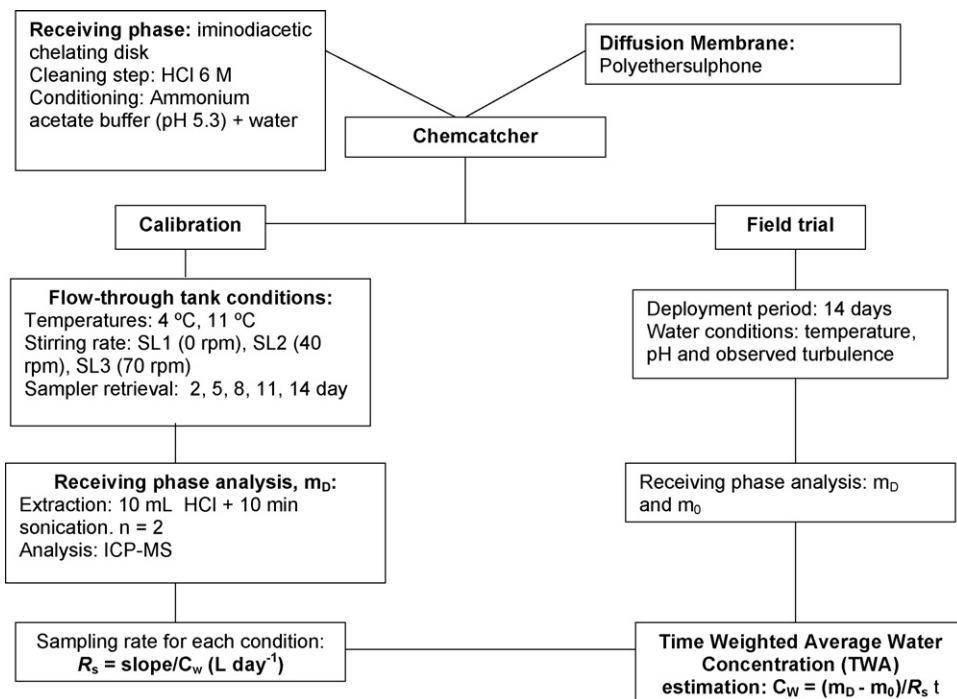


Fig. 1. Analytical protocol for calibration and field trial studies.

and receiving phase is determined as the ratio of mass of analyte accumulated in the receiving phase or diffusion membrane during deployment and the mass accumulated in the receiving phase in the absence of a diffusion membrane (Fig. 2). These AF provide a measure of the effects of the diffusion membrane on uptake by the receiving phase. These membranes varied in nature, pore size and thickness, and as expected Hg was bound to all of them to different degrees. The membranes tested have a moderately hydrophilic nature which favours the accumulation of ionic Hg, but some permeates through their structure allowing its accumulation in the receiving phase. The observed AF values indicate that all of the candidates could potentially be used as diffusion membranes. However, the D membrane was discarded because is prone to biodegradation in the field and provides the lowest accumulation in the chelating disk.

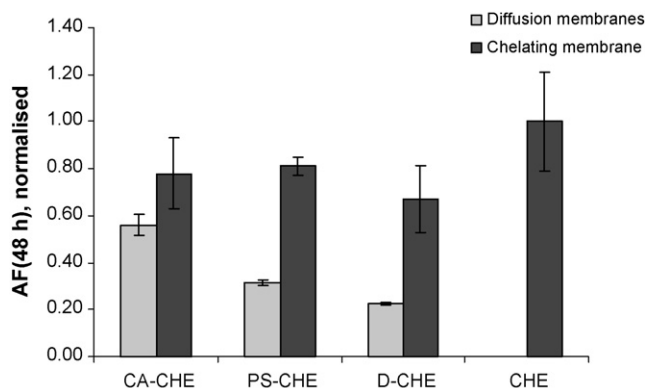


Fig. 2. Normalized accumulation factors (AF) after 48 h deployment for membranes and receiving phase with respect to the naked receiving phase (CHE) (AF = 1). Samplers were deployed at the bottom of the calibration tank at a water temperature of 11 °C and a turbulence level of SL1. Hg concentration $2 \mu\text{g L}^{-1}$ ($n = 3$). Key: CA: cellulose acetate, PS: polyethersulphone, D: cellulose dialysis and CHE: chelating.

Subsequently the accumulation of Hg by the configurations CHE-CA and CHE-PS was measured over a longer period of time (7 days) at 11 °C, SL1 and a Hg concentration of $4 \mu\text{g L}^{-1}$. Linear accumulation with time was observed for both samplers; however the lag time (time necessary to saturate the diffusion membrane with analyte before its subsequent accumulation in the receiving phase) was shorter for the CHE-PS configuration, and this was used in all subsequent experiments.

3.3. Sampler uptake rates of Hg in tank studies

Reviews of the principles governing the uptake of an analyte by different designs of passive sampling device constructed from a receiving phase and a diffusion membrane, including the Chemcatcher, have been published [27–31]. Briefly, the uptake of a chemical into a sampler can be divided into three stages: linear, curvilinear and finally equilibrium state. During initial deployment accumulation is approximately linear. At this stage, the mass of analyte in the receiving phase is directly proportional to the concentration to which the system has been exposed, deployment time and effective sampling rate (R_s); following the equation:

$$m_D = m_0 + C_W R_s t \quad (1)$$

where m_D = mass (ng) of target analyte accumulated in the receiving phase, m_0 = initial mass (ng) of the analyte in the receiving phase, C_W = TWA analyte concentration in water (ng L^{-1}), R_s = effective sampling rate of the device (L day^{-1}) and t = deployment time (days). R_s represents the equivalent volume of water cleared of analyte per unit of time and is analyte specific:

$$R_s = k_e K_{DW} V_D \quad (2)$$

where k_e is an overall exchange rate constant, K_{DW} is the receiving phase-water distribution coefficient and V_D is the volume of the receiving phase. R_s can be determined experimentally using a flow-through calibration tank at a fixed concentration of analyte (C_W). After exposure the uptake curve is obtained as the amount

Table 2

Calibration curve fits and estimated sampler uptake rate (R_s) for inorganic Hg at different combinations of water temperature and water turbulence in the flow-through tank. Results are expressed as mean R_s (L day^{-1}) \pm coefficient of variation ($n=3$). Two or three replicates were retrieved after 2, 5, 8, 11 and 14 days of exposure. SL1: samplers at the bottom of the tank. SL2: samplers rotating at 40 rpm. SL3: samplers rotating at 70 rpm. Nominal Hg concentration was $0.4 \mu\text{g L}^{-1}$ for 4°C and $0.2 \mu\text{g L}^{-1}$ for 11°C .

Water temperature ($^\circ\text{C}$)	Stirring level	Slope (ng h^{-1})	Regression coefficient (R^2)	Sampler uptake rate, R_s (L day^{-1})
4	SL2	1.69	0.99	0.080 ± 0.018
	SL3	1.43	0.95	0.070 ± 0.016
11	SL1	0.44	0.83	0.029 ± 0.009
	SL2	0.70	0.94	0.084 ± 0.019
	SL3	0.76	0.97	0.091 ± 0.020

of analyte accumulated in the receiving phase versus the sampler exposure time. Where the sampler operates within the linear region of the calibration curve (up to approximately the half time to reach equilibrium), R_s is calculated by dividing the slope of the calibration curve by the aqueous analyte concentration during the exposure period. R_s could be affected by environmental variables such as water temperature and turbulence.

In order to measure the effects of temperature and turbulence on the performance of the CHE-PS Chemcatcher for the sampling of Hg, samplers were deployed in the calibration tank for up to 14 days at two water temperatures, three levels of turbulence (Table 1) and at a constant concentration (C_w) of Hg (0.2 or $0.4 \mu\text{g L}^{-1}$). After exposure, the amount of analyte (m_D) accumulated in the receiving phase was measured. Each calibration experiment yielded an uptake curve from which the sampling rate (R_s) for Hg could be calculated. Satisfactory linear regression fits of the Eq. (1) were obtained for most conditions tested. Table 2 summarizes the calibration data for each of the five experiments and the calculated sampling rates (R_s).

Linear uptake was observed over a deployment period of 14 days at a relatively high concentration (0.2 or $0.4 \mu\text{g L}^{-1}$) of Hg in the tank. This provides evidence that the sampler is operating in a region far from equilibrium. This is consistent with the high capacity (about 45 mmol/disk of divalent metal) of the Empore chelating disk, and its strong complexation with Hg. Additional experiments (data not shown) indicate that even after 30 days of deployment the uptake was still linear.

The rate of uptake of Hg into the receiving phase, and therefore the R_s value obtained, is affected by two diffusion barriers: the water boundary layer (typically about 1 mm in stagnant conditions) and the membrane (ca. 0.15 mm thickness). In more turbulent conditions, the thickness of the boundary layer decreases (to about 0.001 – 0.1 mm in fast flowing conditions) [28] which may have a significant effect on sampling rate. These effects are evident under the conditions of 11°C and SL1 (i.e. static conditions) where a low value of R_s (0.029 L day^{-1}) was obtained. Lag-time is another important factor that affects the rate of uptake of analytes over the deployment period, and will be particularly influential for short deployments. This will increase with the thickness of the water boundary layer. The lag-time effect is higher at lower water temperatures, where no measurable uptake was achieved. At 11°C and higher levels (SL2 and SL3) of turbulence the lag-phase was considered smaller (less than 1 day). These results suggest that accumulation at low turbulence levels was mainly affected by diffusion through an aqueous boundary layer, and to a lesser extent by diffusion across the PS membrane. The R_s values obtained from laboratory-based calibrations, except those using quiescent conditions, should allow a reasonable estimation of TWA concentrations in flowing field waters. Values of R_s were in the range 0.070 – 0.091 L day^{-1} , and therefore the volume of water sampled during a typical 14-day field deployment would be 0.98 – 1.27 L . No significant effects of temperature on uptake were found between 4 and 11°C , and similar behaviour would be expected to even at the

slightly higher water temperatures found in river water in summer.

3.4. Quality control and method quantification limits

The application of appropriate quality control (QC) procedures is mandatory for the use of any passive sampler. Appropriate QC samples should be prepared to quantify background levels in the receiving phase, and possible contamination during transport, deployment, retrieval, storage, processing and analysis. Apart from the commonly used reagent and procedural blanks, two different types of QC Chemcatchers are used: fabrication blanks and field blanks. Fabrication blanks are prepared in parallel to samplers for deployment and are kept refrigerated and filled with deionised water in the laboratory during the sampling campaign. Field blanks are samplers that account for contamination during transport to and from each sampling location. They are transported under the same conditions as deployed samplers and are exposed to ambient air during both deployment and retrieval. During the whole sampling period these samplers are kept refrigerated and filled with deionised water. Another factor to be considered is the number of samplers deployed, and the number of blanks to be used at each field location. The number of samplers used will depend on the required confidence level for the data obtained. It is generally recommended that 2–3 field and laboratory blanks and 4–6 exposure Chemcatcher samplers are used at each location. The difference in concentration between replicates was usually less than 10% for QC blanks and less than 20% for exposure samplers. Another factor that contributes to the overall uncertainty of the method is the reliability of the estimates of Hg concentration in the water of the calibration tank during the 14 days exposures. The variability of the measured concentration over the duration of the experiments was in the range 10–20%.

The quantification limit depends on the sampling rate, the exposure period and the detection limit of the analytical technique. The overall method detection limit (MDL), was calculated as the minimum aqueous concentration (C_w) of Hg detectable by the sampler after a typical 14-day field exposure. This was calculated by substituting into Eq. (1) the FI-ICP-MS instrumental detection limit for a blank sampler (calculated as three times the standard deviation based on 10 replicates) in the mass accumulated (m_D) term, and using the different uptake rates (R_s) (Table 2). The MDL ranged between 2.2 and 2.9 ng L^{-1} (as Hg) at the two water temperatures and at medium (SL2) and high (SL3) water turbulences tested. The method quantification limit (MQL) ranged between 7.3 and 9.7 ng L^{-1} (as Hg). These concentrations are low enough to enable monitoring levels of Hg by the developed passive sampler in most contaminated aquatic environments.

3.5. Field trial at Valdeazogues River, Almadén, Spain

A field study at the Valdeazogues River (Almadén, Spain) between 1974 and 1977 showed that the concentration of Hg

Table 3

Concentration of Hg in spot water samples ($n=3$) collected from the Valdeazogues River at location 1 during the field deployment of the passive sampling devices. S.D. = standard deviation.

Time (day)	Concentration of Hg (ng L^{-1})	Mean concentration of Hg \pm S.D. (ng L^{-1})
0	909	883 ± 27
	856	
	884	
7	421	454 ± 41
	440	
	500	
14	64	60 ± 4
	56	
	60	

in unfiltered water samples ranged between 1.64 and 3.0 $\mu\text{g L}^{-1}$. Twenty years later (1995–1997), a study performed at similar sampling points showed that the water concentration had decreased (<0.11 – $1.13 \mu\text{g L}^{-1}$) [5]. The latter level is below the maximum in-stream concentration (2.4 $\mu\text{g L}^{-1}$ Hg) allowed by the US Environmental Protection Agency [2] and similar to the average monthly maximum allowable concentration (1.0 $\mu\text{g L}^{-1}$ total Hg) for inland surface waters [3]. It has been reported that the river sediments in this area contain high concentrations of Hg (typically 0.01–0.05 $\mu\text{g g}^{-1}$), being about one order of magnitude higher than those commonly considered as representative of global background levels [26,32]. Monitoring data also show a quite serious pollution problem with phosphate, nitrate and ammonium with values up to 5.9, 1.42 and 12.0 mg L^{-1} , respectively. This area was therefore deemed as a suitable site to evaluate the field performance of the newly developed variant of the Chemcatcher passive sampler.

Two field sites along the Valdeazogues River were selected for the 2-week deployment of the samplers. Spot water samples and measured parameters were taken at days: 0, 7 and 14 of the trial. The water temperature was 10, 9.5 and 12 °C at both sites and water pH was 6.9, 6.5 and 6.3 at the first sampling point and 7.6, 7.2 and 7.0 at the second during the trial. At both locations biofouling of the diffusion membrane of the samplers was minimal; however, some deposition of silt was observed on the diffusion surface on retrieval of the devices.

Concentrations of total Hg found in spot water samples collected in the section between the Valdeazogues river and the La Serena dam (location 1) are shown in Table 3. The concentration of total Hg in unfiltered water samples collected 15 km downstream of the above location (location 2) was, as expected, much lower, being below the analytical detection limit ($<1.2 \text{ ng L}^{-1}$). The levels found at location 1 (883–60 ng L^{-1}) are in agreement with other data for the river in the same season and with similar water flows [5]. The differences in concentration (more than one order of magnitude) between the start and the end of the trial were probably due to a period of heavy rainfall at the end of the first week that increased the river flow and diluted the concentration of Hg in the water samples. These data demonstrate the difficulties in the use of irregular spot sampling procedures to estimate meaningful concentrations of aquatic pollutants.

The mass of Hg found in the receiving phase of Chemcatcher after deployment at the two sampling points and the estimated TWA concentrations interval (C_w) are given in Table 4. The temperature was about 11 °C and the turbulence of the river water during this season was assumed to be equivalent to the SL2–SL3 turbulence range of the calibration tank experiments. Therefore, for TWA estimated concentration, R_s value in the range 0.084–0.091 L day^{-1} was used. The different concentrations of Hg found in the spot

water samples at the two sampling points were also reflected in the amount of Hg accumulated by the samplers.

At location 1, the estimated TWA concentration of Hg (85–92 ng L^{-1}) measured by Chemcatcher was much lower than that found in spot water samples collected over the same period (mean value of 466 ng L^{-1} Hg). However, at the end of the trial (day 14) the average spot water concentration of Hg was $60 \pm 4 \text{ ng L}^{-1}$, that is lower than the TWA concentration measured by the sampler. The concentration in the river water may have been even lower immediately after the rain event than that measured at the end of the trial. However, no information is available on this, and it exemplifies the difficulties in comparing aqueous concentrations measured by the two techniques and shows the potential advantages of the use of passive sampling device in obtaining an improved overall picture of water quality [12,13].

Calibrations were performed in tap water with relatively high amounts of chloride and sulphate ions, and Hg^{2+} was introduced in the systems as HgCl_2 ($\log \beta_1 = 6.6$ and $\log \beta_2 = 13.2$), it could be expected that the effective uptake rate was representative of free and hydrated ions, and also of weak Hg complexes that could diffuse through the PS membrane (200 nm pore size). This behaviour is similar to that postulated for other passive samplers which sequester mainly the ionic and kinetically labile unbound fraction of metals present in the water [17–20,22,28]. Some fractions would have readily formed complexes with dissolved organic matter (fulvic and humic acids) or be bound to particulate material in the unfiltered water samples. The pore size of the membrane will exclude some but not all of these fractions. The calibration data are based on solutions containing only very low concentrations of organic matter. In the field there will be wide variation in the concentrations and properties of the organic material present. It is not feasible to take this into account this wide variability in routine laboratory-based calibrations. However, this should be taken into consideration when interpreting field data. Further work is needed in this area for all types of passive sampler (for both organic and inorganic pollutants). At location 2, the Chemcatcher was able to sequester measurable amounts of Hg where the spot sample water concentration was below the detection limit.

The performance of Chemcatcher for Hg can be also compared with the DGT passive sampling device developed for Hg [18]. These devices differ in their design, materials of construction and geometry. Like the DGT, Chemcatcher, sequesters only inorganic ions and labile fractions of metals that are able to diffuse across the diffusion layers. As for DGT, the Chemcatcher sequestration capability should allow an *in situ* fractionation of Hg species by the application of different membranes varying in pore size.

Table 4

Mass of Hg accumulated in the 47 mm Empore chelating receiving phase of the Chemcatcher at the two sampling sites on the Valdeazogues River after the 14-day trial and the calculated TWA concentration. The TWA concentration (C_w) of Hg was calculated using the R_s interval of 0.084–0.091 L day^{-1} (water temperature 11 °C, and water turbulence levels SL2 and SL3).

Sampler number	Location 1 (ng disk^{-1})	Location 2 (ng disk^{-1})
Field blank \pm S.D. ($n=3$) ^a	28.4 \pm 2.3	26.4 \pm 0.9
1	102.2	50.1
2	180.5	40.0
3	125.2	43.3
4	147.1	30.2
5	137.3	33.5
6	125.4	36.8
Mean	136.3 \pm 26.4	39.0 \pm 7.1
TWA (C_w) (ng L^{-1})	84.7–91.7	9.9–10.7

^a The mass of Hg in the field blank was subtracted from the mass of Hg found in the disk after deployment to calculate the TWA concentration.

4. Conclusions

The passive sampler developed and evaluated in the current work for the measurement of Hg in surface waters increases the range of applications of the Chemcatcher technology. The device, based on an iminodiacetic chelating receiving phase and a PS membrane provides a sampling rate high enough to detect Hg species at environmentally relevant levels. One important advantage of this variant of the Chemcatcher is that it uses low cost, commercially available components that are easy to pre-condition and assemble into the PTFE sampler body. The TWA concentration range estimated by this sampler in the field trial was about an order of magnitude less than estimates derived from spot samples. This reflects a difference between the two methods where the passive sampler measures only the inorganic ions and the weak complexes of Hg that are able to diffuse across the water boundary layer and PS membrane, whereas the spot sampling (unfiltered) measures the total Hg content of the water. Despite these differences the passive samplers provide useful data that give information concerning concentrations of pollutants in the water between infrequent spot sampling events. This technology could yield complementary data that would increase confidence in the information from routine regulatory water monitoring programmes.

Acknowledgements

We acknowledge the financial support of the European Commission (STAMPS: Contract No. EVK1-CT-2002-00119) and Ministerio de Educación y Ciencia (CTQ2004-20349-E/PPQ) for this work (<http://www.port.ac.uk/research/stamps/>).

References

- [1] European Communities Council Decision 2455/2001/EC, Office for Official Publications of the European Communities.
- [2] Report EPA 816-F-03-016 June 2003, National Drinking Primary Water Standards, United States. <http://www.epa.gov/safewater/consumer/pdf/mcl.pdf>. Last accessed September 2007.
- [3] WHO Guidelines for Drinking-Water Quality, World Health Organisation, 2005.
- [4] J.E. Sánchez Uría, A. Sanz Medel, Talanta 47 (1998) 509.
- [5] J.J. Berzas-Nevaldo, L.F. Garcia-Bermejo, R.C. Rodríguez Martín-Doimeadios, Environ. Pollut. 122 (2003) 261–271.
- [6] F. Bakir, Science 191 (1973) 230–241.
- [7] C. Neal, R.J. Williams, M. Neal, L.C. Bhardwaj, H. Wickham, M. Harrow, L.K. Hill, Sci. Total Environ. 251 (252) (2000) 441–457.
- [8] I.J. Allan, B. Vrana, R. Greenwood, G.A. Mills, B. Roig, C. Gonzalez, Talanta 69 (2006) 302–322.
- [9] S. Kahle, P.H. Becker, Chemosphere 39 (1999) 2451–2457.
- [10] J. Burger, K.F. Gaines, C.S. Boring, W.L. Stephens, J. Snodgrass, M. Gochfeld, Environ. Res. 87 (2001) 108–118.
- [11] F. Stuer-Lauridsen, Environ. Pollut. 136 (2005) 503–524.
- [12] B. Vrana, I.J. Allan, R. Greenwood, G.A. Mills, E. Dominiak, K. Svensson, J. Knutsson, G. Morrison, TrAC-Trend Anal. Chem. 24 (2005) 845–868.
- [13] J. Namiéśnik, B. Zabiegala, A. Kot-Wasik, M. Partyka, A. Wasik, Anal. Bioanal. Chem. 381 (2005) 279–301.
- [14] A. Södergren, Environ. Sci. Technol. 21 (1987) 855–859.
- [15] T. Górecki, J. Namiéśnik, TrAC-Trend Anal. Chem. 21 (2002) 276–291.
- [16] D.W. Brumbaugh, J.D. Petty, T.W. May, J.N. Huckins, Chemosphere: Global Change Sci. 2 (2000) 1–9.
- [17] W. Davison, H. Zhang, Nature 367 (1994) 546–547.
- [18] M.C. Alfaro-De la Torre, P.Y. Beaulieu, A. Tessier, Anal. Chim. Acta 418 (2000) 53–68.
- [19] H. Docekalová, P. Divis, Talanta 65 (2005) 1174–1178.
- [20] J.K. Kingston, R. Greenwood, G.A. Mills, G.M. Morrison, L.B. Persson, J. Environ. Monit. 2 (2000) 487–495.
- [21] L.B. Persson, G. Morrison, J.U. Friemann, J. Kingston, G. Mills, R. Greenwood, J. Environ. Monit. 3 (2001) 639–645.
- [22] B. Vrana, G.A. Mills, M. Kotterman, P. Leonards, K. Booi, R. Greenwood, Environ. Pollut. 145 (2007) 895–904.
- [23] R. Aguilar-Martínez, R. Greenwood, G.A. Mills, B. Vrana, M.A. Palacios-Corvillo, M.M. Gómez-Gómez, Intern. J. Environ. Anal. Chem. 88 (2008) 75.
- [24] B. Vrana, G.A. Mills, E. Dominiak, R. Greenwood, Environ. Pollut. 142 (2006) 333–343.
- [25] P. Higuera, R. Oyarzun, J.C. Sánchez Hernández, J.A. Molina Abril, J. Lillo, S. Lorenzo, J.M. Esbrí, J.E. Gray, M.E. Hines, VII Congreso Nacional de Medio Ambiente, Madrid, 2004.
- [26] P. Higuera, R. Oyarzun, J. Lillo, J.C. Sánchez-Hernández, J.A. Molina Abril, J.M. Esbrí, S. Lorenzo, Sci. Total Environ. 356 (2006) 112–124.
- [27] L.P. Yu, X.P. Yan, Trends Anal. Chem. 22 (2003) 245–253.
- [28] K. Booi, B. Vrana, J.N. Huckins, in: R. Greenwood, G.A. Mills, B. Vrana, D. Barceló (Eds.), Comprehensive Analytical Chemistry, vol. 48, Elsevier, Amsterdam, 2007, pp. 251–278.
- [29] J.N. Huckins, G.K. Manuweera, J.D. Petty, D. Mackay, J.A. Lebo, Environ. Sci. Technol. 27 (1993) 2489–2496.
- [30] B. Vrana, G.A. Mills, R. Greenwood, J. Knutsson, K. Svensson, G. Morrison, J. Environ. Monit. 7 (2005) 612–620.
- [31] J.N. Huckins, J.D. Petty, K. Booi, Monitors of Organic Contaminants in the Environment: Semipermeable Membrane Devices XV, Springer Verlag, Germany, 2006, p. 223.
- [32] M.S. Gustin, G.E. Taylor, T.L. Leonard, Environ. Health Perspect. 102 (1994) 772–778.



Research into conditions of quantity in the determination of carboniles in complex air matrices by adsorptive solid phase microextraction

E. Gómez Alvarez^{a,*}, M. Valcárcel^{b,1}

^a *Fundación Centro de Estudios Ambientales del Mediterráneo (CEAM), Charles Darwin, 14, Parque Tecnológico, 46980 Paterna, Valencia, Spain*

^b *Department of Analytical Chemistry, Marie Curie Annex Building, Campus de Rabanales, University of Córdoba, E-14071 Córdoba, Spain*

ARTICLE INFO

Article history:

Received 11 March 2008

Received in revised form 9 September 2008

Accepted 21 September 2008

Available online 5 October 2008

Keywords:

Solid phase microextraction fibres

Displacement effects

Quantitative air sampling

Carboniles

PFBHA derivatisation

EUPHORE

ABSTRACT

This study focuses on certain aspects of the quantity of adsorptive solid phase microextraction when applied in the form of on-fibre derivatisation with *O*-(2,3,4,5,6)-pentafluorobenzyl-hydroxylamine hydrochloride (PFBHA) for the determination of carboniles in air samples of relevance in the atmosphere. The study was performed in the high-volume outdoor atmospheric simulation chambers (EUPHORE) located in Valencia (Spain). At short sampling times, the adsorption profiles obtained when only benzaldehyde was inserted in the chamber coincided with those obtained when other carbonylic compounds were also introduced at the same concentration, and this was also the case when the concentration of all the gaseous mixture components was increased considerably from one experiment to another. In a number of experiments applying different conditions, it was proven that all the extraction profiles belonged to the same regression when the fibre responses were plotted against the concentration–time product. A number of calibrations were obtained for benzaldehyde introduced in the chamber alone and in a mixture with three other carboniles at similar concentration values. A statistical test is applied to confirm that they all belonged to the same regression since they shared homogeneous variances. After these tests, the method of SPME on-fibre derivatisation for the determination of carboniles was considered to be safely applicable to quantification. Moreover, the concentration levels at which certain unwanted effects, i.e., displacement, saturation and competition, were observed are a few orders of magnitude higher than their occurrence levels in atmospheric processes.

© 2008 Elsevier B.V. All rights reserved.

1. Introduction

The analytical determination of carboniles generated as intermediate degradation products in atmospheric reactions poses important difficulties and their quantification in atmospheric matrices constitutes an analytical challenge. Carboniles are polar and volatile, a fact that negatively affects their chromatographic behaviour [1]. Tropospheric mixing ratio ranges for OVOs are highly variable [2–4] and generate at low concentration levels as products of atmospheric reactions, thus adding more complexity to the determination. With the exception of formaldehyde and acetaldehyde, which can be present at relative high concentration levels in ambient air, the concentration of the rest can be expected low [5]. As an example, benzaldehyde concentration (target compound in the present study) in ambient air has been estimated at

low values, i.e., 0.1–1 ppbV in urban ambient air. Carboniles are highly reactive with atmospheric oxidants (and especially with the OH radical, which is the major oxidizing agent in the atmosphere) [6]. Their atmospheric relevance also comes from their absorption of light in the 290–400 nm region that producing the radicals RO₂, HO₂, and OH. In the drier parts of the atmosphere, this source of OH radicals, primarily from formaldehyde and acetone, can become the dominant source [5,7].

Derivatisation with dinitrophenyl hydrazine (DNPH) – normally used in conjunction with HPLC analysis – [8,9] and PFBHA is usually applied to the determination of carboniles in air. Both types of derivatisation are performed after sampling with cartridges (gas phase) and/or filters (particles) and are followed by lengthy and aggressive sample treatment steps, which could potentially alter the sample composition. Silica gel cartridges impregnated with DNPH have been used for over two decades for carbonile measurements [10]. This technique enables relatively easy sample collection in the field but suffers from low time resolution. However, it requires substantial sample preparation since the derivative products need to be isolated prior to chromatography through lengthy solvent extraction steps. In addition, derivatisation with

* Corresponding author. Tel.: +34 96 131 8227; fax: +34 96 131 8190.

E-mail addresses: elena@ceam.es (E.G. Alvarez), qa1meobj@uco.es (M. Valcárcel).

¹ Tel.: +34 957 218616; fax: +34 957 218616.

DNPH presents serious difficulties in the determination of certain carboniles, especially dicarboniles, due to the inefficiency of derivatising both groups simultaneously.

PFBHA derivatisation applied to solid phase microextraction [11–13] provides a number of exceptional advantages. Derivatisation takes place immediately on PFBHA anchored to the fibre following a simple procedure consisting of simply exposing the fibre to the headspace of a high PFBHA concentration solution. As the fibre is directly introduced in the liner/injector of a gas chromatograph, analytes are thermally desorbed and carried into the column, thus avoiding dilution by solvents and sample alteration due to sampling treatment steps. In addition, the methodology can resolve and quantify stereoisomers individually. It is particularly sensitive to dicarboniles (these carboniles that pose the greatest problems for determination by DNPH derivatisation, as outlined above), since the carbonylic groups are efficiently derivatised, providing high molecular weight oximes. In an atmospheric simulation chamber, the methodology can be conducted *in situ* from the chamber, thus avoiding sampling tubes and lines. The combination of both advantages has resulted in the quantification of dicarbonylic intermediates of aromatic photo-oxidation [14].

The main difficulty is calibration. A few approaches have been developed. Martos and Pawliszyn [11] developed an approach based on the physico-chemical properties of the coating, applied to liquid fibres, i.e., when the extraction mechanism is absorption. Górecki et al. [15] developed a theoretical calibration procedure for adsorption-type fibres based on the Langmuir adsorption isotherm.

Sampling with adsorptive materials is by definition competitive. Sampling of a mixture of compounds with adsorptive fibres could constitute the real limitation of SPME. This modality of SPME is also much more sensitive and achieves significantly better LOD than sampling with liquid fibres. The amount of the analyte extracted by the fibre from a sample can be significantly affected by the sample matrix composition [15–17]. In addition, bibliographical reports [18] different adsorption profiles, i.e., differing profiles of adsorbed mass versus sampling time (min), at different concentrations are of concern since this fact adds new difficulties to calibration. These facts have led us (1) to explore variations in the methodology which could lead to improving its performance and (2) to conduct studies aimed at evaluating the quantitivity of the methodology in the experimental conditions applied to atmospheric studies. In the present work, the emphasis is placed on the elucidation of such effects in the determination of carboniles of relevance to atmospheric studies.

On the positive side, the results obtained by our group in an intercomparison exercise [19] proved that the SPME methodology could yield quantitative measures for the analytes tested. Among the analytes tested in this exercise was benzaldehyde, the target compound in the present study. The experimental work described herein was carried out in preparation for our participation in the intercomparison exercise.

The present study reports the experimental conditions in which the methodology of SPME on-fibre derivatisation with PFBHA is best applied to the determination of carboniles in gaseous atmospheric matrixes, with the aim of improving the quality of the results obtained in terms of sensitivity and quantitivity, as well as the conditions under which competition between analytes can be avoided. Benzaldehyde, the analyte studied in this work, was scrutinized in different mixtures at different concentrations of the component analytes and under different experimental conditions applied to the sampling. The aim was to search for conditions in which unwanted effects that may affect quantitivity could be avoided and establishing upper concentration levels at which quantitative determinations could be obtained. For that reason a conscious choice of concentrations considerably higher than ambi-

ent levels of compounds into the chamber was made. Although these are not realistic concentration levels, they usually constitute working conditions in atmospheric simulation chambers, in order to match the limits of detection of the range of analytical methodologies involved. In addition, the feasibility of calibrating and applying the calibrations on different days and under different experimental conditions was explored. The development of calibration procedures that do not depend on the matrix composition was also dealt with in the present work.

2. Experimental

2.1. Technical description of the European photo-reactors (EUPHORE) chambers

Each of the two simulation chambers is formed by 32 individual segments welded together to form a half-spherical shaped Teflon bag with a volume of about 200 m³. The chambers are made of a fluorine-ethene-propene (FPE) foil with a thickness of 0.13 mm. This foil can transmit over 80% of incident light in the near UV and the visible range between 280 and 640 nm, which is the important range for the photo-oxidation processes. Each chamber is self-stabilising against wind distortions when operated with an excess pressure of 100–200 Pa. A floor cooling system integrated in the chamber floor compensates heating of the chamber by solar radiation. Ports for input of the reactants and sampling lines for the different analytical instruments are located on the floor of the chamber. Two mixing fans of 67 m³ min⁻¹ air throughput are mounted inside the chamber to ensure homogeneous mixing of the volume. They provide an interior air velocity of approximately 4 m s⁻¹. This fact is of extraordinary importance and could be the basis for the sensitive determination that the SPME methodology has achieved in determining the intermediates of the reactions conducted in the simulators.

The air that fills the chamber is passed through a compressor and after through a condensate trap to separate oil and water from the air. The emulsion is separated in an oil water separator. The air is dried in absorption driers with an air throughput of ca. 500 m³/h. These driers are filled with a special molecular sieve. A pressure dew point of -70 °C is reached and the CO₂ content is reduced significantly. By means of a special charcoal adsorber NO_x is eliminated and oil vapour and non-methane hydrocarbons are reduced to a limit of <0.4 µg/m³.

In addition to conventional analytical instrumentation (GC, GC-MS, HPLC, O₃, NO_x and NO_y analysers, actinometers for measurement of photolysis frequencies of different chemical species – J (O₃), J (O¹D) and J (NO₂)) the chamber is equipped with state-of-the-art *in situ* measurement techniques (long-path Differential Optical Absorption Spectrometry (DOAS), long-path Fourier Transformed Infrared Spectrometry, Tunable Diode Laser).

A FTIR spectrometer (NICOLET, MAGNA 550, resolution of 1 cm⁻¹, MCTβ detector) is used to determine at any time the concentration of compounds introduced in the chamber (and their products when that is the case). It is used for the trace gas detection in the infrared spectral range between 400 and 4000 cm⁻¹, in combination with a long-path absorption system. Liquid N₂ (Praxair) is used to cool down the detector.

Losses in the chamber volume caused by the variety of sampling equipment and instruments connected on-line to the chamber, are compensated by a replenishment flow that maintains an overpressure in the chamber. This causes a dilution, for which SF₆ (sulfur hexafluoride) is added as a dilution tracer. This is an inert compound that yields a strong band between 955 and 935 cm⁻¹ in the infrared spectrum. In each experiment, 6.5 ml of SF₆ was injected

into the chamber through one of the ports integrated in a flange for the input of reactants. The absorption peak produced by this compound is integrated throughout the course of the reaction. A graphical plot of the decay (as a natural logarithm over time of the ratio of absorbance at any given time with respect to the initial absorbance recorded just after the introduction of the tracer in the chamber) provides the dilution rate. Typical values in chamber B of the EUPHORE facilities are between $(5-7) \times 10^{-6} \text{ s}^{-1}$.

Additional information on technical aspects of the chambers operation is provided in four EUPHORE Reports [20–23]. PDF copies of the reports can be downloaded from the Web site http://www.physchem.uni-wuppertal.de/PC_WWW_Site/Publications/Publications.html.

2.2. Reagents and materials

The following reagents were used: acetaldehyde (Fluka, Milano, Italy), para-formaldehyde (also called polyoxymethylene) (Fluka, Milano, Italy) a polymer of formaldehyde, benzaldehyde (Aldrich, St. Louis, MO, USA), O-(2,3,4,5,6) pentafluorobenzylhydroxylamine hydrochloride (Fluka). Weighed amounts of each one of the compounds were inserted in the chamber according to the concentration level desired. The compounds were weighed, introduced in an impinger, heated to volatilisation and finally carried by an air stream inside the chamber.

The SF₆, introduced in the chamber to monitor dilution was purchased from Abelló Linde, S.A., Gases Técnicos, Barcelona.

Polydimethylsiloxane/divinylbenzene (PDMS/DVB) 65 μm SPME fibres were purchased from Supelco (Lund, Sweden). 4 ml amber headspace Vials for SPME with Silicone Septa were also purchased from Supelco.

2.3. Instrumentation and methods

For the analysis of SPME fibres, a 6890 HP Gas Chromatograph equipped with a HP-5MS capillary column (crosslinked 5% PHME siloxane, 30 m × 0.25 μm × 0.25 μm) which was coupled to a flame ionization detector (FID) and an inlet liner with a narrow internal diameter (0.75 mm i.d. pre-drilled thermogreen LB-2 septa for SPME) were also purchased from Supelco.

The conditions that achieved the best resolution of peaks, sensitivity and speed of analysis were as follows: oven temperature: start-up at 80 °C, held for 2 min, followed by a ramp of 20 °C/min to 200 °C, held for 2 min (total analysis time, 11 min). Injector: 270 °C. The system was operated in splitless mode. After 1 min, a 9.1 ml/min split flow was started. The column flow was set at 2 ml/min.

At working chromatographic conditions, the oxime HCHO-PFBHA eluted at 3.57 min and the excess of PFBHA at 4.5 min approximately. Acetaldehyde and benzaldehyde yielded two isomeric oximes at retention times of approximately 4.60 and 4.66 min for the former and 9.24 and 9.33 min for the latter. Quantification of the oximes was performed by adding up the peak areas of the two oximes formed on derivatisation.

2.4. Fiber conditioning and application of derivatising agent on fibre

Previous to their initial use, the fibres were conditioned by inserting them in the injector of the gas chromatograph at 250 °C for half an hour according to manufacturer's instructions. Every day, the fibres are pre-conditioned by keeping them in the injector of a gas chromatograph for about 15 min. The fibres are used continuously, i.e., the fibre that is injected is directly taken out of the injector of a gas chromatograph to sample the next sample. By

doing so, every analysis also constitutes pre-conditioning for the following sampling step avoiding fibre contamination.

The derivatising reagent was loaded on the 65-μm thick PDMS/DVB fibre. Loading was performed from the headspace of a 4 ml opaque amber vial containing a well-agitated 17 mg/ml aqueous solution of PFBHA. The septum was punctured with the fibre sheath to a depth of 0.5 cm, as the loading of the derivatising agent is performed from the headspace. After 2 min, the fibre was retracted and removed from the vial. The needle was again adjusted to full length.

2.5. Calculation of concentration of carboniles in the chamber

The number of molecules or volumes of a given gaseous species, i.e., mixing ratios, forms the basis of units in atmospheric chemistry; in aqueous chemistry, mass rather than volume is used as the basis for expressing concentrations in ppm [5]. For gas-phase species, the most commonly used units are parts per million (ppm), parts per billion (ppb) and parts per trillion (ppt).

From the amount (mass) of compound introduced in the chamber, the concentration in molecules/cm³ is calculated by dividing by the MW of the compound, and the resulting amount in moles divided between the chamber volume (204,500 l) to obtain the concentration of the compound introduced in the chamber in mol/l. By applying a volume conversion factor (1 l = 10E+03 cm³), and the Loschmid number (6.02E+23 molecules mol⁻¹), the concentration in mol/l can be easily transformed in molecules/cm³.

$$\frac{(1/MW) \times (m(\text{mg})/1000)}{204,500(\text{l})/1000} \times 6.023 \times 10^{23}$$

In order to calculate the mixing ratios from the concentrations introduced in the chamber, the concentration in mol/l, calculated before, needs to be multiplied by the molar volume (22.4 l) and a correction for pressure and temperature (when not in normal conditions) applied. This will provide the volume (l) of compound per litres of dry air in the chamber. From the definition of ppm as the number of pollutant molecules per 10⁶ molecules of air (or 10⁹ in the case of ppb), the resulting amount should be divided by 10⁶ to obtain the mixing ratio in ppm, or 10⁹ to obtain the mixing ratio in ppb.

$$\frac{((1/MW) \times (m(\text{mg})/1000))/(204,500(\text{l})/1000) \times (22.4(\text{l})/1000) \times (T/273.15) \times (1013.25/\text{P})}{10^9}$$

Alternatively, a more accurate estimation of the concentration of the different analytes in the chamber can be obtained by FTIR, with the additional advantage of its good sampling acquisition capability. The concentrations of the different analytes in the chamber were obtained applying the corresponding factor to the absorption region or peak height as compared with previously recorded reference spectra. The concentration of a given analyte corresponding to a reference spectrum can be accurately determined by applying cross-section values obtained through a number of independent insertions of the compound in the chamber. The concentration of a compound in the chamber, cross-sections and chamber path-length are related to absorbance through the Lambert–Beer law. The cross-section is a measure of the effective surface area seen by the impinging radiation beam and, as such, has units of surface area (usually cm²). The concentration of HCHO during the course of the experiment was calculated by the peak height at 1746 cm⁻¹. The concentration of acetaldehyde was calculated by the analysis of the peak areas in the region 1053:1156 cm⁻¹, where acetaldehyde presents a characteristic band. Reference spectra were available from previous experiments. Finally, the exact concentration of

Table 1

Sequence of experiments and experimental conditions applied to set conditions of quantity in studies conducted in the environmental chambers EUPHORE.

Aim of the experiment	Composition of gaseous mixture in chamber ^b	Quantities introduced in chamber	<i>P</i> ^a	<i>T</i> ^a
(1) Optimization of derivatising reagent PFBHA concentration	500 ± 150 ppbV benzaldehyde	425 mg	1002.24	296.85
(2) Post-sampling derivatisation	505 ± 151 ppbV benzaldehyde	420 mg	1002.30	300.02
(3) Study of fibre saturation. Competitive and displacement effects. Comparison between benzaldehyde adsorption profiles when introduced alone in the chamber and in a mixture with other components				
(a) Benzaldehyde alone in chamber. Adsorption profiles (Fig. 2A and B)	1241 ± 372, 608 ± 182 and 163 ± 49 ppbV of benzaldehyde on different days. Adsorption profiles plotted (interval of sampling times: [10 s to 10 min]. 12 h for concentrations of 1241 ± 372 and 608 ± 182 ppbV	1 ml (1045 mg approximately)	1003.89	296.84
		500 µl (522 mg approximately) by dilution of last	1003.94 1003.94	290.86 290.86
(b) Mixture of aldehydes. Focus on just benzaldehyde (Fig. 3A and B)	(b.1) 617 ± 185 ppbV benzaldehyde alone 617 ± 185 ppbV benzaldehyde with 360 ± 108 ppbV formaldehyde, 1096 ± 329 ppbV acetaldehyde	522 mg benzaldehyde 86 mg formaldehyde 386 mg acetaldehyde	1003.94	295.21
	(b.2) (focuses on short sampling times) 150 ± 45 ppbV benzaldehyde alone 150 ± 45 ppbV benzaldehyde (25 ± 7 ppbV formaldehyde and 150 ± 45 ppbV acetaldehyde) 617 ± 185 ppbV benzaldehyde alone	by dilution of last	1003.94	294.86
(c) Study of mixtures focusing on all components (Fig. 4A and B)	(c.1) formaldehyde, 360 ± 108 ppbV acetaldehyde, 1096 ± 329 ppbV benzaldehyde, 617 ± 185 ppbV Adsorption profiles covering wide range of sampling times (up to several hours) (Fig. 4A) A window from the beginning of the x-axis of last profile, focusing on shorter sampling times (Fig. 4B)	86 mg formaldehyde 386 mg acetaldehyde 522 mg benzaldehyde	1003.94	294.86
	(c.2) Significant reduction of mixture components formaldehyde, 25 ± 7 ppbV acetaldehyde, 150 ± 45 ppbV benzaldehyde, 150 ± 45 ppbV	by dilution of last		
(d) Exploring conditions that permit obtaining common adsorption profiles in different experimental conditions. Sampling mixtures with significant reduction of sampling times (Fig. 5)	Day 1 314 ± 94 ppbV formaldehyde 311 ± 93 ppbV acetaldehyde Day 2 833 ± 250 ppbV formaldehyde 1221 ± 366 ppbV acetaldehyde Day 3 883 ± 265 ppbV formaldehyde 897 ± 269 ppbV acetaldehyde In all cases 50, 100, and 200 µl benzaldehyde successively added into the chamber providing increases of concentration levels of 65 ± 19, 125 ± 37 and 250 ± 75 ppbV approximately Sampling steps performed at 5, 15, 30, 45, 60 and 120 s	75 mg formaldehyde 109 mg acetaldehyde 198 mg formaldehyde 425 mg acetaldehyde 210 mg formaldehyde 313 mg acetaldehyde	1003.94 mbar 1007.8 mbar 1000.6 mbar	295 K 299 K 296 K
(e) Calibrations	(e.1) 500 ± 150 ppbV of benzaldehyde introduced in chamber alone (no other component introduced) Introduction repeated on four successive days and the corresponding four calibrations obtained	Benzaldehyde alone: 457 mg 476 mg 474 mg 437 mg	998.8 mbar 1004.72 mbar 1006.23 mbar 996.82 mbar	298.43 K 294.9 K 294.27 K 294.43
	(e.2) 479 ± 144 ppbV benzaldehyde 727 ± 218 ppbV butyraldehyde 468 ± 140 ppbV trimethylacetaldehyde Calibration performed and compared with the other four	(e.2) Calibration of benzaldehyde in mixture 416 mg benzaldehyde 444 mg butyraldehyde 320 mg trimethylacetaldehyde	992.86 mbar	293 K

^a *P*, *T* at introduction of components into the chamber.^b An error in the estimation of concentrations of 30% is attributed to unique additions of compounds into the chamber.

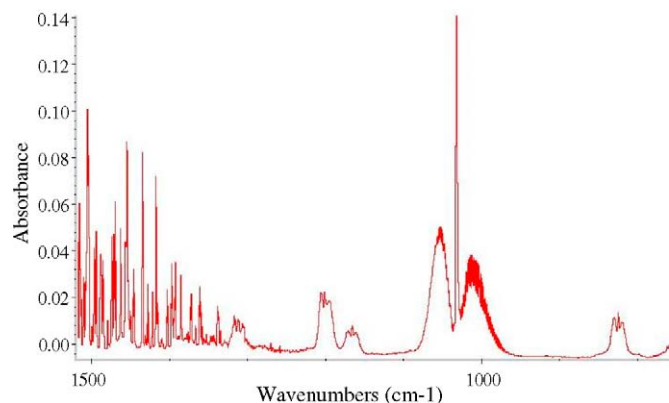


Fig. 1. FTIR reference spectrum of benzaldehyde in the area used in quantification introduced in the chamber at a concentration of approximately 120 ± 36 ppbV ($100 \mu\text{l}$).

benzaldehyde in the chamber was calculated by applying a similar approach in the region $1146:1228 \text{ cm}^{-1}$ where benzaldehyde presents a characteristic band. Fig. 1 shows the area of the FTIR benzaldehyde reference spectra in the region of interest obtained after inserting in the chamber $100 \mu\text{l}$ of benzaldehyde. The figure shows the band selected for quantification purposes because of its clear definition and less potential interference from other overlapping bands of the spectra coming from the rest of the carboniles introduced in the chamber.

The concentrations provided in Table 1 have been calculated as per above using the compound mass introduced in the chamber and the pressure and temperature at the time of its introduction. To calculate the function used in the plots to describe the concentration of benzaldehyde in the chamber, the concentration values obtained in the comparison of FTIR with reference spectra were graphically displayed. This allowed us to obtain the decay in benzaldehyde through the course of the experiments versus time and the calculation of the integral of the best-fitted concentration equation with time.

2.6. Planning and description of experiments

The sequence of experiments conducted and the experimental conditions applied are summarised in Table 1.

The initial tests aimed at optimising the experimental conditions related to the derivatisation reaction, in terms of the concentrations of derivatising agent solution used to load PFBHA on the fibre. The derivatisation process was also investigated to see if a change in the sequence of events could have the effect of diminishing the extent of some unwanted effects.

The next set of experiments aimed at assessing both the saturation phenomena on the fibre and the variation of adsorption profiles in the sampling of carboniles. For this, adsorption profiles were obtained for benzaldehyde introduced alone in the chamber at different concentration levels.

Then, benzaldehyde was inserted in the chamber in combination with other carboniles, and the adsorption profiles obtained for benzaldehyde alone were compared with those corresponding to benzaldehyde in a mixture. Initially, attention was focused only on benzaldehyde (and not on the rest of the gaseous mixture).

Monitoring of all the species in the sample mixture followed, to look for relevant information about the processes taking place. Next we established a comparison with the results obtained in a different test in which the concentration of all the components of the gaseous mixture was significantly reduced.

The next stage was to inquire into the effects that the presence of very volatile carboniles could have on the sampling of the target analytes.

Once we verified the presence of interactions between analytes co-existing in a gaseous sample, we focused on finding sampling methodologies and protocols that could avoid the observed variations with sample composition. One possible way would be to reduce the sampling times [17,18]. The concentration of the potentially interfering analytes was doubled in a subsequent trial, and sampling at short times was performed in the new set of conditions.

Finally, calibration in the initial stage was attempted in different conditions, i.e., analyte alone and in a mixture. These sets of tests were divided in the following stages:

- (a) Comparison between adsorption profiles when benzaldehyde was introduced in the chamber alone or in a mixture with other compounds.

Benzaldehyde was introduced in the chamber at concentration levels of 1241 ± 372 , 608 ± 182 and 163 ± 49 ppbV on different days and the corresponding adsorption profiles were obtained (adsorption of benzaldehyde oxime on the fibre at different sampling times ranging from 10 s to 10 min). Then, adsorption profiles at longer sampling times (of up to 12 h) were performed for the concentrations of 1241 ± 372 and 608 ± 182 ppbV. In all these, the GC-FID area responses were represented versus the concentration in the chamber. The analyte concentration in bulk air (C_g) was considered constant when short sampling times were applied. When this was not the case, the integral of the function $\int C_g dt$ describing the variation of the concentration with time (due to dilution) was plotted.

- (b) Mixture of aldehydes:

- (b.1) The adsorption profiles obtained by introducing 617 ± 185 ppbV alone was compared with those obtained when the same amount of benzaldehyde was inserted in the chamber together with other carboniles (360 ± 108 ppbV formaldehyde and 1096 ± 329 ppbV acetaldehyde).

- (b.2) Comparison of adsorption profiles obtained for benzaldehyde alone (at a concentration level of 150 ± 45 ppbV) with those corresponding to the same amount of benzaldehyde introduced in the chamber together with formaldehyde (25 ± 7 ppbV formaldehyde) and acetaldehyde (150 ± 45 ppbV acetaldehyde). In the same graph, another series of two experiments was also compared, i.e., those corresponding to 617 ± 185 ppbV benzaldehyde alone with the adsorption profile provided by benzaldehyde in a mixture of the following composition: 617 ± 185 ppbV benzaldehyde, 360 ± 108 ppbV formaldehyde and 1096 ± 329 ppbV acetaldehyde.

- (c) Follow-up of the remaining sample components.

- (c.1) Another series of experiments was carried out in which a mixture of aldehydes was inserted in the chamber in the following order: acetaldehyde, formaldehyde and benzaldehyde at concentration levels of approximately 360 ± 108 ppbV (formaldehyde), 1096 ± 329 ppbV (acetaldehyde), 617 ± 185 ppbV (benzaldehyde). This time, the SPME responses to all the sample components were traced.

- (c.2) Significant reduction of mixture components: in parallel to the last test, another test was conducted with a significant reduction in the concentration of the remaining sample components to the following levels: formaldehyde, 25 ± 7 ppbV; acetaldehyde, 150 ± 45 ppbV; benzaldehyde, 150 ± 45 ppbV.

- (d) Superposition of adsorption profiles obtained at varying concentrations of gaseous matrices and different experimental conditions.

Approximately, 109 mg of acetaldehyde (approximately 311 ± 93 ppbV) were introduced in the chamber followed by 75 mg of formaldehyde (approximately 314 ± 94 ppbV). In a separate experiment, the amounts of acetaldehyde and formaldehyde introduced in the chamber were increased significantly (198 mg formaldehyde and 425 mg acetaldehyde) providing concentrations in the chamber of 833 ± 250 ppbV formaldehyde and 1221 ± 366 ppbV acetaldehyde. In all cases 50, 100, and 200 μ l of benzaldehyde were successively added to the chamber. Sampling at 5, 15, 30, 45, 60 and 120 s was performed. The objective of these series of experiments was to establish the conditions under which sampling in the chamber could be performed quantitatively in a real case.

- (e) Calibration curves. ANOVA test applied (proof of homogeneity of variances).

In order to test the validity of this approach, a number of calibration experiments were carried out. Initially, just 450 mg of benzaldehyde (slight variations from 1 day to another) were introduced in the chamber, yielding an approximate concentration of 518 ± 155 ppbV. This calibration curve was repeated four successive days ($n = 4$). During the course of the calibration experiments, a decrease in regression coefficients was observed together with a lower loading of PFBHA, generating a lower oxime formation which decreased the sensitivity of the analysis. It was then observed that the fibre used had turned an intensely dark colour. New fibres were used for the rest of the analysis. On a different day, 416 mg of benzaldehyde, 444 mg of butyraldehyde and 320 mg of trimethylacetaldehyde were introduced in the chamber. The composition of the gaseous mixture was not relevant since the study focused on benzaldehyde alone. The mixture composition was changed to these other compounds that were less harmful and less affected by the derivatising agent background.

3. Results and discussion

3.1. Optimisation of derivatisation and blank experiments

Certain aspects of the experimental procedure have been thoroughly tested and reported in the literature [17], such as the loading of the derivatising agent directly from solid reagents, decomposition of the reagent in the fibre coating and changes in loading behaviour of the coating with repeated use. In general terms, they are in good agreement with our observations. In this section, we report the results of a number of aspects related to the experimental procedure applied to derivatisation.

Different concentrations of PFBHA solutions were assayed to achieve the highest loading on the fibre without considerably increasing the loading time. High concentrations of PFBHA should be applied on the fibre in order to avoid as far as possible binding of the pure compound. The concentrations assayed were 17 g/l, as reported in the literature [12]. In addition, a saturated solution of PFBHA (concentration approximately 89 g/l) was assayed. The loss of stability of the saturated solution over time was noticeable, since the intensity of the interfering peaks increased within a few days. The solution of derivatising agent should be prepared daily and not stored from 1 day to the next. Working with clean fibres is crucial at low concentrations of the compounds of interest or at low sampling times.

Different loading times were assayed, causing the amount of PFBHA on the fibre to increase consistently. Using the 89 g/l solution, the mass load was higher for the same loading times, when

compared with the 17 g/l solution. This resulted in an approximately 3% increase in oxime formation. However, it also increased the intensity of the interfering peaks, which increases the procedural limits of detection (LOD) significantly for compounds whose oximes co-elute with the most intense peaks. This is the case of formaldehyde, acetone (also reported in Refs. [17,24,25]) and acetaldehyde, and it would hinder their quantitative determination especially at low concentration levels (low ppbV).

In order to account for these interfering peaks, a number of chromatographic tests were obtained upon the application of derivatising agent on the fibre (control samples). The origin of the peaks observed is not completely understood. Control samples are obtained twice a day, before the first sampling step from the chamber, and at the end of the day, after all sampling steps are concluded. This provides an indication of whether PFBHA is being contaminated during the progression of the experiments. In addition, background samples are taken, i.e., chromatograms resulting from sampling of zero air from the chamber. These three chromatograms were generally in good agreement. This allows concluding that the net change in response could be attributed to the change in concentration of target compounds (benzaldehyde) into the chamber.

It should be clarified that problems due to impurities in the derivatising agent and reactivity of PFBHA affect mainly the determination of small carbonyls, but not significantly the quantitative determination of other bigger carboniles, such as benzaldehyde, target analyte in this study.

As stated above the exact origin of such contamination is not completely understood. The work by Reisen et al. [25] suggests that the derivatising agent should be loaded on the fibre under a nitrogen atmosphere to minimize contamination from, for example, acetone in the laboratory air and thus avoid problems in the determination of some of the small carbonyls due to the background contamination with some of the ubiquitous carbonyls in ambient air, such as formaldehyde, acetaldehyde and acetone.

It has been suggested that in some instances it could come from the water used for the preparation of the derivatising solution. In fact, Wang et al. [17] comment on the possibility of decomposition of the reagent in the fibre coating. The authors report that background contamination peaks were observed, most notably for formaldehyde, as had previously been noted by other researchers [17,24] also describe the calculations followed in order to calculate the procedural LOD, i.e., a value of the limit of detection that takes into account the signal provided by the derivatising reagent loaded on the fibre. When PFBHA was used, the limit of detection was calculated as the concentration that yields a peak height twice the signal-to-noise ratio.

It is also possible that when the derivatising agent is loaded on the fibre, it fragments into smaller size components that elute at different retention times, generating high backgrounds at different positions of the chromatogram and affecting the procedural limits of detection.

In the present study, at longer sampling times, the higher the concentration of derivatising agent used, the higher the amount of oxime was observed. However, at short sampling times, the amount of oxime formed at both concentration levels of derivatising solution was quite similar. In both cases, there was an important excess of PFBHA. The higher oxime formation at higher concentrations of derivatising agent could be due to the higher number of available binding sites available that become occupied by the analyte when long enough times are allowed.

Additional tests were carried out to quantify desorption of derivatising agent from fibres at room temperature. After 14 h, 28.37% of the PFBHA loaded on the fibre from a 17 g/l solution had desorbed.

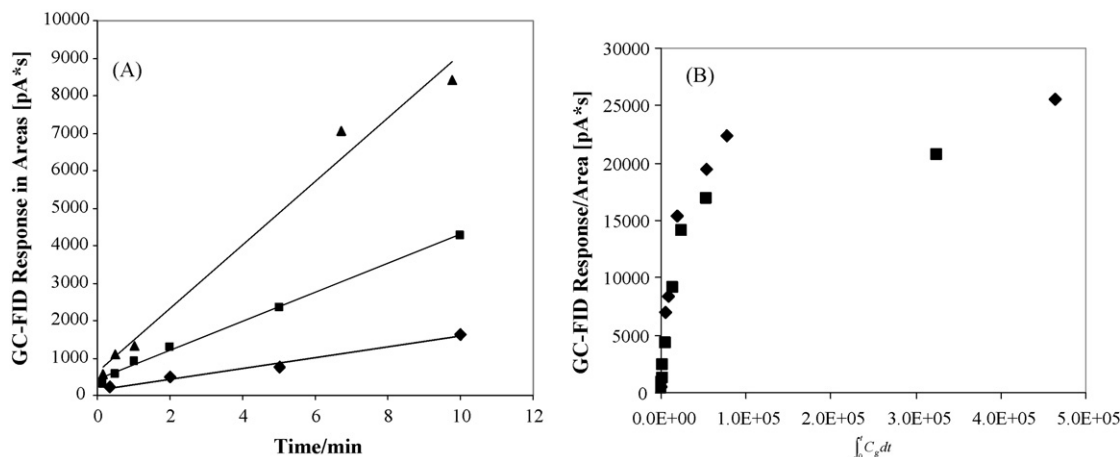


Fig. 2. (A) Adsorption profiles for benzaldehyde alone in the chamber at sampling times of up to 10 min and at three different concentration levels. (♦) Conc = 163 ± 49 ppbV; (■) Conc = 608 ± 182 ppbV; (▲) Conc = 1241 ± 372 ppbV. (B) Adsorption profiles for benzaldehyde at two different concentration levels when just benzaldehyde is introduced in the chamber. (■) 608 ± 182 ppbV; (♦) 1241 ± 372 ppbV. Sampling times of up to 12 h.

Finally, sampling of benzaldehyde introduced in the chamber at a concentration level of 500 ppbV was carried out at different times ranging from a few seconds to 2 h. After each sampling step, a 2 min headspace loading of PFBHA was performed. Post-sampling derivatisation was essayed as a test to determine if the reaction rate of the carbonile group with the derivatising reagent could be limiting the extent to which the reaction takes place. Derivatising after sampling would allow enough time for the compound to react after sampling has been carried out. The final oxime formation was lower than that obtained when loading the derivatising reagent onto the fibre before sampling. In line with Wang's et al. [17] observations, the reaction rate with the derivatising reagent is not expected to limit the overall reaction rate.

3.2. Evaluation of competitive effects in the determination of carboniles in air samples

In order to elucidate the dependence of analyte uptake on the fibre with the presence and concentration of other analytes in the sample matrix, a series of tests were carried out. Benzaldehyde

alone is introduced in a first instance in the chamber at two concentration levels (Fig. 2A and B). A number of sampling steps were performed at different times (up to a maximum of 12 h). In a second experiment, the same types of profiles are obtained when a combination of benzaldehyde, formaldehyde and acetaldehyde is placed in the chamber at two concentration levels (Fig. 3A and B).

The profiles of analyte uptake versus sampling time at longer sampling times displayed in Figs. 2B and 3A are typical of equilibrium situations in which a maximum of analyte adsorption is reached, upon which no further increase in analyte uptake is observed. The maximum response is dependent on the concentration of analyte in the sample matrix (Fig. 2B). However, the tests showed an aspect of sampling with SPME fibres, also pointed out by Koziel et al. [18], which is of concern due to its potential to hinder quantitative determinations, i.e., analyte uptake at equilibrium depends on the composition of the sample matrix. Sampling in non-equilibrium (prior to equilibrium) could minimize this effect. In fact, at short sampling times, there is good agreement between the uptake profiles at two concentration levels (Fig. 3B). It should be

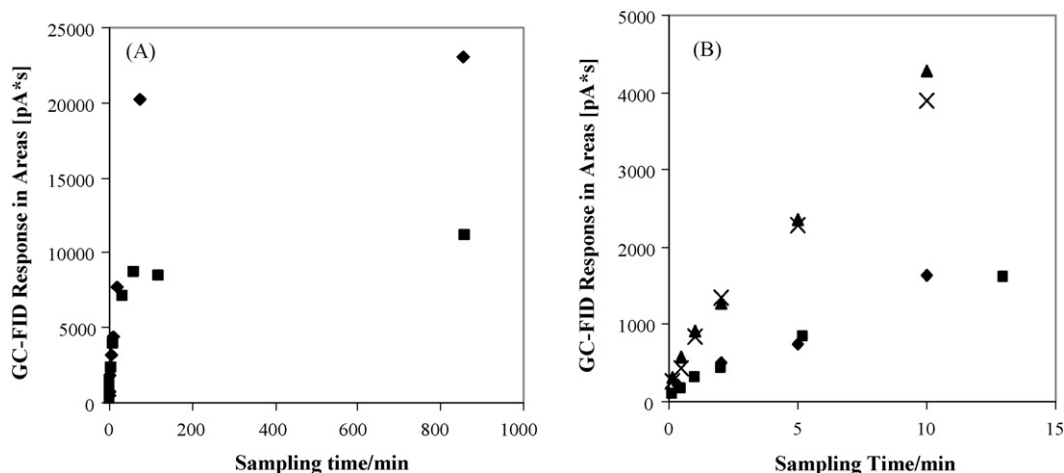


Fig. 3. (A) Adsorption profiles obtained for benzaldehyde as the only carbonile in the chamber and in a mixture of aldehydes at a concentration level of roughly 617 ± 185 ppbV. (♦) Just benzaldehyde in the chamber; (■) benzaldehyde in a mixture of aldehydes. 617 ± 185 ppbV benzaldehyde (360 ± 108 ppbV formaldehyde and 1096 ± 329 ppbV acetaldehyde). (B) Adsorption profiles for sum of benzaldehyde oximes when just benzaldehyde was introduced in the chamber and in a mixture with other gaseous compounds (focuses on short sampling times). (♦) Just benzaldehyde at 150 ± 45 ppbV; (■) 150 ± 45 ppbV of benzaldehyde in gaseous mixture (25 ± 7 ppbV formaldehyde and 150 ± 45 ppbV acetaldehyde); (▲) just benzaldehyde at 617 ± 185 ppbV; (×) 617 ± 185 ppbV of benzaldehyde in mixture (360 ± 108 ppbV formaldehyde and 1096 ± 329 ppbV acetaldehyde).

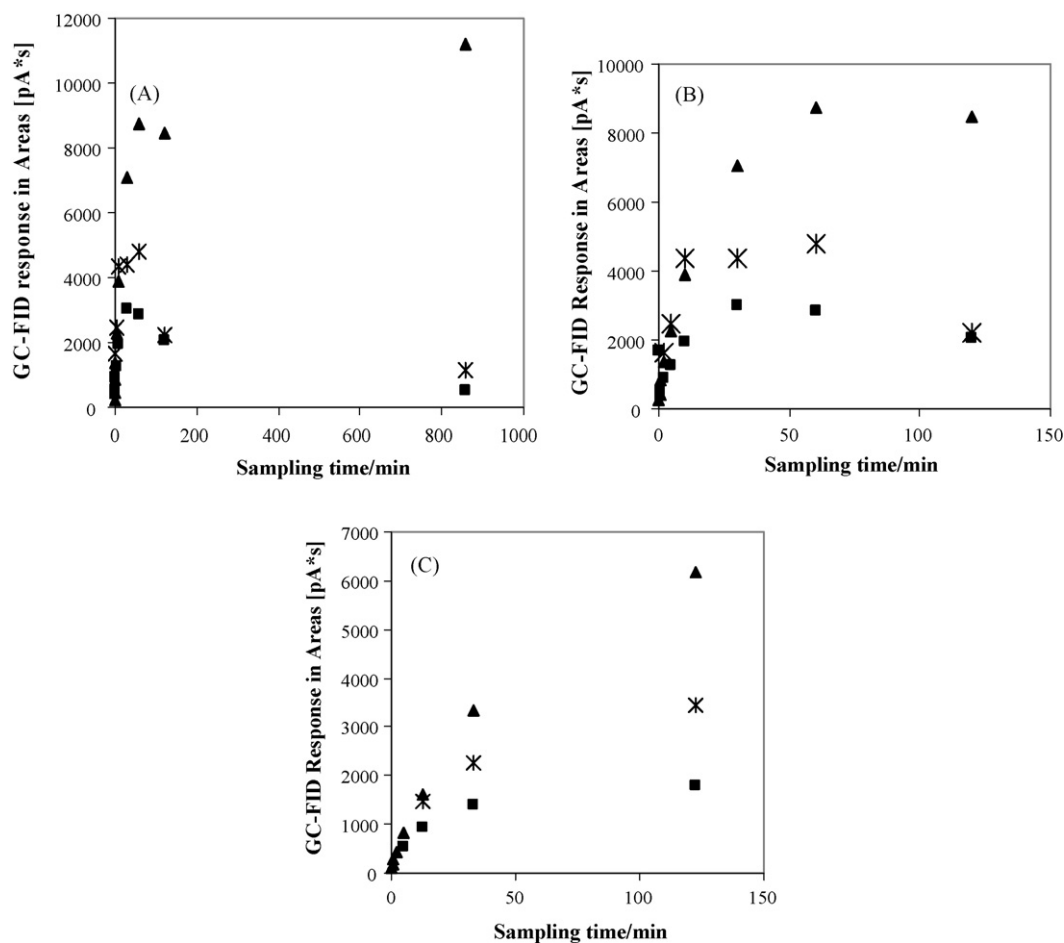


Fig. 4. (A) Adsorption profiles at long sampling times of the following aldehydes in a gaseous mixture: (X) formaldehyde 360 ± 108 ppbV; (■) acetaldehyde 1096 ± 329 ppbV; (▲) benzaldehyde 617 ± 185 ppbV. (B) Adsorption profiles at short sampling times of the following aldehydes in a gaseous mixture (window from the beginning of the x-axis of last profile, focusing on shorter sampling times): (X) formaldehyde 360 ± 108 ppbV; (■) acetaldehyde 1096 ± 329 ppbV; (▲) benzaldehyde 617 ± 185 ppbV. (C) Adsorption profile for the sum of oximes of different aldehydes in a gaseous mixture: (X) formaldehyde 25 ± 7 ppbV; (■) acetaldehyde 150 ± 45 ppbV; (▲) benzaldehyde 150 ± 45 ppbV.

kept in mind that with 12 h sampling times, a certain desorption of oximes and PFBHA (as stated in Section 3.1) can take place and this could derive in a certain decrease of response for which no correction has been applied.

With the aim of looking more deeply into the processes taking place, tests with mixtures of the three analytes were carried out and the responses to the different analytes were followed individually. The profiles obtained for formaldehyde and acetaldehyde show a decrease in response with sampling times (Fig. 4A). Fig. 4B zooms into the previous profile focusing on shorter sampling times (up to 2 h). The above-mentioned decrease in response for formaldehyde and acetaldehyde can also be appreciated at shorter sampling times. An additional test carried out to obtain more information on this aspect was to significantly reduce the concentration of all components in the mixture. Fig. 4C was obtained at considerably lower concentration levels of the mixture components, i.e., formaldehyde, 25 ± 7 ppbV; acetaldehyde, 150 ± 45 ppbV; benzaldehyde, 150 ± 45 ppbV, and sampling time spans of over 2 h. The decrease in response observed previously for formaldehyde and acetaldehyde is not observed in this plot. The response obtained for benzaldehyde increased significantly (if concentration differences are accounted for) with respect to the previous plot.

The experiments carried out to this point verified the occurrence of certain undesirable effects, reported in the literature, that could negatively affect the quantitative determination of carboniles by

SPME. In the following sets of experiments, focus was placed on investigating the conditions that would allow us to obtain single adsorption profiles despite the composition of the gaseous sample, a requirement for calibration. In the first of these tests, the concentrations of potentially interfering species in the determination of the target analytes were gradually increased to unusually high levels for atmospheric studies. The aim was to set upper limits to the concentrations of species that can potentially impair the quantitative determination. Sampling was performed at very short sampling times, the most advantageous conditions in kinetic studies for obtaining enough samples to picture reaction profiles. Fig. 5 shows that at low concentration levels and low sampling times, the occurrence of different adsorption profiles at different concentrations was avoided (agreement of adsorption profiles-GC-FID response versus $\int C_g dt$). The points lay around a straight line corresponding to the initial region of the adsorption profile, i.e., the points obtained before the plateau.

These very positive results were taken as the starting point for developing calibration methods that can be applied in practice. A set of experiments was designed as a test to check whether the application of our methodology yielded the same calibration curve for the pure compound (benzaldehyde) alone in the chamber as for benzaldehyde in a mixture. This would avoid obtaining one calibration curve when the composition of the gaseous mixture varies, which would be the case if the different regressions (best-fit equation) shared the same variances.

Table 2
ANOVA test applied on a number of calibration curves obtained.

Replicate	Equation	R^2	Number of points eliminated by study of residuals	Total number of points	F	Sig.	α	β
Rep I	$Y = 0.404x + 26.344$	0.97	0	10	309.9	0.000	0.000	0.006
Rep II	$Y = 0.5786x - 10.521$	0.93	1	10	98.19	0.000	0.000	0.576
Rep.III	$Y = 0.404x + 38.955$	0.89	0	8	48.17	0.000	0.000	0.066
Rep IV	$Y = 0.484x - 17.613$	0.87	2	11	46.10	0.000	0.000	0.430
<i>In a mixture</i>								
Rep. V	$Y = 0.535x - 5.599$	0.96	1	12	227.8	0.000	0.000	0.587
Combining all	$Y = 0.450x + 15.251$	0.96	9	51	594.5	0.000	0.000	0.008
Eliminating last two (Rep III and Rep IV, compound alone in the chamber)	$Y = 0.45x + 15.251$	0.96	2	28	594.5	0.000	0.000	0.008

ANOVA was applied to the statistical validation of the test. Some of the assumptions of the statistical test are summarised here for completeness. According to this test, the initial assumption (all regressions share the same variances) can be accepted if F is high and $\alpha \leq 0.05$. This was applied to each of the calibration curves individually and to the assembly of the points obtained in the different calibrations.

According to the statistical test, the optimum values for the coefficients would be:
Slope $a = 1; \alpha = 0$ (or $\alpha \leq 0.05$).

Y -intercept $b = 0; \beta \geq 0.95$ (statistical requirement, experimentally $\beta \geq 0.5$ is accepted).

The fulfilment of the first requirement constitutes the mathematical proof of linearity while the second determines the need to use a blank for calibration.

The test also integrates the outliers identified in the study of residuals. Points with a value of $Z_{res} > 1.96$ have to be discarded, in which case the whole validation has to be applied again to the remaining points.

Four calibrations were obtained at short sampling times (15 s) and benzaldehyde alone in the gas matrix and one of benzaldehyde in a mixture with the other gaseous analytes. The lower regression coefficients correspond to calibrations performed with an older fibre, which was subsequently discarded. The statistical test was

applied sequentially, first to all curves and then to just those with better R^2 values. Individually, all curves met the test requirements although three of them showed the need to include a blank in the calibration. When the test was applied to the assembly of all curves, nine points had to be eliminated based on the study of residuals. However, the test permits eliminating up to 11 points (2/9 of the total number, which was 50). After proceeding in this way, the test yielded a good combined $R^2 = 0.96$ (corresponding to all the points included in the analysis).

When applied to just the three curves with the best R^2 values, only two points had to be rejected (outliers), and the same value of R^2 (0.96) was obtained (again showing the need to include a blank for calibration). Table 2 presents the results obtained in this validation. They prove that all the calibration curves obtained for benzaldehyde – on its own and in a mixture – share homogeneous variances.

4. Conclusions

The aim of this work was to assess the potential of SPME with solid fibres to provide quantitative data. This study was focused on the on-fibre derivatisation with PFBHA of a mixture of carbonile compounds in gaseous samples, products of a number of reactions commonly studied in the degradation mechanisms of relevant compounds in atmospheric chemistry reactions. An important fact, and the starting point of this study, was that different adsorption profiles were obtained for the same compound at different concentration levels [18].

The extractive capacity of adsorptive fibres is quite high, as can be inferred from a number of facts, one of them being that increasing exposure to the headspace of high concentration solutions of derivatising agent, resulted in increasing mass adsorbed on the fibre. For this step a loading time of two minutes was chosen to guarantee a sufficient excess of derivatiser to generate quantitative results. The derivatising agent was loaded on the fibre in high amounts, which kept increasing with loading time. Despite this, the fibres could still bind the pure, underderivatised analyte. Therefore, it would seem that the apparent equilibrium/saturation could be related to the way the analyte transfer takes place.

To ensure quantitivity, it is important to work at low concentration levels and for low sampling times. These conditions are applicable and advisable in atmospheric studies. The tests carried out as part of the present work guarantee that the regressions performed in different experimental conditions and gaseous mixture compositions, share homogeneous variances. The experimental procedure is simplified by eliminating the need to calibrate at each particular set of experimental conditions.

The tests were carried out in extreme conditions, i.e., the concentrations of analytes used were considerably higher than those that would be present in normal atmospheric conditions. This study

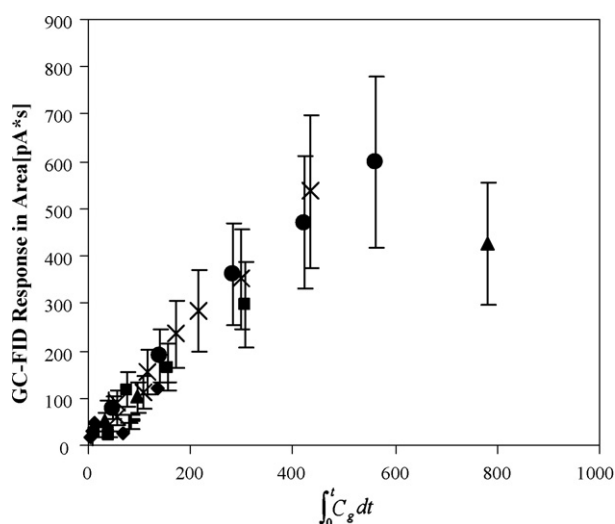


Fig. 5. Adsorption profile presented by benzaldehyde adsorbed on PDMS-DVB 65 μm fibres at three different levels of concentration and in two different situations in which the concentration of the rest of the components of the gaseous mixture was doubled in two sets of experiments with respect to a first set. Symbols represent the following concentrations of benzaldehyde: (\times) 65 \pm 19 ppbV, Day 1; (\times) 125 \pm 37 ppbV, Day 1; (\bullet) 250 \pm 75 ppbV, Day 1; (\blacklozenge) 65 \pm 19 ppbV, Day 2; (\blacksquare) 125 \pm 37 ppbV, Day 2; (\blacktriangle) 250 \pm 75 ppbV, Day 2; ($+$) 65 \pm 19 ppbV, Day 3; ($-$) 125 \pm 37 ppbV, Day 3. See Table 1 for the concentrations the remaining components of the gaseous mixture on the different days.

shows that unwanted effects which could affect quantity in sampling with SPME PFBHA on-fibre derivatisation, are unlikely to occur at realistic concentration levels in the air.

In addition, the decrease of fibre efficiency due to deterioration or depletion of the polymeric phase of the fibre, was also subjected to study in the present work as a potential aspect to impair quantitative analysis. While it is important to be aware of these facts, the results provided were still within the methodology variability determined in this study.

Acknowledgments

Financial support of the European Commission, Generalitat Valenciana and Fundació Bancaixa is gratefully acknowledged. The author is grateful to Esther Borrás for helpful discussions on the statistical model used to validate calibrations. This research work has been funded by the program CONSOLIDER-INGENIO 2010 (Proyecto Graccie).

References

- [1] A. Vairavamurthy, J.M. Roberts, L. Newman, *Atmos. Environ.* 26 (11) (1992) 1965.
- [2] D. Riemer, P. Willer, P. Milne, C. Farmer, R. Zika, E. Apel, K. Olszyna, T. Kliendienst, W. Lonneman, S. Bertman, P. Shepson, T. Starn, *J. Geophys. Res.* 103 (1998) 111–128.
- [3] H.B. Singh, M. Kanakidou, P.J. Crutzen, D.J. Jacob, *Nature* 378 (1995) 50–54.
- [4] H.B. Singh, et al., *J. Geophys. Res.* 99 (1994) 1805–1819.
- [5] B.J. Finlayson-Pitts, J.N. Pitts Jr., *Chemistry of the Upper and Lower Atmosphere*, Academic Press, San Diego, CA, 2000.
- [6] R. Atkinson, *J. Phys. Chem. Ref. Data*, Monograph No. 2, 1–216.
- [7] P.O. Wennberg, T.F. Hanisco, L. Jaeglé, D.J. Jacob, E.J. Hints, E.J. Lanzendorf, J.G. Anderson, R.-S. Gao, E.R. Keim, S.G. Donnelly, L.A. Del Negro, D.W. Fahey, S.A. McKeen, R.J. Salawitch, C.R. Webster, R.D. May, R.L. Herman, M.H. Proffitt, J.J. Margitan, E.L. Atlas, S.M. Schauffler, F. Flocke, C.T. McElroy, T.P. Bui, *Science* 279 (1998) 49–53.
- [8] H. Nishikawa, T. Sakai, *J. Chromatogr. A* 710 (1995) 159.
- [9] E. Koivusalmi, E. Haatainen, A. Root, *Anal. Chem.* 71 (1999).
- [10] K. Fung, D. Grosjean, *Anal. Chem.* 53 (2) (1981) 168–171.
- [11] P.A. Martos, J. Pawliszyn, *Anal. Chem.* 69 (1997) 206–215.
- [12] P.A. Martos, J. Pawliszyn, *Anal. Chem.* 70 (1998) 2311–2320.
- [13] J.A. Koziel, J. Noah, J. Pawliszyn, *Environ. Sci. Technol.* 35 (2001) 1481–1486.
- [14] E. Gómez Alvarez, J. Viidanoja, A. Muñoz, J. Hjorth, *Environ. Sci. Technol.* 41 (2007) 8362–8369.
- [15] T. Górecki, X. Yu, J. Pawliszyn, *Analyst* 124 (1999) 643–649.
- [16] R.A. Murray, *Anal. Chem.* 73 (2001) 1646–1649.
- [17] Q. Wang, J. O'Reilly, J. Pawliszyn, *J. Chromatogr. A* 1071 (2005) 147–154.
- [18] J. Koziel, M. Jia, J. Pawliszyn, *Anal. Chem.* 72 (2000) 5178–5186.
- [19] E.C. Apel, T. Brauers, R. Koppmann, R. Tillmann, C. Holzke, R. Wegener, J. Boßmeyer, A. Brunner, T. Ruuskanen, M. Jocher, C. Spirig, R. Steinbrecher, R. Meier, D. Steigner, E. Gómez Alvarez, K. Müller, S.J. Solomon, G. Schade, D. Young, P. Simmonds, J.R. Hopkins, A.C. Lewis, G. Legreid, A. Wisthaler, A. Hansel, R. Blake, K. Wyche, A. Ellis, P.S. Monks, *J. Geophys. Res.*, 113, D20307, doi:10.1029/2008JD009865, 21 October 2008.
- [20] EUPHORE Report I. The European Photoreactor EUPHORE: Design and Technical Development of the European Photoreactor and First Experimental Results. Final Report of the EC-Project. Contract: EV5V-CT92-0059. Editor: Karl H. Becker, February 1996.
- [21] EUPHORE Report II. Euphore Report, 1997 (2nd Report). Editors: Ian Barnes, Bergische Universität-GH, Wuppertal, Germany and John Wenger, University College Dublin, Ireland. Institute of Physical Chemistry, Bergische Universität-GH Wuppertal, December 1998.
- [22] EUPHORE Report III. The European Photoreactor EUPHORE. 3rd Report. Editors: Ian Barnes and Howard Sidebottom. Institute of Physical Chemistry, Bergische Universität Wuppertal, Germany, December 2001.
- [23] EUPHORE Report IV. The European Photoreactor EUPHORE, 4th Report, 2001. Editor: Ian Barnes. Institute of Physical Chemistry, Bergische Universität Wuppertal and Fundación Centro de Estudios Ambientales del Mediterráneo, Valencia, February 2004.
- [24] J.W. Munch, D.J. Munch, S.D. Winslow, *Proceedings of the Water Quality Technology Conference*, San Diego, CA, November 1–4, 1998, p. 898.
- [25] F. Reisen, S.M. Aschmann, R. Atkinson, J. Arey, *Environ. Sci. Technol.* 37 (2003) 4664–4671.



Electrochemistry and chemiluminescence techniques compared in the detection of NADPH oxidase activity in phagocyte cells

A. Ashkenazi^a, K. Abu-Rabeah^a, R.S. Marks^{a,b,c,*}

^a Department of Biotechnology Engineering, Ben-Gurion University of the Negev, P.O. Box 653, Beer-Sheva 84105, Israel

^b National Institute for Biotechnology in the Negev, Ben-Gurion University of the Negev, P.O. Box 653, Beer-Sheva 84105, Israel

^c ILSE Katz Center for Meso and Nanoscale Science and Technology, P.O. Box 653, Beer-Sheva 84105, Israel

ARTICLE INFO

Article history:

Received 25 May 2008

Received in revised form 4 September 2008

Accepted 21 September 2008

Available online 30 September 2008

Keywords:

Neutrophils

PLB 985

Electrochemistry

Superoxide

Hydrogen peroxide

Chemiluminescence (CL)

ABSTRACT

Several methodologies have been used in clinical chemistry for real-time assessment of NADPH oxidase primary product superoxide anion which dismutates to hydrogen peroxide. Among these methodologies, isoluminol chemiluminescence (CL) is considered to be one of the more sensitive and reliable techniques for the assessment of NADPH oxidase activity in neutrophils. The electrochemical technique was recently designed and also applied for real-time detection of NADPH oxidase activity in neutrophils but its reliability and sensitivity has not been investigated so far. In this study, isoluminol CL and electrochemical techniques were investigated and compared by monitoring the generation of superoxide and hydrogen peroxide in both PLB 985 cell line differentiated into neutrophil-like cells and human neutrophils. The electrochemical technique was shown to be as sensitive as that of CL and able to detect the reactive oxygen species (ROS) release of as low as 500 cells. Thus, the electrochemical technique could be used as an alternative to optical techniques for the evaluation of extracellular ROS in phagocyte cells.

© 2008 Elsevier B.V. All rights reserved.

1. Introduction

Chemiluminescence (CL) is a well-investigated diagnostic tool based on light active compounds excited by reactive oxygen species (ROS) release energy in the form of light [1]. In clinical chemistry CL is often used in the analysis and assessment of ROS production in human neutrophils [2–5]. In a previous study carried out in our laboratory a novel, computerized, multi-sample, temperature-controlled luminometer for a fiber array-based biosensor was built to monitor circulating neutrophil activity. This fiber-based chemiluminescent sensor provides timely and clinically relevant diagnostic and management information for patients experiencing infection [6]. Several techniques were developed and applied to monitor cellular ROS production like: photometry, fluorometry and luminometry. Among them the CL technique was shown to be sensitive, easy to perform and specific for a particular oxygen metabolite [7].

Recently, an electrochemical amperometric technique was developed for real-time detection of extracellular hydrogen peroxide generation from neutrophils by measuring the current resulting from the oxidation of the electroactive species, hydrogen peroxide [8]. The electrochemical method can follow the activity of NADPH oxidase, a major enzyme in ROS generation principally producing superoxide anion which dismutates to hydrogen peroxide in phagocyte cells [9,10].

Few research efforts have been dedicated to explore whether electrochemical techniques are sensitive and able to give reliable results for NADPH oxidase activity, as compared to that of the well-established CL technique. In order to approach this question, the electrochemical and CL techniques were used to analyze the NADPH oxidase activity in the human promyelocytic leukemia cell line PLB 985. PLB 985 cells do not have an active oxidative system but are capable of generating ROS after differentiation into neutrophil-like phenotype, which is induced by dimethyl sulfoxide (DMSO) [11–13]. PLB 985 cells are able to develop NADPH oxidase components during DMSO differentiation [14–16] but the enzyme activity has not yet been fully characterized and compared to that of human neutrophils. In the CL technique, isoluminol was used as an extracellular chemiluminogenic probe, as the amino group localized on the aromatic ring increases the molecule hydrophilicity preventing it from crossing biological membranes [17]. An additional peroxidase, such as horseradish peroxidase (HRP), is introduced to the monitoring system for real-time detection of superoxide gen-

Abbreviations: CL, chemiluminescence; DMSO, dimethyl sulfoxide; DPI, diphenyleneiodonium chloride; FACS, fluorescence-activated cell sorter; MPO, myeloperoxidase; HRP, horseradish peroxidase; KRP, Krebs Ringer phosphate buffer; PBS, phosphate-buffered saline; PH, peak height; PMA, phorbol myristate acetate; PT, peak time; ROS, reactive oxygen species; SOD, superoxide dismutase.

* Corresponding author at: Department of Biotechnology Engineering, Ben-Gurion University of the Negev, P.O. Box 653, Beer-Sheva 84105, Israel.

Tel.: +972 8 6477182; fax: +972 8 6472857.

E-mail addresses: ashkenaa@bgu.ac.il, rsmarks@bgu.ac.il (R.S. Marks).

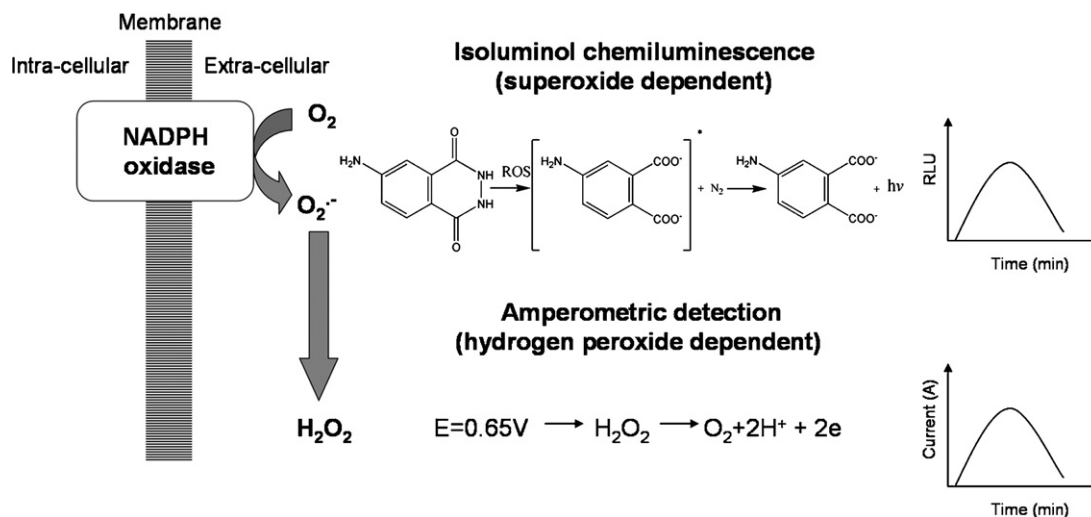


Fig. 1. Experimental design of extracellular superoxide and hydrogen peroxide detection by the isoluminol CL and electrochemical techniques in phagocyte cells. The chemical reactions which are involved in the light and current generation events are also described.

eration, to amplify the light emission of isoluminol [18]. In the electrochemical technique, the amperometric setup was designed to monitor and follow the release of hydrogen peroxide without any additives (Fig. 1).

This study compares the performances of the isoluminol CL and electrochemistry to detect NADPH oxidase activity in human neutrophils and neutrophil-like PLB 985 cells by examining both techniques kinetic parameters (reaction profile during measurement time, total capacity to produce ROS, maximum velocity (V_{max}), response time and sensitivity).

2. Experimental

2.1. Separation of human neutrophils

Neutrophils were separated from the blood of healthy human volunteers by the Histopaque (Sigma 10771) gradient technique. Each 10-mL blood sample was mixed with 10 mL of phosphate-buffered saline (PBS). The diluted blood samples were layered over 12.5 mL of Histopaque, at a density of 1.077 g/mL, followed by centrifugation ($400 \times g$) for 30 min at room temperature. Top layers were separated and the resulting pellet was diluted within PBS. Dextran (Sigma D4876) solution of 0.9% salinity was added to the diluted pellet to a final Dextran concentration of 1.5% and sedimentation was performed for 30 min. Then the separated volume was centrifuged ($400 \times g$) at 4 °C, followed by hypotonic lysis of erythrocytes. The viability, determined by trypan blue (Biological Industries 031021B) assay, of the separated neutrophils was generally greater than 98%.

2.2. Cell cultures

Human promyelocytic leukemia PLB 985 cells (generously given by Prof. Rachel Levy, Department of Clinical Biochemistry, Ben-Gurion University, Israel) were passed twice weekly in RPMI medium (Sigma R8758) supplemented with 10% (v/v) heat-inactivated fetal calf serum (Biological Industries 041211), 100 U/mL penicillin, 100 μ g/mL streptomycin (Biological Industries 030311B), 2 mM L-glutamine (Biological Industries 030201C) and a HEPES buffer (Biological Industries 030251B). The cells were incubated in a humidified atmosphere at 37 °C containing 5% (v/v) CO_2 .

In order to induce neutrophil differentiation, PLB 985 cells were seeded at 2.5×10^5 cells/mL in growth medium supplemented with

1.25% (v/v) DMSO (Sigma D2650). The cells were allowed to differentiate for (4–6 days) without replacement of growth medium.

2.3. Preparation of reagents and solutions

Krebs Ringer phosphate buffer (KRP) was composed of 119 mM NaCl, 4.75 mM KCl, 0.420 mM $CaCl_2$, 1.19 mM $MgSO_4 \cdot 7H_2O$, 16.6 mM sodium phosphate buffer, pH 7.4 and 5.56 mM glucose. The following stock solutions were dissolved in KRP and kept at -20 °C: 200 U/mL of horseradish peroxidase (HRP) (Sigma P6782), 4000 U/mL of superoxide dismutase (SOD) from bovine erythrocytes (Sigma S2515). The following stock solutions were dissolved in DMSO and kept at -20 °C: 1 mM of phorbol myristate acetate (PMA) (Sigma P8139), 0.1 M of isoluminol (Sigma A8264), 1 mM of diphenyliodonium chloride (DPI) (Sigma D2926). Hydrogen peroxide (Sigma 323381) kept at 4 °C, diluted in KRP just before the experiment.

2.4. Chemiluminescence measurement

CL was measured in a 96 microplate Luminoskan Ascent (Thermo Labsystems). Isoluminol was used to amplify the CL activity and diluted in KRP prior to the experiment. The reaction mixture for CL in each well contained: cells in concentrations of 5×10^5 cells per well, KRP buffer, different concentrations of isoluminol and 5 U/mL HRP. Each well contained 200 μ L and the reaction mixture was held in equilibration for 5 min at 37 °C. In order to activate the system 20 μ L of PMA (final concentration of 1 μ M PMA per well) were added and CL kinetics were measured. Each sample was tested twice. All measurements were carried out at a constant temperature of 37 °C. The measurement interval was set from 1 to 60 s, running time up to 60 min. In addition, the total area under the curve (AUC) was calculated and resembled the capacity of the cells to generate ROS [4].

2.5. Electrochemical measurements

The amperometric detection of extracellular hydrogen peroxide was performed by PalmSens (Palm Instruments BV), a hand-held battery-powered instrument for use with electrochemical sensors. The instrument was equipped with a microprocessor having low noise and a low-current potentiostat controlling the applied potential, and enabling measurement of the current response. The

Table 1

The specificity of the amperometric and isoluminol-HRP CL techniques towards superoxide anion and hydrogen peroxide.

	DPI inhibitor (10 μ M)	SOD scavenger (300 U/mL)	Catalase scavenger (3000 U/mL)	Control (no scavengers or inhibitors)
Isoluminol CL activity (% from control)	3 \pm 1 ^a	10 \pm 3 ^a	80 \pm 4 ^a	100
Amperometric activity (% from control)	3 \pm 2 ^a	235 \pm 50 ^a	40 \pm 17 ^a	100

Human neutrophils (5×10^5 cells) were activated with PMA and ROS production was measured in the presence of NADPH oxidase inhibitor (DPI) and in the presence of ROS scavengers (SOD or catalase). The activity of isoluminol-HRP CL and electrochemistry was determined by calculation of the total area under the curves (light or current). Values are means \pm standard deviation (S.D.) of three experiments of the percentage of the activity (with the addition of scavengers/inhibitors) from the control (without scavengers/inhibitors).

^a $p < 0.05$ vs. control (no inhibition).

instrument was operated by a suitable PC program (PSlite). A handmade vial was designed and used for the hydrogen peroxide measurements from phagocyte cells. This vial was set upon screen-printed carbon electrodes. The working and counter electrodes consisted of carbon and the reference electrode consisted of silver. The total volume of the reaction mixture was 200 μ L inside the electrochemical vial and contained 5×10^5 cells within KRP solution. The reaction mixture was held in equilibrium at 37 $^\circ$ C for 5 min and, to activate the system 20 μ L of PMA (final concentration of 1 μ M PMA) were added. The potential applied at the working electrode was 0.65 V vs. the reference electrode. At this potential, hydrogen peroxide was oxidized on the working electrodes surface and the current was recorded and presented by the PSLite. A calibration curve of the current resulted with different concentrations of hydrogen peroxide (0.1–200 μ M) showing a linear graph tendency ($R^2 = 0.99$). All H_2O_2 measurements were performed at 37 $^\circ$ C. The measurement interval was 1 s and running time was up to 80 min. The AUC was also calculated in the electrochemical technique.

2.6. Determination of differentiation markers

Determination of a CD11b membrane marker was used to evaluate the percentage of functional neutrophil-like PLB 985 cells and human blood neutrophils [19] in the electrochemical and CL measurements. Thus, all the CL and electrochemical measurements were normalized by the percentage of functional phagocyte cells. The CD11b analysis was determined by flow cytometry: briefly, one million cells were harvested and centrifuged and washed with cold phosphate-buffered saline (PBS), pH 7.2. The pellet resuspended in 50 μ L PBS, incubated for 30 min on ice with 10 μ L (dilution 1:2) of monoclonal antibody:PE-labeled IgG1 mouse anti human CD11b (eBioscience 12-0018). After incubation the pellet was washed twice and resuspended with 1 mL of cold PBS. The analysis was performed using a Fluorescence-activated cell sorter (FACS) (FACSVantage SE, BAKETLAB). Control experiments were done with a PE-labeled isotype-specific irrelevant monoclonal antibody (eBioscience 12-4714).

Only 3 \pm 2% of the non-induced PLB 985 cells expressed a CD11b marker. After 6 days of induction by DMSO, CD11b expression increases dramatically to 86 \pm 2% in neutrophil-like PLB 985 cells. Human blood neutrophils expression of CD11b was 93 \pm 1%.

3. Results and discussion

3.1. The specificity of isoluminol CL and electrochemical techniques towards superoxide anion and hydrogen peroxide

Isoluminol without any additives had a minor detection signal from human neutrophils and the addition of HRP to the monitoring system amplified the light response more than 10 times in our experiments, which correlates with a previous report [17]. Several CL probes were sensitive to different oxygen radicals in the oxidative burst of neutrophils. Table 1 shows that the addition

of 300 U/mL of the ROS scavenger enzyme, SOD, which catalyses the dismutation of superoxide to hydrogen peroxide, inhibited the activity of isoluminol-HRP CL, at a relatively high rate of 90% in human neutrophils. This inhibition proves the strong dependence of the isoluminol-HRP system on superoxide anion as previously reported [7]. But the addition of SOD into the electrochemical monitoring system increased the activity by more than half, implying a preference for hydrogen peroxide. In order to further strengthen these observations, 3000 U/mL of the ROS scavenger enzyme, catalase, which catalyses the decomposition of hydrogen peroxide to water and oxygen, were introduced to both monitoring systems. The activity of the isoluminol-HRP CL was almost not affected; but that of the electrochemical technique was decreased by 60%. The role of NADPH oxidase in generating current or light in both monitoring systems was tested by the addition of 10 μ M of DPI, an NADPH oxidase inhibitor, which abolished the activity of both isoluminol-HRP CL and electrochemical techniques (Table 1). DPI was added to the reaction mixture after the activation of the cells with PMA since the inhibition mechanism of this compound is significantly higher after the turnover of the enzyme [20].

3.2. Isoluminol CL kinetics of human neutrophils and neutrophil-like PLB 985 cells

Both electrochemical and CL techniques enable the detection of ROS kinetic release from neutrophils but they are based on different chemical concepts (Fig. 1). In order to make a comparison between both techniques, analyses of the kinetic parameters were performed. Furthermore, the comparison between the kinetic parameters of both techniques was examined on more than one cell type (human neutrophils and neutrophil-like PLB 985 cells) to better understand their performances regarding NADPH oxidase activity. The isoluminol kinetics for superoxide detection of both human neutrophils and neutrophil-like PLB 985 are presented in Fig. 2. In both types of cells the concentration of the isoluminol probe and the phorbol myristate acetate (PMA) stimulant was similar. In human neutrophils the peak of the CL response was higher, and was reached after a peak time (PT) of 3 min; in neutrophil-like PLB 985 cells the CL peak is lower, and was reached after a PT of 6 min. However, the duration response of neutrophil-like PLB 985 cells is longer, continuing over 40 min from cell stimulation. The area under the isoluminol CL curves (CL capacity) which reflects the total amount of ROS produced was calculated. Neutrophil-like PLB 985 cells ROS production was twice as much as human neutrophils (Fig. 2 inset).

3.3. Electrochemical kinetics of human neutrophils and neutrophil-like PLB 985 cells

The superoxide anion generated by the NADPH oxidase dismutates rapidly to hydrogen peroxide, easily measured directly via electrochemical detection. A calibration curve was prepared to correlate between the apparent current in the system and the

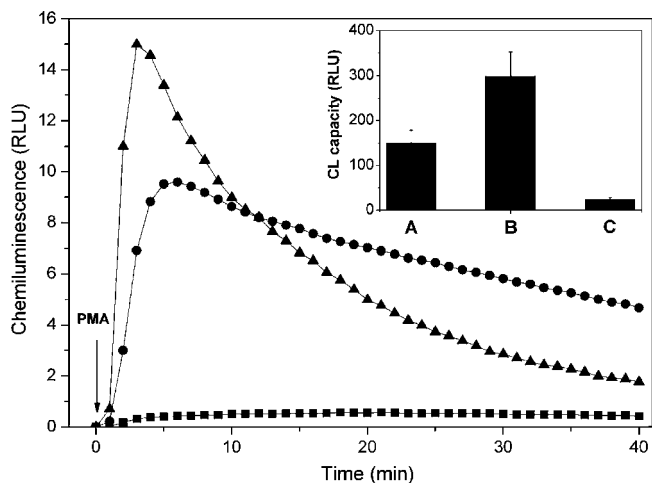


Fig. 2. Isoluminol CL of stimulated neutrophils and neutrophil-like PLB 985 cells. 5×10^5 cells in KRP were mixed with $56 \mu\text{M}$ of isoluminol and 5 U/mL of HRP and stimulated with $1 \mu\text{M}$ of PMA. (■) Non-induced PLB 985 cells; (●) DMSO-induced PLB 985 cells; (▲) human neutrophils. The CL kinetic curve is a representative curve out of three determinations which were analyzed from different blood donors. Inset plot: Total isoluminol CL capacity of neutrophils (A), DMSO-induced PLB 985 cells (B) and non-induced PLB 985 cells (C). Cells were mixed with $56 \mu\text{M}$ of isoluminol and 5 U/mL of HRP, activated with PMA and the light measurements were performed for 60 min to calculate the total area under the curves which resembles the CL capacity. Results are presented as means \pm S.D. of three determinations.

hydrogen peroxide concentration produced by the cells. Fig. 3 presents the concentration of hydrogen peroxide released from human neutrophils and neutrophil-like PLB 985 cells evaluated by electrochemical detection. Similar to the isoluminol CL, the peak of the hydrogen peroxide release is higher in the human neutrophils case and also achieved faster compared to neutrophil-like PLB 985. Maximal hydrogen peroxide concentration is about $5.5 \mu\text{M}$ in human neutrophils, achieved after PT of 6 min; whereby in neutrophil-like PLB 985 cells, the maximal hydrogen perox-

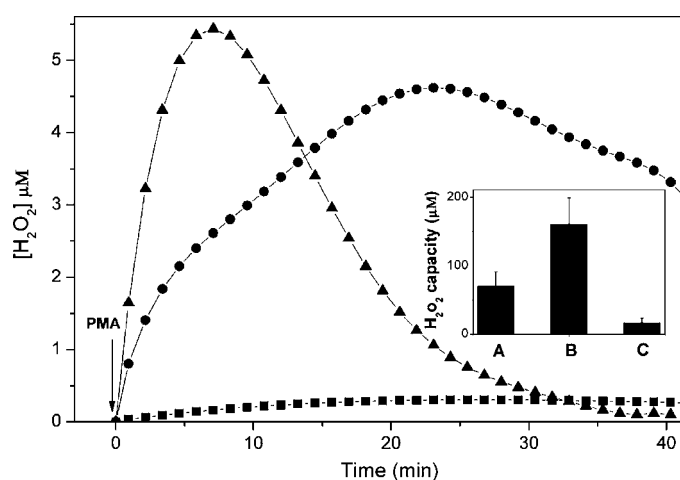


Fig. 3. Electrochemical detection of hydrogen peroxide release by stimulated neutrophils and neutrophil-like PLB 985 cells. 5×10^5 cells in KRP were stimulated with $1 \mu\text{M}$ of PMA during a constant voltage of 0.65 V . The current in the vial during the time resulted in a transformation to a hydrogen peroxide concentration by calibration curve. (■) Non-induced PLB 985 cells; (●) DMSO-induced PLB 985 cells; (▲) human neutrophils. The electrochemical kinetic curve is a representative curve from three determinations which were analyzed from different blood donors. Inset plot: Total hydrogen peroxide capacity of neutrophils (A), DMSO-induced PLB 985 cells (B) and non-induced PLB 985 cells (C). Hydrogen peroxide from stimulated cells was measured during a constant voltage of 0.65 V for 90 min to calculate the total area under the curves which resembles the hydrogen peroxide capacity. Results are presented as means \pm S.D. of three determinations.

ide concentration is almost $4.5 \mu\text{M}$, achieved after PT of 25 min. However, the difference between the PT in the electrochemical detection is much higher than the isoluminol CL response. PMA stimulant causes specific degranulation with full activation of the phagocyte redox metabolism [3]. Thus, there is also degranulation of hydrogen peroxide consuming enzymes, such as myeloperoxidase (MPO), to the extracellular matrix. This resulted in the levels of hydrogen peroxide detected by the electrode being the difference between hydrogen peroxide generation and consumption by NADPH oxidase and MPO, respectively. DMSO-induced promyelocytic leukemia cell lines have several deficiencies in MPO activity [21,22]. These findings may explain the delayed hydrogen peroxide PT in DMSO-induced PLB 985 cells. In addition, the decomposition rate of hydrogen peroxide is much lower in DMSO-induced PLB 985 cells compared to human neutrophils (Fig. 3). This observation correlates with the hypothesis regarding MPO-deficient activity in DMSO-induced PLB 985 cells. Besides the detection of NADPH oxidase metabolite, hydrogen peroxide, the electrochemical technique was shown to give information regarding hydrogen peroxide consuming enzymes. In the amperometric detection the area under the curve (hydrogen peroxide capacity) was also calculated for neutrophil-like PLB 985 cells and human neutrophils (Fig. 3 inset) and was approximately twice as much as human neutrophils. This tendency correlates with that of isoluminol CL.

3.4. Isoluminol CL and electrochemical kinetic parameters evaluation

Stimulated NADPH oxidase in phagocyte cells generates superoxide and hydrogen peroxide; in the isoluminol CL technique at least some of the superoxide yields electronically excited products which relax with photon emission. The luminescence velocity can be determined by

$$V = \frac{dh\nu}{dt} = \frac{PH}{PT} \quad (1)$$

The velocity is expressed by photons or RLU per minute and can be calculated in the isoluminol system by peak height (PH) divided by the PT [4]. In both human neutrophils and neutrophil-like PLB 985 cells, the increasing concentrations of isoluminol were followed by increasing PH in the CL response. Based on previous publications [23–25] the theory of Henri–Michaelis Menten was chosen to build and describe the (isoluminol probe)–(phagocyte)–(CL), like a (substrate)–(enzyme)–(product) condition. Isoluminol was considered as a substrate for the Henri–Michaelis Menten analysis. The double reciprocal plot describing CL velocity vs. isoluminol concentrations is presented in Fig. 4B for both human neutrophils and neutrophil-like PLB 985 cells. Maximum velocity value assigned by V_{max} of the CL response, is calculated from the plot, Fig. 4B shows the V_{max} of human neutrophils is 3.8 times higher than the V_{max} of neutrophil-like PLB 985 cells. Since isoluminol CL is superoxide dependent (Fig. 2), the ratio value could be correlated with the activity rate of NADPH oxidase in human neutrophils, when compared to the same in PLB 985 cells. Henri–Michaelis Menten analysis can also be applied to the electrochemical technique, if examining the linear increase in hydrogen peroxide during the first minutes after PMA stimulation, when the oxidase is in full capacity to produce hydrogen peroxide. Unlike the isoluminol CL, the amperometric detection enables direct measurement of hydrogen peroxide which is a product of the oxidase. The velocity of the electrochemical response can be determined by

$$V = \frac{d[\text{H}_2\text{O}_2]}{dt} \quad (2)$$

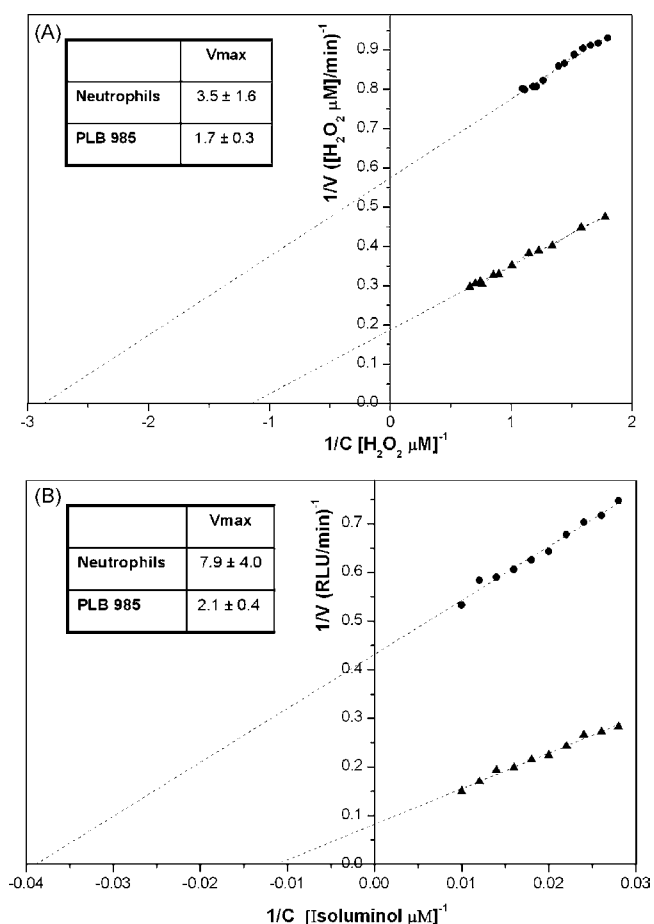


Fig. 4. (A) Double reciprocal plot[†] for electrochemical velocity vs. hydrogen peroxide concentrations. The maximum velocity ($V_{\text{max}}^{\ddagger}$) is given by $[\text{H}_2\text{O}_2 \mu\text{M}]/\text{min}$. (●) DMSO-induced PLB 985 cells and (▲) human neutrophils. (B) Double reciprocal plot[†] for isoluminol velocity vs. isoluminol concentrations. The maximum velocity ($V_{\text{max}}^{\ddagger}$) is given by RLU/min . (●) DMSO-induced PLB 985 cells and (▲) human neutrophils. [†]Both reciprocal plots are representative of three different experiments. [‡]The given values of V_{max} are average values from three different experiments which were analyzed from different blood donors or different differentiation experiments.

The velocity presents the hydrogen peroxide concentration per time unit. The double reciprocal plot for the velocity vs. hydrogen peroxide concentrations is shown in Fig. 4A for both human neutrophils and neutrophil-like PLB 985 cells. In that case, the V_{max} of human neutrophils is 2.1 times higher than the V_{max} of neutrophil-like PLB 985 cells. The difference between the ratio of V_{max} in the electrochemical and chemiluminescent techniques may be caused by differences in the yield of converting superoxide into hydrogen peroxide in different phagocyte cells. In the case of human neutrophils the hydrogen peroxide production rate (V_{max}) was 84 nmole/h per 10^6 cells (Fig. 4A). This value is close to a previous report about human neutrophils [8]. In the case of DMSO-

induced PLB 985 cells the hydrogen peroxide generation rate (V_{max}) of 41 nmole/h per 10^6 cells (Fig. 4A) was found and reported for the first time.

3.5. Isoluminol CL and electrochemical techniques sensitivity

Since it was already shown that the electrochemical and isoluminol CL methods can detect and follow the principle products of NADPH oxidase (superoxide and hydrogen peroxide), further analysis was made regarding the sensitivity of these two real-time techniques. Table 2 summarizes the dynamic parameters used for detection in the electrochemical and CL techniques. Response time was defined as the lag time starting from the stimulation of the cells until the first increase in the measuring signal in both detecting systems (light or current). The response time of isoluminol CL was shown to be faster than the electrochemical technique in both neutrophils and DMSO-induced PLB 985 cells. In addition, DMSO-induced PLB 985 cells are slower in response time than human neutrophils in both measuring techniques. Despite the extended response time of the electrochemical technique, the ratio between response time of electrochemistry and CL technique was similar for both neutrophils and PLB 985 (Table 2). Thus, the extended electrochemical response time can be explained by the order of kinetic reactions (superoxide generated before hydrogen peroxide) and not by low sensitivity of the electrochemical detection. The detection limit is also calculated in both techniques by reducing the number of cells in the measuring vial until there is no further kinetic response. Table 2 shows that both electrochemical and CL techniques were able to measure the kinetic response in as low as 500 cells.

4. Conclusions

Finally, the isoluminol CL and electrochemical techniques were shown to follow the release kinetics of superoxide anion and hydrogen peroxide, respectively, in phagocyte cells. More importantly, a quantitative approach has been applied to monitor the extracellular NADPH oxidase activity in both neutrophil-like PLB 985 cells and human neutrophils. The CL is a well-known technique used in many laboratories around the world for real-time assessment of ROS production from phagocyte cells due to its sensitivity, fast response time and low noise levels. The principle of detection is based on several compounds, that after being excited by different oxygen radicals, release energy (light). This study shows that the electrochemical technique could be used as an alternative for real-time assessment of ROS production from phagocyte cells as it is sensitive and gives comparable results to that of CL and enables direct measurements without any additives.

Acknowledgments

This Research was supported by the Institute for Future Defense Technologies Research at the Technion named for the Medvedi, Shwartzman and Gensler families. The authors would like to thank

Table 2

The sensitivity of the electrochemical and isoluminol CL techniques to detect ROS in human neutrophils and DMSO-induced PLB 985 cells.

	Isoluminol CL		Electrochemistry	
	Human neutrophils	DMSO-induced PLB 985	Human neutrophils	DMSO-induced PLB 985
Response time (s) [†]	8 ± 2	32 ± 3	17 ± 6	52 ± 12
Limit of detection [‡]		500 cells		500 cells

[†]Response time is determined by the time lag from the stimulation of 5×10^5 cells by $1 \mu\text{M}$ PMA until the increase of the first signal (light/current). Results are presented as average of three different determinations ± S.D. [‡]The limit of detection is the lower number of cells that gives a kinetic response after stimulation with $1 \mu\text{M}$ PMA. A reaction vial without cells was used as a negative control.

Dr. Boris Rogachev for the collection of blood samples and to Dr. Sebastien Herrmann for helpful discussion on this manuscript.

References

- [1] C. Dodeigne, L. Thunus, R. Lejeune, *Talanta* 51 (2000) 415.
- [2] L.R. Dechatelet, G.D. Long, P.S. Shirley, D.A. Bass, M.J. Thomas, F.W. Henderson, M.S. Cohen, *J. Immunol.* 129 (1982) 1589.
- [3] H. Lundqvist, P. Follin, L. Khalfan, C. Dahlgren, *J. Leukoc. Biol.* 59 (1996) 270.
- [4] H. Hasegawa, K. Suzuki, S. Nakaji, K. Sugawara, *J. Immunol. Methods* 210 (1997) 1.
- [5] M. Magrisso, M.L. Alexandrova, V.I. Markova, B.G. Bechev, P.G. Bochev, *Luminescence* 15 (2000) 143.
- [6] M. Magrisso, O. Etzion, G. Pilch, A. Novodvoretz, G. Perez-Avraham, F. Schlaeffer, R.S. Marks, *Biosens. Bioelectron.* 21 (2006) 1210.
- [7] C. Dahlgren, A. Karlsson, *J. Immunol. Methods* 232 (1999) 3.
- [8] X. Liu, J.L. Zweier, *Free Radic. Biol. Med.* 31 (2001) 894.
- [9] M.B. Hampton, A.J. Kettle, C.C. Winterbourn, *Blood* 92 (1998) 3007.
- [10] J. El-Benna, P.M. Dang, M.A. Gougerot-Pocidallo, C. Elbim, *Arch. Immunol. Ther. Exp. (Warsz)* 53 (2005) 199.
- [11] S.J. Collins, F.W. Ruscetti, R.E. Gallagher, R.C. Gallo, *Proc. Natl. Acad. Sci. U.S.A.* 75 (1978) 2458.
- [12] K.A. Tucker, M.B. Lilly, L. Heck Jr., T.A. Rado, *Blood* 70 (1987) 372.
- [13] R. Dana, T.L. Leto, H.L. Malech, R. Levy, *J. Biol. Chem.* 273 (1998) 441.
- [14] R. Levy, D. Rotrosen, O. Nagauker, T.L. Leto, H.L. Malech, *J. Immunol.* 145 (1990) 2595.
- [15] E. Pedruzzi, M. Fay, C. Elbim, M. Gaudry, M.A. Gougerot-Pocidallo, *Br. J. Haematol.* 117 (2002) 719.
- [16] R. Van Bruggen, E. Anthony, M. Fernandez-Borja, D. Roos, *J. Biol. Chem.* 279 (2004) 9097.
- [17] H. Lundqvist, C. Dahlgren, *Free Radic. Biol. Med.* 20 (1996) 785.
- [18] S. Kopprasch, J. Pietzsch, J. Graessler, *Luminescence* 18 (2003) 268.
- [19] E. Feuk-Lagerstedt, E.T. Jordan, H. Leffler, C. Dahlgren, A. Karlsson, *J. Immunol.* 163 (1999) 5592.
- [20] B.V. O'Donnell, D.G. Tew, O.T. Jones, P.J. England, *Biochem. J.* 290 (Pt 1) (1993) 41.
- [21] G.R. Pullen, C.S. Hosking, *Clin. Exp. Immunol.* 62 (1985) 304.
- [22] M. Yamada, K. Kurahashi, *J. Biol. Chem.* 259 (1984) 3021.
- [23] R.C. Allen, *Methods Enzymol.* 133 (1986) 449.
- [24] J. Genius, J. Fandrey, *Free Radic. Biol. Med.* 29 (2000) 515.
- [25] A. Van Nerom, M. Desmidt, R. Ducatelle, F. Haesebrouck, *J. Biolumin. Chemilumin.* 12 (1997) 207.



Determination of ultra-trace amount methyl-, phenyl- and inorganic mercury in environmental and biological samples by liquid chromatography with inductively coupled plasma mass spectrometry after cloud point extraction preconcentration

Jianguo Chen^{a,b}, Hengwu Chen^{a,*}, Xianzhong Jin^b, Haiting Chen^b

^a Department of Chemistry, Zhejiang University, Zijing'gang Campus, Hangzhou 310058, China

^b Ningbo Entry-exit Inspection and Quarantine Bureau, Ningbo 315012, China

ARTICLE INFO

Article history:

Received 3 August 2008

Received in revised form

11 September 2008

Accepted 12 September 2008

Available online 23 September 2008

Keywords:

Cloud point extraction

Mercury speciation

HPLC

ICP-MS

Water samples

Biological samples

ABSTRACT

The cloud point extraction (CPE) preconcentration of ultra-trace amount of mercury species prior to reverse-phase high performance liquid chromatography (HPLC) with inductively coupled plasma mass spectrometry (ICP-MS) detection was studied. Mercury species including methyl-, ethyl-, phenyl- and inorganic mercury were transformed into hydrophobic chelates by reaction with sodium diethyldithiocarbamate, and the hydrophobic chelates were extracted into a surfactant-rich phase of Triton X-114 upon heating in a water bath at 40 °C. Ethylmercury was found partially decomposed during the CPE process, and was not included in the developed method. Various experimental conditions affecting the CPE preconcentration, HPLC separation, and ICP-MS determination were optimized. Under the optimized conditions, detection limits of 13, 8 and 6 ng l⁻¹ (as Hg) were achieved for MeHg⁺, PhHg⁺ and Hg²⁺, respectively. Seven determinations of a standard solution containing the three mercury species each at 0.5 ng ml⁻¹ level produced relative standard deviations of 5.3, 2.3 and 4.4% for MeHg⁺, PhHg⁺ and Hg²⁺, respectively. The developed method was successfully applied for the determination of the three mercury species in environmental water samples and biological samples of human hair and ocean fish.

© 2008 Elsevier B.V. All rights reserved.

1. Introduction

It is well known that the toxicity of mercury is highly dependent on its chemical forms, and alkylmercury compounds are deemed to be the most toxic substances among the various mercury species. The determination of mercury species in environmental and biological samples has attracted much attention of chemical analysts [1–3].

The common analytical techniques used for mercury speciation are based on coupling chromatographic separation to mercury specific detection [4–7]. Compared with gas chromatography, high performance liquid chromatography (HPLC) is the preferred separation technique used for mercury speciation, because the mercury species need not to be derived to volatile compounds before HPLC separation. Thus, HPLC has been coupled to various atomic spectrometric techniques for mercury speciation in the past several decades [2–4]. Since the concentration of mercury species

in non-polluted environmental and biological samples is usually at tens ng l⁻¹ or pg g⁻¹ levels, inductively coupled plasma mass spectrometry (ICP-MS) is, among various elemental specific detection techniques, the most preferable detection technique for mercury speciation due to its excellent detectability for mercury [8–10]. Thus, various coupled HPLC-ICP-MS systems [11–21] have in recent years been reported for the determination of mercury species in environmental or biological samples since the first work reported by Bushee [18]. Even so, determination of mercury species in water samples with HPLC-ICP-MS is still challenging, because the detection limits of mercury species obtained by the HPLC-ICP-MS are usually in the range of 0.x–0.0x μg l⁻¹. Therefore, preconcentration of mercury species prior to HPLC-ICP-MS determination is sometimes required. It has been reported that solid-phase extraction preconcentration of mercury species with diethyldithiocarbamate-immobilized C18 [12] or dithiocarbamate resin [19], and of insoluble diethyldithiocarbamate chelates of mercury species [11] with C18 before HPLC-ICP-MS determination lowered the detection limits down to several ppt levels.

Cloud point extraction (CPE) [22–23], which is based on the temperature induced phase-transfer of non-ionic surfactants in

* Corresponding author. Tel.: +86 571 88206773; fax: +86 571 88206773.
E-mail address: hwchen@zju.edu.cn (H. Chen).

aqueous solution, is an efficient and analyst/environment-friendly alternative for sample pretreatment. Compared with conventional solvent extraction, it greatly reduces the extraction time, solvent consumption and waste-disposal costs. Thus, CPE has in recent years been used for preconcentration of various trace metal ions with posterior quantification by an atomic spectrometric technique [23]. However, only a few works have been reported on CPE preconcentration of mercury species. de Wuiloud et al. [24] reported a CPE approach for preconcentration of trace inorganic mercury in tap water samples with chelating reagent 2-(5-bromo-2-pyridylazo)-5-diethylaminophenol and non-ionic surfactant polyethyleneglycolmono-*p*-nonylphenylether prior to flow injection cold vapor generation inductively coupled plasma optical emission spectrometry, and achieved a detection limit of 4 ng l^{-1} inorganic mercury. Li and Hu [25] developed a non-chromatographic technique for the speciation of methylmercury and inorganic mercury in seafood by sequential CPE combined with inductively coupled plasma optical emission spectrometry, obtaining the detection limits of 56.3 and 94.6 ng l^{-1} for Hg^{2+} and MeHg^+ (as Hg), respectively. Yin [26] reported a dual CPE technique for capillary electrophoresis (CE) speciation of mercury. In their method, mercury species were first extracted into Triton X-114 surfactant-rich phase as hydrophobic 1-(2-pyridylazo)-2-naphthol (PAN) chelates, which were then back extracted to aqueous phase by forming hydrophilic mercury complexes of cysteine. Using a CE system with UV detector for posterior separation and determination, the author reported detection limits of 47.5 , 45.2 , 4.1 , and $10.0 \mu\text{g l}^{-1}$ (as Hg) for methyl-, ethyl-, phenyl-, and inorganic mercury, respectively. Yu [27] developed a CPE approach for preconcentration of methyl-, ethyl-, phenyl-, and inorganic mercury species as their pyrrolidinedithiocarbamate (APDC) chelates prior to HPLC-cold vapor generation-atomic fluorescence spectrometry (CV-AFS) for speciation of mercury in fish. The author claimed detection limits ranging from 2 to 9 ng l^{-1} (as Hg) for the methyl-, ethyl-, phenyl-, and inorganic mercury. To the best of our knowledge, however, no report about coupling of CPE preconcentration to HPLC-ICP-MS for speciation of ultra-trace mercury has been published.

The purpose of the present work is to develop a sensitive, analyst/environment-friendly and cost-effective method for the determination of ultra-trace mercury species in environmental waters and biological samples by coupling CPE preconcentration to HPLC-ICP-MS system.

2. Experimental

2.1. Instrumentation

A model 7500a ICP-MS (Agilent, USA) was used in this work. An Agilent 1100 HPLC system (Agilent, Germany) consisted of a degassing system, a triple-gradient pumping system and a Rheodyne Model 7725 injection valve was employed. Separation was performed on a Discovery C18 column ($4.6 \text{ mm i.d.} \times 15 \text{ mm}$, $5 \mu\text{m}$) (Supelco, PA, USA). The outlet of the LC column was directly connected to the sample introduction system of ICP-MS via a 30 cm of 0.18 mm i.d. Teflon tubing. The optimized chromatographic and ICP-MS operating conditions are summarized in Table 1. The HPLC-ICP-MS system worked at time resolved analysis mode, and Software B 03.03 ICP-MS chemstation was used to control the system, and the collected data were processed with the Version C. 01.00 Chromatographic Data Analysis software provided by the manufacturer.

A Biofuge Primo R7500 centrifuge (Kendro laboratory, GmbH, Hanau, Germany) was used to accelerate the phase separation dur-

Table 1
Operational parameters of the HPLC-ICP-MS system.

HPLC part	
Column	Discovery C18, $4.6 \text{ mm i.d.} \times 15 \text{ mm}$, $5 \mu\text{m}$
Mobile phase	35% methanol–40% acetonitrile–25% water containing $1.0 \times 10^{-4} \text{ mol l}^{-1}$ DDTC
Flow rate of the mobile phase	0.8 l min^{-1}
Sampling volume	$20 \mu\text{l}$
ICP-MS part	
Forward power	1500 W
Reflect power	<5 W
Spray chamber temperature	-5°C
Plasma gas and its flow rate	Ar, 15 l min^{-1}
Auxiliary gas and its flow rate	Ar, 0.2 l min^{-1}
Carrier gas and its flow rate	Ar, 0.5 l min^{-1}
Make up gas and its flow rate	Ar, 0.4 l min^{-1}
Optional gas and its flow rate	Ar/O ₂ = 4:1 in volume, 0.3 l min^{-1}
Sampling depth	11 mm
Monitoring masses	Hg, $m/z = 202$
Acquisition mode	Time resolved analysis
Integration time	1 s

ing CPE. All the vessels used for trace analysis were soaked in 10% nitric acid for 24 h and subsequently rinsed at least three times with pure water.

2.2. Reagents

All reagents were of analytical or better grade, and pure water ($18.2 \text{ M}\Omega \text{ cm}$) obtained from MILLI-Q elemental-grade water purification system (Millipore Corp., Molsheim, France) was used throughout the work. Triton X-114 (>93%) was obtained from Acros Organics (New Jersey, USA) and used without further purification. A 0.05 mol l^{-1} sodium diethyldithiocarbamate (DDTC) was prepared by dissolving the reagent (Shanghai No. 3 Reagent Factory, China) in methanol–water (1:1, v/v). Methanol and acetonitrile (HPLC grade) were obtained from Tedia (Tedia Inc., OH, USA).

A stock standard solution of $1000 \text{ mg l}^{-1} \text{ Hg}^{2+}$ prepared in 5% nitric acid was obtained from National Standard Material Center (GSB G 62069-90, Beijing, China). Stock standard solutions of MeHg^+ , EtHg^+ , and PhHg^+ at 1000 mg l^{-1} (as Hg) were prepared by individually dissolving appropriate amounts of methylmercury chloride ($\geq 95\%$), ethylmercury chloride ($\geq 95\%$), both from Alfa Aesar (A Johnson Matthey Company, MA, USA), and phenylmercuric acetate (98%, Acros Organics, New Jersey, USA) in methanol, respectively. All these stock solutions were stored in plastic bottles and kept at 4°C . Working standard solutions were prepared from the corresponding stock solutions by stepwise dilution with water just before use. Standard reference material of human hair was obtained from National Standard Material Center (GBW 07601, Beijing, China), and the ocean bonito fish was purchased from local ocean fish market.

2.3. Procedure for cloud point extraction

Aliquots of 25 ml water samples or standard solutions were pipetted to 50 ml plastic centrifuge tubes. Then, 1 ml of 0.05 mol l^{-1} borate buffer (pH 9.0), 0.4 ml of 5% Triton X-114 and 0.4 ml of 0.05 mol l^{-1} DDTC were sequentially added and completely mixed with the sample or standard solutions. The centrifuge tubes containing the mixed solutions were heated in a thermostatic water bath at 40°C for 10 min. Separation of the aqueous and surfactant-rich phases was accomplished by centrifuging at 4000 rpm for 10 min. The supernatant aqueous waste in the tubes was removed with a pipette. Then, 0.5 ml of methanol was added to dilute the

surfactant-rich phase. After mixing, the diluted surfactant-rich solutions were ready for mercury speciation by HPLC–ICP–MS. If the prepared concentrates were not immediately subjected to the determination, they were stored in refrigerator (4 °C).

2.4. Sample preparation

2.4.1. Water sample

Water samples were subjected to the analysis soon after their collection. Before CPE, they were filtered through a membrane of 0.45 μm pore size, and the filtrated water was adjusted to pH 8–9 with a dilute sodium hydroxide solution. A 25 ml aliquot of the water sample was pipetted into centrifuge tube and subjected to the CPE as described in the above section. If the water samples were not analyzed after collection, they should be acidified to pH < 2 with dilute hydrochloric acid and stored at –4 °C.

2.4.2. Biological sample

An improved sonication-assisted acid leaching procedure was adopted from Ref. [27]. About 0.1 g human hair (a standard reference material) or 0.2 g mashed and homogenized fish sample was accurately weighed into a 50 ml plastic centrifuge tube. Then 3 ml of 5 mol l⁻¹ HCl was added, extraction was performed in sonicated water bath for 30 min at room temperature. After centrifugation, the clear supernatant was collected into another 50 ml plastic centrifuge tube. The residue was extracted again as described above, and the supernatant was combined with the first one. The residue was then extracted with 5 ml pure water for 30 min at room temperature under sonification, and the supernatant water was again mixed with the combined acidic supernatant. After vortex mixing, the extractant solution was filtered through a membrane of 0.45 μm pore size into a 100 ml volumetric flask, and diluted to the mark with water. A 25 ml aliquot of the prepared solution was pipetted to a 50 ml plastic centrifuge tube, and then subjected to CPT as described in Section 2.3.

3. Results and discussion

3.1. Optimization of the HPLC–ICP–MS system coupled with CPE

In the previously reported works on coupling reversed-phase HPLC to ICP–MS for mercury speciation, the mobile phases were usually the aqueous solutions containing ammonium acetate buffer, methanol or acetonitrile and complex reagent such as 2-mercaptoethanol and cysteine that was used to on-column transform the mercury species to their corresponding complexes. The total content of methanol or acetonitrile in the mobile phase was usually less than 3%, so that stable plasma discharge could be maintained. Such type of mobile phase provided appropriate elution strength for the 2-mercaptoethanol or cysteine complexes of mercury species, because these complexes were quite hydrophilic. Nevertheless, such a mobile phase is not suitable for the present work, because CPE preconcentration of mercury species requires the water-soluble mercury species be transformed to water-insoluble chelates with suitable chelating reagent, and the subsequent separation of such hydrophobic chelates with reverse-phase HPLC needs a mobile phase with high organic solvent content [28]. In our tests, when a methanol–water binary solvent system containing 70% methanol was used, it took about 30 min to elute the most hydrophobic DDTC chelate of Hg²⁺, Hg(DDTC)₂, out of the column. When a ternary mobile phase containing 40% methanol–40% acetonitrile–20% water was used at the flow rate of 0.8 ml min⁻¹, the DDTC chelates of MeHg⁺, EtHg⁺, PhHg⁺ and Hg²⁺ were eluted within 10 min, with the peaks for EtHg⁺ and PhHg⁺ being partially overlapped. Baseline separation of the four

species was achieved within 14 min when a mobile phase of 35% methanol–40% acetonitrile–25% water running at the same flow rate was used. Thus, this ternary system was used as the optimized separation condition in the following work.

Since the HPLC eluant was directly introduced into the ICP source, the use of mobile phase with high organic content would create problems of plasma instability and carbon particle deposition in the sampling and skimming cones. To solve these problems, some special measures were adopted in the present work. Firstly, plasma forward power as high as 1500 W was used to maintain stable plasma discharge. Secondly, temperature of spray chamber was kept at –5 °C with the help of a Peltier cooling system to remove as much organic solvent as possible from the sample aerosol. Thirdly, an optional gas flow containing oxygen was applied to reduce the risk of carbon deposition on the surface of sampling cone [29]. It was observed that the color of the plasma was green when a standard solution of Hg²⁺ prepared with a mobile phase containing 35% methanol and 40% acetonitrile was aspirated into the plasma without the optional gas flow. Under this condition, carbon deposition occurred on the sampling cone after the solution was continuously aspirated for less than 10 min. While an optional gas (argon containing 20% O₂) was applied and its flow rate gradually increased from 0 to 0.4 l min⁻¹, the color of the plasma turned from green to light blue. As shown in Fig. 1, the signal of mercury increased with the increase of the optional gas flow up to 0.2 l min⁻¹ after which gradually decreased, meanwhile the background detected at ²⁰⁶Pb was continuously depressed with the increase of the optional gas flow. As a result, the signal-to-noise ratio of mercury reached maximum at the optional gas flow rate of 0.3 l min⁻¹. Under this condition, carbon deposition could hardly be observed on the sampling cone after the HPLC–ICP–MS system had been run with a mobile phase containing 35% methanol and 40% acetonitrile for a period of more than 8 h.

At the conditions of the plasma forward power being kept at 1500 W and optional gas flow rate at 0.3 l min⁻¹, the nebulizer gas flow rate and sampling depth were optimized respectively. The maximum signals for the mercury species reached at the flow rate of 0.5 l min⁻¹ that was lower than the previously reported ones [13,15]. This may be ascribed to that the eluant introduced into the nebulizer contained a high content of organic solvent on one hand, and that the total carrier gas flow for aerosol delivery was supplemented by the optional gas on the other hand. The influence of sampling depth ranging from 9 mm to 13 mm on the signals of the mercury species was also investigated. It was found that the sampling depth did not significantly affect the ion signals despite

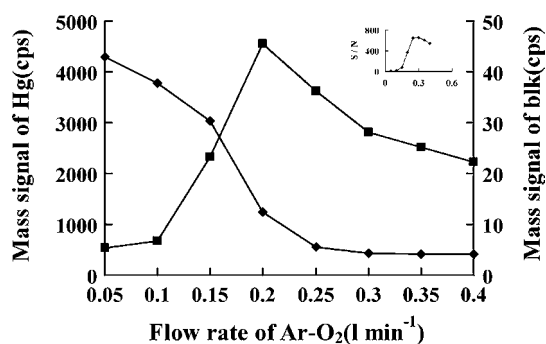


Fig. 1. Effect of operation gas flow rate on the mass signals of mercury. 10 μg l⁻¹ Hg²⁺ in the 35% methanol–40% acetonitrile–25% water was directly aspirated into the nebulizer of the ICP–MS system. ■, mass signals of mercury; ♦, background observed with the m/z 206. The insert shows the effect of the operation-gas flow-rate on the ratio of signal to noise (S/N). Other operational conditions for ICP–MS were the same as described in Table 1.

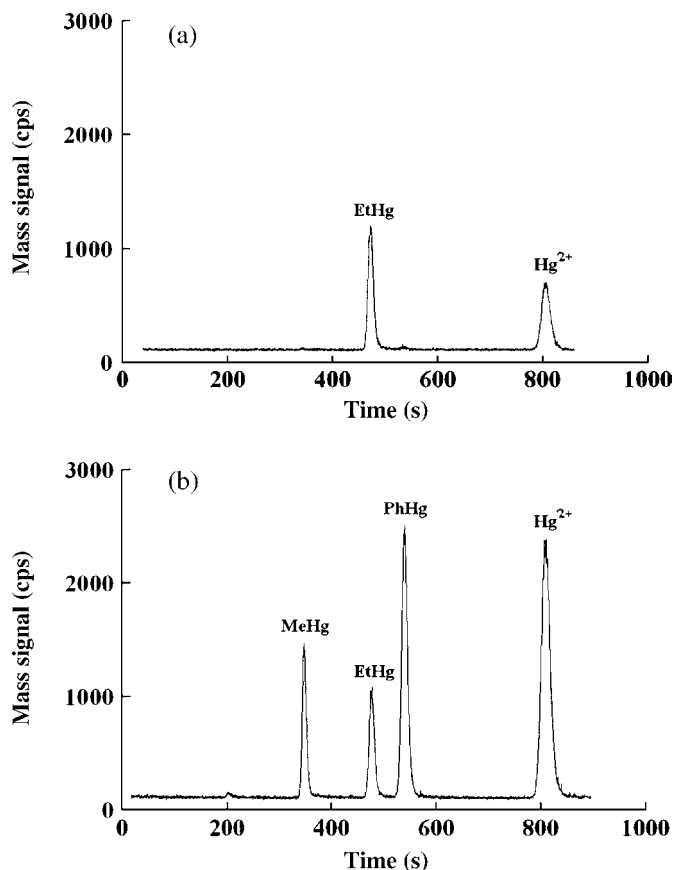


Fig. 2. Chromatograms of HPLC-ICP-MS analysis for mercury species after CPE. (a) ethylmercury alone; (b) methyl-, ethyl-, phenyl- and inorganic mercury. The concentration of each mercury species was $1 \mu\text{g l}^{-1}$ (as Hg) in all the tests. Experimental conditions for CPE: acidity of the medium, pH 9.0; DDTC concentration, $8 \times 10^{-4} \text{ mol l}^{-1}$; Triton X-114 concentration, 0.08% (w/v); incubation temperature and time, 40°C for 10 min. The operational conditions for HPLC separation and ICP-MS detection were described in Table 1.

that the highest signals for the three species were observed in the sampling depth of 11 mm that was adopted for the determinations.

3.2. Cloud point extraction

CPE is based on the temperature induced phase-transfer phenomenon of non-ionic surfactants in aqueous solution. When a non-ionic surfactant micelle solution is heated to above its cloud point temperature, the solution becomes turbid. With centrifugation, the turbid solution may be separated into two liquid phases: a surfactant-rich phase (usually with small volume of several hundred micro litres) and another aqueous phase. Hydrophobic species in the sample solutions can be solvated into the non-ionic surfactant micelle phase, and enriched in the surfactant-rich phase upon the phase transferring. For CPE preconcentration of trace metal species, the water-soluble metal ions should be transferred into water-insoluble chelates via complex with a suitable chelating agent. Therefore, the CPE efficiency for metal species mainly depends on the behavior of the non-ionic surfactant and the complex formation between the metal ion and chelating agent. In the present work, Triton X-114 was selected as the non-ionic surfactant for CPE of the mercury species due to its low cloud point temperature ($\sim 25^\circ\text{C}$), which was in favor of the phase transition at relative low temperature ($30\text{--}40^\circ\text{C}$) to prevent the mercury species and their chelates from decomposing during the incubation step. DDTC was used as the chelating agent, because it can quickly com-

plex to mercury species with favorable formation constants and to form water-insoluble chelates, whereas the agent itself is highly water-soluble.

3.2.1. Stability of the mercury species

In the previously works on CPE preconcentration of mercury species with chelating reagent of either PAN [26] or APDC [27] prior to CE separation with UV detection [26] or HPLC separation with CV-AFS detection [27], no observation on the decomposition of the mercury species has been reported. However, in our tests in CPE of the mercury species with DDTC, EtHg⁺ was found partially decomposed. It was observed that two fully resolved peaks appeared in the chromatogram when a test solution containing single EtHg⁺ was subjected to CPE and subsequent HPLC-ICP-MS. As shown in Fig. 2a, the first peak with the retention time of about 8 min was assigned to the DDTC-EtHg species, while the second one possessed the same retention time as Hg(DDTC)₂. For comparison, the chromatogram obtained with a mixed solution of the four mercury species was shown in Fig. 2b. The Hg(DDTC)₂ species was

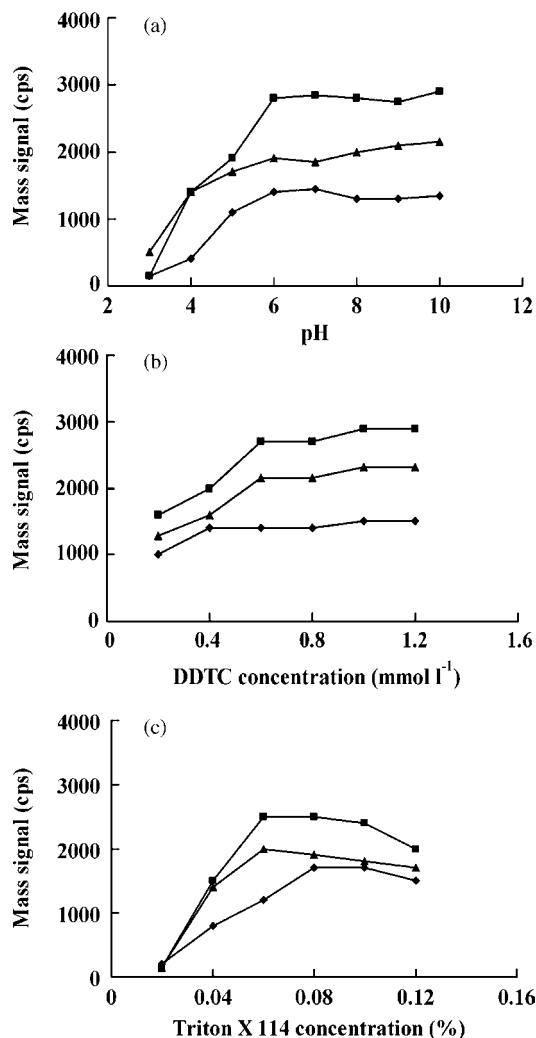


Fig. 3. Effects of chemical conditions for the CPE on the HPLC-ICP-MS signals of the mercury species. (a) The influence of pH. Buffers: pH3-5, phthalate; pH6-7, phosphate; pH 8-10, borate. Except for the medium pH, all other experimental conditions were the same as in Fig. 2. (b) Influence of DDTC concentration, all other experimental conditions were the same as described in Fig. 2. (c) Influence of Triton X-114 concentration. Except for the concentration of Triton X-114, all other experimental conditions were the same as described in Fig. 2. ♦, MeHg; ■, PhHg; ▲, Hg²⁺.

Table 2

Analytical performances of the HPLC–ICP–MS system for the determination of mercury species after cloud point extraction.

Analytical performances	MeHg ⁺	PhHg ⁺	Hg ²⁺
Retention time (min)	6.24	9.22	13.38
The numbers of theoretical plates	2.8×10^4	3.1×10^4	3.2×10^4
Enhancement factor ^a	18	46	57
Detection limits (ng l ⁻¹)	13	8	6
Dynamic linear range (μg l ⁻¹)	0.02–2.00	0.02–2.00	0.02–2.00
Linear regression equation ^b	$I = 140637c + 3206$	$I = 430316c + 6728$	$I = 469354c + 198$
Correlation coefficient	0.9986	0.9998	0.9999
Relative standard deviation (%) (0.5 μg l ⁻¹ , n = 7)	5.3	2.3	4.4
(0.05 μg l ⁻¹ , n = 3)	14.2	11.4	19.5

^a The ratio of sensitivities observed with HPLC–ICP–MS of DDTC chelates of the mercury species after and before CPE.^b I, peak area; c, concentration in ng ml⁻¹.

thought to be transformed from the DDTC–EtHg, which might be instable under the experimental conditions, and the ethyl group of which could be substituted by the excess DDTC. The decomposition also occurred when the chelating reagent DDTC was replaced by APDC. Neither MeHg⁺ nor PhHg⁺ was found decomposed during the CPE process. Langseth [28] reported, in his study on HPLC speciation of mercury species after solvent extraction of the species as alkylthiocarbamate chelates, that the organomercury compounds partly decomposed to Hg²⁺ when extracted from acidic solution, being most pronounced for PhHg⁺ and hardly observable for MeHg⁺, but the extraction from basic solution, for instance in pH 9.5 medium, was quantitative. In the present CPE system where the extraction was performed in pH 9.0, the decomposition of EtHg⁺ could most possibly be ascribed to the heating process for phase isolation. Detail study on the mechanism of the decomposition of the mercury compound during CPE is currently progressing. Since EtHg⁺ seldom exists in non-polluted waters and biological samples, it was then excluded from the analyte list of the present study.

3.2.2. Optimization of experimental conditions for CPE

In the present study, the effect of experimental conditions such as sample acidity, DDTC concentration and Triton X-114 concentration on the CPE efficiency were investigated and optimized based on univariate design. Considering that the formation and precipitation of surfactant-rich phase is mainly depends on the behavior (for instance the cloud point temperature) of the employed non-ionic surfactant, such conditions as the temperature (40 °C) and time duration (10 min) used for incubation of the test solutions and that for centrifugation of the surfactant-precipitated suspension were directly adopted from our previous work [30] where the non-ionic surfactant and sampling volume used for CPE preconcentration

were the same as used in the present work. The influence of acidity on the HPLC–ICP–MS signals of the MeHg⁺, PhHg⁺ and Hg²⁺ was investigated in the range of pH 3–10 while the DDTC and Triton X-114 concentrations in the CPE media were kept at 8×10^{-4} mol l⁻¹ and 0.08%, respectively. As shown in Fig. 3a, the HPLC–ICP–MS signals for the three mercury species increased with the increase of pH value up to 6, thereafter they were approximately kept at the same levels. Considering that the chelating reagent DDTC is much more stable in slightly alkaline medium than in acidic or neutral medium [31], pH 9.0 was finally selected for CPE of the mercury species and a borate buffer was used to control the acidity of the CPE medium. While the pH of the CPE media was kept at pH 9.0 and Triton X-114 concentration at 0.08%, the influence of DDTC concentration on HPLC–ICP–MS signals of the post-CPE determination was demonstrated in Fig. 3b. As the constant maximum signals for MeHg⁺, PhHg⁺ and Hg²⁺ were observed at the DDTC concentrations higher than 6×10^{-4} mol l⁻¹, a DDTC concentration of 8×10^{-4} mol l⁻¹ was adopted. At the optimized pH 9.0 and 8×10^{-4} mol l⁻¹ DDTC concentration, the influence of Triton X-114 concentration on the HPLC–ICP–MS signals was shown in Fig. 3c, and the maximum mass signals of the three mercury species were obtained at Triton X-114 concentration of 0.08% (w/v) in the test solution. Under this condition, about 200 μl of Triton X-114 rich phase could be collected after phase separation.

Under the optimized CPE conditions, the extraction efficiency, defined as the percentage of the mercury species transferred from the aqueous test solution into the surfactant-rich phase, of $39.9 \pm 0.3\%$, $95.9 \pm 0.4\%$ and $93.6 \pm 3.4\%$ (mean ± S.D., n = 3) were observed for MeHg⁺, PhHg⁺, and Hg²⁺, respectively. It is understandable if one takes it in mind that the hydrophobic property of the DDTC chelate of MeHg⁺ (Me–Hg–DDTC) is much poorer

Table 3

Analytical results of the mercury species in water samples and of the spike-recovery tests.

Water sample	Spiked (μg l ⁻¹)			Measured (μg l ⁻¹ , mean ± S.D., n = 3) and average recovery (%; in the parallel)		
	MeHg ⁺	PhHg ⁺	Hg ²⁺	MeHg ⁺	PhHg ⁺	Hg ²⁺
Tap water	–	–	–	ND	ND	ND
	0.050	0.050	0.050	0.042 ± 0.006 (84)	0.044 ± 0.005 (88)	0.041 ± 0.008 (82)
	0.50	0.50	0.50	0.52 ± 0.073 (104)	0.42 ± 0.072 (85)	0.46 ± 0.024 (91)
Water from Beidou River	–	–	–	ND	ND	0.23 ± 0.02
	0.10	0.10	0.10	0.094 ± 0.0044 (94)	0.092 ± 0.0035 (92)	0.34 ± 0.012 (110)
	1.00	1.00	1.00	1.08 ± 0.049 (108)	1.06 ± 0.057 (106)	1.18 ± 0.083 (95)
Water from Baixi Reservoir	–	–	–	ND	ND	ND
	0.10	0.10	0.10	0.094 ± 0.001 (94)	0.098 ± 0.001 (98)	0.090 ± 0.007 (90)
	1.00	1.00	1.00	0.95 ± 0.009 (95)	1.02 ± 0.033 (102)	1.04 ± 0.003 (104)
Seawater from Bailun coast	–	–	–	ND	ND	ND
	0.020	0.020	0.020	0.023 ± 0.002 (115)	0.019 ± 0.002 (94)	0.022 ± 0.002 (108)
	2.00	2.00	2.00	1.97 ± 0.027 (98)	1.74 ± 0.045 (87)	1.97 ± 0.087 (98)

ND: not detected.

than the chelate of PhHg^+ (Ph-Hg-DDTC) and that of Hg^{2+} (DDTC-Hg-DDTC).

3.3. Interference

Under the optimized conditions for CPE, interference studies were carried out by individually spiking gradually increased amounts of foreign metal ions into the test standard solutions containing three mercury species (each at $1.0 \mu\text{g l}^{-1}$ level) before subjected to the cloud point extraction, and a deviation greater than $\pm 10\%$ from the signals observed in absence of any foreign metals was used as the criterion of interference occurring. It was found that K^+ and Na^+ in at least 10 mg ml^{-1} , Ca^{2+} and Mg^{2+} in 1 mg ml^{-1} , Fe^{3+} and Zn^{2+} in 5 mg l^{-1} , Al^{3+} and Cr^{3+} in 1 mg l^{-1} , Pb^{2+} , Cd^{2+} , Cu^{2+} , Ni^{2+} , Co^{2+} and Mn^{2+} in 0.1 mg l^{-1} did not cause significant interference. Thus, the interference tolerance levels of the proposed method meet the requirement of analyzing non-polluted waters such as tap water, fresh water, and seawater.

3.4. Analytical figures of merit

Under the optimized conditions, the obtained analytical characteristic data such as dynamic linear ranges, linear regression equations, signal-enhancement factors, detection limits (defined as the concentrations that gave triple the peak-to-peak noise of the baseline signals, $S/N = 3$), and precisions are summarized in Table 2. Thus, the detection limits obtained by the present method were not only improved by 1–2 orders of magnitude in comparison to the methods without any preconcentration step [13–17,20], but also comparable to those [11,12,19] observed with methods including a solid-phase extraction preconcentration procedure.

3.5. Applications

Due to the decomposition of EtHg^+ occurring in the process of CPE, the present approach is only suitable for the samples containing negligible amount of EtHg^+ , say one order of magnitude less than the content of Hg^{2+} . Therefore, it is important to inspect whether or not the peak for EtHg^+ appears in the chromatogram after a chromatogram of an unknown sample is obtained. If EtHg^+ present in a sample, a positive error may be introduced into the analytical result of inorganic mercury. Fortunately, EtHg^+ is usually absent or much less than those of MeHg^+ and Hg^{2+} in non-polluted environmental water samples and biological samples. With this warning being taken in mind, the proposed method was first applied to the determination of MeHg^+ , PhHg^+ , and Hg^{2+} in water samples (fresh water and seawater). Experiment results showed that all the analyzed water samples contained no detectable EtHg^+ . The accuracy of the proposed method was examined with spike-recovery tests. Two concentrations (one in ppb level and the other in sub-ppb level) of mercury species (MeHg^+ , PhHg^+ and Hg^{2+}) were spiked into various water samples, and the concentrations of the mercury species in spiked and non-spiked samples were measured against a calibration curve made with a series of standard solutions that were subjected to the same procedures as the samples. The analytical results for the water samples, together with the

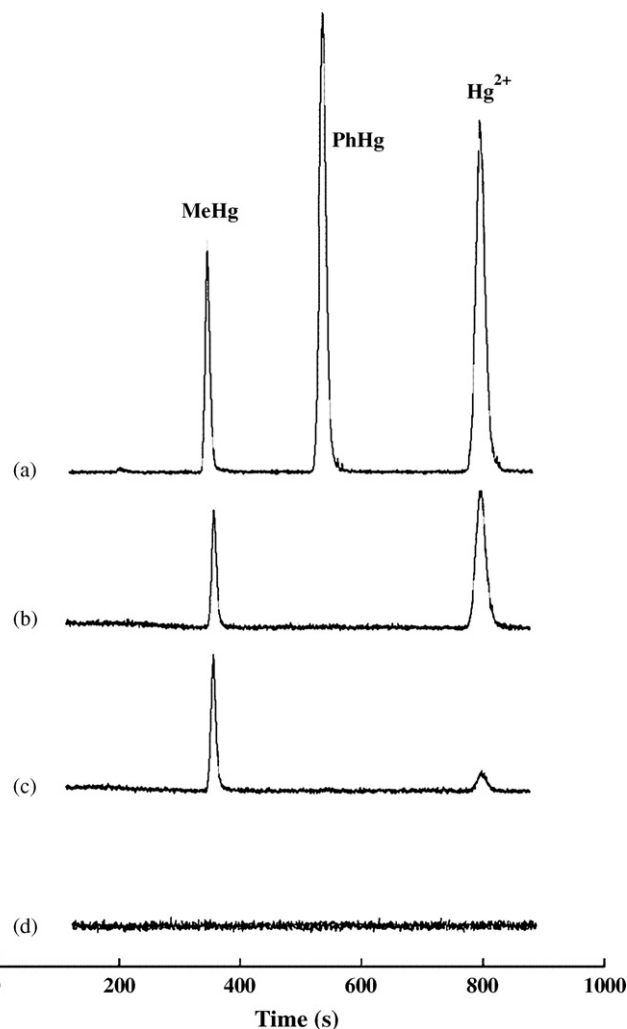


Fig. 4. Chromatograms of (a) a standard solution containing methyl-, phenyl-, and inorganic mercury, each at $1 \mu\text{g l}^{-1}$, (b) human hair standard material, (c) a sample of ocean bonito, and (d) the reagent blank. The experimental conditions for HPLC-ICP-MS and CPE were described in Fig. 2.

recoveries of spiked mercury species, are listed in Table 3. Thus, recoveries ranging from 82% to 115% were obtained from all of the tested water samples, demonstrating satisfactory accuracy of the proposed method for determination of mercury species in non-polluted water samples. It was noticed that when seawater samples were analyzed with the proposed method, the test solutions, upon warming at 40°C , turned turbid more quickly than the test solutions of fresh water samples. After centrifugation, the interface between the surfactant-rich phase and supernatant aqueous phase was clearer for seawater samples than that for fresh water samples. These observations could be ascribed to the effect of salt-assisted phase separation. Nevertheless, no significantly poor recoveries of the spiked mercury species were obtained for the seawater samples as listed in Table 3.

Table 4
Analytical results of the mercury species in biological samples (in ng g^{-1}).

Sample	Measured by this work (mean \pm S.D., $n = 3$)		Certified Total Hg	Measured by CV-AFS Total Hg	Reported by references	
	MeHg^+	Hg^{2+}			MeHg^+	Hg^{2+}
Human hair (GBW 07601)	227 ± 30	151 ± 19	360 ± 50	–	180 ± 50 [32]	200 ± 10 [32]
Ocean bonito	282 ± 9	38 ± 6	–	240 ± 50	–	–

When the developed method was used to determine mercury species in a human hair sample (a standard reference material issued by National Standard Material Center of China) and a fish meat sample, an acid leaching procedure adopted from Ref. [27] was employed to extract the mercury species from the ground or mashed solid samples prior to CPE. For the human hair sample, only MeHg⁺ and Hg²⁺ were detected, and no peak for EtHg⁺ appeared in the chromatogram (see Fig. 4). Analytical results for the standard reference material are listed in Table 4. As only total mercury content in the human hair was certified, reference-reported data for the mercury speciation obtained are also listed in the Table 4. Thus, both the total mercury content and the individual contents of MeHg⁺ and Hg²⁺ species observed with the developed method are basically in agreement with the certified and reported values. Also listed in Table 4 is the analytical result for the fish meat sample of ocean bonito. Only MeHg⁺ and Hg²⁺ species were found, and the sum of the MeHg⁺ and Hg²⁺ mercury contents determined with the present approach is in good agreement with the total mercury content obtained with the National Standard Procedure (GB/T 5009.17-2003, cold-vapor generation-atomic fluorescence method).

4. Conclusions

The cloud point extraction of mercury species with chelating agent DDTC and non-ionic surfactant Triton X-114 can be used for preconcentration of MeHg⁺, PhHg⁺ and Hg²⁺, but is not suitable for the preconcentration of EtHg⁺ because the species is subjected to partial decomposition during the extraction process. The separation of the concentrated DDTC chelates of mercury species by reverse-phase HPLC requires an eluant containing organic solvent as high as 75% to elute all the DDTC chelates within 15 min. Consequently, special measures such as high plasma forward power, cooling spray chamber and oxygen-containing optional gas flow are required for stabilization of the ICP discharge when the high-solvent-eluant is directly introduced into the ICP-MS system. Under the optimized conditions, the detection limits for MeHg⁺, PhHg⁺ and Hg²⁺ observed with the developed cloud point extraction-HPLC-ICP-MS reaches down to 6~13 ng l⁻¹ levels, 1~2

orders of magnitude lower than the reported values obtained with HPLC-ICP-MS without any preconcentration step. The developed method can be used to determine MeHg⁺, PhHg⁺ and Hg²⁺ in non-polluted water samples that contain negligible EtHg⁺ species.

References

- [1] J.E. Sánchez Uría, A. Sanz-Medel, *Talanta* 47 (1998) 509.
- [2] A.M. Carro, M.C. Mejuto, *J. Chromatogr. A* 882 (2000) 283.
- [3] M. Leermakers, W. Baeyens, P. Quevauviller, M. Horvat, *Trends Anal. Chem.* 24 (2005) 383.
- [4] C. Sarzanini, E. Mentasti, *J. Chromatogr. A* 789 (1997) 301.
- [5] Y. Cai, *Trends Anal. Chem.* 19 (2000) 62.
- [6] B. Welz, *Spectrochim. Acta B* 53 (1998) 169.
- [7] X.P. Yan, Z.M. Ni, *Spectrosc. Spectr. Anal.* 21 (2001) 129.
- [8] S.J. Hill, L.J. Pitts, A.S. Fisher, *Trends Anal. Chem.* 19 (2000) 120.
- [9] M. Montes-Bayón, K. DeNicol, J.A. Caruso, *J. Chromatogr. A* 1000 (2003) 457.
- [10] G.K. Zoorob, J.W. McKiernan, J.A. Caruso, *Mikrochim. Acta* 128 (1998) 145.
- [11] R. Falter, G. Ilgen, *Fresenius J. Anal. Chem.* 358 (1997) 401.
- [12] R.M. Blanco, M.T. Villanueva, J.E. Sánchez Uría, A. Sanz-Medel, *Anal. Chim. Acta* 419 (2000) 137.
- [13] S.C. Hight, J. Cheng, *Anal. Chim. Acta* 567 (2006) 160.
- [14] A. Castillo, A.F. Roig-Navarro, O.J. Pozo, *Anal. Chim. Acta* 577 (2006) 18.
- [15] C.S. Chiou, S.J. Jiang, K.S.K. Danadurai, *Spectrochim. Acta B* 56 (2001) 1133.
- [16] M. Wang, W.Y. Feng, J.W. Shi, F. Zhang, B. Wang, M.T. Zhu, B. Li, Y.L. Zhao, Z.F. Cai, *Talanta* 71 (2007) 2034.
- [17] B. Vallant, R. Kadnar, W. Goessler, *J. Anal. At. Spectrom.* 22 (2007) 322.
- [18] D.S. Bushee, *Analyst* 113 (1988) 1167.
- [19] M.J. Bloxham, A. Gachanja, S.J. Hill, P.J. Worsfold, *J. Anal. At. Spectrom.* 11 (1996) 145.
- [20] J. Morton, V.A. Carolan, P.H.E. Gardiner, *J. Anal. At. Spectrom.* 17 (2002) 377.
- [21] C.W. Huang, S.J. Jiang, *J. Anal. At. Spectrom.* 8 (1993) 681.
- [22] C.D. Stalikas, *Trends Anal. Chem.* 5 (2002) 343.
- [23] E.K. Paleologos, D.L. Giokas, M.I. Karayannis, *Trends Anal. Chem.* 24 (2005) 426.
- [24] J.C.A. de Wuilloud, R.G. Wuilloud, M.F. Silva, R.A. Olsina, L.D. Martinez, *Spectrochim. Acta B* 57 (2002) 365.
- [25] Y.J. Li, B. Hu, *Spectrochim. Acta B* 62 (2007) 1153.
- [26] X.B. Yin, *J. Chromatogr. A* 1154 (2007) 437.
- [27] L.P. Yu, *J. Agric. Food Chem.* 53 (2005) 9656.
- [28] W. Langseth, *Fresenius Z. Anal. Chem.* 325 (1986) 267.
- [29] C.F. Harrington, T. Catterick, *J. Anal. At. Spectrom.* 12 (1997) 1053.
- [30] J.G. Chen, H.W. Chen, S.H. Chen, L. Lin, Y.Y. Zhong, *Chem. Res. Chinese U.* 23 (2007) 143.
- [31] K.L. Cheng, K. Ueno, T. Imamura, *Handbook of Organic Analytical Reagents*, CRC Press, Boca Raton, FL, 1982.
- [32] W.Y. Feng, Z.F. Chai, Q.F. Qian, *J. Radioanal. Nucl. Chem.* 212 (1996) 61.



High throughput screening various abused drugs and metabolites in urine by liquid chromatography–heated electrospray ionization/tandem mass spectrometry

Chung-Yu Chen^a, Chien-Chun Shen^a, Tzung-Jie Yang^a, Yan-Zin Chang^b, Maw-Rong Lee^{a,*}

^a Department of Chemistry, National Chung Hsing University, 250 Kuo-Kung Rd., Taichung, Taiwan, ROC

^b Institute of Medical and Molecular Toxicology, Chung-Shan Medical University, Taichung, Taiwan, ROC

ARTICLE INFO

Article history:

Received 30 June 2008

Received in revised form

10 September 2008

Accepted 11 September 2008

Available online 18 September 2008

Keywords:

High-throughput screening

Abused drugs

Heated electrospray ionization

Tandem mass spectrometry

Urine

ABSTRACT

An integrated method of liquid chromatography–heated electrospray ionization/tandem mass spectrometry was evaluated for high throughput screening of various abused drugs in urine. Chromatographic analysis was performed on a C18 reverse phase column using a linear gradient of 10 mM ammonium acetate containing 0.1% formic acid–methanol as mobile phase and the total separation time was 7 min. A simple and rapid sample preparation method used was by passing urine samples through a 0.22 μm PVDF syringe filter. The detection limits of the studied abused drugs in urine were from 0.6 ng mL^{-1} (ketamine) to 9.0 ng mL^{-1} (norcodeine). According to the results, the linear range was from 1 to 1200 ng mL^{-1} with relative standard deviation (R.S.D.s) value below 14.8% (intra-day) and 24.6% (inter-day). The feasibility of applying the proposed method to determine various abused drugs in real samples was examined by analyzing urine samples from drug-abused suspects. The abused drugs including ketamines and amphetamines were detected in suspected urine samples. The results demonstrate the suitability of LC–HESI-MS/MS for high throughput screening of the various abused drugs in urine.

© 2008 Elsevier B.V. All rights reserved.

1. Introduction

Using of abused drugs is increasing worldwide, and millions of individuals are reported to be current users of cocaine, amphetamine-like stimulants, ketamine, and other new abused drugs, with significant consequences for human health and social behavior [1]. Drug abuse that alters human behavior and leads to crimes has become a serious problem throughout the world. The determination of various classes of abused drugs is important in many fields of analytical toxicology, such as forensic analysis, workplace drug testing, and antidoping analysis [2,3]. A forensic toxicology analytical method must provide a rapid, simple, high reliability and accuracy for screening drugs and metabolites of toxicological interest in suspected biological samples.

An effective analytical protocol for the detection of abused drugs in urine should consist of (1) a sensitive initial screening procedure to identify specimens with negative results and to select presumptive specimens with positive results for further testing; (2) a highly specific confirmatory technique that is at least as sensitive as the

initial screen for confirmation of presumptive positive results. In generally, enzyme immunoassay (EIA) generally designed for single substances or classes of substances are very common in forensic laboratories as a screening technique because its relatively fast analysis time for high throughput screening [4,5]. However, there are several disadvantages in use of EIA for abused drugs screening such as high cost for EIA reagent, a relative high false positive rate caused by cross-reactivity of the EIA reagent, and not flexible enough to accommodate the analysis of new abused drugs because of EIA reagents for these drugs are unavailability [6,7]. Separation techniques such as high performance liquid chromatography (HPLC) coupled to diode-array detector (DAD) or electrochemical array detector [8–10], capillary electrophoresis coupled with electrospray ionization-mass spectrometry (CE-ESI-MS) [11], and gas chromatography (GC) coupled to mass spectrometry (MS) have been used for determination various abused drugs in different biological matrixes such as plasma, urine, oral fluid or hair [12–16]. Recently, the GC/MS technique is the most commonly used to separate and determine abused drugs and their metabolites due to its high specificity, sensitivity, and cost. But the derivatization process in GC/MS analysis is required to increase the volatility of many polar analytes. This derivatization step is costly, time consuming, and susceptible to errors that affect the quality of the analytical results [17].

* Corresponding author. Tel.: +886 4 2285 1716; fax: +886 4 2286 2547.
E-mail address: mrlee@dragon.nchu.edu.tw (M.-R. Lee).

Nowadays, liquid chromatography coupled with mass spectrometry (LC–MS) has become popular and been successfully applied to detect a wide variety of drugs in biological matrices due to its high selectivity and excellent sensitivity. LC–MS, unlike GC–MS, is not limited by several factors such as nonvolatility and high molecular weight. Most importantly, LC–MS enables the determination of both lipophilic parent drugs and hydrophilic metabolites without doing for any derivatization or hydrolysis process. Recently, introduction of tandem mass spectrometry coupled to liquid chromatography (LC–MS/MS) has largely improved the performance of the technique by enhancing sensitivity and analyte identification, therefore, LC–MS/MS has led to increase usage in high-throughput analysis. The LC–MS and LC–MS/MS are currently the techniques of choice for the screening of abused drugs in different matrixes [7,18–24].

In this study, a simple and sensitive high throughput analytical method for determination of various abused drugs including amphetamine and its analogues; ketamine and its metabolite; cocaine and morphine and some new abused drugs in human urine was developed by using LC–MS/MS. A novel heated electrospray ionization (HESI) source coupled to selected reaction monitoring (SRM) scan mode was used in this study. The detection limits, precision and linear range of this procedure for various abused drugs are discussed. The feasibility of applying the method to analyze the amount of abused drugs in real urine samples from suspects was also examined.

2. Experimental

2.1. Chemicals and reagents

The reference standards of alprazolam, cocaine, codeine, dihydrocodeine, ketamine (K), lorazepam, lysergic acid diethylamine (LSD), 3,4-methylenedioxyamphetamine (MDA), 3,4-methylenedioxyamphetamine (MDMA), 3,4-methylenedioxyamphetamine (MDEA), *p*-methoxyamphetamine (PMA), methadone, midazolam, morphine, norketamine (NK), norcodeine, available as solution in methanol or acetonitrile at concentration of 1 mg mL⁻¹, were purchased from Cerilliant (Round Rock, TX, USA). Amphetamine (AM) and methamphetamine (MA) were purchased from Sigma Chemical Co. (St. Louis, MO, USA). Dehydronorketamine (DK) was obtained from Pfizer (Ann Arbor, MI,

USA). Ketamine-d₄ (100 µg mL⁻¹ in methanol) as internal standard was purchased from Cerilliant. HPLC-grade methanol and formic acid were purchased from Merck (Darmstadt, Germany). Ammonium acetate (ACS grade) was purchased from Riedel-de Haën (Seelze, Germany). The laboratory purified water (>18 MΩ) was obtained from a Milli-Q system located in the laboratory (Millipore simplicity®, Millipore, France).

2.2. Preparation of standard stocks, working solution and urine samples

Individual standard stock solutions concentration 200 µg mL⁻¹ were prepared by direct diluted liquid standards by using methanol and prepared by accurately weighted amount of powder standards then dissolved in methanol, respectively. Then the prepared stock solutions were stored in colored vials at –30 °C in a refrigerator. Working solutions of different concentration for all analytes were diluted from the stock solutions with purified water and with drug-free urine for finding out the optimum ionization conditions of concentration of 1 µg mL⁻¹ and for calibration standard of concentration ranged from 1 to 1200 ng mL⁻¹. The quality control (QC) samples were at the concentration of 20, 200 and 400 ng mL⁻¹. The spiked urine sample was filtered by a 0.2 µm PVDF filter (Millipore, USA) before analysis.

2.3. Chromatographic conditions

LC analyses were carried out on an Agilent 1100 series HPLC system consisting of binary gradient pump (Agilent Technologies, Palo Alto, CA, USA). Chromatographic separation was performed on a Waters Xterra RP18 (2.1 mm × 50 mm, 3.5 µm particle size) LC column (Waters Corp., Milford, MA, USA), which was preceded in-line by a precolumn filter of 3 mm frit (Supelco, Bellefonte, PA, USA). The mobile phase was filtered using a Nylon 66 membrane filter (0.2 µm) and degassed by using vacuum followed by sonication. The mobile phase was composed of 10 mM ammonium acetate containing 0.1% formic acid (pH 3.44) as solvent A and methanol as solvent B. A short linear gradient was used, starting at 5% solvent B held for 1 min, changing to 100% solvent B for 1 min and held for 3.5 min then back to 5% solvent B for 0.5 min held until the end of gradient. The flow rate was 0.3 mL min⁻¹ and the total chromatographic separation time was 7 min.

Table 1
Tandem mass spectrometry parameters for SRM determination of abused drugs and metabolites.

Compound	Retention time (min)	Parent ion (<i>m/z</i>)	Quantitation ion (<i>m/z</i>) and collision energy (%)	Confirming ion (<i>m/z</i>) and collision energy (%)
Alprazolam	3.74	309	205 (39)	165 (37)
AM	2.11	136	91 (20)	119 (10)
Cocaine	3.32	304	182 (19)	105 (34)
Codeine	2.06	300	165 (36)	215 (25)
Dihydrocodeine	1.84	302	199 (34)	201 (27)
DK	3.09	222	205 (11)	142 (23)
K	3.23	238	125 (30)	207 (13)
Lorazepam	3.78	321	275 (20)	303 (15)
LSD	3.41	324	223 (22)	208 (31)
MA	2.35	150	91 (20)	119 (10)
MDA	3.02	180	135 (19)	163 (10)
MDEA	3.20	208	163 (14)	135 (21)
MDMA	3.10	194	163 (12)	135 (20)
Methadone	3.62	310	265 (16)	105 (32)
Midazolam	3.61	326	209 (32)	244 (28)
Morphine	1.05	286	165 (34)	201 (20)
NK	3.23	224	125 (25)	207 (12)
Norcodeine	2.31	286	165 (52)	181 (33)
PMA	3.14	166	121 (18)	149 (11)
Ketamine-d ₄	3.22	242	129 (30)	211 (13)

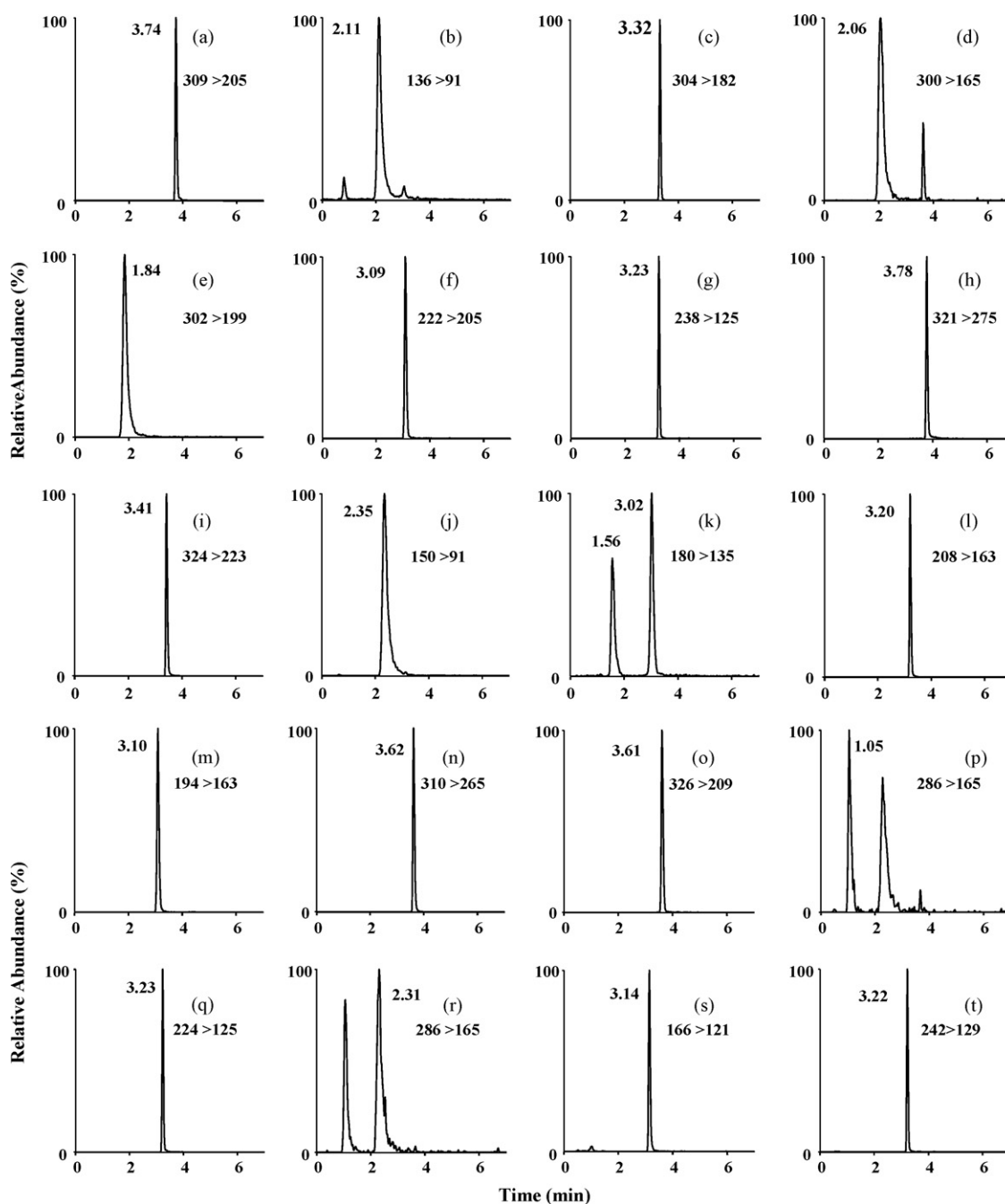


Fig. 1. Mass ion chromatogram of the spiked 200 ng mL⁻¹ abused drugs in blank urine produced by LC–HESI–MS/MS. (a) Alprazolam; (b) AM; (c) cocaine; (d) codeine; (e) dihydrocodeine; (f) DK; (g) K; (h) lorazepam; (i) LSD; (j) MA; (k) MDA; (l) MDEA; (m) MDMA; (n) methadone; (o) midazolam; (p) morphine; (q) NK; (r) norcodeine; (s) PMA; (t) ketamine-d₄.

2.4. Mass spectrometry conditions

Mass spectrometry was performed on a Thermo Finnigan TSQ Quantum Ultra EMR triple quadrupole mass spectrometer (ThermoFisher, San Jose, CA, USA) calibrated in the positive ion mode using a 1,3,6-polytyrosine. The heated-electrospray ionization (HESI) was used as ionization source with positive mode in this study. Nitrogen was used as the sheath gas, auxiliary gas, and ion sweep gas. The optimal ionization and ion transmission conditions were tuned by an automated tuning procedure to maximize the signal for the intensity of ion monitored and the optimal values

were shown as follows: spray voltage was 3500 V; vaporizer temperature was 250 °C; sheath gas, ion sweep gas and auxiliary gas pressure were 45, 12, and 4 arbitrary units, respectively; capillary temperature was 270 °C; tube lens offset and skimmer offset were 65 and 0 V, respectively. Detection of the analytes was performed in the selected reaction monitoring (SRM) mode with a signal time segment. Argon was used as collision gas at a pressure of 1.5 mTorr. The scan width for SRM was 0.7 *m/z*, scan time was 0.01 s, and the peak width settings (FWHM) for both Q1 and Q3 were 0.7 *m/z*. Data processing was proceeded using Thermo Xcalibur Version 2.0 software.

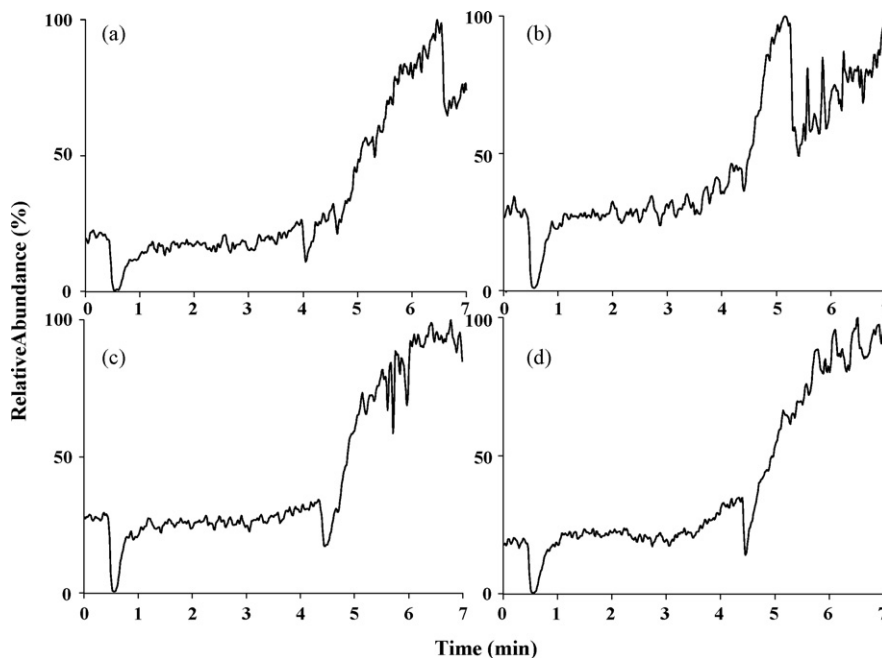


Fig. 2. Ion suppression was studied by monitoring the signal for transition (a) 286 > 165 (morphine); (b) 136 > 91 (AM); (c) 238 > 125 (K); (d) 326 > 209 (midazolam) during post-column infusion of 200 ng mL⁻¹ of morphine, AM, K, and midazolam, respectively.

2.5. Method validation

The method was validated for linearity, limit of detection (LOD), limit of quantification (LOQ), and precision. Urine calibration standards were prepared daily by diluting the stock solution with drug-free urine to provide final concentrations of all analytes ranging from 1 to 1200 ng mL⁻¹. Three replicate analyses were performed for each concentration to evaluate linearity and the peak areas were used for quantification through the calibration curves of all analytes. LOD and LOQ were defined as concentrations in a urine sample resulting in peak area with signal-to-noise ratios of 3 and 10, respectively. Precision of the assay was determined by generating intra-day and inter-day variability data from spiked QC samples of three different concentrations. The intra-day precision was evaluated by performing five replicates of the QC samples including sample preparation procedures; the inter-day precision was evalu-

ated by performing five replicates of the QC samples on each of five different days within a 5-day period.

3. Results and discussion

3.1. Evaluated ion transition in SRM mode

To evaluate the ion transition of all abused drugs in the SRM mode, the individual drug standard working solution of 1 μg mL⁻¹ was infused into HESI source by using a syringe pump at the flow rate of 5 μL min⁻¹ and ionized in positive ionization mode. All abused drugs in this study were successful ionized by using positive HESI ionization mode and the protonated molecule, [M+H]⁺, was the base peak for all abused drugs in the full scan spectrum. The protonated molecule for each analyte was chosen as parent ion and tuned for daughter ion scan automatically by instrumental function

Table 2
Analytical characteristics of LC–HESI–MS/MS method for various abused drugs in urine samples.

Compound	Linear range (ng mL ⁻¹)	Linear equation	Correlation coefficient (R^2)	Limit of Detection (ng mL ⁻¹)	Limit of Quantification (ng mL ⁻¹)
Alprazolam	5–400	$Y = 0.0094X - 0.0466$	0.9992	1.1	3.8
AM	5–400	$Y = 0.0032X - 0.0006$	0.9993	3.6	12.1
Cocaine	1–1200	$Y = 0.0287X - 0.0146$	0.9996	0.7	2.3
Codeine	10–400	$Y = 0.0008X - 0.0162$	0.997	4.6	15.2
Dihydrocodeine	10–400	$Y = 0.0028X - 0.0405$	0.9973	2.3	7.7
DK	5–1200	$Y = 0.0032X + 0.002$	0.9981	4.5	15.1
K	1–1200	$Y = 0.0054X + 0.013$	0.9996	0.6	2.1
Lorazepam	5–400	$Y = 0.0026X - 0.014$	0.9989	1.4	4.6
LSD	5–800	$Y = 0.0134X + 0.0022$	0.9992	1.4	4.6
MA	5–400	$Y = 0.0112X - 0.0687$	0.9987	1.9	6.4
MDA	5–400	$Y = 0.0013X - 0.0069$	0.9993	4.9	16.3
MDEA	5–400	$Y = 0.00114X + 0.0159$	0.9993	1.6	5.4
MDMA	5–400	$Y = 0.0102X - 0.037$	0.9988	1.4	4.5
Methadone	5–400	$Y = 0.0369X - 0.0416$	0.9995	0.8	2.7
Midazolam	5–800	$Y = 0.0022X - 0.0071$	0.9994	1.7	5.7
Morphine	5–400	$Y = 0.0002X - 0.0019$	0.9941	4.0	13.3
NK	5–800	$Y = 0.003X + 0.0021$	0.9998	0.9	2.8
Norcodeine	10–400	$Y = 0.0002X + 0.0017$	0.9981	9.0	30.0
PMA	5–400	$Y = 0.0045X - 0.0148$	0.9992	1.0	3.4

Table 3

Intra- and inter-day precision of the QC samples (20, 200 and 400 ng mL⁻¹) of various drugs in urine expressed by relative standard deviation (%).

	Intra-day (n = 5)			Inter-day (n = 5)		
	20	200	400	20	200	400
Alprazolam	10.5	6.5	4.8	14.4	10.3	8.0
AM	11.1	6.9	6.5	14.7	11.3	9.0
Cocaine	6.6	4.3	3.2	11.5	6.6	3.3
Codeine	11.8	6.3	5.3	16.7	6.4	5.5
Dihydrocodeine	9.2	5.2	4.4	19.7	9.3	6.7
DK	6.1	6.6	5.5	10.4	9.6	5.8
K	6.5	2.9	2.9	9.9	7.2	3.9
Lorazepam	12.2	5.3	4.0	18.4	12.0	7.1
LSD	6.9	6.3	5.8	19.0	9.1	7.2
MA	12.1	8.5	7.5	21.7	9.4	8.1
MDA	14.8	12.1	11.7	23.3	17.1	14.6
MDEA	5.0	3.0	2.7	10.9	7.0	3.7
MDMA	7.6	5.2	4.9	16.4	11.8	9.3
Methadone	10.8	7.3	5.5	14.3	10.6	8.6
Midazolam	9.3	5.0	3.6	14.1	13.2	11.9
Morphine	16.5	10.7	7.4	24.6	9.4	5.6
NK	6.4	4.7	4.1	8.8	7.3	6.6
Norcodeine	14.8	7.7	4.5	18.0	7.2	6.7
PMA	11.3	8.7	6.3	18.6	15.2	14.6

under 1.5 mTorr argon gas used as collision gas in collision chamber. According to the automatic daughter ion scan tuning results, the two major ion transitions for each analyte and the optimal collision energy for each ion transition were summarized in Table 1. The separation and detection result of analyzed urine spiked 19 kinds of abused drugs by using the optimum LC–HESI-MS/MS conditions were shown in Fig. 1. From the Fig. 1, the 19 kinds of abused drugs in urine sample were successfully detected by proposed method. Ion suppression from injection of filtered urine study was observed for the signal from the infused morphine, AM, K, and midazolam (Fig. 2). The results shown that the ion suppression by urine matrix is obtained in the early retention time, but it does not have any significant effect for the signal of the compounds studied.

3.2. Linearity, limits of detection and quantification, and precision

The linearity, limits of detection, and limits of quantification for analyzing the various abused drugs by LC–HESI-MS/MS were calculated under the optimum separation and detection conditions described previously. Triplicate injections were performed. A linear

regression was used to plot the peak area ratio of analyte to internal standard against analyte concentration. The linearity of proposed method was studied within 1–1200 ng mL⁻¹. The square correlation coefficients (r^2 value) were ranged from 0.9941 for morphine to 0.9998 for norketamine. The linear range experiments provided the necessary information to estimate limits of detection and limits of quantification, based on the peak of the lowest concentration in the linear range with a single-to-noise ratio (S/N). LODs and LOQs were evaluated by S/N of three and ten, respectively. The LODs and LOQs obtained for determination of all abused drugs in urine can be down to the ng mL⁻¹ level. The LODs and LOQs for analyzing all abused drugs were ranged from 0.6 to 9.0 ng mL⁻¹ and from 2.1 to 30.0 ng mL⁻¹, respectively. Comparing to prior literature [18,22,25,26], the LODs and LOQs of ketamines, amphetamines, morphine, cocaine, and codeine of proposed method are lower than the results of published method. The summary of analytical characteristics of LC–HESI-MS/MS method for all abused drugs in urine sample was shown in Table 2. Intra-day precision of the proposed method was evaluated by analyzing five replicates of spiked QC urine sample at three concentration levels (40, 200 and 400 ng mL⁻¹) in the same day. Inter-day precision was evaluated by analyzing five replicates of three QC urine samples on each of five different days within a 5-days period. The intra-day and inter-day precisions of the method were calculated as the relative standard deviation (R.S.D.). The intra-day precision was ranged from 5.0 to 16.5% for low concentration (40 ng mL⁻¹) QC sample; 2.9–12.1% for middle concentration (200 ng mL⁻¹) QC sample; 2.7–11.7% for high concentration (400 ng mL⁻¹) QC sample. The inter-day precision was ranged from 8.8 to 24.6% for low concentration QC sample; 6.4–17.1% for middle concentration QC sample; 3.3–14.6% for high concentration QC sample. The results of intra-day and inter-day were summarized in Table 3. These results indicated that the method has acceptable precision for high throughput screening.

3.3. Application in real suspected urine analysis

This study also examined the effectiveness of the proposed method for practical application by analyzing the actual specimens obtained from drugs abused suspects. The real suspected urine samples obtained from Drug Testing Laboratory of Chung Shan Medical University Hospital were stored at –30 °C in a refrigerator before analyzed. The suspected urine samples were diluted

Table 4

Abused drugs concentrations (ng mL⁻¹) in real samples produced by LC–HESI-MS/MS.

	S ₁	S ₂	S ₃	S ₄	S ₅	S ₆	S ₇
Alprazolam	N.D.	N.D.	N.D.	N.D.	N.D.	N.D.	N.D.
AM	180.6	233.7	N.D.	99.8	28.5	38.7	N.D.
Cocaine	N.D.	N.D.	N.D.	N.D.	N.D.	N.D.	N.D.
Codeine	N.D.	N.D.	N.D.	N.D.	N.D.	N.D.	N.D.
Dihydrocodeine	N.D.	N.D.	N.D.	N.D.	N.D.	N.D.	N.D.
DK	2685.0	5424.0	7115.3	N.D.	N.D.	8.7	1745.2
K	145.5	199.2	250.0	N.D.	N.D.	11.8	712.1
Lorazepam	N.D.	N.D.	N.D.	N.D.	N.D.	N.D.	N.D.
LSD	N.D.	N.D.	N.D.	N.D.	N.D.	N.D.	N.D.
MA	763.6	462.1	N.D.	346.3	222.9	359.7	N.D.
MDA	104.0	215.4	N.D.	69.1	N.D.	N.D.	N.D.
MDEA	N.D.	N.D.	N.D.	N.D.	N.D.	N.D.	N.D.
MDMA	503.8	454.9	N.D.	N.D.	N.D.	N.D.	N.D.
Methadone	N.D.	N.D.	N.D.	N.D.	N.D.	N.D.	N.D.
Midazolam	N.D.	N.D.	N.D.	N.D.	N.D.	N.D.	N.D.
Morphine	N.D.	N.D.	N.D.	N.D.	N.D.	N.D.	N.D.
NK	757.4	1027.6	694.5	N.D.	N.D.	9.8	854.1
Norcodeine	N.D.	N.D.	N.D.	N.D.	N.D.	N.D.	N.D.
PMA	N.D.	N.D.	N.D.	N.D.	N.D.	N.D.	N.D.

N.D.: not detected.

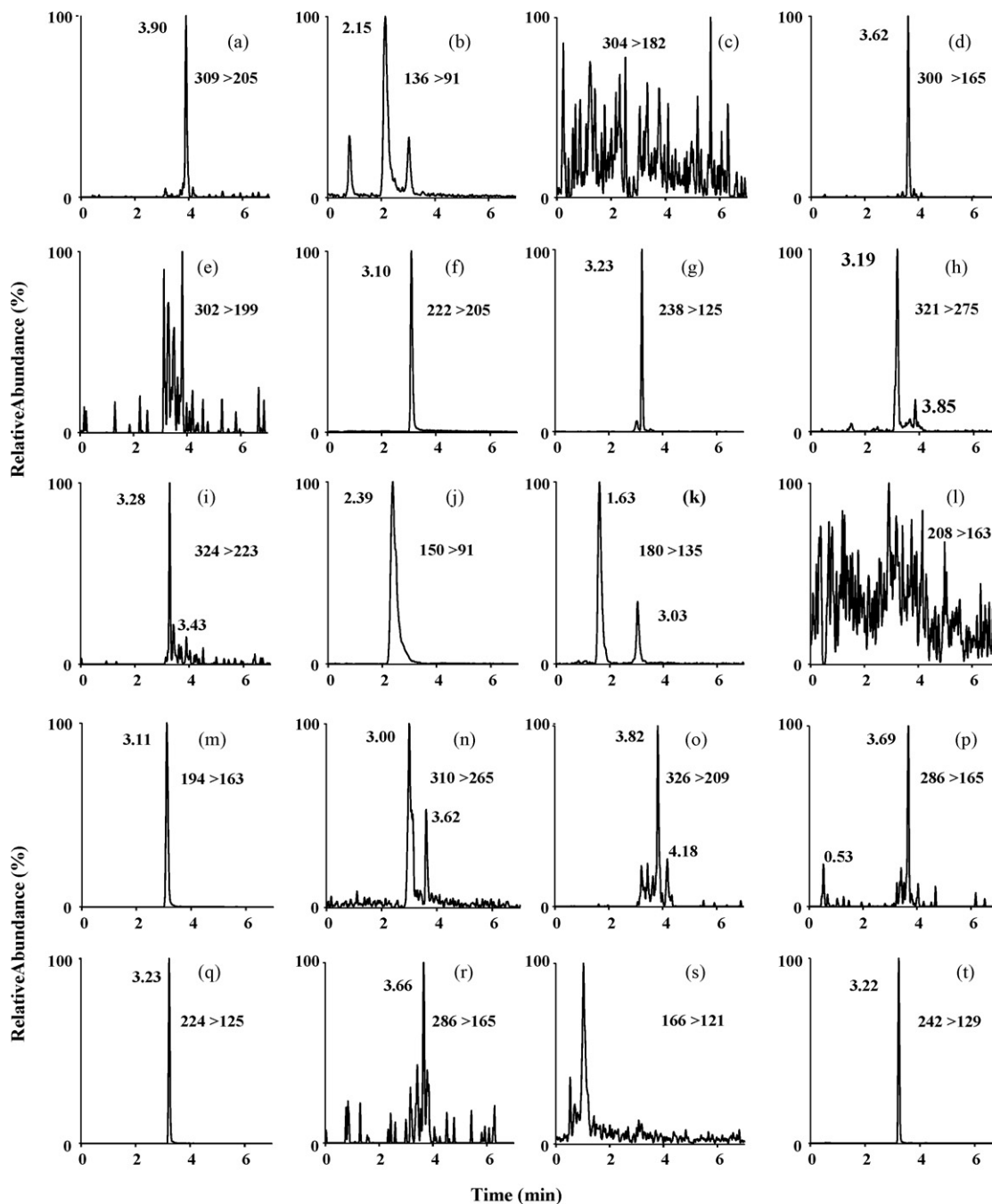


Fig. 3. Mass ion chromatogram of the S_1 sample produced by LC-HESI-MS/MS. (a) Alprazolam; (b) AM; (c) cocaine; (d) codeine; (e) dihydrocodeine; (f) DK; (g) K; (h) lorazepam; (i) LSD; (j) MA; (k) MDA; (l) MDEA; (m) MDMA; (n) methadone; (o) midazolam; (p) morphine; (q) NK; (r) norcodeine; (s) PMA; (t) ketamine- d_4 .

with drug-free urine by suitable multiple then analyzed by the LC-HESI-MS/MS method described above. Triple replicate analysis was performed for each sample. The mass ion chromatograms of suspect S_1 urine sample were shown in Fig. 3. Fig. 3 indicated that amphetamine, methamphetamine, MDA, MDMA, ketamine, norketamine, and dehydronorketamine were found in the urine of suspect S_1 . The analytical results were summarized in Table 4. From the results, amphetamine, methamphetamine, MDA, MDMA, ketamine, norketamine, and dehydronorketamine were found in suspected urines and concentrations of these drugs were calculated range from 28.5 to 233.7, 222.9 to 763.6, 69.1 to 215.4, 454.9 to 503.8, 11.8 to 712.1, 9.8 to 1027.6 and 8.7 to 7115.3 ng mL^{-1} , respectively. The results obtained from real case studies clearly indicate the pro-

posed method is simple, rapid, and sensitive enough to be used for high throughput screening various abused drugs in suspected urines.

4. Conclusions

This study evaluated the LC-HESI-MS/MS to apply on high throughput screening for the various abused drugs in urine sample. The total analytical time was 7 min by using a 5 cm Xterra RP18 LC column and SRM scan mode. The limits of detection and limits of quantification for proposed method were below 9.0 and 30.0 ng mL^{-1} , respectively. Furthermore, this method has been applied to screen of various abused drugs in suspected urine

samples. The amphetamines and ketamines compounds were found in these suspected urine samples concentration ranged from 28.5 to 763.6 ng mL⁻¹ and 8.7 to 7115.3 ng mL⁻¹, respectively. In the view of the simplicity, rapidity, sensitivity, and selectivity, the proposed method is recommendable for the high throughput screening various abused drugs in urine in the forensic science.

Acknowledgements

The authors would like to thank the financial supports from National Science Council of Taiwan under contract no. NSC. 95-2113-M-005-019-MY3 and from National Bureau of Controlled Drugs, Department of Health, ROC under contract no. DOH96-NNB-1005.

References

- [1] E.J. Cone, *Forensic Sci. Int.* 121 (2001) 7.
- [2] P. Hemmersbach, R. de la Torre, *J. Chromatogr. B* 687 (1996) 221.
- [3] E.J. Cone, P. Welch, B.D. Paul, J.M. Mitchell, *J. Anal. Toxicol.* 15 (1991) 161.
- [4] L. Kroener, F. Musshoff, B. Madea, *J. Anal. Toxicol.* 27 (2003) 205.
- [5] G. Cooper, L. Wilson, C. Reid, D. Baldwin, C. Hand, V. Spiehler, *J. Forensic Sci.* 50 (2005) 928.
- [6] R. Valdes Jr., S.A. Jortani, *Clin. Chem.* 48 (2002) 405.
- [7] W.C. Cheng, T.S. Yau, M.K. Wong, L.P. Chan, V.K.K. Mok, *Forensic Sci. Int.* 162 (2006) 95.
- [8] D.R. Stoll, C. Paek, P.W. Carr, *J. Chromatogr. A* 1137 (2006) 153.
- [9] A.S. Yazdi, Z. Es'haghi, *J. Chromatogr. A* 1094 (2005) 1.
- [10] P. Huettli, S. Koester, L. Hoffer, G.A. Gerhardt, *Electroanalysis* 11 (1991) 313.
- [11] M. Himmelsbach, C.W. Klampfl, W. Buchberger, *J. Sep. Sci.* 28 (2005) 1735.
- [12] M.R. Lee, Y.S. Song, B.H. Huang, C.C. Chou, *J. Chromatogr. A* 896 (2000) 267.
- [13] D.W. Lachenmeier, L. Kroener, F. Musshoff, B. Madea, *Rapid Commun. Mass Spectrom.* 17 (2003) 472.
- [14] T. Gunnar, K. Ariniemi, P. Lillsunde, *J. Mass Spectrom.* 40 (2005) 739.
- [15] S. Strano-Rossi, F. Molaioni, F. Rossi, F. Botrè, *Rapid Commun. Mass Spectrom.* 19 (2005) 1529.
- [16] M. Miguez-Framil, A. Moreda-Pineiro, P. Bermejo-Barrera, P. Lopez, M.J. Taberero, A.M. Bermejo, *Anal. Chem.* 79 (2007) 8564.
- [17] A. Leinonen, T. Kuuranne, R. Kostianen, *J. Mass Spectrom.* 37 (2002) 693.
- [18] B. Maralikova, W. Weinmann, *J. Chromatogr. B* 811 (2004) 21.
- [19] M. Wood, M. Laloup, M.D.R. Fernandez, K.M. Jenkins, M.S. Young, J.G. Ramaekers, G. De Boeck, N. Samyn, *Forensic Sci. Int.* 150 (2005) 227.
- [20] C.C. Chou, M.R. Lee, *Anal. Chim. Acta* 538 (2005) 49.
- [21] M. Concheiro, A. de Castro, O. Quintela, M. Lopez-Rivadulla, A. Cruz, *J. Chromatogr. B* 832 (2006) 81.
- [22] R. Kronstrand, I. Nyström, J. Strandberg, H. Druid, *Forensic Sci. Int.* 145 (2004) 183.
- [23] C.Y. Chen, M.R. Lee, F.C. Cheng, G.J. Wu, *Talanta* 72 (2007) 1217.
- [24] M. Huerta-Fontela, M.T. Galceran, F. Ventura, *Anal. Chem.* 79 (2007) 3821.
- [25] M. Andersson, E. Gustavsson, N. Stephanson, O. Beck, *J. Chromatogr. B* 861 (2008) 22.
- [26] T. Legrand, S. Roy, C. Monchaud, C. Grondin, M. Duval, E. Jacqz-Aigrain, *J. Pharm. Biomed. Anal.* 48 (2008) 171.



Screen anticancer drug in vitro using resonance light scattering technique

Zhanguang Chen^{a,*}, Guoliang Liu^{a,b}, Meizhen Chen^b, Benjie Xu^b, Yurui Peng^a,
Maohuai Chen^c, Mingyao Wu^c

^a Department of Chemistry, Shantou University, Shantou 515063, China

^b Department of Biology, Shantou University, Shantou 515063, China

^c Medical College, Shantou University, Shantou 515041, China

ARTICLE INFO

Article history:

Received 17 July 2008

Received in revised form 5 September 2008

Accepted 10 September 2008

Available online 18 September 2008

Keywords:

Resonance light scattering

Screen in vitro

Anticancer drug

3-(4,5-Dimethylthiazol-2-yl)-2,5-diphenyl
tetrazolium bromide

Hepatocellular carcinoma cell of mouse

ABSTRACT

An in vitro screening model using resonance light scattering (RLS) technique with 3-(4,5-dimethylthiazol-2-yl)-2,5-diphenyl tetrazolium bromide (MTT) reagent as the reactive probe to target cancer cell was firstly developed. In this model, MTT was reduced by viable cancer cells to produce a purple formazan. Cell viability was proportional to the number of formazan induced strong light scattering signal. The inhibition rate of anticancer drug was found to vary inversely with the H₂₂-MTT system RLS intensity. So it was intuitive to see the sequence of the tumor suppressive activity of six anticancer drugs without data processing by RLS/MTT screening spectra. Compared with the traditional MTT method, this method has high sensitivity, low detection limit and quite intuitive screening results which were identical to those obtained from the MTT colorimetric assay.

© 2008 Elsevier B.V. All rights reserved.

1. Introduction

In vitro anticancer drug screening has always been one of the most popular domains of cancer research, which is the key to the development of anticancer agents [1,2]. So an effective anticancer drug-screening method is the starting point and decisive step of the innovative drug research. Hepatocellular carcinoma is one of the most common malignancies worldwide [3,4]. Screening novel anticancer drug for hepatocellular carcinoma is vital. Herein, a new method of screening anticancer drug in vitro that can screen anticancer drugs and simultaneously determine their relative anti-tumor efficiencies against hepatocellular carcinoma cell of mouse (H₂₂ cell) by resonance light scattering (RLS) technique was developed.

The conventional methods for screening antineoplastic agents in vitro mainly included MTT colorimetric assay [5], ATP bioluminescence assay [6], ³H-TdR incorporation method [7], sulforhodamine B (SRB) assay [8], Acid Phosphatase Enzyme (APA) method [9], and Clonogenic Assay [10]. However, most of these methods have their unavoidable drawbacks: for instance, there are expensive reagents in ATP bioluminescence assay, radioactive elements and expensive apparatus in ³H-TdR incorporation method, and cumbersome oper-

ation in SRB assay and Clonogenic Assay. Moreover, relatively high cost is a common disadvantage of these traditional screening methods. Resonance light scattering, an elastic scattering, occurs when the incident beam is close in energy to an absorption band. Since Pasternack et al. established the RLS technique to study the aggregations of porphyrins with an ordinary fluorescence spectrometer [11,12], RLS studies have attracted great interest among researchers because its experimental apparatus is simple, rapid, and sensitive. In recent years, RLS has been used to determine nucleic acid [13–17], protein [18–21], amino acid [22], inorganic ions [23], and medicines [24–26]. In this paper, it was the first time that RLS technique was used to implement anticancer drugs screening in vitro to target cancer cells.

3-(4,5-Dimethylthiazol-2-yl)-2,5-diphenyl tetrazolium bromide (MTT) was reduced by mitochondrial dehydrogenase in viable cancer cells to produce the purple formazan. Cell viability was proportional to the number of formazan, certain diameter particle, which induced remarkable RLS signal with the RLS theory [27–29]. Light scattering is caused by the presence of proper diameter particles. Because the dimension of formazan particle is much less than the incident wavelength, it should be in accordance with the Rayleigh light scattering formula [27,28]. Therefore, RLS intensity is proportional to the number of particles or the concentration of cancer cell. It is the theoretical basis for the method of screening anticancer drug in vitro using RLS technique.

* Corresponding author. Tel.: +86 754 8290 2767; fax: +86 754 8290 2767.
E-mail address: kqlu@stu.edu.cn (Z. Chen).

In this paper, the screening assays of six anticancer drugs were implemented by the RLS/MTT screening method. The result demonstrated that there were the intuitively remarkable differences among RLS intensities of the H₂₂-MTT systems with the maximum peak located at 393.0 nm in the RLS/MTT screening spectra after treated with anticancer agents at the proper peak plasma concentration (ppc) for 48 h. The difference of RLS intensities represented the differentiation of the inhibition rates of six anticancer agents against H₂₂ cells. Meanwhile, the intuitive results of anticancer drugs were obtained by RLS/MTT method and were consistent with the traditional MTT colorimetric spectrophotometry.

2. Experimental

2.1. Tumor cell line and culture

Hepatocellular carcinoma cell of mouse (H₂₂ cell) was used in RLS/MTT screening assay and the traditional screening assay. H₂₂ cell was one kind of nonadherent cell lines which was usually used to be as a model in drug-screening programs in vitro and was obtained from the medical college of Shantou University (Shantou, Guangdong Province, China). Prior to use in the screening assay, the cancer cells were grown in culture medium RPMI 1640 (Hyclone, Northumberland, UK), supplemented with 10% heat-inactivated fetal bovine serum (FBS) (Sigma Chemical Co., St. Louis, MO), 10% glutamine, 10% penicillin-streptomycin (all from GIBCO, Life Technologies, Roskilde, Denmark) and incubated in a 5% CO₂ humidity incubator at 37 °C. And it was periodically examined using an inverted microscope (Nikon, Japanese).

2.2. Reagents and drugs treatment

MTT was purchased from Sigma Company, USA. The MTT solution (5.0 mg mL⁻¹) was prepared by dissolving certain MTT in phosphate buffered saline (pH 7.2) and stocked in 1.0 mL aliquots at 4 °C in the dark. Cisplatin (DDP), mitomycin (MMC), 5-fluorouracil (5-FU), etoposide (VP-16), cytarabine (AraC), vincristine (VCR) was obtained from Bristol Myers Co. Ltd., New York, America. All drugs were dissolved with physiological saline and stored at -20 °C. The drugs were diluted with RPMI 1640 plus 10% fetal bovine serum just prior to each experiment.

In this paper, H₂₂ cell was treated with DDP, MMC, 5-FU, VP-16, AraC and VCR. Peak plasma concentration (ppc) was the highest level of drug that was obtained in the blood. 1.0 ppc of DDP, MMC, 5-FU, VP-16, AraC, and VCR was 10.0, 3.0, 10.0, 10.0, 10.0, and 4.0 μg mL⁻¹, respectively [30,31]. Concentrations of 0.1, 1.0, and 10 ppc were chosen for the drug treatment experiments.

All chemicals used were of analytical grade or the best grade commercially available, and double-distilled water was used throughout.

2.3. RLS/MTT screening assay

Logarithmically grown H₂₂ cells were standardized to the cell suspension at the density of 6.0 × 10⁶ cells mL⁻¹. Then they were diluted to 1.5 × 10⁵, 3.0 × 10⁵, 4.5 × 10⁵, 6 × 10⁵, 7.5 × 10⁵, 9 × 10⁵, 1.05 × 10⁶, 1.2 × 10⁶ cells per well with fresh culture medium. Each well of a U-shaped 24-well microtiter plate (Falcon, Becton Dickinson, Mountain View, CA, USA) received 1.0 mL of H₂₂ cell suspension. Meanwhile, the chemotherapeutic drugs DDP, MMC, 5-FU, VP-16, AraC, and VCR at the concentrations of 0.1, 1.0, 10 times of peak plasma concentration were added to the experimental wells which received 1.0 mL logarithmically grown H₂₂ cells suspension at the density of 6.0 × 10⁵ cells mL⁻¹. The plates after treated with anticancer drugs were incubated in a 5% CO₂ humidity incubator at

37 °C for 24, 48, and 72 h, respectively. Triplicate wells were used for each experimental condition. Twenty microliters of the MTT solution (5.0 mg mL⁻¹) were then added to each experimental well, and the plates were incubated for 8 h at 37 °C. The samples were diluted to 5.0 mL with PBS (pH 7.2). The RLS spectra were measured with a Model LS-55 spectrofluorometer (Perkin-Elmer, USA) with a quartz cuvette (1 cm × 1 cm). The RLS spectra were obtained by scanning simultaneously the excitation and emission monochromators ($\Delta\lambda = 0.0$ nm) with the excitation and emission slits 5.0 nm. The RLS intensity was measured at 393.0 nm. In the experiment the RLS intensity increment (ΔI_{RLS}) of the H₂₂-MTT system was written down. The enhanced RLS intensity of H₂₂-MTT system was represented as $\Delta I_{\text{RLS}} = I_{\text{RLS}} - I_{\text{RLS}}^0$ (I_{RLS} and I_{RLS}^0 were the RLS intensities of the H₂₂-MTT system with and without H₂₂ cell).

3. Results and discussion

3.1. Spectral characteristics

The RLS spectra of the H₂₂-MTT systems are shown in Fig. 1. It can be seen that both MTT and H₂₂ cell have very weak RLS signals when they exist separately in the whole scan range of 250–700 nm. However, the weak RLS signal of MTT can be remarkably enhanced when small amount of H₂₂ cell was added with the maximum peak located at 393.0 nm under the same circumstances. The addition of increasing H₂₂ cells to the MTT solution led to the gradual enhancement in RLS intensity, which disclosed a concentration-dependent relationship.

The RLS/MTT screening spectra of the H₂₂-MTT system after treated with anticancer drugs DDP, MMC, 5-FU, VP-16, AraC, and VCR at the concentration of 1.0 ppc for 48 h are shown in Fig. 2. The first curve is the blank group which is the MTT solution without adding H₂₂ cells. The eighth curve is the control group which is mainly the mixture of H₂₂ cells and MTT without adding any anticancer drug. It is intuitive to see the sequence of RLS intensities at 393.0 nm as follows: Control > VCR > AraC > VP-16 > 5-FU > MMC > DDP > Blank in the RLS/MTT screening spectra (Fig. 2). The higher the inhibition rate of anticancer drug on H₂₂ cells, the lower the RLS intensity was. Therefore, it was easy to obtain the sequence of the tumor suppressive activity of six anticancer drugs as follows: VCR < AraC < VP-16 < 5-FU < MMC < DDP by RLS/MTT screening spectra. This result was consistent with the traditional screening assay and the pharmacodynamics evaluation report of the clinical application of anticancer agents [32,33].

In principle, the sharp RLS intensities of H₂₂ cells treated with anticancer drugs at the maximum scattering peak wavelength pro-

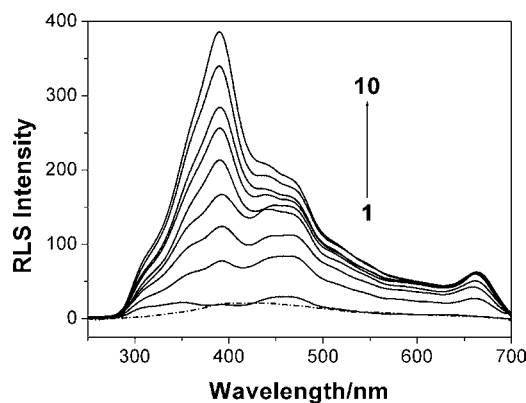


Fig. 1. The RLS spectra of H₂₂-MTT system. Conditions: $C_{\text{MTT}} = 20 \mu\text{g mL}^{-1}$, $C_{\text{H}_{22}\text{cell}}$ (cells mL⁻¹): (1) 2.4 × 10⁵ (without MTT); (2) 0; (3) 3 × 10⁴; (4) 6 × 10⁴; (5) 9 × 10⁴; (6) 1.2 × 10⁵; (7) 1.5 × 10⁵; (8) 1.8 × 10⁵; (9) 2.1 × 10⁵; (10) 2.4 × 10⁵; pH 7.2.

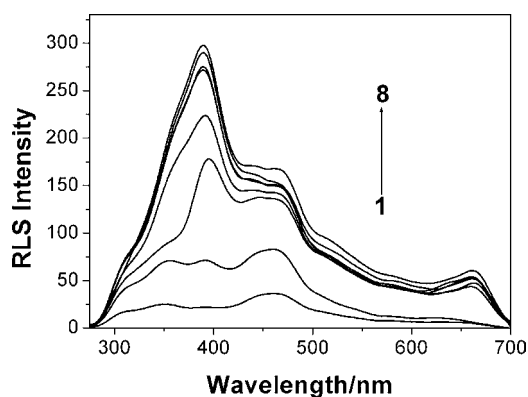


Fig. 2. The RLS/MTT screening spectra of anticancer drugs. Conditions: $C_{H_{22}cell} = 1.2 \times 10^5$ cells mL^{-1} , $C_{MTT} = 20 \mu g mL^{-1}$; (1) the blank group; (8) the control group; (2–7) DDP, MMC, 5-FU, AraC, VP-16, and VCR at 1.0 ppc for 48 h, respectively; pH 7.2.

vided excellent differentiation among six anticancer agents, giving information about the relative anticancer strengths of different anticancer drugs. The differentiation of antitumor effects of different anticancer agents was intuitively seen in RLS/MTT screening spectra without calculation (Fig. 2). So a method of screening anticancer drug in vitro using RLS technique was developed.

3.2. Effect of cell concentration

It is shown that there is a good linear relationship between RLS intensity of H_{22} -MTT system and H_{22} cell concentration when the H_{22} cell concentration ranges from 3.0×10^4 to 2.1×10^5 cells mL^{-1} (Fig. 3). The linear regression equation using the least square method is $\Delta I_{RLS} = 12.58 + 17.462C_{H_{22}cell}$ ($r = 0.997$). So 1.2×10^5 cells mL^{-1} of H_{22} cells was chosen for the RLS/MTT screening assays.

3.3. Effect of MTT concentration

Fig. 4 displays the effect of MTT concentration on RLS intensity. It can be clearly seen that MTT concentration had a great influence on RLS intensity. The RLS intensity increased with the increase of the concentration of MTT. Moreover, the RLS intensity of the H_{22} -MTT system reached the maximum and kept constant when the concentration of MTT is in the range 18–30 $\mu g mL^{-1}$. Therefore, 20 $\mu g mL^{-1}$ of MTT solution was selected for the further screening assays in this paper.

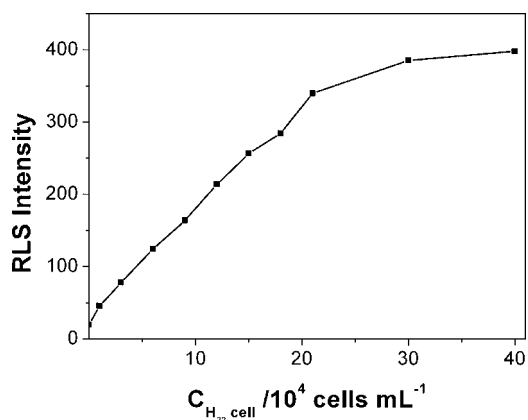


Fig. 3. The effect of H_{22} cell concentration on the RLS intensity. Conditions: $C_{MTT} = 20 \mu g mL^{-1}$; pH 7.2.

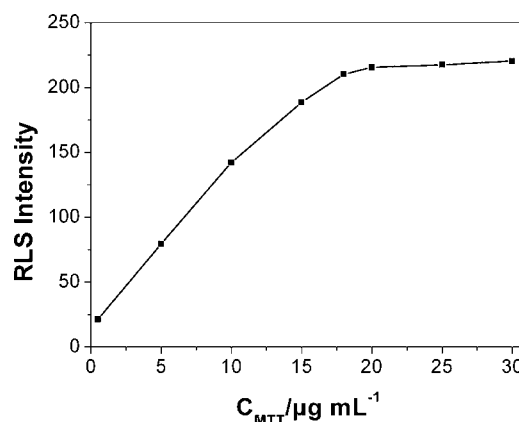


Fig. 4. The effect of MTT concentration on the RLS intensity. Conditions: $C_{H_{22}cell} = 1.2 \times 10^5$ cells mL^{-1} ; pH 7.2.

3.4. Effect of anticancer drugs concentrations

The effect of anticancer drugs concentrations on the RLS signal was studied and shown in Fig. 5. The first curve is the blank group; the fifth curve is the control group. It is clearly seen that the difference of RLS signal of H_{22} -MTT system treated with DDP at concentrations of 0.1, 1.0, and 10 ppc for 24 h is quite remarkable, which discloses the difference of the inhibition rates of the anticancer drug at different concentrations against the same cancer cell (Fig. 5). The inhibitory effect of anticancer drug against H_{22} cells increases with the increase of the concentration of anticancer drug, which leads to the ability of H_{22} cells to produce the formazan declined. It reflects the decrease of RLS intensity in the RLS spectra.

The inhibitory effects of various anticancer drugs were expressed in the form of the inhibition rate of viability according to the following formula [34]:

$$\text{inhibition rate (\%)} = \left[1 - \frac{I_{\text{treated}} - I_{\text{blank}}}{I_{\text{control}} - I_{\text{blank}}} \right] \times 100$$

where I_{treated} is the average RLS intensity of H_{22} -MTT in wells treatment with drugs; I_{blank} is the average RLS intensity of MTT reagent in wells with RPMI 1640 medium without adding H_{22} cells; and I_{control} is the average RLS intensity of H_{22} -MTT in wells with H_{22} cells without adding any anticancer agents.

Fig. 6 displayed the effect of drug concentration on the inhibition rates of H_{22} -MTT system treated with DDP, MMC, 5-FU, VP-16, AraC, and VCR for 48 h. It can be easily seen that the difference of

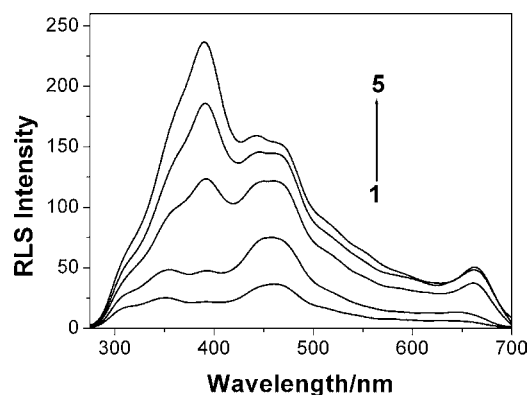


Fig. 5. The RLS spectra of H_{22} -MTT system treated with DDP at different concentrations. Conditions: $C_{H_{22}cell} = 1.2 \times 10^5$ cells mL^{-1} , $C_{MTT} = 20 \mu g mL^{-1}$; (1) the blank group; (5) the control group; (2–4) inhibition rates after treatment with DDP at 10, 1.0, 0.1 ppc for 24 h, respectively; pH 7.2.

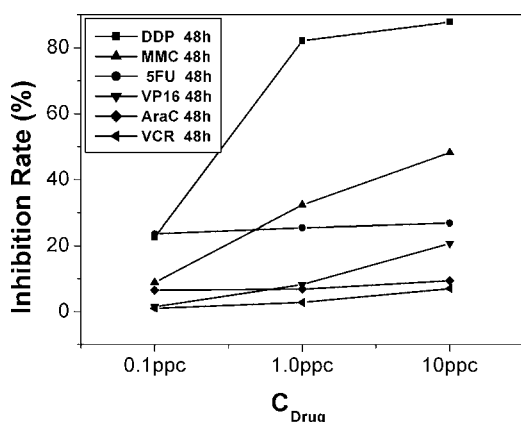


Fig. 6. The effect of drug concentration on the inhibition rate. Conditions: $C_{H_{22}cell} = 1.2 \times 10^5$ cells mL^{-1} , $C_{MTT} = 20 \mu g mL^{-1}$; pH 7.2. Comparison of cytotoxicity in H_{22} cell treated with DDP, MMC, 5-FU, VP-16, AraC, and VCR by RLS/MTT screening method. The effect of DDP on the inhibition rate of cell viability was more significant than others for 48 h.

inhibition rates of anticancer drugs became significant when the concentrations of anticancer drugs reached 1.0 ppc for 48 h. So 1.0 time that of peak plasma concentration (ppc) was chosen for the anticancer drugs screening assays.

3.5. Effect of reactive time

As shown in Fig. 7, the reactive time between H_{22} cell and anticancer drug influenced significantly on the RLS intensity of H_{22} -MTT system treated with DDP at 1.0 and 10 ppc for 24, 48, and 72 h. With treatment from 24 to 72 h, there was no change in inhibition rate of DDP at 0.1 ppc (data not shown). The inhibition rate of anticancer drug enhanced with the increase of the reactive

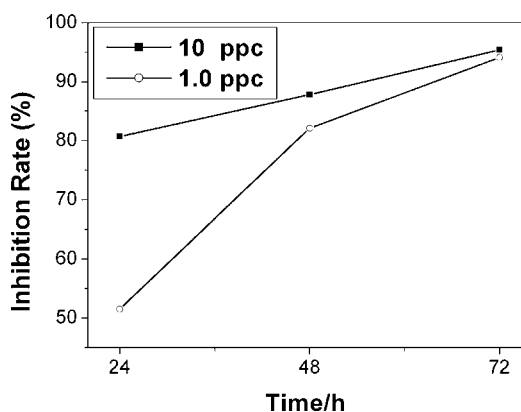


Fig. 7. The effect of reactive time on the RLS intensity of H_{22} -MTT system treated with DDP. Conditions: $C_{H_{22}cell} = 1.2 \times 10^5$ cells mL^{-1} , $C_{MTT} = 20 \mu g mL^{-1}$; pH 7.2.

Table 1
Comparison of IC_{50} value and relative antitumor activity (peak plasma concentration/ IC_{50}) among four anticancer drugs against H_{22} cell by RLS/MTT method and MTT method.

Anticancer drugs	Exposure time (h)	IC_{50} value ($\mu g mL^{-1}$)		Relative antitumor activity	
		RLS/MTT method	MTT method	RLS/MTT method	MTT method
DDP	48	3.98 ± 0.05	4.12 ± 0.06	2.51	2.42
	72	1.49 ± 0.08	1.83 ± 0.08	6.71	5.46
MMC	48	32.0 ± 0.02	33.5 ± 0.07	0.09	0.089
	72	25.1 ± 0.18	26.9 ± 0.21	0.12	0.11
5-FU	72	110.2 ± 0.22	121.3 ± 0.31	0.09	0.08
VP-16	72	252.0 ± 0.35	275.1 ± 0.45	0.04	0.036

Table 2

Comparison analytical parameters of two screening methods under the optimum conditions.

Screening in vitro methods	Linear regression equation	Detection limit (cells mL^{-1})	Correlation coefficient (r)
RLS/MTT method	$Y = 12.580 + 17.462C_{H_{22}cell}$	800	0.997
MTT method	$Y = 0.075 + 0.084C_{H_{22}cell}$	1500	0.995

time which proved the exposure time-dependent manner of inhibition rate of anticancer drug. However, the difference of inhibition rate became smaller as the increase of the reactive time. Therefore, 48 h was selected for the RLS/MTT screening assays.

3.6. Verification test

To validate the accuracy of RLS/MTT screening method, similarly treated H_{22} cells were plated for MTT colorimetric assay [35] with some modification. Briefly, each well of round-bottom 96-well microtiter plates (Falcon, Becton Dickinson, Mountain View, CA, USA) received 100 μL of H_{22} cells suspension. 20 μL of MTT solution was added to each well and incubated for 4 h. The microtiter plates were centrifuged ($1400 \times g$, $15^\circ C$, 5 min) and the untransformed MTT was removed carefully by an Eppendorf pipette. Each well was added to 200 μL of a DMSO working solution (180 μL DMSO with 20 μL 1.0 mol L^{-1} HCl), and the absorbance (A) was determined at 570.0 nm using an ELISA plate reader (Dynatech, Guernsey, UK) after 15 min.

According to the FDA, IC_{50} represents the concentration of a drug that is required for 50% inhibition in vitro. The IC_{50} value was determined based on inhibition rates of H_{22} cell by SPSS12.0 Probit regression method. The experiments were repeated five times for each drug. The relative antitumor activity was calculated by the following formula [36], which was used to compare the antitumor effect of each drug:

$$\text{relative antitumor activity} = \frac{\text{peak plasma concentration} (\mu g mL^{-1})}{IC_{50} \text{ value} (\mu g mL^{-1})}$$

As shown in Table 1 the result of RLS/MTT screening method was consistent with that of MTT assay, which proved the method accuracy. Meanwhile, DDP has higher antitumor activity than other anticancer drugs by the relative antitumor activity value, which suggests DDP has more antitumor effect than others against H_{22} cell. Table 2 displayed that the slope of linear regression equation of RLS/MTT method was larger than that of the traditional MTT colorimetric method, which disclosed this method has higher sensitivity. Therefore, the RLS/MTT screening method is a useful tool to be used in practical applications.

3.7. Mechanism of the reactive

MTT was reduced by viable cancer cells to produce the formazan which induces RLS signal. Cells viability was proportional to the

number of formazan. As different anticancer drugs caused cancer cells varying degrees of growth inhibition or even death, the ability of H₂₂ cells after treated with different anticancer drugs to produce the formazan was different. It reflected the differentiation of RLS intensity at the maximum scattering peak in the RLS/MTT screening spectra. The different RLS intensities represented the differentiation of inhibition rates of six anticancer agents against H₂₂ cells. The inhibition rate of anticancer drug was found to vary inversely with RLS intensity of the H₂₂-MTT system. Moreover, the antitumor effectiveness of different anticancer drugs is properly ordered in the RLS/MTT screening spectra, only even looking at the raw data without manipulation. Therefore, an intuitive method of screening anticancer drug in vitro using RLS technique was proposed in this contribution.

4. Conclusion

The RLS/MTT screening assay was developed for rapidly screening anticancer drugs in vitro. The result showed that the RLS/MTT screening assay was an inexpensive, simple and fast procedure which required only measuring the RLS intensity. It can be intuitive to see the differentiation of the tumor suppressive activity of anticancer drugs without data processing in RLS/MTT screening spectra. Compared with the traditional MTT method, this method has higher sensitivity. In addition, this method can be easily adapted to high throughput drug screening in vitro, which can also be used to screen potential anticancer drug from large candidate libraries.

Acknowledgments

All authors express their sincere thanks for the support from the National Natural Science Foundation of China (No. 39670298) and the Municipal Science Foundation of Shantou (No. S02023).

References

- [1] J.M. Padrón, C.L. Wilt, K. Smid, S.W. Evelien, H.J. Backus, P.E. Pizao, G. Giaccone, G.J. Peters, *Crit. Rev. Oncol. Hemat.* 36 (2000) 141–157.
- [2] M. Suggitt, M.C. Bibby, *Clin. Cancer Res.* 11 (2005) 971–981.
- [3] L. Lu, Z.H. Yang, B.H. Zhu, S.H. Fang, X. Yang, W. Cai, C.Y. Li, J.X. Ma, G.Q. Gao, *Cancer Lett.* 257 (2007) 97–106.
- [4] A.B. Rogers, E.J. Theve, Y. Feng, R.C. Fry, K. Taghizadeh, K.M. Clapp, C. Boussahmain, K.S. Cormier, J.G. Fox, *Cancer Res.* 67 (2007) 11536–11546.
- [5] P. Skehan, R. Storeng, D. Scudiero, A. Monks, J. McMahon, D. Vistica, J. Natl. Cancer Inst. 82 (1990) 1107–1112.
- [6] W.T.Y. Loo, J.H.M. Fong, M.N.B. Cheung, L.W.C. Chow, *Biomed. Pharmacother.* 59 (2005) S337–S339.
- [7] N. Miyazaki, H. Ohkura, N. Kajimura, N. Okazaki, *Eur. J. Cancer* 28 (1992) 1419–1422.
- [8] P. Houghton, R. Fang, L. Techatanawat, G. Steventon, P.J. Hylands, C.C. Lee, *Meth. Ods* 42 (2007) 377–387.
- [9] A.R. Friedrich, W. Eder, J. Castaneda, M. Doss, E. Huber, R. Ebner, J. *Biomol. Screen.* 12 (2007) 925–937.
- [10] M.N. Kirstein, K.M. Wieman, B.W. Williams, J.E. Fisher, P.H. Marker, C.T. Le, D. Yee, R.A. Kratzke, *Lung Cancer* 58 (2007) 196–204.
- [11] R.F. Pasternack, P.J. Collings, *Science* 269 (1995) 935–939.
- [12] R.F. Pasternack, C. Bustamante, P.J. Collings, A. Giannetto, E.J. Gibbs, *J. Am. Chem. Soc.* 115 (1993) 5393–5399.
- [13] C.Z. Huang, K.A. Li, S.Y. Tong, *Anal. Chem.* 68 (1996) 2259–2263.
- [14] Z.G. Chen, W.F. Ding, F.L. Ren, J.B. Liu, Y.Z. Liang, *Anal. Chim. Acta* 550 (2005) 204–209.
- [15] J. Li, Y.L. Wei, L.M. Guo, C.H. Zhang, Y. Jiao, S.M. Shuang, C. Dong, *Talanta* 76 (2008) 34–39.
- [16] J.H. Zheng, X. Wu, M.Q. Wang, D.H. Ran, W. Xu, J.H. Yang, *Talanta* 74 (2008) 526–532.
- [17] H.Y. Wang, Y.F. Li, C.Z. Huang, *Talanta* 72 (2007) 1698–1703.
- [18] Z.G. Chen, J.B. Liu, Y.Z. Liang, F.L. Ren, J. *Biomol. Screen.* 11 (2006) 400–406.
- [19] Z.G. Chen, J.B. Liu, Y.L. Han, *Talanta* 71 (2007) 1246–1251.
- [20] L.J. Dong, X.G. Chen, Z.D. Hu, *Talanta* 71 (2007) 555–560.
- [21] H.C. Pan, X.C. Tao, C.J. Mao, J.J. Zhu, F.P. Liang, *Talanta* 71 (2007) 276–281.
- [22] Z.G. Chen, J.B. Liu, Y.L. Han, L. Zhu, *Anal. Chim. Acta* 570 (2006) 109–115.
- [23] X.F. Long, S.P. Bi, H.Y. Ni, X.C. Tao, N. Gan, *Anal. Chim. Acta* 501 (2004) 89–97.
- [24] S.P. Liu, H.Q. Luo, N.B. Li, Z.F. Liu, W.X. Zheng, *Anal. Chem.* 73 (2001) 3907–3914.
- [25] P. Feng, W.Q. Shu, C.Z. Huang, Y.F. Li, *Anal. Chem.* 73 (2001) 4307–4312.
- [26] M.H. Xiang, X. Xu, D.X. Li, F. Liu, N. Li, K.A. Li, *Talanta* 76 (2008) 1207–1211.
- [27] Y.F. Li, C.Z. Huang, X.L. Hu, *Chin. J. Anal. Chem.* 26 (1998) 1508–1515.
- [28] J. Anglister, I.Z. Steinberg, *J. Chem. Phys.* 74 (1981) 786–791.
- [29] G.A. Miller, *J. Chem. Phys.* 82 (1978) 616–618.
- [30] X.L. Zhang, W. Wang, W.T. Yu, Y.B. Xie, X.H. Zhang, Y. Zhang, X.J. Ma, *Biotechnol. Prog.* 21 (2005) 1289–1296.
- [31] T. Kusumoto, Y. Sakaguchi, Y. Maehara, T. Nakashima, M. Furusawa, K. Sugimachi, *Oncology* 49 (1992) 343–346.
- [32] M.L. Slevin, *Cancer* 67 (1991) 319–329.
- [33] P.J. Houghton, P.J. Cheshire, L. Myers, C.F. Stewart, T.W. Synold, J.A. Houghton, *Cancer Chemoth. Pharm.* 31 (1992) 229–239.
- [34] O. Yuichiro, N. Kazuhiko, F. Yasuhiro, S. Yasutsuna, M. Koichi, B. Masami, *Cancer Res.* 49 (1989) 4098–4102.
- [35] T. Mosmann, *J. Immunol. Meth.* 65 (1983) 55–63.
- [36] N. Horiuchi, K. Nakagawa, Y. Sasaki, K. Minato, Y. Fujiwara, K. Nezu, Y. Ohe, N. Saijo, *Cancer Chemoth. Pharm.* 22 (1988) 246–250.



Combining biofunctional magnetic nanoparticles and ATP bioluminescence for rapid detection of *Escherichia coli*

Yuxiao Cheng, Yajun Liu, Jingjing Huang, Kang Li, Wen Zhang, Yuezhong Xian, Litong Jin*

Department of Chemistry, East China Normal University, Shanghai 200062, PR China

ARTICLE INFO

Article history:

Received 11 June 2008

Received in revised form 1 September 2008

Accepted 9 September 2008

Available online 18 September 2008

Keywords:

Escherichia coli (*E. coli*)

Biofunctional magnetic nanoparticles

(BMNPs)

Antibody

Amine-functionalized magnetic nanoparticles

ATP bioluminescence

ABSTRACT

A rapid, specific and sensitive method for assay of *Escherichia coli* (*E. coli*) using biofunctional magnetic nanoparticles (BMNPs) in combination with adenosine triphosphate (ATP) bioluminescence was proposed. The BMNPs were fabricated by immobilizing a specific anti-*E. coli* antibody on the surface of amine-functionalized magnetic nanoparticles (about 20 nm in diameter), and then was applied to capture the target bacteria *E. coli* from samples. The BMNPs exhibited high capture efficiency to *E. coli*. Transmission electron microscope (TEM) images showed that the BMNPs were bound to the surface of entire *E. coli* cells. The target bacteria became magnetic so that could be isolated easily from the sample solution by employing an external magnetic field. The concentration of *E. coli* captured by the BMNPs was then detected by an ATP bioluminescence method. The optimization of ATP measurement was carried out to improve the detection sensitivity. The proposed method was applied to detect the *E. coli* inoculated into pasteurized milk with low detection limit (20 cfu/mL) and short detection time (about 1 h).

© 2008 Elsevier B.V. All rights reserved.

1. Introduction

Escherichia coli (*E. coli*), which are found in large numbers among the intestine of humans and other warm-blooded animals spread abroad in natural environment, are the major cause of infection outbreaks with serious consequences. In particular, the serotype O157:H7 associate with several human diseases including diarrhoea, hemorrhagic colitis and hemolytic-uremic syndrome [1]. One of the largest outbreaks occurred in Japan in 1996, where over 10,000 people were infected and 11 died [2]. Conventional microbiological methods for *E. coli* detection relying on the cell culture are still the most definite method, but the incubation period needed is too long (24–48 h) to meet the need of real-time microbial detection [3]. More recently, several rapid assays for detecting *E. coli* based on different measuring principles, such as polymerase chain reaction [4–7], immunoassay [8,9], optical assay [10,11] etc., have been developed. Although these methods shortened the detection time varying from several hours to 1 day, many of these methods are still time-consuming and poor in sensitivity.

In the recent years, with the rapid development of nanostructured materials and nanotechnology in the fields of biotechnology

and pathogen detection, magnetic nanoparticles (MNPs) especially receive considerable attention. Due to their numerous attributes, such as magnetic properties, low toxicity and biocompatibility, they are attractive and strong candidates for applications in diagnosis, separations, and magnetic resonance imaging for detection [12–16]. In particular, some important progress in pathogen detection [17–21] has been made based on well-synthesized and functionalized iron oxide nanoparticles. For example, El-Boubbou et al. had demonstrated magnetic glyco-nanoparticle (MGNP)-based system to not only detect *E. coli*, but also remove up to 88% of the target bacteria from the medium [18]. Gao et al. combined fluorescent probes and magnetic nanoparticles for rapid detection of traces of bacteria in human blood within 2 h [19]. Lin et al. employed vancomycin-modified magnetic nanoparticles as affinity probes to selectively trap Gram-positive pathogens from sample solutions [20]. The bacteria isolated from sample solution by applying a magnetic field could be detected rapidly by MALDI-MS analysis.

The detection of the bacterial number by the adenosine triphosphate (ATP) bioluminescence method is known to be highly in accordance with the plate count method [23,24], and the ATP bioluminescence can estimate the concentration of viable bacterial within minutes. However, since ATP is ubiquitous in all living cells, the measurement does not provide sufficient information on the identity of target cells. In the present work, we had functionalized magnetic nanoparticles by immobilizing anti-*E. coli* antibody on the surface of amine-functionalized magnetic nanoparticles to

* Corresponding author. Tel.: +86 21 62232627; fax: +86 21 62232627.
E-mail address: ltjin@chem.ecnu.edu.cn (L. Jin).

fabricate BMNPs, which could concentrate traces of *E. coli* from sample solution with high capture efficiency. The BMNPs conjugated with the target bacteria were easily isolated from the solution by applying an external magnet, and the separated bacteria were detected by using the ATP bioluminescence. Due to the extraordinary properties of the BMNPs, the proposed method possessed high specificity, low detection limit and short assay time.

2. Experimental

2.1. Reagents and apparatus

Avidin, N-hydroxysuccinimide (NHS) and 1-ethyl-3-(3-dimethylaminopropyl) carbodiimide (EDC) were purchased from Sigma Company (St. Louis, MO, USA). Goat anti-*E. coli* polyclonal antibody and rabbit anti-*E. coli* polyclonal biotin-labeled antibody were obtained from Abcam (Cambridge, UK). $\text{FeCl}_3 \cdot 6\text{H}_2\text{O}$, 1,6-hexanediamine, bovine serum albumin (BSA), N-(2-Hydroxyethyl) piperazine-N'-2-ethanesulfonic acid (Hepes), magnesium acetate, dithiothreitol, EDTA, dodecyl trimethyl ammonium bromide (DTAB) and α -cyclodextrin were purchased from Shanghai Chemical Reagent Company (Shanghai, China). *E. coli* (BL21) was a gift from School of Life Sciences, East China Normal University (Shanghai, China).

Extracellular ATP eliminator reagent, luciferase from firefly and D-luciferin were purchased from Shenyang Zhongke Liangma Bio-engineering Co. Ltd. (Shenyang, China). Intracellular extraction reagent was prepared by dissolving different concentration of DTAB in Tris-EDTA buffer. Luciferin-luciferase bioluminescence reagent was prepared in 5 mL Hepes buffer (50 mM, pH = 7.8) contained 0.5 mg/mL of luciferase, 0.3 mM luciferin, 10 mM magnesium acetate, 10 mg of BSA, 1.0 mM dithiothreitol, 1.0 mM EDTA and 2% β -cyclodextrin.

Transmission electron microscopy (TEM) images of the *E. coli* captured by BMNPs were obtained on JEOL 2100 electron microscopes (JEOL Ltd., Tokyo, Japan). Fourier transform infrared (FTIR) spectrum was acquired at ambient temperature using a NEXUS470 optical bench (Nicolet). The ATP bioluminescence intensity was read on Model 3560 ($10\times$) Microluminometer (New Horizons Diagnostics Corporation, Columbia, USA).

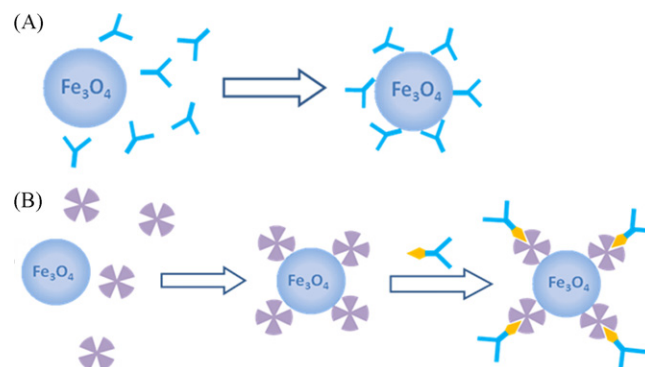
2.2. Preparation of amine-functionalized magnetic nanoparticles

The amine-functionalized Fe_3O_4 were prepared by a facile one-pot method according to the literature [25]. Briefly, a solution of anhydrous sodium acetate (2.0 g), 1,6-hexanediamine (7.0 g) and $\text{FeCl}_3 \cdot 6\text{H}_2\text{O}$ (1.0 g) dissolved in 30 mL glycol was stirred vigorously at 50 °C to get a transparent solution. The as-prepared solution was transferred into a Teflon-lined autoclave and reacted at 200 °C for 6 h. The magnetite nanoparticles were collected by applying an external magnetic field and rinsed with water and ethanol to remove the solvent and unbound 1,6-hexanediamine. Then, the nanoparticles were dried at 50 °C before characterization and application.

2.3. Fabrication of BMNPs

2.3.1. Strategy A

3 mg amine-functionalized magnetic nanoparticles were dispersed in 6 mL PBS buffer solution (10 mM, pH 7.4) by ultrasound irradiation technology. Then, polyclonal antibody (250 μL) at a concentration of 4 mg/mL, EDC (2.3 mg) and NHS (5.2 mg) was added into the magnetic nanoparticles solution. The magnetic nanoparticles were incubated at 37 °C with gentle agitation for 24 h. After the



Scheme 1. Schematic representation of strategies A and B used to prepare the BMNPs.

reaction was completed, the forming BMNPs were isolated under an external magnetic field and washed with PBS buffer twice. The BMNPs were resuspended in 3.0 mL PBS, and stored at 4 °C until use.

2.3.2. Strategy B

Avidin conjugation to magnetic nanoparticles (3 mg) used the above procedure except that the antibody was changed to avidin. After the separation and wash steps, the avidin conjugated magnetic nanoparticles were resuspended in 2.5 mL PBS, and added with 50 μL of biotin-labeled antibody at a concentration of 4 mg/mL. The mixture was gently stirred for 1 h, and washed with PBS by magnetic field separation to remove the free biotin-labeled antibody. Scheme 1 shows the processes of the fabrication of BMNPs by two strategies.

2.4. Cultivation of *E. coli*

E. coli (BL21) cultures were grown overnight in LB medium at 37 °C with aeration by shaking, which allowed the growing stationary phase to be reached. For detecting the density of *E. coli*, the stationary phase *E. coli* cultures were serially diluted (10-fold steps) 10^7 times with LB medium, and 100 μL diluted solution of *E. coli* was plated on LB agar plates. After incubation at 37 °C for 24 h, *E. coli* colonies on plates were counted to determine the number of colony-forming units per milliliter (cfu/mL).

2.5. Capture of *E. coli* by BMNPs

Pure culture of the *E. coli* at the stationary phase was centrifuged at 12,000 g for 10 min to remove the growth medium. The reserved bacterial pellets were resuspended in PBS (0.01 M, pH 7.4) and then serially diluted from 10^3 to 10^8 cfu/mL. 120 μL of BMNPs prepared above was added into 1 mL of *E. coli* solution with serial concentration. The mixture was gently shaken for 1 h at room temperature and the *E. coli* captured by BMNPs were separated by an external magnet.

2.6. ATP bioluminescence measurement

50 μL of *E. coli* solution or *E. coli* binding with BMNPs solution was placed into the bioluminescence cell, and 50 μL of extracellular eliminator reagent was added to remove all non-bacterial ATP. Then, 50 μL of 0.2% DTAB as ATP extractant was added to release ATP of bacteria cells. Finally, luciferin-luciferase was added to generate the bioluminescence which was detected by microluminometer in the form of relative light units (RLUs).

2.7. Sample preparation and detection

Pasteurized milk was purchased from the local supermarket. 10 ml of pasteurized milk was inoculated with *E. coli* at a concentration of 5×10^6 cfu/mL. The inoculated sample was then taken through a 10-fold serial dilution in uninoculated pasteurized milk to obtain samples at the concentration ranging from 5×10^1 to 5×10^6 cfu/mL. A similar method was adopted for pasteurized apple juice and tap water. Ground beef was purchased from a grocery store. 1 g ground beef was mixed with 10 mL *E. coli* solution at the concentration of 1×10^5 cfu/mL. Then, the samples were homogenized by vigorously shaking for 5 min.

240 μ L of BMNPs were added into 2.0 mL of milk, apple juice, tap water and ground beef samples prepared above. After gentle shaking at 37 °C for 1 h, the *E. coli* cells captured by the BMNPs were isolated magnetically and resuspended in 50 μ L of PBS. The suspension of *E. coli* binding with BMNPs was placed into the bioluminescence cell and the ATP bioluminescence was measured.

3. Results and discussion

3.1. Characterization of amine-functionalized magnetic nanoparticles

The amine-functionalized magnetic nanoparticles were prepared by a facile one-pot strategy using $\text{FeCl}_3 \cdot 6\text{H}_2\text{O}$ as a single iron source and 1,6-hexadecylamine as a ligand. Transmission electron microscope (TEM) observation indicates that the as-prepared magnetic nanoparticles are about 20 nm in diameter (Fig. 1). Compared to magnetic beads (1–5 μ m in diameter) used in biological separation, the magnetic nanoparticles possess high surface/volume ratio, which can provide more contact surface area for attaching antibody and for capturing pathogens [17]. Moreover, the small size of magnetic nanoparticles allows the affinity of multiple MNPs onto a bacterial cell rendering easy magnet-mediated separation [17,22] and fast detection.

Fourier transform infrared (FTIR) spectroscopy was used to characterize the amine-functionalized magnetite nanoparticles. As can be seen from Fig. 2, The strong IR band at 584cm^{-1} was characteristic of the Fe–O vibrations [26], and the appearance of peak around 1624 and 1457cm^{-1} can be attributed to the existence of the free $-\text{NH}_2$ group on the nanoparticles, which proved that the amine groups had been functionalized on the surface of

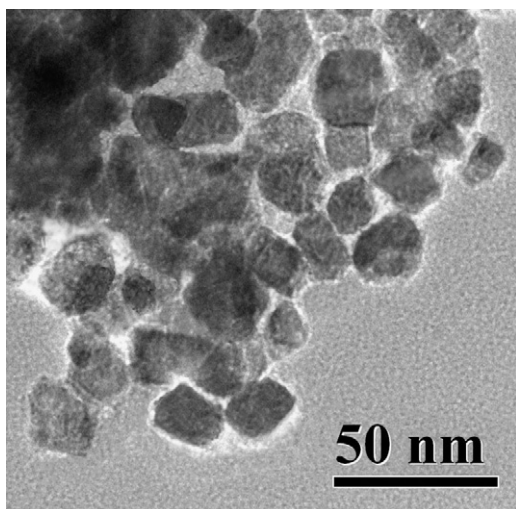


Fig. 1. TEM image of amine-functionalized magnetic nanoparticles.

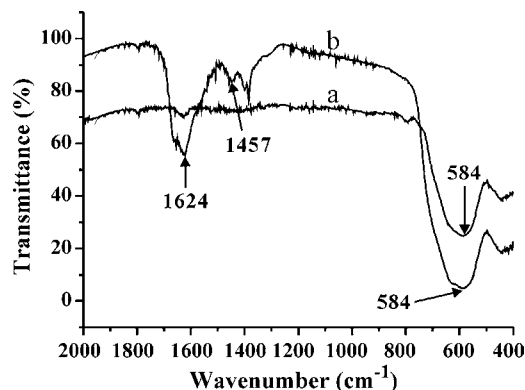


Fig. 2. FTIR spectra of unmodified (a) and amine-functionalized (b) magnetic nanoparticles.

magnetic nanoparticles. The magnetic nanoparticles coated with amine groups made them convenient to bioconjugate with biological macromolecules, such as protein, nucleic acid, antibody, etc.

3.2. Preparation of BMNPs

To prepare the BMNPs, the appropriate antibody should be selected. The range of specificity and type of antigen to conjugate with the antibody were considered. For detection of *E. coli* in drinking water and food sample, polyclonal antibody was necessary in contrast to monoclonal antibodies because the types of *E. coli* in drinking water and food samples were diverse. The antibodies were immobilized on the surface of the magnetic nanoparticles by two strategies. In strategy A, anti-*E. coli* antibodies were directly immobilized onto the magnetic nanoparticles using carbodiimide chemistry [27,28] to cross-link free carboxylic acid groups on antibodies with amine-containing nanoparticles; in strategy B, avidin was first linked on the surface of magnetic nanoparticles as a bridge molecule [29], then the biotin-antibodies were immobilized onto avidin. For strategy A, antibodies were attached onto the magnetic nanoparticles at random. Thus, some of the antigen binding sites of the antibody may be blocked. Whereas, in strategy B, the biotin labeled antibody was bound to the bridge molecule avidin, which ensured that the antibody recognition sites were oriented away from the surface of magnetic nanoparticles. Furthermore, avidin, which has four capturing sites for biotin, provided both sufficient binding opportunity and binding strength for biotin labeled antibody. So, antibodies on the surface of magnetic nanoparticles could be bound to the target bacteria easily and avidin-labeled magnetic nanoparticles may capture more cells. The BMNPs prepared by two different methods were used to capture the *E. coli* (2×10^5 cfu/mL) in the PBS. We found that the capture efficiency of BMNPs prepared by strategy B (about 90%) exhibited better binding performance than those by strategy A (about 75%). Therefore, the BMNPs prepared by strategy B were used for the further work.

3.3. Capture of *E. coli* by BMNPs

Fig. 3 presents the TEM image that was obtained by employing the BMNPs to capture the target bacteria in *E. coli* solution. Inset of Fig. 3 is one of the magnified TEM images of *E. coli* binding with BMNPs. The result showed that the shape of *E. coli* was ellipse with about 2 μ m long and the BMNPs were bound to the surface of entire *E. coli* cells. The target bacteria *E. coli* became magnetic and could be isolated easily from the sample solution by employing an external magnetic field.

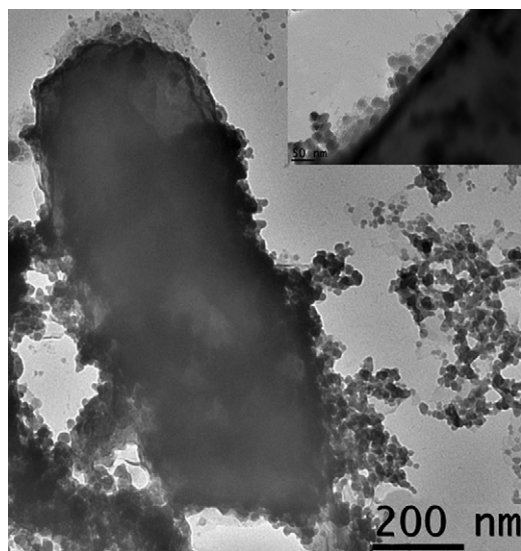


Fig. 3. TEM image of *E. coli* binding with BMNPs. Inset is the magnified TEM image of *E. coli* binding with BMNPs.

Because the BMNPs were applied to capture the *E. coli* and improve the specificity of ATP measurement, the capture efficiency was important to get accurate results and high sensitivity. 1.0 mL of *E. coli* with different concentrations in PBS was added with 120 μ L of BMNPs (1 mg/mL). The mixture was incubated with gentle shaking at room temperature for 1 h. Then, the *E. coli* captured by BMNPs were concentrated by external magnet, and suspended in 1.0 mL PBS solution. The ATP bioluminescence of the captured *E. coli* were measured and compared with that obtained without BMNPs captured. As can be seen from Table 1, the capture efficiency of BMNPs to *E. coli* exceeds 90% at the low concentration. As the increase of the density of *E. coli*, the capture efficiency decreased gradually, which may be because that the BMNPs reach a saturation of bacterial binding. However, it still remained 80% at the concentration of 2×10^6 cfu/mL. Compared to the normal-size magnetic particles, the nano-size BMNPs allowed the attachment of more magnetic particles onto the bacterial cells, which resulted in better capture performance. Liu [30] and Fu [31] have reported that the capture efficiency of normal-size magnetic particles was about 50%. These results showed that the BMNPs possessed excellent capture performance to *E. coli*, which made traces of bacteria can be concentrated from sample and improved the sensitivity of the bioluminescence detection.

3.4. Optimum conditions for the ATP bioluminescence measurement

Before the bioluminescence assay it is necessary to extract ATP from the bacterial cells because the intracellular ATP level can

Table 1
Capture efficiency of BMNPs to *E. coli*.

<i>E. coli</i> sample (cfu/mL)	ATP bioluminescence of total <i>E. coli</i> (RLU)	ATP bioluminescence of <i>E. coli</i> captured by BMNPs (RLU)	Capture efficiency (%)
2×10^4	1,650	1,573	95.3
2×10^5	7,930	7,210	90.9
2×10^6	31,203	24,971	80.0

Capture efficiency was described as the ratio of *E. coli* captured by BMNPs to original *E. coli* sample in the form of ATP bioluminescence. ATP bioluminescence intensity was given as relative light units (RLUs).

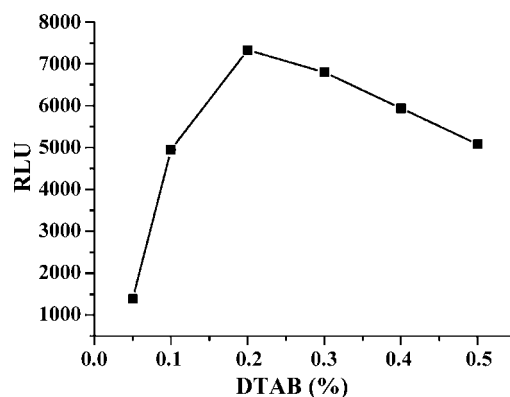


Fig. 4. Effect of DTAB concentration on the ATP bioluminescence intensity of 2×10^5 cfu/mL *E. coli*.

not be measured without extraction. Trichloroacetic acid (TCA) was often used as an ATP extractant [32]. However, TCA strongly interferes with the subsequent luciferase–luciferin assay unless the extract was highly diluted prior to assay, which decreased the sensitivity of intracellular ATP measurement. In this work, DTAB was chosen as the extractant in that quaternary ammonium compounds give higher ATP yield than TCA according to the report [33]. In addition, the β -cyclodextrin can be used to neutralize the DTAB [34], which minimize the interference to luciferase–luciferin assay, and improved the detection sensitivity.

The extraction performance of DTAB at various concentrations (0.05, 0.1, 0.2, 0.5, 1, 2%) was investigated in 2×10^5 cfu/mL *E. coli* sample. As can be seen from Fig. 4, the ATP bioluminescence increased as the concentration of DTAB increased. However, an increase in the DTAB concentration over 0.2% did not enhance the ATP bioluminescence intensity; on the contrary, the bioluminescence intensity decreased because that the DTAB may inactivate firefly luciferase. Thus, 0.2% DTAB was chosen as the optimum DTAB concentration. On the other hand, the effect of β -cyclodextrin (0.5, 1, 2, 5, 10%) on the response of bioluminescence was also studied. The result obtained was that the optimum β -cyclodextrin concentration was 2%.

3.5. Detection of *E. coli* in real samples

The method combining BMNPs with ATP bioluminescence was applied to detect *E. coli* in pasteurized milk and apple juice. As

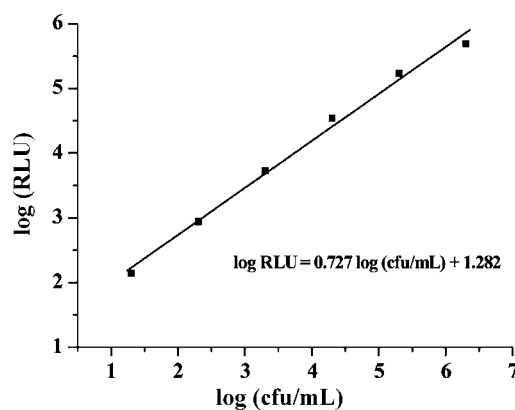


Fig. 5. ATP bioluminescence intensity of *E. coli* at different concentrations captured by BMNPs from pasteurized milk. The *E. coli* binding with BMNPs separated from 2 mL of original *E. coli* solution was resuspended in 50 μ L PBS, and then detected by ATP bioluminescence assay.

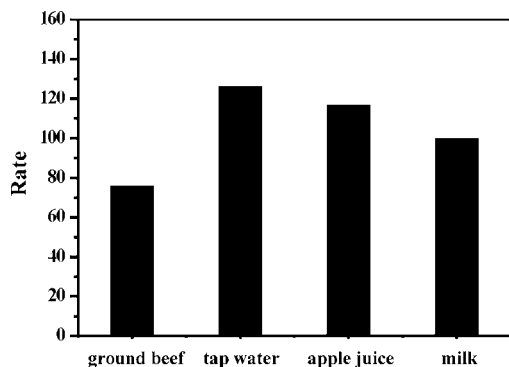


Fig. 6. Comparison of various real samples artificially contaminated with *E. coli* (1×10^5 cfu/mL). The rates obtained were compared to the milk (1×10^5 cfu/mL) which was regarded as 100%. Detection was performed as described in Fig. 5.

shown in Fig. 5, *E. coli* can be determined in the range of 2×10^1 to 2×10^6 cfu/mL with a detection limit of 20 cfu/mL. The whole procedure for detecting the *E. coli* took about 1 h. The detection limit and assay time obtained in this work were found to be superior to other techniques. For example, a fluorescent bacteriophage assay (FBA) for the detection of *E. coli* was developed by Goodridge et al. [35], 10–100 cfu/mL of *E. coli* in contaminated raw milk were detectable after a 10 h enrichment step. Tims and Lim reported that *E. coli* was determined at the 10^3 cfu/mL level in less than 10 h using optical immunoassay, enrichment, and PCR steps [36]. A flow-type antibody sensor was applied to detect *E. coli* in various food samples ranging from 1.7×10^5 to 8.7×10^7 cfu/mL within 30 min [37]. Gehring et al. developed an enzyme-linked immunomagnetic chemiluminescence method to detect *E. coli* in pristine buffered saline yielding detection limits of approximate 1×10^5 to 1×10^6 of live cfu/mL for 1.5 h [38].

Ground beef, apple juice and tap water were also tested by contaminating the samples with *E. coli*. Fig. 6 shows the rates for beef, apple juice, and tap water samples, which was compared to the milk. The rate for the apple juice (117%) and tap water (126%) samples were higher than that of milk (100%). However, in the case of ground beef, the rate (76%) was less than that of the milk. Although the method was used for beef, apple juice, milk, and tap water samples in this work, it has the potential to be employed in other kind of food or drink sample. Variation in the detection from one kind of sample to another can be avoided by calibrating in the same matrix as the samples.

4. Conclusion

In this work, BMNPs were prepared by attaching the antibody on the amine-functionalized magnetic nanoparticles, and were further applied to detect the *E. coli* in pasteurized milk. The BMNPs exhibited high capture efficiency to *E. coli*. The *E. coli* cells were separated from the sample and detected by ATP bioluminescence assay. The proposed method could detect *E. coli* in pasteurized milk ranging from 2×10^1 to 2×10^6 cfu/mL with a detection limit of 20 cfu/mL,

and the total detection time was about 1 h. Since the preparation of surface functionalization magnetic nanoparticles is low-cost and reproducible, the method combining the BMNPs with ATP bioluminescence illustrated much potential in bacterial detection.

Acknowledgements

This work was supported by Science and Technology Commission of Shanghai Municipality (No. 06dz05824), the National Natural Science Foundation of China (No. 20475017) and Ph.D. Program Scholarship Fund of ECNU (2008).

References

- [1] F. Villani, F. Russo, G. Blaiotta, G. Moschetti, D. Ercolini, *Meat Sci.* 70 (2005) 181.
- [2] www.city.sakai.osaka.jp/city/info/o157prpt/index.html.
- [3] L. Clesceri, A. Greenberg, A. Eaton, *Standard Methods of the Examination of Water and Wastewater*, 20th ed., American Public Health Association, American Water Works Association and Water Environment Federation, Washington, DC (1998).
- [4] J.M. Simpson, D.V. Lim, *Biosens. Bioelectron.* 21 (2005) 881.
- [5] D.R. Lazaro, M. Hernandez, R. Esteve, J. Hoofar, M. Pla, *J. Microbiol. Meth.* 54 (2003) 381.
- [6] C. Bischoff, J. Lüthy, M. Altwegg, F. Baggi, *J. Microbiol. Meth.* 61 (2005) 335.
- [7] T. Mohammadi, R.N.I. Pietersz, C.M.J.E. Vandenbracke-Grauls, P.H.M. Savelkoul, H.W. Reesink, *Transfusion* 45 (2005) 731.
- [8] C. Ruan, L. Yang, Y. Li, *Anal. Chem.* 74 (2002) 4814.
- [9] L. Yang, Y. Li, *J. Microbiol. Meth.* 64 (2006) 9.
- [10] S.O. Van Poucke, H.J. Nelis, *Appl. Environ. Microbiol.* 61 (1995) 4505.
- [11] K. Geissler, M. Manafi, I. Amoros, L. Alonso, *J. Appl. Microbiol.* 889 (2000) 280.
- [12] S.G. Penn, L. He, M. Natan, *Curr. Opin. Chem. Biol.* 7 (2003) 609.
- [13] P.S. Doyle, J. Bibette, A. Bancaud, J. Viovy, *Science* 295 (2002) 2237.
- [14] S.I. Stoeva, F.W. Huo, J.S. Lee, C.A. Mirkin, *J. Am. Chem. Soc.* 127 (2005) 15362.
- [15] Y.W. Jun, Y.M. Huh, J.S. Choi, J.H. Lee, H.T. Song, S. Kim, S. Yoon, K.S. Kim, J.S. Shin, J.S. Suh, J. Cheon, *J. Am. Chem. Soc.* 127 (2005) 5732.
- [16] Y.M. Huh, Y.W. Jun, H.T. Song, S. Kim, J.S. Choi, J.H. Lee, S. Yoon, K.S. Kim, J.S. Shin, J.S. Suh, J. Cheon, *J. Am. Chem. Soc.* 127 (2005) 12387.
- [17] H. Gu, K. Xu, C. Xu, B. Xu, *Chem. Commun.* (2006) 941.
- [18] K. El-Boubbou, C. Gruden, X. Huang, *J. Am. Chem. Soc.* 129 (2007) 13392.
- [19] J. Gao, L. Li, P. Ho, G.C. Mak, H. Gu, B. Xu, *Adv. Mater.* 18 (2006) 3145.
- [20] Y. Lin, P. Tsai, M. Weng, Y. Chen, *Anal. Chem.* 77 (2005) 1753.
- [21] H. Gu, P.L. Ho, K.W.T. Tsang, L. Wang, B. Xu, *J. Am. Chem. Soc.* 125 (2003) 15702.
- [22] X. Zhao, L.R. Hilliard, S.J. Mechery, Y. Wang, R.P. Bagwe, S. Jin, W. Tan, *Proc. Natl. Acad. Sci. U.S.A.* 101 (2004) 15027.
- [23] J. Lee, R.A. Deininger, *J. Rapid Methods Autom. Microbiol.* 7 (1999) 135.
- [24] D. van der Kooij, H.R. Veenendaal, C. Baars-Lorist, D.W. van der Klift, Y.C. Drost, *Water Res.* 29 (1995) 1655.
- [25] L. Wang, J. Bao, L. Wang, F. Zhang, Y. Li, *Chem. Eur. J.* 12 (2006) 6341.
- [26] I.J. Bruce, J. Taylor, M. Todd, M.J. Davies, E. Borioni, C. Sangregorio, T. Sen, *J. Magn. Magn. Mater.* 284 (2004) 145.
- [27] K. Ho, P. Tsai, Y. Lin, Y. Chen, *Anal. Chem.* 76 (2004) 7162.
- [28] M. Mikhaylova, D.K. Kim, C.C. Berry, A. Zagorodni, M. Toprak, A.S.G. Curtis, M. Muhammed, *Chem. Mater.* 16 (2004) 2344.
- [29] F. Mavre, M. Bontemps, S. Ammar-Merah, D. Marchal, B. Limoges, *Anal. Chem.* 79 (2007) 187.
- [30] Y. Liu, Y. Li, *J. Microbiol. Meth.* 51 (2002) 369.
- [31] Z. Fu, S. Rogelj, T.L. Kieft, *Int. J. Food Microbiol.* 99 (2005) 47.
- [32] N. Hattori, T. Sakakibara, N. Kajiyama, T. Igarashi, M. Maeda, S. Murakamia, *Anal. Biochem.* 319 (2003) 287.
- [33] S. Hoffner, C. Jimenez-Misasl, A. Lundin, *Luminescence* 14 (1999) 255.
- [34] A. Lundin, J. Anson, *Method for extraction of intracellular components*, (1997) EP0566625.
- [35] L. Goodridge, J. Chen, M. Griffiths, *Int. J. Food Microbiol.* 47 (1999) 43.
- [36] T.B. Tims, D.V. Lim, *J. Microbiol. Meth.* 55 (2003) 141.
- [37] N. Kim, I. Park, *Biosens. Bioelectron.* 18 (2003) 1101.
- [38] A.G. Gehring, D.M. Albin, P.L. Irwin, S.A. Reed, S.I. Tu, *J. Microbiol. Meth.* 67 (2006) 527.



Trace determination of short-chain aliphatic amines in biological samples by micellar electrokinetic capillary chromatography with laser-induced fluorescence detection

Ying-Hua Deng^{a,b}, Hong Wang^a, Lu Zhong^c, Hua-Shan Zhang^{a,*}

^a Department of Chemistry, Wuhan University, Wuhan 430072, China

^b Department of Chemistry and Life Science, Hubei University of Education, Wuhan 430205, China

^c Wuchang Shipyard Workers' Hospital, Wuhan 430060, China

ARTICLE INFO

Article history:

Received 18 June 2008

Received in revised form 7 September 2008

Accepted 9 September 2008

Available online 18 September 2008

Keywords:

Aliphatic amines

Biological samples

Capillary electrophoresis

Derivatization

Laser-induced fluorescence detection

N-Hydroxysuccinimidyl

fluorescein-*O*-acetate

ABSTRACT

In this study, a new capillary electrophoresis (CE) method is described originally for the sensitive and selective determination of short-chain aliphatic amines in biological samples. These amines were converted into their *N*-hydroxysuccinimidyl fluorescein-*O*-acetate (SIFA) derivatives and measured by micellar electrokinetic capillary chromatography with laser-induced fluorescence detection. The derivatization conditions and separation parameters for the aliphatic amines were optimized in detail. The SIFA-labeled amines were fully separated within 8.5 min using 25 mM pH 9.6 boric acid electrolyte containing 60 mM sodium dodecyl sulfate (SDS). The parameters of validation such as linearity of response, precision and detection limits were determined. The detection limits were obtained in the range from 0.02 to 0.1 nM, which was the lowest value reported by CE methods. The developed method was successfully employed to monitor aliphatic amines in serum and cells samples. After comparison of other CE methods using different fluorescent probes, the present method represents a powerful tool for the trace determination of aliphatic amines in complex biological samples.

© 2008 Elsevier B.V. All rights reserved.

1. Introduction

Short-chain aliphatic amines like methylamine (MA), ethylamine (EA), *n*-propylamine (PrA), *n*-butylamine (BA), *n*-pentylamine (PA), are industrial important chemicals with a wide range of applications. They are used as raw materials or as chemical intermediates in the production of pharmaceuticals, pesticides, polymers, detonator, dyestuffs, emulsifier, rubber products and corrosion inhibitors [1–3]. As we all know, these amines not only have unpleasant smell but also possess hazards, because they are strongly irritant to eye, nose, skin, mucous membranes and respiratory tract, and some are precursors of *N*-nitrosamines, which are carcinogenic substances [4,5]. In addition, most aliphatic amines are common components of biological systems as biodegradation products of organic mater such as proteins, amino acids, and other nitrogen-containing compounds [6,7]. Thus, these amines also exist in biological samples besides in foods and environmental samples. Consequently, the accurate determination of aliphatic

amines at trace levels is highly significant for toxicology, clinical chemistry, environment science, food quality, biomedical research, and so on.

Until now, many analytical methods have been developed to determine aliphatic amines mostly involving spectrofluorimetry [8,9], thin-layer chromatography [10,11], gas chromatography [12–14], and high performance liquid chromatography (HPLC) [15–18]. However, these methods usually have limitations such as low sensitivity, ghosting peaks, long analytical time, complex extraction process, and relatively large sample volume of requirement [18–20]. In recently years, capillary electrophoresis (CE) has become a popular analytical tool because both electric field and chemical equilibria are used in the separation process. Thus, the separation of CE relies on mobility differences between the analytes interaction with additives [21]. On the other hand, laser-induced fluorescence (LIF) detection is one of the most sensitive detection techniques in CE, which is capable of achieving the concentration detection limits below 10^{-13} M and the mass detection limits less than 10 molecules [22,23]. Due to the advantages of high sensitivity, rapid resolution, high separation efficiency and small sample size, CE-LIF system has been demonstrated to be powerful for the determination of low-concentration aliphatic amines in biological samples.

* Corresponding author. Tel.: +86 27 87218924; fax: +86 27 68754067.
E-mail address: hshzhang@whu.edu.cn (H.-S. Zhang).

However, aliphatic amines are rather insensitive towards LIF detector owing to the absence of chromophores in most of them. For this reason, chemical derivatization prior to analysis by CE-LIF is necessary to transform the aliphatic amines into derivatives that can be more easily isolated, resolved and detected. This leads to the appearance of many derivatization reagents in CE methods, e.g., *o*-phthalaldehyde (OPA) [24], fluorescein isothiocyanate (FITC) [25,26], naphthalene-2,3-dicarboxaldehyde (NDA) [27] and 6-oxy-(*N*-succinimidyl acetate)-9-(2'-methoxycarbonyl) fluorescein (SAMF) [20]. The proposed method used OPA as a labeling reagent for aliphatic amines is not applied to the detection of them in real samples [24]. The other CE methods available using derivatization with FITC, NDA and SAMF are applied to the determination of aliphatic amines in foods and environmental samples such as water, atmospheric aerosol and beers. While in biological samples, as far as we know, no studies have been published in the literature on the application of CE to the determination of aliphatic amines.

N-Hydroxysuccinimidyl fluorescein-*O*-acetate (SIFA) was synthesized in our laboratory for amine labeling [28]. Because of its high fluorescence quantum efficiency, fast labeling reaction, mild derivatization conditions and few side products, SIFA has been successfully used for the analysis of a series of amino compounds with HPLC and CE in our previous research [28–33]. The aim of this work was to establish a sensitive and selective method for the trace determination of short-chain aliphatic amines using SIFA as a labeling reagent with CE-LIF in biological samples. This work deals with the optimization conditions of CE separation and chemical derivatization. Under the optimized conditions, five labeled aliphatic amines can be well separated within 8.5 min. Using the proposed CE-LIF method, aliphatic amines in human prostate carcinoma DU-145 cells, serum of healthy volunteer and hypertension patient were quantified with satisfactory recoveries varying from 93.5 to 103.5%. To the best of our knowledge, this is the first time to determine aliphatic amines in biological samples by CE-LIF system.

2. Experimental

2.1. Instrumentation

CE experiments were carried out on a P/ACE MDQ Capillary Electrophoresis System (Beckman–Fullerton, CA, USA) with an LIF detector and a photo DAD (190–600 nm). An argon ion laser (3 mW) was used as excitation source (488 nm) and the electropherograms were recorded by monitoring the emission intensity at 520 nm. The DAD was set at 235 nm for the electroosmotic flow (EOF) marker, thiourea. Electrophoretic separation was performed in an uncoated fused-silica capillary (60.2 cm, 50 cm to the detector, 75 μ m I.D., Yongnian Optic Fiber, Hebei, China) at 25 °C. Samples were introduced into the capillary from the anodic side by pressure of 0.5 psi for 5 s and the injection volume was approximately 25 nL. Separation was performed at a constant voltage of 25 kV.

New capillaries were successively preconditioned with methanol, H₂O, 0.1 M HCl, H₂O, 0.1 M NaOH and H₂O for 5, 5,

10, 5, 30, 5 min, respectively. Each day before starting the measurements, the capillary was rinsed with 0.1 M NaOH for 5 min, H₂O for 5 min, and then running buffer for 10 min using a pressure of 20 psi. Between analyses it was flushed with 0.1 M NaOH for 5 min, H₂O for 5 min, and the running buffer for 5 min.

The pH values of solutions were measured using a DELTA 320 pH meter (Mettler-Toledo, Shanghai, China). The biological samples were treated using a refrigerated centrifuge (Mikro 22R, Hettich, Germany).

2.2. Chemicals and reagents

All the chemicals were of analytical reagent grade, unless specially stated otherwise. SIFA was synthesized in our laboratory and a 3×10^{-2} M solution was prepared in anhydrous acetonitrile. Methylamine, ethylamine, *n*-propylamine, *n*-butylamine, *n*-pentylamine, *n*-hexylamine (HA), thiourea and all amino acids were purchased from Shanghai Chemicals Company (Shanghai, China). Sodium dodecyl sulfate (SDS) and histamine were obtained from Sigma (St. Louis, MO, USA). Spermine, spermidine and putrescine, in the form of hydrochloride salts, were obtained from Acros Organics (Belgium).

All aqueous solutions were prepared from deionized water purified with a Milli-Q system (Millipore, Bedford, MA, USA). Stock solution of aliphatic amines was prepared in water at a concentration of 1×10^{-3} M and diluted sequentially to the required concentration when used. The running buffer was prepared by dissolving certain concentrations boric acid and SDS into deionized water and the pH of the solution was adjusted by dropwise adding 0.1 M NaOH. Before used, the buffer solutions were filtered through 0.22 μ m membrane filters and degassed in an ultrasonic bath for 1 min. PBS consisted of 8.0 g/L NaCl, 0.2 g/L KCl, 2.88 g/L Na₂HPO₄ and 0.2 g/L K₂HPO₄, and the pH was adjusted to 7.4 by adding 0.1 M HCl.

2.3. Derivatization procedure

The chemical structure of SIFA and its reaction with aliphatic amines are shown in Fig. 1. The derivatization procedure is similar to our previous works [27,28,32]. To the standard solution containing appropriate amount of aliphatic amines, 50 μ L of boric acid buffer (pH 8.5) and 10 μ L of 3×10^{-2} M SIFA solution were added, and the total volume was diluted to 1 mL with deionized water. Then, the mixture was homogenized and incubated at 45 °C for 30 min.

2.4. Sample preparation

Human blood samples were collected from healthy volunteer and hypertension patient treated at the Hospital of Wuchang Shipyard Workers. All the blood samples were obtained by venipuncture and centrifuged at 10,000 rpm for 10 min after standing for 2 h at room temperature. The obtained sera were stored at –35 °C until analysis. When use, the serum sample was thawed and

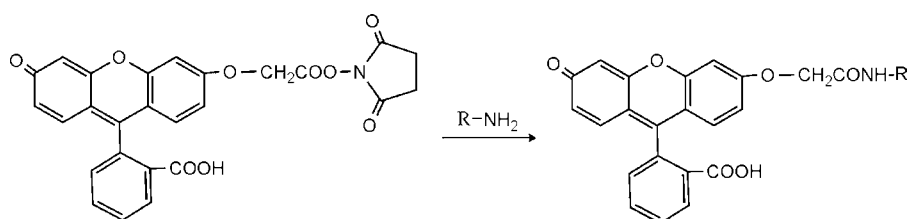


Fig. 1. The reaction of SIFA with aliphatic amines.

deproteinized by adding 150 μL of acetonitrile to 100 μL sample. After vigorously shaking for 2 min, the mixture was centrifuged at 10,000 rpm for 8 min at 4 °C. Aliquots of the supernatant were used for the derivatization as described above.

The human prostate carcinoma DU-145 cells were generously provided by Min Xie (Department of Chemistry, Wuhan University, Wuhan, China). The DU-145 cells were adherent on the wall. Before analysis, the growth medium was spilled and roughly 2×10^6 DU-145 cells were left on the wall. About 1 mL of 0.25% trypsin-EDTA solution was added to the flask and placed in the bioculture box for 1 min to digest the cells. Then, about 2×10^5 DU-145 cells were collected by centrifugation at approximately 1000 rpm for 5 min at room temperature. Subsequently, the cells were washed three times with cold PBS buffer and resuspended in 0.1 mL of water. The mixture was ultrasonic vibrated for 5 min to lyse the cells and then was centrifuged at 5000 rpm for 10 min. The supernatant was collected and an equal volume of chloroform was added, mixed, and shaken vigorously to precipitate proteins. After centrifugation at 10,000 rpm for 15 min, the supernatants were derivatized according to the same procedure as mentioned above to determine aliphatic amines.

3. Results and discussion

3.1. Optimization of CE separation conditions

Taking into account of the size of the derivatization agent compared to those of the analyzed amines, it is obvious that all the considered amines – SIFA would have the same electrophoretic mobility (the same ratio charge/size) and thus any separation in capillary zone electrophoresis was doomed to failure. Consequently, micellar electrokinetic capillary chromatography (MEKC), which involves the use of charged micelles to separate uncharged and charged molecules by means of a micellar pseudo-phase that is created through hydrophobic interactions between molecules and surfactant, was employed in this experiment. Various separation variables including background electrolyte (BGE) and applied voltage were optimized in order to ensure good sensitivity and selectivity.

3.1.1. The effect of surfactant concentration

In MEKC separation, the concentration of surfactant added in the running buffer plays a key role in amelioration of separation resolution. The most popular anionic surfactant for MEKC is SDS. So, the effect of SDS concentration on resolution was first examined in this study. It was found that the labeled MA migrated together with the hydrolysate of SIFA (fluorescein-*O*-acetic acid, FOAA) when the concentration of SDS was equal to or less than 50 mM (see Fig. 2A). With the increase of SDS concentration, the separation selectivity was improved. As demonstrated in Fig. 2B, the complete resolution of the five derivatives was achieved with 60 mM SDS. Further increasing the SDS concentration did not improve resolution significantly but resulted in excessively long migration times. Accordingly, 60 mM concentration of SDS was adopted for further investigation.

3.1.2. The influence of buffer concentration

The ionic strength of running buffer is a significant factor for CE separation. In this work, boric acid buffer was chosen as BGE because it provides much smaller current and smoother baseline than borate buffer when the electrolytes are at the same concentration and pH value. To explore different buffer conditions, boric acid buffer at 15, 20, 25, 30, and 40 mM were evaluated with 60 mM SDS. As the buffer concentration increased, improvement of the separation of aliphatic amines was observed due to the decrease of EOF.

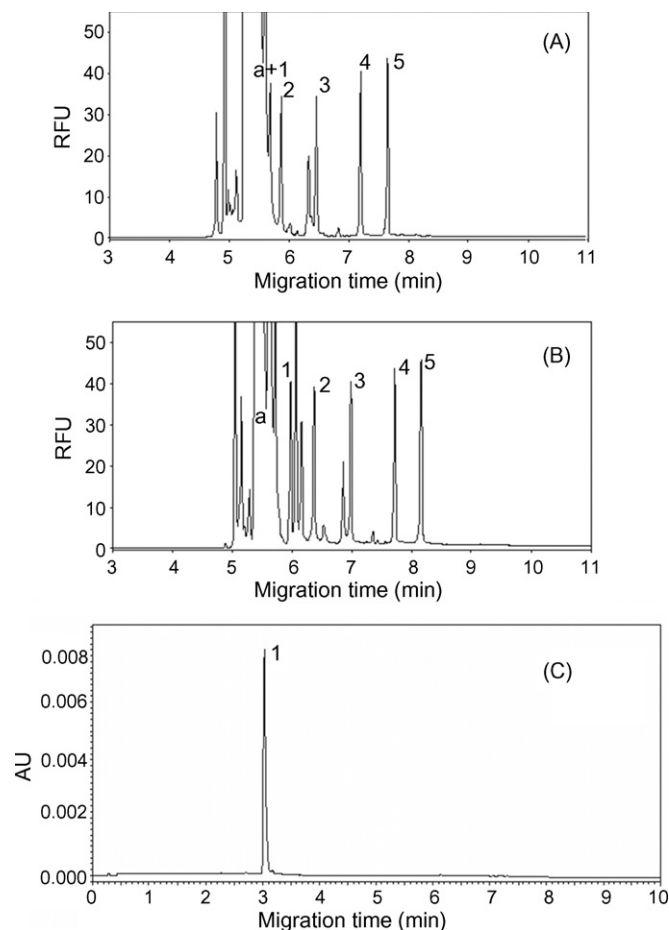


Fig. 2. Electropherograms obtained for separation of SIFA labeled aliphatic amines with different running buffer and electropherogram of the EOF marker, thiourea. (A) Peaks: (a) FOAA, (1) SIFA-MA; (2) SIFA-EA; (3) SIFA-PrA; (4) SIFA-BA; (5) SIFA-PA; running buffer: 25 mM H_3BO_3 , 50 mM SDS, pH 9.6; voltage: 25 kV; capillary temperature: 25 °C; injection 5 s at 34.5 mbar. Amine concentration: 1 μM ; (B) peaks as in (A), running buffer: 25 mM H_3BO_3 , 60 mM SDS, pH 9.6; other conditions as in (A). (C) Peaks: (1) Thiourea. Detection: DAD, 235 nm. Marker concentration: 1 mM. Other conditions as in (B).

When the concentration of boric acid buffer reached 25 mM, SIFA labeled aliphatic amines were fully separated in relatively short time. Nevertheless, higher concentrations could result in tedious analysis time. Considering both the resolution and the analysis time, 25 mM boric acid was chosen as the optimum buffer concentration.

3.1.3. The effect of buffer pH

pH value of running buffer, which can influence the mobility of analytes by adjusting the velocity of EOF and the charges of analytes, has been regarded as one of the most important parameters for CE separation. The effect of pH values of boric acid electrolyte on the separation was also investigated. It was found that the peak of labeled EA was not baseline separated with an unwanted peak when pH value was less than 9.4. The satisfactory resolution of the five amines can be achieved at pH 9.6 as well as 9.8 and 10.2. But the migration times were prolonged and the derivative peaks became worse, when higher pH values were employed. Based on the results, pH 9.6 boric acid electrolyte was used in this experiment.

3.1.4. Effect of other separation parameters

Other separation parameters such as sample injection, separation voltage and capillary temperature were further optimized.

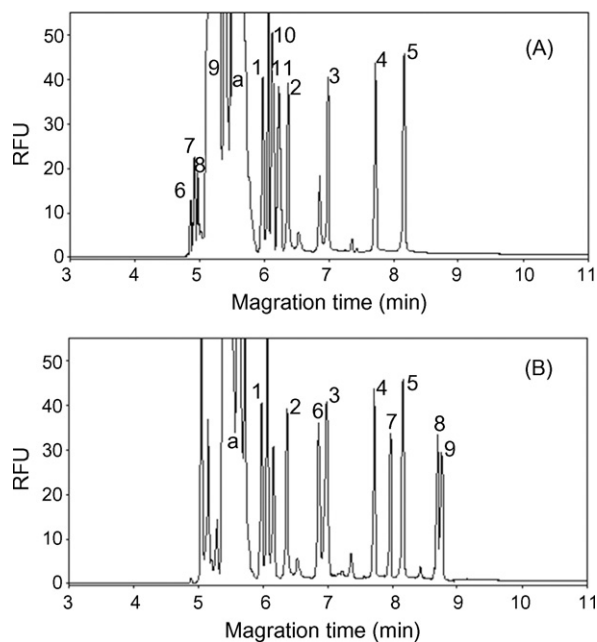


Fig. 3. Electropherograms of the separation of SIFA labeled aliphatic amines in the presence of other amino compound. Peaks 1–5 and electrophoretic conditions were the same in Fig. 2B. (A) Peaks: (6) Lysine; (7) Histidine; (8) Arginine; (9) all neutral amino acids; (10) Glutamate; (11) Aspartate. (B) Peaks: (6) Histamine; (7) Putrescine; (8) Spermine; (9) Spermidine.

After compared pressure and electrokinetic injection mode, pressure injection mode was chosen in this study. Increasing voltage could speed up separation and improve selectivity until it reached 25 kV. Optimization of the capillary temperature led to the selection of 25 °C.

In summary, 25 mM H₃BO₃ (pH 9.6) containing 60 mM SDS was used for the best separation. The voltage applied was 25 kV, and the capillary temperature selected was 25 °C. Under the optimized conditions, the five SIFA tagged aliphatic amines were completely resolved within 8.5 min in the order of MA, EA, PrA, BA and PA, as shown in Fig. 2B. Moreover, Fig. 2C shows the EOF marker, thiourea, using a DAD at 235 nm under the above-mentioned separation conditions.

3.2. Selectivity of the method

Because SIFA can react with amino acids that usually exist in biological samples, their existence may interfere with the determination of aliphatic amines. In order to assess the selectivity of the developed method toward the five short-chain aliphatic amines, a mixture of common amino acids was analyzed under the optimized conditions. As shown in Fig. 3A, the migration time of alkaline and

neutral amino acid derivatives were much shorter than those of the aliphatic amines, and the two acidic amino acids (glutamate and aspartate) migrated between MA and EA. Furthermore, since spermine, spermidine, putrescine and histamine have been detected in cell samples [34–36], the interference from these biogenic amines was also investigated under the above chosen conditions (Fig. 3B). The migration time of labeled spermine and spermidine was found to be longer than that of PA. Putrescine migrated between BA and PA, and histamine eluted between EA and PrA. Therefore, the peaks of amino acids and biogenic amines did not co-migrate with the targets of interest and did not make any interference. That is to say, the proposed method provided high selectivity toward the five short-chain aliphatic amines and allowed their quantitative determination in biological samples.

3.3. Analytical calibration

The linearity of the present method was determined by analyzing standard solutions of five aliphatic amines containing known concentrations ranging from 2×10^{-9} to 2×10^{-6} M under the optimum separation and derivatization conditions. The corresponding calibration curves were constructed by plotting the peak area against the analyte concentration. The results are listed in Table 1. The correlation coefficients for each aliphatic amine were from 0.9985 to 0.9997, which indicated good linearity over three magnitude orders.

In order to ensure the reproducibility of the method, the capillary should be washed with NaOH, water, and running buffer between each run, since this washing process can effectively eliminate the adsorption of analytes onto the capillary wall. The reproducibility of the method was evaluated with six sequential runs of derivatized standard amine solution. Table 1 also shows inter-day and intra-day repeatability in terms of relative standard deviation (RSD) in migration time and peak area. RSD for migration time was excellent for both intra-day ($\leq 0.75\%$) and inter-day ($\leq 1.95\%$). Fairly good intra-day ($\leq 1.42\%$) and inter-day ($\leq 4.26\%$) reproducibility for peak area was achieved.

The limits of detection (LOD) were taken as concentration that gave a signal to noise ratio of 3. The LOD for the aliphatic amines was between 0.02 and 0.1 nM, which was lower than LOD obtained from the previously reported CE method [20,24–27].

3.4. Determination of aliphatic amines in biological samples

The present method was used to determine aliphatic amines in serum of hypertension patient and healthy volunteer, as well as human prostate carcinoma DU-145 cells. Fig. 4 illustrates the typical electropherograms of the biological samples. In order to identify the peak of aliphatic amines, standard addition approach was employed as shown Fig. 4. The analytical results of samples are summarized in Table 2. As seen in the table, some amounts of

Table 1
Calibration range, regression equation, correlation coefficients, RSDs, and LOD

Analyte	Calibration range (μM)	Regression equation ^a	<i>r</i>	RSD (%; <i>n</i> = 6) ^b				LOD (nM)
				Intra-day		Inter-day		
				MT	PA	MT	PA	
MA	0.002–2	$y = (7.46 \pm 0.03) \times 10^6 x + (8.77 \pm 0.3) \times 10^4$	0.9995	0.35	1.01	0.37	2.27	0.02
EA	0.002–1	$y = (6.09 \pm 0.02) \times 10^6 x + (5.17 \pm 0.1) \times 10^3$	0.9985	0.75	1.42	1.95	4.26	0.1
PrA	0.006–2	$y = (7.19 \pm 0.01) \times 10^6 x - (3.97 \pm 0.08) \times 10^4$	0.9993	0.74	0.54	0.76	1.26	0.1
BA	0.002–2	$y = (8.56 \pm 0.04) \times 10^6 x + (5.41 \pm 0.2) \times 10^4$	0.9994	0.68	1.17	0.70	1.25	0.04
PA	0.005–1	$y = (8.28 \pm 0.03) \times 10^6 x - (3.44 \pm 0.09) \times 10^4$	0.9997	0.72	0.80	1.78	2.14	0.05

^a *x*, concentration of aliphatic amines (μM); *y*, peak area of aliphatic amine derivatives in electropherogram.

^b MT, migration time; PA, peak area.

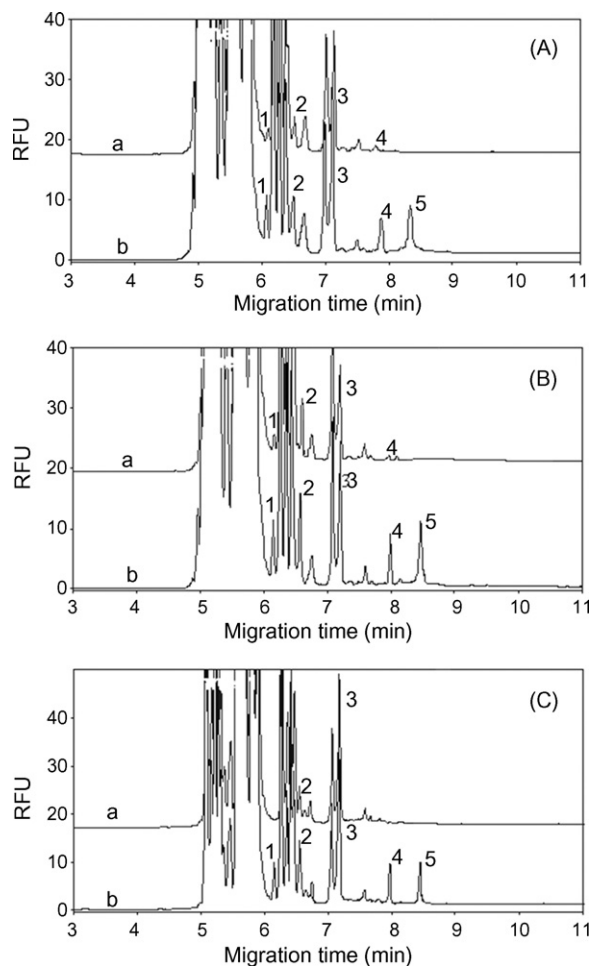


Fig. 4. Electropherograms obtained from three samples. (A) are serum of hypertension patient, (B) are serum of healthy volunteer, (C) are Du-145 cell. (a) the sample, (b) the same sample spiked with 0.2 μM of standard amines. Electrophoretic conditions and peaks were the same in Fig. 2B.

MA, EA, PrA and BA were detected in serum samples, only EA and PrA were identified in DU-145 cells. In addition, PA did not exist in all of the three samples. The recoveries ranged from 93.5% to 103.5% and the RSDs from 1.69% to 5.01%, which elucidated satisfactory recoveries and acceptable reproducibility of the developed method.

3.5. Comparison of the present method with other CE methods for the determination of aliphatic amines

Up to now, there are four derivatizing reagents used to label aliphatic amines in CE, including OPA, FITC, NDA and SAMF. The overall comparison of the present method using SIFA with other CE ones is given in Table 3. As can be seen, SIFA exhibits the lower reaction velocity than OPA, NDA and SAMF, but higher reaction velocity than FITC, which is widely used dye for amino compounds. The current method offers the shortest separation time and the highest sensitivity in all the methods summarized here. Moreover, the developed method has been successfully applied to the determination of aliphatic amines in biological samples such as serum and cells, while other CE methods have detected them in foods and environmental samples. To the best of our knowledge, this is first report on the use of CE-LIF system to determine aliphatic amines in biological samples.

Table 2
Analytical results of samples

Analytes	Serum of hypertension patient		Serum of healthy volunteer		Du-145 cells		Recovery (%; n = 5)
	Added (μM)	Found (μM)	Added (μM)	Found (μM)	Added (μM)	Found (μM)	
MA	0	0.0556	0	0.0582	0	0	101.0 \pm 1.4
	0.20	0.246	0.20	0.258	0.20	0.202	
EA	0	0.115	0	0.232	0	0.163	103.5 \pm 2.0
	0.20	0.321	0.20	0.419	0.20	0.370	
PrA	0	0.650	0	0.454	0	0.969	99.5 \pm 2.3
	0.20	0.851	0.20	0.661	0.20	1.168	
BA	0	0.0223	0	0.0267	0	0	97.5 \pm 1.2
	0.20	0.217	0.20	0.216	0.20	0.195	
PA	0	0	0	0	0	0	98.5 \pm 1.6
	0.20	0.196	0.20	0.208	0.20	0.197	

Table 3
Comparison of the present method with other CE ones

Reagent	Derivatization			Separation		Detection	LOD (nM)	Sample	Reference
	T	Time	Medium	Electrophoretic buffer	Time (min)				
SIFA	45 °C	30 min	pH 8.5 H ₃ BO ₃ buffer	25 mM H ₃ BO ₃ , 60 mM SDS, pH 9.6	8.5	Ar ⁺ LIF, 488 nm	0.02–0.1	Serum, cells	This work
SAMF	30 °C	6 min	pH 8.0 H ₃ BO ₃ buffer	25 mM H ₃ BO ₃ , 24 mM SDS 12.5% v/v CH ₃ CN, pH 9.0	15	Ar ⁺ LIF, 488 nm	0.08–0.4	Beer	[20]
OPA	r.t. ^a	2–3 min	0.1 M tetraborate	20 mM sodium tetraborate, 100 mM SDS, 5% acetonitrile, 10 mM β-CD, pH 9.0	17	He–Cd LIF, 325 nm	89–460	Standards	[24]
FITC	r.t.	16–48 h	0.3 M NaHCO ₃	30 mM H ₃ PO ₄ , 25% CH ₃ OH, pH 7.0	25	Ar ⁺ LIF, 488 nm	1	Water	[25]
FITC	21 °C	12 h	pH 8.8 NaHCO ₃	20 mM borate, 20% acetone, 5 mM DM-β-CD	9.3	Ar ⁺ LIF, 488 nm	0.9–5	Atmospheric aerosol	[26]
NDA	r.t.	0.3–2 min	pH 7.7 H ₃ PO ₄ –Na ₂ B ₄ O ₇	10 mM Tris–H ₃ PO ₄ , pH 4.0	11.3	Amperometric	51–380	Water	[27]

^a r.t.: room temperature.

4. Conclusions

The proposed CE-LIF method based on derivatization with SIFA appears to be suitable for the rapid and sensitive determination of aliphatic amines in biological samples. Optimum separation was obtained using 25 mM H₃BO₃ (pH 9.6) containing 60 mM SDS within 8.5 min. Detection limits for aliphatic amines of 0.02–0.1 nM were achieved. The efficient labeling and high quantum efficiency of SIFA offers this CE-LIF method with outstanding advantages than previous reported ones. With its simplicity, rapidity, low cost, high sensitivity and good specificity, this approach displays great potential for the trace determination of aliphatic amines in complex biological samples.

Acknowledgments

This work was supported by the National Natural Science Foundation of China (No. 20575047, 30770550 and 20775058, Beijing, China). We express our thanks for Prof. Zhao-Rui Zeng and Dr. Min Xie's assistance (Department of Chemistry, Wuhan University, Wuhan, China).

References

- [1] J. Chodkowski, Dictionary of Chemistry WP, Warsaw, WP, Warsaw, Poland, 1995 (in Polish).
- [2] S. Meseguer-Lloret, C. Molins-Legua, P. Campins-Falco, J. Chromatogr. A 978 (2002) 59.
- [3] J. Namieśnik, A. Jastrzębska, B. Zygmont, J. Chromatogr. A 1016 (2003) 1.
- [4] H. Greim, D. Bury, H.J. Klimisch, M. Oeben-Negele, K. Ziegler-Skylakakis, Chemosphere 36 (1998) 271.
- [5] J. Verdú-Andrés, P. Campins-Falcó, R. Herráez-Hernández, Analyst 126 (2001) 1683.
- [6] M. AbalosM, J.N. Bayona, F. Ventura, Anal. Chem. 71 (1999) 3531.
- [7] M. Akyüz, Ş. Ata, J. Chromatogr. A 1129 (2006) 88.
- [8] Z.M. Siddiqi, D. Pathania, Talanta 60 (2003) 1197.
- [9] M.R. Hadjimohamadi, M.J. Chaichi, P. Biparva, K. Alizadeh, Spectrochim. Acta Part A 70 (2008) 358.
- [10] S. Bardocz, T. Karsai, P. Elodi, Chromatographia 20 (1985) 23.
- [11] L. Simon-Sarkadi, A. Kovacs, E. Mincsovcics, J. Planar Chromatogr. 10 (1997) 59.
- [12] K. Kuwata, E. Akiyama, Y. Yamazaki, H. Yamazaki, Y. Kuge, Anal. Chem. 55 (1983) 2199.
- [13] M. Kaykhaii, S. Nazari, M. Chamsaz, Talanta 65 (2005) 223.
- [14] M. Akyüz, Atmos Environ. 42 (2008) 3809.
- [15] B. Sahasrabuddhey, A. Jain, K.K. Verma, Analyst 124 (1999) 1017.
- [16] S.M. Lloret, C.M. Legua, J.V. Andrés, P.C. Falcó, J. Chromatogr. A 1035 (2004) 75.
- [17] J.-S. Li, H. Wang, L.-W. Cao, H.-S. Zhang, Talanta 69 (2006) 1190.
- [18] S. Lamba, A. Pandit, S.K. Sanghi, V.S. Gowri, A. Tiwari, V.K. Baderia, D.K. Singh, P. Nigam, Anal. Chim. Acta 614 (2008) 190.
- [19] K.-A. Da Costa, J.J. Vrbanc, S.H. Zeisel, Anal. Biochem. 187 (1990) 234.
- [20] L.-W. Cao, H. Wang, H.-S. Zhang, Electrophoresis 26 (2005) 1954.
- [21] J. Kraly, M.A. Fazal, R.M. Schoenherr, R. Bonn, M.M. Harwood, Anal. Chem. 78 (2006) 4097.
- [22] K. Swinney, D.J. Bornhop, Electrophoresis 21 (2000) 1239.
- [23] Y. Dong, H. Chen, Y. Chen, Y. Hui, X. Chen, Z. Hu, J. Sep. Sci. 29 (2006) 2049.
- [24] W. Maruszak, J. High Resol. Chromatogr. 22 (1999) 126.
- [25] W.C. Brumley, V. Kelliher, J. Liq. Chromatogr. Rel. Technol. 20 (1997) 2193.
- [26] E. Dabek-Zlotrzynska, W. Maruszak, J. Chromatogr. B 714 (1998) 77.
- [27] L.-Y. Zhang, Y.-M. Liu, Z.-L. Wang, J.-K. Cheng, Anal. Chim. Acta 508 (2004) 141.
- [28] H. Wang, J. Li, X. Liu, T.-X. Yang, H.-S. Zhang, Anal. Biochem. 281 (2000) 15.
- [29] H. Wang, J. Li, X. Liu, H.-S. Zhang, Anal. Chim. Acta 423 (2000) 77.
- [30] H. Wang, J. Li, T.-X. Yang, H.-S. Zhang, J. Chromatogr. Sci. 39 (2001) 365.
- [31] Y.-H. Deng, R.-J. Li, H.-S. Zhang, X.-L. Du, H. Wang, Anal. Chim. Acta 601 (2007) 118.
- [32] Y.-H. Deng, H.-S. Zhang, X.-L. Du, H. Wang, J. Sep. Sci. 31 (2008) 990.
- [33] Y.-H. Deng, H.-S. Zhang, H. Wang, Anal. Bioanal. Chem. 392 (2008) 231.
- [34] M. Du, V. Flanigan, Y.-F. Ma, Electrophoresis 25 (2004) 1496.
- [35] G.-S. Liu, J.-N. Chen, Y.-F. Ma, J. Chromatogr. B 805 (2004) 281.
- [36] L.-W. Cao, H. Wang, H.-S. Zhang, Electrophoresis 27 (2006) 827.



Improving the spectrophotometric determination of the alkylating activity of anticancer agents: A new insight into the mechanism of the NBP method

Karen M.E. Dierickx^a, Fabrice Journé^a, Pascal Gerbaux^b, Renato Morandini^a,
Jean-Michel Kauffmann^c, Ghanem E. Ghanem^{a,*}

^a Laboratoire d'Oncologie et Chirurgie Expérimentale (L.O.C.E.), Institut J. Bordet, Rue Héger-Bordet 1, Université Libre de Bruxelles, 1000 Bruxelles, Belgium

^b Laboratoire de Chimie Organique, Centre de Spectrométrie de Masse, Université de Mons-Hainaut, Mons, Belgium

^c Laboratoire Chimie Analytique Instrumentale et Bio-électrochimie, Institut de Pharmacie, Université Libre de Bruxelles, Bruxelles, Belgium

ARTICLE INFO

Article history:

Received 29 July 2008

Received in revised form 9 September 2008

Accepted 10 September 2008

Available online 18 September 2008

Keywords:

Modified NBP method

Bischloroethyl alkylating agents

Epstein reaction

Stability chromophore

ABSTRACT

In this paper, the mechanism of the nitrobenzylpyridine (NBP) method to measure the alkylating activity of drugs originally described by Epstein et al. [J. Epstein, R.W. Rosenthal, R.J. Ess, *Anal. Chem.* 27 (1955) 1435–1439] and modified later by others was revisited using melphalan, *m*-sarcolysin, chlorambucil, cyclophosphamide and ifosfamide. Its direct application to determine the activity of these drugs in human serum and aqueous media is described and discussed.

This method, based on the formation of a chromophore due to the reaction between the alkylating agent and NBP, was significantly improved by extracting as quickly as possible the reaction product(s) into chloroform before adding alkali to develop the color. This significantly limited the degradation by hydrolysis of the products and enhanced the yield of the end chromophore in the organic phase. The reaction time was optimized by monitoring each compound color development.

The best reaction time for each compound was selected and a higher stability of the extracted color over at least 1 h was obtained (compared to a couple of minutes in previous studies). Most interestingly, water evaporation due to heating had little or no effect on the linearity of standard curves evaluated in the micromolar concentration range. Both the sensitivity and reproducibility of the method were therefore significantly improved.

There appears to be a direct correlation between compound hydrolysis and alkylation activity; the relative reactivity is different among the compounds owing to the rate of (i) production, (ii) the relative proportions and (iii) the hydrolysis of the intermediates. A general mechanism for the nucleophilic competitive substitution is proposed.

© 2008 Elsevier B.V. All rights reserved.

1. Introduction

Alkylating agents were the first compounds identified to be useful in cancer chemotherapy. Among the routinely used today in cancer therapy are the nitrogen mustards alias (2-chloroethyl)amino group such as melphalan, chlorambucil, cyclophosphamide and ifosfamide. Once in the body, each chloroethyl side-chain undergoes an intermolecular cyclization with the release of a chloride anion. The highly reactive ethylene ammonium derivative so formed can interact with DNA mainly through the seven nitrogen atom of guanine and other residues thereby adding alkyl groups at oxygen, nitrogen, phosphorous, or sulphur atoms [1]. This interaction, called

cross-linking, prevents DNA strands from being separated for synthesis and RNA transcription. The alkylating groups are known to be temperature sensitive and undergo a rather rapid hydrolysis of the chloroethyl groups making them inactive [2].

Various analytical procedures to monitor these alkylating drugs in biological samples are described using TLC, LC or GC [3]. Although the GC methods are very sensitive, they often require a derivatization procedure with, e.g. diethyldithiocarbamic acid (DDTC), trifluoroacetic anhydride (TFAA) or esterification with diazomethane or heptafluorobutyric acid prior to analysis. The development of LC/GC coupled to MS markedly improved the selectivity and sensitivity [3].

One suitable rapid simple technique that is highly selective to determine the activity of bis(chloroethyl)containing alkylating compounds is the colorimetric NBP assay [4,5] originally designed as a semi-quantitative visualization on TLC and later adapted for quantification in aqueous and biological samples [6–9].

* Corresponding author. Tel.: +32 2 541 32 96.

E-mail addresses: karen.dierickx@bordet.be (K.M.E. Dierickx), gghanem@bordet.be (G.E. Ghanem).

The colorimetric assay employs nitrobenzyl pyridine (NBP, Epstein reagent) that acts as a substrate for the electrophilic binding of the chloroethyl group. The reaction occurs at high temperature (100 °C) and in low acidic media. A violet chromophore is obtained by adjusting the solution at a basic pH value. The original method was substantially modified by Friedman and Boger [6] as follows: (i) an acetate buffer (pH 4.6, 0.025 M) replaced the phthalate buffer (pH 4.6, 0.025 M) to improve the drug reactivity with the Epstein reagent; (ii) a heat denaturation step was applied to remove proteins before adding the Epstein reagent; (iii) NaOH replaced K₂CO₃ or triethylamine to improve the yield of the end colored chromophore; (iv) at the end of the reaction, instead of measuring directly the absorbance of the final mixture, an ethyl acetate extraction step was included to substantially increase the chromophore yield and give more reproducible blanks [6].

Others, like, e.g. Christian et al. [8], adapted the Friedman and Boger's procedure by using a higher concentration of Epstein reagent, no ethylacetate extraction and triethylamine instead of NaOH to determine cyclophosphamide in mouse plasma.

The NBP method was already used to analyse mechlorethamine [6], melphalan [10], cyphenmustine [11], chlorambucil [12], 1-(2-haloethyl)-1-nitrosoureas [7], cyclophosphamide [8] and ifosfamide [13,14]. The methods, however, suffered from the high instability of the colored end product requiring the absorbance measurement to be done within 3–5 min.

Our interest to have a reliable method for assessing the overall alkylating activity of the chloroethyl group is related to several conditions: (i) the difficulty to easily separate the hydrolyzed chloroethyl groups of many drugs even by LC; (ii) the measurement of the alkylating activity of the drug and its active metabolites; and (iii) the determination of the alkylating activity in complex media such as human serum and cell culture media.

While applying the NBP method to the determination of the overall alkylating activity of a chlorinated compound and its active metabolites, we made a series of observations that led us to revisit the procedure and propose several critical modifications in order

to: (i) optimize the different experimental conditions; (ii) markedly improve the stability of the chromophore; and (iii) improve the sensitivity and reproducibility of the drug determination in biological fluids and cell culture media.

2. Experimental

2.1. Reagents and solutions

Group 1: melphalan (Alkeran[®], GlaxoSmithKline, Belgium), chlorambucil (Sigma–Aldrich, Belgium) and meta-sarcolysin (kindly provided by PTC Pharma AG, CH) were dissolved in ethanol/0.1 M HCl (50/50; v/v) solution and further diluted in saline (0.9% NaCl, 0.154 M). Group 2: cyclophosphamide (Endoxan[®], Baxter, Belgium) and ifosfamide (Holoxan[®], Baxter, Belgium) were dissolved and diluted in saline (Table 1). Stock solutions of 5% or 10% 4-(4-nitrobenzyl)pyridine (Sigma–Aldrich, Belgium) were prepared in methanol.

2.2. Apparatus

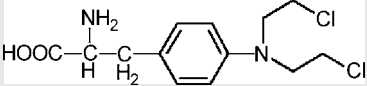
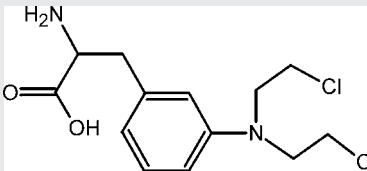
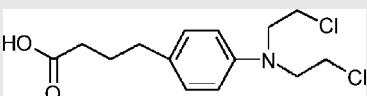
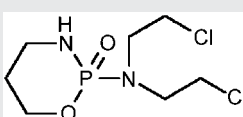
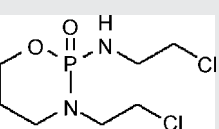
Absorbance was measured by a Beckman spectrophotometer (DU-65 Beckman, Germany). LC analysis was performed on a Gilson apparatus using a C18 column (150 mm × 4.6 mm) (Grace, Belgium). For compounds of group 1, the run was performed under acetonitrile/H₂O gradient (30–70% acetonitrile over 30 min) containing 0.01% TFA (trifluoroacetic acid). The injection volume was 20 µl and the UV detection was done at 254 nm.

2.3. Determination of the chemical alkylating activity

2.3.1. Melphalan, m-sarcolysin and chlorambucil (group 1)

One ml of the test sample containing the alkylating agent or blank in saline, 0.2 M acetate buffer pH 5.0 and/or diluted serum was incubated in a dry oven pre-heated at 100 °C for 30 min with a 5% (w/v) solution of 4-(4-nitrobenzyl) pyridine in sealed

Table 1
Compound structure and conditions of the NBP method used for bischloroethyl alkylating drug measurement.

Name	MW	Structure	Time, temp., λ _{max}	Chromophore extraction	Ref.
Melphalan	305.2		15 min, 85 °C, 565 nm.	Triethylamine/acetone	[10]
m-Sarcolysin	305.2		–	–	–
Chlorambucil	304.2		20 min, 56 °C, 578–594 nm.	Triethylamine/propylene glycol	[12]
Cyclophosphamide	261.1		20 min, 100 °C, 575 nm.	Triethylamine/acetone	[8]
Ifosfamide	261.1		40 min, 100 °C, 540 nm. 20 min, 100 °C, 575 nm.	Triethylamine in diethylether/acetone Triethylamine/acetone	[13] [14]

glass tubes and cooled to room temperature for 15 min. Next, 1 ml of chloroform and 1 ml of 3 M NaOH solution were successively added. After each step the samples were immediately vortexed thoroughly. Samples were let to rest for 10 min and centrifuged for 2 min at $1500 \times g$. The violet colored chloroform layer (1 ml) was removed and the associated spectra were recorded at a drug concentration of $82 \mu\text{M}$. The maximum absorbance wavelength for all compounds was 545 nm. Each experiment was performed in triplicate and a blank was subtracted from each sample.

2.3.2. Cyclophosphamide and ifosfamide (group 2)

These compounds were diluted in saline then 10% of Epstein reagent was added and the mixture heated in a dry oven at 100°C for 60 min. Subsequently, chloroform and NaOH were added and spectra were recorded at a drug concentration of 0.94 mM. The maximum absorbance wavelength for both compounds was at 545 nm. Each experiment was performed in triplicate and a blank was subtracted from each sample.

2.4. Stability studies of the chromophore

The end product stability was monitored by performing: (i) a comparison between chloroform and ethyl acetate/acetone (5:2) mixture for chromophore extraction [6]: a $82 \mu\text{M}$ solution of melphalan, *m*-sarcolysin, chlorambucil and a 0.95 mM cyclophosphamide and ifosfamide in saline were analyzed as described above and the stability of the absorbance of the organic phase was monitored over a time frame of 60 min. Results were expressed as relative absorbance to time 0. (ii) An investigation of the difference in stability of the colored chromophore by changing the sequence of addition of NaOH and chloroform. The alkylating activity of $82 \mu\text{M}$ chlorambucil and melphalan solutions was determined by adding NaOH prior to the chloroform and conversely. For practical reasons, the reaction was stopped after 15 min at 100°C instead of 30 min and the stability of the colored product was monitored over 60 min.

2.5. Determination of molar extinction coefficient, linearity, sensitivity

2.5.1. Melphalan, *m*-sarcolysin and chlorambucil

Linearity studies were realized in saline, in acetate buffer (0.2 M pH 5.0)/saline (1:1) or in a serum/saline/acetate buffer 0.2 M pH 5.0 (1:1:2) mixture spiked with each of the compounds. Concentrations of each compound ranging from 0.33 to $164 \mu\text{M}$ (0.1–50 $\mu\text{g/ml}$) were analyzed as described above to determine the alkylating activity.

2.5.2. Cyclophosphamide and ifosfamide

Concentration ranging from $10 \mu\text{M}$ to 0.94 mM for cyclophosphamide and $10 \mu\text{M}$ to 1.9 mM for ifosfamide were analyzed as described above.

The respective correlation and molar extinction coefficients, as well as detection limits, were calculated. The latter was defined as the mean value $\pm 3\text{S.D.}$ that was statistically different from the blank.

2.6. Epstein reaction rate

The reaction rate was determined by monitoring absorbance values at 545 nm over time for a given concentration and at 100°C . A $164 \mu\text{M}$ solution of chlorambucil, *m*-sarcolysin, melphalan or a 0.95 mM ifosfamide solution diluted in saline was incubated for 5, 10, 15, 30 and 60 min at 100°C in the presence of 5% (v/v) Epstein

reagent. The alkylating activity was determined as described above. The reaction rate of a 0.95 mM solution of cyclophosphamide was monitored after incubation for 5, 15, 30, 60 and 120 min at 100°C with a 10% (v/v) Epstein solution.

2.7. Hydrolysis rate of the compounds at 100°C

In order to compare the stability of the compounds at 100°C , a $164 \mu\text{M}$ solution of melphalan, *m*-sarcolysin and chlorambucil was monitored by LC as previously described [15] before and after incubation during 7 or 10 min at 100°C . Each compound was analyzed in two or three independent experiments.

The stabilities of cyclophosphamide (0.47 mM) and ifosfamide (0.95 mM) were determined by a derivatization method with DDTC described by Kaijser et al. [16]. After incubation at 100°C for 0, 10 or 30 min, 0.5 ml of the compound was mixed with 0.5 ml sodium phosphate buffer pH 8.0 and 100 μl of a 0.1 g/ml diethyldithiocarbamate (DDTC) solution (dissolved in water and filtered before use). This mixture was heated for 30 min at 70°C in a warm-bath and immediately cooled at 0°C . Then 20 μl was injected on the C18 LC column. The LC was performed under isocratic conditions with a mobile phase of acetonitrile/water 32/68 (v/v) and a flow rate of 0.750 ml/min. UV detection of the mono-derivatized and di-derivatized product was done at 280 nm. The disappearance of these derivatives was evaluated to estimate the rate of hydrolysis. Each compound was analyzed in two or three independent experiments.

3. Results

3.1. Chloroform extraction

In their reported method, Friedman et al. used an ethyl acetate/acetone (5:2) extraction. They also claimed that the absorbance readings should be performed within 2–5 min in the absence of light in order to obtain reproducible results [6]. At variance, in our modified method, using chloroform instead of acetate/acetone extraction resulted in a relatively stable absorbance between 15 and 60 min except for melphalan (Fig. 1).

The yield of the extracted chromophore was significantly higher when the extraction step was performed by first adding chloroform and then NaOH, rather than extracting the basified solution. In other words, the reaction product(s) were highly unstable in alkaline media and needed to be as quickly as possible extracted into the organic phase. This was clearly observed for chlorambucil and to a lower extent for melphalan (Fig. 2). The spectrum of the colored chloroform phase was recorded for a wavelength range between 400 and 900 nm. All compounds showed a maximum absorbance at 545 nm (Fig. 3).

3.2. Determination of linearity, precision and accuracy in saline, pH 5 acetate buffer and diluted serum

Standard curves were calculated by linear regression from serial dilution of a standard stock solution and performed in triplicates. Table 2 gives a summary of the coefficient of correlation (r^2), detection limit (DL) and the molar extinction coefficient (ϵ) for each studied compound. There was a linear relationship between the concentration of the parent compound and the measured absorbance of the chromophore(s) in the organic layer. A detection limit of $33 \mu\text{M}$ was achieved for group 1 compounds and was slightly lower in the presence of buffer. The molar extinction coefficients were different for all compounds, with chlorambucil showing the highest and *m*-sarcolysin the lowest. Group 2 compounds

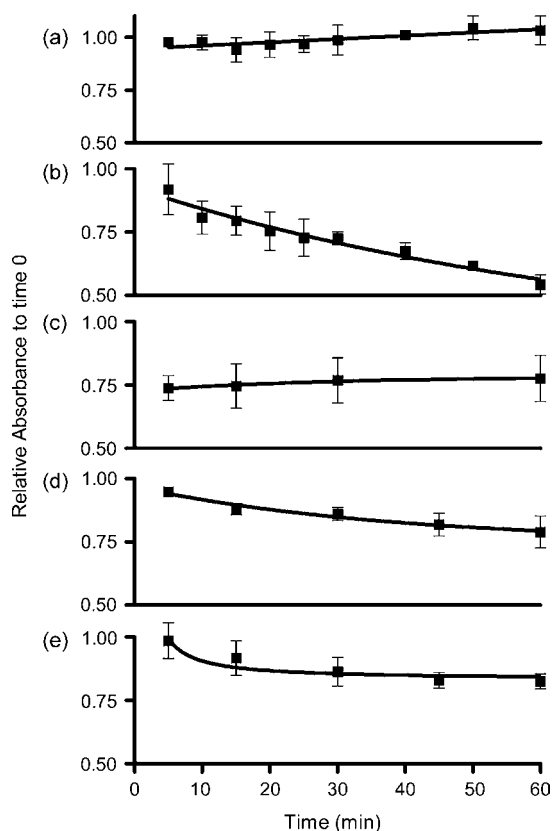


Fig. 1. Stability of the chloroform extracted chromophore of 82 μM of (a) chlorambucil, (b) melphalan, (c) *m*-sarcolysin and 0.95 mM of (d) ifosfamide and (e) cyclophosphamide. Results are expressed as relative absorbance to time zero.

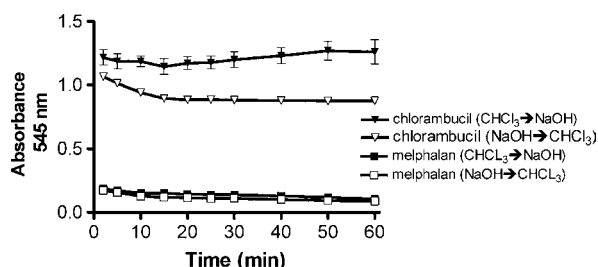


Fig. 2. Difference in colored product yield between first adding chloroform and then NaOH or conversely with 82 μM chlorambucil or melphalan (15 min reaction).

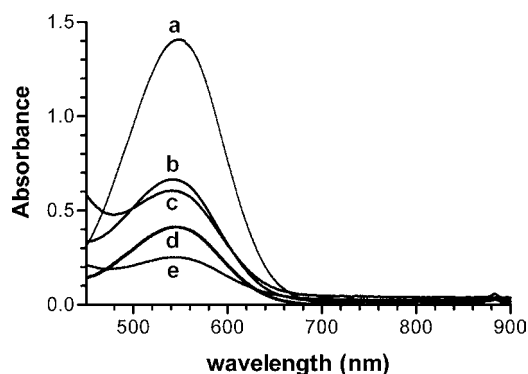


Fig. 3. Compared spectra of (a) chlorambucil, (b) cyclophosphamide, (c) ifosfamide, (d) melphalan and (e) *m*-sarcolysin chromophores in chloroform.

Table 2

Linear regression correlation coefficient (r^2), detection limit (DL) and molar extinction coefficient (ϵ) with 'relative standard deviation' (R.S.D.) of melphalan, *m*-sarcolysin and chlorambucil in saline, pH 5.0 buffer (0.2 M acetate) and acidified (acetate) serum 3:1 and of cyclophosphamide and ifosfamide in saline.

	r^2	DL (μM)	ϵ	R.S.D.
Melphalan				
Saline	0.99	33	6,002	9.6
Buffer pH 5.0	0.99	3	4,903	1.6
Acidified serum 3:1	0.98	33	3,776	7.6
<i>m</i> -Sarcolysin				
Saline	0.99	33	3,333	8.6
Buffer pH 5.0	0.99	3	3,755	6.6
Acidified Serum 3:1	0.99	33	879	18.6
Chlorambucil				
Saline	0.97	3	17,454	4.6
Buffer pH 5.0	0.99	0.3	9,129	6.3
Acidified Serum 3:1	0.98	33	5,327	2.3
Cyclophosphamide				
Saline	0.99	47	674	4.8
Ifosfamide				
Saline	0.99	38	664	5.5

had a much lower molar extinction coefficients than those of group 1.

3.3. Determination of the reaction rate with melphalan, *m*-sarcolysin, chlorambucil and ifosfamide

In accordance with the reactivity observed for chlorambucil, melphalan and *m*-sarcolysin, the reaction rate for chlorambucil was the highest followed by melphalan and *m*-sarcolysin. When monitoring the reaction at 100 °C for a 164 μM solution of each compound ($n=3$) using a 5% (v/v) Epstein solution, the reaction maximum was reached after 30 min at 100 °C. As expected, ifosfamide showed to be far less reactive towards the Epstein reagent and after 120 min the maximum was not yet reached. Even by doubling the Epstein concentration, when monitoring the reaction rate of ifosfamide (data not shown) and cyclophosphamide (Fig. 4), the reaction did not reach a maximum although the absorbance measured was doubled.

3.4. Hydrolysis of melphalan, *m*-sarcolysin and chlorambucil monitored at 100 °C by LC

Table 3 summarizes the percentage of loss, for the different compounds, by hydrolysis after 7, 10 or 30 min of incubation at 100 °C. The data confirmed that group 1 was much more sensitive to hydrolysis than group 2.

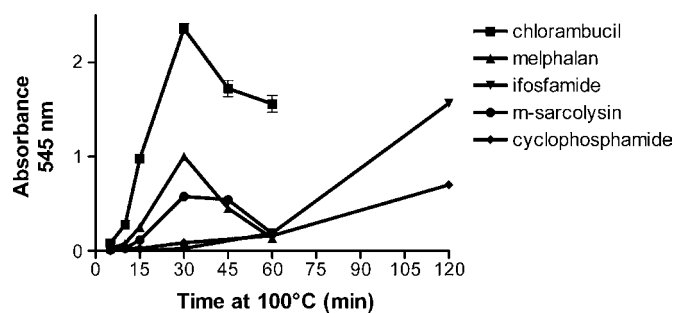


Fig. 4. Alkylating activity of melphalan, *m*-sarcolysin, chlorambucil (164 μM) and ifosfamide (0.94 mM) measured after different times of incubation at 100 °C with 5% Epstein reagent and of cyclophosphamide (0.95 mM) incubated with 10% Epstein reagent.

Table 3

Hydrolysis rate of 164 μ M melphalan, *m*-sarcolysin, chlorambucil, 0.47 mM cyclophosphamide and 0.94 mM ifosfamide at 100 °C (expressed as mean percent \pm S.D.).

Compound	7 min	10 min	30 min
Melphalan	64 \pm 20	83 \pm 5	–
<i>m</i> -Sarcolysin	50 \pm 14	90 \pm 3	–
Chlorambucil	72 \pm 10	97.2 \pm 0.4	–
Cyclophosphamide	–	0	43 \pm 2
Ifosfamide	–	0	2.4 \pm 0.6

4. Discussion

In the present study, we observed important differences in reactivity of alkylating agents towards the NBP reagent that prompted us to optimize the experimental conditions and led us to propose a complement to the known reaction mechanism. We investigated known alkylating agents namely melphalan and its isomer *m*-sarcolysin, chlorambucil, cyclophosphamide and ifosfamide.

The first examined parameter was the stability of the chromophore. Although the modified NBP-method described by Friedman and Boger [6] proved to be a very useful technique with high selectivity and low background, the high instability of the colored product required to sequentially measure the absorbance of the samples every 2–5 min in the absence of light. Our first modification was the replacement of ethyl acetate by chloroform and changing the sequence of base addition at the extraction step. This resulted in a stable color over at least 60 min and pointed out the need to minimize the residence time of the reaction product in alkaline media due to chromophore instability. This was demonstrated for, e.g. chlorambucil which gave a 22% gain in color intensity and a reasonable 60 min stability. The use of chloroform extraction had other benefits: it resulted in very low blanks and precise results, because here, a constant volume for extraction was maintained in contrast to volume reduction due to evaporation at 100 °C [4].

The different compounds gave reaction product(s) with similar absorbance maxima at 545 nm but with different molar extinction coefficients. Unlike the reference method, where each reacted

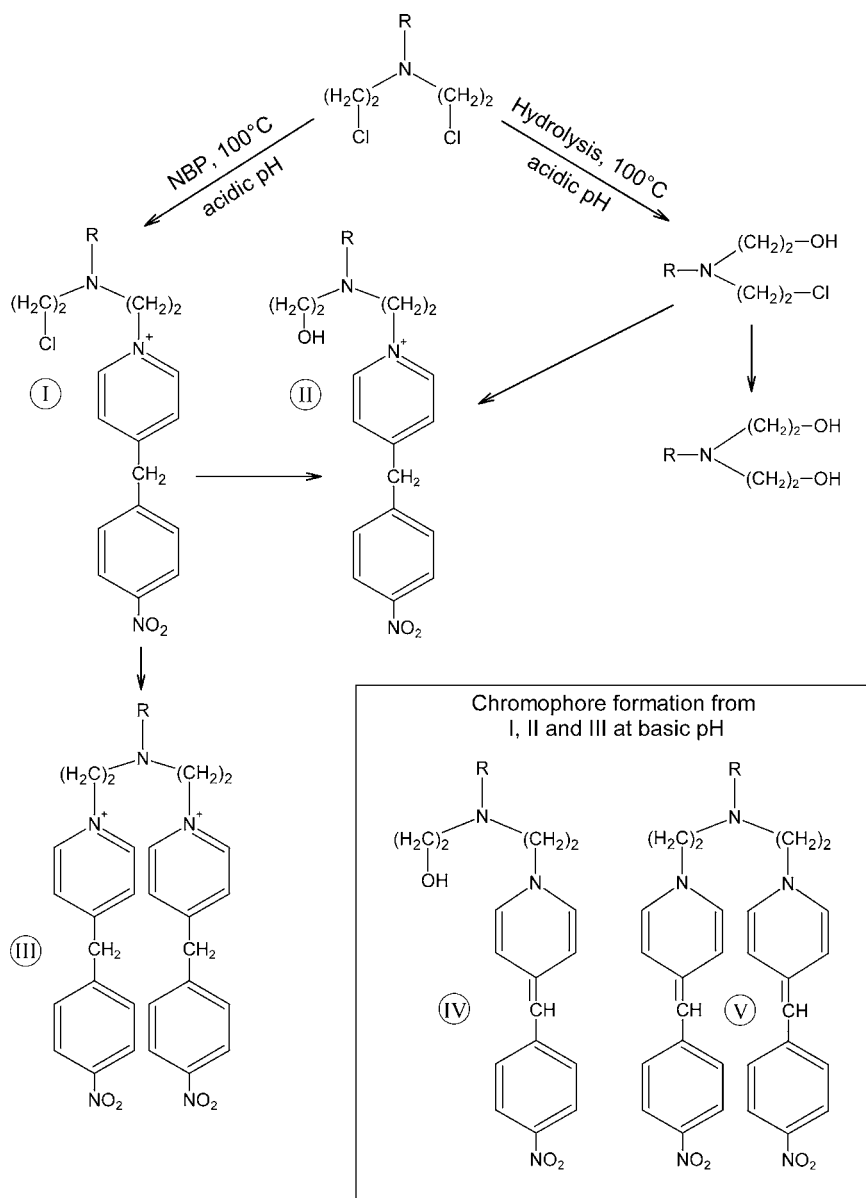


Fig. 5. Proposed mechanism for NBP method. At basic pH, two chromophores (IV and V) are formed from the three products (I–III).

compound had a different maximal wavelength, the proposed chloroform extraction most probably yielded the same chromophore(s) suggesting a better exclusion of interfering products.

On the other hand, we observed that even structurally similar compounds such as melphalan and its positional isomer *m*-sarcolysin used at the same molarities had different chromophore yields, clearly suggesting a difference in reactivity with NBP reagent. For all the studied compounds, we found different kinetics that can be divided into two groups: (group 1) melphalan, *m*-sarcolysin and chlorambucil and (group 2) cyclophosphamide and ifosfamide, with reaching the maximum yield at 30 and beyond 60 min, respectively. These data suggested a parallelism of behavior between hydrolysis and alkylating activity of the studied molecules. This prompted us to further investigate the hydrolysis of all compounds also bearing in mind that the high sensitivity to hydrolysis of the chlorine groups of such compounds, especially at high temperatures, is very well known [2]. Hydrolysis should normally reflect the relative reactivity of the compounds with NBP. In the absence of the latter, more than 80% of each of melphalan, *m*-sarcolysin and chlorambucil was hydrolyzed after 10 min at 100 °C while 43% of cyclophosphamide and only 3% of ifosfamide were hydrolyzed at 60 min.

By comparing the hydrolysis and chromophore formation kinetics, three clear conclusions can be drawn: (i) the alkylating potential of each compound towards NBP seems directly related to its hydrolysis rate; (ii) there must be a preferential competition between the two reactions favoring NBP-bound product formation; (iii) the basic pH accelerates the hydrolysis of the chromophore at least for the most reactive members of group 1. Therefore, we tentatively propose a more detailed mechanism for the overall process (Fig. 5) where a mixture of mono- or di-substituted drug can be generated. The formation of the latter was probably favored by the sustained heating. Hydrolysis of the reaction products, at least for group 1, could also occur under prolonged heating. At basic pH, two chromophores (IV and V) were formed from the three products (I–III) of group 1 since the monochlorinated product (I) was rapidly hydrolyzed. Hydrolysis of the formed chromophores could also take place that can explain the gradual disappearance of the color and their relative better stability in a non-aqueous medium. The organic phase extraction efficiency may be related to differences water solubility of the reaction products also depending on the structure of the parent drug.

With respect to the reactivity towards NBP reagent, it might be postulated that the lateral chain R of the nitrogen linked to the bischloroethyl group exerted a marked influence. The possible delocalization of the nitrogen lone electron pair into the benzyl ring of the drug compound made the nitrogen more positively charged resulting in a facilitated release of the chloride ions and higher reactivity towards the NBP reagent. Such a delocalization of the nitrogen electrons was not inferred for group 2 and the delocalization was

easier for melphalan than for the isomer *m*-sarcolysin likely due to the para-position of the alanine substituent.

In conclusion, our results support a multiparameter process that are critical for the yield and the nature of the produced chromophores: (i) the stability/hydrolysis of the chlorine atoms influenced by the charge conferred by the remaining of the molecule at a given pH; (ii) the heating duration, first favoring a mono-substituted, then a bi-substituted product followed by its hydrolysis; (iii) the stability of the chromophore formed at basic pH that can be substantially improved by chloroform extraction. The present work, in addition to improved analytical aspects, emphasizes on the distinct behavior of several alkylating compound in the Epstein reaction and proposes a more detailed reaction scheme than shown in the literature.

With some limitations, such as avoiding the use of ecotoxic chloroform and replace it, e.g. by dichloromethane, this modified NBP assay can be a useful and easy method to estimate the overall alkylating activity of bischloroethyl containing anticancer drugs in aqueous media and sera.

Acknowledgments

The authors would like to thank Yildirim S., Mersch P. and Borsu I. for their excellent technical assistance and Mrs. Angelina de Beer (Dept. of Pharmacy) for kindly providing cyclophosphamide and ifosfamide. Pascal Gerbaux is Research Associate of the Fonds National de la Recherche Scientifique (FRS-FNRS Belgium).

References

- [1] D.B. Ludlum, in: F.F. Becker (Ed.), *Cancer: A Comprehensive Treatise*, vol. 5, Plenum Press, New York, 1977, pp. 285–307.
- [2] A. Norda, U. Loos, M. Sastry, J. Goehl, W. Hohenberger, *Cancer Chemother. Pharmacol.* 43 (1) (1999) 35–42.
- [3] A. Paci, A. Rieutord, F. Brion, P. Prognon, *J. Chromatogr. B* 764 (2001) 255–287.
- [4] J. Epstein, R.W. Rosenthal, R.J. Ess, *Anal. Chem.* 27 (1955) 1435–1439.
- [5] O. Klatt, A.C. Griffin, J.S. Stehlin, *Proc. Soc. Exp. Biol. Med.* 104 (1960) 629–631.
- [6] O.M. Friedman, E. Boger, *Anal. Chem.* 33 (7) (1961) 906–910.
- [7] G. Wheeler, B.J. Bowdon, J.A. Grimsley, H. Lloyd, *Cancer Res.* 34 (1974) 194–200.
- [8] R.A. Christian, S.K. Chaffee, G.J. Hovick, W.J. Steele, *Life Sci.* 27 (1980) 2595–2599.
- [9] P.G. Penketh, K. Shyam, A.C. Sartorelli, *Anal. Biochem.* 231 (1995) 452–455.
- [10] A.K. Taha, R.A. Ahmad, D.W. Rogers, J. Pritchard, H.J. Rogers, *Cancer Chemother. Pharmacol.* 10 (1983) 212–216.
- [11] U. Sanyal, S. Bhattacharya, U. Sadhu, S. Dutta, H. Das, M. Ghosh, *Cancer Lett.* 70 (1993) 1–6.
- [12] M.I. Jesson, J.B. Johnston, E. Robotham, A. Begleiter, *Cancer Res.* 15 (49) (1989) 7031–7036.
- [13] C. Aeschlimann, A. Küpfer, H. Scheffer, T. Cerny, *Drug Metab. Dispos.* 26 (9) (1998) 883–890.
- [14] J. Ninane, R. Baurain, J. De Kraker, A. Ferster, A. Trouet, G. Cornu, *Cancer Chemother. Pharmacol.* 24 (1989) S2–S6.
- [15] K. Dierickx, R. Morandini, T.H. Nguyen, F. Salès, J.M. Kauffmann, G.E. Ghanem, *Pigment Cell Melanoma Res.* 21 (4) (2008) 439–451.
- [16] G.P. Kaijser, J.H. Beijnen, E. Rozendom, A. Bult, W.J.M. Underberg, *J. Chromatogr. B* 686 (1996) 249–255.



Determination of aminoglutethimide enantiomers in pharmaceutical formulations by capillary electrophoresis using methylated- β -cyclodextrin as a chiral selector and computational calculation for their respective inclusion complexes

Abdalla A. Elbashir^a, Fakhr Eldin O. Suliman^b, Bahruddin Saad^{a,*}, Hassan Y. Aboul-Enein^{c,**}

^a School of Chemical Sciences, Universiti Sains Malaysia, Penang 11800, Malaysia

^b Department of Chemistry, College of Science, Sultan Qaboos University, Box 36, Al Khod 123, Oman

^c Pharmaceutical and Medicinal Chemistry Department, National Research Centre, Tahrir Street, Dokki, Cairo 12311, Egypt

ARTICLE INFO

Article history:

Received 25 August 2008

Received in revised form

11 September 2008

Accepted 12 September 2008

Available online 27 September 2008

Keywords:

Aminoglutethimide

Chiral analysis

Capillary electrophoresis

Computational calculations

ABSTRACT

A capillary electrophoretic method for the separation of the aminoglutethimide (AGT) enantiomers using methylated- β -cyclodextrin (M- β -CD) as chiral selector is described. Several parameters affecting the separation were studied, including the type and concentration of chiral selector, buffer pH, voltage and temperature. Good chiral separation of the racemic mixture was achieved in less than 9 min with resolution factor $R_s = 2.1$, using a fused-silica capillary and a background electrolyte (BGE) of tris-phosphate buffer solution (50 mmol L⁻¹, pH 3.0) containing 30 mg mL⁻¹ of M- β -CD. The separation was carried out in normal polarity mode at 25 °C, 16 kV and using hydrostatic injection. Acceptable validation criteria for selectivity, linearity, precision, and accuracy/recovery were included. The proposed method was successfully applied to the assay of AGT enantiomers in pharmaceutical formulations. The computational calculations for the inclusion complexes of the R- and S-AGT-M- β -CD rationalized the reasons for the different migration times between the AGT enantiomers.

© 2008 Elsevier B.V. All rights reserved.

1. Introduction

Aminoglutethimide (\pm AGT) \pm -3-(4-aminophenyl)-3-ethyl-2,6-piperidinedione (Fig. 1) is used clinically for the treatment of hormone-dependent metastatic breast cancer [1]. This drug is marketed as a racemic mixture and it was reported that the (+)-R-isomer had the most steroidogenesis inhibitory activity (two or three times more potent than the racemate), while the (–)S-isomer had very little activity at dose levels tenfold higher [1].

High performance liquid chromatography (HPLC) methods for the direct chiral separation of AGT enantiomers in biological fluid and in bulk were reported [2–5], however these methods are time-consuming and expensive. Cesur et al. [1] have developed an indirect LC method for the determination of AGT enantiomers in tablets formulations. However the method is time consuming as it requires a derivatization step and the retention time is over

30 min. Recently Ali et al. [6] separate piperidine-2,6-dione analogues on Chiralpak IA and Chiralpak IB columns by using HPLC. Enantioseparation of aminoglutethimide by high-speed counter-current chromatography using carboxymethyl- β -cyclodextrin as chiral selector was reported by Ai et al. [7].

The last two decades have witnessed the emergence of capillary electrophoresis (CE) as a powerful analytical technique for the separation of chiral compounds. This has largely been attributed to its remarkable efficiency, low consumption of sample and reagent and versatility. In CE, chiral separation is simply achieved by adding to the background electrolyte (BGE) appropriate chiral selectors, mainly cyclodextrin (CD) and their derivatives [8,9]. A survey through the literature revealed scattered reports on the chiral separation of AGT using different CE modes with various chiral selectors [10–20]. Abushoffa et al. [20] employed native cyclodextrins in single and dual systems to determine the affinity constants for AGT enantiomers. However, a full validated CE method and applications for the determination of AGT enantiomers in pharmaceutical formulations have not been reported.

Thus, the aim of this study is to develop a CE method for the separation of the enantiomers of AGT using derivatives CD as a chiral selector for the separation of the enantiomers of AGT. The

* Corresponding author.

** Corresponding author. Tel.: +20 103678948; fax: +20 233370931.

E-mail addresses: bahrud@usm.my (B. Saad), enein@gawab.com (H.Y. Aboul-Enein).

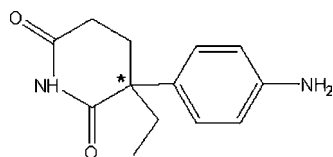


Fig. 1. Chemical structure of AGT, the asterisk indicates the chiral center.

proposed procedure was applied for the determination of AGT enantiomers in commercial tablets. Furthermore, molecular modeling techniques, using semi-empirical calculations, were used to understand the mechanism of the chiral separation by methylated- β -cyclodextrin (M- β -CD). This was performed by the analysis of the inclusion complexes of the two enantiomers with cyclodextrin using the well-known Parametric Model (PM3).

2. Experimental

2.1. Chemicals and reagents

Aminoglutethimide (AGT), (\pm)-3-(4-aminophenyl)-3-ethyl-2,6-piperidinedione and tris(hydroxymethyl)aminomethane were purchased from Sigma–Aldrich (St. Louis, USA). 2-Hydroxypropyl- β -cyclodextrin (HP- β -CD), hydroxypropyl- α -cyclodextrin (HP- α -CD), 2-hydroxypropyl- γ -cyclodextrin (HP- γ -CD) and, M- β -CD were obtained from Fluka (Buchs, Switzerland). Commercial pharmaceutical preparation in the form of tablet (claimed to contain 250 mg active ingredient) was purchased from a local drug-store. Milli-Q water was used thought the studies.

2.2. Instrumentation and electrophoretic conditions

The analysis was carried out on a Waters Capillary Ion Analyzer (Milford, MA, USA) which was interfaced to a Waters PC 800 Workstation. Uncoated fused-silica capillary (total length, 35 cm and internal diameter, 50 μ m) was used for the enantiomeric separation. The separation were carried out at 25 °C and using a voltage of 12 kV. Samples were injected hydrostatically for 25 s. Detection was achieved at 254 nm.

New uncoated fused-silica capillary was conditioned by flushing with 1 molL⁻¹ NaOH for 30 min, then 0.1 molL⁻¹ NaOH for 10 min and water and buffer each for 15 min. The running buffer consisted of 50 mmolL⁻¹ H₃PO₄ that had been adjusted to the desired pH with 1 molL⁻¹ Tris solution. The BGE was passed through 0.2 μ m cellulose nitrate membrane filter (Whatman International, Maidstone, England) and was degassed by sonication prior to use.

Prior to each analysis, the capillary column was rinsed with 0.1 molL⁻¹ NaOH for 1 min, and then purified water, followed by the BGE, each for 2 min between the runs.

2.3. Stock and standard solutions

Standard stock solution (1000 μ g mL⁻¹) of racemic AGT was prepared in water and was kept refrigerated. Working standard solutions were prepared daily by diluting suitable aliquots of the stock solution with water. The standard solutions were stored in brown glass vial to protect from light.

2.4. Pharmaceutical sample preparation

Five tablets were weighed, ground and mixed in a mortar. Appropriate amount of the powder equivalent to 50 mg of racemic AGT was taken and dissolved in 25 mL of water by ultrasonic for 3 min and diluted to 100 mL with water. The sample was filtered through

a membrane (0.22 μ m) and 1 mL of the filtrate was diluted with water to 10 mL. This solution was introduced to the CE system for the separation.

2.5. Computational methodology

The initial geometry of AGT is optimized using the PM3 (Parametric Model) level of theory. The M- β -CD structure was built on the molecular structure of the parent β -CD molecular structure that is generated on the basis of the crystallographic parameters provided by the Structural Data Base System of the Cambridge crystallographic Data center [21,22]. The inclusion complexes were constructed from the separately optimized M- β -CD and the enantiomers of AGT. The starting geometries were constructed using CS Chem 3D Ultra (Version 8.0, CambridgeSoft.com) and were fully optimized with the parametric method PM3. The coordinate system used to define the process of complexation is based on placing the glycosidic oxygen atoms of the M- β -CD onto the XY plane with their center defined as the center of the coordination system. Two different inclusion orientations were considered. In the first orientation (model A) the substituted phenyl group was docked into the narrower rim of the cyclodextrin with the bond connecting the two rings coincident with the Z-axis. While in the second orientation (model B) the substituted phenyl ring was docked into the wider rim of the cyclodextrin. Multiple starting positions were generated for both enantiomers by moving the connecting bond along the Z-axis. The relative position of the host and the guest are measured by the position of the carbon atom on the phenyl ring that is connected to the piperidinedione ring. The inclusion complexes were emulated by moving the guest molecule from 10 to -10 Å, at 1 Å intervals, and by rotating the guest from 0° to 360° at 20° intervals in the two orientations. The complexation energy ΔE_{comp} is calculated for the minimum energy structures by the following equation:

$$\Delta E_{\text{comp}} = E_{\text{comp}} - E_{\text{AMG}} - E_{\text{M-}\beta\text{-CD}} \quad (1)$$

where E_{comp} , E_{AMG} , and $E_{\text{M-}\beta\text{-CD}}$ represents the total energy of the complex, the free guest molecule and the free host molecule, respectively. The magnitude of the energy change would be an indication of the driving force towards complexation. The more negative the complexation energy change is the more thermodynamically favorable is the inclusion complex.

3. Results and discussion

3.1. Optimization of separation conditions

AGT enantiomers had been successfully separated by CE [14,20] using native CD in single and dual systems; γ -CD provided the highest selectivity [20]. In this paper, AGT enantiomers were separated using derivatized CDs, namely HP- α -CD, HP- β -CD, HP- γ -CD and M- β -CD in order to find cheap suitable chiral selector that can be used for routine work. Tris-phosphate buffer (pH 3.0) was used for preliminary studies. All the CDs used were able to separate AGT enantiomers; however M- β -CD provided the highest selectivity and was thus used for further studies.

pH is an important parameter to be optimized as it affects the ionization of the silanol group of the capillary wall, which in turn affects the magnitude of the electroosmotic flow (EOF). A successful enantioseparation of basic drugs is possible using acidic buffer conditions [23]. At lower pH, cationic drugs and their complexes migrate towards the cathode and the free CDs are uncharged and move with EOF, which is very low and directed to the anode [24]. In this study, the effect of pH on the resolution over the range 2.0–3.5,

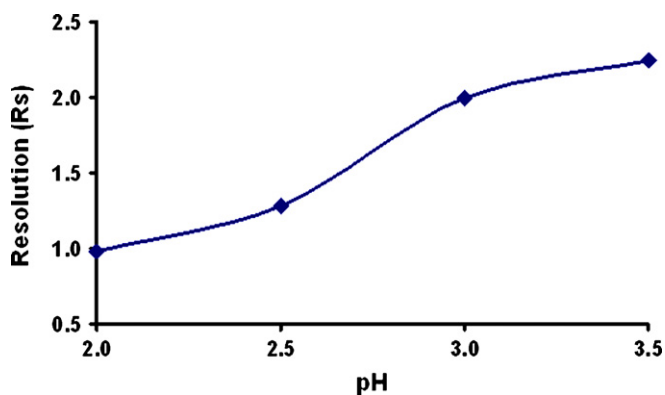


Fig. 2. Effect of pH on resolution of AGT enantiomer (buffer concentration, 50 mM; M- β -CD concentration, 30 mg mL⁻¹; temperature, 25 °C; and applied voltage, 16 kV).

using 50 mmol L⁻¹ buffer solution prepared at different pH containing 20 mg mL⁻¹ M- β -CD were investigated. The results are shown in Fig. 2.

CD concentration is an essential parameter to be optimized in chiral separations. The effects of different concentration of M- β -CD (10–40 mg mL⁻¹) on the resolution and migration times were investigated. Chiral separation was achieved for all concentrations (Fig. 3) tested. Increasing the concentration of M- β -CD causes the resolution and migration time to increase (data not shown). This is probably due to the favorable complexation with the chiral selector under these conditions. M- β -CD 30 mg mL⁻¹ was chosen as a compromise between resolution and speed of analysis.

The effect of applied voltage was also investigated, as it is known that increasing the voltage gives rise to shorter migration times [25]. However generation of Joule heat may limit the theoretical gain in the resolution and efficiency when the voltage is increased. In this study, voltages over the range 14–20 kV were investigated. Resolution with good peak shape and reasonable migration time was found when operated at 16 kV.

The influence of temperature (19–28 °C) on the peak efficiency was also studied. Best peaks were obtained when separated at 25 °C.

The selected electrophoretic conditions are summarized in Table 1. Fig. 4 shows the electropherogram corresponding to a standard solution of 50 μ g mL⁻¹ of AGT under the selected conditions. From this electropherogram, it can be ascertained that the selected electrophoretic procedure provides a good separation of AGT enantiomers ($R_s = 2.13$).

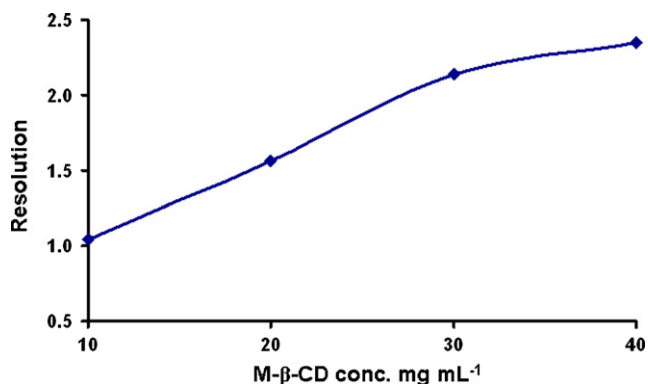


Fig. 3. Effect of M- β -CD concentration on the resolution of AGT enantiomer (buffer concentration 50 mM; temperature 25 °C, and applied voltage, 16 kV).

Table 1
Optimum CE operating conditions.

Background electrolyte	50 mmol L ⁻¹ Tris-phosphate buffer; pH 3.0; M- β -CD, 30 mg mL ⁻¹
Applied voltage	16 kV
Sample injection	Hydrostatic, 10 s
Capillary Temperature	25 °C
Fused-silica capillary	35 cm total length (27.5 cm effective length) \times 50 μ m, i.d.
Detection wavelength	254 nm

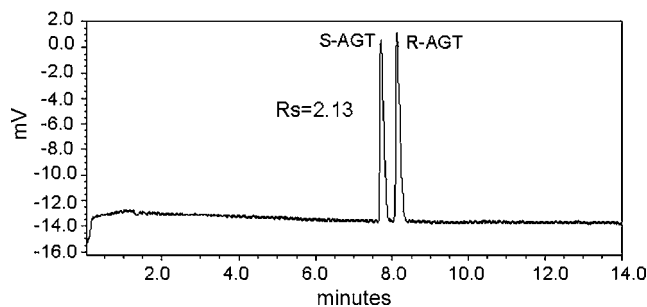


Fig. 4. Electropherogram obtained from the injection of standard racemic AGT, please refer to Table 1 for CE conditions.

3.2. Validation of the analytical methods

3.2.1. Selectivity

No interference from the formulation excipients could be observed at the migration times of the enantiomers. The S-enantiomer migrated first and this was confirmed by spiking the S-enantiomer standards.

3.2.2. Precision

Intraday precision was assessed by injecting racemic AGT standards at three different concentrations (10, 40, and 60 μ g mL⁻¹) six times. In all cases, the relative standard deviation (R.S.D.) for migration times and corrected peak area were less than 4.67 and 3.67%, respectively (Table 3). The interday precision was assessed by introducing three concentrations of the standard (10, 40, and 60 μ g mL⁻¹) six times for 3 consecutive days. In all cases, good precision as evidenced from R.S.D. for migration time and corrected peak area of less than 4.52 and 3.75%, respectively was found (Table 2).

3.2.3. Accuracy

The accuracy of the method was evaluated by conducting recovery studies on placebos. Several aliquots of the racemic AGT at three different concentrations (20, 40, and 60 μ g mL⁻¹) were added

Table 2
Within days and interday reproducibility for the repeated injection of different concentration of racemic AGT standard.

Factor conc. (μ g/mL)	R.S.D. (%)			
	Migration time		Corrected peak areas	
	S-AGT	R-AGT	S-AGT	R-AGT
Intraday precision (n = 6)				
10	3.97	4.67	3.05	3.67
40	2.48	2.57	1.06	3.28
60	1.00	1.1	2.59	1.53
Interday precision (n = 18)				
10	4.17	4.52	3.8	3.3
40	3.146	3.50	2.2	1.9
60	3.67	4.20	3.75	3.6

Table 3

Recoveries obtained from the determination of AGT in placebos that contained different levels of spiked standards.

Sample	Racemic AGT ($\mu\text{g/mL}$)	Recovery (%) (mean \pm S.D.)	
		S-AGT	R-AGT
1	20	100.64 \pm 0.65	99.28 \pm 2.5
2	40	99.51 \pm 4.8	100.33 \pm 1.21
3	60	99.92 \pm 2.0	100.89 \pm 4.33

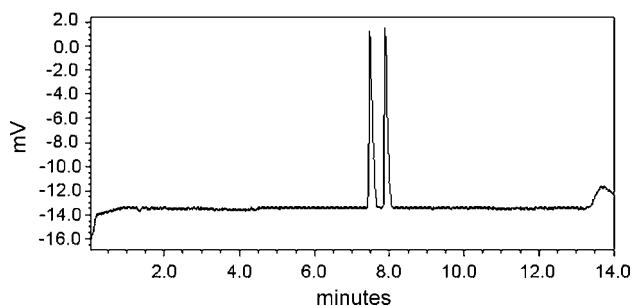


Fig. 5. Electropherogram obtained from the injection of tablet containing racemic AGT.

to an analytical placebo prepared from the excipients. The results are summarized in Table 3. Recoveries between 99.28 and 100.89% were obtained.

3.2.4. Linearity

The calibration curve was constructed by plotting the corrected peak area (y) as a function of analyte concentration (x) in $\mu\text{g mL}^{-1}$. Six standard solutions containing 10–100 $\mu\text{g mL}^{-1}$ racemic AGT were injected. The linear regression equations obtained are summarized below:

$$\text{S-AGT: } y = (67.2 \pm 1.1)x + (1396 \pm 20.72), \quad r^2 = 0.9987$$

$$\text{R-AGT: } y = (70.1 \pm 1.67)x + (1296 \pm 72.17), \quad r^2 = 0.9996$$

3.2.5. Limit of detection (LOD) and quantitation (LOQ)

The LOD of S-AGT and R-AGT enantiomers were 2.20 and 2.13 $\mu\text{g mL}^{-1}$ for both enantiomers. This was obtained by multiplying the standard deviation of AGT known concentration by 3. The LOQ, estimated by multiplying the standard deviation of AGT of known concentration by 10, were 4.25 and 4.15 $\mu\text{g mL}^{-1}$ for S-AGT and R-AGT, respectively.

3.3. Analysis of pharmaceutical formulations

The validated method was applied for the determination of AGT enantiomers in commercial pharmaceutical preparation. Results of the determinations are shown in Table 4. In all cases, good agreement between the total values as claimed by the manufacturer and the proposed CE method were obtained. Fig. 5 shows typical electropherogram of the pharmaceutical formulation.

Table 4

Analysis results for the pharmaceutical formulations containing racemic AGT.

Sample no.	Manufacturer's claim (mg)	S-AGT \pm S.D.	R-AGT \pm S.D.	Total active ingredient (mg) \pm S.D.
1	250	127.55 \pm 2.89	122.87 \pm 1.59	250.42 \pm 4.48
2	250	121.94 \pm 2.40	125.31 \pm 1.89	247.25 \pm 4.39
3	250	124.06 \pm 2.64	126.49 \pm 1.25	250.55 \pm 3.90
4	250	128.02 \pm 2.52	125.92 \pm 1.57	253.22 \pm 4.12

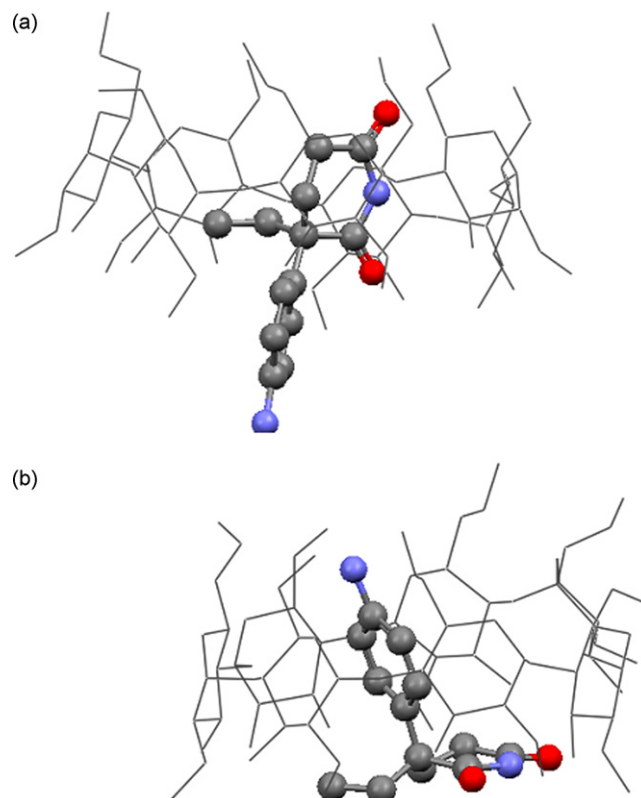


Fig. 6. Structure of R-AGT/M- β -CD complexes with the minimum energy obtained from PM3 calculations. Complexation of R-AGT through entering of the substituted phenyl group via (a) the narrow rim of M- β -CD (model A) and (b) the wider rim (model B).

3.4. Molecular modeling

The addition of cyclodextrins resulted in the separation of AGT enantiomers, with M- β -CD giving the best separation. This could be mainly due to the stronger complexation of AGT by M- β -CD. To investigate further the mechanism of separation we utilized the methods of theoretical semi-empirical calculation using PM3 level of theory. The main theoretical results obtained for the optimized geometries are shown in Table 5. The large negative binding energies upon complexation clearly indicate that the M- β -CD can form stable complexes with both S- and R-AGT. For the R-isomer it is clear from Table 5 that the complexation process is favorable for both models. The complexation energy favors, by 14.6 kJ mol^{-1} , the formation of the complex by entering of the substituted phenyl group via the wider rim of the cyclodextrin (model B) to the inclusion of the complex via the narrower rim. The optimized geometries for both models A and B of the inclusion complexes for R-AGT are shown in Fig. 6. It is obvious from Fig. 6 that the guest molecule in both models is well included in the cavity through both sides.

On the other hand complexation for the S-AGT is also favorable for both orientations. It can be seen from Fig. 7 that S-AGT pene-

Table 5
PM3 calculated parameters of M- β -CD, AGT and their complexes.

	R-AGT	S-AGT	M- β -CD	Model A		Model B	
				R-AGT/M- β -CD	S-AGT/M- β -CD	R-AGT/M- β -CD	S-AGT/M- β -CD
E (kJ/mol)	350.64	348.96	-5815.24	-5595.51	-5597.27	-5610.11	-5643.53
ΔE (kJ/mol)				-130.91	-131.00	-145.5	-168.3
HOMO-LUMO gap (eV)	7.88	8.10	12.21	8.41	8.36	8.27	8.46
Dipole moment (Debye)	19.48	20.2	1.73	13.0	16.7	12.25	10.63

trates well into the cavity of the cyclodextrin in both structures. The PM3 calculations, however, show that the inclusion of the substituted phenyl group through the wider rim (model B) is energetically more favorable by $37.39 \text{ kJ mol}^{-1}$. Interestingly, it can also be seen from Table 5 that the S-AGT inclusion complex is significantly more favorable than that of the R-AGT complex by an energy difference of 22.8 kJ mol^{-1} for model B. This indicates that S-AGT fits more tightly into the M- β -CD based on the PM3 theoretical calculations. We also observed from Fig. 6 that R-AGT tilt towards the Z-axis in model B when it enters the cyclodextrin cavity, probably to enhance the stability of the formed complex. This phenomenon was not observed for the inclusion of S-AGT in the cyclodextrin.

It has been reported that host-guest C-H...O interactions resulting from fitting small molecules in cyclodextrin cavities play an important role in the binding energies of a number of cyclodextrin inclusion complexes [21,22]. It is also reported that the C-H...O hydrogen bond energies were around $2\text{--}8 \text{ kJ mol}^{-1}$ and these energies are smaller than hydrogen bonding energies but are appreciably higher than van der Waals interactions [26,27]. Investigation of C-H...O interactions for the two inclusion complexes revealed the presence of a number of short host-guest C-H...O (distance $< 3 \text{ \AA}$) interactions. The S-isomer was found to possess more

of these short range bonds than the R-isomer. These interactions are weak but are considered as an additional force beside van der Waals forces and hydrogen bonding adding extra stability of the inclusion complexes.

It has been argued that the main contributor to the enantioselectivity is the Columbic forces, whereas van der Waals forces, the major contributor to the binding energy, govern the orientation of molecules [28]. The electrostatic factor, especially the C-H...O interactions determine the most stable inclusion complex between the chiral molecules and the cyclodextrin. Therefore, the enantiomeric separation using cyclodextrin is probably achieved via preferential electrostatic interaction of the host molecule with each of the enantiomers. The results obtained by the theoretical calculations seem to contradict the experimental results where the S-isomer is eluted first. This could be due to the fact that these calculations were performed in the gas phase and the effect of the solvent is not considered. Similar results were reported recently for the chiral separation of (+)-catechin and (-)-epicatechin [29]. It can be concluded from these calculations that the stability of the inclusion complexes between the enantiomers and the cyclodextrin are different leading to different migration times.

4. Conclusion

An easy, cost effective and rapid CE method with a simple background electrolyte and normal polarity mode have been developed and proposed for the enantioselective separation of AGT enantiomer. The use of M- β -CD as single chiral selector for the separation of S and R enantiomers offer significant advantages over previous work that uses dual chiral selector [20] and furthermore is cheaper than the use of gamma CD [14,20]. The proposed method is therefore recommended to be adopted as quality control in pharmaceutical industries. Furthermore, the computational calculations for the inclusion complexes for AGT enantiomers and M- β -CD were performed. The results of these calculations showed the difference in the stability of these complexes which lead to different migration times of the AGT enantiomers.

Acknowledgment

Financial support of the work by a Universiti Sains Malaysia Research University scheme is gratefully acknowledged.

References

- [1] N. Cesur, T. Idil Apak, H.Y. Aboul-Enein, S. Ozkirimli, *J. Pharm. Biomed. Anal.* 28 (2002) 487.
- [2] H.Y. Aboul-Enein, M.R. Islam, *J. Chromatogr. Sci.* 26 (1988) 616.
- [3] H.Y. Aboul-Enein, M.R. Islam, *Chromatographia* 30 (1990) 223.
- [4] H.Y. Aboul-Enein, M.R. Islam, in: S. Ahuja (Ed.), *Chiral Separation by Liquid Chromatography*, American Chemical Society, Washington, DC, 1991, p. 203 (Ch. 12).
- [5] H.Y. Aboul-Enein, *Arch. Pharm.* 337 (2004) 453.
- [6] I. Ali, L. Naim, A. Ghanem, H.Y. Aboul-Enein, *Talanta* 69 (2006) 1013.
- [7] P. Ai, J.C. Liu, M. Zi, Z.H. Deng, Z.H. Yan, L.M. Yuan, *Chin. Chem. Lett.* 17 (2006) 787.
- [8] R. Vespalec, P. Bocek, *Electrophoresis* 20 (1999) 2579.

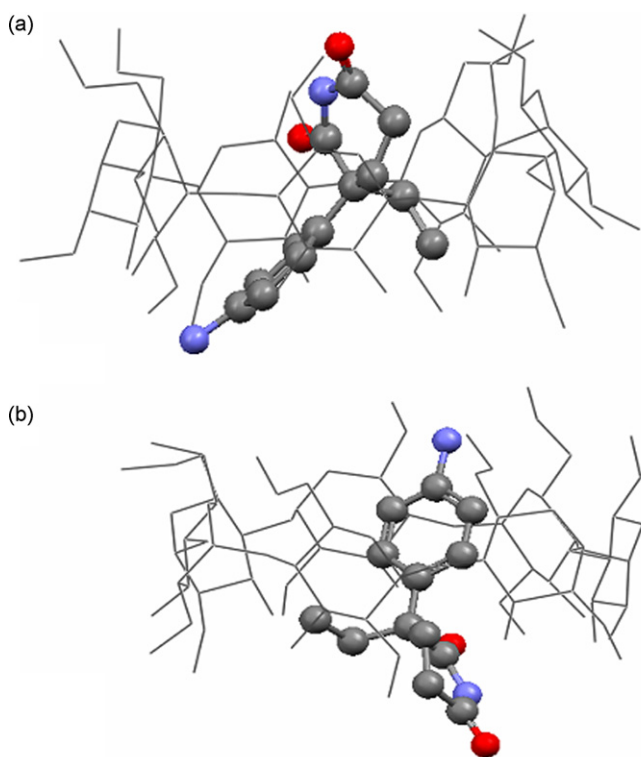


Fig. 7. Structure of S-AGT/M- β -CD complexes with the minimum energy obtained from PM3 calculations. Complexation of R-AGT through entering of the substituted phenyl group via (a) the narrow rim of M- β -CD (model A) and (b) the wider rim (model B).

- [9] B. Koppenhoefer, Z. Xiaofeng, A. Jakob, S. Wuerthner, B. Lin, J. Chromatogr. A 875 (2000) 135.
- [10] E. Francotte, S. Cherkaoui, M. Faupel, Chirality 5 (1993) 516.
- [11] V.C. Anigbogu, C.L. Copper, M. Sepaniak, J. Chromatogr. A 705 (1995) 343.
- [12] A.M. Stalcup, K.H. Gahm, Anal. Chem. 68 (1996) 1360.
- [13] M.E. Swartz, J.R. Mazzeo, E.R. Grover, P.R. Brown, H.Y. Aboul-Enein, J. Chromatogr. A 724 (1996) 307.
- [14] M. Jung, E. Francotte, J. Chromatogr. A 755 (1996) 81.
- [15] E. Francotte, M. Jung, Chromatographia 42 (1996) 521.
- [16] H. Nishi, K. Nakamura, H. Nakai, T. Sato, J. Chromatogr. A 757 (1997) 225.
- [17] D. Lee, S.A. Shamsi, Electrophoresis 23 (2002) 1314.
- [18] M. Girod, B. Chankvetadze, G. Blaschke, J. Chromatogr. A 887 (2000) 455.
- [19] L. Chankvetadze, I. Kartoziya, C. Yamamoto, B. Chankvetadze, G. Blaschke, Y. Okamoto, Electrophoresis 23 (2002) 486.
- [20] A.M. Abushoffa, M. Fillet, R.D. Marini, P. Hubert, J. Crommen, J. Sep. Sci. 26 (2003) 536.
- [21] T. Aree, N. Chaichit, Carbohydr. Res. 337 (2002) 2487.
- [22] T. Aree, N. Chaichit, Carbohydr. Res. 338 (2003) 1581.
- [23] S. Terabe, K. Otsuka, H. Nishi, J. Chromatogr. A 666 (1994) 295.
- [24] M. Fillet, I. Bechet, P. Chiap, P. Hubert, J. Crommen, J. Chromatogr. A 717 (1995) 203.
- [25] J.E. Melanson, N.E. Baryla, C.A. Lucy, TrAC-Trends Anal. Chem. 20 (2001) 365.
- [26] E. Alivera, J.I. García, J.A. Mayoral, Chem. Phys. 240 (1999) 101.
- [27] C. Yan, Z. Xiu, X. Li, C. Hao, J. Mol. Graph. Model. 26 (2007) 420.
- [28] G.R. Desiraju, Acc. Chem. Res. 29 (1996) 441.
- [29] Th. Steiner, Chem. Commun. (1997) 727.



Preparation and application of the titania sol–gel coated anodized aluminum fibers for headspace solid phase microextraction of aromatic hydrocarbons from water samples

Khalil Farhadi^{a,*}, Raheleh Tahmasebi^a, Ramin Maleki^{a,b}

^a Department of Chemistry, Faculty of Science, Urmia University, Urmia, Iran

^b Food & Chemical Analysis Research Lab., Jihad-e-Daneshgahi, Urmia, Iran

ARTICLE INFO

Article history:

Received 2 July 2008

Received in revised form 30 August 2008

Accepted 1 September 2008

Available online 13 September 2008

Keywords:

Titania sol–gel

Solid phase microextraction

Anodized aluminum

BTEX

ABSTRACT

A novel titania sol–gel coating, including tetrabutyl orthotitanat (TBOT) as initial alkoxide, tri-ethanolamine (TEA) as stabilizer, nitric acid as acid catalyst, and polyethylene glycol (PEG, 6000) as binder was prepared for the first time on an anodized aluminium wire and subsequently applied to headspace solid phase microextraction (HS-SPME) of benzene, toluene, ethylbenzene and xylenes (BTEX) with gas chromatography flame ionization detection (GC-FID). The analytical characteristics of the proposed porous titania sol–gel derived TBOT/PEG/TEA (41.6:16.0:42.4) fiber were comparable with reported fibers. The extraction temperature, extraction time, effect of salt addition, desorption temperature and desorption time were optimized. Under the optimized conditions and for all BTEX components, the linearity was from 20 to 800 $\mu\text{g L}^{-1}$, the RSD was below 8.2% and limit of detections (LODs) were between 5.4 and 14.8 $\mu\text{g L}^{-1}$. The recovery values were from 86.7% to 94.2% in water samples. The proposed HS-SPME-GC-FID method was successfully applied for the analysis of BTEX compounds from petrochemical wastewater samples.

© 2008 Elsevier B.V. All rights reserved.

1. Introduction

The volatile aromatic compounds such as benzene, toluene, ethylbenzene and xylenes (BTEX) are fuel components commonly found in ground water contamination. The determination of BTEX in aqueous is usually accomplished by chromatographic techniques and involves preliminary steps like sampling, extraction and pre-concentration [1–3]. Development and/or modifying of sample preparation techniques usually leads to more reproducible results, decreases the use of organic solvents, provides cleaner extracts for instrumental measurement and does everything more quickly and at less cost.

Solid phase microextraction (SPME) is based on the partitioning of analytes between the stationary phase on a fused silica fiber and/or on the inner surface of a capillary and the sample matrix [4]. Therefore, the key part of the SPME technique is the fiber coating and it is clear that future advancements in SPME technology would greatly depend on new developments in the areas of sorbent chemistry and coating technology.

Besides the commercially available SPME fiber, some new types of fibers such as non-polar silica particles bonded with C8, C18 [5], polydimethylsiloxane (PDMS) [6], polyacrylate (PA) [7], carbowax:template resin [8], nafion perfluorinated resin [9], polyimide [10], polypyrrole [11], molecularly imprinted polymer (MIP) [12], poly(3-methylthiophene) [13], activated charcoal [14], filter paper [15], inorganic carbopack [16], gold [17], anodized aluminum wire [18], pencil lead [19], alkyldiol-silica [20] and polyvinyl chloride (PVC) [21,22] have also been developed by several research groups. However, in the most of these fibers the lack of proper chemical bonding between the coated compound and fiber surface may be responsible for the low thermal, chemical stability and short lifetime. Sol–gel coating technology has solved these problems [23–26] and has been used for the preparation of some SPME fibers with high thermal stability in development of methodology for volatile and semi-volatile organic compounds analysis [27–30]. The sol–gel process usually involves catalytic hydrolysis of the alkoxide precursors and polycondensation of the hydrolyzed products and other sol–gel active components present in the sol solution to form a macromolecular network structure of sol–gel materials [31,32]. On the other hand, due to the fragility of fused silica, commonly used as the support for polymeric coating in SPME, the use of a metal support offers a promising alternative to silica rods beside sol–gel coating technology. To the best of our knowledge, the only report about the preparation of the microporous titania-coated alu-

* Corresponding author. Fax: +98 441 3445410.

E-mail addresses: khalil.farhadi@yahoo.com, kh.farhadi@mail.urmia.ac.ir (K. Farhadi).

mina using sol–gel technique has been described by Kermanpur et al. without analytical applications [33]. They utilized tetraethylorthotitanate (TEOT) as an initial alkoxide, diethanolamine (DEA) as a stabilizer and, polyvinyl alcohol (PVA) as a binder for the production of titania sol.

We have recently introduced PVC based SPME fibers for analysis of ethanol, methanol and acetone in human body fluids [22,34] and a titania sol–gel based SPME fiber for aromatic hydrocarbon analysis [3]. In this work, a novel titania sol–gel including tetrabutyl orthotitanate (TBOT), triethanolamine (TEA), and polyethylene glycol (PEG, 6000) was prepared for the first time and was used as a suitable coating on the anodized aluminum wires. The proposed sol–gel fiber was then applied to headspace solid phase microextraction (HS-SPME) of BTEX from water samples.

2. Experimental

2.1. Apparatus

Agilent 6890N gas chromatograph equipped with a FID detector, split/splitless injector and Chemstation software was used for this study. A Rtx-5 capillary column (60 m × 0.25 mm i.d., film thickness 0.1 μm) was utilized. A laboratory made SPME device was used in all experiments. A Leo 440i scanning electron microscope (Leo Electron Microscopy, Cambridge, England) was used for the investigation of the fiber surface.

2.2. Reagents

Benzene, toluene, ethylbenzene, xylene isomers, TBOT, and other chemicals were all from E. Merck (Darmstadt, Germany). Polyethylene glycol was purchased from Scharlau. Nitrogen and hydrogen 99.999% purity was from Roham Gas Co. (Middle East Dubai, United Arab Emirates). Aluminum wires were prepared from EMMC industrial group (Foshan City, Guangdong Province, China) and were anodized by direct current in a solution of sulfuric acid (2 mol L⁻¹) at room temperature [18]. The anodized wires were conditioned at 500 °C for 1 h.

2.3. Fiber preparation

To obtain a stable and homogeneous sol solution, different routes were carried out. The optimized route was found as follows: 1 mL of TBOT as initial alkoxide was dissolved in 5 mL of isopropanol as solvent. This solution was slowly added to a solution containing mixture of 5 mL of isopropanol and 4.3 mL deionized water under vigorous stirring in a Teflon beaker for 10 min. To this mixture, 1 mL of TEA as stabilizer and 0.4 g of PEG as binder were added and the pH of mixture was adjusted at 2 using sufficient amount of 1 mol L⁻¹ nitric acid. In the resulting solution the molar ratios of the deionized water/alkoxide, nitric acid/alkoxide, and TEA/alkoxide were adjusted 50.2, 2.3 and 1.6, respectively. The mixture was stirred at 3000 rpm for about 2 h to obtain a viscous suspension at 22 ± 1 °C.

A 1 cm length of anodized aluminum wire (total length 2 cm) was washed with acetone and placed in a laboratory-made SPME device and then it was dipped vertically into the sol–gel solution for 10 min. For each fiber, this coating process was repeated several times until the desired thickness of the coating (about 25 μm) was obtained. The proposed SPME fiber was then conditioned at 180 °C for 8 h to remove any fiber contaminations.

2.4. GC operating conditions

The initial column temperature was maintained at 40 °C for 1 min and then raised at 5 °C min⁻¹ to 70 °C and held for 5 min.

Nitrogen was used as carrier and makeup gas, which their flow rates are 1.0 and 45 mL min⁻¹, respectively. The injector and detector temperature was held at 180 and 250 °C, respectively. Injections of analytes were made in splitless mode.

2.5. Headspace sampling of BTEX from aqueous samples

Twenty milliliters of water sample was placed in a 25 mL vial containing 1.0 g NaCl, then the vial sealed with a silicone septum and solid phase microextraction from headspace of the sample was carried out at 60 °C. After 20 min, the SPME fiber was removed from the vial and was immediately inserted into the hot injection port of GC in splitless mode and stayed for 12 s. The analytes were thermally desorbed and moved through the capillary column by nitrogen as carrier gas and finally detected by FID.

3. Results and discussion

Two important reactions take place during the sol–gel processing: (1) hydrolysis of the precursor and (2) polycondensation of hydrolyzed products in the presence of suitable acid or base as a catalyst to the formation of a three-dimensional polymeric network. In this work, we used TBOT as the precursor and nitric acid as the catalyst. In our study, PEG was used for several purposes. First, selection of this polymer aimed at chemically binding the PEG stationary phase to the growing titania network at polycondensation step and also to increase in sample capacity for polar and non-polar compounds [35]. Second, in order to eliminate the crack formation and thermal stability, PEG was used to improve the adhesive strength of coating [33] and finally, the use of PEG and TEA as ingredients was caused to obtain a more porous structure and a large surface area. The proposed fiber coated on anodized aluminum was applied as SPME-HS fiber in determination of BTEX from aqueous samples. During the HS-SPME procedure, the distribution and adsorption equilibrium of the analytes must be established between the aqueous and the gaseous phase, and between the gaseous and solid phase. The equilibrium is affected by various factors, such as the extraction temperature, the identity of the analytes, the nature of the fiber, and the extraction time. The optimal experimental conditions should be investigated for each compound and for the fiber selected.

3.1. Optimization of coating composition

In sol–gel based SPME fibers, the coating composition has great influence on the extraction efficiency and selectivity. Therefore, the effect of coating compositions on extraction efficiency (to obtain better repeatability and higher sensitivity) was studied by using BTEX as model extracts. For this purpose, fibers with various compositions of coating material (weight percent) were prepared, and extraction of BTEX from gas phase was performed. The obtained results are shown in Fig. 1. As can be seen among four prepared compositions, fiber no. 2 (41.6% TBOT, 16.0 PEG, 42.4% TEA) shows maximum extraction efficiency for each compound in comparison to the other compositions. Fig. 2 represents the micrograph of the sol–gel fiber no. 2 obtained by scanning electron microscopy (SEM). As can be seen from the graph, the sol–gel coating possesses a porous structure. A high surface area will be able to provide large stationary phase loading and therefore, high extraction capacity. This behavior is probably related to the formation of a homogenous coating layer on fiber no. 2, so it was selected as optimum fiber in further experiments.

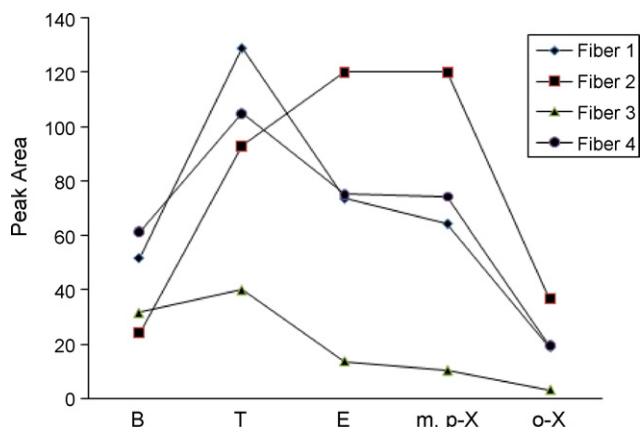


Fig. 1. Effect of sol-gel coating composition (%w/w) on BTEX extraction (fiber 1, 33.8% TBOT, 32.2 PEG, 34.0% TEA; fiber 2, 41.6% TBOT, 16.0 PEG, 42.4% TEA; fiber 3, 42.7% TBOT, 12.0 PEG, 45.3% TEA; fiber 4, 44.2% TBOT, 8.2 PEG, 47.6% TEA).

3.2. Optimization of the microextraction temperature

In headspace SPME, the use of high temperature is suitable for increasing volatility of analytes and establishing the analytes distribution equilibrium between the fiber and gaseous phase but adsorption of the analytes on the fiber is undesirable at high temperatures. However, optimization of the extraction temperature is necessary. For this purpose, extraction of BTEX was performed from 20 mL aqueous samples containing 40 ng L^{-1} of each compound at various temperatures. The obtained peak areas were plotted vs. temperature, and are presented in Fig. 3. As seen, most of components have been extracted using proposed fiber at 60°C . Therefore, 60°C was selected as a suitable experimental temperature for further studies.

3.3. Optimization of microextraction time

Exposure time of the fiber in gaseous samples is an important parameter in achieving distribution equilibrium of analytes between fiber and sample; it is a decisive factor for improving the extraction efficiency. Therefore, the proposed extraction procedure was carried out at different times, ranging from 5 to 20 min. Fig. 4 shows the plot of peak areas vs. exposure times. From these results, it was concluded that equilibrium was reached in 20 min. Thus, in

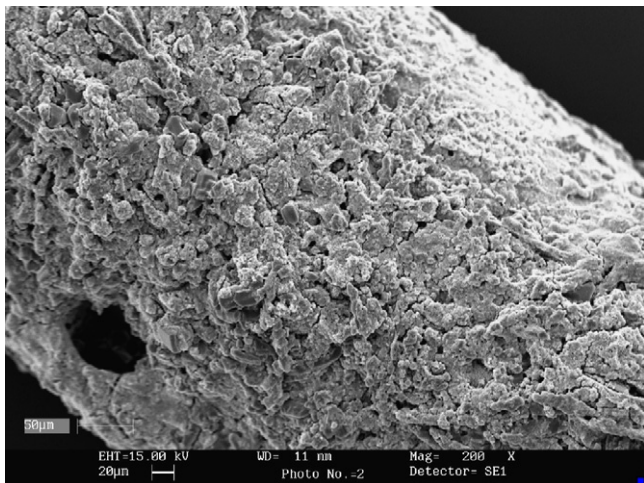


Fig. 2. Scanning electron micrograph of the sol-gel TBOT/PEG/TEA fiber.

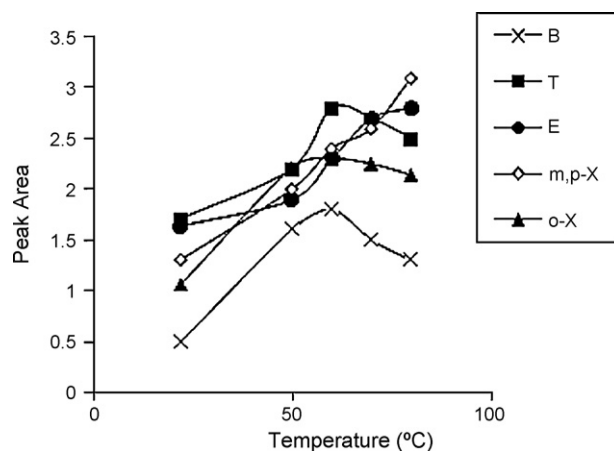


Fig. 3. Effect of temperature on the transfer of BTEX to headspace of water samples.

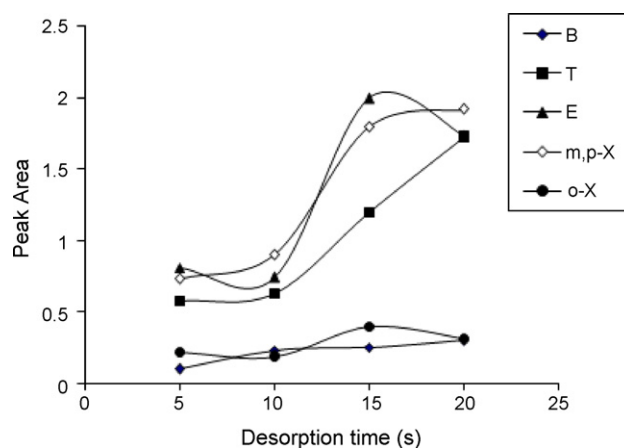


Fig. 4. Effect of time on BTEX extraction.

further extractions the fiber was exposed to headspace of sample for 20 min.

3.4. Optimization of desorption temperature and time

For optimization of desorption temperature, injections were carried out at various temperatures ranging from 100 to 200°C . As can be seen from Fig. 5, all of components are completely desorbed at 180°C , so it was selected as optimum desorption temperature. The desorption time profile is illustrated in Fig. 6. All analytes which

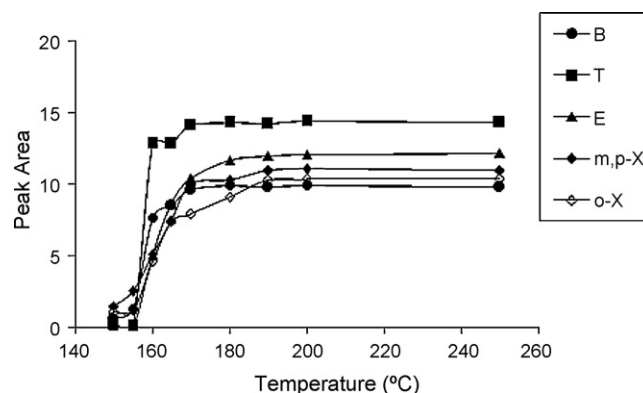


Fig. 5. Effect of desorption temperature.

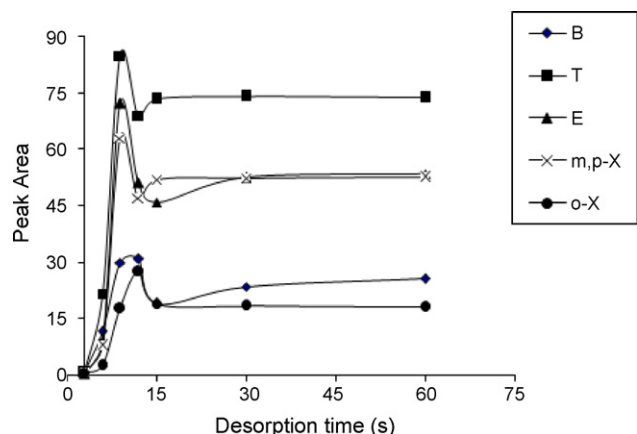


Fig. 6. Effect of time on de-sorption of the analytes from the fiber at 180 °C.

were adsorbed by the porous layer diffuse rapidly from fiber into carrier gas. As Fig. 6 shows, the time required to complete desorption process is less than 12 s for all analytes. Such short desorption equilibration times arise from the porous structure of the sol-gel TBOT/PEG/TEA fiber and result in a short analysis time as well as sharp chromatographic peaks.

3.5. Effect of salt

It is well understood that the water solubility of an organic compound is reduced by adding a salt (usually sodium chloride) to an aqueous solution of the substance. Ions of the dissolved salt attract and hold water molecules, thus make them less free to interact with the solute. This effect lowers the solubility of the solute molecules, with consequent separation or precipitation. To study the salting-out effect, the extraction is performed in the presence of different concentrations of NaCl. The results (Fig. 7) demonstrate that salting-out is most effective and 1 g NaCl (0.85 mol L⁻¹) for each vial was chosen for further studies.

3.6. Study of the microextraction efficiency and other characteristics of proposed fiber

In this case, 10 sequential extractions were performed on a single sample. The extraction efficiency of the analytes was obtained between 18.67% and 21.56% in the first extraction of BTEX compounds. It was well known that SPME is an equilibrium method and

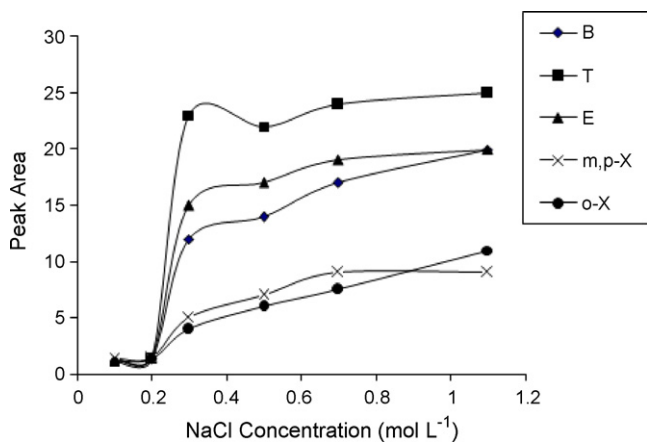


Fig. 7. Influence of NaCl concentration on microextraction efficiency of the SPME fiber.

Table 1

Quantities characteristics of the proposed method for water samples.

Compound	Calibration curve equation	R ^a	LOD ^b	LDR ^c
Benzene	Y = 12.55x + 0.07 ^d	0.995	7.2	20–800
Toluene	Y = 55.21x + 0.05	0.995	5.4	15–80
Ethylbenzene	Y = 96.81x + 0.35	0.998	6.3	10–800
o-Xylene	Y = 81.14x + 0.04	0.998	14.8	40–800
m,p-Xylene	Y = 79.03x + 0.13	0.991	8.1	20–800

^a Correlation coefficient.

^b Limit of detection (μg L⁻¹).

^c Linear dynamic range (μg L⁻¹).

^d Y and x are peak area and concentration of the analytes (μg L⁻¹), respectively.

quantitative extraction of the analytes leads to low detection limits. From the experiments above, we can see that the proposed fiber has a high extraction capacity for BTEX components. The porous coating structure significantly increases the available surface area on the fiber.

It should be mentioned that the proposed sol-gel TBOT/PEG/TEA coated on the anodized aluminium fiber shows no sign of bleeding even at the high temperature of 300 °C. Such a high operating temperature is probably related to strong adhesion of the coating to the alumina surface through chemical bonding. As another advantage, the high thermal stability of sol-gel TBOT/PEG/TEA fiber can provide efficient desorption of extracted analytes without carry over by using a high injection temperature.

3.7. Reproducibility of the proposed method

Further experiments have been performed to assess the repeatability of the method. Thus, five replicate determinations were done using a single fiber and the relative standard deviations were calculated. The obtained results showed that the RSD% of the method was less than 8.2% for all BTEX compounds, which indicates that the proposed method is repeatable. Also reproducibility studies were performed on three different fibers, and the fiber to fiber relative standard deviation was calculated 13.5 ± 2.6% for all compounds.

3.8. Quantitative characteristics of the proposed method and analytical application

To demonstrate the suitability of proposed method for the quantitative analysis of BTEX in aqueous samples, we studied the recovery of BTEX compounds from water samples. The obtained results clearly showed that the matrix effect is negligible, so quantitative characteristics of the proposed method such as calibration curve equations, correlation coefficients, limit of detection (LODs) and linear dynamic ranges (LDRs) were studied. The results are summarized in Tables 1 and 2. The linearity is ideal in the dynamic range: 20–800 μg L⁻¹ for benzene, 15–80 μg L⁻¹ for toluene, 10–800 μg L⁻¹ for ethylbenzene, 40–800 μg L⁻¹ for o-xylene and 20–800 μg L⁻¹ for m,p-xylene. For these compounds, LODs are between 5.4 and 14.8 ng mL⁻¹. The high correlation coefficients (>0.991) and low detection limits as well as wide LDRs are the other advantages of the proposed method. The analytical performance characteristics of the proposed method were summarized in Table 2 and compared with some of other reported GC-SPME methods in literature. As can be seen, the proposed method using sol-gel TBOT/PEG/TEA fiber for the determination of BTEX in this work, showed a low or similar LOD and RSD in most cases, or even superior in some cases, to the previously reported methods. Also, the proposed sol-gel fiber has a high extraction capacity toward BTEX in comparison to the reported fibers and this behavior is very remarkable.

Table 2

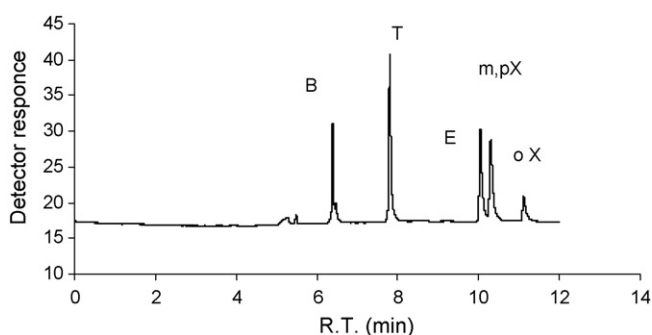
Comparison of analytical characteristics for proposed fiber with other fibers in determination of BTEX compounds.

Reference	Fiber	LDR	LOD	RSD%	Matrix
[36]	PDMS fiber from supelco	–	100 $\mu\text{g L}^{-1}$	<10%	Water
[37]	PDMS fiber and disposable ILcoated fiber	0.4–120 $\mu\text{g mL}^{-1}$	56–271 $\mu\text{g g}^{-1}$	11%<	Paints
[38]	PDMS/DVB	10–2000 $\mu\text{g L}^{-1}$	1.5 $\mu\text{g L}^{-1}$	5.4–8.3%	Aqueous sample
[39]	Lead dioxide fiber	0.1–100 $\mu\text{g L}^{-1}$	0.012 $\mu\text{g L}^{-1}$	–	Well water
[40]	Carboxen/PDMS	–	0.2–0.4 $\mu\text{g L}^{-1}$	12%	Water and air
[3]	Silica rod coated with sol–gel	100–1000 ng g^{-1}	8–20 ng g^{-1}	5–7.9%	Soil
This work	Anodized aluminum coated with titania sol–gel	10–800 $\mu\text{g L}^{-1}$	5.6–12.4 $\mu\text{g L}^{-1}$	<8.2%	Water

Table 3

Results obtained from the analysis of west water samples.

Compound	Concentration in west water sample (ng g^{-1}) ^a	RSD%
Benzene	34.2 ± 2.4	7.02
Toluene	96.5 ± 3.8	3.94
Ethylbenzene	161 ± 11	6.83
Para-xylene	199 ± 10	5.03
Meta-xylene	147 ± 12	8.2
Ortho-xylene	123 ± 9	7.3

^a Average of three replicate determinations.**Fig. 8.** A typical gas chromatogram of BTEX assay in headspace of water sample.

To evaluate the efficiency of the proposed method, it was used for BTEX analysis in Bandar Emam Petrochemical Company (IRAN) wastewater samples. The obtained results are shown in Table 3 and also a typical chromatogram is presented in Fig. 8.

4. Conclusion

A new sol–gel coated SPME fiber based on inorganic polymeric matrix (titania sol and polyethylene glycol) which is coated on anodized aluminum wire is introduced. Probably because of chemical bonding between the sol–gel TBOT/PEG/TEA and the aluminum oxide on the surface aluminum support, these sol–gel coated fibers exhibit higher thermal stability and allows the use of high-injection temperatures for efficient desorption of less-volatile analytes. The porous structure of sol–gel coating increases the surface area on the fiber, the speed of extraction and desorption steps and sample capacity. The coating exhibited a strong hydrophobic character in this work, as shown by the capability of extraction of apolar aromatic compounds, which, surprisingly, was comparable with commercial fibers. The proposed SPME fiber has a high extraction capacity and a good mechanical and thermal stability and can

be used for more than 30 samplings. It has a number of advantages such as simplifying sample preparation, preconcentration and increasing reliability.

References

- [1] R. Giampiccolo, S. Pulvirenti, M. Buratti, A. Colombi, J. Chromatogr. B 723 (1999) 105.
- [2] R. Kubinec, V.G. Berezkin, R. Górová, G. Addová, H. Mračnová, L. Soják, J. Chromatogr. B 800 (2004) 295.
- [3] K. Farhadi, M. Mamaghaniana, R. Maleki, J. Hazard. Mater. 152 (2008) 677.
- [4] J. Pawliszyn, Application of Solid Phase Microextraction, R.S.C. Chromatography Monograph, Cambridge, 1999, p. 573.
- [5] Y. Liu, Y.F. Shen, M.L. Lee, Anal. Chem. 69 (1997) 190.
- [6] A.F. Oliveira, C.B. Silveria, E. Carasek, S.D. Campos, E.A. Campos, Mater. Res. Bull. 34 (1999) 1661.
- [7] W.H.J. Vaes, C. Hamwijk, E.U. Ramos, H.J.M. Verhaar, J.L.M. Hermens, Anal. Chem. 68 (1996) 4458.
- [8] A.A. Boyd-Boland, J. Pawliszyn, Anal. Chem. 68 (1996) 1521.
- [9] T. Gerecki, P. Martos, J. Pawliszyn, Anal. Chem. 70 (1998) 19.
- [10] C.L. Arthur, J. Pawliszyn, Anal. Chem. 62 (1990) 2145.
- [11] J. Wu, W.M. Mullett, J. Pawliszyn, Anal. Chem. 74 (2002) 4855.
- [12] E.H.M. Koster, C. Crescenzi, W. Hoedt, K. Ensing, G.J. Jong, Anal. Chem. 73 (2001) 3140.
- [13] T.P. Gbatu, O. Ceylan, K.L. Sutton, J.F. Rubinson, A. Galal, A. Caruso, H.B. Mark, Anal. Commun. 36 (1999) 203.
- [14] D. Djozan, Y. Assadi, Microchem. J. 63 (1999) 276.
- [15] A.H. Ackerman, R.J. Hurtubise, Anal. Chim. Acta 474 (2002) 77.
- [16] D.W. Potter, J. Pawliszyn, Environ. Sci. Technol. 28 (1994) 298.
- [17] F. Guo, T. Gorecki, D. Irish, J. Pawliszyn, Anal. Chem. 33 (1996) 361.
- [18] D. Djozan, Y. Assadi, S.H. Haddadi, Anal. Chem. 73 (2001) 4054.
- [19] H.B. Wan, H. Chi, M.K. Wong, C.Y. Mok, Anal. Chim. Acta 298 (1994) 219.
- [20] W.M. Mullett, J. Pawliszyn, Anal. Chem. 74 (2002) 1081.
- [21] M.A. Farajzadeh, A.A. Matin, Anal. Sci. 18 (2002) 77.
- [22] R. Maleki, K. Farhadi, A.A. Matin, Anal. Sci. 22 (2006) 1253.
- [23] S.L. Chong, D. Wang, J.D. Hayes, B.W. Wilhite, A. Malik, Anal. Chem. 69 (1997) 3889.
- [24] D.X. Wang, S.L. Chong, A. Malik, Anal. Chem. 69 (1997) 4566.
- [25] S. Bigham, J. Medlar, A. Kabir, C. Shende, A. Alli, A. Malik, Anal. Chem. 74 (2002) 752.
- [26] J.D. Hayes, A. Malik, J. Chromatogr. B 695 (1997) 3.
- [27] C. Wan, P.de B. Harrington, D.M. Davis, Talanta 46 (1998) 1169.
- [28] M. Azenha, C. Malheiro, A.F. Silva, J. Chromatogr. A 1069 (2005) 235.
- [29] D. Wang, J. Xing, J. Peng, C. Wu, J. Chromatogr. A 1005 (2003) 1.
- [30] D. Budziak, E. Martendal, E. Carasek, J. Chromatogr. A 1187 (2008) 34.
- [31] J. Livage, M. Henry, C. Sanchez, J. Solid State Chem. 18 (1988) 259.
- [32] A. Malik, Electrophoresis 23 (2002) 3973.
- [33] A. Kermanpur, E. Ghassemali, S. Salemezadeh, J. Alloys Compd. 461 (2008) 331.
- [34] A.A. Matin, R. Maleki, M.A. Farajzadeh, K. Farhadi, R. Hosseinzadeh, A. Jouyban, Chromatographia 66 (2007) 383.
- [35] Z. Wang, C. Xiao, C. Wu, H. Han, J. Chromatogr. A 893 (2000) 157.
- [36] B.T.U. Isacson, J. Chromatogr. A 1137 (2006) 15.
- [37] J.F. Liu, N. Li, G.B. Jiang, H.M. Liu, J.A. Jonsson, M.J. Wen, J. Chromatogr. A 1066 (2005) 27.
- [38] J.J. Deng, W. Shen, X. Zhang, Talanta 69 (2006) 894.
- [39] A. Mehdinia, M.F. Mousavi, M. Shamsipur, J. Chromatogr. A 1134 (2006) 24.
- [40] K. Demeestere, J.D.B. Dewitte, H.V. Langenhove, J. Chromatogr. A 1153 (2007) 130.



Biosensor based on laccase and an ionic liquid for determination of rosmarinic acid in plant extracts

Ana Cristina Franzoi^a, Jairton Dupont^b, Almir Spinelli^a, Iolanda Cruz Vieira^{a,*}

^a Departamento de Química, Universidade Federal de Santa Catarina - UFSC, CEP 88040-970, Florianópolis, SC, Brazil

^b Instituto de Química, Universidade Federal do Rio Grande do Sul - UFRGS, PO Box 15003, CEP 91501-970, Porto Alegre, RS, Brazil

ARTICLE INFO

Article history:

Received 10 July 2008

Received in revised form 3 September 2008

Accepted 4 September 2008

Available online 17 September 2008

Keywords:

Biosensor

Ionic liquid

Rosmarinic acid

Plant extract

ABSTRACT

Novel biosensors based on laccase from *Aspergillus oryzae* and the ionic liquids (ILs) 1-*n*-butyl-3-methylimidazolium hexafluorophosphate (BMIPF₆) and 1-*n*-butyl-3-methylimidazolium tetrafluoroborate (BMIBF₄) were constructed for determination of rosmarinic acid by square-wave voltammetry. The laccase catalyzes the oxidation of rosmarinic acid to the corresponding *o*-quinone, which is electrochemically reduced back to rosmarinic acid at +0.2 V vs. Ag/AgCl. The biosensor based on BMIPF₆ showed a better performance than that based on BMIBF₄. The best performance was obtained with 50:20:15:15% (w/w/w/w) of the graphite powder:laccase:Nujol:BMIPF₆ composition in 0.1 mol L⁻¹ acetate buffer solution (pH 5.0). The rosmarinic acid concentration was linear in the range of 9.99×10^{-7} to 6.54×10^{-5} mol L⁻¹ ($r = 0.9996$) with a detection limit of 1.88×10^{-7} mol L⁻¹. The recovery study for rosmarinic acid in plant extract samples gave values from 96.1 to 105.0% and the concentrations determined were in agreement with those obtained using capillary electrophoresis at the 95% confidence level. The BMIPF₆-biosensor demonstrated long-term stability (300 days; 920 determinations) and reproducibility, with a relative standard deviation of 0.56%.

© 2008 Elsevier B.V. All rights reserved.

1. Introduction

Ionic liquids (ILs), in particular those derived from imidazolium cation possess unique association of physicochemical properties such as excellent ionic conductivity, high chemical and thermal stability, negligible vapor pressure and wide electrochemical windows [1–3]. These liquids have been widely used in biocatalysis, liquid–liquid extraction processes, materials science, catalysis and organic synthesis [1]. In particular, properties such as non-flammability, high ionic conductivity and electrochemical and thermal stability make ILs ideal electrolytes in electrochemical devices like in batteries, capacitors, fuel cells, photovoltaics, actuators and electrochemical sensors [4–15].

The first carbon paste electrode (CPE) was proposed by Adams in 1958 [16] and since then is widely used in the electroanalytical methods because it offers several important advantages, including controlled bulk modification, ease of construction, low cost, versatility, renewability and low background current [16–18]. It consists of electrically conducting graphite powder and a nonconducting organic liquid as the binder. Nujol and paraffin are the most used

binder components of pastes [16–18]. Recently, the replacement of traditionally used binders by ILs has been shown to be an attractive and efficient alternative due to the high ionic conductivity and sensitivity of the resulting electrodes [4–15].

One of the most important enzymes in terms of applicability and versatility in industry is laccase. It is a multicopper oxidase, one of the extracellular glycoprotein enzymes expressed by white-rot fungi and other organisms that play a crucial role in the terrestrial carbon cycle by aiding the degradation of lignocellulosic materials such as wood. Laccase acts on phenolic substrates by catalyzing the oxidation of their phenolic hydroxyl groups to phenoxy radicals while molecular oxygen is reduced to water [19–21]. The general application of this enzyme has been reported [19–26]. However, biosensors based on the laccase and ionic liquids for the determination of phenolic compounds have not been described in the literature. There is only one report on the use of biosensor containing laccase from *Trametes versicolor* and ionic liquid for the inhibition of laccase activity by halide ions [27] and there are two other reports on the use of glucose oxidase and laccase from *Coriolor versicolor* immobilized at multiwalled carbon nanotubes-ionic liquid gel modified electrodes used as catalysts of anode and cathode of biofuel cells [28,29].

Rosmarinic acid is an ester of caffeic acid and 3,4-dihydroxyphenylacetic acid. It has a number of interesting biological activities

* Corresponding author. Tel.: +55 48 3721 6844; fax: +55 48 3721 6850.
E-mail address: iolanda@qmc.ufsc.br (I.C. Vieira).

such as inhibiting the HIV-1 virus and blood clots, it is also antihepatitis (protecting the liver), antibacterial, antiviral, and anti-inflammatory and it can act as an astringent. It is one of the most efficient natural antioxidants, hence its application in the food industry [30,31]. High performance liquid chromatography is a method commonly used for determination of this substance [32]. However, this generally necessitates lengthy analysis, expensive materials and preliminary steps to prepare the sample before injection. Capillary electrophoresis has been used since it offers considerable reductions in terms of sample preparation, analysis time and reagent consumption [33–36]. Recently, Santhiago et al. [37] have developed a biomimetic sensor based on a dinuclear Fe(III)Zn(II) mimetic complex for the active site of purple acid phosphatase for determination of rosmarinic acid. The rosmarinic acid concentration was linear in the range of 2.98×10^{-5} to $3.83 \times 10^{-4} \text{ mol L}^{-1}$ with a detection limit of $2.30 \times 10^{-6} \text{ mol L}^{-1}$. The coupling of electroanalytical methods with the selectivity and sensitivity of enzymatic reactions is one the most attractive, elegant and promising techniques for the construction of biosensors. Rosmarinic acid is found in many plants and in leaf material of lemon balm (*Melissa officinalis*) it is the majority component. It is added as antioxidant in the cosmetic formulations; however, there are no standard methods for its quantification. So, it is important to develop methods with this main goal.

In this study, biosensors based on laccase from *Aspergillus oryzae* and the ionic liquids 1-butyl-3-methylimidazolium hexafluorophosphate (BMIPF₆) and 1-butyl-3-methylimidazolium tetrafluoroborate (BMIBF₄) were constructed and evaluated. The influence of different experimental parameters including the Nujol:BMIPF₆ ratio, enzyme percentage, and solution pH, along with the frequency, pulse amplitude and increment for the square-wave voltammetry, were investigated in order to optimize the performance of the biosensors employed in the determination of rosmarinic acid. The results obtained in the determination of this substance in plant extract samples using the selected biosensor compared favorably with those obtained using the capillary electrophoresis method.

2. Experimental

2.1. Reagents and solutions

Laccase from *A. oryzae* was purchased from Novozymes (Denilite® II BASE) in the form of microspheres. The ionic liquids 1-butyl-3-methylimidazolium hexafluorophosphate and 1-butyl-3-methylimidazolium tetrafluoroborate were synthesized as previously described in the literature [38,39]. Graphite powder (grade #38) and Nujol were supplied by Fisher Scientific and Aldrich, respectively. Adrenaline, caffeic acid, catechin, chlorogenic acid, ferulic acid, gallic acid, hesperetin, hesperidin, luteolin, *m*-coumaric acid, *p*-coumaric acid, rosmarinic acid, sinapic acid, syringic acid, tannic acid, rutin and vanillic acid were purchased from Sigma. Eriodictyol-7-O-glucoside was purchased from Extrasynthese. Acetate buffer (0.1 mol L⁻¹, pH 5.0) solution was used as the supporting electrolyte. For the capillary electrophoresis analysis, chlorogenic acid (internal standard) was prepared in methanol at 800 mg L⁻¹. Lemon balm (*Melissa officinalis* L.) plant extracts (A, A': Melissa HG FS 157660705 and B, B': Melissa 18745–100%), used for the manufacture of cosmetic products, were obtained from Farma Service Bioextract (São Paulo, SP, Brazil). All reagents were of analytical grade and used without further purification. Ultrapure water (18.2 M Ω) was obtained from a Milli-Q purification system and used throughout the experiments.

2.2. Instrumentation

Voltammetry measurements were carried out using an Autolab PGSTAT12 potentiostat/galvanostat (Eco Chemie, The Netherlands) connected to data processing software (GPES, software version 4.9.006, Eco Chemie). The three-electrode system was composed of a biosensor (geometric area 1.0 mm²) based on laccase and ionic liquids (BMIPF₆ and BMIBF₄) as the working electrode, a platinum wire as the auxiliary electrode and an Ag/AgCl (3.0 mol L⁻¹ KCl) as the reference electrode. Electropherograms were obtained with an Agilent Technologies automated HP^{3D}CE capillary electrophoresis apparatus (Palo Alto, CA, USA), equipped with a diode array detector. The measurements were performed at 25 °C on an uncoated fused-silica capillary (48.5 cm \times 50 μ m I.D. \times 375 μ m O.D., 8.5 cm of effective length) obtained from Microtube (Araraquara, SP, Brazil). The acquisition software for data treatment was HP Chemstation®.

2.3. Construction of biosensors

The biosensors were prepared by hand-mixing laccase (40.0 mg; 20%, w/w) and graphite powder (100.0 mg; 50%, w/w) in a mortar for 20 min to ensure uniform dispersion. Nujol (30.0 mg; 15%, w/w) and BMIPF₆ or BMIBF₄ (30.0 mg; 15%, w/w) were added to this mixture which was then mixed for at least 20 min to produce the final paste. A portion of the resulting paste was packed firmly into the cavity of a syringe and the electrical contact was established via a copper wire. The biosensors were stored at room temperature when not in use. The carbon paste electrode without laccase was prepared following the same steps.

2.4. Electrochemical and capillary electrophoresis measurements

Square-wave voltammetry and cyclic measurements were carried out in an unstirred, non-de-aerated acetate buffer solution (pH 5.0) at 25.0 ± 0.5 °C and all potentials were measured and reported vs. Ag/AgCl (3.0 mol L⁻¹ KCl). In a typical run, 10 mL of the supporting electrolyte was transferred to a clean, dry cell and the required volume of the rosmarinic acid or sample of the plant extract was added by micropipette. After a stirring period of 60 s to homogenize the solution, a square wave or cyclic voltammograms were recorded.

Electropherograms were obtained using the injection pressure of 50 mbar (5.25 Pa) for 5 s and UV detection at 340 nm. The applied separation voltage was 30 kV, negative polarity. The background electrolyte (BGE) consisted of $10.0 \times 10^{-3} \text{ mol L}^{-1}$ (pH 9.3) of sodium tetraborate. At the start of each new working session, the capillary was conditioned at 25 °C and flushed with 1.0 mol L⁻¹ sodium hydroxide for 10 min, followed by deionized water for 5 min and finally with the BGE for 10 min. Between runs with the same buffer, the capillary was rinsed for 0.5 min with BGE. At the end of the analysis the capillary was rinsed for 5 min with 1.0 mol L⁻¹ sodium hydroxide and for 10 min with deionized water.

3. Results and discussion

3.1. Enzymatic reaction and voltammetric study of the biosensors

Reactions catalyzed by enzymes have long been used for the determination of different analytes. Numerous biosensors based on laccase have been described in the literature [24–27]. This is one of the blue copper oxidases which catalyze the four-electron reduction of molecular oxygen to water and the oxidation of a variety of aromatic compounds. In this study, laccase immobilized on the biosensor catalyzes the oxidation of rosmarinic acid present in

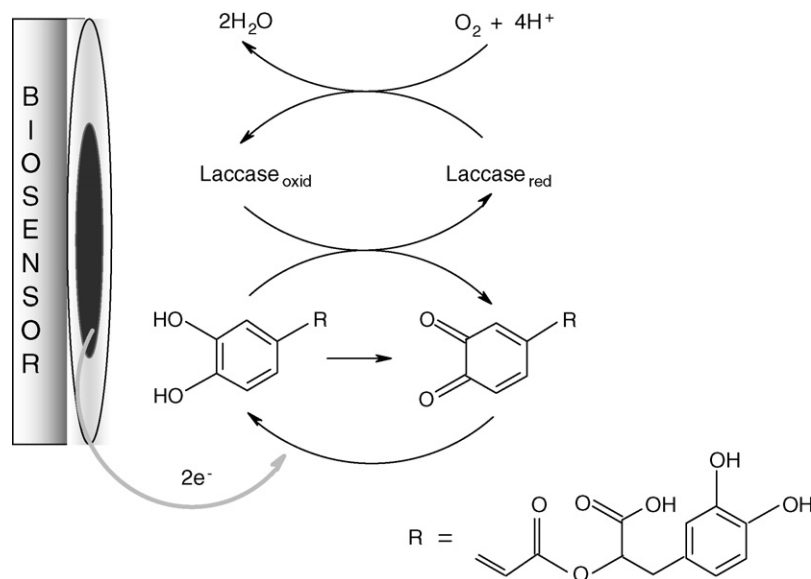


Fig. 1. Schematic representation of the reaction involving rosmarinic acid and laccase on the BMIPF₆-biosensor surface.

the solution to the corresponding *o*-quinone. This product is electrochemically reduced back to rosmarinic acid on the surface of the biosensor as shown in Fig. 1. The resulting reduction current is used as the analytical response for rosmarinic acid determination.

The electrochemical behavior of rosmarinic acid using the bare CPEs and biosensors based on laccase and BMIPF₆ or BMIBF₄ as binders was investigated by square-wave voltammetry in the potential range of +0.5 to −0.5 V vs. Ag/AgCl. Fig. 2 shows the voltammograms obtained using (a') BMIBF₄-CPE, (a) BMIBF₄-biosensor, (b') BMIPF₆-CPE and (b) BMIPF₆-biosensor in a $6.10 \times 10^{-5} \text{ mol L}^{-1}$ rosmarinic acid solution in acetate buffer (0.1 mol L^{-1} , pH 5.0). As can be seen, for the BMIPF₆-biosensor, a higher response for the reduction wave of *o*-quinone to rosmarinic acid at a potential of +0.2 V was observed when compared with the BMIBF₄-biosensor at a potential of +0.1 V and CPEs containing ILs. A plausible explanation for the better performance of the BMIPF₆-biosensor compared to the BMIBF₄-biosensor is that the use of PF₆[−] as the counter ion for the *N,N*-dialkyl sub-

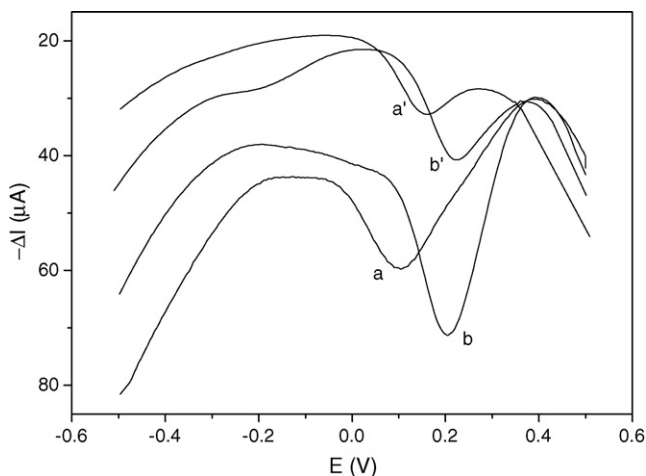


Fig. 2. Square-wave voltammograms obtained using (a') BMIBF₄-CPE, (a) BMIBF₄-biosensor, (b') BMIPF₆-CPE and (b) BMIPF₆-biosensor with $6.10 \times 10^{-5} \text{ mol L}^{-1}$ rosmarinic acid in 0.1 mol L^{-1} acetate buffer solution (pH 5.0); pulse amplitude 100 mV, frequency 30 Hz and scan increment 5.0 mV.

stituted imidazolium cation causes the resulting structure to be hydrophobic. As a consequence, it has a greater stability, good electrochemical conductivity and a wide electrode potential window in aqueous solutions [8]. On the other hand, the BF₄[−] forms a hydrophilic structure with the same cation and thus, for the construction of biosensors, it is unstable in aqueous solutions [1]. The miscibility in water of ILs based on anions such as BF₄[−] is dependent on the structure of the cations. The miscibility decreases with an increase in the cation chain length [1–3]. Therefore, the BMIPF₆-biosensor was chosen for the development of this study.

3.2. Optimization of the biosensor construction and experimental parameters for square-wave voltammetry

Parameters regarding the biosensor composition were investigated in order to build a biosensor with adequate performance. The Nujol:BMIPF₆ ratios (a) 100:0; (b) 75:25; (c) 50:50; (d) 25:75 and (e) 0:100% (w/w) were studied and the biosensor responses in the rosmarinic acid determination by (A) cyclic voltammetry and (B) square-wave voltammetry are compared in Fig. 3. All the biosensors had the same graphite powder:laccase ratio. As can be observed in the cyclic voltammograms (Fig. 3A), the background current increased with an increase in the BMIPF₆ content. It has been reported in the literature [9,13,15] that the addition of ILs to CPEs modifies the microstructure of the paste and that the charge transfer resistance decreases and charge transfer rate increases, due to the higher conductivity of the ILs. The response of the proposed biosensor did not follow this behavior. It can be clearly observed that the background current (due principally to the capacitive current) increased considerably when BMIPF₆ represents over 50%. The same behavior was reported [8] for the oxidation of acetaminophen on carbon paste electrodes modified with different ILs. When the contribution of the capacitive current was suppressed (square-wave voltammograms showed in Fig. 3B; inset shows the current values for each biosensor composition), an increase in the current reduction peak was observed up to a Nujol:BMIPF₆ ratio of 50%. After this, the current decreased significantly. These results are in accordance with those obtained by cyclic voltammetry and confirm the efficiency of the BMIPF₆ as a binder when used in a suitable amount. Additionally, it is clearly observed that the sensitivity of

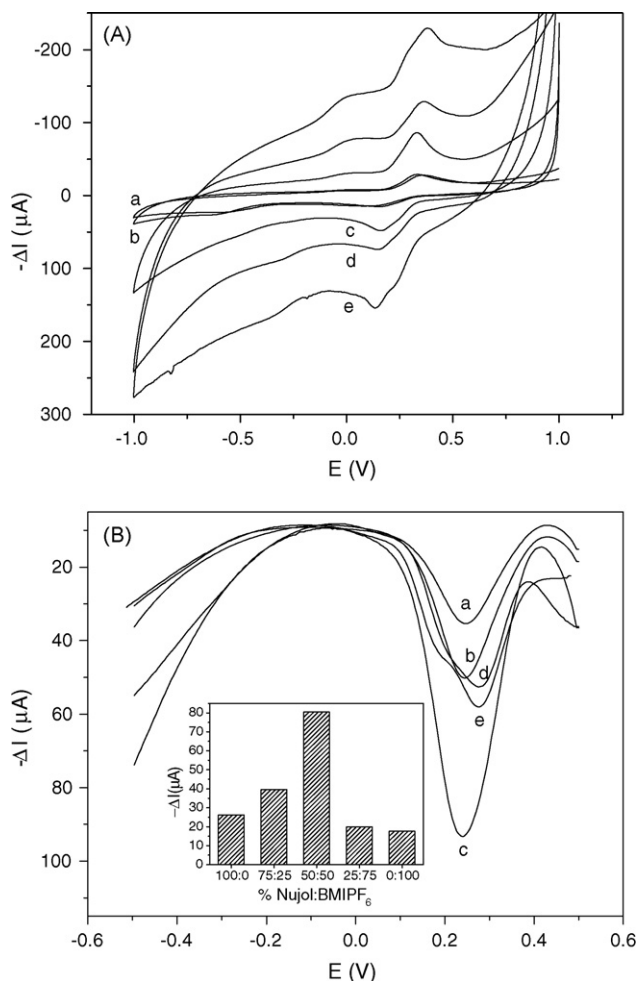


Fig. 3. (A) Cyclic and (B) square-wave voltammograms obtained using different Nujol:BMIPF₆ ratios in the carbon paste modified with laccase immersed in 6.10×10^{-5} rosmarinic acid solution and 0.1 mol L^{-1} acetate buffer solution (pH 5.0) at (A) 100 mV s^{-1} and (B) same conditions as in Fig. 2. Inset: current values for each biosensor composition.

the biosensor was greatly enhanced when the Nujol:BMIPF₆ ratio used was 50:50% (w/w) together with square-wave voltammetry. Therefore, this proportion was used for subsequent biosensor construction and square-wave voltammetry analysis for the determination of rosmarinic acid.

The effect of laccase in percentages of 10–30% (w/w) on the modified carbon paste electrode was investigated. The analytical signals (cathodic peak currents) increased with increases in the enzyme composition up to 20.0% (w/w). Consequently, this enzyme composition was selected for further studies and a composition of 50:20:15:15% (w/w/w/w) graphite powder:laccase:Nujol:BMIPF₆, respectively, was used in the construction of the BMIPF₆-biosensor.

After the optimization of the biosensor composition, other important experimental parameters were investigated, including solution pH (4.0–8.0) and square-wave voltammetry parameters (frequency of 10–100 Hz, pulse amplitude of 10–100 mV and scan increment of 1.0–5.0 mV) in order to obtain the best response for the proposed BMIPF₆-based biosensor. The response was analyzed on the cathodic peak current for a $6.10 \times 10^{-5} \text{ mol L}^{-1}$ rosmarinic acid solution. Table 1 summarizes the range over which each variable was investigated and the optimal value found. The best experimental conditions were selected for subsequent experiments.

Table 1
Optimization of the experimental conditions

Parameter investigated	Range studied	Optimal value
Nujol:BMIPF ₆ (% w/w)	100:0–0:100	50:50
Laccase (% w/w)	10–30	20
pH	4.0–8.0	5.0
Frequency (Hz)	10–100	30.0
Pulse amplitude (mV)	10–100	100
Scan increment (mV)	0.5–5.0	5.0

3.3. Reproducibility and stability of the biosensor

To investigate the precision of the determination, the same biosensor was used for six parallel determinations of $6.10 \times 10^{-5} \text{ mol L}^{-1}$ rosmarinic acid solution in acetate buffer solution (0.1 mol L^{-1} ; pH 5.0). The relative standard deviation was calculated as 0.94%. Four biosensors were constructed using the same procedure and were independently used for the determination of rosmarinic acid under the conditions described above. All the biosensors showed an acceptable reproducibility with a relative standard deviation of 0.56%, indicating that the results obtained with the proposed biosensor have a good reproducibility.

The lifetime and stability of the biosensor are very important features, and thus these parameters were also investigated. The biosensor was used for consecutive measurements without surface renewal over a 300-day period (over 920 samples were determined for each quantity of carbon paste used in the syringe). The response was recorded (cathodic peak currents) in a $6.10 \times 10^{-5} \text{ mol L}^{-1}$ rosmarinic acid (pH 5.0) solution. When the biosensor was stored at room temperature and measurements taken every 1–2 days in solutions of the same composition, no notable changes were observed in its response, indicating good stability and long lifetime.

3.4. Square-wave voltammograms and analytical curve

Under the selected conditions mentioned above, the analytical curve obtained was linear from 9.99×10^{-7} to $6.54 \times 10^{-5} \text{ mol L}^{-1}$ of rosmarinic acid and the regression equation found was $I_{pc} = -1.1210 + 0.5630 \times 10^6 [\text{rosmarinic acid}]$ (I_{pc} : μA ; [rosmarinic acid]: mol L^{-1} ; $r = 0.9996$). The detection limit (three times the blank signal/slope) was calculated using this calibration curve and was found to be $1.88 \times 10^{-7} \text{ mol L}^{-1}$. Fig. 4 shows these voltammograms and the corresponding analytical curve can be seen in the inset. The experiments were carried out in triplicate and the results shown in the inset correspond to the mean of the measurements.

3.5. Selectivity and interference study

Phenolic compounds, such as adrenaline, caffeic acid, catechin, chlorogenic acid, ferulic acid, gallic acid, luteolin, *p*-coumaric acid, rosmarinic acid, syringic acid, sinapic acid, tannic acid, rutin and vanillic acid were investigated, in order to determine the selectivity of the proposed biosensor. The sensor was more sensitive to rosmarinic acid (100%), adrenaline (63.0%), caffeic acid (25.0%), chlorogenic acid (22.0%), catechin (10.0%) and rutin (9.0%). No response was observed for the other phenolic compounds studied.

The effects of other substances on the determination of rosmarinic acid in lemon balm plant extracts, such as caffeic acid, eriodictyol-7-O-glucoside, hesperetin, hesperidin, *m*-coumaric acid, naringenin and naringin, were investigated using square-wave voltammetry. The ratios of the concentration of rosmarinic acid to those of the possible interferents were fixed at 1.0 and 5.0. Of these substances, only the caffeic acid and eriodictyol-

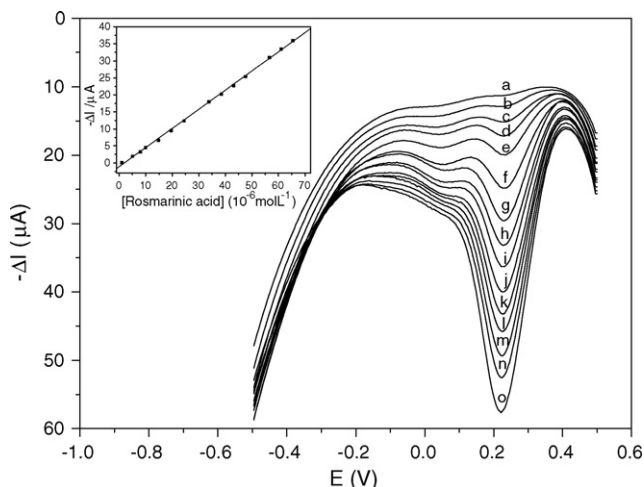


Fig. 4. Square-wave voltammograms obtained using the proposed biosensor for (a) blank in acetate buffer solution (0.1 mol L⁻¹; pH 5.0) and rosmarinic acid solutions at the following concentrations: (b) 9.99×10^{-7} mol L⁻¹; (c) 4.98×10^{-6} mol L⁻¹; (d) 7.94×10^{-6} mol L⁻¹; (e) 9.90×10^{-6} mol L⁻¹; (f) 1.48×10^{-5} mol L⁻¹; (g) 1.96×10^{-5} mol L⁻¹; (h) 2.44×10^{-5} mol L⁻¹; (i) 3.38×10^{-5} mol L⁻¹; (j) 3.85×10^{-5} mol L⁻¹; (k) 4.31×10^{-5} mol L⁻¹; (l) 4.76×10^{-5} mol L⁻¹; (m) 5.66×10^{-5} mol L⁻¹; (n) 6.10×10^{-5} mol L⁻¹; (o) 6.54×10^{-5} mol L⁻¹; other conditions are the same as in Fig. 2. Inset: the analytical curve of rosmarinic acid.

7-O-glucoside showed electrochemical activity on the proposed biosensor. Nevertheless, the concentrations of these compounds in the plant extracts were very low and did not interfere in the determination of rosmarinic acid. These data were agreement with those reported recently by Dastmalchi et al. [40] using high performance liquid chromatography and a biomimetic sensor [37].

3.6. Recovery study and analytical application

Recoveries of 96.1–105.0% for rosmarinic acid present in the plant extract samples ($n=3$) were obtained using the biosensor. In this study 3.57, 10.48, 17.15 and 23.56 mg L⁻¹ of rosmarinic acid solutions were successively added to each sample and the cathodic current peak analyzed. The recovery results obtained were satisfactory, as shown in Table 2, indicating an absence of matrix effects in the rosmarinic acid determinations using the proposed biosensor. Also, the results obtained with the BMIPF₆-based biosensor were compared with those obtained using the capillary electrophoresis method. The results for the two determination methods are shown in Table 3. A good agreement was obtained at the 95% confidence level, within an acceptable range of error, indicating that the biosensor is suitable for the determination of the antioxidant rosmarinic acid in plant extracts.

Table 2
Recoveries of rosmarinic acid solution in plant extracts using the biosensor proposed

Sample	Rosmarinic acid (mg L ⁻¹)		Recovery (%)
	Added ^a	Found	
A	3.57	3.66 ± 0.02	102.5
	10.48	10.78 ± 0.01	102.9
	17.15	17.31 ± 0.02	100.9
	23.56	22.63 ± 0.03	96.1
B	3.57	3.61 ± 0.02	101.1
	10.48	11.01 ± 0.02	105.0
	17.15	17.68 ± 0.03	103.0
	23.56	22.97 ± 0.01	97.5

^a $n=3$.

Table 3

Determination of rosmarinic acid in plant extracts using the BMIPF₆-biosensor and capillary electrophoresis

Sample	Rosmarinic acid (mg L ⁻¹)		Relative error (%) ^a
	Capillary electrophoresis ^b	BMIPF ₆ -biosensor ^b	
A	229.5 ± 0.1	230.7 ± 0.2	+0.5
A'	229.5 ± 0.1	229.9 ± 0.1	+0.2
B	230.2 ± 0.1	215.9 ± 0.2	-6.2
B'	230.2 ± 0.1	212.2 ± 0.1	-7.8

^a BMIPF₆-biosensor vs. capillary electrophoresis.

^b $n=3$; confidence level of 95%.

4. Conclusions

In this study, we present novel biosensors based on laccase from *A. oryzae* and the ionic liquids 1-butyl-3-methylimidazolium hexafluorophosphate or 1-butyl-3-methylimidazolium hexafluoroborate used as the binder. The IL-based biosensors were used for the determination of rosmarinic acid in plant extracts. The BMIPF₆-based biosensor showed more favorable analytical features such as high sensitivity, linear calibration range, low detection limit, rapid response, good reproducibility and long-term stability. In addition, the low cost, renewability, simplicity and fast construction of the biosensor, using square-wave voltammetry as the analysis method, make it superior to other techniques for rosmarinic acid determination. The results indicated that the antioxidant was successfully determined and the results obtained were satisfactory when compared with the capillary electrophoresis method.

Acknowledgments

Financial support from CNPq (Process 472169/2004-1 and 472541/2006-4), MCT/CNPq/PADCT, NOVOZYMES, Farma Service Bioextract and also a scholarship granted by CNPq to ACF are gratefully acknowledged.

References

- [1] D. Wei, A. Ivaska, *Anal. Chim. Acta* 607 (2008) 126.
- [2] J. Dupont, P.A.Z. Suarez, *Phys. Chem. Chem. Phys.* 8 (2006) 2441.
- [3] M. Galiński, A. Lewandowski, I. Stepniak, *Electrochim. Acta* 51 (2006) 5567.
- [4] Y. Zhang, J.B. Zheng, *Electrochim. Acta* 52 (2007) 7210.
- [5] A. Safavi, N. Maleki, F. Tajabadi, *Analyst* 132 (2007) 54.
- [6] S.F. Wang, H.Y. Xiong, Q.X. Zeng, *Electrochem. Commun.* 9 (2007) 807.
- [7] S. Wei, W. Dandan, G. Ruifang, J. Kui, *Electrochem. Commun.* 9 (2007) 1159.
- [8] M. Musameh, J. Wang, *Anal. Chim. Acta* 606 (2008) 45.
- [9] N. Maleki, A. Safavi, F. Tajabadi, *Electroanalysis* 19 (2007) 2247.
- [10] H.Y. Xiong, T. Chen, X.H. Zhang, S.F. Wang, *Electrochem. Commun.* 9 (2007) 2761.
- [11] G. Shul, J. Sirieix-Plenet, L. Gaillon, M. Opallo, *Electrochem. Commun.* 8 (2006) 1111.
- [12] H. Liu, P. He, Z. Li, C. Sun, L. Shi, Y. Liu, G. Zhu, J.H. Li, *Electrochem. Commun.* 7 (2005) 1357.
- [13] N. Maleki, A. Safavi, F. Tajabadi, *Anal. Chem.* 78 (2006) 3820.
- [14] A. Safavi, N. Maleki, F. Tajabadi, E. Farjami, *Electrochem. Commun.* 9 (2007) 1963.
- [15] S. Wei, Y. Maoxia, J. Kui, *Anal. Bioanal. Chem.* 389 (2007) 1283.
- [16] R.N. Adams, *Anal. Chem.* 30 (1958) 1576.
- [17] I.R.W.Z. Oliveira, A. Neves, I.C. Vieira, *Sens. Actuators B* 129 (2008) 424.
- [18] I.R.W.Z. Oliveira, R.E.M.B. Osório, A. Neves, I.C. Vieira, *Sens. Actuators B* 122 (2007) 89.
- [19] P. Widsten, A. Kandelbauer, *Enzyme Microb. Technol.* 42 (2008) 293.
- [20] S.R. Couto, J.L.T. Herrera, *Biotechnol. Adv.* 24 (2006) 500.
- [21] A.M. Mayer, R.C. Staples, *Phytochemistry* 60 (2002) 551.
- [22] A. Jarosz-Wilkolazka, T. Ruzgas, L. Gorton, *Talanta* 66 (2005) 1219.
- [23] A. Jarosz-Wilkolazka, T. Ruzgas, L. Gorton, *Enzyme Microb. Technol.* 35 (2004) 238.
- [24] Y. Zhang, G.M. Zeng, L. Tang, D.L. Huang, X.Y. Jiang, Y.N. Chen, *Biosens. Bioelectron.* 22 (2007) 2121.
- [25] C. Mousty, L. Vieille, S. Cosnier, *Biosens. Bioelectron.* 22 (2007) 1733.
- [26] S.C. Fernandes, I.R.W.Z. Oliveira, O. Fatibello-Filho, A. Spinelli, I.C. Vieira, *Sens. Actuators B* 133 (2008) 202.
- [27] Y. Liu, L. Huang, S. Dong, *Biosens. Bioelectron.* 23 (2007) 35.

- [28] Y. Liu, S. Dong, *Biosens. Bioelectron.* 23 (2007) 593.
- [29] Y. Liu, S. Dong, *Electrochem. Commun.* 9 (2007) 1423.
- [30] M. Petersen, M.S.J. Simmonds, *Phytochemistry* 62 (2003) 121.
- [31] B. Tepe, *Bioresource Technol.* 99 (2008) 1584.
- [32] M. Križman, D. Baričević, M. Prošek, *J. Pharm. Biomed. Anal.* 43 (2007) 481.
- [33] S. Başkan, N. Östekin, F.B. Erim, *Food Chem.* 101 (2007) 1748.
- [34] Y. Peng, J. Ye, J. Kong, *J. Agric. Food Chem.* 53 (2005) 8141.
- [35] Y. Peng, J. Yuan, F. Liu, J. Ye, *J. Pharm. Biomed. Anal.* 39 (2005) 431.
- [36] Z. Tang, Y. Zeng, Y. Zhou, P. He, Y. Fang, S. Zang, *Anal. Lett.* 39 (2006) 2861.
- [37] M. Santhiago, R.A. Peralta, A. Neves, G.A. Micke, I.C. Vieira, *Anal. Chim. Acta* 613 (2008) 91.
- [38] P.A.Z. Suarez, J.E.L. Dullius, S. Einloft, R.F. DeSouza, J. Dupont, *Polyhedron* 15 (1996) 1217.
- [39] C.C. Cassol, G. Ebeling, B. Ferrera, J. Dupont, *Adv. Synth. Catal.* 348 (2006) 243.
- [40] K. Dastmalchi, H.J.D. Dorman, P.P. Oinonen, Y. Darwis, I. Laakso, R. Hiltunen, *LWT* 41 (2008) 391.



Assessment of a dynamic hollow-fibre liquid phase microextraction system for human blood plasma samples

Helena Hansson, Ulrika Nilsson*

Department of Analytical Chemistry, Stockholm University, 106 91 Stockholm, Sweden

ARTICLE INFO

Article history:

Received 4 April 2008

Received in revised form 15 August 2008

Accepted 4 September 2008

Available online 11 September 2008

Keywords:

Supported liquid membrane
Liquid phase microextraction
Hollow fibre
Nitrophenols
Human blood plasma

ABSTRACT

A dynamic liquid phase microextraction (LPME) system, based on hollow-fibre supported liquid membrane (SLM) extraction, was developed for extracting ionisable xenobiotics from human plasma, and its performance was evaluated (in terms of extraction efficiency, reproducibility, durability and carry-over) using nitrophenolic compounds as model analytes at concentrations of 0.1–0.5 $\mu\text{g mL}^{-1}$ in aqueous standards. The efficiency and repeatability were tested also on spiked human plasma. The system is non-expensive, convenient, requires minimal manual handling and enables samples with volumes as small as 0.2 mL to be extracted. For plasma samples extraction efficiencies of between 30 and 58% were achieved within 20 min, including washing steps. The limit of detection (LOD) values were in the range 0.02–0.03 $\mu\text{g mL}^{-1}$. The developed system can provide enrichment factors up to eight, based on the injection-to-acceptor volume ratio (in this case 0.2–0.025 mL). The same hollow-fibre membrane was used up to 8 days with no loss of efficiency. Carry-over was lower than detection limit.

© 2008 Elsevier B.V. All rights reserved.

1. Introduction

In analyses of biological samples, such as plasma, extensive clean up is required to minimize signal suppression by matrix components in the detection step, especially when using ESI-MS. For plasma samples the available sample volumes are also often limited, and thus an extraction method that can handle small sample volumes is desirable. Membrane extraction methods provide many of the benefits of classic liquid–liquid extraction, but they consume less solvents, can be miniaturized and are often less laborious. They are also versatile and can be used in either two- or three-phase systems.

Membrane extraction has been reviewed by Jönsson and Mathiasson [1], and the associated mass transfer kinetics has been carefully examined [2]. On-line membrane extraction/LC/UV [3] and semi-automated membrane extraction/GC/MS [4] systems have also been described recently. The used membranes are microporous and either planar or tubular (i.e. hollow fibre). The hollow-fibre technique is usually referred to as liquid phase microextraction (LPME) or hollow-fibre LPME (HFLPME) and has recently been reviewed by Pedersen-Bjergaard and Rasmussen [5]. The technique can be used in different ways. The most commonly reported is the liquid–liquid–liquid system, based on extraction

from an aqueous donor, via a supported organic liquid membrane (SLM) to an aqueous acceptor, but it can also be used for extraction in liquid–liquid systems from aqueous donors to organic solvents. Another approach is HF-supported headspace-LPME [6–8]. HFLPME has mostly been performed in static mode, which was previously applied to nitrophenols present at trace levels in water samples with large volumes, yielding enrichment factors of several thousands [9]. Also several works using HFLPME in dynamic mode [7,10] and automated systems [11,12] have been published.

Liquid–liquid–liquid HFLPME systems can be efficient for extracting ionisable species and metal ions [13], as long as pH of both donor and acceptor is appropriate. Organic solvents with long chain hydrocarbons like *n*-undecanone or more polar solvents like dihexylether [1], or a mixture of two different organic compounds are often used. Additives, such as ion-pairing agents, have also been used to enhance mass transfer over the membrane [1]. The driving force in such a system is the concentration gradient, which is dependent on the diffusion rates and partitioning coefficients of the analytes in the different liquid phases. The temperature in the system affects both diffusion and partition coefficient [14].

The aim of this study was to develop and evaluate an alternative approach to dynamic HFLPME for extracting ionisable xenobiotics, such as nitrophenolic compounds, from human plasma. The device used is a miniaturized version of the XT-extractor [15] previously presented by our group. In the cited study, the extractor was used

* Corresponding author.

E-mail address: ulrika.nilsson@anchem.su.se (U. Nilsson).

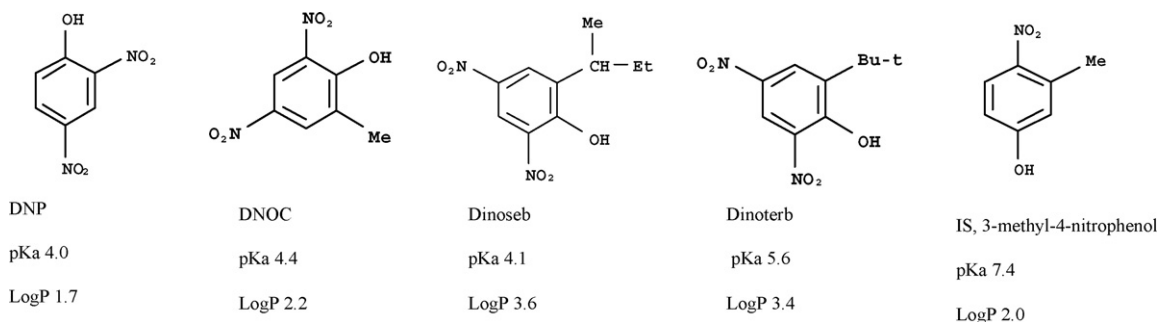


Fig. 1. Chemical structures, log *P* and pK_a of the investigated model compounds.

for three-phase extraction of pharmaceuticals in urine, but it has also been applied to two-phase extraction of organophosphate triester flame-retardants in human plasma [16]. The extraction method requires a minimum of manual handling with a reusable membrane and the design makes it straightforward to couple to analytical instruments, such as LC/MS. To automate the extraction, however, the stability and durability of the membrane as well as carry-over have to be considered. In the present study, the device has been miniaturized to increase the surface area-to-sample volume ratio of the membrane, which was expected to increase the extraction efficiency. Nitrophenolic compounds in both plasma and aqueous samples were selected as model analytes. They comprise a group of toxic compounds that have various industrial uses, and some have been globally used as herbicides, although the latter use is now banned by both the US Environmental Protection Agency (EPA) and the European Union (EU) [17,18]. Exposure limits of 10 µg mL⁻¹ for serum and 5 µg mL⁻¹ for whole blood have been proposed [19], and the EU Directive 75/440/EEC has set a maximum permissible level to 5 µg L⁻¹ for the sum of pesticides in tap water [20]. For individual phenols in surface water, used for production of drinking water, the maximum permissible levels range between 1 and 100 µg L⁻¹ [21].

2. Experimental

2.1. Chemicals and material

The standard compounds, 4,6-*o*-dinitroresol (DNOC), 2-*sec*-butyl-4,6-dinitrophenol (Dinoseb), 2-*tert*-butyl-4,6-dinitrophenol (Dinoterb), 2,4-dinitrophenol (DNP) and 3-methyl-4-nitrophenol (IS) were all of 98% purity and purchased from Sigma-Aldrich (Seelze, Germany). The studied compounds are shown in Fig. 1.

Dihexylether (97%) and acetonitrile (analytical grade) were from Sigma-Aldrich (Steinheim, Germany). Sodium hydrogen carbonate, sulphuric acid, sodium hydroxide and sodium chloride were obtained from Merck (Darmstadt, Germany). Formic acid

(98–100%) was bought from Scharlau Chemie S.A (Barcelona, Spain), and acetone (Normapure) from VWR international (Lutterworth, UK). All aqueous solution used and buffers were made from water purified using a MilliQ device (Millipore, Billerica, MA, USA). Accurel polypropylene (PP 50/280) hollow fibre was purchased from Membrana GmbH (Wuppertal, Germany). Polyetheretherketone (PEEK) T-connectors, low-pressure polyacetal fittings, o-rings and PTFE tubing (OD 1/16 in., id 0.5 mm), were obtained from Vici Jour (Schenkon, Switzerland), cyanoacrylate glue from Casco AB (Stockholm, Sweden) and fused silica capillary tubing (TSP 100245) from Polymicro Technologies Inc. (Phoenix, AZ, USA).

2.2. The extractor

The extraction device, called the SLM extractor, used in this study is very similar in construction to a previously described device, the XT-extractor [15], but contains a membrane with smaller dimensions (wall thickness 50 µm, inner diameter 280 µm). The extractor is easily assembled by hand without any tools. As shown in Fig. 2, it consists of two PEEK T-connectors connected by PTFE tubing (1/16 in. OD, 0.5 mm id) housing a 12-cm long piece of hollow fibre that is stuck, at both ends, to an overlapping, 6 cm fused silica capillary (TSP 100245) tube by cyanoacrylate glue. The PTFE tubing is flanged at both ends and attached to each T-connector with low-pressure polyacetal fittings (1/16 in. OD, 1/4"-28) and o-rings (1/16 in. OD, PP). The fused silica capillaries are tightly connected to a ferrule at their unglued ends. To prevent twisting, the fittings and connectors are tightly connected at one end, while the hollow fibre is free to move at the other. The fibre and the fused silica capillary overlap by about 3–4 mm, to avoid the glue entering the capillary. The device is connected to a syringe pump (Harvard apparatus, pump 22, MA, USA), equipped with two syringes (Hamilton, Bonaduz, Schweiz), one of which supplies the system with the donor phase (aqueous solution of 0 or 200 mM sodium chloride, pH 5 adjusted with sulphuric acid) while the other supplies the acceptor phase (62 mM sodium hydrogen carbonate, pH 10 adjusted with sodium hydroxide).

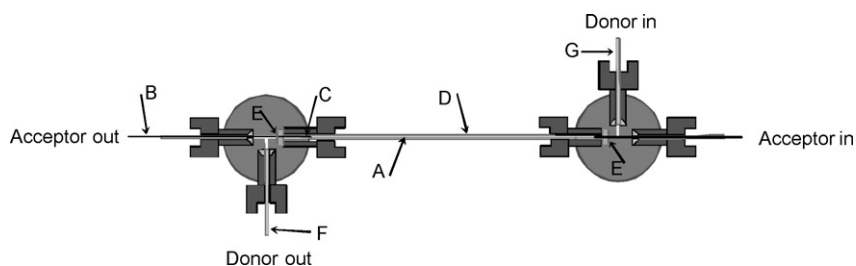


Fig. 2. The extractor used in this study. (A) Polypropylene fibre, (B) fused silica capillary, (C) fibre/capillary overlap, (D) PTFE-tubing, (E) flanged endings, (F/G) donor out/ in through the PTFE-tubing.

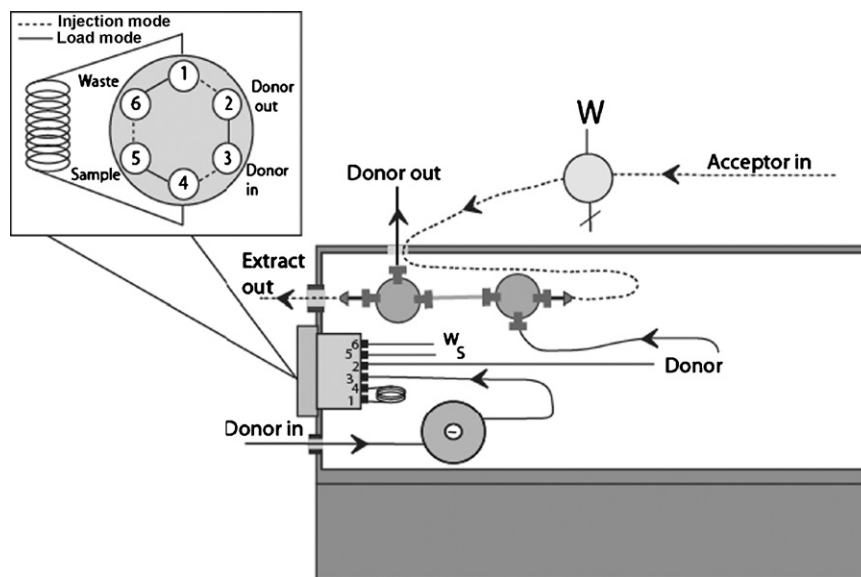


Fig. 3. The extractor and column heater set-up. (A) Heating block, (B) injection valve, (C) extractor, (D) manual low-pressure valve, (W) waste.

2.3. Preparation of the hollow-fibre membrane

Before the hollow fibre was mounted in the PTFE tubing, it was thoroughly washed with acetone. The fibre was then connected to a fused silica capillary connected to a 5-mL syringe filled with acetone, which was manually pushed, at high pressure, through the fibre channel and pores. The syringe was then placed in a syringe pump, which passed acetone through the fibre at a flow rate of 2 mL min^{-1} for 5 min. The acetone was then evaporated from the pores of the fibre, which was subsequently glued to the fused silica capillary with a 3–4 mm overlap, mounted in the PTFE tube and finally attached to the T-connectors.

The next step was to prepare the organic liquid membrane, by saturating the fibre pores with dihexylether. For this purpose, the extractor was clamped vertically and a small amount of dihexylether (approximately 0.2 mL) was delivered by hand from a glass syringe, connected to the fused silica capillary by a small piece of PTFE tubing. The length of the fused silica capillary was then cut to approximately 3 cm to minimize the backpressure in the extractor.

The extractor was finally connected to the syringe pump and 50 mL min^{-1} flows of both donor and acceptor phases were delivered for 40 min to eliminate excess dihexylether. To detect any leakage through the liquid membrane, the pH of both the acceptor and donor phases was monitored at the outlet.

2.4. Extraction set-up

In order to control the temperature the extractor (C) was mounted in a column heater as shown in Fig. 3. The donor phase (aqueous solution of 0 or 200 mM sodium chloride, pH 5) was passed through heating block (A) shortly after entering the column heater. The syringe pump, which provided the system with both donor and acceptor flows, was placed outside the column heater. The flow rates of the donor and acceptor phases were set to 100 and $25 \mu\text{L min}^{-1}$, respectively. The samples were injected using an injection valve (B, Rheodyne, Cotati, CA, USA) mounted in the heater wall and equipped with either a 100-, 200- or $500 \mu\text{L}$ PEEK loop. The acceptor flow was passed through a low-pressure manual valve (D) before entering the column heater and extractor, allowing the acceptor flow to be switched off for static extraction.

2.5. Sample preparation

Stock solutions of the individual reference compounds were prepared by dissolving the weighed substances in acetonitrile:water (1:9) to a final concentration of $60 \mu\text{g mL}^{-1}$. The stock solutions were stored in the refrigerator at 5°C until use.

Non-spiked plasma was obtained from Karolinska Hospital (Stockholm, Sweden) and was kept at -20°C until shortly before use, when it was thawed at room temperature. Aliquots of 2 mL plasma and 0.5 mL of diluted standard (at a concentration of $0.1\text{--}0.5 \mu\text{g mL}^{-1}$ of each analyte) were mixed for 30 min on a mixing table. For blank samples, 0.5 mL of water was added to the plasma. After mixing, 1.8 mL water, 0.2 mL isopropanol and two drops of sulphuric acid was added to each plasma sample, and gently mixed then ultrasonically agitated for 1 min. After this, the plasma samples were kept at room temperature during the day of analysis.

2.6. Evaluation of the extraction parameters

The effects of three extraction parameters (extraction temperature, presence of salt in the donor phase, and flow rates) were evaluated using a full factorial experimental design with the experimental matrix shown in Table 1. The results were then evaluated with Modde 6.0 software (Umetrics, Umeå, Sweden).

The following variable settings were applied in all subsequent experiments. The acceptor phase flow rate throughout the experiments was set at a quarter of the donor phase flow rate by using a syringe with a 4-fold smaller cross-section (2.5 mL , 2.5-MDF-LL-GT/SGE) for the donor phase than the one for the acceptor phase (10 mL , 10-MDF-LL-GT/SGE). During the extraction, the acceptor phase was static in the extractor, and the acceptor flow was led to waste. The sample was injected via the $200 \mu\text{L}$ injector loop, and for

Table 1
Experimental design, $n=3$.

Variable	Low	Mid	High
Donor flow rate	$50 \mu\text{L min}^{-1}$	$75 \mu\text{L min}^{-1}$	$100 \mu\text{L min}^{-1}$
Acceptor flow rate	$12.5 \mu\text{L min}^{-1}$	$19 \mu\text{L min}^{-1}$	$25 \mu\text{L min}^{-1}$
Temperature	20°C	35°C	50°C
NaCl in donor	0 mM	–	200 mM

Table 2
Plasma sample treatments.

Method	Plasma treatment	Analyte concentration in plasma (ng μL^{-1})	Total volume (mL)
1	2 mL plasma, 0.5 mL std (0.5 ng μL^{-1}), 1 mL formic acid (100%)	0.07	3.5
2	1 mL plasma, 0.5 mL std (0.5 ng μL^{-1}), 1 mL ultra pure water, sulphuric acid to pH 2	0.1	2.5
3	1 mL plasma, 0.1 mL std (10 ng μL^{-1}), 0.9 mL ultra pure water, sulphuric acid to pH 2	0.5	2.0
4	1 mL plasma, 0.1 mL std (10 ng μL^{-1}), 0.9 mL ultra pure water, ultrasonicate 30 min, sulphuric acid to pH 2	0.5	2.0
5	1 mL plasma, 0.1 mL std (10 ng μL^{-1}), 0.9 mL ultra pure water, ultrasonicate 1 min, sulphuric acid to pH 2	0.5	2.0
6	1 mL plasma, 0.1 mL std (10 ng μL^{-1}), 0.9 mL ultra pure water, ultrasonicate 1 min, sulphuric acid to pH 1	0.5	2.0
7	2 mL plasma, 1 mL std (0.5 ng μL^{-1}), 0.2 mL isopropanol, ultrasonicate 1 min, sulphuric acid to pH 1	0.16	3.2
8	Classic LLE	6.0	3.0

a donor flow rate of 100 $\mu\text{L min}^{-1}$ the entire sample volume passed through the extractor (on the external side of the membrane) in 4.5 min. The acceptor flow was then started and the extract from the inner volume of the membrane was collected in a vial over 1 min. An aliquot of 10 μL of the internal standard solution (3-methyl-4-nitrophenol) was added to the vial and the resulting solution was vortex-mixed for a few seconds. After the extraction the donor and acceptor solutions were pumped through the system for 4.5 min to clean the extractor. The time needed for a total extraction cycle, including extraction, sample collection and wash, was proportional to the donor flow rate.

2.7. Plasma sample treatment

Plasma samples were treated in different ways (method 1–7 in Table 2) before SLM extraction and compared to classic liquid extraction (method 8). Different pH values and denaturation methods were tested, in order to minimize possible plasma matrix effects on the extraction.

All samples contained 1–2 mL human plasma, 0.1–1 mL standard solution (0.5–10 $\mu\text{g mL}^{-1}$ of each analyte for samples, and 0.0 $\mu\text{g mL}^{-1}$ for blanks). For comparison, standard liquid–liquid extraction was also performed with 2 mL blank plasma and 1 mL dihexylether in a 10-mL test tube. The phases were shaken for 9 min and this procedure was repeated once. The extracts were pooled, centrifuged at 3000 rpm for 2 min and the resulting supernatant was then extracted twice with 1 mL of acceptor phase.

To evaluate the influence of the extraction time, amount and concentrations of the analytes injected on extraction efficiency,

injection loops of three sizes (0.1, 0.2 and 0.5 mL) and two sample concentrations (0.1, 0.5 $\mu\text{g mL}^{-1}$) were tested.

2.8. LC/ESI-MS

HPLC was performed using an LC 10 AD vp chromatograph equipped with a SIL-10 AD vp autoinjector (Shimadzu, Japan) and a Hypersil-Gold C₁₈ column (50 mm \times 2.1 mm id, 3.5 μm particle size; Thermo, Cheshire, UK). In each case the injection volume was 5 μL , the (isocratic) mobile phase was 45% acetonitrile in water with 0.01% formic acid, flow rate 200 $\mu\text{L min}^{-1}$, and the total run time was 18 min.

The HPLC system was coupled to an ESI triple quadrupole API 2000 mass spectrometer from Applied Biosystems (MDS SCIEX, Foster City, Canada). The resulting quasi-molecular ions $[\text{M}-\text{H}]^-$ (m/z 152 for IS, 183 for DNP, 197 for DNOC and 239 for both Dinoseb and Dinoterb) were measured in negative ion, selected ion monitoring (SIM) mode with the following settings: desolvation temperature 350 $^{\circ}\text{C}$, declustering potential -40V , focusing potential -400V , entrance potential -10V , nebulizer gas 10 psi, curtain gas 20 psi, ion spray voltage -4500V , and ion source gases 20 psi. Typical mass chromatograms for plasma samples are shown in Fig. 4.

The instrumental linearity for the analytes was investigated in the range of 0.3–3 ng and no curvature was detected.

To calculate the extraction efficiency a volumetric internal standard and single-point calibration with an external standard were used. The response curve within the investigated concentration range was linear for both internal standard and analytes.

3. Results and discussion

3.1. Aqueous samples

3.1.1. Extraction procedure

The results of the experimental matrix with aqueous samples (Table 1) showed that the extraction efficiency for the studied compounds was highest with the lowest flow rate of the donor phase (50 $\mu\text{L min}^{-1}$), salt added to the donor phase, and the highest tested temperature (50 $^{\circ}\text{C}$). For practical reasons no higher temperatures were tested, to avoid possible coagulation and clogging of the membrane pores. Donor flow rates lower than 50 $\mu\text{L min}^{-1}$ were not tested, since short extraction times were desired. The

Table 3

SLM extraction efficiency for the tested dinitrophenols in aqueous standards.

Pesticide	Day 1	Day 2	Day 3	Day 8
DNP	73 (4)	71 (3)	73 (3)	76 (2)
DNOC	89 (4)	79 (10)	85 (3)	95 (2)
Dinoseb	67 (10)	62 (4)	69 (5)	74 (6)
Dinoterb	62 (10)	65 (6)	72 (7)	81 (7)

Coefficients of variation in % are shown within brackets, $n = 3$. The same membrane was used in all extractions.

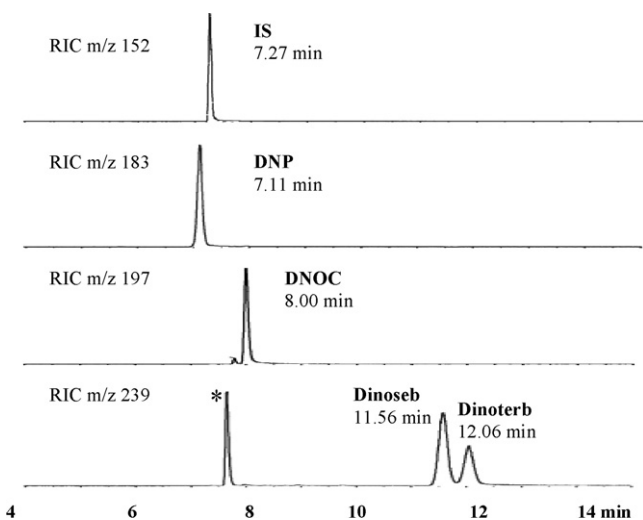


Fig. 4. Chromatograms obtained by LC/ESI-MS of spiked plasma samples in SIM mode, monitoring the $[\text{M}-\text{H}]^-$ ions. 100 μL plasma samples, 0.5 ng μL^{-1} extracted. *Unknown compound detected in all plasma samples.

Table 4
Plasma sample treatment, efficiency and R.S.D.

Method	<i>n</i>	DNP efficiency % (R.S.D.%)	DNOc efficiency % (R.S.D.%)	Dinoseb efficiency % (R.S.D.%)	Dinoterb efficiency % (R.S.D.%)
1	3	3 (36)	9 (17)	2 (22)	2 (21)
2	3	14 (3)	23 (4)	14 (12)	25 (19)
3	3	16 (3)	25 (7)	19 (15)	36 (21)
4:1	1	23	36	24	44
4:2	1	23	36	24	45
5:1	1	29	37	24	55
5:2	1	27	38	24	56
6:1	1	25	34	29	66
6:2	1	25	35	22	48
7	3	46 (3)	58 (3)	30 (10)	33 (10)
8	3	84 (3)	83 (7)	70 (7)	79 (11)

See Table 2 for a key to the treatment methods. Method 1–7 are SLM methods and method 8 classic LLE extraction. Samples 4–6 were made in duplicate (*n* = 2).

Table 5
Extraction efficiency and R.S.D.s obtained for different sample volumes, extraction times, concentrations and sample amounts, *n* = 3 (the membrane was used at least three times).

Sample volume	Extraction time (min)	Amount injected (ng)	DNP efficiency % (R.S.D.%)	DNOc efficiency % (R.S.D.%)	Dinoseb efficiency % (R.S.D.%)	Dinoterb efficiency % (R.S.D.%)
100 μ L loop 0.5 ng μ L ⁻¹	4.5	50	44 (5)	64 (4)	32 (6)	36 (6)
500 μ L loop 0.1 ng μ L ⁻¹	22.5	50	58 (7)	71 (7)	40 (9)	43 (8)

same set of parameters was subsequently used for all samples. After 5 min wash there were no detectable levels of the analytes in the acceptor. However, a 9-min wash was applied in all experiments. The total time required for an extraction cycle, including extraction, sample collection and wash, was 20 min at a donor flow rate set to 50 μ L min⁻¹. In evaluating the system, we obtained a relatively flat response surface indicative of sufficient robustness for the method.

3.1.2. Investigation of extraction efficiency, reproducibility, durability and LOD

The extraction performance of the system, in terms of extraction efficiency, reproducibility and durability of the membrane, was initially investigated for aqueous samples. The extraction efficiency is defined as the number of moles of the analyte collected in the acceptor phase, divided by the number of moles injected into the system [1] and is thus dependent on both the fraction of free ionised analyte in the acceptor phase and the recovery of the extraction. However, in this study the efficiency was considered rather than the enrichment factor.

In previous studies a similar, but larger extractor (the so-called XT-extractor), was used for 30 extractions with no significant reduction in efficiency [15]. Similarly, our investigations of the extraction reproducibility for the miniaturized device used in the present study, showed that the same liquid membrane could be used for several days with no loss of efficiency (Table 3). The results also show that, although the compounds have widely varying log *P* values (as listed in Table 1), the extraction efficiency was only slightly lower for Dinoseb and Dinoterb, the most lipophilic compounds, than for the other compounds.

The method limit of detection (LOD) of the analytical procedure, including the extraction and LC/ESI-MS, was determined for each of the analytes in aqueous samples, using a *S/N* ratio of 3, and found to range between 0.02 and 0.03 μ g mL⁻¹. Although quite low enrichment factors can be achieved with the current SLM device, the LODs achieved are 50-fold lower than the exposure limit for DNOc in whole blood, which is set to 1 μ g mL⁻¹ [19]. Blood levels above 20 μ g mL⁻¹ may give symptoms of poisoning [19]. In all cases, carry-over was below LOD.

3.2. Plasma samples

3.2.1. Effect of sample pre-treatment and sample volume on extraction efficiency

The extraction efficiency was investigated for plasma samples pre-treated in different ways prior to SLM extraction (see Table 2 for details). The efficiency was compared with that obtained for classic liquid–liquid–extraction, which yielded values between 70 and 84%, as shown in Table 4. The rather high efficiency implies that interactions between the analytes and plasma proteins are not a major problem. For SLM extractions, method 7 was found to yield the best efficiency (see Table 4). This method involves denaturation of plasma proteins by addition of isopropanol and adjustment of pH to 1 with sulphuric acid. A lower pH is to be preferred, most likely to neutralise as many analytes as possible in the donor phase, rather than disrupting interactions with proteins. Addition of isopropanol was advantageous, instead of pure water or formic acid. This may be explained by a higher diffusion rate in a sample with more organic solvent, and is probably not due to the denaturation effect itself. The lower efficiency obtained for plasma samples compared to spiked aqueous samples (Table 3) may also be due to the higher viscosity of the former.

Method 7 also gave the best repeatability, with R.S.D.s \leq 10% for all of the analytes. Carry-over was below LOD. Method 7 was chosen for all subsequent experiments.

Two different sample volumes (same amount of analytes), in terms of different injection loops, were compared since this determines the duration time of the sample in the extractor. The results are presented in Table 5. A 5-fold increase of the sample volume, and thus the extraction time of the sample plug in the extractor, only slightly improved the efficiency. This further indicates that the most important parameter limiting the efficiency is the diffusion in the sample, and not in the organic liquid membrane. In all cases the repeatability was high, with R.S.D. values of 10% or lower.

4. Conclusions

The described inexpensive and simple set-up provides a convenient means for the liquid–liquid extraction of weak acids such as

those tested in samples with small volumes. The principle is the same, with comparable recoveries and repeatability as with the HFLPME methods published so far. However, the design is different with a reusable membrane and this study indicates that the system should be well suited for on-line coupling, since carry-over was in all experiments below detection limits. The presented device provides scope to minimize manual handling, solvent consumption as well as sample volume. In addition, there were no problems with protein clogging and the system can be used across large pH and temperature ranges, since none of the parts are very pH or temperature sensitive. The robustness of the system was high when tested on aqueous standards, using the same membrane during several days. However, the robustness with plasma has to be further investigated, although extraction of plasma samples could be performed in at least triplicates without loss of performance.

It was found to be beneficial for the extraction efficiency to dilute the plasma samples, most likely due to a decrease in viscosity. The pH level in the donor phase was also important. Acceptable efficiencies and high repeatability were achieved after a 20-min extraction cycle for plasma samples diluted with isopropanol and adjusted to pH 1. If increased extraction efficiency is desired, the extraction time should be prolonged by decreasing the flow rate.

For some applications, it may be desirable to extract smaller sample volumes than those handled in this work. This may require lower flow rates to achieve comparable efficiencies.

Acknowledgments

We thank Dr. Maria Athanasiadou (Department of Environmental Chemistry, Stockholm University, Sweden) for advice and for providing the plasma samples. Dr. Magnus Åberg for the setup and

evaluation of the experimental design, and Prof. Bo Karlberg for reviewing the manuscript (both from the Department of Analytical Chemistry, Stockholm University, Sweden).

References

- [1] J.Å. Jönsson, L.J. Mathiasson, *J. Chromatogr. A* 902 (2000) 205–225.
- [2] J.Å. Jönsson, P. Lökvist, G. Audunsson, G. Nilvé, *Anal. Chim. Acta* 277 (1993) 9–24.
- [3] X. Wang, D. Kou, S. Mitra, *J. Chromatogr. A* 1089 (2005) 39–44.
- [4] S. Müller, M. Möder, S. Schrader, P. Popp, *J. Chromatogr. A* 985 (2003) 99–106.
- [5] S. Pedersen-Bjerggaard, K.E. Rasmussen, *J. Chromatogr. A* 1184 (2008) 132–142.
- [6] G. Shen, H. Lee, *Anal. Chem.* 75 (2003) 98–103.
- [7] G. Ouyang, W. Zhao, J. Pawliszyn, *J. Chromatogr. A* 1138 (2007) 47–54.
- [8] S.-P. Huang, S.-D. Huang, *J. Chromatogr. A* 1176 (2007) 19–25.
- [9] T. Berhanu, J. Liu, R. Romero, N. Megersa, J.Å. Jönsson, *J. Chromatogr. A* 1103 (2006) 1–8.
- [10] L. Hou, G. Shen, H. Lee, *J. Chromatogr. A* 985 (2003) 107–116.
- [11] G. Ouyang, J. Pawliszyn, *Anal. Chem.* 78 (2006) 5783–5788.
- [12] D. Pezo, J. Salafraña, C. Nerin, *J. Chromatogr. A* 1174 (2007) 85–94.
- [13] J.Å. Jönsson, L. Mathiasson, *Trends Anal. Chem.* 18 (5) (1999) 318–325.
- [14] L. Chimuka, M.M. Nindi, M.E.M. ElNour, H. Frank, C. Velasco, *J. High Resol. Chromatogr.* 22 (1999) 417–420.
- [15] O.B. Jonsson, U. Nordlöf, U.L. Nilsson, *Anal. Chem.* 75 (2003) 3506–3511.
- [16] O. Jonsson, U. Nilsson, *Anal. Bioanal. Chem.* 377 (2003) 182–188.
- [17] EPA, Decision and Emergency Order Suspending the Registrations of all Pesticides Containing Dinoseb, *Feb Reg.* 51 (1986) 36634.
- [18] UNEP, FAO, Inclusion of Chemicals in the Interim Prior Informed Consent Procedure—Review of Notifications of Final Regulatory Actions to Ban or Severely Restrict A Chemical—Dinoseb, UNEP/FAO/PIC/ICRC.3/15, Geneva, 2001.
- [19] A. Moretto, in: T.C. Marrs, B. Ballantyne (Eds.), *Pesticide Toxicology and International Regulation*, Wiley, Chichester, England, 2004, p. 457.
- [20] European Council, Council Directive 75/440/EC of 3 November 1998 on the quality of water intended for human consumption.
- [21] European Council, Council Directive 98/83/EEC of 16 June 1998 concerning the quality required of surface water intended for the abstraction of drinking water in the Member States.



An improved method for the simultaneous analysis of phenolic and steroidal estrogens in water and sediment

A. Hibberd, K. Maskaoui, Z. Zhang, J.L. Zhou*

Department of Biology and Environmental Science, School of Life Sciences, University of Sussex, Falmer, Brighton BN1 9QG, UK

ARTICLE INFO

Article history:

Received 28 April 2008

Received in revised form 29 August 2008

Accepted 4 September 2008

Available online 12 September 2008

Keywords:

Endocrine disrupting chemicals

Phenols

Steroids

Solid-phase extraction

Microwave-assisted extraction

Gas chromatography–tandem mass spectrometry

ABSTRACT

This paper describes an improved method for the extraction and analysis of seven endocrine disrupting chemicals with wide-ranging polarities from water and sediments using gas chromatography–tandem mass spectrometry (GC–MS/MS). The analytes were 4-*tert*-octylphenol, 4-nonylphenol, bisphenol A, estrone, 17 β -estradiol, 17 α -ethynylestradiol and 16 α -hydroxyestrone. The optimised GC–MS/MS method produces increased selectivity and sensitivity compared to GC–MS, with limit of detection ranging from 0.01 to 0.49 ng L⁻¹ in water and from 0.05 to 0.14 ng g⁻¹ in sediment. Extraction from aqueous samples was performed by solid-phase extraction (SPE) and from sediment samples by microwave-assisted extraction (MAE). The improved method for the clean-up of sediment extracts carried out by SPE enhanced EDC recovery (86–102%) while reducing matrix interference and sample drying time. Derivatisation of final sample extracts was achieved using *N,O*-bis(trimethylsilyl)trifluoroacetamide and pyridine, and their stability was enhanced by reconstituting the derivatised extracts with hexane. The method was validated by spiking experiments which showed good recovery and reproducibility. The method was applied to samples taken from the Medway estuary in Kent, UK, where non-conservative behaviour of EDCs was demonstrated.

© 2008 Elsevier B.V. All rights reserved.

1. Introduction

Endocrine disrupting chemicals (EDCs) are of worldwide concern due to their observed effects on the reproductive systems in fish [1,2], other wildlife and possibly even human [3,4]. They are able to do this by blocking or mimicking the normal effect of hormones, affecting their synthesis or metabolism, and changing hormone receptor levels. Chemicals that show endocrine disrupting properties come from a range of chemical groups that are both natural and synthetic in origin. Natural EDCs include estrone (E1), 17 β -estradiol (E2) and 16 α -hydroxyestrone (HE1). These steroidal hormones are excreted by both humans and livestock and are deposited into river systems via sewage treatment works (STW) outfall [5,6] and run-off from agricultural land [7]. The most potent man-made EDC is 17 α -ethynylestradiol (EE2) which is a synthetic hormone used in female contraceptive pills. In addition, important EDCs include 4-*tert*-octylphenol (OP), 4-nonylphenol (NP) and bisphenol A (BPA), all of which are used in household products such as detergents, industrial processes and in the production of plastics. These chemicals are generally found in the ng L⁻¹ range in the aquatic environment [8–10] but even at these low levels estro-

genic effects, such as feminisation and vitellogenin production have been observed in male fish [11]. Phenolic and steroidal EDCs also have the potential to adsorb onto sediments and colloids [12–14]. From these sinks they have the potential to bioaccumulate in, and cause endocrine disruptions to, benthic invertebrates and enter the food chain. It is therefore essential that methods are developed that can simultaneously extract and accurately quantify large groups of these chemicals from complex environmental samples.

The determination of these and other estrogenic compounds in the sediments of river courses is a necessary step towards assessing their potential risk to biota. There are, however, severe difficulties associated with extracting and determining trace level steroidal and phenolic compounds from a complex matrix such as sediments. Extracted sediment samples from rivers typically have a high loading of natural organic matter (NOM) such as humic substances and pigments. An inefficient clean-up stage will allow these products and other contaminants to pass into the final sample extracts. Our earlier work [15] showed that NOM made it difficult to dry sample extracts during the derivatisation procedure, and caused over-loading of the capillary column and severe interferences in compound identification and quantitation. An efficient clean-up of the samples is therefore an important requisite of the extraction procedure. This step has traditionally been carried out using non-deactivated silica gel columns [16,17] and deactivated neutral alumina columns [18] which are time consuming to prepare,

* Corresponding author. Tel.: +44 1273 877318 fax: +44 1273 678937.
E-mail address: j.zhou@sussex.ac.uk (J.L. Zhou).

difficult to clean after use and not always successful in purifying very complex extracts. Solid-phase extraction (SPE) cartridges (e.g., LiChrolut) have also been used for clean-up for the determination of NP [19] and BPA [20] although they only focused on NPs and phthalate esters. Other methods used to clean up sediment samples include high performance liquid chromatography (HPLC) [8] and an LC–LC column switching system [21] although they are complicated and expensive to set up.

Extraction of phenolic and steroidal EDCs from sediments has been accomplished using various methods including acid digestion [22], liquid extraction [16] and Soxhlet extraction [13], and more recently microwave-assisted extraction (MAE) [17]. The MAE method has the benefits of low solvent volume, reduced extraction time, complete decomposition of organic matter, and multiple sample extractions. However, the presence of small particles and NOM in sample extracts from MAE should be removed as completely as possible to achieve a satisfactory separation and prevent false positive signals, a key objective to be achieved in this work.

Previously, gas chromatography–mass spectrometry (GC–MS), LC–MS and LC–tandem MS have been used for the analysis of these compounds [13,23–28]. In comparison GC–tandem MS is a more selective analytical method that can prevent false positive identification and should deliver lower detection limits. An additional objective of this work was to further develop methods for the simultaneous separation and determination of a wide group of EDCs from river water and sediment that gave good recovery and reproducibility and also lower detection limits than GC–MS. The methods were then used to determine the environmental levels of EDCs in river water and sediment samples from the River Medway, a major river in Kent and Sussex, UK, which has not been studied for EDCs, yet rich in wildlife.

2. Experimental

2.1. Chemicals and standard solutions

All of the solvents used in this work including methanol, ethyl acetate, pyridine and dichloromethane were of distilled-in-glass grade and were purchased from Rathburn, UK. Standards of OP, NP, BPA, E1, E2, EE2 and HE1, two internal standards (BPA- d_{16} , and E2- d_2) and the derivatisation agent *N,O*-bis(trimethylsilyl)trifluoroacetamide (BSTFA) containing 1% of trimethylchlorosilane, were all purchased from Sigma–Aldrich, Dorset, UK.

Separate stock solutions of individual compounds were made up at a concentration of 1000 mg L^{-1} in methanol and from these working standards of 10 mg L^{-1} were created. A separate solution of the two internal standards was also prepared at 10 mg L^{-1} in methanol. All of the solutions were stored in the dark at -18°C . Ultra-pure water was supplied from a Maxima HPLC/LS water purification system (USF Elga, UK).

2.2. Aqueous sample preparation

Aqueous samples (2.5L) were taken from below the surface micro-layer in pre-cleaned, glass bottles and preserved by adding 5 mL L^{-1} of 2M sodium azide as a broad spectrum biocide. The samples were filtered within 24 h through pre-ashed (400°C for 4 h) Whatman GF/F filter papers ($0.7 \mu\text{m}$ pore size), using a Büchner apparatus, before 100 ng of internal standards were added by a micro-syringe.

Waters Oasis HLB (hydrophilic–lipophilic–balanced) SPE cartridges (200 mg), with a 6-mL sample reservoir, were held in place on a 12-port Visiprep vacuum manifold (Supelco, USA) and con-

ditioned prior to use by passing through 5 mL of ethyl acetate to remove residual bonding, followed by 10 mL of methanol, which was drawn through under very low vacuum to ensure thorough soaking of the sorbent for 5 min. The cartridges were then washed with $3 \times 5 \text{ mL}$ of ultra-pure water at $1\text{--}2 \text{ mL min}^{-1}$. Between conditioning and sample extraction the cartridges were kept wet with ultra-pure water. The samples were then drawn through the SPE column at $<20 \text{ mL min}^{-1}$, which is three times faster than that used in our earlier methods [25,29].

Following extraction, the cartridges were dried thoroughly under vacuum for at least 30 min before the bound chemicals were eluted by gravity into glass sample bottles (PerkinElmer, UK) using 15 mL of ethyl acetate. The extracts were then reduced in volume to 0.5 mL using a gentle N_2 stream before being transferred by Pasteur pipette to 3 mL reaction vials along with three rinses of ethyl acetate. These were again concentrated by N_2 to 0.5 mL and stored at 4°C until derivatisation.

2.3. Derivatisation

The extracts were first completely dried under a gentle stream of N_2 , to which $50 \mu\text{L}$ each of BSTFA and pyridine (dried with KOH solid) were added before being mixed by percussion. The samples were then allowed to react on a heating block for 30 min at $60\text{--}70^\circ\text{C}$, left to cool to room temperature, dried again with N_2 , before finally being reconstituted with $100 \mu\text{L}$ of hexane. Following derivatisation, the samples were transferred by Pasteur pipette into GC vials with a $300 \mu\text{L}$ fused insert (Anachem, UK) before $1 \mu\text{L}$ was injected by auto-sampler for GC–MS/MS analysis.

2.4. Sediment sample preparation

The sediment samples were taken with a stainless-steel Van Veen grab. Upon collection, the top oxic fraction of the samples were removed and transferred into pre-cleaned glass jars by a solvent rinsed stainless steel spoon. The samples were frozen on return to the laboratory before being freeze-dried (Heto Powerdry PL3000) for 4 d. After lyophilisation the samples were ground and sieved to $<500 \mu\text{m}$ and then stored in the dark in the original glass jars at room temperature until extraction. Dried samples (3 g) were transferred into glass, Teflon lined, extraction vessels and spiked with 100 ng of internal standards. The samples were then left for at least 1 h to allow sorption processes to occur, as in nature. To all the samples methanol (25 mL) and 2 g of copper granules (Sigma–Aldrich) were added before MAE.

2.5. MAE

Sediments were extracted using microwave, similar to our earlier approach [16]. The vessels were put into the MARS-X Laboratory Microwave Accelerated Extraction system (CEM Corp., USA) and heated to 110°C for 15 min, with a 7-min ramp, at 200 psi. After cooling to room temperature for 1 h, the supernatants were decanted into 250 mL round bottomed flasks along with $3 \times 15 \text{ mL}$ sample rinses of methanol. With each rinse addition, the samples were stirred thoroughly and allowed to settle before decanting. The combined supernatants were reduced in volume to 1 mL using a Büchi Rotavapor R-205 rotary evaporator. The water bath was set at 40°C and the sample flask was spun at 50 rpm .

2.6. Sediment clean-up

An improved clean-up process was used in this work by decanting the sediment extracts (1 mL) into 500 mL of ultra-pure water along with $3 \times 10 \text{ mL}$ ultra-pure water rinses. The EDCs in the

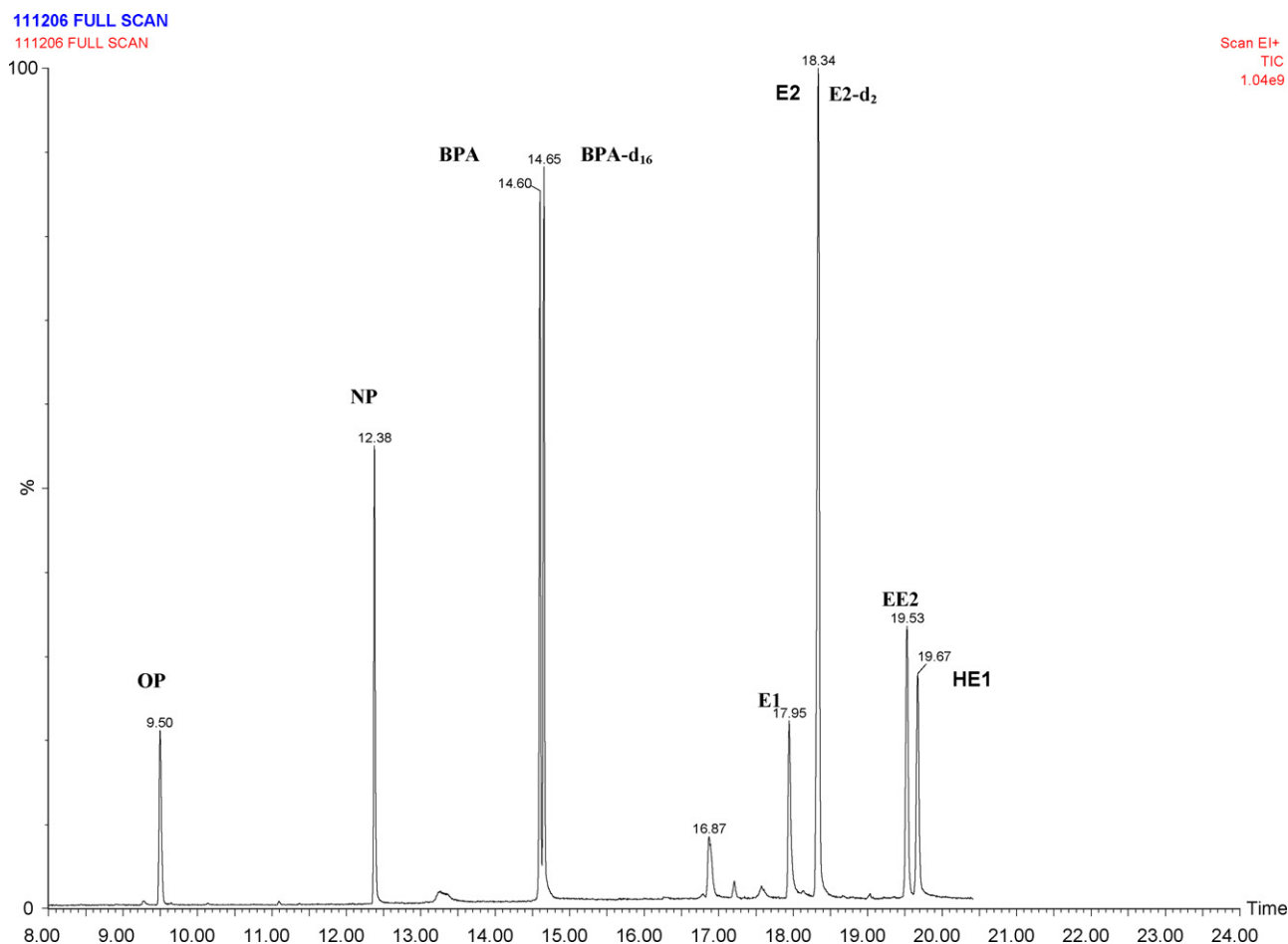


Fig. 1. Full scan of the target compounds and internal standards in GC–MS/MS.

extracts were dissolved back into an aqueous solution while allowing particles such as silt and sand to sink to the bottom. The aqueous samples were then extracted by SPE through Waters Oasis HLB SPE cartridges, as explained earlier. This procedure effectively removed most extraneous material and left the final extract clear in colour. The analytes were subsequently eluted from the SPE cartridges and prepared for analysis exactly as previously outlined for water samples.

2.7. GC–MS/MS analyses

GC–MS/MS analysis was performed using a 6890N network gas chromatograph (Agilent Technologies, USA) interfaced with a tandem quadrupole mass spectrometer (Quattro Micro, Micromass, USA). An Agilent HP-5 capillary column (30 m) with a 0.25-mm internal diameter and a 0.25- μ m film thickness was used. The carrier gas was helium was maintained at a constant flow rate of 1.0 mL min⁻¹. The GC column temperature was programmed from 100 (initial equilibrium time 1 min) to 200 °C via a ramp of 10 °C min⁻¹, 200–260 °C via a ramp of 15 °C min⁻¹, 260–300 °C via a ramp of 3 °C min⁻¹ and maintained at 300 °C for 2 min.

The MS was by positive electron impact ionisation and was operated in full scan mode from m/z 50 to 600 for qualitative analysis (Fig. 1). For quantitative analysis, multiple reaction monitoring (MRM) mode was used (Fig. 2). The inlet and MS transfer line temperatures were maintained at 280 °C and the ion source temperature was 250 °C. Sample injection (1 μ L) was in splitless mode. The electron impact energy used was 70 eV. The collision gas used was argon. Precursor and product ions are shown in Table 1.

2.8. Validation of the method

The linear concentration range of the GC–MS/MS analytical technique was examined by a series of 1 μ L injections of the target compounds with 11 different concentrations (0.01, 0.05, 0.1, 0.5, 1, 3, 5, 10, 20, 50 and 100 ng μ L⁻¹) for each compound, with three replicates per concentration. The linear range for all compounds was found to be between 0.01 and 5 ng μ L⁻¹, with the correlation coefficients varying between 0.95 and 0.99. The reproducibility was also good, as the relative standard deviation of all replicate analyses was within 20%.

3. Results and discussion

3.1. Mass spectra of the silylated EDCs

The TMS⁺ ion (m/z 73) was found in the spectra for all of the compounds investigated. Wherever possible, the molecular ion of the silylated derivative was chosen as the parent ion for the compound. In the case of OP the parent ion chosen was m/z 280 ($M+1$)⁺ which at the loss of two methyl groups gave the daughter ion m/z 249. The confirmation ion m/z 265 ($M-15$)⁺ was a slightly less intense peak that corresponded to the loss of one methyl group. Previous GC–MS studies have used the ion m/z 207 for quantification of OP [17,25] but during this work it was found that this ion is a common fragment to all of the compounds under investigation and so it was avoided. For NP, the molecular ion at m/z 292 was used as the parent and the daughter ion at m/z 179 can be attributed to the loss of C₈H₁₇. BPA

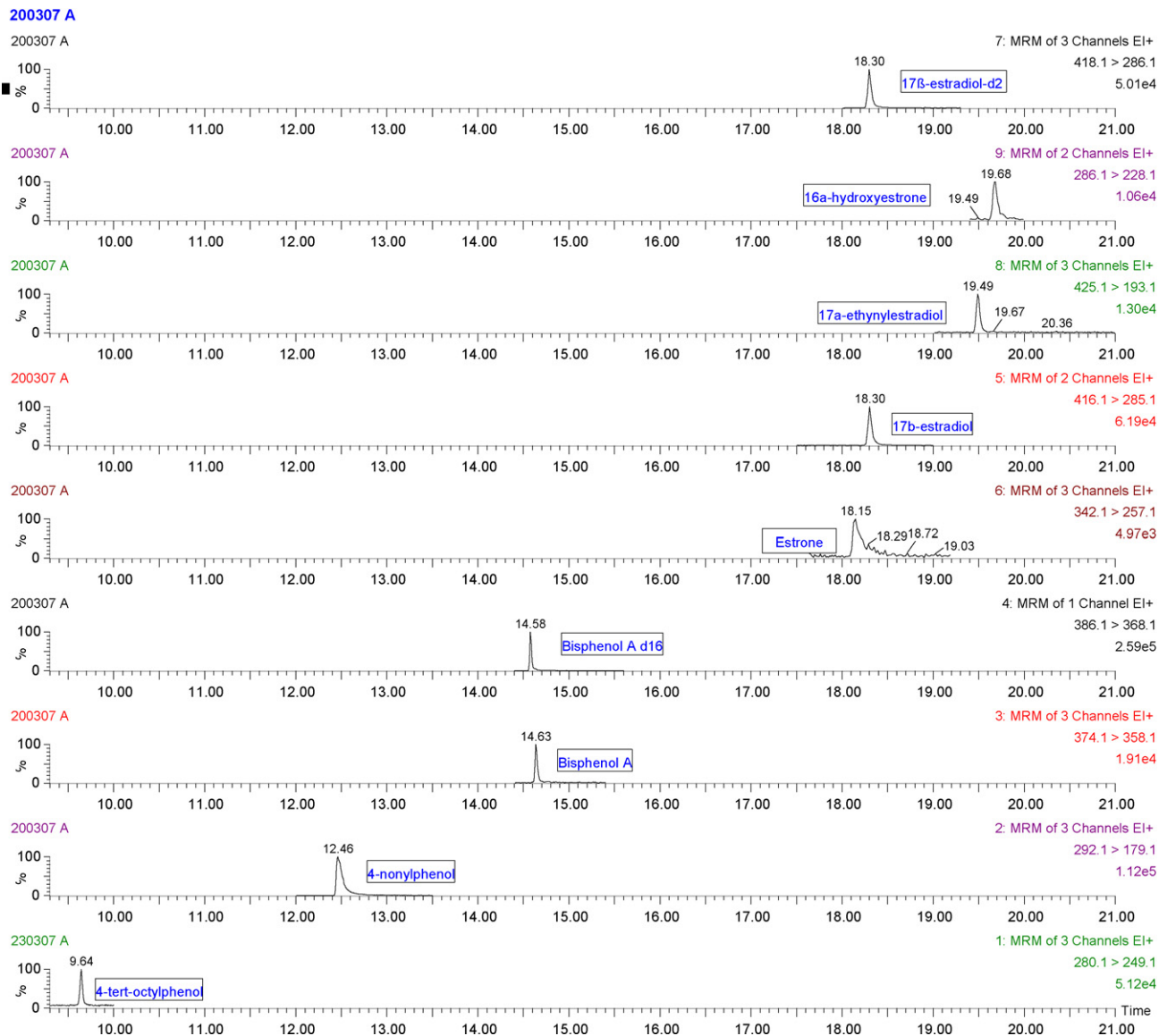


Fig. 2. Chromatograms of the extracted and overlapped MRM of the target compounds.

again made use of the molecular ion m/z 374 as the parent ion, with the stable fragment m/z 358 corresponding to the loss of one oxygen as the daughter. Confirmation ions were provided by the loss of a methyl group (m/z 359) and the loss of an OH group (m/z 357). For E1, the molecular ion of the mono-TMS derivative (m/z 342) was used as the parent ion with m/z 257 ($M-85$)⁺ as the quantitative

daughter. The confirmation was supplied by m/z 205 ($M-37$)⁺. In the case of E2, the di-TMS derivative was formed as evidenced by the molecular ion at m/z 416. This parent ion fragmented to give the daughter ion m/z 285. For EE2 the transition used was m/z 425 > m/z 193 with confirmation by m/z 231. This transition was also used by Ternes et al. [5] who found that the effect of the co-elution of EE2, possibly from humic substances [16,17], could be avoided with this transition. This example of the specificity of GC-MS/MS shows that the method has reduced probability of giving rise to false positives due to its increased selectivity. Finally, HE1 was quantified using the parent ion m/z 286, which corresponds to the unsilylated molecular ion of the compound, with the daughter m/z 228. Good determination and separation was achieved by this method when the seven compounds and two internal standards were analysed as a mixture (Fig. 2).

To determine the optimum collision energy used by the GC-MS/MS for fragmentation, a standard containing all seven compounds and internal standards was analysed by GC-MS/MS using different collision energy from 5 to 30 eV. The collision energy for the individual compounds that gave the peak with the largest area

Table 1
GC-MS/MS parameters for the target EDCs

Compound	Retention time (min)	Molecular mass	Precursor ion (m/z)	Product ion (m/z)
OP	9.64	206	280	249
NP	12.46	220	292	179
BPA	14.60	228	374	358
BPA-d ₁₆	14.65	244	386	368
E1	18.15	270	342	257
E2	18.30	272	416	285
EE2	19.49	296	425	193
HE1	19.68	286	286	228
E2-d ₂	18.30	274	418	286

Table 2

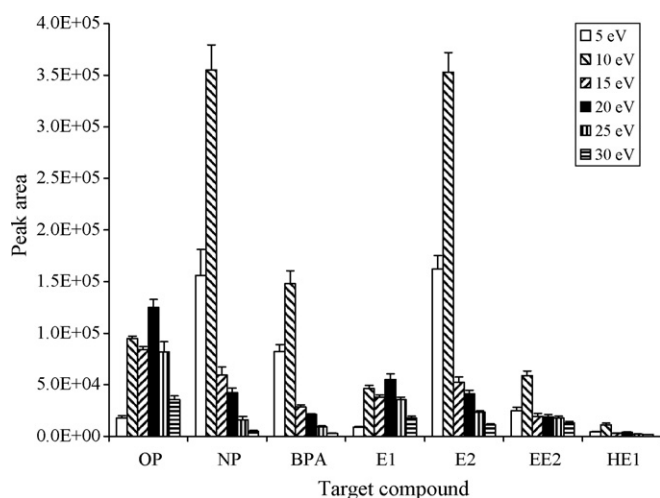
Recovery of the target EDCs from river water: pH 7.9, salinity = 0‰

Spiked level (ng L ⁻¹)	OP	NP	BPA	E1	E2	EE2	HE1
50	65 ± 5	109 ± 8	100 ± 1	89 ± 8	106 ± 3	99 ± 4	91 ± 7
100	99 ± 28	77 ± 6	96 ± 4	72 ± 5	79 ± 4	99 ± 8	113 ± 2
200	82 ± 22	78 ± 14	112 ± 3	119 ± 11	94 ± 2	75 ± 1	116 ± 12

Table 3

Mean recovery (±S.D.) of the EDCs during clean up of sample extracts by silica gel and SPE method

	OP	NP	BPA	E1	E2	EE2	HE1
SPE clean-up (%)	94 ± 4	102 ± 4	100 ± 7	90 ± 1	102 ± 16	86 ± 1	99 ± 20
Silica gel clean-up (%)	86 ± 8	114 ± 2	56 ± 6	60 ± 8	92 ± 2	132 ± 7	50 ± 13

**Fig. 3.** Optimisation of the collision energy for MRM in GC–MS/MS. Error bar = standard deviation.

was chosen as the optimum (Fig. 3). It was found that the collision energy of 10 eV was the optimum for NP, BPA, E2, EE2 and HE1, while the collision energy of 20 eV was optimum for OP and E1.

3.2. Recovery from water and sediment samples

Recovery experiments were carried out by spiking 1 L river water samples with a known amount of the standard mixture (50, 100 and 200 ng L⁻¹). Unspiked sub-samples were also extracted and analysed so that background levels of the analytes could be subtracted from those found in the spiked samples. Good recoveries were obtained ranging from 65 to 119% (Table 2). In comparison to our earlier method [25], the recovery for NP has been clearly improved.

Freeze dried sediment samples from the River Ouse, Sussex, UK, that were known to have a very high NOM content and previ-

Table 4

Inter- and intra-day repeatability of RRF

RRF	Intra-day (n = 6)			Inter-day (n = 4)		
	Mean	S.D.	R.S.D.	Mean	S.D.	R.S.D.
OP	0.18	0.02	11.10	0.20	0.04	20.00
NP	0.38	0.03	7.89	0.40	0.07	17.5
BPA	0.82	0.01	1.23	0.88	0.01	1.22
E1	0.63	0.05	7.94	0.62	0.04	6.45
E2	0.41	0.07	17.07	0.46	0.05	10.87
EE2	0.25	0.04	16.00	0.25	0.01	4.00
HE1	0.26	0.01	3.85	0.30	0.01	3.33

ously given poor recovery results, were spiked with EDCs (100 ng), extracted and then purified using both the SPE and silica gel methods. As shown in Table 3, improved recoveries (86–102%) were obtained by the SPE method in comparison to the silica gel method.

3.3. Quality assurance

To assess the repeatability of the method and to examine the stability of derivatised EDCs, derivatised EDC standards and internal standards at 1 ng μL⁻¹ were analysed consecutively by GC–MS/MS over the next 6 h, as well as daily for 4 d. As shown in Table 4, the relative response factor (RRF) for the EDC derivatives was highly stable over the 4 d period, which is a major improvement compared to our earlier method [25]. Slightly better stability was found within the same d.

The limit of detection (LOD) is the lowest concentration that can be measured with specified certainty. It is calculated as three times the standard deviation, at zero concentration, of a blank sample in 10 independent performances. As shown in Table 5, the LOD values ranged from 0.01 to 0.49 ng L⁻¹ in water, and 0.05 to 0.14 ng g⁻¹ in sediments, which are an improvement from our earlier methods [17,25]. Similarly the limit of quantification (LOQ) was also improved. In addition, the LOD values are comparable to those achieved by LC–tandem MS [28]. Throughout the work analysis was conducted in the linear range of the method.

Table 5

Limit of detection and limit of quantification for the target EDCs

Compound	LOD in water (ng L ⁻¹)		LOQ in water (ng L ⁻¹)		LOD in sediment (ng g ⁻¹)		LOQ in sediment (ng g ⁻¹)		Linear range (ng μL ⁻¹)
	This work	[25]	This work	[25]	This work	[17]	This work	[17]	
OP	0.10	2.6	0.32	8.5	0.14	0.5	0.47	1.7	0.01–5
NP	0.01	0.8	0.04	2.6	0.08	0.5	0.27	1.7	0.01–5
BPA	0.49	5.3	1.63	17.4	0.13	1.0	0.44	3.4	0.01–5
E1	0.25	1.7	0.84	5.6	0.05	0.3	0.17	0.9	0.01–5
E2	0.28	3.4	0.95	11.2	0.06	0.3	0.21	0.9	0.01–5
EE2	0.27	0.8	0.90	2.6	0.14	0.4	0.47	1.4	0.01–5
HE1	0.22	0.3	0.72	1.0	0.05	0.2	0.17	0.5	0.01–5

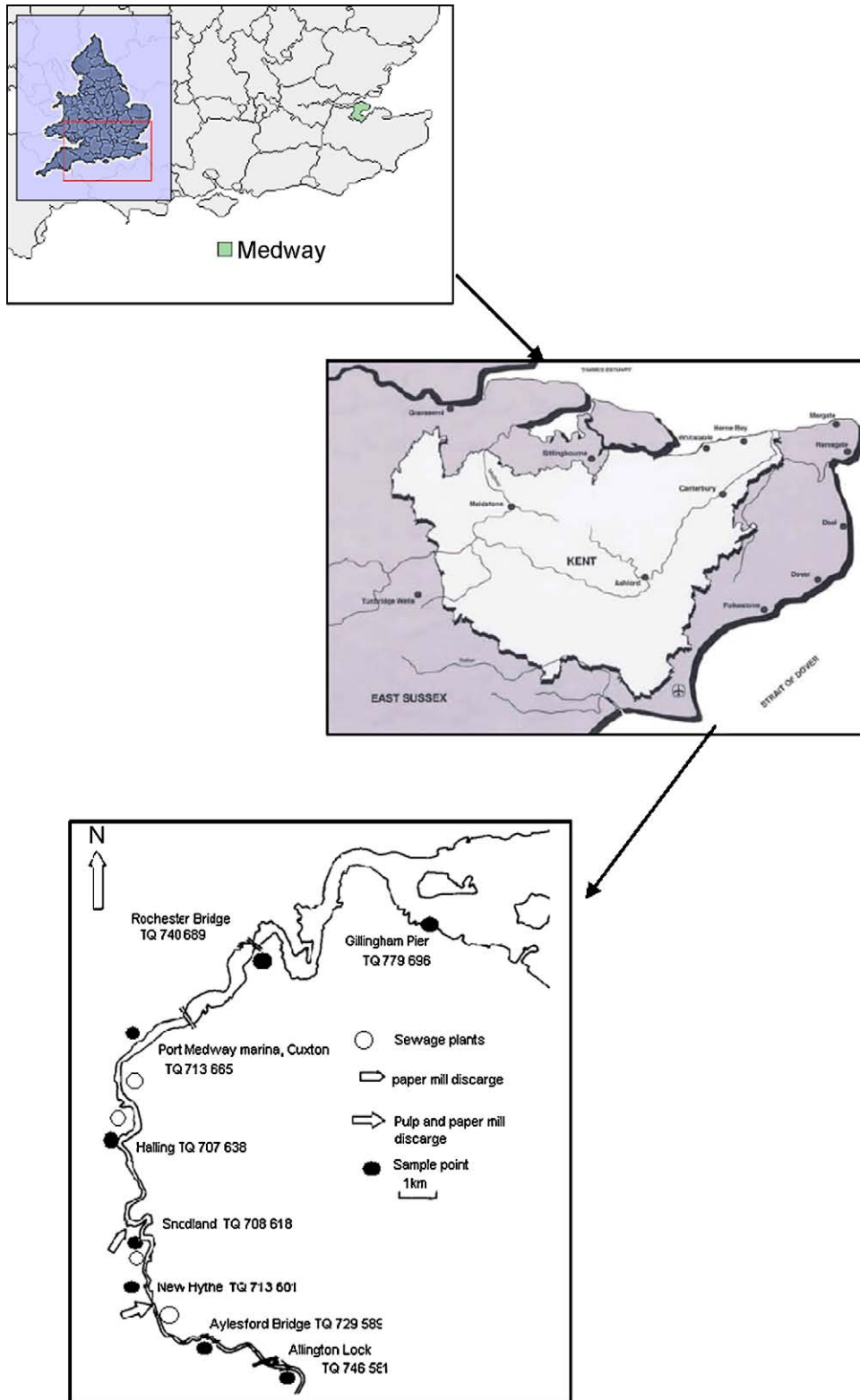


Fig. 4. The Medway estuary, Kent, UK showing sites of sampling for water and sediments.

3.4. Application of the methods to environmental samples

As shown in Fig. 4, the River Medway in Kent, UK was sampled from eight stations between the tidal limit at Allington Lock (51°17'44.36"N, 0°30'18.81"E) and the estuary at Gillingham pier

(51°23'56.02" N, 0°33'19.92" E) in May, August and November 2005. This section of the river was chosen for sampling because it had not been studied for EDCs before and also had four STW (Aylesford, Ham Hill, Halling and Cuxton) that are sources of EDC inputs, with several more STW further down in the estuary. The Medway in this

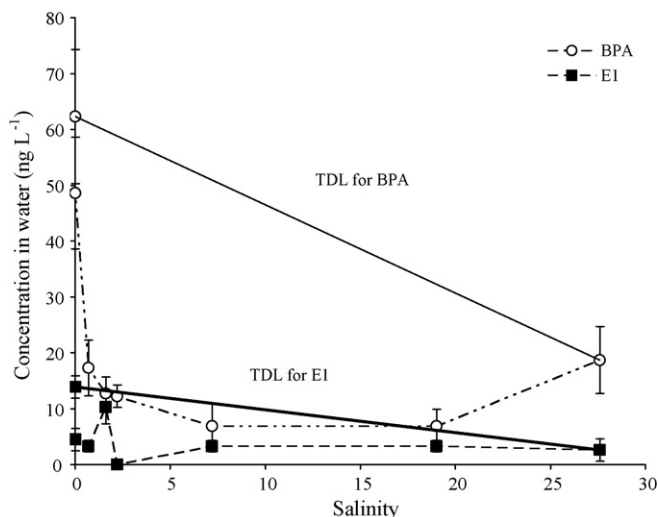


Fig. 5. Salinity profiles of BPA and E1 in the Medway estuary, UK, in August 2005: (TDL) theoretical dilution line. Error bar = standard deviation.

section is free of major industries apart from two large paper mills and some small industrial companies at New Hythe and Snodland. The largest conurbation is at Rochester, while the rest of the estuary is bordered by marshes, fields and small villages.

The levels for EDCs found in the water samples from the River Medway are in accordance with those detected from other rivers and streams with indications that the contamination are derived from STW along the river [30,31]. OP and BPA were found at their highest levels (37.6 and 69.3 ng L⁻¹, respectively) in May at New Hythe. These chemicals were found at levels above the LOD in every sample. The other analytes that were detected in all samples were E1 (0.6–14.3 ng L⁻¹) and E2 (3.1–21.4 ng L⁻¹). In contrast, EE2 was only found in one sample taken from Gillingham Pier in May (1.5 ng L⁻¹). NP (LOD–4.4 ng L⁻¹) was found in two-thirds of the samples, with the highest level being found at Cuxton in November. HE1 was found at its highest level (5.8 ng L⁻¹) at Aylesford Bridge in August which was about twice the level found at the same station in May (2.4 ng L⁻¹). These results are quite possibly associated with the STW at Aylesford. The only other high level found for HE1 was from Cuxton where there is also a STW with an outfall into the river.

In sediments, contamination was also widespread by OP (4.7–31.3 ng g⁻¹), BPA (7.7–56.1 ng g⁻¹), E1 (<LOD–5.8 ng g⁻¹) and E2 (<LOD–11.2 ng g⁻¹) along the entire section of river. NP levels were found to be between <LOD (in 11 of the 24 samples)–11.0 ng g⁻¹ at Allington lock in November. EE2 was not found above LOD in any of the samples. Finally HE1 levels were in the range <LOD–5.0 ng g⁻¹ with contamination only being found in five of the samples and the two highest levels found at Cuxton, close to STW.

The plots of EDC concentrations in water against salinity showed that the concentrations of both BPA and E1 decreased with an increase in salinity, suggesting river Medway as a key source of EDCs to the estuary (Fig. 5). In addition, the concentrations of BPA and E1 at different salinities all fell below the theoretical dilution line (TDL), indicating that these two compounds had been removed due to potential sorption to sediments and biodegradation, and therefore behaved non-conservatively. The findings highlight the potential of estuarine mixing zone as a sink for EDCs, which may become a secondary source in future.

4. Conclusions

In this work a trace analytical method was developed for the determination of seven potent EDCs in water and sediments, based on SPE and MAE followed by GC–MS/MS. The method was optimised for collision energy and provides increased selectivity and sensitivity with a lower limit of detection than earlier methods based on GC–MS. Improved clean-up procedure has removed matrix interferences and increased recovery in sediment samples. The derivatisation technique has been shown to have improved the stability of EDC derivatives over a period of 4 d with good repeatability. The method has been successfully used to determine the concentrations of the target EDCs in water and sediment samples from the Medway estuary during 2005, which are broadly in agreement with levels of EDCs in other rivers and estuaries. The salinity profile of EDCs demonstrates a non-conservative behaviour, consistent with their sorption to sediments and degradation by microbes.

Acknowledgements

This work was funded by an EU Interreg project (grant: 162/039/096) and a Marie Curie Fellowship (contract: MIF1-CT-2006-021556).

References

- [1] S. Jobling, D. Sheahan, J.A. Osborne, P. Matthiessen, J.P. Sumpter, *Environ. Toxicol. Chem.* 15 (1996) 194.
- [2] L.B. Bjerregaard, B. Korsgaard, P. Bjerregaard, *Ecotoxicol. Environ. Safety* 64 (2006) 321.
- [3] J. Auger, J.M. Kunstmann, F. Czyglik, P. Jouannet, *N. Engl. J. Med.* 332 (1995) 281.
- [4] D.L. Davis, M.B. Gottlie, J.R. Stampnitzky, *JAMA* 279 (1998) 1018.
- [5] T.A. Ternes, M. Stumpf, J. Mueller, K. Haberer, R.D. Wilken, M. Servos, *Sci. Total Environ.* 225 (1999) 81.
- [6] Z.L. Zhang, A. Hibberd, J.L. Zhou, *Anal. Chim. Acta* 607 (2008) 37.
- [7] Y. Tashiro, A. Takemura, H. Fujii, K. Takahira, Y. Nakanishi, *Mar. Pollut. Bull.* 47 (2003) 143.
- [8] O.P. Heemken, H. Reincke, B. Stachel, N. Theobald, *Chemosphere* 45 (2001) 245.
- [9] M. Kawaguchi, Y. Ishii, N. Sakui, N. Okanouchi, R. Ito, K. Inoue, K. Saito, H. Nakazawa, *J. Chromatogr. A* 1049 (2004) 1.
- [10] J. Hu, H. Zhang, H. Chang, *J. Chromatogr. A* 1070 (2005) 221–224.
- [11] S.J. Brennan, C.A. Brougham, J.J. Roche, A.M. Fogarty, *Chemosphere* 64 (2006) 49.
- [12] R.D. Holbrook, N.G. Love, J.T. Novak, *Environ. Sci. Technol.* 38 (2004) 4987.
- [13] X. Peng, Z. Wang, C. Yang, F. Chen, B. Mai, *J. Chromatogr. A* 1116 (2006) 51.
- [14] J.L. Zhou, R. Liu, A. Wilding, A. Hibberd, *Environ. Sci. Technol.* 41 (2007) 206.
- [15] A. Hibberd, Ph.D. Thesis, University of Sussex, UK, 2008.
- [16] T.A. Ternes, H. Andersen, D. Gilberg, M. Bonerz, *Anal. Chem.* 74 (2002) 3498.
- [17] R. Liu, J.L. Zhou, A. Wilding, *J. Chromatogr. A* 1038 (2004) 19.
- [18] S. Valsecchi, S. Polesello, S. Cavalli, *J. Chromatogr. A* 925 (2001) 297.
- [19] E.B.L. Cortazar, A. Delgado, N. Etxebarria, L.A. Fernandez, A. Usobiaga, O. Zuloaga, *Anal. Chim. Acta* 534 (2005) 247.
- [20] L. Patrolecco, S. Capri, S. De Angelis, S. Polesello, S. Valsecchi, *J. Chromatogr. A* 1022 (2004) 1.
- [21] M. Petrovic, S. Tavazzi, D.A. Barceló, *J. Chromatogr. A* 971 (2002) 37.
- [22] D. Li, J.R. Oh, J. Park, *J. Chromatogr. A* 1012 (2003) 207.
- [23] R. Espejo, K. Valter, M. Simona, Y. Janin, P. Arrizabalaga, *J. Chromatogr. A* 976 (2002) 335.
- [24] X.-Y. Xiao, D.V. McCalley, J. McEvoy, *J. Chromatogr. A* 923 (2001) 195.
- [25] R. Liu, J.L. Zhou, A. Wilding, *J. Chromatogr. A* 1022 (2004) 179.
- [26] R.A. Trenholm, B.J. Vanderford, J.C. Holady, D.J. Rexing, S.A. Snyder, *Chemosphere* 65 (2006) 1990.
- [27] L. Yang, T. Luan, C. Lan, *J. Chromatogr. A* 1104 (2006) 23.
- [28] I.-C. Beck, R. Bruhn, J. Gandrass, W. Ruck, *J. Chromatogr. A* 1090 (2005) 98.
- [29] Z.L. Zhang, A. Hibberd, J.L. Zhou, *Anal. Chim. Acta* 577 (2006) 52.
- [30] C.H. Koh, J.S. Khim, D.L. Villeneuve, K. Kannan, J.P. Giesy, *Environ. Pollut.* 141 (2006) 39.
- [31] M.R. Servos, D.T. Bennie, B.K. Burnison, A. Jurkovic, R. McInnis, T. Neheli, A. Schnell, P. Seto, S.A. Smyth, T.A. Ternes, *Sci. Total Environ.* 336 (2005) 155.



A rapid, simple method for determining formaldehyde in drinking water using colorimetric-solid phase extraction

April A. Hill, Robert J. Lipert, James S. Fritz, Marc D. Porter*

Institute for Combinatorial Discovery, Ames Laboratory-USDOE, and Department of Chemistry, Iowa State University, Ames, IA 50011, USA

ARTICLE INFO

Article history:

Received 13 June 2008

Received in revised form

12 September 2008

Accepted 16 September 2008

Available online 24 September 2008

Keywords:

Colorimetric-solid phase extraction (C-SPE)

Formaldehyde

Purpald

Diffuse reflectance spectroscopy

ABSTRACT

Formaldehyde has been detected in drinking water supplies across the globe and on board NASA spacecraft. A rapid, simple, microgravity-compatible technique for measuring this contaminant in water supplies using colorimetric-solid phase extraction (C-SPE) is described. This method involves collecting a water sample into a syringe by passage through a cartridge that contains sodium hydroxide, to adjust pH, and Purpald, which is a well-established colorimetric reagent for aldehydes. After completing the reaction in the syringe by agitating for 2 min on a shaker at 400 rpm, the 1.0-mL alkaline sample is passed through an extraction disk that retains the purple product. The amount of concentrated product is then measured on-disk using diffuse reflectance spectroscopy, and compared to a calibration plot generated from Kubelka–Munk transformations of the reflectance data at 700 nm to determine the formaldehyde concentration. This method is capable of determining formaldehyde concentrations from 0.08 to 20 ppm with a total work-up time of less than 3 min using only 1-mL samples.

© 2008 Elsevier B.V. All rights reserved.

1. Introduction

Formaldehyde can enter drinking water supplies by the oxidation of natural organic (humic) matter during water treatment [1,2], or by leaching from polyacetal plastic fittings if the protective coating is breached [3]. Since chronic exposure by ingestion leads to adverse gastrointestinal effects, the EPA has set health advisory levels for formaldehyde in drinking water for a 1-day exposure at 10 ppm, or a 1 ppm lifetime exposure [4]. Moreover, trace levels of this hazardous compound have recently been detected in several water samples collected on International Space Station (ISS) [5]. Two major sources of formaldehyde on ISS have been identified: (1) off-gassing of polymeric materials, and (2) by-products of metabolic processes. Once present in the spacecraft cabin air, formaldehyde can contaminate drinking water through humidity condensate, which has been found to contain up to 9 ppm formaldehyde [6]. To safeguard crew health, NASA has set spacecraft water exposure guidelines that limit formaldehyde concentrations to 20 ppm for a 1–10 day exposure and 12 ppm for a 100–1000 day mission [6].

The quality of spacecraft drinking water is currently evaluated using samples collected on ISS and returned to Earth. This pro-

cess often results in a gap of several months between sample collection and analysis, which raises sample degradation issues and prevents the timely implementation of correction scenarios. These factors underscore the need for rapid, on-board methods for monitoring trace levels of critical components in spacecraft drinking water supplies. Furthermore, these methods must have sufficient selectivity and sensitivity to measure analytes at low concentrations, be user-friendly, small, and lightweight, and be capable of operation in microgravity. As recent reports from our laboratory have shown [7–12], colorimetric-solid phase extraction (C-SPE) has demonstrated the ability to meet many of these requirements.

Colorimetric-solid phase extraction is a novel sorption-spectrophotometric technique that combines colorimetric chemistry with SPE to determine analyte concentration by measuring the color change of single-use SPE membranes. Notably, the use of reagents that have either been impregnated in the extraction membrane or immobilized using inert media (i.e., filter paper) eliminates the need to handle solvents and chemicals during sample workup. Thus, C-SPE functions in a “reagentless” format, minimizing exposure to hazardous materials. A hand-held diffuse reflectance spectrophotometer is used to rapidly quantify membrane-bound analytes using the Kubelka–Munk (KM) function [13,14]. The complete procedure typically requires only 1–2 min. Assessments of the performance of these methods in C-9 microgravity flight simulations [8,10,15] have recently shown excellent agreement with concurrent ground-based analyses of the spacecraft biocides iodine and silver(I) [16]. Due to the success of these

* Corresponding author at: Departments of Chemistry, Chemical Engineering and Bioengineering, University of Utah, Salt Lake City, UT 84108, USA.

Tel.: +1 801 587 1505; fax: +1 801 585 0575.

E-mail address: marc.porter@utah.edu (M.D. Porter).

initial tests, NASA plans to launch C-SPE in the first quarter of 2009 for a 6-month performance test on ISS.

This work extends the scope of C-SPE by demonstrating, for the first time, the measurement of an organic compound in water. Specifically, we have developed a method that is capable of monitoring formaldehyde concentrations from 0.08 to 20 ppm in aqueous samples using Purpald [17–23] as the colorimetric reagent, which has been shown to be both extremely sensitive and specific [18,24]. In addition, Purpald reacts at room temperature and is stable, making it an attractive alternative to both chromotropic acid, which requires heat, and dinitrophenylhydrazine, which is an explosion hazard [25,26]. As described by Dickinson and Jacobsen [21], Purpald combines with formaldehyde in alkaline solution to form a colorless intermediate that is oxidized by ambient oxygen to form an intensely purple tetrazine, which serves as the colorimetric product.

Commercially available formaldehyde test kits that use Purpald suffer from several disadvantages when compared with the method reported herein. First and foremost, all these test kits lack compatibility with operation in microgravity, which is paramount to NASA missions. These kits, including those manufactured by Merck under the names Spectroquant, Aquamerck, Reflectoquant, and Merckoquant, would have to be extensively modified for in-flight water quality monitoring. Also, the added hazards and costs associated with the transport and storage of the concentrated sodium hydroxide solution is a significant drawback to carrying such kits on shuttle missions. Finally, most of these kits are only semi-quantitative and, as such, are unable to accurately determine formaldehyde concentrations in NASA's target range for potable water.

This paper details the development of a C-SPE method that uses Purpald and sodium hydroxide; both immobilized within a filter holder that serves as a reagent cartridge. Procedurally, a water sample is loaded into a 3-mL syringe by passage through the reagent cartridge. Air (~1 mL) that occupies the dead volume of the cartridge is also drawn into the syringe, providing oxygen for the required oxidation. The sample is then agitated on a shaker for only ~2 min. This approach yielded a method capable of detecting formaldehyde from 0.08 to 20 ppm within ~3 min. The developed method is not only applicable to NASA's water quality monitoring needs, but is more user-friendly, provides improved quantitation with a lower detection limit, and requires smaller samples when compared to existing test kits for monitoring formaldehyde in Earth-bound applications.

2. Experimental

2.1. Reagents and chemicals

All solutions were prepared daily with deionized water that was purified by a Millipore Milli-Q water purification system. Solutions with formaldehyde concentrations up to 20 ppm were prepared in Nalgene bottles by diluting the appropriate mass of a formalin solution (37% (wt) formaldehyde, Sigma-Aldrich) with deionized water.

2.1.1. Extraction cartridges

Empore™ Anion Exchange-SR 47-mm extraction membranes (3M) were used as received to collect the colorimetric complex. The membranes were cut into 13-mm disks to fit into Swinnex polypropylene filter holders (Fisher), and placed on top of the support screen located in the bottom portion of the holder. The holder was then assembled by sealing against a silicone gasket.

2.1.2. Reagent cartridges

A 2.0-mL aliquot of 6.0 M NaOH was poured over a 45-mm diameter Millipore Media Pad (Fisher) that was placed in a 50-mm glass Petri dish. Once saturated with liquid, the pad was cut into 10-mm disks and dried gently on a hot plate for ~12 h. When dry, each disk was mounted in place of the support screen in the bottom of a Swinnex holder.

Purpald confinement was accomplished by loading a 13-mm diameter disk, cut from Whatman #1 filter paper, into the top portion of a Swinnex holder (with gasket) and placing 6 mg of the reagent onto the center of the disk. A second filter paper disk was used to cover the reagent and the top and bottom (containing the NaOH disk) portions of the holder were then mated. This step secured the reagent between the two filter paper disks.

2.2. Instrumentation and software

Sample agitation experiments were carried out using an NBS model C24 benchtop shaker. A BYK-Gardner color-guide sphere ($d/8^\circ$) diffuse reflectance spectrophotometer (Model LCB-6830) was employed to measure the diffuse reflectance spectra (DRS) of the disks after extraction of the colored product. This hand-held spectrophotometer is small, lightweight, battery-operated, and can acquire reflectance data in under 2 s over the visible spectral range (400–700 nm) at 20-nm intervals [10]. Once collected, the DRS are downloaded to a personal computer and analyzed using BYK-Gardner QC-Link software that was modified in-house to calculate the Kubelka–Munk function ($F(R)$) [12]. The KM function is given by $F(R) = (1 - R)^2 / 2R$, where R is the diffuse reflectance of the sample relative to a reflectance standard. Note that $F(R)$ is directly related to the concentration of the complex in the membrane, C , by $F(R) = 2.303\epsilon C/s$, where ϵ is the molar absorptivity of the colorimetric product and s is the scattering coefficient of the sample surface. The solution concentration of the analyte is determined by means of a calibration plot of $F(R)$ at a given wavelength versus analyte concentration.

2.3. Experimental procedures

The reagent cartridges are connected to 3-mL Luer Lock polypropylene syringes and aqueous solutions of formaldehyde are drawn into the syringes through the cartridges. During collection, the liquid sample first passes through the NaOH disk, which raises the pH above 10, facilitating the dissolution of the immobilized Purpald. In addition to the liquid sample, the air (~1 mL) that occupies the dead volume of the holder is drawn into the syringe, providing a source of oxygen for formation of the purple product. When filled, the 3-mL syringes contain ~1 mL of air and ~2 mL of sample solution. Immediately after sample collection, the syringes are capped and placed on a shaker with a maximum speed of 400 rpm. After agitating (see below) the sample in the syringe for 2 min total, the air and excess liquid are expelled and the remaining 1.0-mL reacted sample is forced through the extraction cartridge. Finally, the membrane is dried by passage of ~60 mL of air, the holder is disassembled, and the spectrum of the disk is acquired.

3. Results and discussion

3.1. Method development and calibration

Though literature reports the absorbance maximum of the product in solution at 549 nm [27], the minimum reflectance for the on-membrane analysis occurs at ~560 nm. Fig. 1 shows reflectance spectra acquired using the BYK-Gardner spectrophotometer for a series of formaldehyde concentrations. We found that the colored

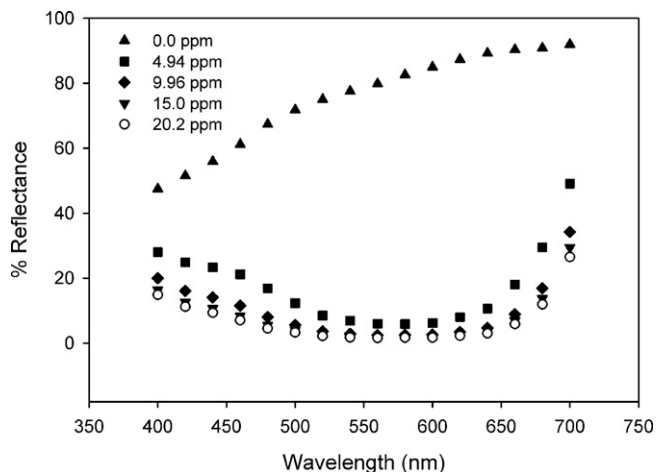


Fig. 1. Diffuse reflectance measurements using C-SPE to analyze solutions containing up to 20 ppm formaldehyde after reacting for 2 min on the shaker.

product is so intensely absorbing that solutions with formaldehyde concentrations above ~ 5 ppm cannot be readily distinguished at 560 nm. An examination of the response at each wavelength revealed that 700 nm was the most effective analytical wavelength; that is, the calibration plot of $F(R)$ vs. concentration at 700 nm exhibited the most linear profile. Moreover, this wavelength yielded a level of performance which surpassed that specified by both EPA and NASA [4,6].

Samples were collected by drawing solution into a syringe through the reagent cartridge and waiting for formation of the purple reaction product. Results indicated that agitation of the contents for ~ 1 min at 400 rpm (in addition to the 1 min required to reach 400 rpm) on a sample shaker increased the rate of air oxidation and purple product formation sufficiently to generate a calibration plot from the KM function of the extraction disks at 700 nm.

The C-SPE calibration plot obtained for the full range targeted by NASA and EPA (i.e., up to 20 ppm) is indicated by the 95% confidence interval shown in Fig. 2 along with the linear regression equation. Analysis of the data obtained from formaldehyde

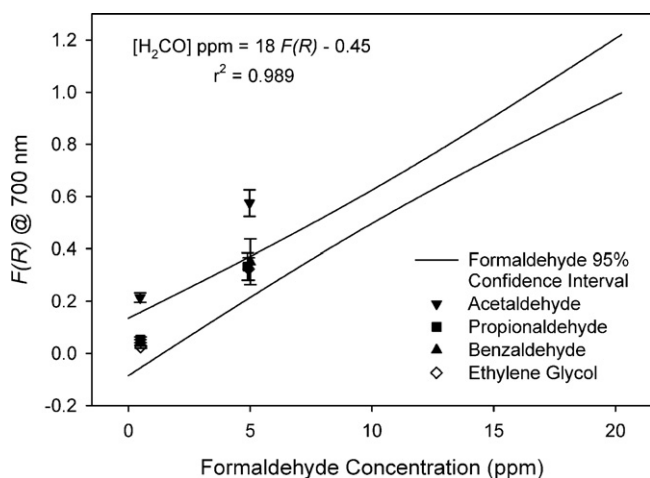


Fig. 2. A plot of the 95% confidence interval for the determination of formaldehyde generated from a Kubelka–Munk transformation of the data at 700 nm. Results obtained from the interference study are also plotted. The $F(R)$ for each solution is plotted against the formaldehyde concentration present in that solution. Each interferent solution contained ~ 5 ppm of the interferent and either ~ 5 or ~ 0.5 ppm formaldehyde.

concentrations up to 1.0 ppm yielded a calculated LOD of 80 ppb. Although the use of the shaker increases the rate of air oxidation, the reaction has not reached completion. Therefore, with such a short reaction interval, small variations in the time between filling the syringe and passing the sample through the extraction membrane can contribute significantly to the deviation in the data. Consequently, the sensitivity and measurement precision are not as high as they might be if the reaction were allowed to reach completion. However, in the interest of developing a rapid analytical technique, the data clearly show that this method has the capability to determine formaldehyde concentrations as low as 80 ppb in less than 3 min.

3.2. Interference study

A study was also conducted of potential interferents. Acetaldehyde and propionaldehyde, as the next two compounds in a homologous series, were tested. Benzaldehyde was included to assess the impact of aromaticity, along with ethylene glycol which is readily oxidized to formaldehyde [28]. The first three substances have been detected, albeit at low (< 8 ppb) levels, in spacecraft water supplies; ethylene glycol has been found at levels up to 1 ppm [5].

The impact of each interferent was examined by generating two sample solutions: one containing a 1:1 ratio of interferent to formaldehyde, and the other a 10:1 ratio. The 1:1 samples consisted of ~ 5 ppm of the interferent and ~ 5 ppm formaldehyde, while the 10:1 samples were composed of ~ 5 ppm interferent and ~ 0.5 ppm formaldehyde. Each solution was tested four times and the average $F(R)$ at 700 nm is plotted in Fig. 2 against the actual concentration of formaldehyde in the solution. The 95% confidence interval for solutions containing only formaldehyde serves as a reference.

Though all of the aldehydes tested are potential interferents in the determination of formaldehyde by Purpald, literature has shown that structural differences in the products formed by different aldehydes lead to variations in their spectra [24,29]. Our findings are consistent with the past work. Acetaldehyde, which differs by only one methyl group, is the strongest interferent, producing a signal that lies well outside the 95% confidence interval for pure formaldehyde. However, the addition of another methyl group, creating propionaldehyde, or the substitution of an aromatic ring, producing benzaldehyde, causes a large decrease in the interfering signal. Formaldehyde measurements with these interferents present fell within the 95% confidence interval determined for pure formaldehyde. Ethylene glycol was found to have the least effect on the determination of formaldehyde by this method. Presumably, at the conditions of the reaction, ethylene glycol is not detectably oxidized to formaldehyde.

4. Conclusions

This work details the development of a C-SPE method for the rapid (~ 3 min) quantification of aqueous formaldehyde from 0.08 to 20 ppm using only a 1.0-mL sample. In addition to its microgravity compatibility, the C-SPE method is more user-friendly, provides better quantitation, has a lower detection limit, and requires smaller samples than existing formaldehyde test kits. These advantages make the C-SPE method attractive for use in many ground-based applications as well, including water quality analysis in underdeveloped regions of the world. In addition to kit development and testing, we will also focus on expanding its usefulness to the detection of glycols, which enter spacecraft water supplies through the use of no-rinse personal hygiene products.

Acknowledgements

The authors would like to thank Jeff Rutz, Dan Gazda and John Schultz of Wyle Laboratories, Houston, TX, USA for their insightful discussions. This work was supported by NASA contract NAG91510. The Ames Laboratory is operated by Iowa State University under U.S. Department of Energy contract DE-AC02-07CH11358.

References

- [1] G. Becher, N.M. Ovrum, R.F. Christman, *Sci. Total Environ.* 117–118 (1992) 509.
- [2] W.H. Glaze, M. Koga, D. Cancilla, *Environ. Sci. Technol.* 23 (1989) 838.
- [3] IPCS, Concise International Chemical Assessment Document No. 40, World Health Organization, Geneva, 2002.
- [4] Toxicological profile for formaldehyde, ATSDR, 1999, Available from: <http://www.atsdr.cdc.gov/toxprofiles/tp111.html>.
- [5] D.K. Plumlee, Proceedings of the 32nd International Conference on Environmental Systems, San Antonio, TX, 2002, SAE Technical Paper #2002-01-2537.
- [6] J.T. McCoy, Formaldehyde, in: *Spacecraft Water Exposure Guidelines for Selected Contaminants*, vol. 2, National Academies Press, 2006, 301 pp.
- [7] M.P. Arena, M.D. Porter, J.S. Fritz, *Anal. Chem.* 74 (2002) 185.
- [8] M.P. Arena, M.D. Porter, J.S. Fritz, P. Mudgett, J. Rutz, J. Schultz, Proceedings of the 32nd International Conference on Environmental Systems, San Antonio, TX, 2002, SAE Technical Paper #2002-01-2535.
- [9] M.P. Arena, M.D. Porter, J.S. Fritz, *Anal. Chim. Acta* 482 (2003) 197.
- [10] D.B. Gazda, R.J. Lipert, J.S. Fritz, M.D. Porter, J. Rutz, P. Mudgett, J. Schultz, Proceedings of the 33rd International Conference on Environmental Systems, Vancouver, B.C., Canada, 2003, SAE Technical Paper #2003-01-2406.
- [11] D.B. Gazda, J.S. Fritz, M.D. Porter, *Anal. Chim. Acta* 508 (2004) 53.
- [12] J.S. Fritz, M.P. Arena, S.A. Steiner, M.D. Porter, *J. Chromatogr. A* 997 (2003) 41.
- [13] G. Kortum, *Reflectance Spectroscopy: Principles, Methods, Applications*, Springer, New York, 1969.
- [14] J.P. Blitz, Diffuse reflectance spectroscopy, in: F.M. Mirabella (Ed.), *Modern Techniques in Applied Molecular Spectroscopy*, John Wiley and Sons, Inc., New York, 1998, p. 185.
- [15] L.M. Ponton, D.B. Gazda, R.J. Lipert, J.S. Fritz, M.D. Porter, J. Rutz, P. Mudgett, D. Dungan, J. Schultz, Proceedings of the 33rd International Conference on Environmental Systems, Vancouver, B.C., Canada, 2003, SAE Technical Paper #2003-01-2408.
- [16] M.D. Porter, J.T. McCoy, A.A. Hazen-Bosveld, R.J. Lipert, J. Nordling, C.J. Shih, D.B. Gazda, J. Rutz, J. Straub, J. Schultz, J. Alverson, Colorimetric solid phase extraction measurements of spacecraft drinking water contaminants, in: *C-9 and Other Microgravity Simulations Summary Report*, 2006.
- [17] G. Zurek, U. Karst, *Anal. Chim. Acta* 351 (1997) 247.
- [18] M.S. Quesenberry, Y.C. Lee, *Anal. Biochem.* 234 (1996) 50.
- [19] J.L. Lambert, J.V. Paukstelis, Y.L. Liaw, Y.C. Chiang, *Anal. Lett.* 17 (1984) 1987.
- [20] M.J. Del Nozal, J.L. Bernal, V. Hernandez, L. Toribio, R. Mendez, *J. Liquid Chromatogr.* 16 (1993) 1105.
- [21] R.G. Dickinson, N.W. Jacobsen, *Chem. Commun.* (1970) 1719.
- [22] R.G. Dickinson, N.W. Jacobsen, *Org. Prep. Proceed. Int.* 6 (1974) 156.
- [23] R.G. Dickinson, N.W. Jacobsen, *Anal. Chem.* 46 (1974) 298.
- [24] H.B. Hopps, *Aldrichim. Acta* 33 (2000) 28.
- [25] A.D. Pickard, E.R. Clark, *Talanta* 31 (1984) 763.
- [26] L. Gollob, J.D. Wellons, *Forest Prod. J.* 30 (1980) 27.
- [27] N.W. Jacobsen, R.G. Dickinson, *Anal. Chem.* 46 (1974) 298.
- [28] E.R. Hess, C.B. Jordan, H.K. Ross, *Anal. Chem.* 28 (1956) 134.
- [29] G. Avigad, *Anal. Biochem.* 134 (1983) 499.



Quantitative determination of chlorogenic acid in *Honeysuckle* using microwave-assisted extraction followed by nano-LC-ESI mass spectrometry

Fengli Hu, Chunhui Deng, Yang Liu, Xiangmin Zhang*

Department of Chemistry, Fudan University, Shanghai 200433, China

ARTICLE INFO

Article history:

Received 24 June 2008

Received in revised form 1 September 2008

Accepted 3 September 2008

Available online 11 September 2008

Keywords:

Nano-liquid chromatography–mass spectrometry

Chlorogenic acid

Microwave-assisted extraction

Honeysuckle

ABSTRACT

The chlorogenic acid (CA) in *Honeysuckle* is determined and identified by nano-liquid chromatography–electrospray ionization mass spectrometry (nano-LC-ESI/MS) after extraction with microwave-assisted extraction (MAE). As a new sample preparation method for *Honeysuckle*, the MAE procedure is optimized, validated and compared with conventional methods including reflux extraction (RE) and ultrasonic extraction (USE). It is found that MAE gives the best result due to the highest extraction efficiency within shortest extraction time (only 4 min). Here, CA is determined by nano-LC-ESI/MS based on the calibration curve of its authentic standard. The method linearity, detection limit, precision and recovery are studied. The results show that the combined MAE and nano-LC-ESI/MS method has a linearity (R^2 0.991, 0.8–20 ng mL⁻¹), a low limit of detection (0.5 ng mL⁻¹), good precision (R.S.D. = 2.54%) and a recovery (84.8%). The experiment has demonstrated that the nano-LC-ESI/MS following MAE is a fast and reliable method for quantitative analysis of CA in *Honeysuckle*.

© 2008 Elsevier B.V. All rights reserved.

1. Introduction

Honeysuckle, the dried flower of *Lonicera japonica* Thunb., is a common Traditional Chinese Medicine (TCM). It has shown a wide spectrum of biological and pharmacological activities such as antibacterial, antiviral [1], antioxidant [2]. *Honeysuckle* contains chlorogenic acid (CA), luteolin-7-O-glucoside, volatile oil, flavone, saponins, polysaccharides, and polyphenolic compound [3]. CA is the major bioactive constituent in the herb. It is necessary to measure CA in *Honeysuckle* for quality of *Honeysuckle*.

Prior to the analysis, the extraction of CA in *Honeysuckle* is required. Reflux extraction (RE) is the most widely used traditional technique for routine herb drug extraction [4–6]. However, RE is laborious, time-consuming, and requires large amounts of solvents. Ultrasonic extraction (USE) is also applied for the CA extraction [7]. However, it does not show satisfactory extraction efficiency. Therefore, a fast, solvent-free and low-cost sample preparation technique for the extraction of CA from TCMs is desirable. Microwave heating involves internal heating based on conduction and dielectric polarization caused by microwave irradiation [8]. Recently, microwave-assisted extraction (MAE) has received more and more attention as a potential alternative to

traditional solid–liquid extraction methods, mainly due to considerable savings in processing time and solvent consumption [9,10]. It is more efficient when compared with traditional heating–reflux since microwave irradiation accelerates cell rupture by sudden temperature rise and internal pressure increase inside the cells of plant sample, which promotes destroy of sample surface [11]. It has been employed for the extraction of various biologically active compounds from different plant matrices [12–17]. In our previous study [18], MAE followed by gas chromatography–mass (GC–MS) has been applied to the TCM analysis.

Recently, remarkable advances in high performance liquid chromatography (HPLC) have been made for the separation and analysis of components in TCMs. Nano-LC as a new powerful analytical tool is carried out in capillaries of small internal diameter (I.D. < 300 μm) containing stationary phases usually employed in HPLC. The nano-LC offers several advantages over classical analytical methods, e.g., rapid separation achieved in a short analysis time with high efficiency, use of minute volumes of mobile phases as well as small amounts of packing materials [19,20], and low sample dilution ratio. However, the method does not prove to be satisfactorily sensitive due to the small volumes of sample injected and the short path length of the detection cell used in UV detection. The combination of nano-LC with mass spectrometry results in a powerful tool increasing the method sensitivity. ESI has now become the most important ionization technique for the on-line coupling of liquid phase separation techniques such as LC with MS

* Corresponding author. Fax: +86 21 65641740.

E-mail address: xmzhang@fudan.edu.cn (X. Zhang).

[21–23]. Advantages of the coupling of LC and ESI/MS are that (a) ESI is the technique of choice for transferring the charged species from liquid phase into gas phase, (b) the hyphenated technique has a broad range of applications from ions and small molecules to macromolecules and (c) ESI-MS allows the detection of multiple charged species originating from high molecular mass molecules. The coupling of both techniques (nano-LC-MS) is easily achieved because of the relatively low flow rate, typical feature of nano-LC system, originated by the employment of small I.D. columns. Thus, nano-LC-MS is often used for the analysis of proteomics [24], pharmaceutical compounds [25] due to its high sensitivity and low limit of detection.

In this study, a MAE followed by nano-LC-ESI/MS is developed for the determination of CA from *Honeysuckle*. This is the first report of hyphenating MAE with nano-LC-MS. The MAE parameters are optimized, and the extraction efficiency by MAE is compared with that by conventional extraction techniques. The method linearity, recovery, precision and detection limit are also studied.

2. Experimental

2.1. Chemical and materials

Methanol, acetonitrile and formic acid were chromatographic grade (Merk, Darmstadt, Germany). Ethanol was analytical grade. Distilled water was purified by a Milli-Q system (Milford, MA, USA). *Honeysuckle* was purchased from local Chinese medicine stores in Shanghai, China. Chlorogenic acid (purity 99.9%) was purchased from the Institute for the Control of Pharmaceutical and Biological Products of China (Beijing, China). Centrifuge was from Christ (Osterode am Harz, Germany).

2.2. LC-MS conditions

The nano LC-ESI/MS system (LC-20ADvp nanopump, SIL-20AC autosampler, Shimadzu, Kyoto, Japan) was equipped with nano-electrospray ionization (ESI) interface. The Zorbax SB-C18 column (150 mm \times 75 μ m, I.D.,) that was packed with 3.5 μ m particles was purchased from Agilent technologies (Santa Clara, CA, USA). The mobile phase consisted of (A) 0.1% formic acid, (B) acetonitrile+0.1% formic acid, with a gradient elution of 5–20% B at 1–16 min, 20–40% B at 16–24 min, then rapidly to 100% B in 1 min, finally holding on 100% B for 4 min. The flow rate was 300 nL min⁻¹. Mass analysis was performed in selected ion monitoring (SIM) and scan modes, respectively. ESI-MS spectra were acquired in positive mode. All mass spectra were acquired on a novel hybrid ion-trap time-of-flight mass spectrometer (Shimadzu LC-MS-IT-TOF) equipped with an ESI source (ESI-IT-TOFMS) in positive ion mode at a resolution of 10000 FWHM. Accurate masses were corrected by calibration using the standard material sodium trifluoroacetate cluster as internal reference. The analytical conditions were as follows: scan range, m/z 200–650; spray voltage, 2.50 kV; detector voltage, 1.65 kV; skimmer voltage, 9.0 V; pressure of TOF region, 1.5×10^{-4} Pa, and temperature, 40 °C; ion source temperature, 200 °C; trap cooling gas (Ar) flow, 94 mL min⁻¹; ion trap pressure, 1.8×10^{-2} Pa; collision gas (Ar) flow, 43 mL min⁻¹; ion accumulated time, 10 ms; precursor ion selected width, 3.0 amu, and selected time, 20 ms; CID collision time, 30 ms; $q = 0.251$.

2.3. Standard solution

The authentic standard of CA was weighted accurately then dissolved in methanol and diluted to 1 mg mL⁻¹. Standard solution was stored in the dark under refrigeration at 4 °C and was found to

be stable for two months. A series of working standard solutions were prepared by the appropriate dilution of the above-mentioned standard solution with water to create CA concentration of 10 and 1 μ g mL⁻¹.

2.4. Comparison of extraction procedures and optimization of MAE parameters

2.4.1. Reflux extraction

One gram of dried *Honeysuckle* was extracted twice with 20 mL of 70% ethanol by reflux for 2 h. The extract was then centrifuged at 15,000 rpm for 15 min. The supernatant was filtered through a 0.45- μ m nylon filter then directly injected into the HPLC. Three replicate injections were analyzed to determine the contents of CA in the herb with the average peak area.

2.4.2. Ultrasonic extraction

One gram of dried *Honeysuckle* powder was weighted accurately to a flask, and then 20 mL of 70% ethanol was added to the tube which was sealed with a glass cap. The powder was extracted in an ultrasonic bath for 30 min. The extract was then centrifuged at 15,000 rpm for 15 min. The supernatant was also filtered through the 0.45- μ m nylon filter and then injected into the HPLC. The contents of CA in *Honeysuckle* were calculated with the mean peak area of three replicate injections.

2.4.3. Microwave-assisted extraction and optimization of MAE parameters

A household microwave oven was modified in our laboratory [26]. The microwave oven operated with a 2450 MHz single-phase output of 700 W. One gram of *Honeysuckle* was placed in a 50 mL flask followed by the addition of 20 mL 70% ethanol. The contents in the flask were vigorously shaken by hand, and then extracted for 4 min at a power level of ca. 400 W. After extraction, the flask was cooled to room temperature before opening. The extract was centrifuged at 15,000 rpm for 15 min and then filtered. 1 μ L of the dilution was injected into the HPLC.

2.5. Method validation

2.5.1. Calibration curve and quantification of samples

The five-point calibration curve of CA was constructed by plotting peak area (y) of CA versus CA amount (x). The regression parameters of slope, intercept and correlation coefficient were calculated by Origin 7.0 software. Concentrations of CA in *Honeysuckle* samples were calculated from the resulting peak area ratios and the regression equation of the calibration curve.

2.5.2. Repeatability and recovery

Five replicate injections of same extract were analyzed by the nano-LC-ESI/MS method to determine variation due to the chromatographic conditions (system precision). Relative standard deviation (R.S.D.) was studied by the analysis of CA content in *Honeysuckle* extracted by MAE. The recovery of CA was studied with *Honeysuckle* spiked with 0.01 μ g CA. The mixture was processed under described sample preparation procedure and analyzed using nano-LC-ESI/MS. Also, the detection limit ($S/N = 3$) of CA was calculated.

3. Results and discussion

3.1. Optimization of HPLC conditions for the separation of CA

Optimized chromatographic conditions are achieved after several trials with acetonitrile, water and formic acid in various

proportions. It is found that the presence of formic acid in the mobile phase has a significant effect on the retention behavior of CA in *Honeysuckle*. Once 1% formic acid is applied instead of pure water, the pH is switched to 4.0, and then the t_R (retention time) of CA on mobile phase is prolonged, avoiding eluting immediately when using water. In this HPLC system, an increase in the percentage of acetonitrile decreases the retention of most compounds. Subsequently, the optimal gradient elution consisting of 1% formic acid is employed, which leads to well-separated resolution, satisfactory peak shape as well as relatively short time for analysis. Eventually, 16 peaks observed within 29 min comprise the fingerprint of *Honeysuckle* obtained by nano-LC-ESI/MS (Fig. 1c, extracted by MAE). Table 1 lists the components separated in the extract of *Honeysuckle*. Component 7 is identified as CA by comparing the retention time and MS spectra with authentic standard (Fig. 1).

3.2. Comparison of microwave-assisted extraction and conventional extraction techniques

According to Table 1, about sixteen components are identified in the extract of MAE while the number in the extract of RE and USE is eight and nine, respectively. Their chromatograms are shown in Fig. 1. It indicates that more components are extracted through MAE. However, two different components (18, 19) are eluted only in the extract by RE at m/z 389.1 and 243.1 while component 17 is only extracted by USE. This difference may be due to the various structure transformation during refluxing, ultrasonic and microwave heating. There are five components which are all identified in the extract of RE, USE, and MAE. The amount of these components are compared in Fig. 2. Except component 6, MAE gives the highest extraction efficiency for the others. Comparison of peak area for CA (Fig. 2,

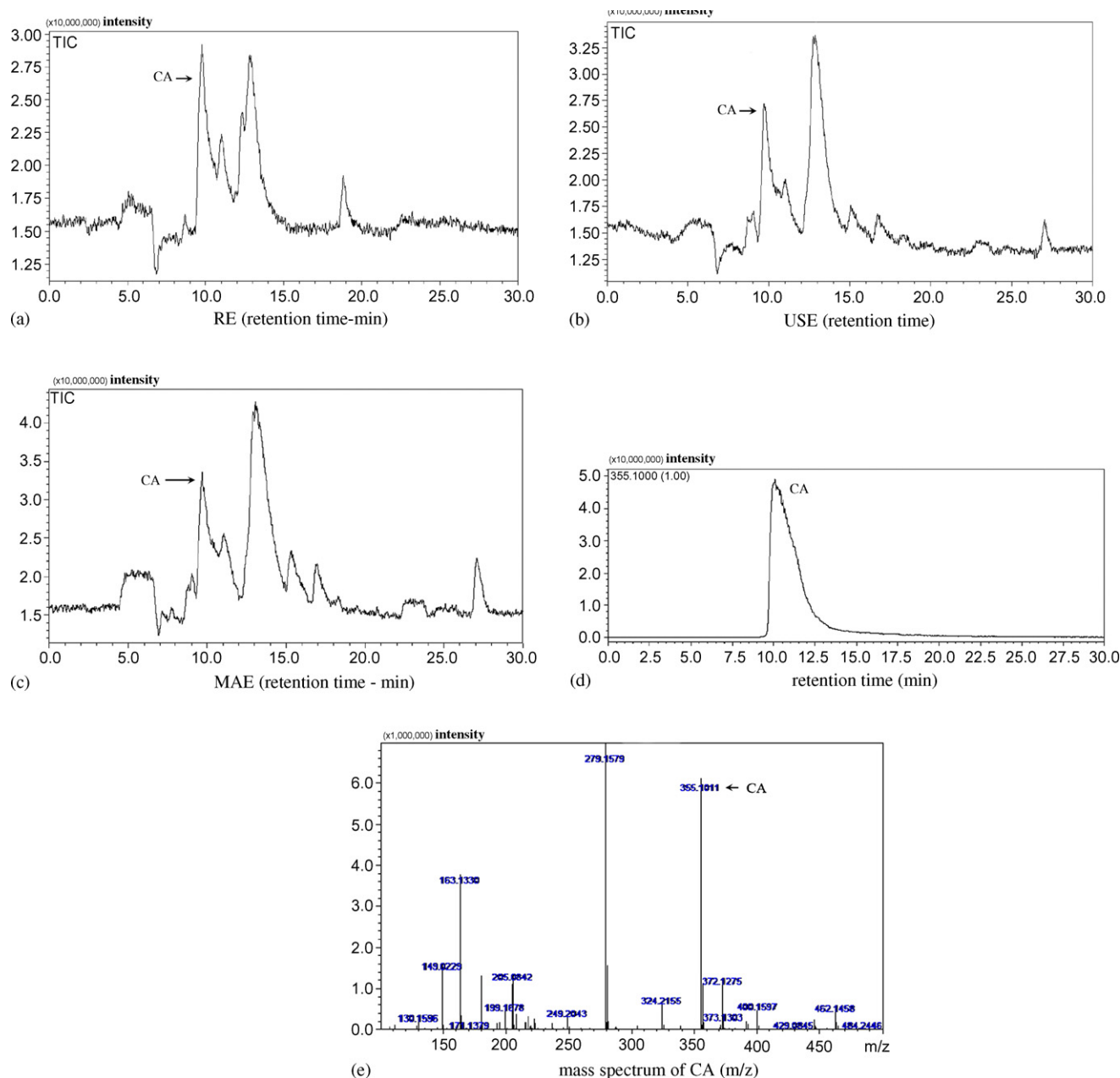


Fig. 1. Chromatograms of *Honeysuckle* extracted by (a) RE, (b) USE and (c) MAE and (d) CA standard together with its (e) mass spectrum.

Table 1
Components separated in the extract of *Honeysuckle* by MAE, RE and USE.

No.	Retention time (min)	Base peak, <i>m/z</i>	Area		
			MAE	RE	USE
1	5.07	359.1	81193663	–	–
2	7.05	316.1	39277182	–	–
3	7.68	446.2	29112818	–	–
4	8.70	404.1	62896168	–	–
5	9.06	214.1	73920664	–	92721527
6	9.64	212.1	399887657	502752323	274641067
7	10.20	354.1	591556301	353803099	326513897
8	10.30	320.1	39142508	–	–
9	11.01	358.1	115915756	116201499	43926068
10	12.82	226.1	1808266849	–	973031165
11	13.82	278.2	380301126	48117017	–
12	15.19	402.2	257652100	64302636	59187301
13	17.00	279.2	51604327	–	–
14	18.27	462.2	33871562	–	–
15	19.80	448.1	24297958	8128749	6684899
16	26.89	416.2	313391484	–	37421157
17	26.47	162.1	–	–	8488602
18	12.34	388.1	–	100947673	–
19	12.82	242.1	–	403154752	–

component 7) shows MAE to be the best extraction technique for CA because it gives the maximum extraction values of it. This proves that the MAE technique is effective for the accurate and reliable determination of CA and main compounds in *Honeysuckle*.

3.3. Optimization of MAE procedure

Effects of microwave power and irradiation time on the extraction are studied (Fig. 3). *Honeysuckle* is extracted at different microwave power (200, 400 and 700 W) and different irradiation time (1, 2, 4 and 6 min), and then further centrifuged. Finally the analytes are analyzed by nano-LC-ESI/MS. As is shown in Fig. 3, with the microwave power of 200, 400 and 700 W, the extraction efficiency of CA is increasing with the exposure time. However, the extraction efficiency decreased when the irradiation time is more than 4 min (while under low power, the time was 2 min). This maybe due to its decomposition at long irradiation time. Generally, the higher extraction temperature is profitable for accelerating reaction and reducing the reaction time of CA. The effect of microwave forward power on the extraction yield is represented in Fig. 3. The experiment results demonstrate that the extraction yield of CA increases when the forward power rises from 200 to 400 W and then the yield decreases at 700 W. Except for extractions irradiated with 1 min, extractions with microwave power of 400 W show the higher content of CA compared with others. Therefore, the best condition for the MAE is performed at a microwave power of 400 W and an irradiation time of 4 min.

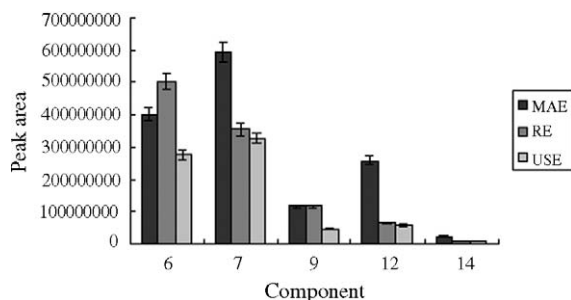


Fig. 2. Comparison of five components identified in the extract of *Honeysuckle* by MAE, RE, and USE, conditions are shown in Section 2.4.

3.4. Method validations

We use the external standard method since it is simple, fast and accurate for sample preparation. The repeatability of retention time about CA during the precision studied is found to be excellent for all solutions. The calibration curve for CA is constructed by analyzing a series of CA standard sample in the concentration range from 0.8 to 20 ng mL⁻¹ and by plotting concentration versus peak area (the simple plot is not shown). The calibration curve shows good linearity in 0.8–20 ng mL⁻¹. The regression equation is $y = 2.82 \times 10^{10}x + 1.69 \times 10^7$. Linear regression analysis of the data yields a correlation coefficient (R^2) of 0.991.

A series of sample analysis are performed to validate the performance of the method. Reproducibility of the combined MAE and nano-LC-ESI/MS method is assessed by the peak area of CA in five replicate analyses of the same extract. The percent R.S.D. value is 2.54%. By spiking the standard solution of CA, the recovery of this component is measured. The amount of the spiked CA is calculated by subtracting the total amount of CA after spiking from the amount in the herb before spiking. The spiking experiments are repeated three times to get the mean amount of CA after spiking. The recovery is 84.8% with R.S.D. 4.64%. The limit of detection (LOD) is 0.5 ng mL⁻¹ ($S/N = 3$).

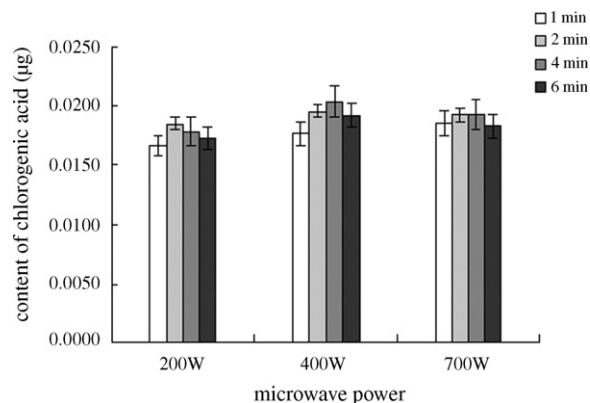


Fig. 3. Effects of microwave power and irradiation time on the amounts of CA extracted from *Honeysuckle*.

When the test solutions of *Honeysuckle* extracts are analyzed by LC–MS under the selected conditions, the calibration curves are used for quantitative analysis.

3.5. Application to the determination of CA in *Honeysuckle's* combination drug

A TCM formula, composed of *Honeysuckle*, *Radix astragali* and *Coptis* is also analyzed. The mixture with 0.1 gram of each herb, dissolved in 30 mL 70% ethanol is extracted by MAE for 4 min at a power level of ca. 400 W. After filtering and centrifuging, 1 μ L extraction is injected into nano-LC-ESI/MS. The quantity of CA is calculated according to the calibration curve. The mean content in combination drug is 1.35 ng with R.S.D. 2.82% (n = 3). The mean amount of CA is calculated with average peak area through three assays.

4. Concluding remarks

An optimized MAE procedure has been developed and manifested more effective than other conventional techniques. For the first time, we report the extraction of CA from *Honeysuckle* using MAE and quantification of this compound by nano-LC-ESI/MS. The MAE method followed by nano-LC-ESI/MS determination, which takes comprehensive effect such as rapid analysis, reduced sample, time and solvent consumption, is a simple, rapid, and reliable method for the quality and quantify assessment of CA in *Honeysuckle*.

Acknowledgment

This paper was supported by 973 Program, 2007CB914100/3, 863 project: 2006AA02A308 and Shanghai Leading Academic Discipline Project, B109.

References

- [1] P.J. Houghton, Z. Boxu, Z. Xisheng, *Phytother. Res.* 7 (1993) 384.
- [2] S.Y. Kim, J.H. Kim, S.K. Kim, M.J. Oh, M.Y. Jung, *J. Am. Oil Chem. Soc.* 71 (1994) 633.
- [3] W.C. Chang, F.L. Hsu, *Prostaglandins Leukot. Essent. Fatty Acids* 245 (1992) 307.
- [4] X.G. Chen, L.H. Hu, X.Y. Su, L. Kong, M.L. Ye, H.F. Zou, *J. Pharm. Biomed. Anal.* 40 (2006) 559.
- [5] H.B. Xiao, X.M. Liang, P.C. Lu, *J. Sep. Sci.* 24 (2001) 186.
- [6] L.H. Hu, X. Li, S. Feng, L. Kong, X.Y. Su, X.G. Chen, F. Qin, M.L. Ye, H.F. Zou, *J. Sep. Sci.* 29 (2006) 881.
- [7] H.B. Xiao, M. Krucker, K. Albert, X.M. Liang, *J. Chromatogr. A* 1032 (2004) 117.
- [8] D.M.P. Mingos, D.R. Baghurst, *Chem. Soc. Rev.* 20 (1991) 1.
- [9] M. Gfrerer, E. Lankmayr, *Anal. Chim. Acta* 533 (2005) 203.
- [10] E. Cortazar, L. Bartolome, A. Delgado, N. Etxebarria, L.A. Fernandez, A. Usobiaga, O. Zuloaga, *Anal. Chim. Acta* 534 (2005) 247.
- [11] B. Zhang, R.Y. Yang, C.Z. Liu, *Sep. Purif. Technol.* 62 (2008) 480.
- [12] M. Zhu, Y. Cao, G.R. Fan, *J. Sep. Sci.* 30 (2007) 67.
- [13] X.J. Pan, G.G. Niu, H.Z. Liu, *Biochem. Eng. J.* 12 (2002) 71.
- [14] A. Sharma, S.C. Verma, N. Saxena, N. Chadda, N.P. Singh, A.K. Sinha, *J. Sep. Sci.* 29 (2006) 613.
- [15] N. Li, C.H. Deng, Y. Li, H. Ye, X.M. Zhang, *J. Chromatogr. A* 1133 (2006) 29.
- [16] Y. Yang, L. Chen, X.X. Zhang, Z.K. Guo, *J. Liq. Chromatogr. Rel. Technol.* 27 (2004) 3203.
- [17] H. Li, B. Chen, L. Nie, S.Z. Yao, *Phytochem. Anal.* 15 (2004) 306.
- [18] C.H. Deng, J. Ji, N. Li, Y.J. Yu, G.L. Duan, X.M. Zhang, *J. Chromatogr. A* 1117 (2006) 115.
- [19] J.P.C. Vissers, H.A. Claessens, C.A. Cramers, *J. Chromatogr. A* 779 (1997) 1.
- [20] G. D'Orazio, Z. Aturki, M. Cristalli, M.G. Quaglia, S. Fanali, *J. Chromatogr. A* 1081 (2005) 105.
- [21] S.H. Hou, J. Zhu, M.Y. Ding, G.H. Lv, *Talanta* 76 (2008) 798.
- [22] R. Guo, Q.F. Zhou, Y.Q. Cai, G.B. Jiang, *Talanta* 75 (2008) 1394.
- [23] H.L. Lee, C.Y. Wang, S. Lin, D.P.H. Hsieh, *Talanta* 73 (2007) 76.
- [24] G. Lochnit, R. Geyer, *Biomed. Chromatogr.* 18 (2004) 841.
- [25] S. Fanali, Z. Aturki, G. D'Orazio, A. Rocco, *J. Chromatogr. A* 1150 (2007) 252.
- [26] C.H. Deng, Y. Mao, F.L. Hu, X.M. Zhang, *J. Chromatogr. A* 1152 (2007) 193.



Palladium–citric acid–ammonium fluoride as a matrix modifier for overcoming of interferences occurring during the direct determination of Sn in *aqua regia* extracts from environmental samples by D₂-ETAAS

Lenka Husáková^{a,*}, Jitka Šrámková^a, Tomáš Černohorský^b, Iva Urbanová-Doležalová^a

^a Department of Analytical Chemistry, Faculty of Chemical Technology, University of Pardubice, nám. Čs. legií 565, Pardubice CZ-532 10, Czech Republic

^b Department of Environmental Protection, Faculty of Chemical Technology, University of Pardubice, nám. Čs. legií 565, Pardubice CZ-532 10, Czech Republic

ARTICLE INFO

Article history:

Received 17 July 2008

Received in revised form

12 September 2008

Accepted 21 September 2008

Available online 1 October 2008

Keywords:

Tin analyte

Chloride matrix

Alumina matrix

ETAAS

Chemical modifiers

Aqua regia extraction

Environmental samples

ABSTRACT

When tin is to be determined in such a complex matrix like *aqua regia* extracts of environmental samples by electrothermal atomic absorption spectrometry (ETAAS), spectral interferences occur when deuterium-lamp (D₂) background correction is used, even using high pyrolysis temperature of 1400 °C achieved with palladium with citric acid chemical modifier. We have found that the further addition of NH₄F to palladium with citric acid chemical modifier is essential for overcoming the above-mentioned problems for which aluminium oxide is most probably responsible. It is supposed, that NH₄F enables volatilization of the alumina matrix formed by hydrolysis from the chloride salt and interfering in a gas phase via the formation of AlF₃ which could be, in contrast to aluminium oxide, removed from the graphite furnace during the pyrolysis stage. Using the proposed chemical modifier, the direct and accurate determination of Sn in *aqua regia* extracts from rocks, soils and sediments is possible even when using matrix free standard solutions. This presumption was confirmed by the analysis of certified reference samples and by the comparison with inductively coupled plasma time of flight mass spectrometry (ICP-TOFMS) method. Characteristic mass and LOD value for the original sample (10- μ L aliquots of sample) was 17 pg and 0.055 μ g g⁻¹, respectively.

© 2008 Elsevier B.V. All rights reserved.

1. Introduction

Direct determination of Sn in environmental samples by electrothermal atomic absorption spectrometry (ETAAS) method is difficult due to the matrix effects [1–10]. Especially chloride matrix is known to interfere seriously onto Sn determination [9]. In the presence of chlorides, several volatile compounds of tin are formed which may be lost during drying and ashing steps and serious gas phase interferences in the atomization stage and spectral effects have occurred [1,9–11]. From this reason the analysis of *aqua regia* extracts from various environmental samples is an extremely difficult analytical task [1].

Up-to-date only a few papers [1,5] have been related to the problems occurring during the direct determination of Sn in *aqua regia* extracts from rocks, soils and sediments, although an *aqua regia* extraction (ISO 11466) [12] is widely used for most of heavy metals and this procedure is often required by regulations to estimate soils contamination. da Silva et al. [1] recommended the use of Ru deposited on a L'vov platform as a permanent modifier for the deter-

mination of Ag, Pb and Sn in *aqua regia* extracts from sediments, nevertheless for Sn, the precision was less satisfactory. This fact was, however, attributed [1] to less efficient extraction for this analyte. The authors [1] have also reported noisy and not symmetrical absorption peaks for Sn in extracts and much higher background absorbance surpassing the correction capability of the continuum source background corrector in comparison with matrix free and 50% v/v *aqua regia* conditions. These differences were attributed not to the common presence of the *aqua regia* in the extract, but to some concomitants of the sample. Arambarri et al. [5] have used Pd modifier for determination of Sn in *aqua regia*-HF extracts from sediments, nevertheless, non-spectral effects were persisted although a full factorial design and central composite design for the optimization of conditions in ETAAS determination have been applied. The use of the “universal chemical modifier” Pd + Mg [13] previously applied successfully to the determination of many elements in different kind of matrices [14] was however less effective in the *aqua regia* medium, e.g. in comparison with Ru permanent modifier [1]. It is clearly evident that several problematic analyses which were not successfully solved up to date using more or less conventional chemical modifiers need the specific treatment evolving the use of chemical modifier to impact effectively and specifically seriously interfering compounds. Of these analyses, the direct determination

* Corresponding author. Tel.: +420 466037029; fax: +420 466037068.
E-mail address: Lenka.Husakova@upce.cz (L. Husáková).

of Sn in *aqua regia* extracts of environmental and geological samples is still a great challenge owing to the above-mentioned problems. Development of methodology for the determination of Sn using instrumentation equipped with D₂ background correction system, which is still the most widely used analytical practice, is described and discussed throughout this work.

2. Experimental

2.1. Reagents

Tin solution (SnCl₄ in HCl 2 mol L⁻¹) of 1 g L⁻¹ Sn was obtained from Merck (Darmstadt, Germany). Nitric acid (65%, w/v) of Selectipur quality (Lach-Ner, Neratovice, Czech Republic) was used. The solution of 1 g L⁻¹ of Pd in 10% (v/v) HCl was obtained from SCP Science (Canada). Solutions of 200 and 100 g L⁻¹ citric acid (p.a.) (Lachema, Brno, Czech Republic) and that of ammonium fluoride (p.p.) (Sigma-Aldrich Chemie GmbH, Steinheim, Germany) were prepared by dissolving these salts in water. Solutions were prepared using deionised water of 0.05 μS cm⁻¹ conductivity using the UltraClear (SG, Germany) pure water system.

2.2. Instrumentation

Measurements were carried out using Avanta P double beam atomic absorption spectrometer (GBC Scientific Equipment Pty. Ltd., Australia) equipped with GF 3000 graphite furnace, auto-sampler PAL 3000 and deuterium arc background corrector. Super lamp (Photron Pty. Ltd., Australia) was the line source (lamp current 15 mA, boost current 18 mA, wavelength 224.6 nm, spectral band-pass 0.5 nm). Peak area absorbance values were measured. Pyrolytically coated graphite tubes (Schunk, Germany, Batch: 1082283) with preinstalled pyrolytic graphite L'vov platform were used. Argon was used as sheating gas; the internal gas flow in the graphite tube was interrupted during the atomization step.

Inductively coupled plasma time of flight mass spectrometer Optimass8000 (GBC Scientific Equipment Pty. Ltd., Australia) [15,16] was used in several cases for comparative measurements.

2.3. Procedure

2.3.1. Samples

Commercially supplied quality control materials of Rocks and Geological Materials and Soils and Sediments, Laterite GBW 07407 and Yellow-red Soil GBW 07405 were purchased from National Research Centre for Certified Reference Materials, NRCRM, China. Samples were prepared by digestion with *aqua regia* according to the ISO Norm 11466 [12] using the same way as described in Ref. [17].

2.3.2. Analytical procedure

When the influence of FeCl₃ or AlCl₃ matrix onto the determination of Sn was studied, 500 pg of Sn and appropriate amounts of individual chloride salt was injected to graphite furnace without or with the use of: (i) 4 μg Pd + 1000 μg citric acid (CA), (ii) 4 μg Pd + 1000 μg CA + 1000 μg ammonium fluoride (AF). For this purpose 4 μL of 1 g L⁻¹ Pd solution or 10 μL of a mixture of 0.4 g L⁻¹ Pd with 100 g L⁻¹ CA was injected and dried at 110 °C to ensure more easily sampling of a sample limited by the use of platform and to protect an intercalation of chloride matrix into graphite [18]. After that, 10 μL aliquot of the solution of 50 μg L⁻¹ Sn and the appropriate volumes of chloride solution and 5 μL of 200 g L⁻¹ AF with or without the use of 5 μL of 200 g L⁻¹ CA were injected as a single deposition on the platform by means of auto-sampler. When *aqua*

regia leaches from GBW 07405 and GBW 07407 samples were analyzed, 10 μL aliquot of the sample and an appropriate volume of modifiers were injected using the same way as described above to ensure the total mass of modifiers injected onto the platform to be 4 μg of Pd + 1600 μg of CA + 1000 μg of AF.

Calibration using five aqueous standards and two standard additions were performed by means of the instrument software. Calibration ranged from the lowest concentration to 200 μg L⁻¹ and was linear through the investigated range.

3. Results and discussion

3.1. Evaluation of interference on Sn determination

We have reported recently [19], that Pd+CA is a very efficient chemical modifier for the elimination of interferences occurring during the direct determination of Tl in *aqua regia* leaches from rocks, soils and sediment samples, especially when combined with Li. However, regarding the determination of Sn, the application of Pd+CA with or without the use of Li, results in overcorrection, and high background values cannot be reduced even at high pyrolysis temperatures as 1400 °C (see Fig. 1). Similar observations were obtained also at other analytical wavelengths being used for Sn determination, i.e. 235.5 and 286.3 nm, even for lowest spectral bandwidth of 0.2 nm achievable with the spectrometer used. It is clear that there must be another source of interference onto Sn determination in comparison with Tl determination and that for this case the composition of a chemical modifier must be adapted. We have found that replacement of Li in Pd+CA+Li mixture by NH₄F can solve all the above-mentioned problems

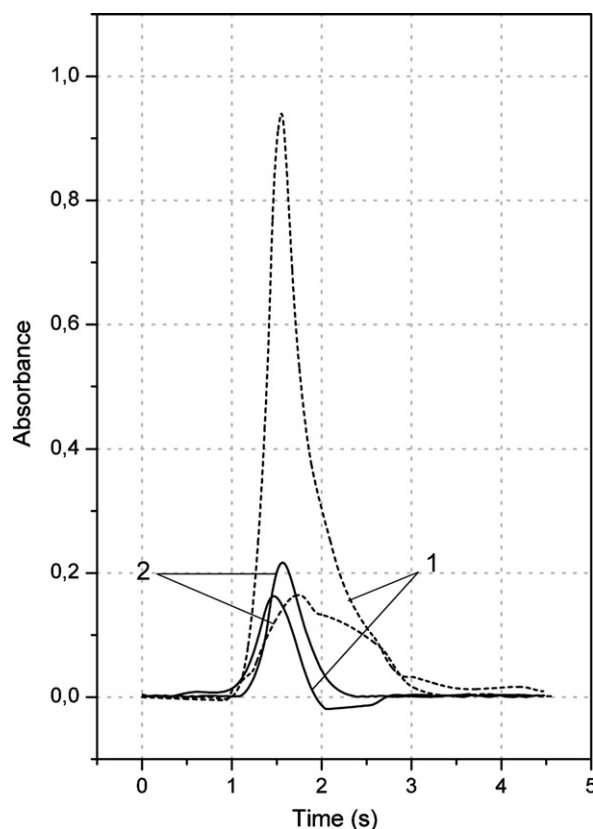


Fig. 1. Atomic (solid lines) and background (dotted lines) absorbance signals for 660 pg of Sn in GBW 07407 sample in the presence of (1) 4 μg Pd + 1000 μg CA and (2) 4 μg Pd + 1000 μg CA + 1000 μg AF. Pyrolysis and atomization temperatures were 1400 and 2200 °C, respectively.

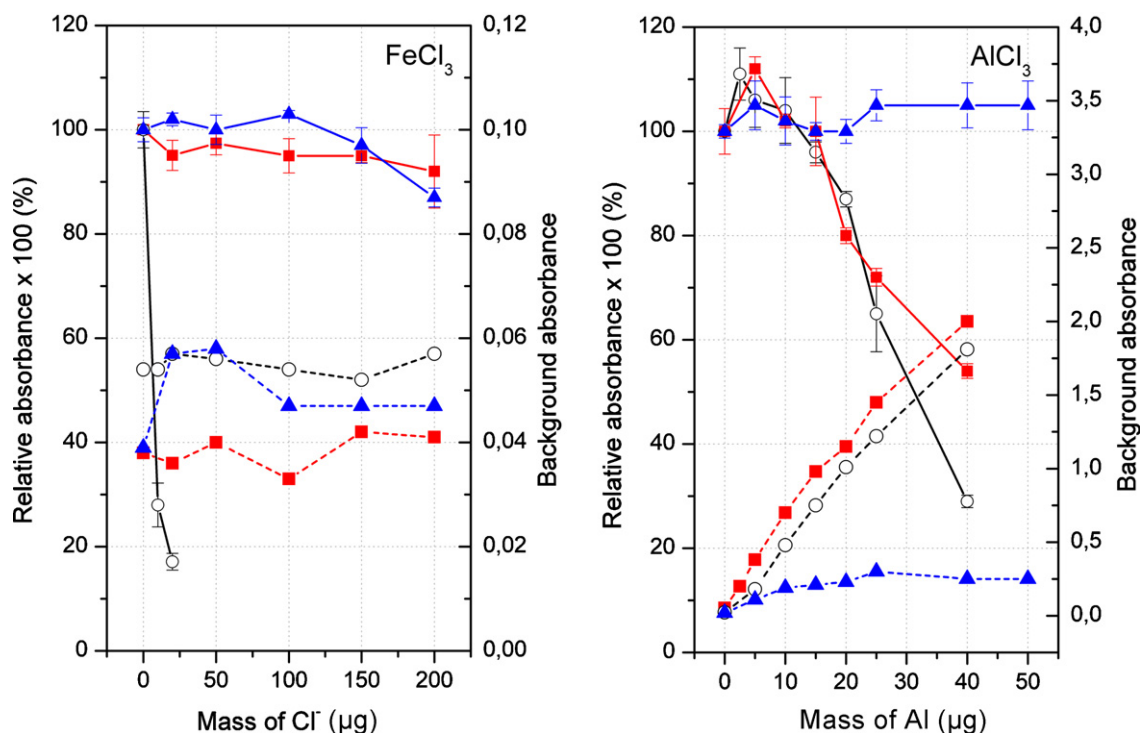


Fig. 2. Influence of FeCl_3 and AlCl_3 matrix on the relative absorbance signal (solid lines) and background absorbance (dotted lines) of 500 pg of Sn in the presence of 4 μg Pd + 1000 μg CA (■), 4 μg Pd + 1000 μg CA + 1000 μg AF (▲) and under modifier free conditions (○). Pyrolysis and atomization temperatures used for measurement are shown in Table 1. The relative absorbance is defined as: integrated absorbance of 500 pg Sn in the presence of chemical modifier and Cl^- or Al within the investigated range/integrated absorbance of 500 pg Sn. Bars indicate the range for each determination ($n = 3$).

observed during the analysis of *aqua regia* leaches from GBW 07405 or GBW 07407. After that, the background is significantly reduced and problems with overcorrection are eliminated (see Fig. 1).

To find which component is the most responsible for the above-mentioned problems, we have studied the influence of increasing amount of FeCl_3 and AlCl_3 onto Sn determination (see Fig. 2) under conditions described in Table 1 since for both GBW 07405 and GBW 07407 the highest values are certified for Fe and Al, respectively. In addition, it was found previously by several authors [8,10] that high aluminium or iron concentrations (3–4 orders of magnitude)

may cause either spectral or chemical (or both) interferences in Sn analysis.

As it can be seen from Fig. 2, the determination of Sn was interfered by the presence of both FeCl_3 and AlCl_3 matrix. A decrease of sensitivity of about 70% was observed for 10 μg of Cl^- in the form of FeCl_3 ; however the interference could be well eliminated by the presence of only Pd + CA. In the presence of this modifier, up to 150 μg of Cl^- in the form of FeCl_3 could be tolerated without significant changes of sensitivity (less than 5%). It is expected that citric acid similarly as ascorbic or oxalic acid [20] helps to decrease the concentration of chlorine atoms in the graphite tube and, consequently, decreases their negative influence on the absorption of Sn. According to Fig. 2 it is evident, that further addition of NH_4F to Pd + CA modifier did not increase the robustness against FeCl_3 matrix and both mixtures were similarly effective in the elimination of FeCl_3 interference, although Fe is known to form very stable soluble complex with fluoride. It follows from Fig. 2 as well that a presence of FeCl_3 matrix did not lead to an increase of background absorbance for Sn 224.6 nm line and similar background absorbance values were obtained at conditions both without and with the presence of both investigated chemical modifiers mixtures. Because an overcorrection was not observed and samples containing only the interferent yielded good blanks without clear atomic peaks, it was concluded that, in presence of FeCl_3 , Sn atomization is suffering mainly by chemical interference and that the spectral ones can be disregarded.

As it is demonstrated in Figs. 2 and 3a, the presence of AlCl_3 matrix interfered in Sn determination, too. In comparison with the presence of FeCl_3 matrix, the background absorbance was significantly increased by the presence of AlCl_3 matrix (Fig. 2). It can be further seen from Figs. 2 and 3b that in the presence of only Pd + CA mixture, the interference from AlCl_3 matrix could not be overcome. However, this problem can be well eliminated by the addition of

Table 1

Optimized electrothermal program for the determination of Sn in *aqua regia* leaches from rocks, soils and sediments.

Step	Temperature ($^{\circ}\text{C}$)	Time (s)		Gas flow (L min^{-1})
		Ramp	Hold	
Injection 1 ^a	65	5	5	3.0
Drying	110	15	0	3.0
Injection 2 ^b	95	15	0	3.0
Drying	180	25	10	3.0
Pyrolysis	^c	5	10	3.0
	^c	0	1	0.0
Atomization	^c	0	2	0.0
Cleaning	2500	1	1	3.0
Cooling down	40	25	5	3.0

^a Injection of appropriate volumes of 1 g L^{-1} of Pd modifier or mixture of Pd with CA.

^b Injection of 10 μL of a sample together with appropriate volume of AF.

^c Pyrolysis and atomization temperatures for measurements when influence of FeCl_3 and AlCl_3 matrix onto Sn determination was studied or when *aqua regia* leaches of rocks, soils and sediments were analyzed were 1400 and 2200 $^{\circ}\text{C}$ in presence of Pd + CA or Pd + CA + AF chemical modifiers. Using the modifier free conditions the pyrolysis and atomization temperatures were 900 and 2100 $^{\circ}\text{C}$.

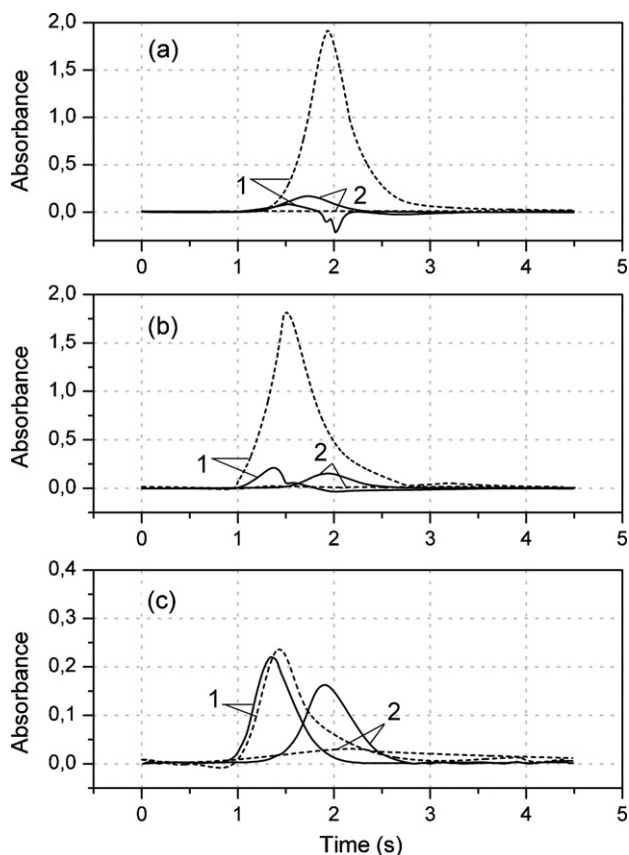


Fig. 3. Atomic (solid lines) and background (dotted lines) absorbance signals for 500 pg of Sn in the presence of (1) 40 µg Al in the form of AlCl₃ and under (2) matrix free conditions: (a) without chemical modifier and in the presence of (b) 4 µg Pd + 1000 µg CA and (c) 4 µg Pd + 1000 µg CA + 1000 µg AF. Pyrolysis and atomization temperatures were in accordance with those given in Table 1.

NH₄F (see Figs. 2 and 3c). Ammonium fluoride significantly reduces the background absorbance and increases the robustness of the chemical modifier to AlCl₃ matrix (Fig. 2). In the presence of 4 µg of Pd + 1000 µg of CA + 1000 µg of AF modifier, 50 µg of Al in the form of AlCl₃ could be tolerated without any change of sensitivity (higher amounts were not studied).

It can be supposed that Al oxide species (probably Al₂O) generated from the solid phase Al₂O₃, which is the most thermally stable condensed phase aluminium oxide [21–23] produced also by thermal behaviour of AlCl₃ matrix as shown previously [21], interfere on Sn determination similarly as described previously during the determination of various elements [24–29] in presence of large amount of alumina matrix and are responsible for negative peak occurring during the analysis of both GBW 07405 and GBW 07407 samples. It can be expected that due to the broad band molecular absorption of alumina oxide species [24] the spectral interference at all the investigated Sn wavelengths, i.e. 224.6, 235.5, 286.3 nm has occurred.

Typical peak profiles derived from the atomization of 500 pg of Sn in the presence of 40 µg of Al in the form of AlCl₃ without any modifier, with applying Pd + CA and with Pd + CA + AF modifier are shown in Fig. 3a-1, b-1 and c-1, respectively. In addition, time-scans of Sn atomic absorption signal without and with the use of modifiers under matrix free conditions are shown for comparison (Fig. 3a-2, b-2 and c-2). Based on the boiling point data available from the literature [30], it can be considered that the elimination of high background absorbance values and an interference observed in the presence of AlCl₃ matrix (Fig. 3a) after the addi-

tion of NH₄F (Fig. 3c) is likely the consequence of a creation of AlF₃ with the sublimation point of 1276 °C, which could be, contrary to aluminium oxide, removed from the graphite furnace during the pyrolysis stage. This presumption can be supported by the studies of Scaccia and Zappa [24] who have applied a halogen assisted thermal purification with the use of Ar + 1% (v/v) CHF₃ internal furnace gas to the determination of Fe in high-purity aluminium to attain a complete volatilization of the matrix without any loss of the analyte. In the presence of fluorinating agent, no aluminium oxide was left in the graphite furnace at and above 700 °C and the authors [24] have reported the formation of solid AlF₃ with the existence in the range of 600 and 1300 °C. The authors [24] have also observed no interfering background within the range of 200–340 nm that was otherwise very intensive without halogenation.

As it can be seen in Fig. 3b and c, in the presence of AlCl₃ matrix, for both Pd + CA and Pd + CA + AF addition, Sn atomic absorption signal appears earlier, i.e. at the lower temperature when compared with matrix free conditions. This fact can be attributed to the less efficient analyte stabilization due to the presence of high amount of the interfering matrix. Possible gas phase reactions of fluorine with the analyte were without practical relevance at the conditions described since no signal suppression was observed after AF addition.

3.2. Application to the analysis of aqua regia extracts

Palladium with citric acid and ammonium fluoride chemical modifier was applied to the determination of Sn in GBW 07407 and GBW 07405 certified reference standards to check accuracy and precision of the method for the purpose of direct analysis of aqua regia extracts of rocks, soils and sediments. 4 µg of Pd, 1600 µg of CA and 1000 µg of AF were used. These amounts were optimized and selected using the same way and the same criteria as described in Ref. [19]. The influence of individual modifier compounds onto specific and non-specific absorbance for both GBW 07407 and GBW 07405 is shown in Fig. 4. The pyrolysis and atomization temperatures used for measurement were 1400 and 2200 °C, respectively. Both temperatures were optimized experimentally by varying the temperature between 900 and 1600 °C for the pyrolysis step and between 1800 and 2300 °C for the atomization step, for both of investigated samples, in the presence of 4 µg Pd + 1600 µg CA + 1000 µg AF. Pyrolysis temperature of 1400 °C was chosen as experiments have shown that maximum temperature of 1500 °C can be tolerated by Sn in both investigated matrices. Optimal atomization temperature of 2200 °C was selected from the plateau area of atomization curves.

As the slopes of calibration lines of the standard additions method for aqua regia extracts from both investigated samples in the presence of 4 µg of Pd + 1600 µg CA + 1000 µg AF were very close to that of the aqueous standard (within 15%), which means that the effect of matrix was under a good control at conditions described, direct aqueous calibration was used for quantification. The equation for direct aqueous calibration, constructed according to the procedure described in Section 2 was as follows: $Q_A = 2.31 \times 10^{-3} (3.9 \times 10^{-5})[\text{Sn}]$ (where Q_A = integrated absorbance and [Sn] is concentration of the analyte in µg L⁻¹; standard deviation of the slope is given in parentheses). It can be seen from Table 2 that a good agreement with values given by the manufacturer of reference materials and with those determined by ICP-TOFMS [16] additionally applied for determination of Sn content in these samples (10-fold or 25-fold diluted) was achieved, which confirms accuracy and reliability of the proposed method.

The precision of the determination expressed as the relative standard deviation of five replicate measurements of 66 µg L⁻¹ of Sn from GBW 07407, and of 51 µg L⁻¹ in 5-fold diluted GBW

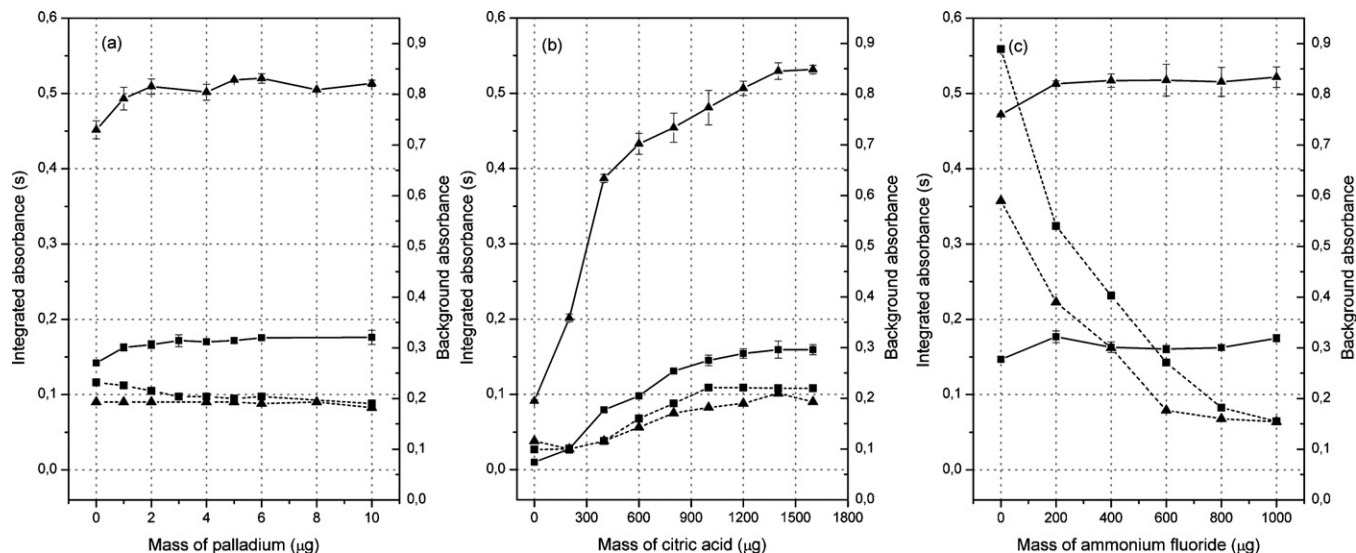


Fig. 4. Influence of the amount of (a) Pd (in presence of 2000 μg of CA and 1000 μg of AF), (b) CA (in presence of 4 μg of Pd and 1000 μg of AF) and (c) AF (in presence of 4 μg of Pd and 1600 μg of CA) on integrated absorbance of Sn (solid line) and background signal (dotted lines) for (■) GBW 07407 and (▲) GBW 07405 samples. Bars indicate the range for each determination ($n = 3$). Pyrolysis and atomization temperature was 1400 and 2200 °C, respectively.

Table 2

Concentrations of Sn in rock, soil and sediment reference samples: comparison of methods.

Reference material	Concentration (mg kg^{-1})		
	Declared	Found ^a	
		ICP-TOFMS	D ₂ -ETAAS
GBW 07407 (Laterite)	3.6 ± 3.2	3.2 ± 0.2	3.3 ± 0.1
GBW 07405 (Yellow-red soil)	17.7 ± 7.3	12.2 ± 0.2	12.7 ± 0.6

^a Mean \pm S.D. for results of independent measurements of three parallels samples.

07405 was 2.6 and 3.2%, respectively. The precision of the method expressed as the relative standard deviation in Sn determination from three independent parallel extractions of GBW 07407 and GBW 07405 was 3.0 and 4.7%, respectively.

Tube life-time given by the typical number of firings for Sn determination in GBW 07407 and GBW 07405 samples was 600–700.

3.3. Figures of merit

Limit of detection (LOD) and limit of quantification (LOQ) defined as the concentration that gives an integrated absorbance equal to three times and 10 times of the standard deviation of 10 measurements of a sample with Sn concentration close to the blank were 1.1 and 3.7 $\mu\text{g L}^{-1}$, respectively. These values, corresponding to 0.055 and 0.19 $\mu\text{g g}^{-1}$ of Sn in the original sample, are sufficiently low so that Sn content in rocks, soils and sediments samples [31] could be determined. As all modifiers components are available in high purity, no problems with contamination were observed even for high amounts of citric acid or ammonium fluoride which impacts positively LOD value. Characteristic mass value of 17.0 ± 0.5 pg was achieved, expressed as the mean \pm S.D. ($n = 4$) from those of GBW 07407 and GBW 07405 calculated from the slopes of the standard additions technique using the equation $m_0 = (0.0044 \times V)/m$, where V is the injection volume (10 μL) and m is the standard additions slope. This value is lower than those reported for Sn previously with different modifiers during the analysis of different environmental samples [2,3,6,7].

4. Conclusions

The mixture of palladium with citric acid and ammonium fluoride has been proved as very effective to overcome the interferences occurring during the direct determination of Sn in *aqua regia* leaches from rocks, soils and sediments by D₂-ETAAS method, of which those caused by aluminium oxide was considered to be the most serious. The application of the modifier to direct determination of Sn in all types of investigated samples has enabled rapid, accurate and interference-free determination in samples with concentration of Sn above 0.19 $\mu\text{g g}^{-1}$. The proposed method offers an effective and simple solution of the problem which up to date was not successfully solved in analytical practice and which is easy to follow for analytical laboratories. It can be expected that high efficiency of the proposed chemical modifier for the modification and removal of the aluminium matrix will result in similar advantage also in case of determination of some other elements strongly sensitive to the presence of alumina matrix.

Acknowledgement

This work was supported by the project MSM 0021627502 of the Ministry of Education, Youth and Sports of the Czech Republic.

References

- [1] J.B.B. da Silva, M.A.M. da Silva, A.J. Curtius, B. Welz, J. Anal. Atom. Spectrom. 14 (1999) 1737.
- [2] P. Bermejo-Barrera, C. Barciela-Alonso, C. González-Sixto, A. Bermejo-Barrera, Fresen. J. Anal. Chem. 357 (1997) 274.
- [3] P. Bermejo-Barrera, M.C. Barciela-Alonso, J. Moreda-Piñeiro, C. González-Sixto, A. Bermejo-Barrera, Spectrochim. Acta Part B 51 (1996) 1235.
- [4] V.I. Slaveykova, M. Hoenig, Analyst 122 (1997) 337.
- [5] I. Arambarri, R. Garcia, E. Millán, Analyst 125 (2000) 2084.
- [6] N.N. Meeravali, S.J. Kumar, J. Anal. Atom. Spectrom. 17 (2002) 704.
- [7] I. López-García, I. Arnau-Jerez, N. Campillo, M. Hernández-Córdoba, Talanta 62 (2004) 413.
- [8] A. Brzezinska-Paudyn, J.C. Van Loon, Fresen. Z. Anal. Chem. 331 (1988) 707.
- [9] E. Lundberg, B. Bergmark, W. Frech, Anal. Chim. Acta 142 (1982) 129.
- [10] M. Tominaga, Y. Umezaki, Anal. Chim. Acta 110 (1979) 55.
- [11] M. Ozcan, S. Akman, Spectrochim. Acta Part B 55 (2000) 509.
- [12] International Organization for Standardization, Soil Quality, Extraction of Trace Elements Soluble in Aqua Regia, ISO 11466, 1995.
- [13] G. Schlemmer, B. Welz, Spectrochim. Acta Part B 41 (1986) 1157.

- [14] B. Welz, M. Sperling, *Atomic Absorption Spectrometry*, 3rd ed., Wiley-VCH, Weinheim, 1999.
- [15] R.E. Sturgeon, J.W.H. Lam, A. Saint, *J. Anal. Atom. Spectrom.* 15 (2000) 607.
- [16] L. Husáková, T. Černohorský, J. Šrámková, L. Vavrušová, *Food Chem.* 105 (2007) 286.
- [17] M. Žemberyová, J. Barteková, I. Hagarová, *Talanta* 70 (2006) 973.
- [18] E. Bulska, H.M. Ortner, *Spectrochim. Acta Part B* 55 (2000) 491.
- [19] L. Husáková, T. Černohorský, J. Šrámková, K. Hubáčková, I. Doležalová, *Anal. Chim. Acta* 614 (2008) 38.
- [20] T. Kántor, *Spectrochim. Acta Part B* 50 (1995) 1599.
- [21] M.A. Castro, K. Faulds, W.E. Smith, A.J. Aller, D. Littlejohn, *Spectrochim. Acta Part B* 59 (2004) 1935.
- [22] M.A. Castro, A.J. Aller, *Spectrochim. Acta Part B* 58 (2003) 901.
- [23] M.R. Shepard, B.T. Jones, D.J. Butcher, *Appl. Spectrosc.* 52 (1998) 430.
- [24] S. Scaccia, G. Zappa, *Spectrochim. Acta Part B* 55 (2000) 1271.
- [25] Z. Slovák, B. Dočekal, *Anal. Chim. Acta* 129 (1981) 263.
- [26] R. Wennrich, W. Frech, E. Lundberg, *Spectrochim. Acta Part B* 44 (1989) 239.
- [27] R. Karwowska, K.W. Jackson, *Spectrochim. Acta Part B* 41 (1986) 947.
- [28] R. Karwowska, K.W. Jackson, *J. Anal. Atom. Spectrom.* 2 (1987) 125.
- [29] V. Tokarová, J. Mareček, *Collect. Czech. Chem. Commun.* 53 (1988) 756.
- [30] D.R. Lide (Ed.), *CRC Handbook of Chemistry and Physics*, 81st ed., CRC Press, Boca Raton, 2000.
- [31] B.J. Alloway (Ed.), *Heavy Metals in Soils*, 2nd ed., Blackie Academic and Professional, London, 1995.



Determination of trace amounts of lead and cadmium using a bismuth/glassy carbon composite electrode

Gil-Ho Hwang^a, Won-Kyu Han^a, Seok-Jun Hong^a, Joon-Shik Park^b, Sung-Goon Kang^{a,*}

^a Department of Materials Science and Engineering, Hanyang University, 17 Haengdang, Seongdong, Seoul 133-791, Republic of Korea

^b Nanomechatronics Research Center, Korea Electronics Technology Institute (KETI), 68 Yatap, Seongnam, Kyunggi 463-816, Republic of Korea

ARTICLE INFO

Article history:

Received 30 July 2008

Received in revised form

17 September 2008

Accepted 18 September 2008

Available online 26 September 2008

Keywords:

Bismuth

Composite electrode

Electrochemical dissolution

Anodic stripping voltammetry

Trace metals

ABSTRACT

We examined the use of a bismuth–glassy carbon (Bi/C) composite electrode for the determination of trace amounts of lead and cadmium. Incorporated bismuth powder in the composite electrode was electrochemically dissolved in 0.1 M acetate buffer (pH 4.5) where nanosized bismuth particles were deposited on the glassy carbon at the reduction potential. The anodic stripping voltammetry on the Bi/C composite electrode exhibited well-defined, sharp and undistorted peaks with a favorable resolution for lead and cadmium. Comparing a non-oxidized Bi/C composite electrode with an in-situ plated bismuth film electrode, the Bi/C composite electrode exhibited superior performance due to its much larger surface area. The limit of detection was 0.41 $\mu\text{g/L}$ for lead and 0.49 $\mu\text{g/L}$ for cadmium. Based on this study, we are able to conclude that various types of composite electrodes for electroanalytical applications can be developed with a prudent combination of electrode materials.

© 2008 Elsevier B.V. All rights reserved.

1. Introduction

Bismuth film electrodes have been recently suggested as an alternative to traditional mercury electrodes for determination of trace metals [1–3]. Bismuth is an environmentally friendly material with very low toxicity and possesses a comparable performance to mercury in stripping analyses. The attractive stripping voltammetric performance of bismuth film electrodes is due to the fused alloys they form with heavy metals [4,5]. Bismuth film electrodes were prepared by an in-situ or ex-situ plating method on various substrates, including gold, platinum [6–7], carbon paste [8,9], glassy carbon [10–12] and carbon fiber [13].

Recently, bismuth-based composite electrodes have been proposed to design mercury-free electrodes for stripping analysis. Major advantages of composite electrodes include their simplicity in sensor preparation and analytical procedures. Bismuth oxide-modified carbon has been studied for the analysis of drinking water, mineral water and urine, [14] and a graphite–epoxy electrode has been mixed with $\text{Bi}(\text{NO}_3)_3$ salt as a built-in bismuth precursor [15]. Carbon electrodes mixed with pure metals have been successfully used for electrochemical analysis. Electroanalytical performance of these electrodes was based on the typical features of the carbon material and electrocatalytical characteristics of doped metals

(Pt, Pd, Ru, etc.) in oxidation of some organic and biological substances [16]. Hocevar et al. reported a bismuth–graphite electrode which was prepared by mixing fine metallic bismuth powder with graphite powder and silicon oil. Incorporated bismuth powders acted as deposition sites of lead and cadmium in the preconcentration step and the resultant configuration exhibited better analytical performance than the bare carbon paste, bismuth paste and bismuth film-coated carbon paste electrode [17].

In contrast with these studies, we utilized a bismuth–glassy carbon (Bi/C) composite electrode with built-in bismuth powders as the source of $\text{Bi}(\text{III})$ ions for the deposition of bismuth on the glassy carbon. The Bi/C composite electrode was electrochemically oxidized and bismuth ions were released from bismuth powders to the supporting electrolyte. The bismuth ions were deposited on the glassy carbon at the reduction potential. The analytical performance of the Bi/C composite electrode was compared with those of a non-oxidized Bi/C composite electrode and in-situ plated bismuth film electrode. In addition, the possibility of using a Bi/C composite electrode for the simultaneous determination of trace amounts of lead and cadmium was evaluated.

2. Experimental procedure

2.1. Apparatus

All electrochemical experiments were performed using a CHI model 750 potentiostat (CH instruments) controlled by a

* Corresponding author. Tel.: +82 2 2220 0404; fax: +82 2 2296 4560.
E-mail address: sgkang@hanyang.ac.kr (S.-G. Kang).

personal computer via CH instruments software. A conventional three electrode cell configuration was employed for the voltammetric measurements, containing a Bi/C composite electrode with diameter of 3 mm as working electrode, platinum mesh (Alfa Aesar) as counter electrode and a saturated calomel electrode (SCE, Fisher Scientific) as reference electrode.

2.2. Reagents

All chemicals used in this study were of analytical reagent grade and used as received. Standard stock solutions of lead and cadmium (1000 mg/L, atomic absorption standard solution) were obtained from Kanto Chemical. Glassy carbon powder, bismuth powder, sodium acetate, and acetic acid were purchased from Aldrich. Supporting electrolyte used in the experiments was 0.1 M acetate buffer (pH 4.5). Terpeneol and ethyl cellulose were purchased from TCI. Epoxy (SJ-52-516) and silver paste (SJ-52-512) were obtained from Sungji Tech. All solutions are prepared with deionized water (18 M Ω cm) from a Milli-Q system (Millipore).

2.3. Electrode preparation

Bi/C composite paste was prepared by mixing bismuth powder and glassy carbon powder with terpeneol containing 5% ethyl cellulose. Silver paste was printed on the alumina plate for the electrical connection and the Bi/C composite paste, which served as the working electrode, was formed onto the silver layer. Finally, the epoxy paste was printed for the insulating layer except on the exposed, 3 mm diameter sensing area. After the printing step, the Ag and the epoxy were baked at 120 °C for 30 min and the Bi/C composite was baked at 150 °C for 30 min.

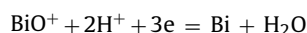
2.4. Procedure

The dissolution of bismuth was performed at 0.3 V (vs. SCE) for 1 min in 0.1 M acetate buffer solution (pH 4.5). For the reduction of the dissolved bismuth ions, a cathodic potential of –1.2 V (vs. SCE) was applied to the working electrode for 3 min, without stirring. After deposition of the bismuth, lead and cadmium standard solutions were added to the cell as required, and a preconcentration potential of –1.2 V was applied to the working electrode for 5 min while stirring. After an equilibration time of 10 s, square wave anodic stripping voltammograms were recorded between –1.2 V and –0.3 V without stirring. For repetitive measurements, the electrode was cleaned at –0.3 V for 30 s under stirring conditions to remove the residual metals. All experiments were done at room temperature.

3. Results and discussion

3.1. Electrochemical characterizations of the Bi/C composite electrode

Fig. 1(a) and (b) shows the cyclic voltammograms of the bismuth and Bi/C composite electrodes containing 50 wt.% bismuth in 0.1 M acetate buffer (pH 4.5), respectively. The scan was conducted from –0.7 V to 0.3 V and then reversed to the initial potential at a rate of 20 mV/s. In the anodic scan, the voltammograms of both the bismuth and Bi/C composite electrodes show significant oxidation peaks at –0.15 V, corresponding to the oxidation of bismuth. In the pH range of 4.0–8.0, the electrochemical reactions can be represented as follows [18]:



Thus, the strong oxidation peaks were associated with the release of bismuth ions from the bismuth powder to the supporting electrolyte. During the cathodic scan, dissolved bismuth ions in the supporting electrolyte were reduced to metallic bismuth on the electrode surface.

At the bismuth electrode (Fig. 1(a)), no significant change of reduction peaks was observed in the cathodic region except for a slight increase of cathodic current at potentials more negative than –0.4 V. This behavior is related to the deposition of dissolved bismuth ions on the electrode surface [19]. In contrast with the bismuth electrode, the Bi/C composite electrode exhibited a couple of redox peaks, which can be clearly seen in Fig. 1(b). This shows that the Bi/C composite electrode was a more suitable substrate for bismuth deposition than metallic bismuth, as the dissolved bismuth ions could easily be deposited on the glassy carbon electrode. Both voltammograms show a crossover between the currents during the anodic and cathodic scans. The presence of the crossover is a typical characteristic of a nucleation and growth process [20,21].

The bismuth electrode was electrochemically oxidized at 0.3 V, which is more positive than the bismuth oxidation potential. The concentration of dissolved bismuth ions was then measured by ICP-MS. The bismuth ions were actually released from bismuth powder to the supporting electrolyte during the dissolution procedure. When the anodic potential was applied to the bismuth electrode with diameter 3 mm in 50 ml of 0.1 M acetate buffer (pH 4.5), the bismuth concentration increased linearly with oxidation time at a rate of 4.27 ppb/min. For the evaluation of the naturally dissolved bismuth, the bismuth electrode was immersed in 50 ml of 0.1 M acetate buffer (pH 4.5) for 1 h and the concentration of bismuth ions was also measured. The concentration of naturally dissolved bismuth was 4.95 ppb. As the bismuth ions were electrochemically

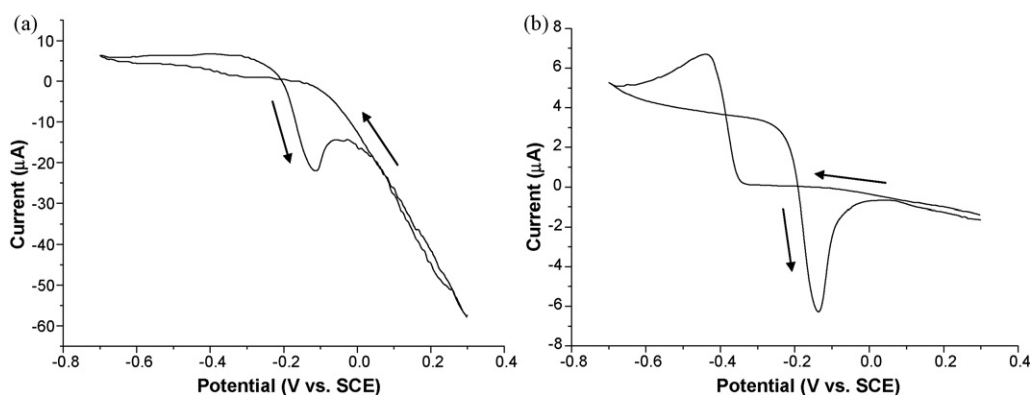


Fig. 1. Cyclic voltammograms of (a) bismuth electrode and (b) Bi/C composite electrode in 0.1 M acetate buffer (pH4.5). Scan rate: 20 mV/s.

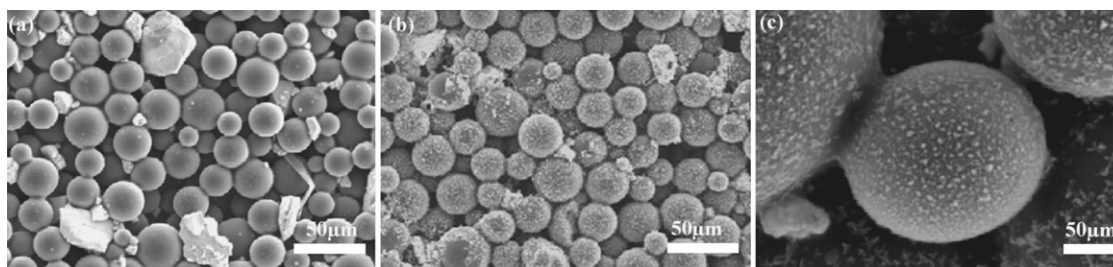


Fig. 2. SEM images for Bi/C composite electrode (a) before and (b) after anodic dissolution and cathodic reduction procedure at 400 \times and (c) at 2500 \times of (b).

released into the supporting electrolyte, only a negligible amount of bismuth in the Bi/C composite electrode was naturally dissolved in the supporting electrolyte and it rarely affected the total bismuth ion concentration. These results are consistent with the literature [17].

3.2. Surface morphologies

Fig. 2(a) is the SEM surface image of the Bi/C composite electrode containing 50 wt.% bismuth before the reduction of released bismuth ions. White particles are bismuth powders with irregular shape and size, and spherical gray particles are glassy carbon powders with 10–40 μm particle size. The SEM surface image of the Bi/C composite electrode after reduction of the released bismuth ions at -1.2 V for 3 min is displayed in Fig. 2(b and c). In Fig. 2(b), it is clearly observed that the glassy carbon surface is covered with bismuth. When the Bi/C composite electrode was oxidized at 0.3 V for 1 min, the concentration of released bismuth ions was not high enough for the deposition of bismuth on glassy carbon. Therefore, it is considered that bismuth ions released from the bismuth powder did not diffuse away from the electrode surface in the still solution. And the local bismuth ion concentration near the electrode surface could be high enough to cover the whole glassy carbon surface with bismuth. When the solution was vigorously stirred, bismuth was not deposited on the glassy carbon surface at all because the dissolved bismuth ions were completely scattered, causing insufficient bismuth ion concentration near the electrode surface. In contrast, too many bismuth ions enhanced the nuclei density of bismuth on the glassy carbon surface and increased the surface coverage of nuclei [21]. Therefore, on the surface of glassy carbon powders adjacent to the bismuth powder, bismuth was deposited in agglomerates, and on the glassy carbon apart from the bismuth powder, bismuth was uniformly deposited. Fig. 2(c), the high magnification of Fig. 2(b), shows bismuth nanoparticles with a size of approximately 300 nm. The white spots and the gray particles with spherical shape represent deposited bismuth and the glassy carbon, respectively. The bismuth nanoparticles were uniformly distributed over the surface in uniform sizes. Similar nucleation behaviors of bismuth have been previously reported; specifically, nitrate solutions of high concentration enhance the nuclei density of bismuth on glassy carbon electrodes [22]. Compared with the nucleation models of Scharifker and Hills, the bismuth nucleation was consistent with the instantaneous nucleation mechanism corresponding to a growth of nuclei on active sites which all are activated at the same time [23]. More detailed investigations were not performed in this study. The presence of bismuth nanoparticles on the glassy carbon resulted in an increase in surface area. This means that the deposition sites of trace metals were increased and the stripping responses were enhanced in anodic stripping analysis. In contrast, an increase of bismuth content in composite electrode could lower the conductivity of the electrode and deteriorate its sensing performance [17].

3.3. Effect of bismuth content in a Bi/C composite electrode

The effect of bismuth content on the stripping response of a Bi/C composite electrode was analyzed in solutions of 100 $\mu\text{g/L}$ lead and cadmium to obtain the highest stripping response (Fig. 3). In the absence of bismuth powder, the pure glassy carbon electrode exhibited a poor performance of $1.32\text{E}-6$ A and $3.98\text{E}-7$ A for lead and cadmium, respectively. As bismuth content in the electrode was increased up to 50 wt.%, the stripping responses increased due to the increase of active sites resulting from the dissolution and reduction of the bismuth powder in the electrode. The bismuth ions released from the electrode formed a large number of nanoparticles on its surface at the reduction potential. The increase in the number of bismuth nanoparticles deposited on the electrode increased the active surface area for the deposition of lead and cadmium, which resulted in higher sensitivity in stripping voltammetry. However, bismuth of more than 50 wt.% in the electrode lowered conductivity and caused agglomeration of bismuth nanoparticles resulting in a smaller active site on the Bi/C composite electrode. As a result, the Bi/C composite electrode with the high bismuth content (above 50 wt.%) showed a lower sensitivity. The pure bismuth powder electrode showed a stripping response similar to that of the Bi/C composite electrode containing 25 wt.% bismuth. Maximum sensitivity of stripping response was obtained at 50 wt.% bismuth, which is equivalent to about 15.7 vol.%. At this composition, bismuth nanoparticles were the most uniformly distributed in individual spherical shapes without agglomeration on the electrode surface.

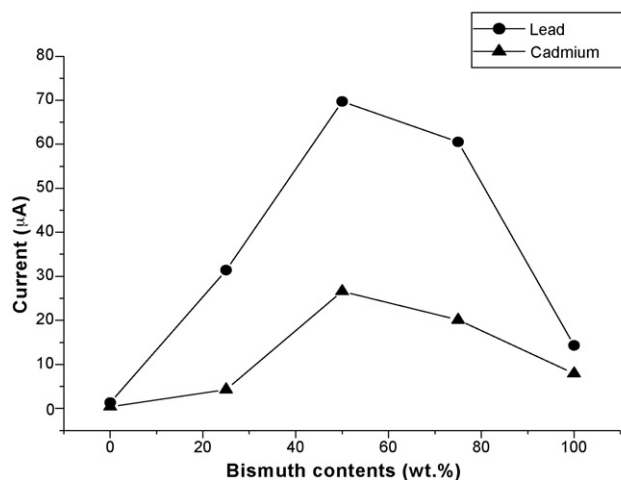


Fig. 3. Effects of bismuth content on the peak height for 100 ppb lead and cadmium. Supporting electrolyte: 0.1 M acetate buffer (pH 4.5); preconcentration potential: -1.2 V; preconcentration time: 300 s; frequency: 50 Hz; pulse height: 50 mV; step increment: 5 mV.

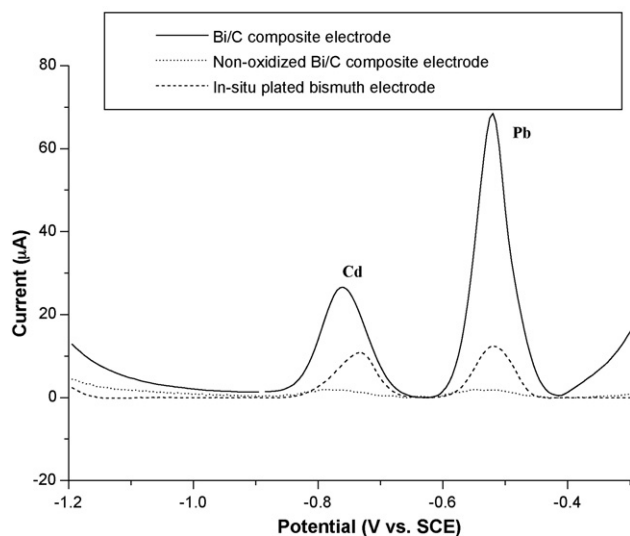


Fig. 4. Square wave stripping voltammograms for 100 µg/L lead and cadmium at Bi/C composite electrode, unoxidized Bi/C composite electrode and in-situ plated bismuth film electrode. Other conditions as in Fig. 3.

Due to the irregular shape and size of bismuth powders, the active area of the deposited bismuth can be changed depending on the electrode preparation. Five different Bi/C composite electrodes containing 50 wt.% bismuth were prepared and their stripping responses were measured under the same conditions. The Bi/C composite showed good reproducibility with standard deviation less than 3% due to the bismuth being redistributed by the dissolution and deposition process.

3.4. Comparison of different bismuth-based electrodes

The stripping responses of two other types of Bi/C composite electrodes are shown in Fig. 4. One was a Bi/C composite electrode in which the dissolution procedure was not used. The cleaning potential of -0.3 V, which is more negative than the oxidation potential of bismuth, was used for the prohibition of bis-

moth dissolution. In this electrode, only bismuth powders mixed in the Bi/C composite electrode served as active sites for the determination of lead and cadmium. The other electrode was an in-situ plated bismuth film electrode. For in-situ plating of bismuth film on the glassy carbon electrode, a 1000 µg/L bismuth ion solution was added to the supporting electrolyte. In the anodic stripping voltammetry performed under the same conditions, all electrodes exhibited well-defined, sharp and undistorted stripping peaks at -0.55 V and -0.75 V for lead and cadmium, respectively. The Bi/C composite electrode exhibited the best performance due to its large active area, followed by the in-situ plated bismuth film electrode and the non-oxidized Bi/C composite electrode. In contrast to the superior electroanalytical performance of the Bi/C composite electrode, the background current increased at a potential more positive than -0.4 V due to the oxidation of bismuth. Furthermore, the hydrogen evolution potential was more positive than that of the in-situ plated bismuth film electrode. These behaviors of the Bi/C composite electrode yielded a narrow potential window. The in-situ plated bismuth film electrode produced the flattest and least noisy baseline and widest potential window, whereas the Bi/C composite electrode exhibited the highest stripping responses to lead and cadmium.

3.5. Calibration data

The simultaneous determination of lead and cadmium with a Bi/C composite electrode was performed and the resulting voltammograms are shown in Fig. 5, together with the corresponding calibration curves. Square wave anodic stripping voltammograms were recorded for increasing levels of lead and cadmium in 20 µg/L steps. In the calibration curves, the plotted values are the average values of five repeated measurements. The calibration curves exhibit excellent linearity with a correlation of 0.999 for lead and 0.998 for cadmium. These results show that lead and cadmium can be simultaneously analyzed by the Bi/C composite electrode. The peak current increased linearly with metal concentration, with a slope of 0.71 µA/µg for lead and 0.26 µA/µg for cadmium. Detection limits of 0.41 µg/L and 0.49 µg/L for lead and cadmium were estimated on the basis of the response for

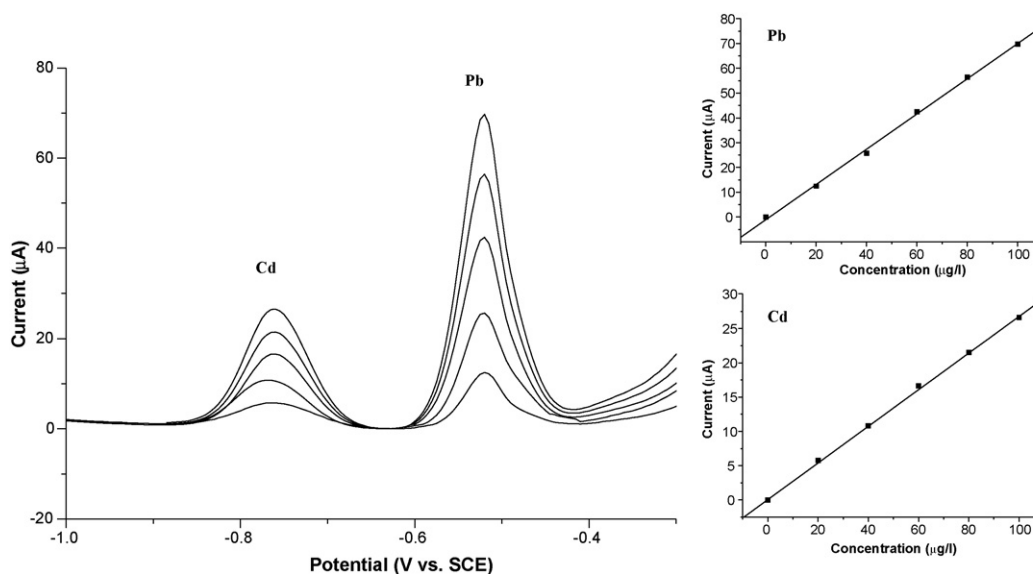


Fig. 5. Square wave stripping voltammograms for increasing concentration of lead and cadmium in 20 µg/L obtained with Bi/C composite electrode. Other conditions as in Fig. 3.

10 µg/L lead and cadmium following a 5 min preconcentration ($S/N=3$).

4. Conclusions

We developed Bi/C composite electrodes to simultaneously determine trace levels of lead and cadmium. Using the developed Bi/C composite electrodes, the external addition of bismuth ions into the measurement solution was not required due to the in-situ generation and deposition of bismuth ions. Whereas bismuth powder showed negligible solubility in 0.1 M acetate buffer (pH 4.5), when the Bi/C composite electrode was electrochemically oxidized at a more positive potential than the bismuth oxidation potential, bismuth ions were released from the bismuth powder to the supporting electrolyte in proportion to the oxidation time. These bismuth ions were deposited on the glassy carbon at the reduction potential. Interestingly, the bismuth ions did not form as a bismuth film, but as bismuth nanoparticles which were uniform in size and uniformly distributed over the surface. These nanoparticles resulted in an increase in the electrode surface area and stripping response for the stripping voltammetry. The analytical performance of the Bi/C composite electrode was superior to the non-oxidized Bi/C composite electrode and the in-situ plated bismuth film electrode. In contrast, the Bi/C composite electrode displayed a narrower potential window than in-situ plated bismuth film electrode. One obvious disadvantage of the Bi/C composite electrode was its decreased conductivity; however, a combination of two separate electrodes, one as the working electrode and the other as the ions supplier, can be an effective solution to this problem. The further studies will be focused on real sample analysis and detection of other metals (zinc, cobalt, chromium, etc.) by combining with different electrochemical technique such as adsorptive stripping voltammetry.

Acknowledgement

This work was supported by the Korea Research Foundation Grant funded by the Korean Government (MOEHRD) (KRF-2007-D00185-102466).

References

- [1] J. Wang, J. Lu, S.B. Hocevar, P.A.M. Farias, *Anal. Chem.* 72 (2000) 3218.
- [2] G. Kefala, A. Economou, M. Sofoniou, *Talanta* 68 (2006) 1013.
- [3] E.A. Hutton, J.T. Elteren, B. Ogorevc, M.R. Smyth, *Talanta* 63 (2004) 849.
- [4] J. Wang, J. Lu, U.A. Kirgoz, S.B. Hocevar, B. Ogorevc, *Anal. Chim. Acta* 29 (2001) 434.
- [5] E.P. Achterberg, C. Braumgardt, *Anal. Chim. Acta* 400 (1999) 381.
- [6] L. Baldrianova, I. Svancara, M. Vlcek, A. Economou, S. Sotiropoulos, *Electrochim. Acta* 52 (2006) 481.
- [7] L. Baldrianova, I. Svancara, A. Economou, S. Sotiropoulos, *Anal. Chim. Acta* 580 (2006) 24.
- [8] G.U. Flechsig, O. Korbout, S.B. Hocevar, S. Thongngamdee, B. Ogorevc, P. Grundler, J. Wang, *Electroanalysis* 14 (2002) 192.
- [9] J. Wang, J. Lu, S.B. Hocevar, B. Ogorevc, *Electroanalysis* 13 (2001) 13.
- [10] E.A. Hutton, B. Ogorevc, S.B. Hocevar, F. Weldon, M.R. Smyth, J. Wang, *Electrochim. Commun.* 3 (2001) 707.
- [11] J. Wang, D. Lu, S. Thongngamdee, Y. Lin, O.A. Sadik, *Talanta* 69 (2006) 914.
- [12] G. Kefala, A. Economou, A. Voulgaropoulos, M. Sofoniou, *Talanta* 61 (2003) 603.
- [13] E.A. Hutton, S.B. Hocevar, B. Ogorevc, *Anal. Chim. Acta* 537 (2005) 285.
- [14] R. Pauliukaite, R. Metelka, I. Svancara, A. Krolicka, A. Bobrowski, K. Vytras, E. Norkus, K. Kalcher, *Anal. Bioanal. Chem.* 374 (2002) 1155.
- [15] M.T. Castaneda, B. Perez, M. Pumerá, M. del Valle, A. Merkoci, S. Alegret, *Analyst* 130 (2005) 971.
- [16] A. Sanchez, A. Zapardiel, F.L. Prado, E. Bermejo, M. Moreno, J.A. Perez-Lopez, M. Chicharro, *Electroanalysis* 19 (2007) 1683.
- [17] S.B. Hocevar, I. Svancara, K. Vytras, B. Ogorevc, *Electrochim. Acta* 51 (2005) 706.
- [18] A.J. Bard, *Encyclopedia of Electrochemistry of the Elements*, vol. 9, Marcel Dekker, 1986, p. 75.
- [19] D. Grujicic, B. Pesic, *Electrochim. Acta* 50 (2005) 4426.
- [20] S.B. Sadale, P.S. Patil, *Solid State Ion.* 167 (2004) 273.
- [21] D. Grujicic, B. Pesic, *Electrochim. Acta* 49 (2004) 4719.
- [22] M. Yang, Z. Hu, *J. Electroanal. Chem.* 583 (2005) 46.
- [23] B. Scharifker, G. Hills, *Electrochim. Acta* 28 (1983) 879.



Stir bar sorptive extraction with in situ derivatization and thermal desorption–gas chromatography–mass spectrometry for trace analysis of methylmercury and mercury(II) in water sample

Rie Ito^a, Migaku Kawaguchi^b, Norihiro Sakui^a, Noriya Okanouchi^a, Koichi Saito^a, Yasuo Seto^c, Hiroyuki Nakazawa^{a,*}

^a Department of Analytical Chemistry, Faculty of Pharmaceutical Sciences, Hoshi University, 2-4-41 Ebara, Shinagawa-ku, Tokyo 142-8501, Japan

^b Bio-Medical Standard Section, National Metrology Institute of Japan (NMIJ), National Institute of Advanced Industrial Science and Technology (AIST), 1-1-1 Umezono, Tsukuba, Ibaraki 305-8563, Japan

^c National Research Institute of Police Science, 6-3-1 Kashiwanoha, Kashiwa-shi, Chiba 277-0882, Japan

ARTICLE INFO

Article history:

Received 22 July 2008

Received in revised form 2 September 2008

Accepted 2 September 2008

Available online 11 September 2008

Keywords:

Methylmercury

In situ derivatization

Stir bar sorptive extraction (SBSE)

Thermal desorption (TD)

Gas chromatography–mass spectrometry

(GC–MS)

ABSTRACT

A method for the trace analysis of methylmercury (MeHg) and Hg(II) in water sample was developed, which involved stir bar sorptive extraction (SBSE) with in situ alkylation with sodium tetraethylborate and thermal desorption (TD)–gas chromatography–mass spectrometry (GC–MS). The limits of quantification of MeHg and Hg(II) are 20 and 10 ng L⁻¹ (Hg), respectively. The method shows good linearity and the correlation coefficients are higher than 0.999. The average recoveries of MeHg and Hg(II) in tap or river water sample are 102.1–104.3% (R.S.D.: 7.0–8.9%) and 105.3–106.2% (R.S.D.: 7.4–8.5%), respectively. This simple, accurate, sensitive, and selective analytical method may be used in the determination of trace amounts of MeHg and Hg(II) in tap and river water samples.

© 2008 Published by Elsevier B.V.

1. Introduction

Mercury (Hg) is a well-known environmental pollutant that exists in three major forms: elemental Hg, a common form in air, inorganic Hg(II), and organic Hg, in particular, methylmercury (MeHg) [1]. However some microbes can convert inorganic forms of mercury into organic forms that can be accumulated by aquatic life. And, it has been reported that MeHg is most toxic to human. To evaluate the potential risks of various Hg species, they must be determined with highly sensitive and reliable methods. In the present study, we focused on the determination of MeHg and Hg(II) in water sample.

The maximum contaminant level goal (MCLG) is a non-enforceable level that is based solely on possible health risks and exposure. In the National Primary Drinking Water Regulations formulated by the Environmental Protection Agency (EPA), MCLG for mercury in drinking water is set at 2 ng mL⁻¹ [2]. Based on this MCLG, EPA has set an enforceable standard called maximum

contaminant level (MCL). MCL for mercury has also been set at 2 ng mL⁻¹ by EPA, since it is the lowest level to which water systems can reasonably be required to remove this contaminant should occur in drinking water. The World Health Organization (WHO) has set the guideline value for inorganic mercury in drinking water at 6 µg L⁻¹ [3]. In Japan, the Ministry of Health, Labour and Welfare of Japan has regulated the standard of water-purity for tap water for mercury species at 0.5 µg L⁻¹ [4].

Gas chromatography (GC) is generally used for the speciation of thermally stable and volatile species of Hg. The method generally involves alkylation of analytes prior to preconcentration [5–9]. Recently, solid phase microextraction (SPME) has been proposed as an alternative to liquid–liquid extraction (LLE) due to simplicity of use, high preconcentration ability, and the ability to extract volatile alkylated species [10]. In addition, the use of headspace solid phase microextraction (HS–SPME) for the determination of MeHg or Hg(II) in water sample has been reported [8,11–14]. More recently, stir bar sorptive extraction (SBSE) was introduced by Baltussen et al. [15], as another preconcentration technique in which a stir bar coated with 50–300 µL of polydimethylsiloxane (PDMS) is employed to extract analytes from a variety of matrices [16–18]. In addition, the use of headspace stir bar sorptive extraction (HS–SBSE) for the trace

* Corresponding author. Tel.: +81 3 5498 5763; fax: +81 3 5498 5062.
E-mail address: nakazawa@hoshi.ac.jp (H. Nakazawa).

Table 1
Figures of merit of SBSE with in situ derivatization and TD–GC–MS

Compound	SIM ^a (<i>m/z</i>)	LOD ^b (ng L ⁻¹)	LOQ ^c (ng L ⁻¹)	Range (μg L ⁻¹)	Correlation coefficient (<i>r</i>)	Amount spiked (0.5 g L ⁻¹)			
						Tap water		River water	
						Recovery (%)	R.S.D. (%) ^d	Recovery (%)	R.S.D. (%) ^d
MeHg	<u>246</u> , 217	5	20	0.02–5	0.999	102.1	7.0	104.3	8.9
Hg(II)	<u>260</u> , 231	2	10	0.01–5	0.999	105.3	7.4	106.2	8.5

^a The underlined number is the *m/z* of the ion used for quantification.

^b LOD: limit of detection (*S/N* = 3).

^c LOQ: limit of quantification (*S/N* > 10).

^d Recoveries and precision were also examined by replicate analysis (*n* = 6) of water samples.

analysis of MeHg and butyltin species in environmental sample has been reported [19]. However, HS-SBSE requires an extraction time of 2 h.

The aim of this study was to determine trace amounts of MeHg and Hg(II) in water samples by SBSE with in situ alkylation with sodium tetraethylborate and TD–GC–MS.

2. Experimental

2.1. Materials and reagents

Methylmercury(II) chloride standard and mercury(II) chloride standard were purchased from Kanto Chemical Co., Inc. (Tokyo, Japan). Other reagents and solvents were purchased from Wako Pure Chemical Inc. (Osaka, Japan). Sodium tetraethylborate (NaBEt₄) was purchased from Hayashi Pure Chemicals Inc. (Osaka, Japan). NaBEt₄ was used as the derivatization reagent, and was dissolved in purified water prior to use. The water purification system was a Milli-Q gradient A 10 equipped with an EDS polisher (Millipore, Bedford, MA, USA).

Calibrators for eight-point calibration (0.02, 0.05, 0.1, 0.2, 0.5, 1, 2, and 5 μg L⁻¹) of MeHg and nine-point calibration (0.01, 0.02, 0.05, 0.1, 0.2, 0.5, 1, 2, and 5 μg L⁻¹) of Hg(II) were prepared by the addition of purified water and calibrators were analyzed by using SBSE with in situ derivatization.

2.2. Instrumentation

TD was performed with a Gerstel TDS 2 thermodesorption system equipped with a Gerstel TDS A autosampler and a Gerstel Cooled Injection System (CIS) 4 programmable temperature vaporization (PTV) inlet. GC–MS was performed with an Agilent 6890N gas chromatograph equipped with a 5973N mass-selective detector with an ultra ion source (Agilent Technologies).

Stir bars coated with a 0.5-mm-thick PDMS layer (24 μL; Twister™) were obtained from Gerstel (Mülheim an der Ruhr, Germany). The stir bars were conditioned for 1 h at 300 °C in a flow of helium. Then, the stir bars were kept in new 2 mL vials until immediately prior to use. The stir bars could be used more than 50 times with appropriate re-conditioning. For the extraction, a 20-mL headspace vial from Agilent Technologies (Palo Alto, CA, USA) was used.

2.3. TD–GC–MS conditions

The TDS 2 temperature was programmed from 20 (held for 1 min) to 200 °C (held for 5 min) at 60 °C min⁻¹. The desorbed compounds were cryofocused in the CIS 4 at –150 °C. After the desorption, the CIS 4 temperature was programmed from –150 to 300 °C (held for 10 min) at 12 °C s⁻¹. Injection was performed in the splitless mode. Separations were conducted on a DB-1 fused silica

column (60 m × 0.25 mm i.d., 1 μm film thickness, J&W Scientific, Agilent Technologies). Oven temperature was programmed from 40 to 220 °C (held for 2 min) at 10 °C min⁻¹. Helium was used as the carrier gas at a flow rate of 1.0 mL min⁻¹. The mass spectrometer was operated in the selected ion-monitoring (SIM) mode with electron ionization (ionization voltage: 70 eV). SIM monitoring ions are shown in Table 1.

2.4. Sample preparation

Ten millilitres of tap water or river water was pipetted into a 20-mL headspace vial. A PDMS stir bar, 2 M sodium acetate buffer (pH 5, 200 μL) for pH adjustment, and NaBEt₄ as the derivatization reagent were added and the vial was crimped with a Teflon-coated silicone septum cap. SBSE with in situ derivatization was performed at room temperature for 15 min while stirring at 1000 rpm. After the extraction, the stir bar was easily removed with forceps (due to magnetic attraction), rinsed with purified water, dried with lint-free issue, and placed inside a glass TD tube. The TD tube was then placed in the TD system where the stir bar was subjected to TD–GC–MS.

3. Results and discussion

3.1. Optimization of GC–MS conditions

Stir bar sorptive extraction with in situ derivatization followed by GC–MS analysis of the standard solutions of MeHg and Hg(II) in the scan mode was performed by EI–MS. The mass spectra of the derivatives of MeHg and Hg(II) are shown in Fig. 1. As shown in Fig. 1, isotopic ions of mercury were observed. As for mercury, the maximum isotopic abundance (approx. 29.86%) is ²⁰²Hg, following to ²⁰⁰Hg (approx. 23.1%).

For SIM, the following ions were monitored: *m/z* 246, 217 for the derivative of MeHg, and *m/z* 260, 231 for the derivative of Hg(II). The underlined number is the *m/z* of the ion used for quantification.

3.2. Optimization of derivatization conditions

One important parameter affecting SBSE with in situ derivatization was the volume of the derivatization reagent. In this regard, optimization of the volume of 0.5% NaBEt₄ solution was performed using 0.5 μg L⁻¹ standard solutions of MeHg and Hg(II). The derivatives of MeHg and Hg(II) in 10 mL of respective standard solutions, which were obtained by SBSE with in situ derivatization, were subjected to TD–GC–MS, and the results are shown in Fig. 2. When the volume of 0.5% NaBEt₄ solution was 10 μL, the derivatives of MeHg and Hg(II) in 10 mL of the respective standard solutions after SBSE with in situ derivatization gave a maximum response. Therefore, 10 μL was considered to be the optimal volume of 0.5% NaBEt₄ solution added.

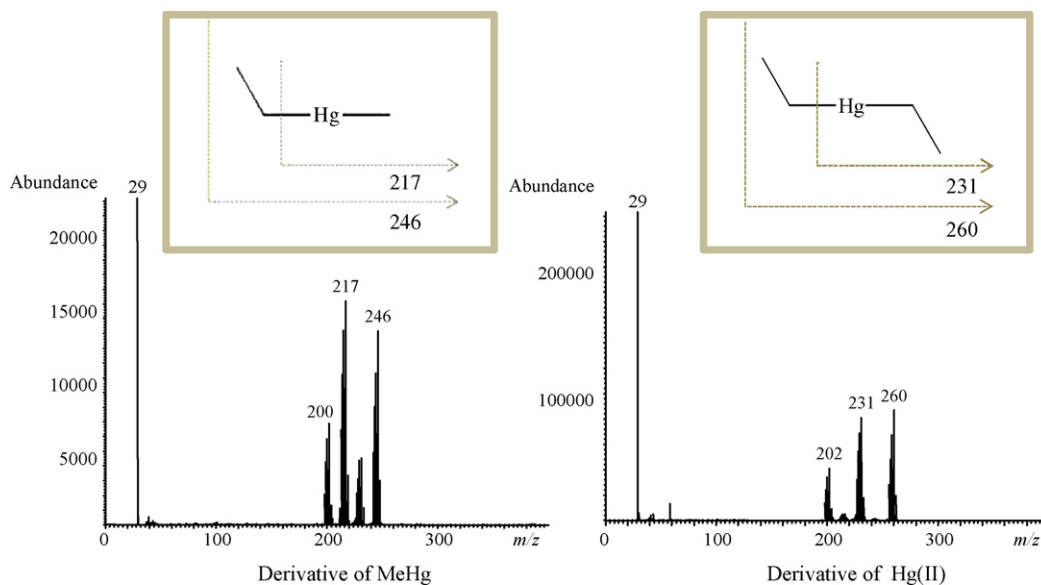


Fig. 1. Mass spectra of derivative of MeHg and Hg(II).

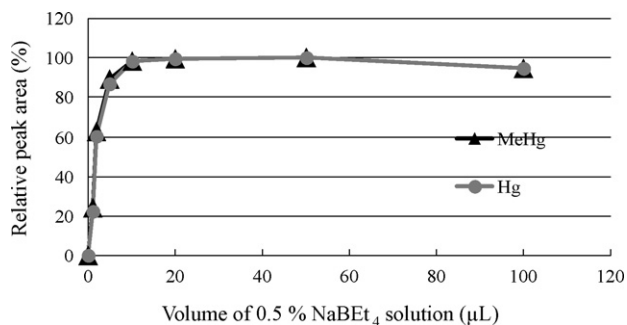


Fig. 2. Optimization of derivatization reagent.

3.3. Optimization of SBSE conditions

One important parameter affecting SBSE with in situ derivatization was the extraction time. To optimize the extraction time, $0.5 \mu\text{g L}^{-1}$ standard solutions of MeHg and Hg(II) were used. The extraction time profiles (0–90 min) of MeHg and Hg(II) in 10 mL standard solutions that were subjected to SBSE with in situ derivatization were determined by TD–GC–MS, and are shown in Fig. 3. The derivatives of MeHg and Hg(II) reached equilibrium after approximately 15 min. Therefore, this condition was used for the determination of MeHg in water samples.

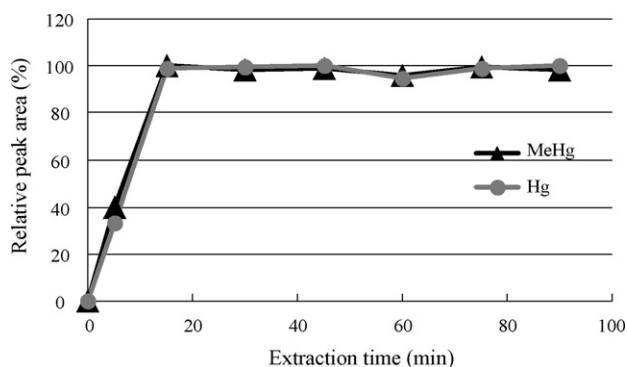


Fig. 3. Optimization of extraction time.

The extraction times of the HS–SBSE method [13] and the present method were 2 h and 15 min, respectively. Clearly, the present method successfully shortened the extraction time.

3.4. Figures of merit of SBSE with in situ derivatization and TD–GC–MS for determination of MeHg

The calculated limits of detection (LOD) of the derivatives of MeHg and Hg(II) were 5 and 2 ng L^{-1} (Hg), respectively, for SBSE with in situ derivatization and TD–GC–MS, with the signal to noise (S/N) ratio being 3. In addition, the limits of quantification (LOQ) of the derivatives of MeHg and Hg(II) when $S/N > 10$ were 20 and 10 ng L^{-1} (Hg), respectively. The method showed good linearity over the calibration range (0.02 – 5 or 0.01 – $5 \mu\text{g L}^{-1}$) and the correlation coefficient (r) was higher than 0.999 for all the analytes. The results are summarized in Table 1. The sensitivity of the present method was approximately the same as that of the HS–SBSE method [19]. Mishra et al. obtained lower LOD in water samples for MeHg but using HS–SPME method [8], however the sensitivity of the present method were better than those obtained by other HS–SPME method [13,14].

The recovery and precision of the method were assessed by replicate analysis ($n=6$) of tap and river water samples fortified

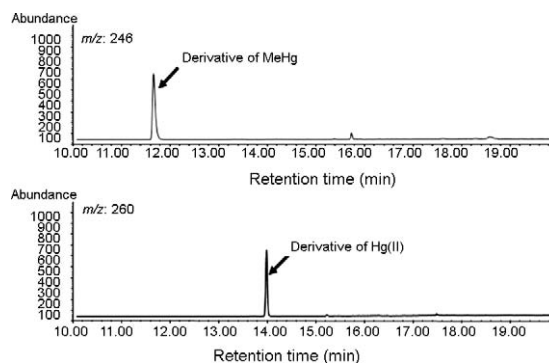


Fig. 4. Typically SIM chromatograms of derivative of MeHg and Hg in river water sample ($0.5 \mu\text{g L}^{-1}$).

at $0.5 \mu\text{g L}^{-1}$ level. The results are shown in Table 1. The average recoveries of MeHg and Hg(II) in tap or river water sample are 102.1–104.3% (R.S.D.: 7.0–8.9%) and 105.3–106.2% (R.S.D.: 7.4–8.5%), respectively. A typical SIM chromatogram of river water sample spiked with $0.5 \mu\text{g L}^{-1}$ MeHg and Hg(II) is shown in Fig. 4. Complete separation was achieved. Therefore, the method may be applicable to the determination of trace amounts of MeHg and Hg(II) in tap and river water samples.

4. Conclusions

The determination of trace amounts of MeHg and Hg(II) in tap or river water samples using SBSE with in situ derivatization and TD–GC–MS was described. The proposed method has many practical advantages, including small sample volume (10 mL) and simplicity of extraction; it is also solvent-free and has high sensitivity. The detection limits of MeHg and Hg(II) were 5 and 2 ng L^{-1} (Hg), respectively. In addition, the present method showed good linearity and high correlation coefficients. The recovery was high and the precision was good for tap and river water samples spiked at $0.5 \mu\text{g L}^{-1}$ level. This simple, accurate, and highly sensitive method is expected to have potential applications in various aqueous samples.

Acknowledgment

This study was supported by Health Sciences Research grants from the Ministry of Health, Labour and Welfare of Japan.

References

- [1] P.J. Craig, *Organometallic Compounds in the Environment: Principles and Reactions*, Longman, Harlow, 1986.
- [2] EPA, National primary drinking water regulations, 2002, 40 CFR Ch.I (7-1-02 Edition): website: <http://www.access.gpo.gov/nara/cfr/waisidx.02/40cfr141.02.html>.
- [3] WHO, WHO Guidelines for drinking water quality, 2005, WHO/SDE/WSH/05.08/10: website: http://www.who.int/water_sanitation_health/dwq/chemicals/mercuryfinal.pdf.
- [4] The Ministry of Health, Labour and Welfare of Japan, 2007, website: <http://www.mhlw.go.jp/topics/bukyoku/kenkou/suido/kijun/dl/k05.pdf> (in Japanese).
- [5] C. Devos, M. Vliegen, B. Willaert, F. David, L. Moens, P. Sandra, J. Chromatogr. A 1079 (2005) 408.
- [6] L. Carrasco, S. Diez, J.M. Bayona, J. Chromatogr. A 1174 (2007) 2.
- [7] A. Delgado, A. Prieto, O. Zuloaga, A. de Diego, J.M. Madariaga, Anal. Chim. Acta 582 (2007) 109.
- [8] S. Mishra, R.M. Tripathi, S. Bhalke, V.K. Shukla, V.D. Puranik, Anal. Chim. Acta 551 (2005) 192.
- [9] V. Kaur, A. Kumar, N. Verma, J. Sep. Sci. 29 (2006) 333.
- [10] C.L. Arthur, J. Pawliszyn, Anal. Chem. 62 (1990) 2145.
- [11] G. Centineo, E. Blanco-González, A. Sanz-Medel, J. Chromatogr. A 1034 (2004) 191.
- [12] Z. Mester, J. Lam, R. Sturgeon, J. Pawliszyn, J. Anal. At. Spectrom. 15 (2000) 837.
- [13] J. Carpinteiro-Botana, R. Rodil-Rodríguez, A.M. Carro-Díaz, R.A. Lorenzo-Ferreira, R. Cela-Torrijos, I. Rodríguez-Pereiro, J. Anal. At. Spectrom. 17 (2002) 904.
- [14] E. Millan, J. Pawliszyn, J. Chromatogr. A 873 (2000) 63.
- [15] E. Baltussen, P. Sandra, F. David, C. Cramers, J. Microcolumn Sep. 11 (1999) 737.
- [16] E. Baltussen, C.A. Gramers, P. Sandra, Anal. Bioanal. Chem. 373 (2002) 3.
- [17] M. Kawaguchi, R. Ito, K. Saito, H. Nakazawa, J. Pharm. Biomed. Anal. 40 (2006) 500.
- [18] F. David, P. Sandra, J. Chromatogr. A 1152 (2007) 54.
- [19] A. Prieto, O. Zuloaga, A. Usobiaga, N. Etxebarria, L.A. Fernández, C. Marcic, A. de Diego, J. Chromatogr. A 1185 (2008) 130.



HPLC–electrospray tandem mass spectrometry for simultaneous quantitation of eight plasma amino thiols: Application to studies of diabetic nephropathy

Zhiting Jiang^{a,b}, Qionglin Liang^b, Guoan Luo^{a,b,*}, Ping Hu^c, Ping Li^d, Yiming Wang^b

^a School of Pharmacy, East-China University of Science & Technology, Shanghai, PR China

^b Key Laboratory of Bioorganic Phosphorus Chemistry & Chemical Biology, Department of Chemistry, Tsinghua University, Beijing, PR China

^c College of Chemical and Molecular Engineering, East-China University of Science & Technology, Shanghai, PR China

^d Clinical Medicinal Research Institute, Chinese-Japanese Friendship Hospital, Beijing, PR China

ARTICLE INFO

Article history:

Received 1 July 2008

Received in revised form 27 August 2008

Accepted 30 August 2008

Available online 7 September 2008

Keywords:

Amino thiol

HPLC–ESI–MS/MS

Diabetic nephropathy

ABSTRACT

It was reported that Hcy was related to the development of kidney disease, but it remains unknown whether Hcy is an independent biomarker for diabetic nephropathy. Analytical method for simultaneous determination of amino thiols among the Hcy metabolic cycle is desirable to discover other potential biomarkers. A high-performance liquid chromatography–electrospray tandem mass spectrometric (HPLC–ESI–MS/MS) method was established for simultaneous quantitation of Cysteine (Cys), total homocysteine (tHcy), S-adenosylmethionine (SAM), S-adenosylhomocysteine (SAH), cystathionine (Cysta), methionine (Met), glutathione (GSH) and cysteinylglycine (Cys-gly) in plasma with N-(2-mercaptopropionyl)-glycine (MPG) as internal standard. The method had simple pretreatment without derivatization and the chromatograms show better separation of the eight amino thiols and the analytic time was 20 min. The results demonstrated that it provided an excellent linearity for all analytes over their respective concentration ranges and illustrated excellent precision and plasma recovery as well. Then, the method was applied in the case–control study of patients with diabetes mellitus (DM) and diabetic nephropathy (DN). In conclusion, it is an effective method to quantitate the concentrations of amino thiols in the human plasma. SAH and SAM were suggested as better potential biomarkers of DM and DN.

© 2008 Elsevier B.V. All rights reserved.

1. Introduction

Diabetes is a complex multisystem disease characterized by defects in insulin action and secretion, resulting in disturbances in the metabolism of amino acids, fatty acids and proteins. The incidence of diabetes increased exponentially and resulted in an epidemic prevalence worldwide during the last two decades. In 2007, the world is estimated to spend at least US\$ 232 billion to prevent and treat diabetes and its complications. By 2025, this lower bound estimate will exceed US\$ 302.5 billion [1]. In times when acute metabolic derangements and infections are no longer the main causes of morbidity and mortality in diabetes, diabetic nephropathy becomes a major cause of end-stage renal disease in diabetic patients. The costs society pays for diabetes care are

mainly related to chronic complications of the disease, such as nephropathy and cardiovascular diseases. As a result of the large preponderance of Type 2 and Type 1 diabetes, the most efficient way to reduce these costs is to promote increased awareness, and implement early detection and aggressive treatment of the accelerated chronic complications of Type 2 diabetes [2].

Endogenous low-molecular weight thiol-containing amino acids play essential roles in a variety of physiological and pathological processes. Increased total plasma homocysteine has been identified as an important risk factor for cardiovascular diseases [3] and it is also associated with the development of nephropathy [4,5]. Homocysteine is either irreversibly catabolized by transsulfuration to cysteine or remethylated to methionine. Despite the recent study by Mann Johannes et al. [6] demonstrated that the development of renal insufficiency was dependent of the plasma tHcy concentration, it remains unknown whether tHcy is an important and independent biomarker in nephropathy or not. Therefore, more attention should be paid to other metabolic intermediates of homocysteine and methionine.

* Corresponding author at: Department of Chemistry, Tsinghua University, Beijing 100084, PR China. Tel.: +86 10 62781688; fax: +86 10 62781688.

E-mail address: luoga@mail.tsinghua.edu.cn (G. Luo).

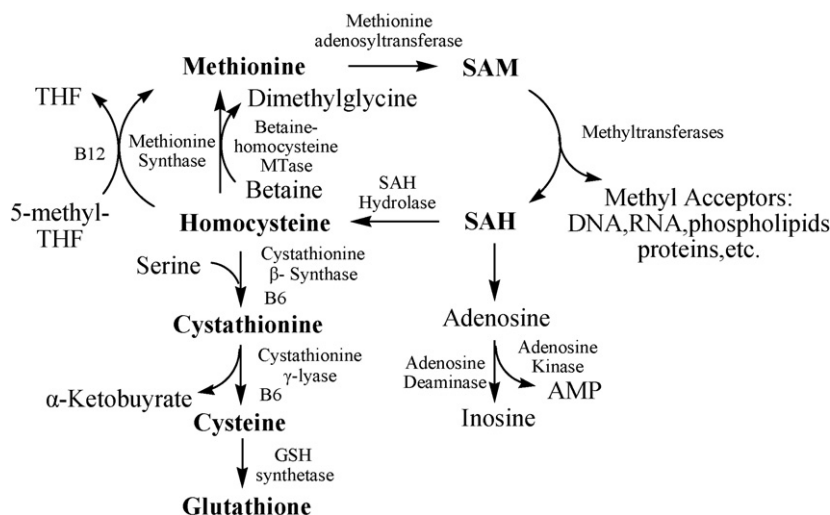


Fig. 1. Aminothiols metabolic pathway with enzymes and vitamins involved.

Under the action of the methionine transferase (MS), Methionine can be regenerated by the remethylation pathway, which is also dependent of the methylenetetrahydrofolate (MTHF) and the cofactor vitamin B12 (Fig. 1). S-Adenosylmethionine (SAM) can be converted to S-Adenosylhomocysteine (SAH) concomitantly by the action of methyltransferases (MT). Because SAH acts as a product inhibitor of MT, the ratio of SAM to SAH is crucial for regulation of methylation. Meanwhile, methylation is essential for a lot of cellular processes, such as epigenetic control of gene expression [7] and regulation of protein function [8]. Cysteine is a non-essential amino acid and is found as the component of most proteins, which is unstable and easily converts into cystine. Otherwise, it is recognized that glutathione provides protection against endogenous oxygen radicals and it is an essential water-phase antioxidant and cofactor for antioxidant enzymes. The data available in other literatures failed to illustrate the interaction and relationship between these aminothiols in physiological and pathological processes, because most reports only pay attention on limited components.

Previous methods reported for the measurement of aminothiols in biological samples mainly include GC–MS [9–11], HPLC with photometric detection [12], fluorescence detection [13–15] or electrochemical detection [16,17], ion-exchange chromatography [18], capillary electrophoresis [19,20] and immunoassays [21]. Each of these methods had basic limitations in terms of cost, complexity of sample pretreatment and/or number of aminothiols simultaneously detected. Most methods depend on derivatization because of lack of the structural features suitable for use of conventional detectors. There is no doubt that derivatization is time-consuming and always has many by-products. Analytical method with simple pretreatment for simultaneous detection and quantitation of these aminothiols is desirable. With the development of tandem

mass spectrometry, HPLC–MS/MS are widely used in the laboratories all over the world. It offers unique advantage in the assay of compounds with chemical instability, high polarity and lack of chromophore. Until now there is no report of simultaneous quantification of Cys, tHcy, SAH, SAM, Cysta, Met, GSH and Cys-gly in human plasma published. The method established using LC–MS/MS can be applied to a study of the pathological mechanism and find potential biomarkers of diabetes and diabetic nephropathy.

2. Experimental

2.1. Reagents and materials

Cysteine (Cys), homocysteine (Hcy), SAM, SAH, cystathionine (Cysta), methionine (Met), glutathione (GSH), cysteinylglycine (Cys-gly), *N*-(2-mercaptopropionyl)-glycine (internal standard, MPG) and dithiothreitol (DTT) standards were purchased from Sigma–Aldrich (St. Louis, MO, USA). The HPLC-grade ammonium formate and formic acid were obtained from Merck (Darmstadt, Germany). The HPLC-grade methanol and the HPLC-MS-grade acetonitrile were purchased from J.T. Baker (Philipsburg, USA). Ultrapure water ($18.2 \text{ M}\Omega \text{ cm}^{-1}$ resistivity) was prepared with a Milli-Q water purification system (Millipore, France). All chemicals were HPLC grade or of the highest purity available.

2.2. Equipment and chromatographic–MS conditions

The concentrations of eight thiol amino acids and an internal standard in plasma were quantified using an HP1100 HPLC system (Agilent Technologies, Palo Alto, CA, USA) and a PE SCIEX API 3000

Table 1
Compound-dependent MS parameters for each analyte.

Compound	MRM transition	DP (V)	FP (V)	EP (V)	CE (V)	CXP (V)
Cys-gly	179.2 → 76.0	24	130	6	22	13
SAH	385.2 → 136.2	35	138	7.5	23.5	15
SAM	399.3 → 250.2	40	160	8.5	22	15
Hcy	136.1 → 90.0	27	125	5.5	16.5	16
Cysta	223.2 → 134.2	33	140	5	20	14
Met	150.0 → 104.0	24	120	5	15	18.5
GSH	308.2 → 179.2	37	160	10	18	10
Cys	122.0 → 76.0	25	135	7	18	13
MPG	164.2 → 76.2	26	130	9	14	13

triple–quadrupole mass spectrometer (PerkinElmer Sciex, Canada) equipped with an electrospray ionization interface used to generate positive ions $[M+H]^+$.

The compounds were separated on a reversed-phase UltimateTM AQ-C18 column (250 mm \times 4.6 mm, 5 μ m particles, Welch Materials, Maryland, USA) connected to an Alltech guard column (7.5 mm \times 4.6 mm, 5 μ m particles) at 30 °C. The two mobile phases consist of (A) 5 mM ammonium formate and 0.15% (v/v) formic acid aqueous solution (pH 2.8) and (B) acetonitrile containing 0.15% (v/v) formic acid. Amino thiols were eluted by a linear gradient over 20 min with 100% A to 80% A at a flow rate of 0.5 mL/min. Approximately, 0.1 mL/min of the effluent was introduced into the interface of the mass spectrometer by a valved three-way split. The turbo ion spray interface was operated in positive ion mode at 5300 V and 350 °C. The operating conditions were optimized by flow injection of a mixture of all analytes as follows: nebulizer gas flow, 8.0 L/min; curtain gas flow, 8.0 L/min; collision gas flow, 6.0 L/min.

In the API3000 system, 5 μ g/mL amino thiols and the internal standard (IS) were respectively, infused into the mass spectrometer to characterize the product ions at a flow rate of 10 μ L/min. These amino thiols were quantified by multiple reaction monitoring (MRM) of the protonated precursor ion and the related product ion using the internal standard method with peak area ratios. The mass transition and parameters for each compound were listed in Table 1. Quadrupoles Q1 and Q3 were set on unit resolution and the analytical data were processed using Analyst software (Applied Biosystems, Foster City, CA, USA) in the API3000 LC–MS/MS system.

2.3. Standards preparation

Each of the analytes was dissolved in methanol–water (50:50, v/v) and IS was dissolved in methanol, all of which were 100 μ g/mL and stored at –20 °C. The standard solutions were serially diluted with mobile phase A (5 mM ammonium formate and 0.15% formic acid aqueous solution) containing 100 μ g/mL DTT to inhibit oxidation. The concentrations of standard working solutions obtained were 0.2, 0.4, 0.8, 1.2, 2, 4, 8 and 16 μ g/mL for Cys-gly and Hcy, 2, 4, 8, 20, 40, 80, 160 and 320 ng/mL for SAH, 4, 8, 16, 24, 40, 80, 160 and 320 ng/mL for SAM, 1, 2, 4, 8, 12, 20, 40 and 80 ng/mL for Cysta, 0.4, 0.8, 1.2, 2, 4, 8, 10 and 16 μ g/mL for Met, 0.1, 0.2, 0.4, 0.6, 1, 2, 4 and 8 μ g/mL for GSH and 1.2, 2, 4, 8, 10, 16, 20 and 32 μ g/mL for Cys.

2.4. Sample and QC preparation

MPG internal standard working stock solution (25 μ g/mL) was prepared and then added 50 μ L into 200 μ L plasma samples, briefly vortex-mixed. Following addition of 100 μ L DTT (15 mg/mL) and 600 μ L methanol, vortex-mixed for 3 min, and then centrifuged at 10000 rpm at 4 °C for 15 min. DTT was used to broke the disulfide bond and stabilize the Hcy monomers, so it is tHcy that was detected in the plasma samples. The supernatant was transferred into a 1.5-mL polypropylene tube and evaporated under gentle stream of nitrogen at room temperature. Before analysis, the residue was reconstituted into 100 μ L of mobile phase A containing 10 μ g/mL DTT by vortex-mixing for 1 min. Finally, 20 μ L of the solution were injected into the column.

Quality control samples were prepared in 200 μ L of blank human plasma by adding 100 μ L of standard solution. Samples were prepared for low, intermediate, and high concentration to evaluate the intra- and inter-day precision and accuracy of the assay method. The treatment of QC was as same as the samples described above.

2.5. Calibration and linearity

Calibration curves were constructed of eight standard concentrations (described in Section 2.3.) of the amino thiols (Cys-gly, SAH, SAM, Hcy, Cysta, Met, GSH and Cys) and analyzed for three runs. For each curve, the absolute peak area ratios of the amino thiol to the IS were calculated and plotted against the nominal amino thiol concentration. The concentrations of each analyte were determined using the equations of linear regression obtained from the calibration curves.

2.6. Method validation

Precision and accuracy were determined by the analysis of QC samples spiked with three concentrations listed in Table 2. Six replicate QC samples at each concentration were evaluated on the same day for intra-day precision, while repeated analysis of medium concentration of QC samples twice per day over three consecutive days for inter-day precision ($n = 6$). The precision of the intra- and inter-day assay validation was estimated using the inverse prediction of the concentration of the quality controls from the calibration curve. Standard deviations and relative standard deviations (% R.S.D.) were calculated from the QC values and used to estimate the inter- and intra-day precision.

The recovery was estimated by analyzing healthy subjects plasma spiked at three concentrations of QC samples and unspiked plasma samples, which can be determined by comparing the nominal amino thiol concentration, calculated as the sum of the concentrations in unspiked plasma and the spiked QC concentration, to their measured concentrations. Measured concentrations were defined as 100%. Means, standard deviations and relative standard deviations were calculated.

The stability of amino thiols for 0, 2, 4, 8, 16 and 24 h at –20 °C in plasma was determined by repeated analysis of the medium concentration QC samples.

2.7. Clinical application

The patients were diagnosed according to the standard of Mogenson [22]. Here, we collected blood of healthy subjects (control, $n = 30$), patients with DM ($n = 20$) and DN ($n = 30$). The blood samples centrifuged to obtain plasma in the hospital and then sent to our laboratory. All the plasma samples were stored at –80 °C until analyzed. The plasma concentrations of all amino thiols were quantified as described above.

A Student's unpaired t -test was performed to assess mean differences between plasma amino thiols concentrations of controls, DM and DN using Excel (version 2003 for Windows XP, Microsoft Office Software). Statistical significance was set at $P < 0.05$.

3. Results and discussion

3.1. Optimization of chromatography conditions

The study of amino thiols separation gives rise to three main difficulties: firstly, they are all high polarity compounds; secondly, most of them are lack of chromophore; lastly, they are unstable. The hydrophilic column was chosen over standard reverse-phase columns due to the better ion-exchange properties, which can help overcoming the minimal retention of amino thiols in reversed-phase HPLC. Prolonged retention on the column is particularly beneficial in analysis of plasma samples in order to avoid co-elution with early eluting endogenous compounds that produce ion suppression. In the research, we evaluated three hydrophilic chromatography columns, including Alltima

Table 2
Precisions and recoveries.

Compound	spiked concentration (ng/mL)	Intra-day (n=6)		Inter-day (n=6) R.S.D. (%)
		Recovery (%)	R.S.D. (%)	
Cys-gly	400	92.56	1.20	6.73
	1,200	90.52	6.04	
	4,000	87.20	9.26	
SAH	4	87.24	7.06	3.82
	40	95.26	1.40	
	160	90.54	5.55	
SAM	8	85.54	4.80	6.91
	24	92.36	6.10	
	80	85.56	9.87	
Hcy	400	88.80	2.60	8.34
	1,200	89.48	7.50	
	4,000	88.82	1.71	
Cysta	4	95.67	4.45	6.07
	12	98.90	4.93	
	40	87.14	5.44	
Met	400	99.09	5.24	6.78
	1,200	104.23	3.25	
	4,000	103.94	3.80	
GSH	200	82.72	2.23	6.44
	600	94.34	6.10	
	2,000	109.71	3.71	
Cys	4,000	86.21	2.40	8.31
	8,000	85.10	7.64	
	16,000	86.25	4.87	

HP HILIC (250 mm × 4.6 mm, 5 μm particles, Alltech Associates, Deerfield, IL, USA), Ultimate AQ-C18 (150 mm × 2.1 mm, 5 μm particles, Welch Materials, Maryland, USA) and Ultimate AQ-C18 (250 mm × 4.6 mm, 5 μm particles, Welch Materials, Maryland, USA). The latter is the most suitable for separate aminothiols we interested. Representative chromatograms of eight aminothiols with IS in the plasma from healthy subjects are shown in Fig. 2. The retention times for Cysta, Cys, Cys-gly, Hcy, SAM, Met, GSH, SAH, and IS were approximately 6.5, 6.9, 8.1, 8.2, 8.7, 12.4, 13.2, 15.6 and 18.5 min, respectively. Most analytes can be completely separated besides Cys-gly and Hcy. Then, 1-μg/mL Hcy standard solution was detected using this method and there were no ion intensities available for Cys-gly. Similarly, 1-μg/mL Cys-gly standard solution was also detected. The results illustrated that the interference between Hcy and Cys-gly was less than 1%. The different precursor ion and product ion were chosen for Cys-gly and Hcy under MRM mode, resulting there is little interference and effect with each other.

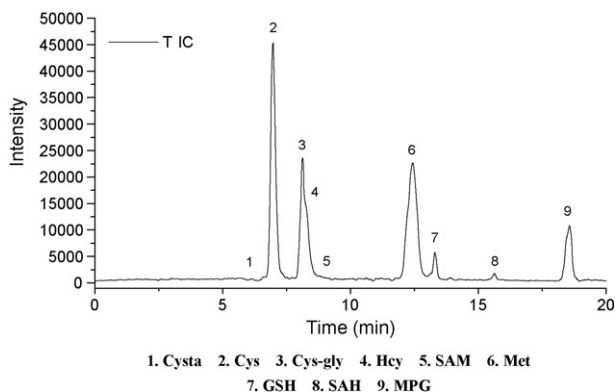


Fig. 2. Total ion chromatogram (TIC) of eight aminothiols and internal standard in plasma: (1) Cysta; (2) Cys; (3) Cys-gly; (4) Hcy; (5) SAM; (6) Met; (7) GSH; (8) SAH; (9) MPG.

The separate of these aminothiols is sensitive to pH value of the mobile phase. The ion intensities are inverse ratio to the pH value, but the use of such acid solution should obtain the pH compatible with the column specifications. After investigating the combination and concentration of formic acid and ammonium formate, 0.15% (v/v) formic acid aqueous solution with 5 mM ammonium formate (mobile phase A) was proved to be the best condition. Addition of 0.15% formic acid to both the mobile phase resulted in greater retention on the column due to ion pairing interaction and without having any effect on ion suppression.

Several reports dealing with the quantitation of endogenous compounds had no internal standard and only relied on linearity of signal versus concentration [23,24], which were no doubt decreasing the accuracy. Cysteamine, *N*-acetylcysteine and *N*-(2-mercaptopropionyl)-glycine are widely used as internal standard of homocysteine and other aminothiols. We found the latter had the most suitable retention time in our chromatography condition, so *N*-(2-mercaptopropionyl)-glycine was chose to increase the precision of analytical method, which is structural analogue of the analytes and has the same efficiency of ESI ionization as the analytes [25].

3.2. Optimization of mass spectrometry conditions

Both positive and negative ion modes were optimized, respectively. We found that most of the aminothiols have provided better sensitivity and lower limit of quantification under positive ion mode. The expected $[M+H]^+$ protonated molecules for Cysta, Cys, Cys-gly, Hcy, SAM, Met, GSH, SAH, and IS observed in the experiment matched the theoretical masses. Optimal MRM transitions were determined as follows: Cysta, 223.2 → 134.2 ($[M+H]^+ - C_3H_7NO_2$); Cys, 122.0 → 76.0 ($[M+H]^+ - HCO_2H$); Cys-gly, 179.2 → 76.0 (glycine); Hcy, 136.1 → 90.0 ($[M+H]^+ - HCO_2H$); SAM, 399.3 → 250.2 (adenosine); Met, 150.0 → 104.0 ($[M+H]^+ - HCO_2H$);

Table 3
Quantification results of control–case study of DM and DN ($P\%=95$).

Compound	Concentration (mean \pm $t \times s/\sqrt{n}$)		
	Control ($n=30$)	DM ($n=20$)	DN ($n=30$)
Cys-gly ($\mu\text{mol/L}$)	8.25 \pm 0.54	6.97 \pm 0.95 ^a	5.56 \pm 0.72 ^a
SAH (nmol/L)	11.04 \pm 1.87	16.25 \pm 3.02 ^a	42.11 \pm 2.75 ^{a,b}
SAM (nmol/L)	29.48 \pm 2.19	35.77 \pm 4.45 ^a	51.41 \pm 6.16 ^{a,b}
Hcy ($\mu\text{mol/L}$)	4.95 \pm 0.60	6.07 \pm 1.20	8.54 \pm 1.03 ^a
Cysta ($\mu\text{mol/L}$)	21.23 \pm 3.51	27.69 \pm 4.93	31.00 \pm 3.20
Met ($\mu\text{mol/L}$)	21.50 \pm 1.87	19.07 \pm 2.67	17.63 \pm 1.34 ^a
GSH ($\mu\text{mol/L}$)	2.94 \pm 0.31	2.46 \pm 0.31	2.16 \pm 0.28 ^a
Cys ($\mu\text{mol/L}$)	72.32 \pm 5.68	89.67 \pm 15.94 ^a	102.98 \pm 13.21 ^a
SAM/SAH	3.75 \pm 0.85	2.59 \pm 0.60	1.28 \pm 0.21 ^{a,b}

^a Compare with control, $P < 0.05$ (Student's unpaired t -test).

^b Compare with DM, $P < 0.05$.

GSH, 308.2 \rightarrow 179.2 (cys-gly); SAH, 385.2 \rightarrow 136.2 (adenine); MPG, 164.2 \rightarrow 76.2 (glycine). They were chosen for quantitation because all the product ions were the most abundant ion. The factors, such as retention times, separations, ion intensities were taken into account and the optimal chromatographic conditions were determined as described in Section 2.2.

3.3. Calibration curves

The linear regression analysis was constructed by plotting the analyte/IS peak-area ratio versus analyte concentration (ng/mL). The range of concentrations was found to be suitable for the analysis of clinical samples. The regression equation of these curves and their correlation coefficients (r^2) were calculated as follows: Cys-gly, $y = 8.12 \times 10^{-4}x - 4.54 \times 10^{-2}$, $r^2 = 0.999$; SAH, $y = 1.22 \times 10^{-3}x + 7.45 \times 10^{-3}$, $r^2 = 0.999$; SAM, $y = 2.62 \times 10^{-3}x - 1.48 \times 10^{-2}$, $r^2 = 0.997$; Hcy, $y = 8.40 \times 10^{-4}x - 7.25 \times 10^{-2}$, $r^2 = 0.997$; Cysta, $y = 1.09 \times 10^{-3}x - 6.65 \times 10^{-4}$, $r^2 = 0.999$; Met, $y = 1.10 \times 10^{-3}x - 1.71 \times 10^{-1}$, $r^2 = 0.999$; GSH, $y = 7.20 \times 10^{-4}x - 2.31 \times 10^{-2}$, $r^2 = 0.999$ and Cys, $y = 1.63 \times 10^{-4}x - 1.20 \times 10^{-2}$, $r^2 = 0.997$. The error for back-calculated concentration of each calibration point was within 10%.

3.4. Limits of detection

Signals three times higher than the peak noise height were regarded as the limit of detection (LOD). The LOD were 0.1 ng/mL for Cys, 0.25 ng/mL for SAH, SAM and Cysta, 0.5 ng/mL for Cys-gly and Met, 1 ng/mL for Hcy and GSH, respectively.

3.5. Precision, extraction recovery and stability

The data from QC samples were calculated to estimate the intra-day precision, inter-day precision, extraction recoveries and stabilities. The results are listed in Table 2.

The QC samples were stored at -20°C and detected at different times over 24 h. No degradation was observed. Therefore, the results showed good stability of these analytes during treatment and storage.

3.6. Case–control study of diabetic nephropathy (DN)

Table 3 summarizes the results of eight amino thiols measured in the controls, patients with DM or DN groups. Concentrations of SAH and SAM showed clear increase in relation to the development of renal function. Increase of plasma concentrations of Cys, tHcy as well as decrease of Cys-gly, Met, and GSH were very common in DN patients. There was no significant change of the plasma Cysta concentration.

The main reason why plasma tHcy in patients with renal failure increased remarkably is that the diminished renal clearance of the plasma. When the plasma is not filtered, the parenchymal cells of kidney do not take up and metabolize the plasma tHcy. According to the Hcy metabolic cycle, Met should be regenerated from Hcy by the remethylation pathway using new methyl groups in the folate coenzyme system, such as N^5 -methyl-THF, or using preformed methyl groups [26]. Met plasma concentration was decreased, while the tHcy concentration was increased in the patients of our study. It is presumed that the disturbed Hcy metabolism in the patients with diabetes or diabetic nephropathy due to the failure of regeneration from Hcy. Hence, tHcy might not be the only biomarker for the development of DN and was also related with the other metabolites in the Hcy metabolic cycle.

SAH concentration was remarkably increased in the patients with DN since that the kidney was reported to be the only route for SAH removal from plasma [27]. Additionally, accumulated Hcy could result in the secondary accumulation of SAH, because of the disturbance of Met synthesis in the Hcy metabolic pathway [28]. Increased SAH concentration could inhibit cellular methyltransferase, leading to SAM accumulation [29]. However, the SAM-dependent methylations are essential for biosynthesis of a variety of cellular components including creatine, epinephrine, carnitine, phospholipids, DNA and RNA. SAM and SAH concentrations in plasma had significant difference between control and DM, as well as between DM and DN group in the experiment. However, tHcy had just conspicuous change between control and DN group. Therefore, SAM and SAH were suggested better potential biomarkers for early diagnosis of DM and DN than tHcy.

The ratio of SAM to SAH, also called “methylation index”, may have an important effect on methyltransferase reactions [30]. The results (Table 3) show a dramatical decrease of SAM/SAH in the patients with nephropathy. These patients were suggested to have less methylation potential in the cell. It corresponded with the hypothesis of Stabler and Allen [31], who indicated that renal failure could result in increasing SAH and decreasing the SAM/SAH ratio.

GSH is given the role in the protection against oxidative stress and detoxification of xenobiotics, and low GSH has been found in plasma from patients with kidney disease [32]. The body's capacity to function with low concentrations of Hcy and Cys is facilitated by its ability to store Cys as GSH. Kidney dysfunction is thought to be associated with disordered metabolism of Cys. GSH and its metabolite, Cys-gly can be a source of Cys to tissues via the action of γ -glutamyltranspeptidase and dipeptidases. The enzymes involved in the Cys catabolism are rapidly decreased, resulting in increasing Cys and tHcy concentrations, as well as depleting GSH and Cys-gly concentrations [33].

4. Conclusion

A few reports have shown some comparison studies among a large number of methods used for Hcy and other aminothiols measurements. It is obvious that HPLC–MS/MS becomes a reference tool since it allows simultaneous detection of several metabolites in a single chromatographic acquisition and it is able to monitor selected mass ions of a fragmented parent ion. The HPLC–ESI–MS/MS method is effective to determine nearly all the aminothiols metabolites simultaneously among the sulfur amino acid metabolic pathway, namely as Cysteine, homocysteine, S-adenosylmethionine, S-adenosylhomocysteine, cystathionine, methionine, glutathione and cysteinylglycine in plasma with N-(2-mercaptopropionyl)-glycine as internal standard. The method offers several attractive features, including increased sensitivity, high specificity, shortened run time, simple sample processing without corrosive and expensive chemicals.

Based on case–control study of aminothiols metabolites, we do not believe Hcy is an independent factor with the development of DM and DN and also associated with other metabolites in the Hcy metabolic cycle. The variability of SAH and SAM with the development of DN is more sensitive than tHcy, suggesting SAM and SAH should be better biomarkers of DM and DN.

Acknowledgements

The investigation received financial assistance from the National Basic Research Development Program of China (973 Program, Nos. 2005CB523503, 2007CB714505) and National Natural Science Foundation of China (No. 90709045).

References

- [1] M. Michael, O. Lut, M. Chantal, *Proteomics Clin. Appl.* 2 (2008) 312.
- [2] M. Michele, *Diab. Med.* 15 (Suppl. 4) (1998) S60.
- [3] O. Nygård, S.E. Vollset, H. Refsum, L. Brattström, P.M. Ueland, *J. Int. Med.* 246 (1999) 425.
- [4] N.S. Anavekar, J.J.V. McMurray, E.J. Velasquez, N. Engl. J. Med. 351 (2004) 1285.
- [5] B.A. Veldman, G. Verwoort, H. Blom, P. Smits, *Diab. Med.* 22 (2005) 301.
- [6] F.E. Mann Johannes, P. Sheridan, M.J. McQueen Matthew, C. Held, J.M.O. Arnold, G. Fodor, S. Yusuf, E.M. Lonn, *Nephrol. Dial. Transplant.* 23 (2008) 645.
- [7] S. Friso, S.W. Choi, *J. Nutr.* 132 (2002) 2382.
- [8] S.B. Vafai, J.B. Stock, *Fed. Eur. Biochem. Soc. Lett.* 518 (2002) 1.
- [9] S.W. Myung, M. Kim, H.K. Min, E.A. Yoo, K.R. Kim, *J. Chromatogr. B* 727 (1999) 1.
- [10] Y. Shinohara, H. Hasegawa, K. Tagoku, T. Hashimoto, *J. Chromatogr. B* 758 (2001) 283.
- [11] J.I. Sigit, M. Hages, K.A. Brensing, U. Frotscher, K. Pietrzik, K. von Bergmann, D. Lutjohann, *Clin. Chem. Lab. Med.* 39 (2001) 681.
- [12] A. Andersson, A. Isaksson, L. Brattstroem, B. Hultberg, *Clin. Chem.* 39 (1993) 1590.
- [13] A.R. Ivanov, I.V. Nazimov, L. Baratova, A.P. Lobazov, G.B. Popkovich, *J. Chromatogr. A* 913 (2001) 315.
- [14] M. Zhang, E.W. Gunter, C. Pfeiffer, *Clin. Chem.* 47 (2001) 966.
- [15] Y.V. Tcherkas, A.D. Denisenko, *J. Chromatogr. A* 913 (2001) 309.
- [16] R. Accinni, S. Bartesaghi, G. De Leo, C.F. Cursano, G. Achilli, A. Loaldi, C. Cellarino, O. Parodi, *J. Chromatogr. A* 896 (2000) 183.
- [17] J.B. Ubbink, *Semin. Thromb. Hemost.* 26 (2000) 233.
- [18] P.M. Ueland, H. Refsum, S.P. Stabler, M.R. Malinow, A. Andersson, R.H. Allen, *Clin. Chem.* 39 (1993) 1764.
- [19] S.H. Kang, W. Wei, E.S. Yeung, *J. Chromatogr. B* 744 (2000) 149.
- [20] A.R. Ivanov, I.V. Nazimov, L.A. Baratova, *J. Chromatogr. A* 895 (2000) 157.
- [21] H.J. Powers, S.J. Moat, *Curr. Opin. Clin. Nutr. Care.* 3 (2000) 367.
- [22] C.E. Mogenson, *The kidney in Diabetes Mellitus*, Livingstone, New York, 1989, p. 19.
- [23] Y. Wang, H.Y. Zhang, Q.L. Liang, H.H. Yang, Y.M. Wang, Q.F. Liu, P. Hu, X.Y. Zheng, X.M. Song, G. Chen, T. Zhang, J.X. Wu, G.A. Luo, *J. Chromatogr. B* 863 (2008) 94.
- [24] W.X. Wang, H.H. Zhou, H. Lin, S. Roy, T.A. Shaler, L.R. Hill, S. Norton, P. Kumar, M. Anderle, C.H. Becker, *Anal. Chem.* 75 (2003) 4818.
- [25] T.D. Nolin, M.E. McMenamin, J. Himmelfarb, *J. Chromatogr. B* 852 (2007) 554.
- [26] R.E. Billings, P.E. Noker, T.R. Tephly, *Arch. Biochem. Biophys.* 208 (1981) 108.
- [27] J.A. Duerre, C.H. Miller, G.G. Reams, *J. Biol. Chem.* 244 (1969) 107.
- [28] P. Yi, S. Melnyk, M. Pogribna, I.P. Pogribny, R.J. Hine, S.J. James, *J. Biol. Chem.* 275 (2000) 29318.
- [29] M. Ehrlich, *J. Cell. Biochem.* 88 (2003) 899.
- [30] K.A. Burren, K. Mills, A.J.N.D.E. Copp, *J. Chromatogr. B* 844 (2006) 112.
- [31] S.P. Stabler, R.H. Allen, *Clin. Chem.* 50 (2004) 365.
- [32] S.H. Jacobson, P. Moldeus, *Clin. Nephrol.* 42 (1994) 189.
- [33] J. Himmelfarb, P. Stenvinkel, T.A. Ikizler, R.M. Hakim, *Kidney Int.* 62 (2002) 1524.



Development of hydrogen peroxide biosensor based on in situ covalent immobilization of horseradish peroxidase by one-pot polysaccharide-incorporated sol–gel process

Feng Li, Wei Chen, Chenfei Tang, Shusheng Zhang*

Key Laboratory of Eco-Chemical Engineering, Ministry of Education, College of Chemistry and Molecular Engineering, Qingdao University of Science and Technology, 53 Zhengzhou Road, Qingdao 266042, PR China

ARTICLE INFO

Article history:

Received 26 June 2008

Received in revised form 31 August 2008

Accepted 3 September 2008

Available online 11 September 2008

Keywords:

Biosensor

Covalent immobilization

Sol–gel

Chitosan

Horseradish peroxidase

Hydrogen peroxide

ABSTRACT

A simple and reliable one-pot approach was established for the development of a novel hydrogen peroxide (H_2O_2) biosensor based on in situ covalent immobilization of horseradish peroxidase (HRP) into biocompatible material through polysaccharide-incorporated sol–gel process. Siloxane with epoxide ring and trimethoxy anchor groups was applied as the bifunctional cross-linker and the inorganic resource for organic–inorganic hybridization. The reactivity between amine groups and epoxy groups allowed the covalent incorporation of HRP and the functional biopolymer, chitosan (CS) into the inorganic polysiloxane network. Some experimental variables, such as mass ratio of siloxane to CS, pH of measuring solution and applied potential for detection were optimized. HRP covalently immobilized in the hybrid matrix possessed high electrocatalytic activity to H_2O_2 and provided a fast amperometric response. The linear response of the as-prepared biosensor for the determination of H_2O_2 ranged from 2.0×10^{-7} to $4.6 \times 10^{-5} \text{ mol l}^{-1}$ with a detection limit of $8.1 \times 10^{-8} \text{ mol l}^{-1}$. The apparent Michaelis–Menten constant was determined to be $45.18 \mu\text{mol l}^{-1}$. Performance of the biosensor was also evaluated with respect to possible interferences. The fabricated biosensor exhibited high reproducibility and storage stability. The ease of the one-pot covalent immobilization and the biocompatible hybrid matrix serve as a versatile platform for enzyme immobilization and biosensor fabricating.

© 2008 Elsevier B.V. All rights reserved.

1. Introduction

The determination of hydrogen peroxide (H_2O_2) is extensively studied in clinical diagnostics, chemical and pharmaceutical industry, environmental control. Amperometric biosensors based on horseradish peroxidase (HRP) have emerged as the most convenient tools for H_2O_2 determination due to the simplicity, high sensitivity and selectivity [1–5]. To improve the performance and long-term stability of the enzyme electrode, effective immobilization of HRP onto the transducer surface through suitable matrix is of great significance.

In recent years, microencapsulation of enzyme in the silica sol–gel matrix has applied as a new platform for the fabrication of biosensors. Typically, those sol–gel matrices possess physical rigidity, chemical inertness, high photochemical biodegradation and negligible swelling in aqueous and organic solutions [2,6–9]. However, silica sol–gel matrices are mainly prepared by using

tetramethoxysilane (TMOS) or tetraethoxysilane (TEOS) as precursor. The poor water solubility of such precursors usually involves enzyme immobilization in organic solvents. Therefore, development of enzyme biosensors based on biocompatible silica sol–gel matrix has attracted increasing attention recently. Despite the effects of designing new precursors with improved water solubility and biocompatibility [2,10], silica-based organic–inorganic hybrids are adopted as attractive materials for biosensor fabricating [7,11].

As a biopolymer containing functional groups of $-\text{OH}$ and $-\text{NH}_2$, chitosan (CS) remains a focus of study as promising matrix for enzyme immobilization due to the unique characteristics [1,11–15]. Recently, CS-based organic–inorganic hybrid materials have been widely developed as functional biomaterials [2,11,16,17]. The formed organic–inorganic hybrid could overcome the disadvantages of pure CS materials such as unsatisfying mechanical property, swelling, and solubility in acidic conditions. For example, Wang and Zhang developed a new amperometric H_2O_2 biosensor based on sol–gel process of THEOS in the presence of CS. HRP entrapped in the hybrid matrix could retain its native biocatalytic activity and provide a fast amperometric response to H_2O_2 [2]. Despite the formation of hydrogen bonds for preparing CS-based

* Corresponding author. Fax: +86 532 84022750.

E-mail address: shushzhang@qust.edu.cn (S. Zhang).

hybrid materials, cross-linked organic–inorganic hybridization using epoxy–siloxane is proposed in the pioneering works of Liu and Shirotsaki [18–20]. In situ cross-linking of CS and the formation of hybrid using the reactivity between amine groups and epoxy groups have been revealed by a set of investigation such as ^{29}Si NMR, scanning and transmission electronic microscopy. Moreover, the hybrid membrane has been proved to possess high hydrophilicity and good cytocompatibility. Very recently, we have developed a new approach for direct preparation of porous functional matrix based on surface imprinting coating technique and such CS-incorporated sol–gel process [21,22].

In this investigation, a novel H_2O_2 biosensor was developed based on in situ covalent immobilization of HRP by one-pot polysaccharide-incorporated sol–gel process. The siloxane with epoxide ring and trimethoxy anchor groups, γ -glycidoxypolytrimethoxysiloxane (GPTMS), was applied as a bifunctional cross-linker. The reactivity between amine groups and epoxy groups offered simple and convenient methodology for covalent incorporation of CS and HRP into inorganic polysiloxane network. Such CS-incorporated sol–gel process was easily carried out in aqueous medium without the addition of any organic solvents. Due to the covalent immobilization of HRP, signal loss resulting from the leaching out of enzyme from the electrode could be avoided. The fabricated H_2O_2 biosensor showed promising performance. The preparation methodology and main characteristics were described and discussed in detail.

2. Experimental

2.1. Reagents

Horseradish peroxidase (EC 1.11.1.7, RZ > 3.0, 250 U mg^{-1}) was obtained from Boao Biotechnology Co. Ltd., China. CS with 98% deacetylation and an average molecular weight of 6×10^4 g mol^{-1} (Yuhuan Biomedical Corp., China) and GPTMS (Alfa aesar) were used in this study. All other chemicals were of analytical reagent grade and used without further purification. Hydrogen peroxide solutions were prepared freshly using a 30% H_2O_2 solution (Nanjing Chemical Reagent Factory, China), and the concentration of H_2O_2 solution was determined by titration with KMnO_4 . The 0.02 mol l^{-1} phosphate buffer solutions (PBS) at various pH values were prepared by first mixing the stock solutions of NaH_2PO_4 and Na_2HPO_4 . Then the pH was adjusted with 0.10 mol l^{-1} NaOH or H_3PO_4 . Double distilled water (DDW) was used throughout this work.

2.2. Apparatus and instrumentations

Amperometric and cyclic voltammetric experiments were performed on a CHI 832B electrochemical analyzer and electrochemical impedance spectroscopy (EIS) was performed on a CHI 660C electrochemical analyzer (Shanghai CH Instrument Company, China). A conventional three-electrode system was used with bare glass carbon electrode (GCE) or modified GCE as the working electrode, Ag/AgCl electrode (saturated with KCl) or saturated calomel electrode (SCE) as the reference electrode, and platinum wire as auxiliary electrode.

2.3. Preparation of the H_2O_2 biosensor

Prior to use, bare GCE was polished with 1.0, 0.3, 0.05 μm $\alpha\text{-Al}_2\text{O}_3$ slurry. The obtained electrode was rinsed with DDW followed by sequential sonicating in acetone, ethanol and DDW. The HRP-modified electrode was prepared by a simple casting method. Briefly, the CS stock solution (2.0 wt%) was firstly prepared by dissolving CS in 0.05 mol l^{-1} acetic acid. After stirring for 1 h, CS/HRP

solution was obtained by blending such CS solution with 5 mg ml^{-1} HRP solution at a volume ratio 2:1 (v/v). Using mass ratio of GPTMS to CS of 3:2, GPTMS was then added. The resulting gel (10 μl) was rapidly deposited onto the pre-treated GCE surface and was dried for 10 min at room temperature. Afterwards, the enzyme electrode was thoroughly immersed in 0.02 mol l^{-1} PBS (pH 7.0) to wash out the non-immobilized enzyme from the electrode surface.

2.4. Characterization of the H_2O_2 biosensor

Cyclic voltammetric experiments were carried out in quiescent solutions with the scan rate of 50 mV s^{-1} . In steady-state amperometric experiments, the potential was set at 0.05 V under magnetic stirring. All potentials were reported versus the Ag/AgCl reference electrode. EIS was performed in 1.0 mmol l^{-1} $\text{K}_3\text{Fe}(\text{CN})_6/\text{K}_4\text{Fe}(\text{CN})_6$ (1:1) mixture containing 0.1 mol l^{-1} KCl with the frequencies ranging from 10^4 to 10^{-1} Hz. Saturated calomel electrode was used as the reference electrode.

3. Results and discussion

3.1. Fabrication of the H_2O_2 biosensor

In the present investigation, in situ covalent immobilization of HRP via one-pot polysaccharide-manipulated sol–gel process was used for the fabrication of HRP/CS/GPTMS/Au biosensor. Due to the possession of epoxy group and trimethoxy anchor groups, GPTMS acted as both inorganic resource and bifunctional cross-linker. On the one hand, polysiloxane network for the organic–inorganic hybrid formed resulting from self-hydrolysis and self-condensation of GPTMS. On the other hand, the reactivity between amine groups and epoxy groups offered simple and convenient methodology for covalent incorporation of CS and HRP into the inorganic framework [18–22].

The advantages of the strategy for fabricating H_2O_2 biosensor come from the following three aspects. Firstly, the proposed strategy was simple and mild. No addition of organic solvents and other catalysts were involved in CS-manipulated sol–gel process [23,24]. It was different from the microencapsulation of enzyme using sol–gel process of TMOS or TEOS. Secondly, a versatile way for the fabrication of biosensors using covalent incorporation of the enzyme was developed. The reactivity of amine groups on the enzyme molecules appears to be universal [25–29]. The reaction between such amine groups and epoxy groups allowed in situ covalent incorporation of HRP and CS into the inorganic polysiloxane network. Thirdly, the CS/GPTMS hybrid materials have been proved to possess high hydrophilicity [20].

3.2. Effect of the mass ratio of GPTMS/CS in casting solution on the characteristics of the biosensor

In the present investigation, the electrode was modified with HRP/CS/GPTMS hybrid film. The characteristics of the deposited hybrid film could be controlled by changing the mass ratio of GPTMS to CS in casting solution. The modified electrodes prepared with different ratio of GPTMS/CS were investigated by evaluating the peak current to 15 $\mu\text{mol l}^{-1}$ H_2O_2 in the presence 1.0 mmol l^{-1} $\text{K}_4\text{Fe}(\text{CN})_6$. The concentration of all CS stock solutions was controlled at 2.0 wt%. Results were shown in Fig. 1. The mass ratios of GPTMS to CS were 1:2, 1:1, 5:4, 3:2, 7:4, 2:1 and 5:2, respectively. As shown, the molar ratios of GPTMS to CS greatly influenced the performance of the biosensor. It was found that too low GPTMS/CS ratio resulted in thin and unstable CS films. With the increase of GPTMS/CS ratio, the thickness of the hybrid films increased and the

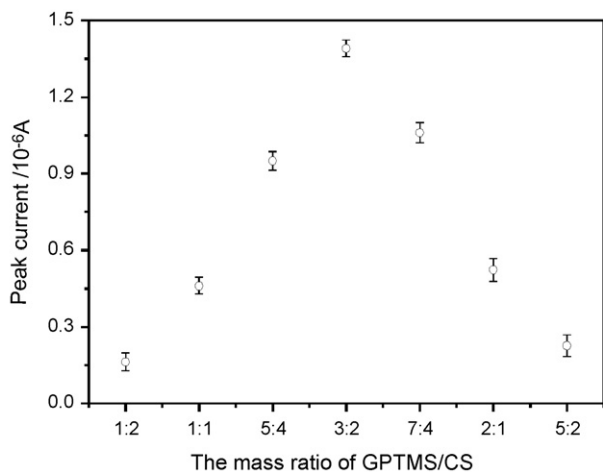


Fig. 1. Effect of the mass ratio of GPTMS/CS on the peak current of the HRP/CS/GPTMS-modified electrode to $15 \mu\text{mol l}^{-1}$ H_2O_2 in 0.02 mol l^{-1} PBS (pH 7.0) containing 1.0 mmol l^{-1} $\text{K}_4\text{Fe}(\text{CN})_6$ at the applied potential of 0.05 V versus Ag/AgCl.

attachment of the films to electrode became tight. However, too thick film by high GPTMS/CS ratio would result in large noise and slow response of biosensors [30]. To make stable biosensors with fast and large response, a mass ratio of GPTMS to CS of 3:2 was selected for further investigation.

3.3. Electrochemical characteristics of the developed H_2O_2 biosensor

The electrocatalytic behavior of HRP covalently incorporated in the hybrid material was evaluated by cyclic voltammetry. Since the proposed HRP electrode did not show direct electron transfer between immobilized HRP and GCE, $\text{K}_4\text{Fe}(\text{CN})_6$ was used as the electron mediator. Cyclic voltammograms (CVs) of the HRP/CS/GPTMS-modified electrode in 0.02 mol l^{-1} PBS (pH 7.0) were given in Fig. 2. When $40 \mu\text{mol l}^{-1}$ H_2O_2 was introduced, an obvious electrocatalytic response was observed with the increase of reduction current and the decrease of oxidation current. The response process of the biosensor may be expressed as

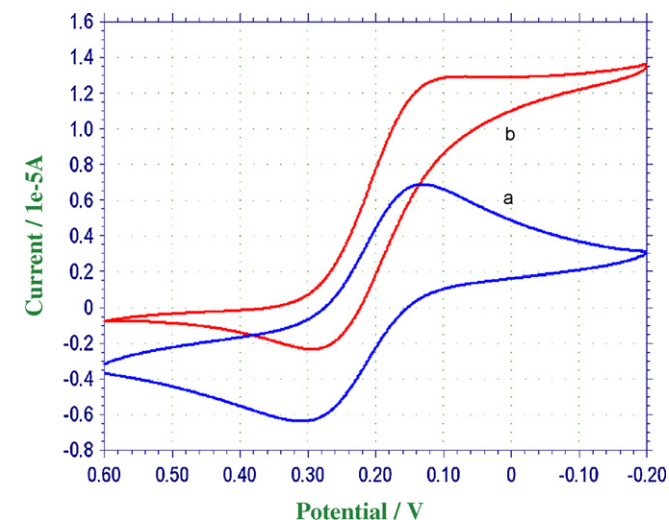


Fig. 2. CVs of the HRP/CS/GPTMS-modified electrode in 0.02 mol l^{-1} PBS (pH 7.0) containing 1.0 mmol l^{-1} $\text{K}_4\text{Fe}(\text{CN})_6$ at a scan rate of 50 mV s^{-1} (a) without H_2O_2 and (b) with $40 \mu\text{mol l}^{-1}$ H_2O_2 .

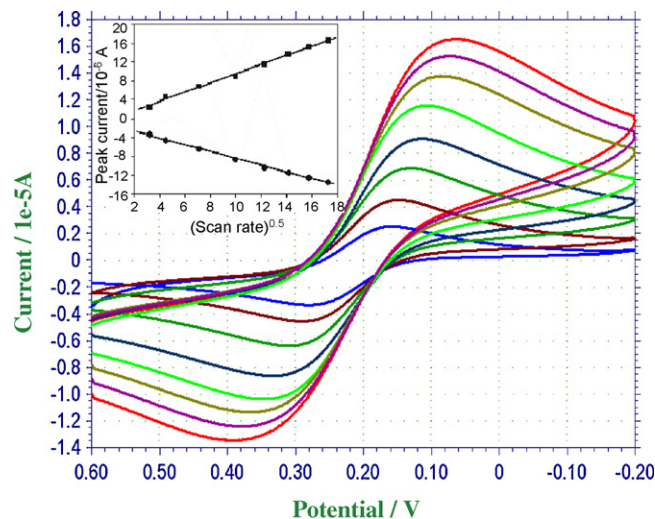
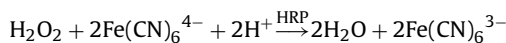


Fig. 3. Typical CVs of the HRP/CS/GPTMS-modified electrode in 0.02 mol l^{-1} PBS (pH 7.0) containing 1.0 mmol l^{-1} $\text{K}_4\text{Fe}(\text{CN})_6$ under different scan rates from 10 to 300 mV s^{-1} . Inset showed the plots of peak current versus the square root of the scan rate.

follows [31,32]:



In the presence of immobilized HRP, $\text{K}_4\text{Fe}(\text{CN})_6$ was oxidized to $\text{K}_3\text{Fe}(\text{CN})_6$ and $\text{K}_3\text{Fe}(\text{CN})_6$ was subsequently reduced at the surface of the electrode.

The CVs of the developed biosensor to various scan rates were also investigated. As shown in Fig. 3, well-characterized redox peaks were observed when scan rate ranged from 10 to 300 mV s^{-1} . In addition, it was found from inset that the peak currents were proportional to the square roots of the scan rates, which showed a typical diffusion-controlled electrochemical behavior.

EIS has been used to characterize the interface properties of the modified electrodes. Fig. 4 showed the typical results of AC impedance spectra of the bare GCE (curve a), CS/GPTMS/GCE (curve b), and HRP/CS/GPTMS/GCE (curve c). The electron transfer resistance (R_{et}) of a bare GCE was estimated to be 1172Ω . After CS/GPTMS hybrid film formed on the surface of GCE, the

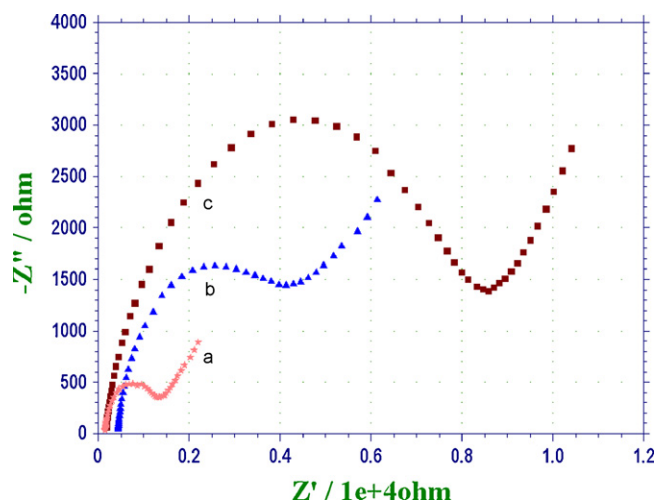


Fig. 4. EIS for (a) bare GCE, (b) CS/GPTMS/GCE, and (c) HRP/CS/GPTMS/GCE in a solution of 0.1 mol l^{-1} KCl containing 1.0 mmol l^{-1} $\text{Fe}(\text{CN})_6^{3-}$ and 1.0 mmol l^{-1} $\text{Fe}(\text{CN})_6^{4-}$ with SCE as the reference electrode.

value of R_{et} was found to be 3703Ω , implying CS/GPTMS hybrid film that obstructs the electron transfer of the electrochemical probe. When HRP was incorporated into the hybrid material, the R_{et} of HRP/CS/GPTMS/GCE electrode was calculated and equalled to 8409Ω . The increase of R_{et} resulted from the hindered pathway of electron transfer by HRP. The results demonstrated that HRP was successfully immobilized into the CS/GPTMS hybrid film.

3.4. Influence of pH and applied potential on biosensor response

The dependence of the biosensor response on pH of the measurement solution was investigated. The pH of the solution ranged from 6.0 to 8.0. The current response increased from pH 6.0 and reached the maximum at pH 7.0. Then, the current response decreased from pH 7.0 to 8.0. Therefore, the suitable pH with the maximum activity of the immobilized HRP was at pH 7.0, which was in agreement with that reported for soluble HRP [2]. The covalent immobilization of HRP and the GPTMS/CS hybrid matrix did not alter the optimal pH value for the catalytic behavior of HRP.

Further studies were performed to investigate the dependence of the biosensor response on the applied potential. Amperometric responses of the proposed biosensor to H_2O_2 at different potentials were examined. Results showed that applied potential possessed significant effect on the response of the biosensor. Little current was seen at 0.20 V, but current was highly increased at 0.10 V. The current response arrived at a maximum value at 0.05 V and a flat step was observed from -0.05 to -0.15 V. As a result, the operating potential of 0.05 V was determined to give a good sensitivity for further study.

3.5. Amperometric response of the developed H_2O_2 biosensor

Amperometric response of the HRP/CS/GPTMS/GCE electrode to successive addition of H_2O_2 in 0.02 mol l^{-1} PBS (pH 7.0) containing 1.0 mmol l^{-1} $K_4Fe(CN)_6$ was given in Fig. 5. The concentration of H_2O_2 in the solution was also indicated in Fig. 5. When H_2O_2 was added to the stirring PBS, the biosensor responded rapidly and 95% of the steady-state current could be obtained within 5 s (Fig. 5a). Such a rapid response could attribute to the fast diffusion of the substrate in the porous and open frameworks of sol–gel hybrid film. Moreover, well-defined current proportional to H_2O_2 concentration has been observed. Fig. 5b displayed calibration curve of the amperometric response of the biosensor to the concentration of H_2O_2 . Inset showed the linear part of the calibration curve. The linear range of the proposed biosensor for the determination of H_2O_2 was found to be 2.0×10^{-7} to $4.6 \times 10^{-5} \text{ mol l}^{-1}$ with a slope of $84.3 \mu\text{A ml mol}^{-1}$ and a correlation coefficient of 0.9991 ($n=26$). The detection limit of $8.1 \times 10^{-8} \text{ mol l}^{-1}$ was estimated at a signal-to-noise ratio of 3.

When H_2O_2 concentration was larger than $4.6 \times 10^{-5} \text{ mol l}^{-1}$, the current response showed a level-off tendency and the curve tended to maximum at $8.8 \times 10^{-5} \text{ mol l}^{-1}$ H_2O_2 , demonstrating the typical Michaelis–Menten kinetic characteristic of enzyme-based electrode.

The apparent Michaelis–Menten constant (K_M^{app}) can give an indication of the enzyme–substrate kinetics. It could be calculated from the electrochemical version of the Lineweaver–Burk equation [33]:

$$\frac{1}{I_{ss}} = \frac{1}{I_{max}} + \frac{K_M^{app}}{I_{max}C}$$

where I_{ss} was the steady-state response current after the addition of substrate, I_{max} was the maximum current measured under saturated substrate conditions, C referred to the bulk concen-

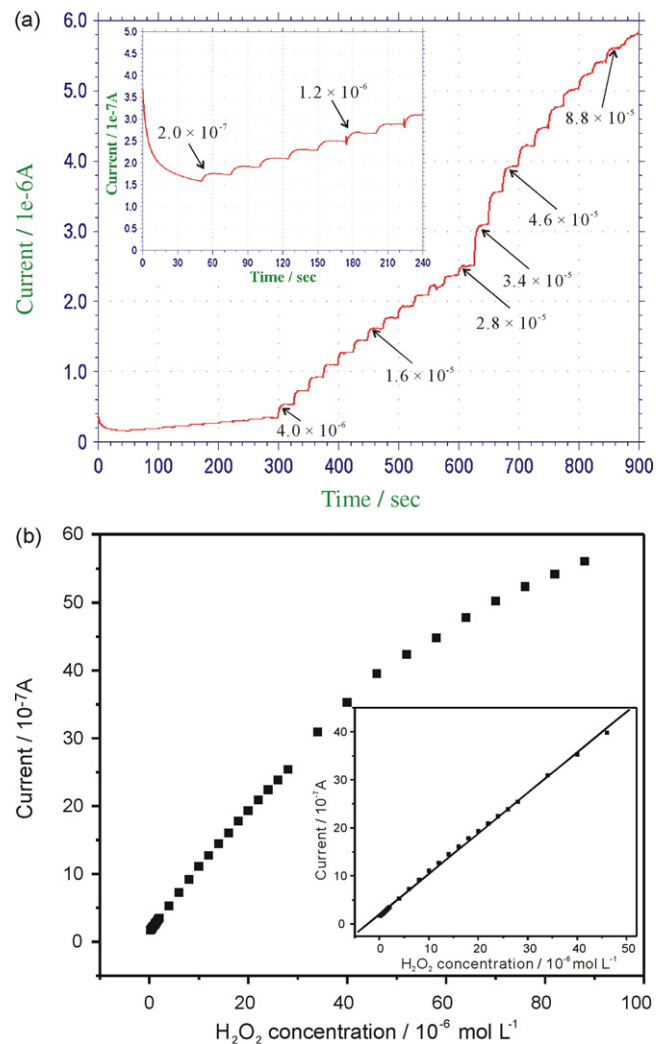


Fig. 5. (a) Typical amperometric response of the fabricated biosensor to successive addition of H_2O_2 into stirring 0.02 mol l^{-1} PBS (pH 7.0) containing 1.0 mmol l^{-1} $K_4Fe(CN)_6$. Applied potential was 0.05 V versus Ag/AgCl and (b) calibration curve between the current and the concentration of H_2O_2 . Inset showed the linear part of the calibration curve.

tration of the substrate. In our work, K_M^{app} was estimated to be $45.18 \mu\text{mol l}^{-1}$. This value was much smaller than HRP entrapped in THEOS–CS gel and TMOS sol–gel [2,34], indicating that the present electrode exhibits a higher affinity for H_2O_2 . The covalent immobilization of HRP for the fabrication of as-prepared electrode appears to be beneficial to improve biosensor's performance.

3.6. Reproducibility and stability of the developed H_2O_2 biosensor

The reproducibility and its storage stability of the developed biosensor in a drying state at 4°C were investigated. Results showed that the current response to $15 \mu\text{mol l}^{-1}$ H_2O_2 was not lowered after the biosensor was tested continuously for 30 times. To evaluate the electrode-to-electrode reproducibility, six biosensors were prepared under the same conditions independently. The R.S.D. (3.1%) obtained with the present method indicated an acceptable electrode-to-electrode reproducibility. The storage stability of the fabricated biosensor was examined by intermittently measuring the current response to H_2O_2 standard solution every 3 days in the period of 2 months. The catalytic current response could maintain about 81% of its original response in 2 months. The good

Table 1
H₂O₂ concentration in real samples tested by the developed H₂O₂ biosensor

C _{Original} (μmol l ⁻¹)	C _{Added} (μmol l ⁻¹)	C _{Found} (μmol l ⁻¹)	Recovery (%)
1.000	1.500	2.469	97.9
8.000	6.000	14.110	101.8
20.000	5.000	25.276	105.5

reproducibility and storage stability were ascribed to the covalent immobilization of HRP in CS/GPTMS hybrid films which provided a biocompatible microenvironment [20,21,35].

3.7. Selectivity and recovery experiments of the developed H₂O₂ biosensor

The selectivity of the developed H₂O₂ biosensor was evaluated by studying the effect of substances that might interfere with the determination of H₂O₂. The current obtained for each potential interfering substance (0.10 mmol l⁻¹) in the presence of H₂O₂ (30.0 μmol l⁻¹) was compared. Glucose, sucrose, ethanol, acetic acid, citric acid and cystine did not cause any observable interference. Only ascorbic acid interfered significantly. Ascorbic acid can reduce the hexacyanoferrate(III) produced in the peroxidase reaction and thus interfered the determination of H₂O₂.

In order to demonstrate the analytical applicability of developed H₂O₂ biosensor, recovery experiments of three real H₂O₂ samples were performed by standard addition method. As listed in Table 1, the recovery rate was in the range 97.9–105.5%. It can be seen that the results in Table 1 were satisfactory.

4. Conclusion

The successful preparation of the H₂O₂ biosensor demonstrated the efficiency of in situ covalent immobilization of enzyme using polysaccharide-incorporated sol–gel process. Such one-pot process offered simple and convenient methodology and could be easily carried out in aqueous medium without the addition of any organic solvents. The enzyme covalently immobilized in such biocompatible hybrid matrix possessed high electrocatalytic activity and fast amperometric response to H₂O₂. The ease of the one-pot covalent immobilization and the biocompatible matrix endowed the electrode with high reproducibility and storage stability. The promising performance of the developed biosensor makes this methodological study and application attractive in enzyme immobilization and fabrication of biosensors.

Acknowledgements

This research was supported by The National Natural Science Foundation of China (Nos. 20775039 and 20775038), The Scientific and Technical Development Project of Qingdao (07-2-3-11-jch) and The National High-tech R&D Program (863 Program, No. 2007AA09Z113).

References

- [1] V. Sanz, S. de Marcos, J. Galban, *Anal. Chim. Acta* 583 (2007) 332.
- [2] G.H. Wang, L.M. Zhang, *J. Phys. Chem. B* 110 (2006) 24864.
- [3] L. Qian, X.R. Yang, *Talanta* 68 (2006) 721.
- [4] A. Morrin, R.M. Moutloali, A.J. Killard, M.R. Smyth, J. Darkwa, E.I. Iwuoha, *Talanta* 64 (2004) 30.
- [5] S.J. Yao, J.H. Xu, Y. Wang, X.X. Chen, Y.X. Xu, S.S. Hu, *Anal. Chim. Acta* 557 (2006) 78.
- [6] F.C.M. Wong, M. Ahmad, L.Y. Heng, L.B. Peng, *Talanta* 69 (2006) 888.
- [7] D. Du, S.Z. Chen, J. Cai, A.D. Zhang, *Talanta* 74 (2008) 766.
- [8] A.M. Massari, I.J. Finkelstein, M.D. Fayer, *J. Am. Chem. Soc.* 128 (2006) 3990.
- [9] F. Li, H.Q. Jiang, S.S. Zhang, *Talanta* 71 (2007) 1487.
- [10] X. Sui, J.A. Cruz-Aguado, Y. Chen, Z. Zhang, M. Brook, J.D. Brennan, *Chem. Mater.* 17 (2005) 1174.
- [11] X.C. Tian, M.J. Li, P.X. Cai, L.J. Luo, X.Y. Zou, *Anal. Biochem.* 337 (2005) 111.
- [12] Y. Zhou, H. Yang, H.Y. Chen, *Talanta* 76 (2008) 419.
- [13] L.H. Zhang, Z.A. Xu, S.J. Dong, *Anal. Chim. Acta* 575 (2006) 52.
- [14] K.J. Feng, Y.H. Yang, Z.J. Wang, J.H. Jiang, G.L. Shen, R.Q. Yu, *Talanta* 70 (2006) 561.
- [15] X.B. Lu, Z.H. Wen, J.H. Li, *Biomaterials* 27 (2006) 5740.
- [16] Q. Xu, C. Mao, N.N. Liu, J.J. Zhu, J. Sheng, *Biosens. Bioelectron.* 22 (2006) 768.
- [17] J. Abdullah, M. Ahmad, L.Y. Heng, N. Karupiah, H. Sidek, *Talanta* 70 (2006) 527.
- [18] Y.L. Liu, Y.H. Su, J.Y. Lai, *Polymer* 45 (2004) 6831.
- [19] Y.L. Liu, Y.H. Su, K.R. Lee, J.Y. Lai, *J. Membr. Sci.* 251 (2005) 233.
- [20] Y. Shiroaki, K. Tsuru, S. Hayakawa, A. Osaka, M.A. Lopes, J.D. Santos, M.H. Fernandes, *Biomaterials* 26 (2005) 485.
- [21] F. Li, X.M. Li, S.S. Zhang, *J. Chromatogr. A* 1129 (2006) 223.
- [22] F. Li, P. Du, W. Chen, S.S. Zhang, *Anal. Chim. Acta* 585 (2007) 211.
- [23] J.E. Meegan, A. Aggeli, N. Boden, R. Brydson, A.P. Brown, L. Carrick, A.R. Brough, A. Hussain, R.J. Ansell, *Adv. Funct. Mater.* 14 (2004) 31.
- [24] Y.A. Shchipunov, T.Y. Karpenko, *Langmuir* 20 (2004) 3882.
- [25] Y.Y. Sun, Y. Bai, W.W. Yang, C.Q. Sun, *Electrochim. Acta* 52 (2007) 7352.
- [26] A. Kumar, R.R. Pandey, B. Brantley, *Talanta* 69 (2006) 700.
- [27] H. Tang, W. Zhang, P. Geng, Q.J. Wang, L.T. Jin, Z.R. Wu, M. Lou, *Anal. Chim. Acta* 562 (2006) 190.
- [28] J.C. Vidal, S. Esteban, J. Gil, J.R. Castillo, *Talanta* 68 (2006) 791.
- [29] Y.T. Kong, M. Boopathi, Y.B. Shim, *Biosens. Bioelectron.* 19 (2003) 227.
- [30] X.L. Luo, J.J. Xu, Q. Zhang, G.J. Yang, H.Y. Chen, *Biosens. Bioelectron.* 21 (2005) 190.
- [31] Y.Q. Miao, S.N. Tan, *Analyst* 125 (2000) 1591.
- [32] C.X. Lei, S.Q. Hu, N. Gao, G.L. Shen, R.Q. Yu, *Bioelectrochemistry* 65 (2004) 33–39.
- [33] R.A. Kamin, G.S. Wilson, *Anal. Chem.* 52 (1980) 1198.
- [34] J. Li, S.N. Tan, H.L. Ge, *Anal. Chim. Acta* 335 (1996) 137.
- [35] J.H. Lin, W. Qu, S.S. Zhang, *Anal. Biochem.* 360 (2007) 288.



Picogram-detection of estradiol at an electrochemical immunosensor with a gold nanoparticle|Protein G-(LC-SPDP)-scaffold

Xiaoqiang Liu, Danny K.Y. Wong*

Department of Chemistry and Biomolecular Sciences, Macquarie University, Sydney, NSW 2109, Australia

ARTICLE INFO

Article history:

Received 12 August 2008
Received in revised form
17 September 2008
Accepted 17 September 2008
Available online 26 September 2008

Keywords:

Estradiol electrochemical immunosensor
Orientation-controlled antibody
immobilisation
Thiolated Protein G-scaffold
Gold nanoparticles on immunosensors

ABSTRACT

Low picograms of the hormone 17 β -estradiol were detected at an electrochemical immunosensor. This immunosensor features a gold nanoparticle|Protein G-(LC-SPDP)¹-scaffold, to which a monoclonal anti-estradiol capture antibody was immobilised to facilitate a competitive immunoassay between sample 17 β -estradiol and a horseradish peroxidase-labelled 17 β -estradiol conjugate. Upon constructing this molecular architecture on a disposable gold electrode in a flow cell, amperometry was conducted to monitor the reduction current of benzoquinone produced from a catalytic reaction of horseradish peroxidase. This current was then quantitatively related to 17 β -estradiol present in a sample. Calibration of immunosensors in blood serum samples spiked with 17 β -estradiol yielded a linear response up to ~ 1200 pg mL⁻¹, a sensitivity of 0.61 μ A/pg mL⁻¹ and a detection limit of 6 pg mL⁻¹. We attribute these favourable characteristics of the immunosensors to the gold nanoparticle|Protein G-(LC-SPDP) scaffold, where the gold nanoparticles provided a large electrochemically active surface area that permits immobilisation of an enhanced quantity of all components of the molecular architecture, while the Protein G-(LC-SPDP) component aided in not only reducing steric hindrance when Protein G binds to the capture antibody, but also providing an orientation-controlled immobilisation of the capture antibody. Coupled with amperometric detection in a flow system, the immunosensor exhibited excellent reproducibility.

© 2008 Elsevier B.V. All rights reserved.

1. Introduction

The hormone, 17 β -estradiol (referred as estradiol hereafter), is known to exhibit a critical impact on the reproductive and sexual functioning, bone structure and some organs (e.g. liver, brain). A deficiency of estradiol is often related to such diseases as menopausal symptoms, heart diseases and osteoporosis [1]. Therefore, detection of estradiol and monitoring of its levels may be necessary in many cases so that appropriate dosage can be administered.

Among the techniques, electrochemical immunosensors [2–4] can offer a specific, sensitive and fast means of detection for estradiol. In this technique, quantitative analysis is performed by measuring the extent of binding between estradiol and its specific capture antibody that has already been immobilised on the immunosensor surface. This is often achieved by evaluating the activity of an enzyme label conjugated to, for example, estradiol. Strong affinity between estradiol and its antibody gives rise to high specificity, while the extent of binding has a major influence on

the sensitivity achievable by an electrochemical immunosensor. To promote efficient antibody–estradiol binding, the anti-estradiol capture antibody must be immobilised on the immunosensor such that its antigenic binding sites are optimally oriented towards estradiol. Several groups [5–7] have hitherto developed electrochemical immunosensors for estradiol in which passively adsorbed immunoglobulin G (IgG) was used to immobilise the antibody. For example, Draisci et al. [5] developed on a glassy carbon electrode a competitive immunoassay for estradiol in bovine serum and obtained a detection limit of 20 pg mL⁻¹. Similarly, in developing an estradiol immunosensor based on a screen-printed carbon electrode, Pamberton et al. [6] relied on passive adsorption to immobilise an anti-mouse IgG layer on the electrode to facilitate interaction with a monoclonal mouse anti-estradiol capture antibody. By calibrating the immunosensor using a competitive immunoassay between an alkaline-phosphatase-labelled estradiol conjugate and free estradiol in serum samples, a dynamic range of 25–500 pg mL⁻¹ and a detection limit of 50 pg mL⁻¹ of estradiol were obtained. More recently, by passive adsorption of anti-rabbit IgG on a graphite working electrode before attaching a polyclonal capture antibody, Volpe et al. [7] achieved a detection limit down to 15 pg mL⁻¹ of estradiol. Nonetheless, the passive adsorption strategy offers limited or no control over the orientation of IgG-bound

* Corresponding author.

E-mail address: Danny.Wong@mq.edu.au (D.K.Y. Wong).

¹ N-succinimidyl-6-[3'-(2-pyridyl)dithio]-propionamido] hexanoate.

antibodies with respect to their antigen binding sites, which would have in turn constrained the achievable sensitivity, dynamic range and detection limit.

To facilitate an orientation-controlled immobilisation of antibody on an electrochemical immunosensor, our group has developed a thiolated Protein G scaffold [8,9]. Protein G is a cell surface protein group C and G *Streptococci* with three antigen-binding domains located near its C-terminal. It is known to exhibit specificity for subclasses of antibodies from many species [10]. A feature of Protein G is a series of lysine residues that are distal from the antibody binding sites. The side-chains of these residues can be chemically converted to thiol functional groups. This then allows the thiolated Protein G to readily self-assemble on a gold electrode, while the free terminal, where the antibody binding sites are located, binds to the non-antigenic site of a capture antibody. In this way, the Protein G scaffold will aid in aligning the capture antibody almost upright with the antigen binding sites readily exposed to interact with an antigen, and will thereby enhance the extent of binding. More recently, our group has demonstrated Protein G thiolated with *N*-succinimidyl-6-[3'-(2-pyridyldithio)-propionamido] hexanoate (denoted as Protein G-(LC-SPDP)) as a superior scaffold to achieve an orientation-controlled immobilisation of a capture antibody on an electrode surface [8]. Notably, the long spacer-arm of LC-SPDP (30 Å) between Protein G and the electrode imparts substantial flexibility on the Protein G-(LC-SPDP) scaffold and facilitates enhanced interaction with the capture antibody.

In electroanalytical chemistry, gold nanoparticles are increasingly incorporated in developing the sensing electrodes because they are easy to prepare. More importantly, gold nanoparticle-coated electrodes have shown an almost 3-fold increase in surface area [11]. Tiny sizes of these particles also aid in achieving good electrical communication with the underlying electrode surface. For example, a 1.4-fold increase in cyclic voltammetric peak current of $\text{Fe}(\text{CN})_6^{3-}$ was observed at a glassy carbon electrode after coating it with a sol-gel-gold nanoparticle film [12]. More recently, colloidal gold nanoparticles were shown to provide an environment similar to the native system of immobilised biomolecules so that the biomolecules efficiently retain their biological activity [13–15]. All these features of gold nanoparticles are expected to aid in improving the analytical performance of electrochemical immunosensors.

In this work, we report the development of an electrochemical immunosensor consisting of a gold nanoparticle|Protein G-(LC-SPDP)-scaffold. A competitive immunoassay between sample estradiol and horseradish peroxidase-labelled estradiol was then established at the immunosensor. Quantitative determination of estradiol was conducted based on the reduction of benzoquinone produced by a reaction catalysed by horseradish peroxidase. We have initially optimised all components of the molecular architecture of the immunosensor using 3-mm diameter gold electrodes so that appreciable changes in the detection signal were measured. Appropriate experimental conditions were then adopted in developing an immunosensor based on disposable 1-mm diameter gold electrodes in a flow cell system to enhance the detection sensitivity. The performance of the immunosensor was evaluated in detecting estradiol in laboratory synthetic solutions and blood serum samples, respectively.

2. Experimental

2.1. Materials

All reagents were of analytical grade unless stated otherwise. Monoclonal mouse anti-estradiol capture antibody (Mab), specific

towards 17β -estradiol-6-(*O*-carboxymethyl)oxime-bovine saline albumin, and a horseradish peroxidase (HRP)-labelled estradiol conjugate (17β -estradiol-6-HRP) were purchased from BiosPacific (Burlingame, CA, USA). They were stored at -20°C until use. In all experiments, a Mab stock (0.47 mg mL^{-1}) and a 17β -estradiol-6-HRP stock (0.1 mg mL^{-1}) were prepared in phosphate buffered saline (PBS)-EDTA (pH 7.4) and stored at 4°C until use. Purified recombinant Protein G (MW 22,600 Da) and LC-SPDP were from Pierce (Illinois, USA). 17β -Estradiol, hydrogen tetrachloro-aurate(III) trihydrate (99.9%), hydroquinone, 30% H_2O_2 (v/v), potassium hydroxide, *L*-cysteine, Bicinchoninic acid (BCA) QuantiPro Protein Assay Kit, dithiothreitol (DTT) and bovine serum albumin (BSA) were all purchased from Sigma-Aldrich (Sydney, Australia). Potassium ferrocyanide and potassium ferricyanide were purchased from BDH Chemicals Ltd. (England). A Superdex 200 PC 3.2/30 size-exclusion column (GE Healthcare, Uppsala, Sweden) was used to purify thiolated Protein G. Microcon centrifugal filtration devices with a 10,000 MW cut-off were purchased from Millipore (Sydney, Australia). The buffers, phosphate buffered saline with EDTA (PBS-EDTA; 10 mM Na_2HPO_4 , 10 mM KH_2PO_4 , 150 mM NaCl, 1 mM EDTA, pH 7.4) and acetate buffer (100 mM CH_3COONa , 100 mM NaCl, pH 4.5) were prepared in Milli-Q water and adjusted to appropriate pH levels using 0.1 M NaOH or 0.1 M HCl. Serum samples were obtained from a Sydney hospital.

2.2. Instrumentation

A three-electrode system, consisting of a 3.0-mm diameter Au disc electrode, a Ag|AgCl (saturated KCl) reference electrode (both from Bioanalytical Systems Inc., West Lafayette, IN, USA) and a Pt counter electrode, was accommodated in a 10-mL electrochemical cell. In amperometric experiments, disposable Au electrodes and a flow cell used were from BVT Technologies (Hudcova, Czech Republic). Each disposable electrode is a single sensor chip consisting of a corundum ceramic base that contained a 1-mm Au working electrode, a Ag|AgCl reference electrode and a Pt counter electrode. The pump and valve were purchased from Extech Equipment Pty Ltd. (Victoria, Australia). Electrochemical experiments were performed using a Powerlab 2120 potentiostat (eDAQ Pty Ltd., Sydney, Australia) interfaced with a PC via a v2.0 EChem software (eDAQ). Prior to all voltammetric experiments, the electrolyte solution was degassed with nitrogen for 10 min and a blanket of nitrogen was maintained over the solution throughout the experiment. In square wave voltammetry, the pulse amplitude was set at 40 mV, frequency 20 Hz and potential step 2 mV. In amperometry, a constant potential of -300 mV was applied to the disposable working electrode, then hydrogen peroxide and hydroquinone were injected in the flow cell ($100\ \mu\text{L min}^{-1}$) after the baseline current has stabilised and the response current was recorded. Scanning electron microscopy of Au nanoparticle-deposited Au electrodes was carried out using JEOL 6480 LA scanning electron microscope (JEOL Optical Laboratory, Japan) at an acceleration voltage of 10 kV and a working distance of 4–5 mm.

2.3. Electrodeposition of gold nanoparticles on Au electrodes

Polycrystalline 3-mm diameter Au electrodes were sequentially polished with aqueous alumina slurries of 1, 0.3 and $0.05\ \mu\text{m}$, before being sonicated in Milli-Q water for 3 min. Cyclic voltammetry of 0.5 M H_2SO_4 was then performed at these electrodes between -0.2 and 1.5 V at 100 mV s^{-1} for 10 min, or until the typical voltammetric characteristics of a clean Au electrode were obtained [16]. Au nanoparticles were then electrodeposited by applying a 15-s potential step from 1.1 to 0 V to each pretreated polycrystalline Au electrode in 1.0 mM HAuCl_4 in 0.5 M H_2SO_4 as

supporting electrolyte [17,18]. Similar procedure was adopted when Au nanoparticles were electrodeposited on disposable Au electrodes, except 0.18 mM HAuCl₄ was used. To estimate the quantity of Au nanoparticles on an electrode, cysteine was adsorbed on the electrode from a 10-mM aqueous cysteine solution for 10 min before cyclic voltammetry was conducted in 0.5 M KOH [19].

2.4. Thiolation of Protein G

A procedure previously described [8] for the thiolation of Protein G using LC-SPDP was adopted. Briefly, 2 mg LC-SPDP was dissolved in 235 μ L dimethylsulfoxide. Then, 10 μ L of the LC-SPDP solution was added to 1 mg Protein G in 0.5 mL PBS-EDTA. After a 30-min incubation at room temperature, excess LC-SPDP and unwanted by-products were removed by two centrifugal filtrations at 12,000 \times g for 30 min using a Microcon centrifugal filtration device and the buffer was exchanged to sodium acetate. DTT was added to the Protein G-(LC-SPDP) solution to obtain a final concentration of 50 mM. This was allowed to react for 30 min at room temperature. Finally, the reaction mixture was purified by size-exclusion high performance liquid chromatography and the purified thiolated Protein G was stored at 4 °C until use. The degree of LC-SPDP-modification of Protein G was evaluated by a spectroscopic pyridine-2-thione assay [20]. In this assay, 100 μ L purified LC-SPDP-modified Protein G was diluted to 1 mL in PBS and the absorbance of this solution was measured at 343 nm against a PBS blank. Then, 10 μ L of 15 mg mL⁻¹ DTT was added and, after 15 min, the absorbance of the reduced sample was measured against a PBS blank again. The absorbance difference was then used to evaluate the molar ratio of LC-SPDP to Protein G as described in Ref. [20].

The quantity of Protein G-(LC-SPDP) bound to the electrode surface was determined after estimating the residual protein content of the wash solution using a BCA-based QuantiPro Protein Assay Kit. Briefly, the assay working reagent was prepared by combining 1 part of protein sample with 1 part of a premixed solution containing 25 parts of bicinchoninic acid solution and 1 part of 4% (w/v) CuSO₄·5H₂O. This reagent was mixed in equal quantities with a blank solution, BSA protein standards, and electrode wash solutions, respectively. The reaction proceeded for 1 h at 60 °C before being quenched in ice water. The absorbance of the violet solutions at 562 nm was measured against the blank. Based on calibration, the absorbance difference was then used to estimate the quantity of Protein G.

2.5. Preparation of electrochemical immunosensors

To prepare an electrochemical immunosensor, a 10- μ L aliquot of Protein G-(LC-SPDP) was applied to a Au electrode immobilised with Au nanoparticles for 1 h at room temperature. Then 5 μ L of 1% (w/v) BSA solution was applied to the electrode for 30 min to prevent non-specific binding of Mab and estradiol-HRP conjugate. Next, 5 μ L of Mab stock solution, diluted 1:50 in PBS, was applied to the electrode surface for 1 h at room temperature. The electrode was rinsed in between steps using washing buffer and distilled water, respectively. A similar procedure was employed in preparing a disposable electrode-based immunosensor, except one-fifth of the volumes of all reagents was used.

To facilitate a competitive immunoassay, the electrode surface was immobilised with a solution containing sample estradiol and 2 μ g mL⁻¹ of estradiol-HRP conjugate. The competition reaction was allowed for 30 min at room temperature prior to rinsing the electrode with PBS and distilled water. Fresh substrate solution containing hydrogen peroxide and hydroquinone was used in each experiment.

2.6. Calibration

Calibration was initially conducted in estradiol standard solutions (25–4000 pg mL⁻¹) in PBS as a supporting electrolyte, whereas that in serum was conducted by spiking estradiol solutions (final concentration 25–1500 pg mL⁻¹) into estradiol-free serum. All correlation coefficients of calibration plots were statistically tested using Student's *t*-test. All errors correspond to the respective 95% confidence intervals.

3. Results and discussion

3.1. Au nanoparticle-coated Au electrodes

Electrodes immobilised with Au nanoparticles were shown to exhibit a 3-fold increase in electrochemically active surface area [11,21]. In developing an electrochemical immunosensor for estradiol using a Au nanoparticle-coated Au electrode, the large surface area will promote an enhanced quantity of antibody-estradiol complex on the electrode surface. This will in turn improve the sensitivity, dynamic range and detection limit of the analysis. In our work, Au nanoparticles were initially deposited by applying a reduction potential step from 1.1 to 0V for a particular duration to an acid-treated 3-mm diameter polycrystalline Au electrode in 1.0 mM HAuCl₄ (0.5 M H₂SO₄ as supporting electrolyte). Among the factors, electrochemical deposition time is critical in forming Au nanoparticles, as discussed further below. Optimum deposition time must be determined to obtain the largest possible increase of electrode surface area. To determine the surface area of Au nanoparticles and therefore the optimum deposition time, we have relied on the specific reductive desorption of thiol-Au bonds to estimate the thiol-Au surface coverage on an electrode [9,22,23] as described below.

Initially, Au nanoparticles were electrochemically deposited on Au electrodes over several deposition times between 5 and 30 s. These electrodes were next immersed in a 10-mM aqueous cysteine solution for 10 min to facilitate adsorption. Cyclic voltammetry at these electrodes was then conducted in 0.5 M KOH and the results obtained are depicted in Fig. 1(a). Two reduction peaks (between -0.8 and -0.9 V, and between -1.05 and -1.15 V) were observed and these results are in agreement with the reductive desorption of alkane thiol self-assembled monolayers from a Au surface [23]. These two peaks were attributed to the reduction of a S-Au bond to R-S⁻ at a terrace and a step site on a rough Au surface. Therefore, the total area under the two reduction peaks is directly proportional to the surface coverage of thiol-Au bond on an electrode. As shown in Fig. 1(a), there was an increase in the surface coverage when the deposition time was increased from 5 to 15 s, indicating an increase in electrode surface area arising from the deposited Au nanoparticles. However, when a deposition time of 30 s was applied, the surface coverage decreased. We attributed this to the agglomeration of Au nanoparticles to form a film similar in area to that of the underlying electrode, and hence a smaller surface coverage compared to that obtained when the nanoparticles were dispersed on the surface. These results indicate that a deposition time of 15 s would yield the largest electrode surface area before the nanoparticles formed a continuous Au film. This is confirmed by the scanning electron micrograph shown in Fig. 1(b). In this figure, the white shining spheres correspond to Au particles dispersed on a relatively smooth bulk Au surface represented by the dark background. Additionally, as gold nanoparticles were deposited on a gold electrode surface, it was difficult to distinguish small gold particles from the gold surface in Fig. 1(b). Typical diameters of these particles were estimated to be 20–200 nm. These results are similar

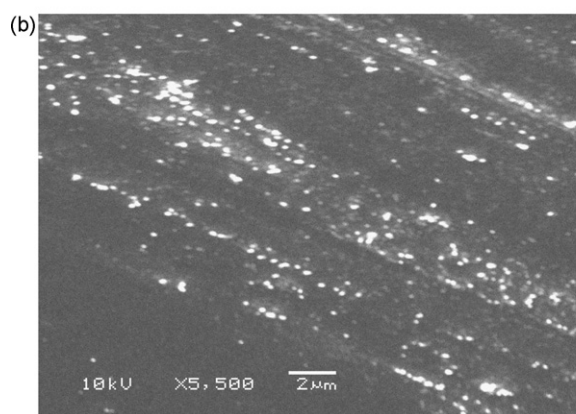
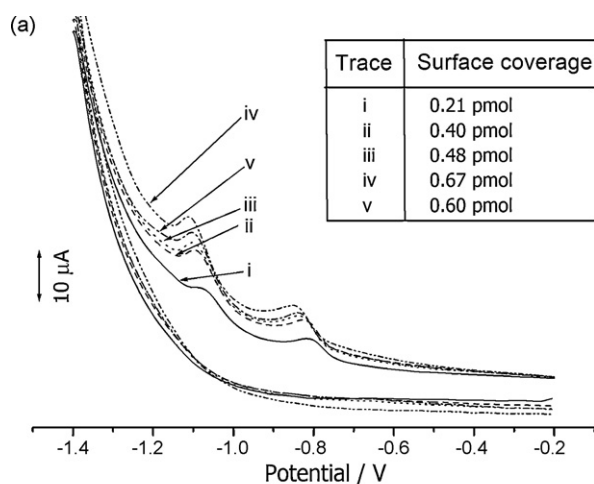


Fig. 1. (a) Cyclic voltammetry of cysteine-adsorbed Au nanoparticle-coated Au electrodes in 0.5 M KOH. Au nanoparticles were electrochemically deposited over a deposition time of (i) 0 s, (ii) 5 s, (iii) 10 s, (iv) 15 s and (v) 30 s. Scan rate: 150 mV s⁻¹. The inset tabulates the surface coverage of thiol-Au bond estimated based on the total area under the two reductive desorption peaks. (b) Scanning electron micrograph of Au nanoparticles electrodeposited on an Au electrode by applying a potential step from 1.1 to 0 V versus Ag|AgCl for 15 s.

to those reported elsewhere [18,19,24]. Compared with the surface coverage determined at bare gold electrodes, the presence of Au nanoparticles has increased the electrochemically active surface area by a factor of approximately 3 ($N=4$).

3.2. Characterisation of Au electrodes with a Protein G-(LC-SPDP) scaffold

Following the deposition of Au nanoparticles on Au electrodes, a Protein G-(LC-SPDP) scaffold was immobilised on the electrodes. To characterise the formation of a Protein G-(LC-SPDP) scaffold, reductive desorption was again conducted. The cyclic voltammogram obtained after desorbing the scaffold in 0.5 M KOH is shown in Fig. 2, which reveals two comparable reductive desorption peaks (between -0.8 and -0.9 V, and between -1.0 and -1.1 V) to those observed in Fig. 1(a), indicating successful immobilisation of the Protein G-(LC-SPDP) scaffold on the electrodes. Using a BCA protein determination kit, we have estimated 1.23 μg (standard deviation 0.15 μg; $N=6$) Protein G-(LC-SPDP) on Au nanoparticle-coated Au electrodes, compared to 0.97 μg (standard deviation 0.13 μg; $N=6$) on bare Au electrodes. These results also indicate successful conversion of amino groups in lysine residues of Protein G to thiol groups required for immobilising Protein G on the Au surface. Based on a spectrometric pyridine-2-thione assay, we found that approximately 42% of the lysine residues was thiolated, compared to 30%,

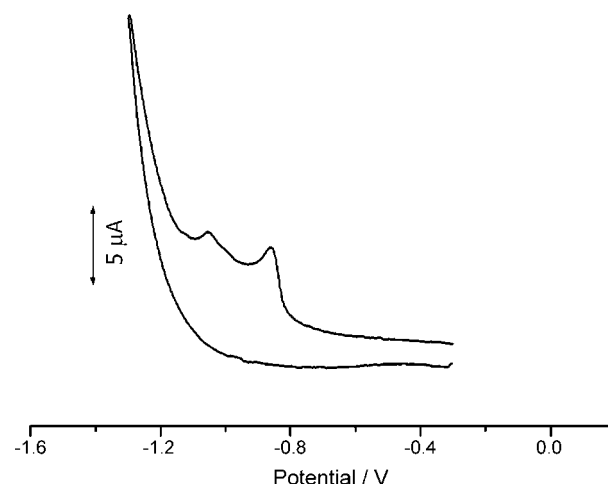
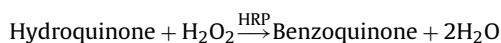


Fig. 2. Cyclic voltammetry of a Protein G-(LC-SPDP)-coated Au electrode in 0.5 M KOH. Scan rate: 150 mV s⁻¹.

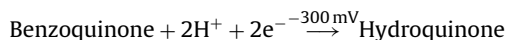
17% and 18% thiolation in Ribonuclease A, amylase and HRP, respectively [20]. Reduced steric hindrance around Protein G-(LC-SPDP) with a long spacer arm has possibly facilitated a higher degree of thiolation.

3.3. Assembling electrochemical immunosensors

With a Au-nanoparticle|Protein G-(LC-SPDP) scaffold on Au electrodes, the next step in assembling the electrochemical immunosensor for estradiol is to immobilise the anti-estradiol antibody, Mab, on the electrodes. The optimum quantity of Mab on the scaffold was determined based on its interaction with estradiol labelled with the enzyme HRP. In the presence of H₂O₂ as a mediator, HRP catalyses the conversion of hydroquinone to benzoquinone:



By applying a reduction potential of -300 mV, benzoquinone is reduced to hydroquinone:



The reduction current generated in square wave voltammetry between 0.1 and -0.4 V is quantitatively related to the 17β-estradiol-6-HRP conjugate and hence the quantity of Mab immobilised on the scaffold. As both Mab and the quantity of estradiol-HRP were expected to affect the magnitude of detection signal of an immunosensor, the interaction between these two factors was studied. In our experiments, electrodes immobilised with a Au nanoparticle|Protein G-(LC-SPDP) scaffold were respectively incubated in Mab solutions of concentration range 0.96–24 μg mL⁻¹. Next, these electrodes were incubated in 17β-estradiol-6-HRP of concentration between 0.2 and 10 μg mL⁻¹, respectively, at 25 °C for 30 min. Finally, each electrode was placed in a cell containing 20 mM PBS. Hydroquinone (final concentration 2.0 mM) and H₂O₂ (final concentration 1.0 mM) were then injected in the cell before square wave voltammetry was conducted. The reduction peak current obtained was used to construct the plots shown in Fig. 3. At each Mab concentration, the reduction peak current increased when increasingly available 17β-estradiol-6-HRP conjugate (as concentration increased from 0.2 to 2 μg mL⁻¹) bound to a fixed quantity of Mab. However, the reduction peak current levelled off at 17β-estradiol-6-HRP conjugate concentration

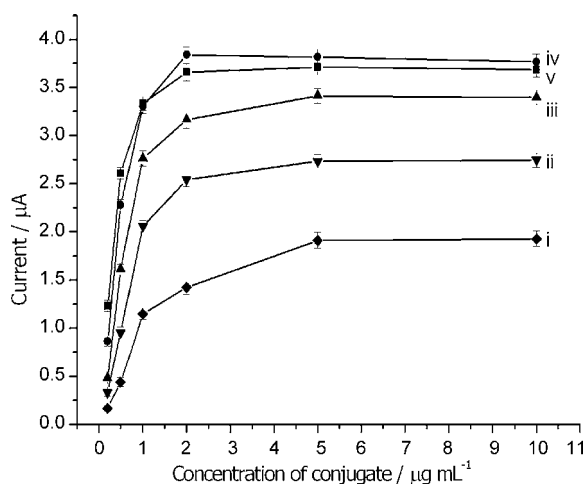


Fig. 3. The current response of the estradiol immunosensor at different combination of antibody and HRP-estradiol conjugate. The concentration for Mab is (i) 0.96, (ii) 2.4 (iii) 4.8, (iv) 9.6, and (v) 24 $\mu\text{g mL}^{-1}$.

higher than $2 \mu\text{g mL}^{-1}$, most likely because 17β -estradiol-6-HRP has saturated the Mab layer and no significant further binding took place between Mab and excess 17β -estradiol-6-HRP. At a fixed 17β -estradiol-6-HRP concentration, the reduction peak current increased rapidly as Mab concentration was increased from 0.96 to $9.6 \mu\text{g mL}^{-1}$, indicating a spontaneous interaction between Mab and 17β -estradiol-6-HRP. However, when the Mab concentration was increased from 9.6 to $24 \mu\text{g mL}^{-1}$, a similar extent of interaction was observed due to a lack of binding between 17β -estradiol-6-HRP and excess Mab present in the system. Moreover, excess Mab would easily lead to crowdedness on the electrode surface, which would in turn cause deactivation of some HRP of the conjugate. Hence, similar binding was observed despite the application of additional Mab. Overall, the results in Fig. 3 indicated an optimum estradiol-HRP conjugate concentration of $2 \mu\text{g mL}^{-1}$ and Mab concentration of $9.6 \mu\text{g mL}^{-1}$ for use in constructing an immunosensor on 3-mm diameter Au electrodes.

At this stage of our development, cyclic voltammetry of a mixture of $2.5 \text{ mM Fe}(\text{CN})_6^{3-}$ and $2.5 \text{ mM Fe}(\text{CN})_6^{4-}$ in 20 mM PBS as supporting electrolyte was also studied at electrodes with a Au nanoparticle|Protein G-(LC-SPDP)-scaffold. The results are shown in Fig. 4. Initially, Trace a shows a well-defined cyclic voltammogram (peak separation of 91 mV and peak current ratio 1.04) at a bare Au electrode. After the electrode was immobilised with Protein G-(LC-SPDP) and $9.6 \mu\text{g mL}^{-1}$ Mab, it yielded a less well-defined voltammogram (peak separation of 210 mV and peak current ratio 0.8), as shown in Trace b. Adsorption of Protein G-(SPDP) and Mab on the electrode surface would have obstructed the electron transfer reaction of the $\text{Fe}(\text{CN})_6^{3-}/\text{Fe}(\text{CN})_6^{4-}$ couple, leading to a more sluggish reaction. A 76% decrease in current was observed in Trace b compared to Trace a. However, when Protein G-(LC-SPDP) and Mab were immobilised on a Au nanoparticle-coated Au electrode, the electron transfer kinetics of $\text{Fe}(\text{CN})_6^{3-}/\text{Fe}(\text{CN})_6^{4-}$ were improved (peak separation of 200 mV and peak current ratio 1.09) and the current was enhanced by 92% (Trace c) relative to that shown in Trace b. Similar to those reported previously [14,25], the small sizes of Au nanoparticles enable them to penetrate the barrier of Protein G-(LS-SPDP) and Mab in this work, forming a tunnel that facilitates the electron transfer of $\text{Fe}(\text{CN})_6^{3-}$ and $\text{Fe}(\text{CN})_6^{4-}$ at the electrode surface. The results obtained support the development of a Au nanoparticle|Protein G-(SPDP)-scaffold for an electrochemical immunosensor in this work.

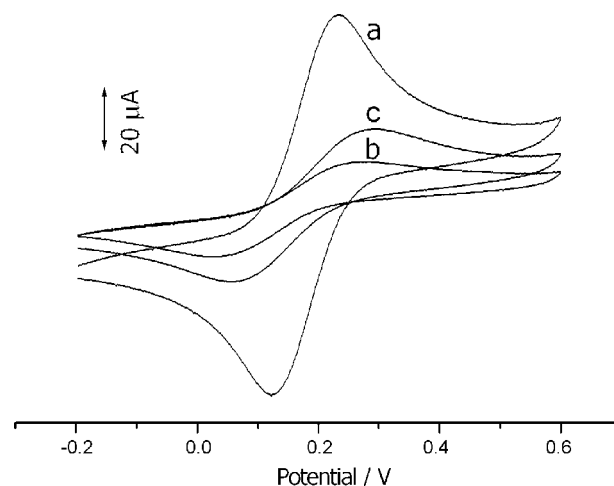


Fig. 4. Cyclic voltammetry of $2.5 \text{ mM Fe}(\text{CN})_6^{3-}$ and $2.5 \text{ mM Fe}(\text{CN})_6^{4-}$ at (a) a bare Au electrode, (b) an Au electrode immobilised with Protein G-(LC-SPDP) and Mab, (c) a Au electrode with a Au nanoparticle|Protein G-(LC-SPD)-scaffold immobilised with Mab, in 0.02 M PBS (pH 7.5). The potential was initially scanned from -0.2 to 0.6 V at a rate of 100 mV s^{-1} .

3.4. Analytical applications of the immunosensor

Due to the small size of the estradiol molecule, a competitive electrochemical immunoassay was adopted at the electrochemical immunosensor for analysis of estradiol. In conjunction with a flow system, disposable 1-mm diameter gold electrodes were used to construct an immunosensor and amperometric detection was carried out in the flow cell system. This is so that we can achieve benefits such as constant analysis conditions, improved fluid handling and stable electrochemical signal. Based on an electrode surface area ratio, a corresponding proportion of the optimised quantity of all components of the molecular structure determined on 3-mm diameter Au electrodes was immobilised on the disposable Au electrodes to construct the electrochemical immunosensors in a flow system. Briefly, Au nanoparticles were deposited by applying a potential step from 1.1 to 0 V to disposable electrodes immersed in 0.18 mM HAuCl_4 (0.5 M H_2SO_4 supporting electrolyte) for 15 s. A 2- μL aliquot of Protein G-(LC-SPDP) was then applied on the electrodes and they were left at room temperature for 1 h. Next, these electrodes were sequentially incubated in 1 μL of 1% (w/v) BSA solution for 30 min, 1 μL of $9.6 \mu\text{g mL}^{-1}$ Mab for 1 h, and 1 μL mixture of estradiol standard solution and estradiol-HRP conjugate for 30 min.

Amperometry was conducted by applying a constant potential of -300 mV . Current versus time plots obtained using estradiol standard solutions in PBS are shown in Fig. 5(a). In these plots, while the concentration of estradiol standard solution was increased from 25 to 4000 pg mL^{-1} , there was a proportional decrease in the quantity of 17β -estradiol-6-HRP conjugate competing to bind to Mab immobilised on the immunosensor scaffold, giving rise to a decrease in the reduction peak current shown in Fig. 5(a). Fig 5(b) shows the calibration plot constructed based on the reduction peak current obtained in the current versus time plot. For this calibration plot, we obtained a correlation coefficient of 0.983, which was found to be statistically significant at a 95% confidence level ($N=5$). The linear relationship can be expressed as

$$\text{Reduction peak current } (\mu\text{A}) = (2.97 \pm 0.38) - (0.68 \pm 0.09) [\text{Estradiol}] (\text{pg mL}^{-1})$$

where the errors represent the 95% confidence intervals. A linear response up to $\sim 1500 \text{ pg mL}^{-1}$ was shown by the immunosensors.

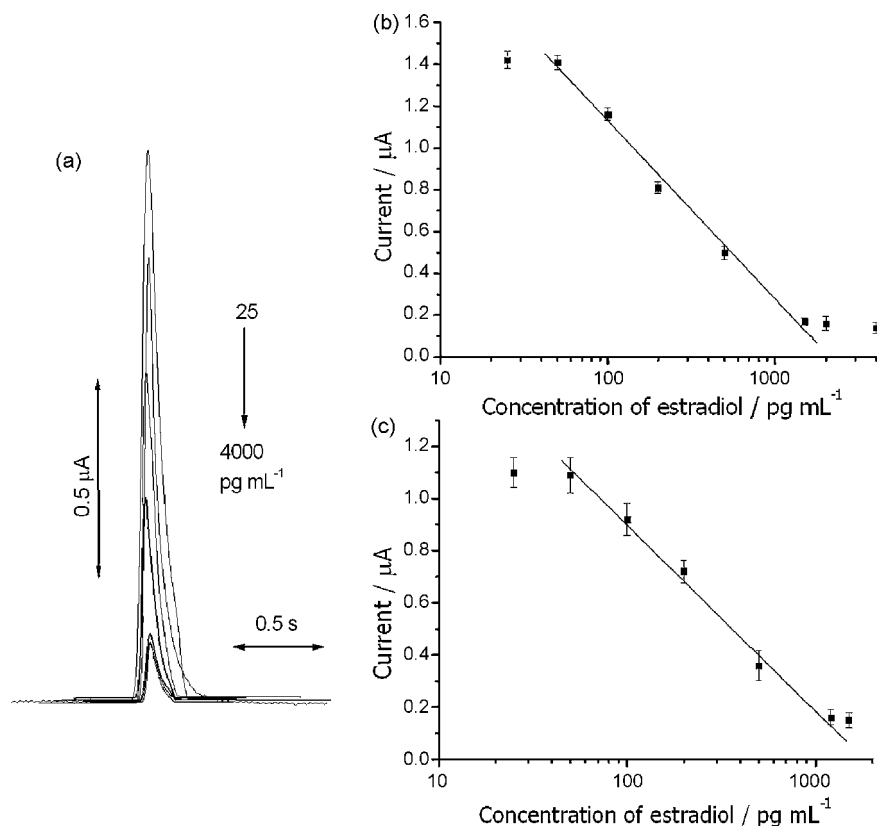


Fig. 5. (a) The current–time plots of the competitive immunoassay for estradiol in PBS, (b) calibration plot obtained using the electrochemical immunosensor in detecting estradiol in PBS, and (c) calibration plot obtained using the electrochemical immunosensor in detecting estradiol spiked in serum samples.

In addition, a sensitivity (denoted by the slope of the calibration plot) of $0.68 \mu\text{A}/\text{pg mL}^{-1}$ was obtained. The detection limit (defined as the difference between the mean blank signal and three times the standard deviation of the blank) [7] was estimated to be 3.5 pg mL^{-1} . For comparison, when calibration experiments were repeated using immunosensors without gold nanoparticles, a correspondingly higher detection limit of 18 pg mL^{-1} was obtained.

In order to further examine the performance of the electrochemical immunosensors, same calibration experiments were repeated by spiking an estradiol standard in blood serum samples collected from a local hospital. The calibration plot (with a statistically significant correlation coefficient of 0.972 at a 95% confidence interval; $N=5$) obtained is shown in Fig. 5(c). In this case, a comparable linear response up to $\sim 1200 \text{ pg mL}^{-1}$, a sensitivity of $0.61 \mu\text{A}/\text{pg mL}^{-1}$, and a detection limit of 6 pg mL^{-1} were obtained. The linear relationship is represented by

$$\text{Reduction peak current } (\mu\text{A}) = (2.39 \pm 0.45) - (0.61 \pm 0.13) [\text{Estradiol}] (\text{pg mL}^{-1})$$

Note that similar sensitivity was obtained at immunosensors calibrated in PBS and in blood serum, reflecting the excellent specificity and selectivity of the immunosensor. Moreover, an improved detection limit of estradiol by an order of magnitude was achieved at the immunosensor, compared to those reported by Draisci et al. [5], Pamberton et al. [6] and Volpe et al. [7], as quoted previously. We attribute this to firstly a large immunosensor surface area using a scaffold consisting of Au nanoparticles, which would have facilitated the immobilisation of a substantial amount of Protein G-(LC-SPDP) and the estradiol capture antibody, Mab, on the

electrode surface for binding to estradiol. Meanwhile, thiolation has also strongly anchored Protein G on the Au surface, leaving its free terminal to bind to the non-antigenic site of Mab. In this way, Protein G-(LC-SPDP) incorporated in the scaffold would aid in an orientation-controlled immobilisation of Mab on the immunosensor to encourage an efficient binding to estradiol. This has resulted in an enhanced reduction current produced via the catalytic enzyme reaction of HRP conjugated to estradiol that bound to Mab. Further, the long spacer arm of LC-SPDP would have reduced steric hindrance in attaching Mab to Protein G. All these features of the Au nanoparticle/Protein G-(LC-SPDP) scaffold, coupled with amperometric detection in a flow system, are expected to have synergistically contributed to the development of an electrochemical immunosensor with low picograms detection limit. Note that a range of $25\text{--}400 \text{ pg mL}^{-1}$ estradiol was usually detected in samples collected during non-menstrual period [25]. This range lies well between the detection limit (6 pg mL^{-1}) and the limit of linearity ($\sim 1200 \text{ pg mL}^{-1}$) of the electrochemical immunosensors.

3.5. Precision and stability study

To further characterise the electrochemical immunosensors, we have conducted several precision and recovery studies. In the precision study, the reproducibility (intra-assay) and repeatability (inter-assay) of the competitive assays were tested at three different estradiol concentrations of 60, 250 and 1000 pg mL^{-1} . Intra-assays of these samples were performed in four duplicates with the same immunosensor and inter-assays with different immunosensors from the same manufactured batch. The results of these studies are summarised in Table 1. For intra-assays, the relative standard deviation (RSD) varied from 3.1% to 7.8%, while that for inter-assay varied

Table 1
Precision of the estradiol immunosensor.

Estradiol (pg mL ⁻¹)	Intra-assay RSD ^a	Inter-assay RSD
60	3.1%	6.8%
250	4.4%	8.6%
1000	7.8%	11.6%

^a RSD = standard deviation/mean; (N=4).

Table 2
Accuracy of the estradiol immunosensor.

Estradiol added (pg mL ⁻¹)	Estradiol found (pg mL ⁻¹)	RSD	Recovery
60	51	7.2	85%
250	284	7.8	113.6%
1000	1097	9.1	109.7%

RSD = Standard deviation/mean; (N=4).

from 6.8% to 11.6%. As expected, the intra-assay variance was lower than the inter-assay variance. Owing to the small current responses, a higher RSD was obtained at 1000 pg mL⁻¹ compared to that at 60 pg mL⁻¹. The small RSDs showed that our immunosensor fabrication procedure is reliable. In addition, amperometric responses of 16 immunosensors were measured after 1 day, 1 week and 2 weeks, respectively, and were compared to those obtained on the first day. We found an average drop of 2.5% in the amperometric response after 1 day, 16% after 1 week and 44% after 2 weeks. This is most likely to be caused by the transient deterioration of the enzyme attached to the estradiol-HRP conjugate.

3.6. Recovery

The accuracy of the immunosensor was studied by measuring the recovery of spiked human serum samples. The concentration selected were 60, 250 and 1000 pg mL⁻¹, representing low, medium and high concentrations, respectively. The recovery was obtained by comparing the concentration calculated based on an independently prepared calibration plot with the actual added concentration. The calibration plot was constructed based on the same experimental conditions as recovery test. As shown in the results tabulated in Table 2, the recovery is relatively high in the highest concentration, and the lowest recovery was given by the lowest concentration. However, the average recovery is 102.7%, indicating the feasibility of using the estradiol sensor to detect samples in serum in the obtained dynamic range.

4. Conclusion

In this work, Au nanoparticles and Protein G thiolated with LC-SPDP were immobilised on Au electrodes to act as a composite scaffold for an estradiol electrochemical immunosensor. A large surface area on the immunosensor surface was provided by the deposited Au nanoparticles to enhance the quantity of Protein G-(LC-SPDP) and capture antibody required in developing an immunosensor for estradiol. Compared with passive adsorption, Protein G-(LC-SPDP) facilitated immobilisation of capture antibody with improved orientation. Coupled with amperometric detection of estradiol in a flow system, the immunosensor exhibited superior linear range, sensitivity and detection limit of estradiol in blood serum samples spiked with estradiol.

References

- [1] H. Kuramitz, M. Matsuda, J.H. Thomas, K. Sugawara, S. Tanaka, *Analyst* 128 (2003) 182–186.
- [2] J.M. Fowler, D.K.Y. Wong, B.H. Halsall, W.R. Heineman, in: X. Zhang, H. Ju, J. Wang (Eds.), *Electrochemical Sensors, Biosensors and their Biomedical Applications*, Academic Press, New York, 2008, pp. 115–234.
- [3] E.P. Medyantseva, E.V. Khaldeeva, G.K. Budnikov, *J. Anal. Chem.* 56 (2001) 886.
- [4] A.L. Ghindilis, P. Atanasov, M. Wilkins, E. Wilkins, *Biosens. Bioelectron.* 13 (1998) 113–131.
- [5] R. Draisci, I. Purificato, F.d. Quadri, G. Volpe, D. Compagnone, G. Palleschi, *Analyst* 125 (2000) 1419–1423.
- [6] R.M. Pemberton, T.T. Mottram, J.P. Hart, *J. Biochem. Biophys. Methods* 63 (2005) 201–212.
- [7] G. Volpe, G. Fares, F.D. Quadri, R. Draisci, G. Ferretti, C. Marchiafava, D. Moscone, G. Palleschi, *Anal. Chim. Acta* 572 (2006) 11–16.
- [8] J.M. Fowler, M.C. Stuart, D.K.Y. Wong, *Biosens. Bioelectron.* 23 (2007) 633–639.
- [9] J.M. Fowler, M.C. Stuart, D.K.Y. Wong, *Anal. Chem.* 79 (2007) 350–354.
- [10] L. Bjorck, G. Kronvall, *J. Immunol.* 133 (1984) 969–974.
- [11] S. Liu, L. Wang, F. Zhao, *J. Electroanal. Chem.* 602 (2007) 55–60.
- [12] G. Maduraiveeran, R. Ramaraj, *J. Electroanal. Chem.* 608 (2007) 52–58.
- [13] F. Yan, J. Chen, H.X. Ju, *Electrochem. Commun.* 9 (2007) 293–298.
- [14] J. Li, J. Yu, F. Zhao, B. Zeng, *Anal. Chim. Acta* 587 (2007) 33–40.
- [15] Y. Zhuo, R. Yuan, Y. Chai, D. Tang, Y. Zhang, N. Wang, X.LiQ. Zhu, *Electrochem. Commun.* 7 (2005) 355–360.
- [16] R.V. Bucur, A. Bartes, V. Mecea, *Electrochim. Acta* 23 (1978) 641–646.
- [17] X. Dai, O. Nekrassova, M.E. Hyde, R.G. Compton, *Anal. Chem.* 76 (2004) 5924–5929.
- [18] M.S. El-Deab, T. Ohsaka, *Electrochem. Commun.* 4 (2002) 288–292.
- [19] M.S. El-Deab, T. Ohsaka, *Electrochim. Acta* 47 (2002) 4255–4261.
- [20] J. Carlsson, H. Drevin, R. Axén, *Biochem. J.* 173 (1978) 723.
- [21] T. Tangkuaram, C. Ponchio, T. Kangkasomboon, P. Katikawong, W. Veerasai, *Biosens. Bioelectron.* 22 (2007) 2071–2078.
- [22] A. Ulman, *Chem. Rev.* 96 (1996) 1533–1554.
- [23] T. Kawaguchi, H. Yasuda, K. Shimazu, M.D. Porter, *Langmuir* 16 (2000) 9830–9840.
- [24] H. Cui, Y. Xu, Z.F. Zhang, *Anal. Chem.* 76 (2004) 4002–4010.
- [25] M. Wheeler, in: D. Wild (Ed.), *The Immunoassay Handbook*, vol. 9, Stockton Press, New York, 1994, pp. 366–378.



Optimized chromatographic and bioluminescent methods for inorganic pyrophosphate based on its conversion to ATP by firefly luciferase

Simone M. Marques, Filipe Peralta, Joaquim C.G. Esteves da Silva*

Centro de Investigação em Química (CIQ-UP), Department of Chemistry, Faculty of Sciences, University of Porto, R. Campo Alegre 687, 4169-007 Porto, Portugal

ARTICLE INFO

Article history:

Received 12 July 2008

Received in revised form 8 September 2008

Accepted 21 September 2008

Available online 27 September 2008

Keywords:

Inorganic pyrophosphate

ATP

Firefly luciferase

Ion-pair-HPLC

Bioluminescence

Experimental factorial design

ABSTRACT

Two new methods for inorganic pyrophosphate (PPI) quantification are described. They are based on the enzymatic conversion of PPI into ATP by firefly luciferase (Luc, E.C. 1.13.12.7) in the presence of dehydroluciferyl-adenylate (L-AMP) followed by the determination of ATP by one of two different procedures, either UV-monitored (260 nm) ion-pair-HPLC (IP-HPLC) (method A) or luciferase-dependent bioluminescence in the presence of its substrate, firefly luciferin (D-LH₂) (method B). These methods were subjected to optimization using experimental design methodologies to obtain optimum values for the selected factors: method A—incubation time ($t_{inc} = 15$ min), inactivation time of the enzyme ($t_{inac} = 2$ min), pH of the reaction mixture (pH 7.50) and the concentrations of L-AMP ([L-AMP] = 40 μ M) and luciferase ([Luc] = 0.1 μ M); method B—concentrations of L-AMP ([L-AMP] = 2 μ M), luciferase ([Luc] = 50 nM) and luciferin ([LH₂] = 30 μ M). Method A has a linear response over the range of 0.1–20 μ M of PPI, with a limit of detection (LOD) of 0.5 μ M and a limit of quantitation (LOQ) of 1.8 μ M. Precision, expressed as relative standard deviation (R.S.D.), is 7.4% at 1 μ M PPI and 5.9% at 8 μ M PPI. Method B has a linear response over the range of 0.75–6.0 μ M of PPI, with LOD and LOQ of 0.624 and 2.23 μ M, respectively, and a R.S.D. of 5.1% at 2.5 μ M PPI and 4.9% at 5 μ M PPI. Under optimized conditions sensitive and robust methods can be obtained for the analysis of PPI impurities in commercial nucleotides and tripolyphosphate (P₃).

© 2008 Elsevier B.V. All rights reserved.

1. Introduction

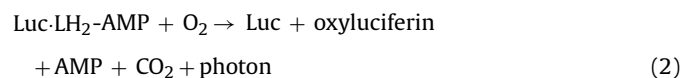
Inorganic pyrophosphate (PPI) is ubiquitous in many metabolic pathways related to ATP bioenergetics [for example, as a coproduct of adenylation reactions, in which the adenylate moiety of ATP (5'-AMP) is transferred to any molecule to "activate" it for subsequent reactions] or in biosynthetic reactions like the synthesis of DNA and RNA and cyclic nucleotides (cAMP and cGMP) [1]. But far from being a by-product PPI has important biological roles, particularly in bacteria [2,3], protists [4] and plants [5,6]. Furthermore PPI is a modulator in the calcification process in humans, and the misregulation of its concentration is associated with pathologies in cartilaginous tissues [7] and in the vascular system [8].

Several methods for detecting and quantifying PPI are described in the literature. Most of them are multistep coupled enzymatic assays, generally employing two or more different enzymes that work sequentially to convert PPI into products that can be measured by means of UV-vis or luminescent techniques [9–20], although colorimetric methods coupled with HPLC detection [21] or capillary

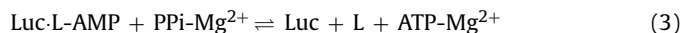
electrophoresis separation [22] were also reported. The development of highly specific chemical sensors for PPI measurement in aqueous medium is also an increasing area of research [23–25].

Enzymatic assays have the advantages of being very specific and sensitive. They allow the quantification of PPI in a wide range of concentrations, from μ M down to pM. A commonly employed enzyme in many of the coupled enzymatic assays is luciferase [12,13,18,20].

Firefly luciferase (Luc, E.C. 1.13.12.7) is an enzyme that produces light through the oxidation of its substrate, luciferin (D-LH₂), in the presence of ATP-Mg²⁺ and oxygen, in a two-step process [26–29] (Eqs. (1) and (2)).



Besides this reaction luciferase also catalyzes the reaction of PPI with dehydroluciferyl-adenylate (L-AMP), previously formed in the oxidation of the intermediate luciferyl-adenylate [LH₂-AMP (1)], yielding dehydroluciferin (L) and regenerating ATP (3) [27,29,30].



* Corresponding author. Tel.: +351 220402569; fax: +351 220402659.
E-mail address: jcsilva@fc.up.pt (J.C.G. Esteves da Silva).

The concentration of the ATP formed can be directly calculated by chromatography or, if D-LH₂ is added to the assay medium, by measuring the bioluminescent emitted light (Eqs. (1) and (2)). Subsequently the ATP content is related to the original amount of PPI in the sample.

This paper presents two optimized methods for PPI quantification based on the luciferase-catalyzed generation of ATP from PPI and L-AMP (3) followed by its measurement by ion-pair-HPLC (IP-HPLC) with detection at 260 nm (method A) or by measuring the light from the bioluminescent reaction (method B). These methods were applied to the determination of PPI content in commercial nucleotide substances.

2. Experimental

2.1. Reagents

Commercial *Photinus pyralis* luciferase (L9506; lot 014K7430), D-luciferin (D-LH₂), HEPES (4-(2-hydroxyethyl)piperazine-1-ethanesulfonic acid) and all the nucleotides (CTP, CDP, CMP, UTP, UDP, UMP, ADP, AMP and ATP for the HPLC standard) were purchased from Sigma (Steinheim, Germany); PPI (Na₄P₂O₇·10H₂O), tripolyphosphate (P₃) (Na₅P₃O₁₀) and MgCl₂ were purchased from Fluka (Buchs, Switzerland); L-AMP was chemically synthesized as described in [31,32]. For the HPLC eluent methanol (liquid chromatographic grade) and Pi (Na₂HPO₄·2H₂O) were purchased from Merck (Darmstadt, Germany) and TBA (tetrabutylammonium bromide) from Fluka. Commercial reagents were used throughout this study without further purification.

A stock solution of luciferase was prepared by dissolving the lyophilized powder in HEPES buffer 0.5 M pH 7.5 (44 μM, or approximately 10 mg/mL) and stored at -20 °C. To ensure that the same conditions were used throughout the work, all stock solutions were prepared in deionized water, divided into small aliquots, and stored at -20 °C.

2.2. Enzymatic assays

2.2.1. Method A

A reaction mixture was prepared in ice and contained MgCl₂ (4 mM), HEPES buffer (100 mM) pH 7.50, L-AMP (40 μM) and the sample or PPI standards. The reaction was initiated by the addition of luciferase (0.1 μM) to obtain a final volume of 20 μL, and the tubes were incubated for 15 min at room temperature (25 °C). To stop the reaction the tubes were transferred to ice, 40 μL of cold deionized water was added and the tubes were heated in a water bath at 100 °C for 2 min to denature the enzyme. Afterwards the tubes were allowed to cool, centrifuged (16,100 × g, 2 min) and the supernatants were analyzed. Controls were prepared by replacing the sample or PPI standard with deionized water and adding denaturated luciferase (100 °C for 2 min).

All values indicated are final concentrations.

2.2.2. Method B

The bioluminescence assays were performed in a homemade luminometer using a commercial photomultiplier tube (HC135, Hamamatsu, Middlesex, USA).

A reaction mixture was prepared in ice into a transparent test tube containing MgCl₂ (2 mM), HEPES buffer (50 mM) pH 7.50, L-AMP (2 μM) and luciferase (50 mM). The reaction was initiated by the injection of 30 μL of D-LH₂ (30 μM), and the mixture was incubated for 30 s. Injections of 50 μL of sample or PPI standards were made to obtain a final volume of 100 μL. The reaction was allowed to proceed for 2 min, throughout the process the emitted light was recorded and integrated over 0.1 s intervals.

All values indicated are final concentrations and the enzymatic reaction took place at room temperature (25 °C).

2.3. Chromatographic instrumentation and conditions

The chromatographic system was constituted by a isocratic pump (Hewlett-Packard 1100 Series, Boeblingen, Germany), a manual sample injection valve with a 20-μL loop (Rheodyne 7725i, Rohnert Park, USA), a silica-based C₁₈ reversed-phase column (Hypersil ODS column 4.6 mm × 100 mm, 5.0 μM, Agilent, Santa Clara, USA) and a photodiode array detector (UV 6000LP with a 50 mm LighPipe flowcell, Thermo Scientific, San Jose, USA). Elutions were performed at a constant flow rate (0.5 mL/min) under isocratic conditions. The mobile phase was composed of methanol in water (20%, v/v), TBA (20 mM) and Pi buffer (60 mM) pH 7.0.

The ATP peaks were identified by their retention time in relation to an ATP standard (ATP 25 μM diluted 1:2 in deionized water) at 260 nm.

2.4. Methods characterization

2.4.1. Method A

To obtain the linear response range calibration curves were made. PPI standard solutions between 0.1 and 20 μM were prepared in deionized water and assayed as described in Sections 2.2.1 and 2.3.

To evaluate precision, assays described in Sections 2.2.1 and 2.3 were performed with PPI standards of 1 and 8 μM (*n* = 6 each), and the precision was expressed as relative standard deviation (R.S.D.) values.

2.4.2. Method B

To obtain the linear response range calibration curves were made. PPI standard solutions between 0.75 and 6 μM were prepared in deionized water and assayed as described in Section 2.2.2.

To evaluate precision, assays described in Section 2.2.2 were performed with PPI standards of 2.5 and 5 μM (*n* = 6 each), and the precision was expressed as R.S.D. values.

2.5. Sample analysis

2.5.1. Nucleotide interference evaluation

To assess the possible interference from nucleoside triphosphate (NTP) and P₃ enzymatic assays were done as described in Sections 2.2.1 and 2.3. The concentration range used was between 500 and 2000 μM for CTP and UTP and between 100 and 400 μM for P₃.

To further confirm that no interference was exerted by the nucleotides a recovery assay was performed by spiking an aqueous solution of CMP (500 μM) with a 2 μM PPI standard solution. A control was made by replacing the nucleotide with deionized water and adding a 6 μM PPI standard solution. Both assays were performed as described in Sections 2.2.1 and 2.3. Curves were obtained by the method of standard additions (PPI standard solutions between 2 and 16 μM).

2.5.2. PPI quantification

The quantification of PPI in nucleotides and P₃ preparations was done by using the method of standard additions. Aqueous solutions of the nucleotides (500 μM in method A and between 200 and 1500 μM in method B) and P₃ (100 μM in method A and between 100 and 200 μM in method B) were prepared and kept in ice. The assays were performed as described in Sections 2.2.1, 2.2 and 2.3 with the addition of PPI standard solutions between 2 and 16 μM

in method A and between 0.75 and 6 μM in method B. In method B PPI standards were co-injected with samples.

If not analyzed immediately the samples were kept at -20°C after the enzymatic reactions.

2.6. Data analysis

Experimental designs and calculations were done using *The Unscrambler*[®] v. 9.2 (CAMO ASA, Oslo, Norway). Evaluation of the global linear model, global quadratic model, quadratic effects and the shape of the response surfaces was done by analysis of variance (ANOVA) through the Fisher-ratio (*F*-ratio), the *p*-value and using the values of a multiple linear regression analysis (regression coefficients and the corresponding standard errors), respectively [33–36]. The criteria for considering a factor as statistically significant were higher *F*-ratios and the regression coefficients higher than the corresponding standard errors. The analysis of the critical effects was done by using the algorithm of Dong [36,37].

All calculations were done with a *Microsoft*[®] *Excel* spreadsheet. From calibration curves set up by means of the least square method the limits of detection (LOD) and limits of quantitation (LOQ) were calculated as the analyte concentrations which fulfill the following criteria: $\text{LOD} = (a + 3S_{y/x})$ and $\text{LOQ} = (a + 10S_{y/x})$, where *a* is the intercept of the calibration curve and $S_{y/x}$ is the random error in the *y*-direction [38].

In both methods (A and B) PPI concentration was obtained by the method of standard additions. In method A regression lines were obtained by plotting the areas of ATP formed (at 260 nm) in the enzymatic reaction as a function of the concentrations of PPI standards added to the samples. The ATP peak areas were integrated using the HPLC software package (*Excalibur*[™] v. 1.4 SR1, Thermo Scientific, San Jose, USA) and the control tubes' areas were subtracted to eliminate the background noise. The PPI concentration in the sample was given by the ratio of the intercept and the slope of the regression lines. In method B regression lines were obtained by plotting the initial velocity of the reaction as a function of the concentrations of PPI standards added to the samples. The initial velocity was obtained for each experimental point by plotting the recorded emitted light as a function of time and calculating the slope of the linear portion of these plots, which corresponds to the first 20 s of reaction (Fig. 3). The PPI concentration in the sample was given by the ratio of the intercept and the slope of the regression lines.

3. Results and discussion

3.1. Factorial analysis of method A

The methodology under development is constituted by an enzymatic reaction coupled to the chromatographic detection of ATP. The IP-HPLC detection of ATP is a well-established analytical procedure and was not subjected to optimization [39]. The important factors identified in the enzymatic assay were the incubation time (t_{inc}), the enzyme's inactivation time (t_{inac}), the assay's pH (pH) and the concentrations of L-AMP ([L-AMP]) and luciferase ([Luc]), which were analyzed to test their importance to the method's sensitivity. Because of the relatively large number of factors to analyze, a screening design (fractional factorial design) with five factors and two levels (plus a center level) was formulated with ten experiments (eight cube experiments plus two samples in center conditions). Table 1 summarizes the experimental design created.

From the analysis of variance (ANOVA) it was concluded that pH, t_{inc} and [L-AMP] have the highest influence over the system's response (data not shown). The analysis of the critical effects using the algorithm of Dong confirmed the ANOVA results. Indeed, taking into consideration the effects of the factors analyzed ($t_{\text{inc}} = 21,440$; $t_{\text{inac}} = 10,000$; pH = 17,000; [L-AMP] = 24,690; and [Luc] = 2177) and that the margin of error is 19,665 and the simultaneous margin of error is 36,513, only the factors t_{inc} and [L-AMP] were considered to be statistically significant [36,37].

From the response surfaces (Fig. 1A–C) it was verified that the better responses could be attained using lower [L-AMP] and higher t_{inc} and pH values. As the maximum value of pH tested is also the optimal value for luciferase activity it was kept constant at 7.50. Furthermore, as [Luc] and t_{inac} do not significantly affect the response they were fixed at the minimum values tested, 0.1 μM and 2 min, respectively.

In order to achieve the optimum (most sensitive) conditions, the factors previously identified as critical, [L-AMP] and t_{inc} , were analyzed under a central composite design constituted by eleven experiments (eight cube experiments plus three samples in center conditions) (Table 1). The analysis of the effects focused on the main effects, two-way interactions and quadratic terms. The ANOVA results (data not shown) and the response surface (Fig. 1D) showed that the longer the t_{inc} the better the results. However, for [L-AMP], a more complex result was obtained since both low and high concentrations originated good and equivalent responses. To

Table 1
Experimental designs, factors and corresponding levels researched.

Factor	Levels				
Method A (HPLC)					
Fractional factorial design					
L-AMP concentration ([L-AMP]) (μM)	80		100		120
Luciferase concentration ([Luc]) (μM)	0.10		0.55		1.00
pH (pH)	7.00		7.25		7.50
Incubation time (t_{inc}) (min)	5		10		15
Inactivation time (t_{inac}) (min)	2		3		4
Central composite design					
[L-AMP] (μM)	41.7	50	70	90	98.2
t_{inc} (min)	8	10	12.3	15	16
Method B (bioluminescence)					
Full factorial design I					
[Luc] (nM)	10		50		90
[L-AMP] (μM)	0.2		0.7		1.2
Full factorial design II					
[L-AMP] (μM)	1		3		5
Luciferin concentration ([LH ₂]) (μM)	10		20		30

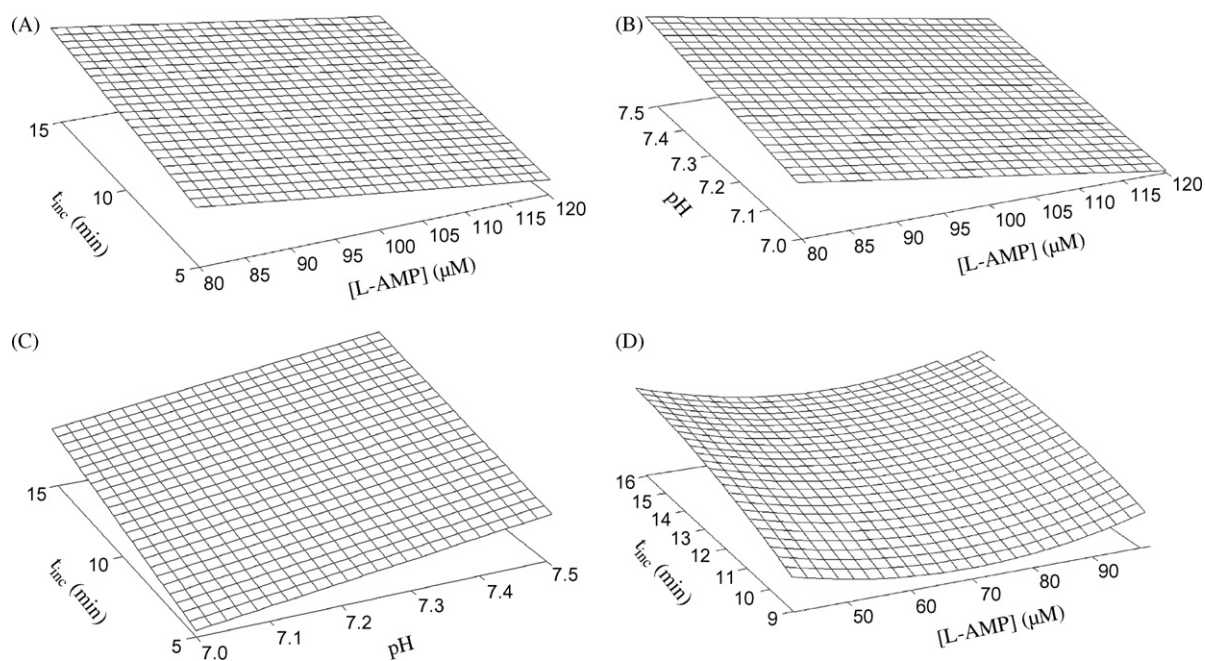


Fig. 1. Response surfaces for the optimization of method A. From (A) to (C), fractional factorial design and (D) central composite design. The surfaces represent the most significant factors to the method's response evaluated by the analysis of variance (ANOVA) in each design. (A) t_{inc} vs [L-AMP]; (B) pH vs [L-AMP]; (C) t_{inc} vs pH; and (D) t_{inc} vs [L-AMP].

check for this result calibration curves with 40 and 90 μM of L-AMP were tested and the results were similar (data not shown). Consequently, the optimum values for the factors analyzed were settled as [L-AMP] = 40 μM and t_{inc} = 15 min.

3.2. Factorial analysis of method B

Method B can be considered experimentally simpler than method A. The key factors were identified as [L-AMP], [Luc] and the concentration of luciferase's substrate, luciferin ([LH₂]). These three factors were analyzed to test about their importance to the method's sensitivity using a two-step approach (Table 1): a three level full factorial design without replicates was used for the analysis of [L-AMP] and [Luc] (nine experiments); and a three level full factorial design with three replicates was used for the analysis of [L-AMP] and [LH₂] and to check if there were any interaction within these two factors (twenty seven experiments). Taking into consideration that luciferase is a quite expensive reagent the first design was planned to be relatively economic (only nine experiments were done).

The ANOVA results (data not shown) and the analysis of the response surfaces (Fig. 2A) showed that [L-AMP] was the most

important factor and the higher was its concentration the higher was the initial velocity of light production. Although [Luc] also affected significantly the method's response there was not a clear trend (Fig. 2A). Taking into consideration the cost of the enzyme and that it was verified an interaction between [Luc] and [L-AMP] (ANOVA, data not shown) its concentration was fixed at 50 nM.

The analysis of the effects of [L-AMP] and [LH₂] on the method's response (Fig. 2B) showed that in the concentration range studied only [LH₂] had a significant effect and the higher the concentration the higher was the bioluminescent signal. Accordingly [LH₂] was fixed at the highest concentration analyzed (30 μM) and [L-AMP] = 2.0 μM (slightly above the maximum [L-AMP] used in the first experimental design). Under these optimized conditions ([L-AMP] = 2 μM ; [Luc] = 50 nM; [LH₂] = 30 μM) the response of the bioluminescent system is proportional to PPI, as can be seen in Fig. 3 for several PPI concentrations.

3.3. Figures of merit of the optimized methods

Using the optimized conditions for method A calibration curves for PPI in water were obtained showing linear trends in the concentration range between 0.1 and 20 μM (correlation coefficients

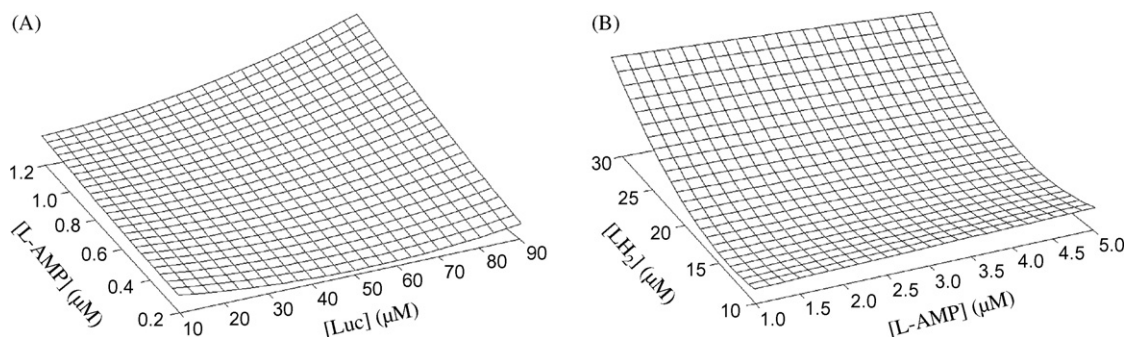


Fig. 2. Response surfaces for the optimization of method B (both full factorial designs). (A) [L-AMP] vs [Luc]; and (B) [LH₂] vs [L-AMP].

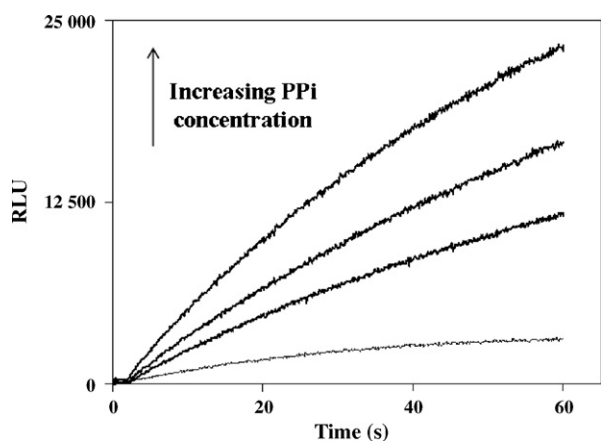


Fig. 3. Time course of the light emitted in the bioluminescent reaction under optimized conditions (method B) for several PPI concentrations: 0.75, 2.25, 3.00, and 4.50 μM . RLU, relative light units.

greater than 0.999). From the calibration curves the LOD and the LOQ were estimated as 0.5 and 1.8 μM , respectively. The precision (R.S.D.) of the method for the assay of PPI in aqueous solutions was 7.4% at 1 μM PPI and 5.9% at 8 μM PPI.

Regarding method B calibration curves for PPI in water showed linear trends in the concentration range between 0.75 and 6 μM (correlation coefficients greater than 0.99), the LOD and the LOQ were estimated as 0.624 and 2.23 μM , respectively, and the precision of the method was 5.1% at 2.5 μM PPI and 4.9% at 5 μM PPI.

3.4. Method A PPI quantification

Several aqueous solutions of nucleotides and P_3 were prepared and analyzed using the optimized assay. Fig. 4 shows responses of the assay as a function of the concentrations of CTP, UTP and P_3 . The analysis of this figure showed that an increase in CTP and P_3 concentrations provoked a marked increase on the ATP enzymatic

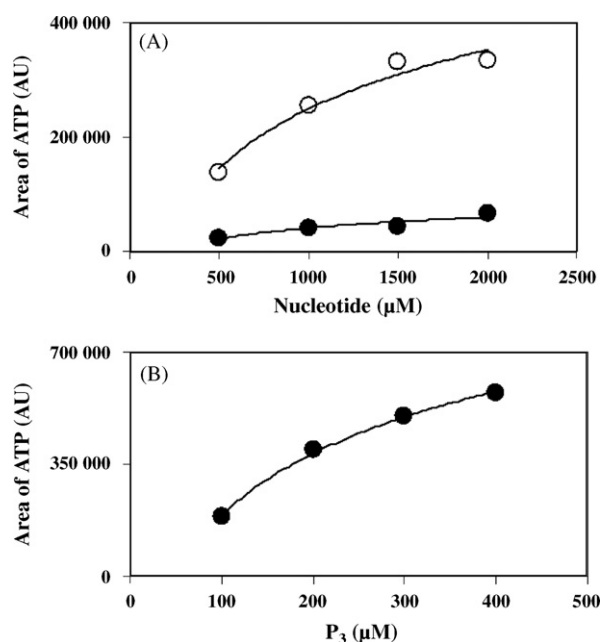
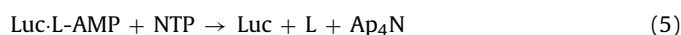
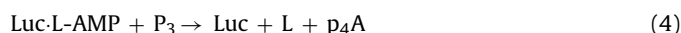


Fig. 4. Effect of (A) NTP [CTP (○) and UTP (●)] and (B) P_3 in the response of the optimized method A. AU, absorbance units.

production while for UTP a relatively constant amount of ATP was produced. Also, the responses for CTP and P_3 were characterized by a slightly curvilinear dependence with their concentration, particularly in relatively high concentrations (above 1.5 mM for CTP and above 400 μM for P_3 , respectively). These results suggested that CTP and P_3 have a higher PPI contamination than UTP and that they interfere with the response.

This interference is due to the reaction of P_3 with L-AMP leading to L and adenosine 5' tetraphosphate [p_4A] (4), a well established dark (lateral) reaction catalyzed by luciferase [30,40]. In fact, luciferase catalyzes the synthesis of adenosine(5')tetraphospho(5')nucleosides (Ap_4N) from any NTP containing an intact terminal pyrophosphate and L-AMP (5) [30,32,40,41]. Although a relatively slow rate of p_4A and Ap_4N production is usually observed in typical luciferase reaction conditions [32], it was observed that the areas of p_4A , which could also be detected by IP-HPLC under method A's assay conditions, increased proportionally with the increase in P_3 concentration (data not shown). In order to avoid this interference and to minimize matrix effects low concentrations of nucleotides, and especially of P_3 , should be used, PPI concentration should be corrected using the area of p_4A formed and the method of standard additions should be applied.



Recovery assays of 2 μM (107.9%) and 6 μM (100.7%) PPI in CMP (500 μM) and in water respectively, using the method of standard additions, confirmed that this approach abrogated the interferences of the analytes in the method's response, and also showed that the new method presents a good accuracy.

Fig. 5A shows typical curves for the determination of PPI in CTP, AMP and P_3 solutions by the method of standard additions. The analysis of this figure clearly showed that CTP and P_3 had a PPI contamination whereas AMP was almost free of PPI, as can be deduced by observing the extension of the curve's extrapolation in the x-axis. Also, a control curve where the samples were replaced with deionized water (Fig. 5A) was parallel to CTP and P_3 curves and superimposed with the AMP curve, thus confirming the referred results. The results of the PPI analysis in the samples were the following (molar percentages): CTP 1.1%; UTP 0.18%; CDP 0.41%; and UDP 0.19%. The nucleotides CMP (0.11%), UMP (0.06%), ADP (0.14%) and AMP (0.14%) have only traces of PPI contamination (values of PPI concentration \leq LOD). The PPI contamination of P_3 was 9.1%.

3.5. Method B PPI quantification

The same nucleotides and P_3 were analyzed for PPI contamination through method B. Fig. 5B presents the curves obtained for CTP, AMP and P_3 plus a control in water. Analogously to method A it was verified a relatively high PPI content in CTP and P_3 and a low PPI contamination in AMP. The results for all the tested compounds were the following (PPI contamination in molar percentages): CTP 0.84%; UTP 0.24%; CDP 0.51%; UDP 0.15%; CMP 0.09%; UMP 0.06%; ADP 0.21%; AMP 0.23%; and P_3 9.4%.

A comparison of the two methods through the PPI percentages calculated by each of them is shown in Fig. 5C. The plot has a linear shape with the following linear least squares fitting equation: $\text{PPI}\% (\text{method A}) = 0.0068 + 0.97 \text{ PPI}\% (\text{method B})$. The correlation coefficient is 0.9993 (nine data points) and the confidence limit at the 95% significance level is for the intercept $[-0.098; 0.11]$ and for the slope $[0.94; 1.0]$. This result showed that the two methods give similar estimates of the PPI content in commercial nucleotides and P_3 preparations without any systematic error [38].

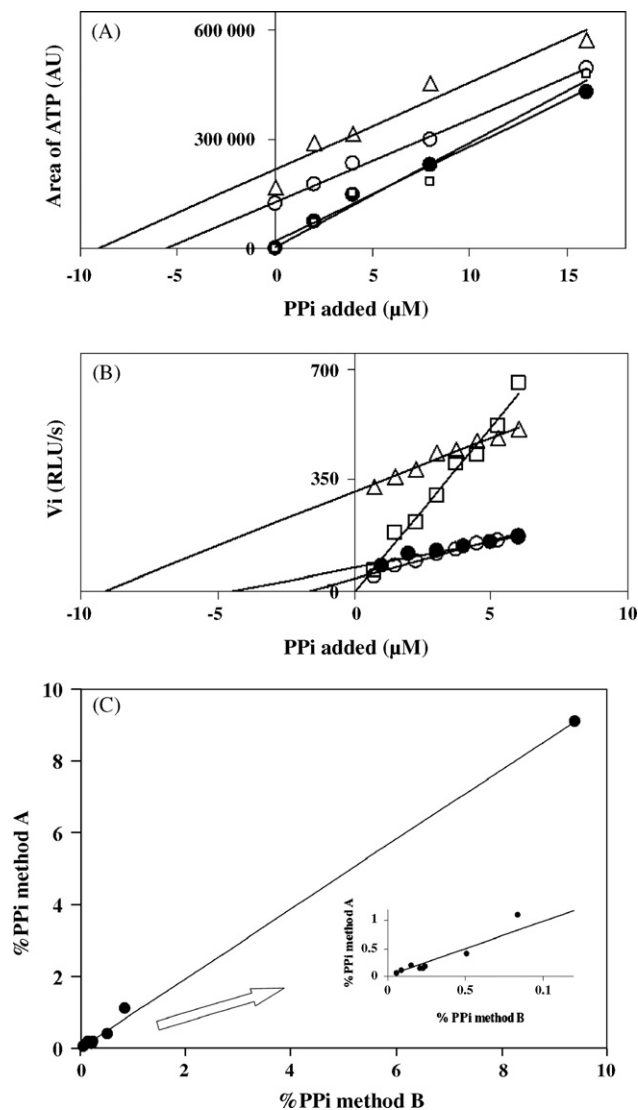


Fig. 5. PPI assay by (A) method A and (B) method B in CTP (\circ), AMP (\bullet) and P_3 (Δ). Controls where samples were replaced with deionized water (\square) are also shown in each method. The curves were obtained by the method of standard additions. (C) Comparison of the two analytical methods by a regression line of the percentages of PPI calculated for both methods. *Inset:* Magnification of the low-range PPI percentages (below 1% PPI content). AU, absorbance units; RLU, relative light units; V_i , initial velocity.

4. Conclusions

In this work two novel optimized methods for PPI measurement are presented. They are enzyme-based assays that use luciferase to catalyze the production of ATP from PPI and L-AMP, followed by the quantification of ATP by IP-HPLC with detection at 260 nm (method A) or by bioluminescence (method B). The success of method A is based on enzymatic and chromatographic selectivity and method B on enzyme selectivity and fast assay time. Another advantageous feature of these new methods is that the enzymatic assay only requires luciferase, whereas in other enzymatic-based methods for PPI quantification a multiple enzyme system is required [9–20], making then costly (not only because enzymes are expensive and sensitive reagents but also because more substrates are needed). These methods were particularly designed to measure PPI present as contaminant in nucleotides and other biochemical substances preparations,

however they can easily be applied to other biochemical samples.

The experimental design methodology used in the methods' optimization allowed, after a relatively small number of experiments, the determination of the experimental factors that make the methods quite sensitive and robust. The limit of detection of PPI in these optimized methods is below the micromolar concentration range, which is the range of normal PPI concentrations in human fluids [9,42], so these new methods could also be applied, for example, to clinical evaluation of PPI.

In conclusion these new assays are suitable for PPI quantification in the micromolar concentration range. They do not require complex experimental procedures and many samples can be handled during the same analysis. Furthermore they can be applied to determine the level of PPI in commercial reagents where the presence of this compound must be detected and quantified.

Acknowledgements

A research grant (to Simone M. Marques) from the Faculty of Sciences of University of Porto is acknowledged. Financial support from University of Porto and Caixa Geral de Depósitos (Project IPG136) and from Fundação para a Ciência e Tecnologia (Lisbon) (FSE-FEDER) (Project PTDC/QUI/71366/2006) is also acknowledged.

References

- [1] J.K. Heinonen, Biological Role of Inorganic Pyrophosphate, Kluwer Academic Publishers, Norwell, 2001, pp. 1–28.
- [2] H.G. Wood, N.H. Goss, Proc. Natl. Acad. Sci. U.S.A. 82 (1985) 312.
- [3] M. Perrotte-Piquemal, A. Danchin, F. Biville, Biochimie 81 (1999) 245.
- [4] J.R. Pérez-Castiñeira, R. Gómez-García, R.L. López-Marqués, M. Losada, A. Serano, Int. Microbiol. 4 (2001) 135.
- [5] A. Dupaix, G. Johannin, B. Arrio, FEBS Lett. 249 (1989) 13.
- [6] A. Mustroph, G. Albrecht, M. Hajirezaei, B. Grimm, S. Biemelt, Ann. Bot. 96 (2005) 717.
- [7] R.A. Terkeltaub, Am. J. Physiol. Cell Physiol. 281 (2001) C1.
- [8] K.A. Lomashvili, S. Cobbs, R.A. Hennigar, K.I. Hardcastle, W.C. O'Neill, J. Am. Soc. Nephrol. 15 (2004) 1392.
- [9] G. Lust, J.E. Seegmiller, Clin. Chim. Acta 66 (1976) 241.
- [10] H.L. Drake, N.H. Goss, H.G. Wood, Anal. Biochem. 94 (1979) 117.
- [11] H. de Groot, H. de Groot, T. Noll, Biochem. J. 230 (1985) 255.
- [12] P. Nyrén, A. Lundin, Anal. Biochem. 151 (1985) 504.
- [13] B.A. Barshop, D.T. Adamson, D.C. Vellom, F. Rosen, B.L. Epstein, J.E. Seegmiller, Anal. Biochem. 197 (1991) 266.
- [14] R.H. Upson, R.P. Haugland, M.N. Malekzadeh, R.P. Haugland, Anal. Biochem. 243 (1996) 41.
- [15] V. Jansson, K. Jansson, Anal. Biochem. 304 (2002) 135.
- [16] M. Tagiri-Endo, Anal. Biochem. 315 (2003) 170.
- [17] V. Jansson, K. Jansson, Anal. Biochem. 317 (2003) 268.
- [18] H. Arakawa, K. Karasawa, T. Igarashi, S. Suzuki, N. Goto, M. Maeda, Anal. Biochem. 333 (2004) 296.
- [19] H. Nakamura, R. Yamazaki, T. Shirai, H. Sano, Y. Nakami, K. Ikebukuro, K. Yano, Y. Nomura, Y. Arikawa, Y. Hasebe, Y. Masuda, I. Karube, Anal. Chim. Acta 518 (2004) 45.
- [20] Y. Sun, K.B. Jacobson, V. Golovlev, Anal. Biochem. 367 (2007) 201.
- [21] N. Yoza, I. Akazaki, T. Nakazato, N. Ueda, H. Kodama, A. Tateda, Anal. Biochem. 199 (1991) 279.
- [22] O. Hénin, B. Barbier, A. Brack, Anal. Biochem. 270 (1999) 181.
- [23] Y.J. Jang, E.J. Jun, Y.J. Lee, Y.S. Kim, J.S. Kim, J. Yoon, J. Org. Chem. 70 (2005) 9603.
- [24] H.K. Cho, D.H. Lee, J.I. Hong, Chem. Commun. 13 (2005) 1690.
- [25] H.N. Lee, K.M.K. Swamy, S.K. Kim, J.-Y. Kwon, Y. Kim, S.-J. Kim, Y.J. Yoon, J. Yoon, Org. Lett. 9 (2007) 243.
- [26] J.W. Hastings, W.D. McElroy, J. Coulombre, J. Cell Comp. Physiol. 42 (1953) 137.
- [27] W.C. Rhodes, W.D. McElroy, J. Biol. Chem. 233 (1958) 1528.
- [28] H. Fraga, J.C.G. Esteves da Silva, R. Fontes, ChemBioChem 5 (2004) 110.
- [29] H. Fraga, Photochem. Photobiol. Sci. 7 (2008) 146.
- [30] R. Fontes, D. Fernandes, F. Peralta, H. Fraga, I. Maio, J.C.G. Esteves da Silva, FEBS J. 275 (2008) 1500.
- [31] L.J. Bowie, Method. Enzymol. 57 (1978) 15.
- [32] H. Fraga, J.C.G. Esteves da Silva, R. Fontes, FEBS Lett. 543 (2003) 37.
- [33] J.C.G. Esteves da Silva, J.R.M. Dias, J.M.C.S. Magalhães, Anal. Chim. Acta 450 (2001) 175.

- [34] P.B.M. Pinheiro, J.C.G. Esteves da Silva, *Anal. Bioanal. Chem.* 382 (2005) 341.
- [35] P.M.S.M. Rodrigues, J.C.G. Esteves da Silva, M.C.G. Antunes, *Anal. Chim. Acta* 595 (2007) 266.
- [36] D.L. Massart, B.G.M. Vandeginste, L.M.C. Buydens, S. de Jong, P.J. Lewi, J. Smeyers-Verbeke, *Handbook of Chemometrics and Qualimetrics: Part A (Data Handling in Science and Technology, vol. 20A)*, Elsevier, Amsterdam, 1997, pp. 643–738.
- [37] F. Dong, *Stat. Sinica* 3 (1993) 209.
- [38] J.N. Miller, J.C. Miller, *Statistics and Chemometrics for Analytical Chemistry*, 4th edition, Dorchester, Pearson Prentice Hall, 2000, pp. 107–150.
- [39] D. Di Pierro, B. Tavazzi, C.F. Perno, M. Bartolini, E. Balestra, R. Calìò, B. Giardina, G. Lazzarino, *Anal. Biochem.* 231 (1995) 407.
- [40] A. Sillero, M.A.G. Sillero, *Pharmacol. Therapeut.* 87 (2000) 91.
- [41] R. Fontes, B. Ortiz, A. de Diego, A. Sillero, M.A.G. Sillero, *FEBS Lett.* 438 (1998) 190.
- [42] D.C. Silcox, D.J. McCarty, *J. Clin. Invest.* 52 (1973) 1863.



Multiple small volume microwave-assisted digestions using conventional equipment for multielemental analysis of human breast biopsies by inductively coupled plasma optical emission spectrometry

J. Millos^b, M. Costas-Rodríguez^a, I. Lavilla^a, C. Bendicho^{a,*}

^a Departamento de Química Analítica y Alimentaria, Área de Química Analítica, Facultad de Química, Universidad de Vigo, As Lagoas-Marcosende s/n, 36310 Vigo, Spain

^b Centro de Apoyo Científico Tecnológico a la Investigación, Universidad de Vigo, As Lagoas-Marcosende s/n, 36310 Vigo, Spain

ARTICLE INFO

Article history:

Received 11 July 2008

Received in revised form

15 September 2008

Accepted 21 September 2008

Available online 27 September 2008

Keywords:

Multiple small volume microwave-assisted digestions

Human breast biopsies

Trace elements

Inductively coupled plasma optical emission spectrometry

ABSTRACT

A multiple microwave-assisted digestion procedure using small PTFE closed vials (6 mL capacity) inserted into conventional microwave digestion vessels has been developed as a fast, efficient and clean methodology for multielemental analysis of human breast biopsies by inductively coupled plasma optical emission spectrometry. This small volume strategy allows drastically diminishing the volume of acid needed for digestion, and in turn, a decrease in sample dilution and an increase in sample throughput is achieved. A 2_{IV}^{4-1} fractional factorial design was used for screening optimization of four variables that can influence the digestion efficiency: (A) nitric acid volume, (B) pre-digestion step, (C) microwave power, and (D) digestion time. A validation study included linearity, precision, detection and quantification limits. Validation against different biological certified reference materials (CRMs) was also performed.

The digestion method is suitable for the determination of Al, Ca, Cu, Fe, K, Mg, Mn, P, S and Zn in small size biological samples such as breast biopsies (<30 mg dry mass). Forty-seven biopsies from 39 women were analyzed: 20 samples from healthy women corresponding to mammoplasties and 27 samples from patients suffering from cancer pathology (19 corresponded to tumour and 8 to adjacent normal tissue). A significant accumulation of Al, Ca, Cu, K, Mg, Mn, P and Zn was found in tumour as compared to healthy tissues. When this comparison is made for tumour and adjacent tissues, a significant accumulation of Al, Mg, P and Zn in tumour tissues was observed. Finally, only Ca significantly accumulates in the adjacent tissues as compared to healthy tissues.

© 2008 Elsevier B.V. All rights reserved.

1. Introduction

Breast cancer is, among women worldwide, the most common cause of cancer. The American Cancer Society estimated 238,510 new female breast cancer cases and 40,460 deaths in 2007 [1]. Many trace elements play an essential role in numerous biological processes, including carcinogenesis. Significant differences in concentration of some elements in cancerous tissues and normal tissues have been observed [2–8]. The role of these elements in the development or inhibition of cancer is still unclear and numerous investigations are carried out on this subject. Many of these studies have focused on metal induced carcinogenicity, oxidative stress caused by metals being the most important mechanism [9]. However, some of these elements are involved at the same time in the antioxidant defense, i.e. taking part of enzymes such as superoxide dismutases [10], and then, it is still under discussion if the

accumulation of these elements is a consequence or a need for the development of the disease [7].

Therefore, in view of the state of the art concerning elements and cancer, the simultaneous determination of several elements in human biopsies is increasingly demanded. Different multielemental analytical techniques have been used for biopsies samples: X-ray fluorescence that has been the most used with this purpose [2,8,11–16], X-ray emission [4–17], instrumental neutron activation analysis [6–18] and more recently, inductively coupled plasma mass spectrometry (ICP-MS) [5,15,19]. Application of non-destructive techniques requires sophisticated and expensive equipment and hence, inductively coupled plasma optical emission spectrometry (ICP-OES) can be an alternative for determining some essential and non-essential elements. Only in a few papers this technique has been applied to the analysis of human biopsies [20–22]. Basle et al. [20] determined Na, K, Mg, Cu, Zn, Fe, Sr, Al, B and Si in cortical bone, Hamada et al. [21] analyzed liver from children with hepatobiliary disease to determine Mg, Zn and Cu and Olszewski et al. [22] determined Al and Pb in tissue biopsies from patients with laryngeal papilloma or cancer.

* Corresponding author. Tel.: +34 986 812281; fax: +34 986 812556.
E-mail address: bendicho@uvigo.es (C. Bendicho).

Microwave-assisted digestion with acids is a sample treatment usually needed when ICP-OES is selected as the determination technique. The small quantity of sample available as well as the low elemental concentration makes the use of conventional digesters troublesome. Usually, the digestions are carried out in large volume PTFE vessels (50–120 mL approximately) and this results in relatively large volumes (e.g. 10–25 mL). Small volume digestion strategies can be necessary when small samples are analyzed to avoid the important loss in sensitivity that occurs because of dilution.

Small vessels for microwave digestion (20 mL) [23], polystyrene or glass liners (15 and 20 mL, respectively) [19–24] and Teflon closed vials (7 mL or 6 mL) into a conventional microwave vessel [15,25–29] have been used for organic and biological microsamples. Many of these liners usually need specific microwave ovens and rotors, and therefore, they cannot be easily amenable to all laboratories. When the number of samples to be analyzed increases, the use of several vials heated in a conventional microwave vessel would significantly increase sample throughput with no changes in the conventional microwave digester.

In a previous work, a microwave-assisted digestion method based on the use of small PTFE vials inserted into a conventional microwave vessel for ultratrace element determination in breast biopsies by ICP-MS was reported [30].

In this work, we extend this method to the determination of essential (Ca, Cu, Fe, K, Mg, Mn, P, S, Zn) and non-essential (Al) elements in breast biopsies by ICP-OES. The effects of the relevant variables involved in the digestion procedure were evaluated by means of a 2_{IV}^{4-1} fractional factorial design. Forty-seven breast biopsies from both healthy women and women with breast cancer pathology were analyzed. A statistical comparison among elemental contents in tumour tissues, adjacent-to-tumour tissues and healthy tissues (i.e. from mammoplasties) was made.

2. Experimental

2.1. Instrumentation

Atomic emission measurements were performed with a PerkinElmer (Überlingen, Germany) model Optima 4300 DV inductively coupled plasma atomic emission spectrometer, equipped with a PerkinElmer autosampler model AS90 plus and WinLab32™ Software. Axial viewing mode was used. The instrumental settings and operating conditions are shown in Table 1.

Digestions of breast biopsies and certified reference materials (CRMs) were carried out with a microwave digestion system Multiwave 3000 Oven (Anton Paar, Graz, Austria) equipped with a rotor of 8 PFA digestion vessels of 100 mL volume. PFA closed vials of 6 mL capacity (Saville, Minnetonka, USA) inserted into 100 mL capacity vessels were used. Fig. 1 shows a cross section of a digestion vessel with the three vials inside. The dimensions of the vials (60 mm height, 10 mm diameter) and those of the microwave vessels (200 mm height, 25 mm diameter) allow inserting three vials, one over the other.

A Retsch (Haan, Germany) mixer mill MM 2000, equipped with 10 mL capacity agate cups and agate balls, was used for grinding biopsy samples.

2.2. Reagents and standards

High-purity deionised water (resistance 18 MΩ cm) from a Milli Q water purification system (Millipore, San Quentin, France) and ultrapure grade HNO₃ (Hyperpur-Plus, Panreac, Barcelona, Spain) were used throughout the work. A multielement standard stock solution containing 10 mg L⁻¹ (Cu, Mg and Mn) and 100 mg L⁻¹ (Al, Ca, Fe, K and Zn) (ICP Multi Element Standard Certipur® VI

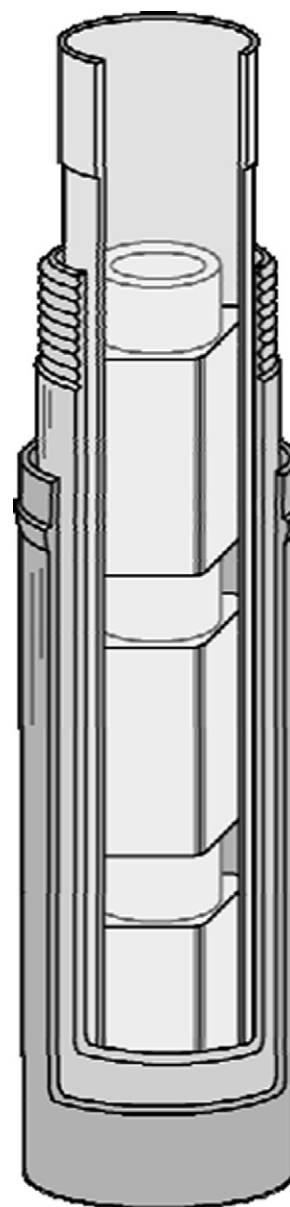


Fig. 1. Teflon perfluoroalkoxy (PFA) small vials inserted into a conventional Teflon PFA microwave vessel.

Merck, Darmstadt, Germany) and single element stock solutions of 1000 mg L⁻¹ (P and S) (CPI International, USA) were used for calibration. Internal standardization was carried out with ¹¹⁵In (2 μg L⁻¹) prepared from a single element standard stock solution of 1000 mg L⁻¹ (Merck). All standards were prepared daily by dilution with HNO₃ 2% (v/v).

In order to avoid contamination, clean procedures during sampling, handling and analysis were adopted. All glassware and polyethylene containers were previously washed and kept for 24 h in 10% (v/v) nitric acid and then were rinsed at least three times with ultrapure water. All manipulations were carried out in a Class 100 laminar flow hood (Cruma, Barcelona, Spain) inside a clean room.

2.3. Sampling and sample preparation

Forty-seven biopsies corresponding to 39 women were provided by the POVISA Hospital (Vigo, Spain). Twenty samples corresponded to healthy women (i.e. mammoplasties). Twenty-seven

Table 1
Instrumental parameters and operating conditions for ICP-OES with Perkin-Elmer Optima 4300 DV.

Radiofrequency power (W)	1500
Plasma gas flow (L min ⁻¹)	15.0
Auxiliary gas flow (L min ⁻¹)	0.2
Nebuliser gas flow (L min ⁻¹)	0.4
Sample flow rate (mL min ⁻¹)	2
Nebuliser	Concentric glass, Meinhard Type K
Spray chamber	Cyclonic
Stabilization time (s)	15
Replicate time (s)	5
Replicates	3
Detection wavelengths (nm)	Al (396.153); Ca (317.933); Cu (327.393); Fe (238.204); K (766.490); Mg (285.213); Mn (257.610); P (213.617); S (181.975); Zn (206.200)

biopsies corresponded to women who had been diagnosed with breast cancer, nineteen of which belonged to tumour tissue and eight to adjacent normal tissues. Patients were mostly resident in the area of Vigo (109 km², 465,000 inhabitants) and entered into this study before any chemotherapy or radiotherapy. The average age of these patients was 59 years, with a range between 29 and 91 years. For the healthy women group, the average age was 39 years (range 21–67). In this area, breast cancer deaths per 100,000 inhabitants were 27.0 in 2002 [31]. This figure is bigger than that corresponding to USA in the same year (24.2) [1].

Among 19 tumour breast biopsies, 15 corresponded to malignant tumours and 4 to benign tumours (fibroadenomas). Among the malignant tumours, 13 corresponded to invasive ductal carcinomas (IDC) and 2 to invasive lobular carcinomas (ILC). Five tumours corresponded to stage I (evidence of tumour growth), seven to stage II (local spread), one to stage III (extensive local and regional spread) and two to stage IV (metastasis).

Once collected, biopsies were subjected to cryogenic freezing for preservation. In the lab, biopsies were rinsed in ultrapure water and dried at 60 °C to constant weight. Then, biopsies were ground with a mixer mill for 3 min and stored in closed polyethylene vessels at 4 °C until analysis.

2.4. Small volume microwave-assisted digestion procedure

A portion of biopsy sample (20–30 mg) was accurately weighed into a Teflon PFA closed vial. A volume of 0.3 mL of concentrated nitric acid was added. Three closed vials were prepared and placed into the Teflon PFA conventional microwave vessel (Fig. 1). Next, 6 mL of water were added to increase the external pressure and facilitate a uniform heating. In total, with eight conventional digestion vessels, 24 digestions can be made in a heating run. After heating and cooling, the digests were made up to volume using 5 mL flasks. With each set of digestions a blank was included. Three subsamples of each biopsy were digested.

Four certified reference materials were employed for validation purposes: BCR 185R (bovine liver) from the Institute for Reference Materials and Measurements (IRMM, Geel, Belgium) and DORM-2 (dogfish muscle), TORT-2 (lobster hepatopancreas) and DOLT-3

(dogfish liver) from the National Research Council Canada (NRCC, Ottawa, Canada).

2.5. ICP-OES determination

Elements were determined by ICP-OES (axial configuration). Non-spectral interferences in the plasma were reduced by careful optimization of the instrumental parameters, use of robust plasma conditions and appropriate wavelengths. The presence of matrix effects was investigated by recovery experiments using the spiked CRM BCR 185R. No interferences were observed for the different elements determined. Then, the determination of elemental concentrations was based on a calibration graph obtained from standard aqueous solutions with addition of In as internal standard. Calibration graphs were built from three replicates measurements.

3. Results and discussion

3.1. Multivariate optimization of digestion procedure

CRM BCR-185R (bovine liver) was used for optimization of digestion procedure. Four variable influencing the digestion were optimized using a 2_{IV}^{4-1} fractional factorial experimental design [32]: (A) volume of nitric acid (0.3 mL level minimum and 0.6 mL level maximum); (B) step of pre-digestion (no, minimum level and yes, maximum level; in the latter, a 450 W power and a 2 min time were employed); (C) power in the digestion step (250 W minimum level and 450 W maximum level); (D) digestion time (15 min minimum level and 30 min maximum level). These values were chosen following preliminary experiments. For any combination of factor levels, the sample was completely digested.

The 2_{IV}^{4-1} experimental design allows assessing the effect of four variables with eight experiments (Table 2). Experiments were run randomly and by triplicate. The emission signal intensity for each experiment was obtained. The significance of variable effects and two-factor interactions (without confusions) was established by comparing their values with twice the statistical error of the design ($2\bar{S}$) and $p < 0.05$. Fig. 2 shows the Pareto bar plots for main effects. As can be observed, neither significant effects nor

Table 2
 2_{IV}^{4-1} fractional factorial design for optimization of small volume microwave-assisted digestion.

Experiment number	Experiment order	Volume of HNO ₃ (mL)	Pre-digestion	Digestion power (W)	Digestion time (min)
1	4	0.3	No	250	15
2	8	0.6	No	250	30
3	6	0.3	Yes	250	30
4	1	0.6	Yes	250	15
5	3	0.3	No	450	30
6	7	0.6	No	450	15
7	2	0.3	Yes	450	15
8	5	0.6	Yes	450	30

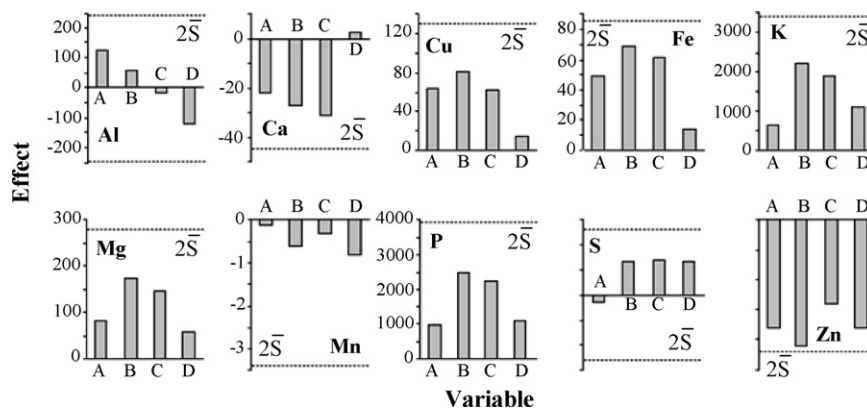


Fig. 2. Main effects obtained for the selected variables (variable A, volume of nitric acid; variable B, pre-digestion step; variable C, microwave power; variable D, time of digestion step). Experimental errors of the design are represented by dashed lines.

significant interactions are present. This allows concluding that any of the studied levels can be used. Criteria of rapidity and economy were selected: (A) 0.3 mL of nitric acid; (B) pre-digestion (longer lifetime of vials and vessels was observed with a 2 min pre-digestion step); (C) 250 W digestion power; (D) 15 min digestion time.

These results indicate an efficient and robust sample digestion methodology. The robustness of this methodology was assessed by comparing the mean concentration value obtained from two sets of results (five independent samples each) obtained with BCR-185R. The first set of data was acquired with proposed operative conditions, while the second one was obtained with different microwave digestion working conditions (0.5 mL of nitric acid, without pre-digestion, 450 W and 20 min). Mean results from the two data sets were compared by means of a *t*-test ($p < 0.05$). The results were statistically comparable and the method is considered to be robust.

3.2. Analytical performance

Table 3 shows validation data: instrumental and procedural limits of detection (LOD) and quantification (LOQ), linearity and repeatability.

Instrumental LODs and LOQs were obtained using the background equivalent concentration (BEC) of the analyte, which was calculated from the ratio of 10 measurements of the blank and the slope of the calibration curve. The LODs were calculated as three times the standard deviation of the blank (3σ criterion) and the LOQs as ten times the standard deviation of the blank (10σ criterion). Procedural LOD and LOQ values in biopsies were determined considering the instrumental LOD and LOQ values and the sample treatment (30 mg of dry sample in 5 mL of solution after digestion and dilution).

Calibration was performed with a series of standard concentrations in the ranges shown in Table 3. In all cases, regression coefficients were higher than 0.999 for calibration curves. Sensitivity was the slope value obtained by least-square regression analysis of the calibration curves.

The precision of the method, expressed as relative standard deviation (RSD), was evaluated in terms of repeatability. RSDs were obtained from five independent digestions and from three replicates of the same digestion. RSDs were lower than 3%.

Different certified reference materials were used to evaluate the accuracy: BCR 185 R (bovine liver), TORT-2 (lobster hepatopancreas), DORM-2 (dogfish muscle) and DOLT-3 (dogfish liver). Table 4 shows the obtained results. Found and certified values were compared using a *t*-test, no significant differences were observed ($t_{\text{exp}} < t_{\text{crit}}$; $n = 5$; $p < 0.05$). For the elements that are not certified in

the different CRMs, recovery experiments with spiked CRM BCR 185R were performed. In all cases, recoveries were in the range 97–104%.

The method displayed adequate analytical characteristics for the elements and samples under study.

3.3. Sample analysis

Forty-seven breast biopsy samples were analyzed following the proposed procedure. Analytical results are summarized in Table 5 as mean, median and range (minimum and maximum) corresponding to tumour, adjacent normal and healthy normal tissues. Three separate digestions of each sample were made. In general, it is possible to observe the accumulation of different elements in tumour breast tissues. This trend can be seen in Fig. 3, where the ratios of average concentration values corresponding to tumour/healthy, tumour/adjacent and adjacent/healthy tissues are plotted. These ratios confirm the order of element concentrations: tumour tissues \geq adjacent normal tissues \geq healthy tissues. Ratios between 1.3 and 5.1 were obtained when the mean values of tumour and healthy tissues are considered, between 1.4 and 3.4 for tumour and adjacent tissues and between 0.9 and 2.0 for adjacent and healthy tissues.

Non-significant correlations were found between element contents and the age of patients for the three groups of biopsies.

The large variability of element concentrations in the different samples indicates that results are not normally distributed (skewness and kurtosis coefficients and their standard errors were calculated for tumour, adjacent and healthy distributions). In order to compare the results, a non-parametric Mann–Whitney *U* test was applied for assessing the differences between cancerous/adjacent, cancerous/healthy and adjacent/healthy tissues. Statistical data analysis was performed with SPSS 14.0. The values for the statistical

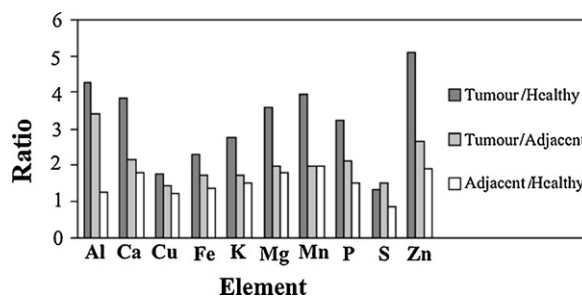


Fig. 3. Elemental concentration ratios of tumour-to-adjacent, tumour-to-healthy and adjacent-to-healthy tissues.

Table 3
Analytical characteristics.

Element	Instrumental		Methodological		Linear range ($\mu\text{g L}^{-1}$)	Slope ($\text{L } \mu\text{g}^{-1}$)	RSD (%)
	LOD ($\mu\text{g L}^{-1}$)	LOQ ($\mu\text{g L}^{-1}$)	LOD ($\mu\text{g g}^{-1}$)	LOQ ($\mu\text{g g}^{-1}$)			
Al	1.71	5.70	0.43	1.43	20–500	97304	2.33
Ca	0.04	0.13	0.01	0.03	100–2500	163252	2.39
Cu	3.12	10.40	0.78	2.60	5–100	105974	2.25
Fe	2.03	6.77	0.51	1.69	50–1000	103803	2.26
K	25.14	83.80	6.29	20.95	100–2500	3952	0.41
Mg	0.23	0.77	0.06	0.19	100–2500	450167	2.12
Mn	0.38	1.27	0.10	0.32	5–100	435474	2.46
P	38.26	127.53	9.57	31.88	100–10000	2282	1.48
S	40.15	133.83	10.04	33.46	100–10000	393	1.04
Zn	1.53	5.10	0.38	1.28	10–250	115899	2.37

Table 4
Validation of the proposed method against different CRMs.

Element	BCR-185R		TORT-2		DORM-2		DOLT-3	
	Found ^b	Certified ^a	Found ^b	Certified ^a	Found ^b	Certified ^a	Found ^b	Certified ^a
Al	9.5 ± 0.9	–	33.1 ± 3.4	–	11.8 ± 1.3	10.9 ± 1.7	27.5 ± 3.0	25 ^c
Ca	143 ± 9	–	3331 ± 242	–	485 ± 43	–	567 ± 29	–
Cu	282 ± 10	277 ± 5	106 ± 8	106 ± 10	2.27 ± 0.17	2.34 ± 0.16	30.7 ± 0.5	31.2 ± 1.0
Fe	179 ± 6	–	102 ± 10	105 ± 11	147 ± 7	142 ± 10	1487 ± 51	1484 ± 57
K	11285 ± 366	–	8065 ± 121	–	14425 ± 287	–	10002 ± 261	–
Mg	649 ± 23	–	1184 ± 87	–	1024 ± 85	–	1275 ± 83	–
Mn	11.52 ± 0.33	11.07 ± 0.29	13.9 ± 0.9	13.6 ± 1.2	3.44 ± 0.31	3.66 ± 0.34	9.01 ± 0.16	–
P	13020 ± 368	–	10332 ± 249	–	10112 ± 228	–	13500 ± 250	–
S	8162 ± 174	–	10430 ± 263	–	7957 ± 272	–	13695 ± 274	–
Zn	142.2 ± 4.6	138.6 ± 2.1	190 ± 12	180 ± 6	25.7 ± 1.2	25.6 ± 2.3	87.6 ± 1.6	86.6 ± 2.4

Results are expressed in $\mu\text{g g}^{-1}$.

–: Values non-certified.

^a Average value ± confidence interval ($p < 0.05$).

^b Average value of five different digestions ± standard deviation.

^c Indicative value.

Table 5
Elemental concentrations in tumour and non-tumour tissues ($\mu\text{g g}^{-1}$).

Element	Tumour tissue ($n = 19$)			Adjacent normal tissue ($n = 8$)			Healthy normal tissue ($n = 20$)		
	Mean	Median	Range	Mean	Median	Range	Mean	Median	Range
Al	82.8	50.0	12.1–297.0	24.2	18.5	8.0–48.00	19.2	13.0	1.0–76.1
Ca	1239.3	785.3	298.2–5195.6	571.5	483.5	66.0–1231.0	322.9	354.5	16.0–781.5
Cu	3.9	3.1	1.1–8.9	2.8	2.3	1.00–6.02	2.2	2.05	0.9–4.4
Fe	80.4	39.0	3.0–337.4	46.9	54.0	3.0–91.0	34.8	14.5	2.3–123.0
K	357.2	286.3	31.2–1725.7	207.4	113.5	34.00–907.0	135.7	116.5	20.1–579.2
Mg	236.4	208.4	61.0–534.0	118.0	72.5	8.00–310.0	65.7	64.0	6.4–124.4
Mn	1.7	0.7	0.1–5.6	0.8	0.51	0.09–2.05	0.4	0.2	0.1–0.9
P	1797.7	1356.5	255.1–4688.5	844.4	577.0	206.0–1533	558.5	520.0	48.2–1266.7
S	3030.8	2851.2	1370.5–6912.7	1983.4	1619.0	370.0–3853.0	2299.1	2322.5	214.5–3915.3
Zn	48.6	43.1	15.2–192.4	17.9	9.8	5.70–63.30	9.5	9.3	4.1–13.9

parameter (δ) corresponding to the above test are shown in Table 6. Significant differences ($p < 0.05$) were obtained for all elements, except for Fe and S, when tumour and healthy tissues were compared. When tumour and adjacent tissues are compared, significant

Table 6
Mann–Whitney test.

Element	δ Tumour/healthy	δ Tumour/adjacent	δ Adjacent/healthy
Al	0.000 ^a	0.009 ^a	0.605
Ca	0.000 ^a	0.254	0.043 ^a
Cu	0.002 ^a	0.137	0.709
Fe	0.175	0.633	0.304
K	0.038 ^a	0.159	0.709
Mg	0.000 ^a	0.022 ^a	0.381
Mn	0.001	0.232	0.281
P	0.000 ^a	0.044 ^a	0.304
S	0.194 ^a	0.071	0.328
Zn	0.000 ^a	0.005 ^a	0.601

^a Significant ($p < 0.05$).

differences were observed for Al, Mg, P and Zn. Only Ca displays significant differences when comparing adjacent and healthy tissues.

The significant accumulation of Ca, both in tumour and adjacent tissue, is indicative of the presence of microcalcifications in both cases, but particularly in tumours. These microcalcifications are one of the most usual diagnostic markers of breast cancer and can be found in benign and malignant lesions. The microcalcification composition can indicate the disease state. Calcium oxalate dehydrate (deposits type I) is associated with benign lesions and calcium hydroxyapatite (deposits type II) with malignant lesions [33]. Calcium hydroxyapatite crystals may play an active role in the extension of cancer in surrounding cells; this can explain the accumulation of Ca in adjacent tissue also. This compound improves mitogenesis in cell lines MCF-7 and Hs578T and also in normal human mammary epithelial cell lines [34].

Aluminium accumulates in the tumour tissue in spite of not being an essential element. Significant differences were obtained for tumour/healthy and tumour/adjacent for this element. Al is

omnipresent in everyday life, and this fact results in an increase of this non-essential metal in the body burden. Aluminium in antiperspirants has been related to a potential role in breast cancer [35,36]. This element is capable of causing both DNA alterations and epigenetic effects. A possible interference in the functioning of intracellular receptors for estrogens has been suggested. These receptors act as ligand-activated zinc finger transcription factors [35]. The aluminium content of breast tissue in the outer regions (axilla and lateral) was found to be higher than in the inner regions, and this can be due to the proximity to the application area of antiperspirant [36].

Zn, Cu and Mn are significantly accumulated in tumour with regard to healthy tissues. For Zn, there are also significant differences between tumour and adjacent tissues. In general, it is possible to consider a role of these elements as cellular growth protectors. Oxidant–antioxidant balance is considered as the principal regulator of growth factors and invasion of tumour cells [9]. Zn, Cu and Mn are cofactors of enzymes with important catalytic functions in the antioxidant defense system as superoxide dismutases. Manganese superoxide dismutase is the major defense mechanism against mitochondrial reactive oxygen species that induce oxidative stress. Cu/Zn superoxide dismutase is known as a scavenger of superoxides. The overexpression of these enzymes inhibits breast cancer growth [37]. Particularly, elevated Zn concentration in mammary tumours has been associated with an upregulated metallothionein expression with an increased metallothionein protein level [4,38].

Metallothioneins are the main detoxification mechanism for protecting the cell against heavy metals. These proteins also take part in the homeostasis of Zn and Cu, and the level of this protein group has been significantly correlated with the contents of Cu and Zn in tumour tissues [39].

The accumulation of Mg, K and P in tumour tissues can be explained by the need of metabolic energy for supporting a higher rate of cell proliferation in the tumourgenesis. These elements are involved in the generation and the transport of the metabolic energy. A wide range of metabolic enzymes involved in the transfer phosphate groups requires Mg. In general, phosphorous as ATP plays a key role in the bioenergetics. The ionic gradients Na–K that originate across the cellular membranes are basic for cellular life.

Table 7

Concentration intervals found in the literature for tumour, adjacent and healthy breast tissues ($\mu\text{g g}^{-1}$).

Element	Tumour	Adjacent	Healthy
Al	10 ^a –78 ^a	10 ^a –36 ^a	0.11 ^b –11.8 ^b
Ca	44 ^c –1719 ^a	9 ^c –575 ^a	–
Cu	0.86 ^d –78.92 ^e	0.29 ^d –48.87 ^e	0.24 ^f –3.05 ^g
Fe	7 ^h –1840 ^a	3 ⁱ –925 ^a	1 ^f –24 ^f
K	85 ⁱ –7630 ^a	17 ⁱ –5050 ⁱ	87 ^f –2230 ^j
Mg	25 ^j –272 ^j	15 ^j –218 ^j	320 ^j –360 ^j
Mn	0.3 ^a –22.2 ^e	0.2 ^a –20.3 ^e	–
P	170 ^j –1002 ^j	48 ^j –424 ^j	–
S	792 ^k –4960 ⁱ	175 ⁱ –415 ⁱ	–
Zn	1.07 ^a –138.95 ^e	2.12 ^d –61.98 ^e	0.5 ^f –9.34 ^g

The sign minus represents non-reported values. Values are expressed in $\mu\text{g g}^{-1}$ wet tissue.

^a Ref. [18].

^b Ref. [35].

^c Ref. [40].

^d Ref. [2].

^e Ref. [4].

^f Ref. [3].

^g Ref. [5].

^h Ref. [7].

ⁱ Ref. [16].

^j Ref. [41].

^k Ref. [8].

Metabolic energy, resulting from the hydrolysis of the ATP upon activation by Mg^{2+} , is needed for the maintenance of this gradient.

Elemental concentrations found in this work compare well with published data (Table 7). Elevated levels of Al and Ca in tumour tissues can be generally seen.

4. Conclusions

Multiple microwave-assisted digestions carried out in small vials inserted into conventional microwave vessels display several advantages: (a) increased sample throughput; (b) suitability for small sample sizes (20–30 mg dry weight); (c) minimum dilution; (d) decreased acid volume for digestion. This methodology has proved accurate and robust and is well suited to the determination of different elements (Ca, Cu, Fe, K, Mg, Mn, P, S and Zn) in biopsies by ICP-OES. Statistically significant differences in concentration were obtained for all elements, except for Fe and S, when tumour and healthy tissues were compared. Ca and Al stand out, since they accumulate to a large extent in tumour tissues. Ca accumulates in tumour due to the formation of microcalcifications, which play an important role in the extension of tumours to adjacent tissues.

Acknowledgements

Financial support from the Spanish Education and Science Ministry (project CTQ2006-04111/BQU) is gratefully acknowledged. The authors thank Dra Pilar Sanmiguel from the anatomy pathological service of the POVISA Hospital (Vigo, Spain) and Dr Jorge Cameselle from the Institute of molecular pathology and immunology (Oporto University, Portugal) for providing the biopsies and their interest in interdisciplinary collaboration.

References

- [1] American Cancer Society, Breast Cancer Facts & Figures 2007–2008, 2008, <http://www.cancer.org>.
- [2] K. Geraki, M.J. Farquharson, D.A. Bradley, *Phys. Med. Biol.* 47 (2002) 2327.
- [3] K. Geraki, M.J. Farquharson, D.A. Bradley, R.P. Hugtenburg, *Nucl. Instrum. Methods Phys. Res. Sect. B* 213 (2003) 564.
- [4] G.J.N. Raju, P. Sarita, M.R. Kumar, G.A.V.R. Murty, B.S. Reddy, S. Lakshminarayana, V. Vijayan, P.V.B.R. Lakshmi, S. Gavaranasa, S.B. Reddy, *Nucl. Instrum. Methods Phys. Res. B* 247 (2006) 361.
- [5] J.G. Ionescu, J. Novotny, V. Stejskal, A. Laetsch, E. Blaurock-Busch, M. Eisenmann-Kleim, *Neuroendocrinol. Lett.* 27 (2006) 36.
- [6] A.M. Ebrahim, M.A.H. Eltayeb, M.K. Shaat, N.M.A. Mohamed, E.A. Eltayeb, A.Y. Ahmed, *Sci. Total Environ.* 383 (2007) 52.
- [7] U. Majewska, D. Banas, J. Braziewicz, S. Gozdz, A. Kubala-Kukus, M. Kucharzewski, *Phys. Med. Biol.* 52 (2007) 3895.
- [8] A. Kubala-Kukús, D. Banás, J. Braziewicz, S. Gózd, U. Majewska, M. Pajek, *Spectrochim. Acta B* 62 (2007) 695.
- [9] M. Valko, C.J. Rhodes, J. Moncol, M. Izakovic, M. Mazur, *Chem. Biol. Interact.* 160 (2006) 1.
- [10] J.M. Mates, C. Pérez-Gómez, I. De Castro, *Clin. Biochem.* 32 (1999) 595.
- [11] G.C. Gregoriadis, N.S. Apostolidis, A.N. Romanos, T.P. Paradellis, *Cancer* 52 (1983) 508.
- [12] S.L. Rizk, H.H. Sky-Peck, *Cancer Res.* 44 (1984) 5390.
- [13] E.N. Drake II, H.H. Sky-Peck, *Cancer Res.* 49 (1989) 4210.
- [14] D. von Czarnowski, E. Denkhaus, K. Lemke, *Spectrochim. Acta B* 52 (1997) 1047.
- [15] I. Varga, A. Szebeni, N. Szoboszlai, B. Kovács, *Anal. Bioanal. Chem.* 383 (2005) 476.
- [16] T. Magalhaes, A. von Bohlen, M.L. Carvalho, M. Becker, *Spectrochim. Acta B* 61 (2006) 1185.
- [17] S.B. Reddy, M.J. Charles, G.J.N. Raju, V. Vijayan, B.S. Reddy, M.R. Kumar, B. Sundareswar, *Nucl. Instrum. Methods Phys. Res. Sect. B* 207 (2003) 345.
- [18] K.H. Ng, D.A. Bradley, L.M. Looi, *Br. J. Radiol.* 70 (1997) 375.
- [19] B. Bocca, A. Lamazza, A. Pino, E. De Masi, M. Iacomino, D. Mattei, S. Rahimi, E. Fiori, A. Schillaci, A. Alimonti, G. Forte, *Rapid Commun. Mass Spectrom.* 21 (2007) 1776.
- [20] M.F. Basle, Y. Mauras, M. Audran, P. Clochon, A. Rebel, P. Allain, J. Bone Miner. Res. 5 (1990) 41.
- [21] C. Hamada, R. Ohi, T. Chiba, Y. Matsumoto, H. Koyama, H. Sato, *Biomed. Res. Trace Elem.* 2 (1991) 135.
- [22] J. Olszewski, J. Latusinski, A. Kita, P. Pietkiewicz, S. Starostecka, J. Majak, *B-ENT* 2 (2006) 47.

- [23] I. Muller, *Atom. Spectrosc.* 19 (1998) 45.
- [24] B. Bocca, A. Alimonti, G. Forte, F. Petrucci, C. Pirola, O. Senofonte, N. Violante, *Anal. Bioanal. Chem.* 377 (2003) 65.
- [25] S. Baldwin, M. Deaker, W. Maher, *Analyst* 119 (1994) 1701.
- [26] M. Deaker, W. Maher, *Anal. Chim. Acta* 350 (1997) 287.
- [27] M. Deaker, W. Maher, *J. Anal. At. Spectrom.* 14 (1999) 1193.
- [28] G. Esslemont, W. Maher, P. Ford, F. Krikowa, *Atom. Spectrosc.* 21 (2000) 42.
- [29] W. Maher, S. Forster, F. Krikowa, P. Snitch, G. Chapple, P. Craig, *Atom. Spectrosc.* 22 (2001) 361.
- [30] J. Millos, M. Costas-Rodríguez, I. Lavilla, C. Bendicho, *Anal. Chim. Acta* 622 (2008) 77.
- [31] Planificación sanitaria, Xunta de Galicia, "A nosa saúde en cifras. Ano 2005", 2005.
- [32] G. Box, S. Hunter, W.G. Hunter, *Statistics for Experiments: Design, Innovation and Discovery*, second ed., Wiley, New Jersey, 2005, p. 236.
- [33] A.S. Haka, K.E. Shafer-Peltier, M. Fitzmaurice, J. Crowe, R.R. Dasari, M.S. Feld, *Cancer Res.* 62 (2002) 5375.
- [34] M.P. Morgan, M.M. Cooke, P.A. Christopherson, P.R. Westfall, G.M. McCarthy, *Mol. Carcinog.* 32 (2001) 111.
- [35] P.D. Darbre, *J. Inorg. Biochem.* 99 (2005) 1912.
- [36] C. Exley, L.M. Charles, L. Barr, C. Martin, A. Polwart, P.D. Darbre, *J. Inorg. Biochem.* 101 (2007) 1344.
- [37] C.J. Weydert, T.A. Waugh, J.M. Ritchie, K.S. Lyer, J.L. Smith, L. Li, D.R. Spitz, L.W. Oberley, *Free Radic. Biol. Med.* 41 (2006) 226.
- [38] R. Lee, W. Woo, B. Wu, A. Kummer, Z. Xu, *Exp. Biol. Med.* 228 (2003) 689.
- [39] B. Florianczyk, J. Osuchowski, R. Kaczmarczyk, T. Trojanowski, M. Stzyjecka-Zimmer, *Folia Neuropathol.* 41 (2003) 11.
- [40] M.K.J. Siddiqui, S. Jyoti, P.K. Singh, K. Mehrotra, R. Singh, Sarangi, *Environ. Int.* 32 (2006) 630.
- [41] S.S. Ranade, V.K. Panday, *Sci. Total Environ.* 41 (1985) 79.



A novel fiber-packed column for on-line preconcentration and speciation analysis of chromium in drinking water with flame atomic absorption spectrometry

Romina P. Monasterio^{a,d}, Jorgelina C. Altamirano^{a,b,c}, Luis D. Martínez^{b,e}, Rodolfo G. Wuilloud^{a,b,c,*}

^a *Laboratory of Environmental Research and Services of Mendoza (LISAMEN), CCT – CONICET – Mendoza, Av. Ruiz Leal S/N Parque General San Martín, CC 131, M 5502 IRA Mendoza, Argentina*

^b *Consejo Nacional de Investigaciones Científicas y Técnicas (CONICET), Argentina*

^c *Instituto de Ciencias Básicas, Universidad Nacional de Cuyo, Mendoza, Argentina*

^d *Departamento de Química, Facultad de Ciencias Exactas y Naturales, Universidad Nacional de La Pampa, Argentina*

^e *Departamento de Química Analítica, Facultad de Química, Bioquímica y Farmacia, Universidad Nacional de San Luis, Argentina*

ARTICLE INFO

Article history:

Received 29 June 2008

Received in revised form 2 September 2008

Accepted 3 September 2008

Available online 11 September 2008

Keywords:

Chromium speciation

Llama fiber

Preconcentration

Flame atomic absorption spectrometry

ABSTRACT

A novel on-line preconcentration and determination system based on a fiber-packed column was developed for speciation analysis of Cr in drinking water samples prior to its determination by flame atomic absorption spectrometry (FAAS). All variables involved in the development of the preconcentration method including, pH, eluent type, sample and eluent flow rates, interfering effects, etc., were studied in order to achieve the best analytical performance. A preconcentration factor of 32 was obtained for Cr(VI) and Cr(III). The levels of Cr(III) species were calculated by difference of total Cr and Cr(VI) levels. Total Cr was determined after oxidation of Cr(III) to Cr(VI) with hydrogen peroxide. The calibration graph was linear with a correlation coefficient of 0.999 at levels near the detection limit and up to at least $50 \mu\text{g L}^{-1}$. The relative standard deviation (R.S.D.) was 4.3% ($C = 5 \mu\text{g L}^{-1}$ Cr(VI), $n = 10$, sample volume = 25 mL). The limit of detection (LOD) for both Cr(III) and Cr(VI) species was $0.3 \mu\text{g L}^{-1}$. Verification of the accuracy was carried out by the analysis of a standard reference material (NIST SRM 1643e “Trace elements in natural water”). The method was successfully applied to the determination of Cr(III) and Cr(VI) species in drinking water samples.

© 2008 Elsevier B.V. All rights reserved.

1. Introduction

Chromium is one of the most abundant elements on earth and is found naturally in rocks, soil, plants, animals, volcanic dust and gases [1]. It can percolate into the soil by leaching and has the potential to contaminate groundwater, which can be a major source of drinking water [2]. In aqueous solution, it is mainly present as Cr(III) and Cr(VI) oxidation states [3–6]. The properties of these species are very different from a chemical and toxicological point of view. Trivalent Cr, the main chemical species found in food, is essential for maintaining normal glucose and lipid metabolism (group 3 of IARC) [1,6,7]. On the other hand, hexavalent Cr-containing compounds are considerably toxic and known to be carcinogenic and mutagenic for humans (group 1 of IARC) [6]. Thus, considerable emphasis has

been given to the development of analytical methodologies for Cr species separation and determination.

Since one of the routes of incorporation of Cr into the human body is water, its determination in this type of samples becomes very important. The Food and Agriculture Organization of the United Nations (FAO) and the World Health Organization (WHO) recommend a guideline value of 0.05 mg L^{-1} Cr for drinking water [6]. Therefore, powerful analytical techniques are required and only few of them show enough sensitivity. Among them, electrothermal atomic absorption spectrometry (ETAAS) and inductively coupled plasma mass spectrometry (ICP-MS) are the most commonly used for trace Cr determination [8]. Despite flame atomic absorption spectrometry (FAAS) continues to be highly employed in routine analytical laboratories, the low concentration levels of Cr that can be found in water are not compatible with the detection limit achieved by this technique.

Therefore, determination of Cr species at trace levels, usually includes preparation and preconcentration steps prior to elemental detection in order to achieve accurate, reliable and sensitive results [9,10]. Some preconcentration methods have used chelation with diphenylcarbazide [11,12] or 4-(2-thiazolilazo)-resorcinol (TAR) [13], as a previous step to metal adsorption on polymeric

* Corresponding author at: Laboratory of Environmental Research and Services of Mendoza (LISAMEN), CCT – CONICET – Mendoza, Av. Ruiz Leal S/N Parque General San Martín, CC 131, M 5502 IRA Mendoza, Argentina. Tel.: +54 261 5244064; fax: +54 261 5244001.

E-mail address: rwuilloud@mendoza-conicet.gov.ar (R.G. Wuilloud).

URL: <http://www.cricyt.edu.ar/lisamen/> (R.G. Wuilloud).

Table 1
Instrumental and experimental conditions

Flame type	Air–C ₂ H ₂
Wavelength	357.9 nm
Slit width	0.7 nm
Lamp current	25 mA
Measurement mode	Peak height
Air flow rate	6 L min ⁻¹
Acetylene flow rate	2 L min ⁻¹
Sample introduction flow rate	9 mL min ⁻¹
Column characteristics	
Effective bed length	43 mm
Internal diameter	3 mm
Fiber amount	70 mg
Preconcentration conditions	
Loading flow rate	2 mL min ⁻¹
Loading volume	25 mL
Eluent	NaOH (1 mol L ⁻¹)
Stopped-flow time	5 min

resins, like XAD [14,15]. On the other hand, ionic exchange materials, like alumina [16,17] and commercial polymeric resin, such as Dowex or Amberlite, have been widely used with good results [1,18,19]. Other techniques, such as precipitation and coprecipitation [20,21], have also been applied for Cr determination at trace levels. However, many of these methodologies were performed in batch, requiring considerable sample volumes in order to reach low detection limits, turning these procedures time-consuming and impractical in routine analysis. This situation has been significantly improved by utilizing on-line preconcentration systems coupled to elemental detectors, such as FAAS [22].

An alternative material for metal retention, especially for remediation purposes, has been wool and/or fiber of animal origin. Fiber proteins have polar and ionizable groups on the side chain of amino acid residues and bind charged species such as metal ions. In fact, feather or silk proteins have been used for purification of heavy metal-contaminated waste water [23]. Studies on wool keratin for binding of heavy metals as well as coloring with metal complexes, such as *o*-*o'*-dihydroxyazo Cr compounds, began in the 1950s [23,24]. However, to date fibers have not been implemented in analytical chemistry to develop metal preconcentration.

In the present work, the novel application of animal fiber for the efficient retention and preconcentration of Cr is showed. An on-line flow injection preconcentration system consisting of a fiber-packed column for Cr(VI) retention was developed and coupled to FAAS detection. Cr(III) and Cr(VI) species were differentiated by oxidation of Cr(III) into Cr(VI) by hydrogen peroxide prior retention of the second species in the fiber-packed column. Therefore, total content of Cr was then evaluated based on Cr(VI) species determination. The analytical parameters for optimal speciation along with the possible mechanisms of Cr retention on the fiber are discussed.

2. Experimental

2.1. Instrumentation

The measurements were performed with a PerkinElmer (Uberlingen, Germany) Model 5100PC atomic absorption spectrometer equipped with a Cr hollow cathode lamp. The FAAS instrumental and operating conditions that provided the best sensitivity for Cr(VI) signal are listed in Table 1.

The flow injection system is shown in Fig. 1. A Gilson (Villiers Le-Bell, France) Minipuls 3 peristaltic pump equipped with tygon-type pump tubes (Gilson) were employed to propel the sample, reagent and eluent. The sample injection was achieved using a six-way rotary valve from Upchurch Scientific (Oak Harbor, WA, USA).

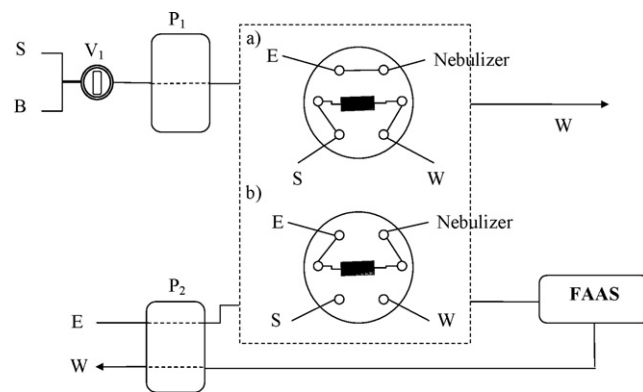


Fig. 1. Schematic diagram of the instrumental setup. S, sample; E, eluent; W, waste; P₁ and P₂, peristaltic pumps; V₁, six-way valve; V₂, six-way valve. (a) Load position and (b) injection position.

2.2. Reagents and chemicals

A stock standard solution of 1000 mg L⁻¹ Cr(III) was prepared from 7.6930 g chromium nitrate (99.99%) (Cr(NO₃)₃·9H₂O) (Merck, Darmstadt, Germany) dissolved in ultrapure water and diluted to 1000 mL with a final HNO₃ concentration of 0.05 mol L⁻¹. Working solutions were prepared by dilution of the stock standard solution.

A stock standard solution of 1000 mg L⁻¹ Cr(VI) was prepared from 2.8287 g potassium dichromate (99.5%) (K₂Cr₂O₇) (Aldrich, Milwaukee, WI, USA) dissolved and diluted to 1000 mL with ultrapure water. Working standard solutions were prepared by appropriate dilution with ultrapure water.

We prepared 1 mol L⁻¹ sodium hydroxide solution from NaOH (Aldrich) and used it for Cr(VI) elution from the column. A nitric acid solution of 1 mol L⁻¹ was prepared from proper dilution of 65% (w/w) HNO₃ (Merck). We prepared these solutions as a carrier for conditioning the column and regeneration.

Ultrapure water (18 MΩ cm) was obtained from a Milli-Q water purification system (Millipore, Paris, France).

All reagents were of analytical reagent grade and the presence of Cr was not detected in the working range.

All bottles used for storing samples and standard solutions, as well as the glassware were washed in 10% (v/v) nitric acid for 24 h and finally rinsed with ultrapure water.

2.3. Preparation of the fiber-packed column

Llama (*lama glama*) fibers with no treatment were purchased at local stores. The llama fiber was washed before using in an ultrasonic bath with a detergent solution followed by 0.5 mol L⁻¹ sodium hydroxide, 1 mol L⁻¹ nitric acid and finally water. The fiber was dried at room temperature until constant weight. A glass column (3 mm i.d. and 55 mm length) was used for preconcentration. An amount of 70 mg of llama fiber was used to pack the column up to an effective bed length of 43 mm. The column was finally washed with ultrapure water followed by conditioning with 0.5 mol L⁻¹ sodium hydroxide and 1 mol L⁻¹ nitric acid.

2.4. Separation and preconcentration procedure

Initially, the column was conditioned for preconcentration at the correct pH with 1 mol L⁻¹ nitric acid, valve V₁ in position B (Fig. 1). The sample solution was then loaded on the fiber-packed column at a flow rate of 2 mL min⁻¹, with valve V₁ in S position and valve V₂ in load position (a). After the loading time, the loading lines and column were washed with 1 mol L⁻¹ nitric acid, with the

valve V_1 again in position B. Finally, valve V_2 was switched to the injection position (b) and the column was loaded with 1 mol L^{-1} sodium hydroxide followed by a 5-min stopped-flow. After this time the retained Cr species was eluted with 1 mol L^{-1} sodium hydroxide solution at a flow rate of 9.5 mL min^{-1} , directly into the nebulizer and subsequently the flame. The procedure was based on the retention of Cr(VI) on the fiber. After oxidation of Cr(III), total Cr was evaluated by applying the preconcentration procedure described above. The concentration of Cr(III) species was calculated as the difference between the total concentration of Cr and that of Cr(VI).

2.5. Oxidation of Cr(III) species

Hydrogen peroxide was used for oxidation of Cr(III) to Cr(VI). A standard solution ($100 \mu\text{g L}^{-1}$ Cr(III)) volume of 70 mL was added with $500 \mu\text{L}$ of 100 vol. hydrogen peroxide. This solution was heated on a thermostatic water bath for 40 min at 93°C and then boiled on a heating plate for 10 min in order to remove any excess of hydrogen peroxide. After this procedure, the resulting solution was cooled to room temperature and then taken up to 100 mL with ultrapure water.

2.6. Sample collection and conditioning

For the collection of tap water samples, domestic water was allowed to run for 20 min and approximately a volume of 1000 mL was collected in a beaker. The water samples were filtered through $0.45 \mu\text{m}$ pore size membrane filters (Millipore) immediately after sampling and acidified to pH 2 with nitric acid. Finally, samples were stored in bottles (Nalgene; Nalge, Rochester, NY, USA) at 4°C .

3. Results and discussion

3.1. Optimization of loading variables

Sample pH value plays an important role with respect to the adsorption of Cr(III) and Cr(VI) onto microcolumns. The pH of media is a critical parameter as Cr speciation is dependant on this factor. Thus, Cr(VI) can exist primarily as chromic acid (H_2CrO_4) and its salts, hydrogen chromate ion (HCrO_4^-) and chromate ion (CrO_4^{2-}). The predominant species are H_2CrO_4 at $\text{pH} < 1$, HCrO_4^- at $\text{pH} 1\text{--}6$, and CrO_4^{2-} at $\text{pH} 6$ [25]. Loading conditions were optimized by monitoring Cr signal with FAAS while changing the pH of the solutions that passed through the column. The effect of pH was evaluated in the range of 1.1–6.1. As can be seen in Fig. 2a, it is evident that Cr(VI) retention resulted optimum at pH 4 and hence, this value was selected for all experiments.

The possibility of using a buffer to keep a constant pH 4 was investigated using a 2-mol L^{-1} sodium acetate/acetic acid solution. Buffer concentrations were in the range of 6.7×10^{-3} to 0.13 mol L^{-1} . However, when this buffer system was used, a considerable drop in sensitivity was observed (Fig. 2b). This phenomenon can be explained considering a possible competition between acetate ion and Cr(VI) anionic species by the active sites of the fiber. Therefore, pH was adjusted by addition of proper amounts of acid or base.

A flow rate ranging between 0.5 and 6 mL min^{-1} was found to be suitable for optimal loading on the fiber-packed column. Higher flow rates did not lead to any improvement of Cr retention. This could be probably due to insufficient contact time between the sample solution and the fiber. A flow rate of 2 mL min^{-1} was selected.

The influence of the column length was investigated between 25 and 115 mm. In the analytical range of this work, increasing the

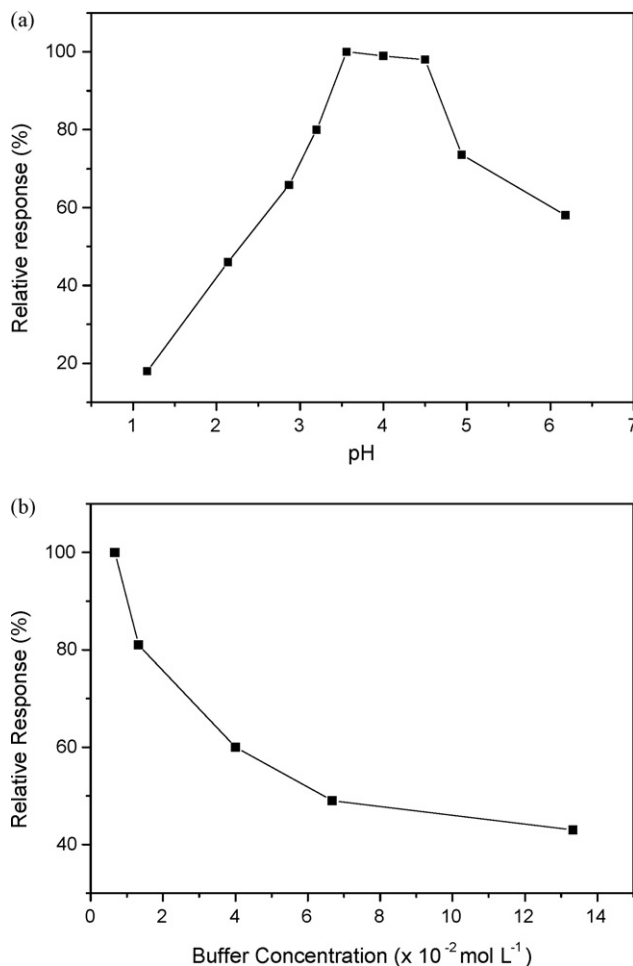


Fig. 2. (a) Dependence of Cr(VI) retention on fiber material with the pH of loading solutions. (b) Relationship between buffer concentration and Cr(VI) retention. Preconcentration of 25 mL of $100 \mu\text{g L}^{-1}$ Cr(VI) at $\text{pH} 4.0$. Other conditions were as shown in Table 1.

fiber amount did not improve the preconcentration and recovery of Cr(VI). Therefore, a fiber bed length of 43 mm was chosen as optimal.

3.2. Optimization of elution variables

In order to elute Cr(VI) species retained on the fiber, hydroxides were used as eluents. The eluting agents were ammonium hydroxide and sodium hydroxide in concentrations ranging from 0.5 to 3 mol L^{-1} . As it is shown in Fig. 3, the highest efficiency for Cr elution from the column was achieved with 1 mol L^{-1} NaOH solution. Higher concentrations of this eluent resulted to be less effective. On the other hand, Cr recoveries obtained with ammonium hydroxide were lower to that of NaOH for each concentration level. Based on these observations, 1 mol L^{-1} NaOH solution was selected as eluent for further experiments.

An important variable to be optimized was the contact time of the eluent solution with the fiber. Thus, it was observed that a minimal contact time was needed in order to achieve total elution of Cr from the column (Fig. 4). Elution was performed by a stopped-flow procedure filling the column with 1 mol L^{-1} NaOH and keeping the eluent for 5 min before injection into FAAS.

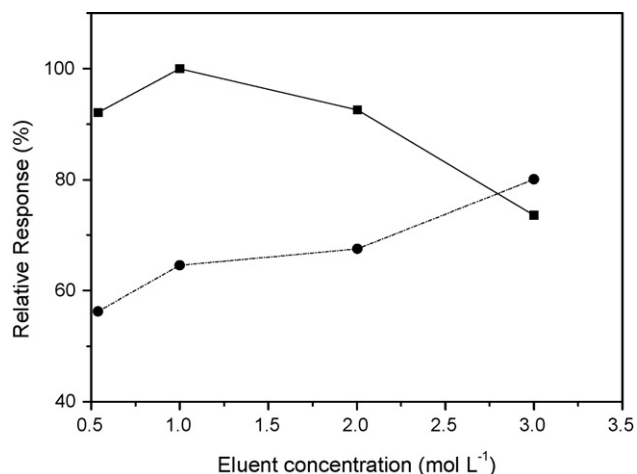


Fig. 3. Effect of types and concentration of eluting agents. (■) Sodium Hydroxide; (●) ammonium hydroxide. Other conditions were as shown in Table 1.

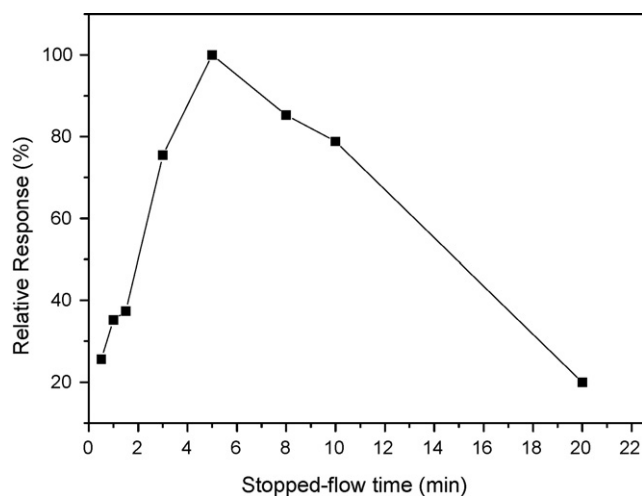


Fig. 4. Effect of stopped-flow time on Cr elution efficiency from the fiber-packed column. Other conditions were as mentioned in Table 1.

3.3. Retention efficiency and preconcentration factor

A retention percentage higher than 99.8% was achieved when the procedure was carried out under optimal experimental conditions (Table 1). Therefore, an enrichment or preconcentration factor of 32 was obtained for a sample volume of 25 mL. The amount of Cr(VI) species retained on the fiber was determined in batch. A 50-mL portion of 60 mg L^{-1} Cr(VI) solution was adjusted to pH 4 with nitric acid and shaken with 100 mg of fiber in a glass flask for 30 min. Adsorption capacity of llama fiber material was found to be $25.2 \text{ mg Cr(VI) g}^{-1}$ of dried fiber. It can be stated that adsorption

capacity of llama fiber is higher than those reported for others ion exchange materials such as alumina [10] and nanometer-sized zirconium oxide immobilized on silica gel [26], but significantly less expensive as compared to these materials.

3.4. Separation of Cr(III) and Cr(VI) species

Oxidation of Cr(III) to Cr(VI) was needed in order to allow Cr(III) retention on the fiber as Cr(VI) species. Hydrogen peroxide was selected as oxidant due to its high oxidation capacity and the possibility of it being eliminated from the reaction media by simple heating of the mixture. Therefore, several hydrogen peroxide concentrations 2.5 , 4.9 and $9.8 \times 10^{-2} \text{ mol L}^{-1}$ and at different pH of the media (pH 4, 8.3, and 11) were assayed. Optimal Cr(III) retention and recoveries were achieved for $4.9 \times 10^{-2} \text{ mol L}^{-1}$ hydrogen peroxide at pH 8.3.

In order to assess the selectivity of the proposed method for Cr(III) and Cr(VI) determination, it was applied to several standard solutions at different concentration ratios of the two oxidation states. Table 2 indicates that Cr(III) and Cr(VI) species were completely separated and quantitatively recovered. The method was thus shown to have an acceptable performance for selective determination of Cr species under different conditions.

3.5. Interferences

The effects of representative potential interfering species (at the concentration levels at which they may occur in the sample studied) were tested. The recovery of the analyte was not influenced by CO_3^{2-} , Cl^- , SO_4^{2-} , PO_4^{3-} and Fe^{3+} ions, probably due to the retention capacity of the fiber that avoided fast saturation of the column. These ions could be tolerated up to at least $2,000 \text{ } \mu\text{g L}^{-1}$.

3.6. Determination of Cr species in water samples

After separation/preconcentration by the proposed procedure, the calibration graphs for FAAS determination of Cr(VI) were linear, achieving a relative standard deviation (R.S.D.) of 4.3% ($C = 5 \text{ } \mu\text{g L}^{-1}$, $n = 10$, sample volume = 25 mL). Linearity of calibration curve was observed at levels near the detection limit and up to at least $300 \text{ } \mu\text{g L}^{-1}$. The calibration graph showed a correlation coefficient of 0.999. The limit of detection (LOD), calculated based on three times the standard deviation of the background signal (3σ), was $0.3 \text{ } \mu\text{g L}^{-1}$. The preconcentration factor was obtained as the ratio of the slopes of the calibration curves for Cr(VI) with and without the preconcentration step. The accuracy of the proposed method was evaluated by analyzing a standard reference material, NIST SRM 1643e "Trace Elements in Water", with a reported Cr content of $20.40 \pm 0.24 \text{ } \mu\text{g L}^{-1}$. Using the proposed methodology the Cr content determined in this SRM was $20.1 \pm 1.9 \text{ } \mu\text{g L}^{-1}$.

The results of the method applied to Cr(III) and Cr(VI) determination in drinking water samples were in the range of $7.3\text{--}14.2 \text{ } \mu\text{g L}^{-1}$ for Cr(VI) and $1.2\text{--}2.4 \text{ } \mu\text{g L}^{-1}$ for Cr(III). The results

Table 2
Evaluation of the separation of Cr(VI) and Cr(III) species

Cr(VI)/Cr(III) ratio	Cr(VI)			Cr(III)		
	Added ($\mu\text{g L}^{-1}$)	Found ($\mu\text{g L}^{-1}$)	Recovery (%)	Added ($\mu\text{g L}^{-1}$)	Found ($\mu\text{g L}^{-1}$)	Recovery (%)
21	42	41.5	99.0	2	1.90	96.5
2.66	32	31.4	98.3	12	11.9	99.8
1	22	21.5	97.7	22	21.8	99.2
0.37	12	11.8	98.3	32	32.8	102
0.05	2	1.90	95.4	42	79.6	99.8

Table 3
Analysis of Cr(VI) and Cr(III) in drinking water samples (95% confidence interval; $n = 6$)

Sample	Cr(VI)			Cr(III)		
	Added ($\mu\text{g L}^{-1}$)	Found ($\mu\text{g L}^{-1}$)	Recovery (%) ^a	Added ($\mu\text{g L}^{-1}$)	Found ($\mu\text{g L}^{-1}$)	Recovery (%) ^a
1	0	10.3 ± 1.5	–	0	2.4 ± 0.3	–
	10	20.1 ± 1.9	99.6	10	12.5 ± 0.9	100.0
2	0	7.3 ± 0.7	–	0	1.2 ± 0.2	–
	10	17.6 ± 1.2	100.0	10	11.0 ± 1.6	98.0
3	0	14.2 ± 1.4	–	0	1.5 ± 0.3	–
	10	24.1 ± 2.3	99.8	10	11.3 ± 1.7	99.6

^a $100 \times ((\text{found} - \text{base}) / \text{added})$.

are shown in Table 3. Concentration levels observed in this work were not significantly different to those reported by Bulut et al. [14], Wuilloud et al. [9], and Saygi et al. [1], for Cr(III) and Cr(VI) species in drinking water samples.

4. Conclusion

The methodology developed in this work provides a novel, simple, and inexpensive approach to achieve high retention and separation of Cr(III) and Cr(VI) species. The results showed that llama fiber has high and reproducible retention capacity of Cr(VI) species and hence, it is proposed as an effective alternative to other more expensive ionic exchanger materials. The preconcentration system provided an enrichment factor of 32 as a consequence of the high Cr retention (99%) on the fiber.

The coupling of an on-line preconcentration system to FAAS increases the speed of the preconcentration and analysis process, while reducing sample consumption and contamination risks. The proposed on-line preconcentration system associated with FAAS detection allowed the separation and determination of Cr(III) and Cr(VI) species in drinking water samples at levels as low as $\mu\text{g L}^{-1}$ with good accuracy and reproducibility.

Acknowledgments

This work was supported by Consejo Nacional de Investigaciones Científicas y Técnicas (CONICET), Agencia Nacional de Promoción Científica y Tecnológica (FONCYT) (PICT-BID) (FONTAR—N° PMT II – CAI/073), and Universidad Nacional de San Luis (Argentina).

References

[1] K.O. Saygi, M. Tuzen, M. Soylak, L. Elci, *J. Hazard. Mater.* 153 (2008) 1009.

- [2] U. Kalbe, W. Berger, J. Eckardt, F.-G. Simon, *Waste Manage.* 28 (2008) 1027.
 [3] A. Manova, S. Humenikova, M. Strelec, E. Beinrohr, *Microchim. Acta* 159 (2007) 41.
 [4] ATSDR, Toxicological profile for chromium (update), Agency for Toxic Substances and Disease Registry U.S. Department of Health and Human Services, Atlanta, 1998.
 [5] IARC, Monographs on the Evaluation of Carcinogenic Risks to Humans, Lyon, 1987, p. 31.
 [6] G.F. Nordberg, B.A. Fowler, M. Nordberg, L. Friberg, *Handbook on the Toxicology of Metals*, Academic Press, Burlington, 2007.
 [7] J.L. Burguera, M. Burguera, C. Rondon, L. Rodriguez, P. Carrero, Y. Petit De Peña, E. Burguera, *J. Anal. Atom. Spectrom.* 14 (1999) 821.
 [8] V. Gomez, M.P. Callao, *Trends Anal. Chem.* 25 (2006) 1006.
 [9] R.G. Wuilloud, G.M. Wuilloud, J.C.A. De Wuilloud, R.A. Olsina, L.D. Martinez, *Atom. Spectrosc.* 23 (2002) 44.
 [10] N. Rajesh, B. Deepthi, A. Subramaniam, *J. Hazard. Mater.* 144 (2007) 464.
 [11] M. Goldoni, A. Cagliari, D. Poli, M.V. Vettori, M. Corradi, P. Apostoli, A. Mutti, *Anal. Chim. Acta* 562 (2006) 229.
 [12] S. Matsuoka, Y. Tennichi, K. Takehara, K. Yoshimura, *Analyst* 124 (1999) 787.
 [13] L.S. De Carvalho, A.C.S. Costa, S.L.C. Ferreira, L.S.G. Teixeira, *J. Braz. Chem. Soc.* 15 (2004) 153.
 [14] V.N. Bulut, C. Duran, M. Tufekci, L. Elci, M. Soylak, *J. Hazard. Mater.* 143 (2007) 112.
 [15] I. Narin, A. Kars, M. Soylak, *J. Hazard. Mater.* 150 (2008) 453.
 [16] M. Sperling, S. Xu, B. Welz, *Anal. Chem.* 64 (1992) 3101.
 [17] P. Bermejo-Barrera, M.C. Barciela-Alonso, B. Perez-Fernandez, A. Bermejo-Barrera, *Spectrochim. Acta B* 58 (2003) 167.
 [18] S.A. Cavaco, S. Fernandes, M.M. Quina, L.M. Ferreira, *J. Hazard. Mater.* 144 (2007) 634.
 [19] S. Kartal, S. Tokahoglu, B. Özkan, *Bull. Kor. Chem. Soc.* 27 (2006) 694.
 [20] K. Prasad, R.S. Praveen, T. Prasada Rao, P. Gopikrishna, G.R.K. Naidu, *Atom. Spectrosc.* 26 (2005) 173.
 [21] T. Minami, Y. Sohrin, J. Ueda, *Anal. Sci.* 21 (2005) 1519.
 [22] G.M. Wuilloud, R.G. Wuilloud, J.C.A. De Wuilloud, R.A. Olsina, L.D. Martinez, *J. Pharmaceut. Biomed.* 31 (2003) 117.
 [23] P. Kar, M. Misra, *J. Chem. Technol. Biotechnol.* 79 (2004) 1313.
 [24] M.J. Richardson, J.H. Johnston, *J. Colloid Interface Sci.* 310 (2007) 425.
 [25] P. Krystek, R. Ritsema, *Int. J. Mass Spectrom.* 265 (2007) 23.
 [26] Y. Ren, Z. Fan, J. Wang, *Microchim. Acta* 158 (2007) 227.



Development and validation of a HPLC method for the determination of buprenorphine hydrochloride, naloxone hydrochloride and noroxymorphone in a tablet formulation

Ali Mostafavi^a, Ghazaleh Abedi^b, Ahmad Jamshidi^b, Daryoush Afzali^a, Mohammad Talebi^{b,*}

^a Department of Chemistry, Shahid Bahonar University of Kerman, Kerman, Iran

^b Novel Drug Delivery Systems Department, Iran Polymer & Petrochemical Institute, P.O. Box 14185-458, Tehran, Iran

ARTICLE INFO

Article history:

Received 30 June 2008

Received in revised form

12 September 2008

Accepted 17 September 2008

Available online 24 September 2008

Keywords:

Buprenorphine hydrochloride

Naloxone hydrochloride

Noroxymorphone

High-performance liquid chromatography

Tablet formulation

ABSTRACT

A simple isocratic reversed-phase high-performance liquid chromatographic method (RP-HPLC) was developed for the simultaneous determination of buprenorphine hydrochloride, naloxone hydrochloride dihydrate and its major impurity, noroxymorphone, in pharmaceutical tablets. The chromatographic separation was achieved with 10 mmol L⁻¹ potassium phosphate buffer adjusted to pH 6.0 with orthophosphoric acid and acetonitrile (17:83, v/v) as mobile phase, a C-18 column, Perfectsil Target ODS3 (150 mm × 4.6 mm i.d., 5 μm) kept at 35 °C and UV detection at 210 nm. The compounds were eluted isocratically at a flow rate of 1.0 mL min⁻¹. The average retention times for naloxone, noroxymorphone and buprenorphine were 2.4, 3.8 and 8.1 min, respectively. The method was validated according to the ICH guidelines. The validation characteristics included accuracy, precision, linearity, range, specificity, limit of quantitation and robustness. The calibration curves were linear ($r > 0.996$) over the concentration range 0.22–220 μg mL⁻¹ for buprenorphine hydrochloride and 0.1–100 μg mL⁻¹ for naloxone hydrochloride dihydrate and noroxymorphone. The recoveries for all three compounds were above 96%. No spectral or chromatographic interferences from the tablet excipients were found. This method is rapid and simple, does not require any sample preparation and is suitable for routine quality control analyses.

© 2008 Elsevier B.V. All rights reserved.

1. Introduction

Buprenorphine (Fig. 1a) is an oripavine derivative possessing partial *mu* agonist and *kappa* antagonist opioid activity with a potency of 20–40 times higher than that of morphine [1,2]. It has been used successfully by intramuscular, intravenous and sublingual routes for the treatment of moderate to severe pain at doses from 0.3 to 0.6 mg [3]. Clinical studies have shown that buprenorphine, like methadone, can also be used for the treatment of opioid addiction and withdrawal patients from heroin [4,5]. It is usually administered in sublingual formulation as either liquid or water-soluble tablets. As such, they can be diverted for illicit intravenous use. In an effort to circumvent this possibility, buprenorphine has now been coformulated in sublingual tablet with the *mu* antagonist, naloxone (Fig. 1b). Recently, sublingual tablets containing a fixed dose combination of buprenorphine hydrochloride (BH) and nalox-

one hydrochloride dehydrate (NH), at a ratio of 4:1 with respect to the free bases, have been approved by the Food and Drug Administration (FDA) for treating opiate dependence [6]. They are available in two strengths: 2 mg/0.5 mg tablets containing 2.16 mg BH (equivalent to 2 mg buprenorphine base) and 0.61 mg NH (equivalent to 0.5 mg naloxone base); and 8 mg/2 mg containing 8.64 mg BH (equivalent to 8 mg buprenorphine base) and 2.44 mg NH (equivalent to 2 mg naloxone base).

A literature survey reveals that there are a number of various analytical methods available for the quantitative individual determination of buprenorphine, or combination with other drugs mainly using chromatographic methods such as gas chromatography with electron-capture [7] or mass spectrometry [8,9] detection and HPLC with fluorescence [10], electrochemical [11] or mass spectrometry detection [12–14]. However, all of these methods involve an extraction and/or derivatization steps, which demand some well-known drawbacks including the possibility of incomplete derivatization, additional chromatographic interferences and increased method complexity and sample preparation time.

The British Pharmacopeia (BP) provides two different potentiometric titration methods for assay of BH and NH. Regarding the related substances, however, two distinct RP-HPLC procedures

* Corresponding author at: Novel Drug Delivery Systems Department, Iran Polymer & Petrochemical Institute, 15 KM Tehran-Karaj Highway, P.O. Box 14185-458, Tehran, Iran. Tel.: +98 21 44580000; fax: +98 21 44580021.

E-mail address: talebi.md@yahoo.com (M. Talebi).

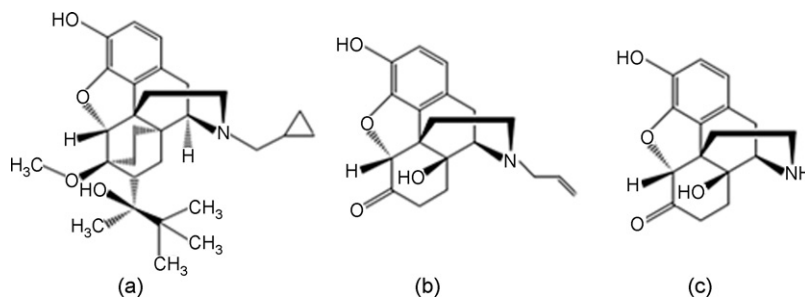


Fig. 1. Chemical structures of buprenorphine (a), naloxone (b) and noroxymorphone (c).

have been proposed, one for buprenorphine using UV detection at 288 nm, and another for naloxone impurities at 230 nm. BP specifies five substances as possible impurities for NH; one of them, noroxymorphone (NM, Fig. 1c), the starting material in NH synthesis, may cause gastric disturbance with nausea, vomiting and constipation and is required to be controlled [15]. In the United States Pharmacopoeia (USP), however; without specifying any other impurities than noroxymorphone hydrochloride, a TLC method is described for the determination of this compound and other NH impurities, yet monograph improvement has been requested [16,17].

It is worth noting the lack of official methods for assays of active ingredients and related substances in pharmaceutical preparations in pharmacopoeia, especially when it is currently possible to find a plethora of methods based on HPLC of these compounds. However, to the best of our knowledge, there are no chromatographic methods in the literature for the analysis of any buprenorphine dosage forms. The only reported analysis of buprenorphine in pharmaceutical products includes a spectrophotometric method based on colored ion-pair formation [18]. Hence, an attempt has been made to develop a simple, efficient and selective method for the determination of BH, NH and its major degradation impurity, NM, in sublingual tablets. In this study, HPLC instrumentation with UV detection, which is readily available in most analytical and pharmaceutical laboratories, was used. The method requires no extraction or derivatization steps reducing the total analysis run time to less than 10 min.

2. Experimental

2.1. Materials

Reference standards were purchased from Macfarlan Smith (Edinburgh, UK) and were checked against European Pharmacopoeia CRS standards (Strasbourg, France). The common tablet excipients and commercial marketed products were provided by Darou Darman Pars (Tehran, Iran). All other reagents were spectrophotometric or HPLC grade obtained from Romil Chemicals (Loughborough, UK). Water purified via a Milli-Q system, Millipore Corp. (Bedford, USA) was used for all purposes.

2.2. Instrumentation and chromatographic conditions

The HPLC system consisted of a Younglin ACME 9000 (Seoul, Korea) equipped with a quaternary pump, online degasser, column heater, autosampler and UV detector. Data collection and analyses were performed using Autochro 2000 software (Younglin). Separation was achieved on C-18 column, Perfectsil Target ODS3 (150 mm × 4.6 mm, 5 μm) with a 10 mm × 4.0 mm, 5 μm guard column (MZ-Analysentechnik, Mainz, Germany). The elution was isocratic with mobile phase of acetonitrile and 10 mmol L⁻¹ potassium phosphate buffer adjusted to pH 6.0 with orthophosphoric

acid (83:17, v/v). The flow rate was 1.0 mL min⁻¹ and yielded a back-pressure of about 740 psi. The column temperature was maintained at 35 °C, the detection was monitored at a wavelength of 210 nm and injection volume was 20 μL.

2.3. Standard solutions and calibration graphs for chromatographic measurement

Stock standard solutions of BH, NH and NM were separately prepared in methanol using individual EP CRS standards to obtain concentrations of 440, 200 and 200 μg mL⁻¹, respectively. If haziness was observed in NM solution, addition of about 0.5%, 0.1 mol L⁻¹ HCl was sufficient to clarify the solution. Calibration standards at eight levels were prepared by appropriately mixed and further diluted stock standard solutions in the concentration range of 0.022–220 μg mL⁻¹ for BH and 0.01–100 μg mL⁻¹ for NH and NM. Similarly, quality control (QC) standard solutions were prepared daily by diluting the corresponding stock standard solutions of individual reference standards for the final QC concentrations of 4.8, 48 and 240 μg mL⁻¹ for BH and 2.4, 24 and 120 μg mL⁻¹ for NH and NM, respectively. Samples in triplicates were made for each concentration and peak areas were plotted against the corresponding concentrations to obtain the calibration graphs.

2.4. Sample preparation

A number of 20 accurately weighed tablets were ground into a fine powder using a glass mortar and pestle. A portion equivalent to about four tablets (typically each contains 2.16 mg BH and 0.61 mg NH) was accurately weighed and transferred to a 20 mL volumetric flask. Approximately 15 mL methanol and about 0.5%, 0.1 mol L⁻¹ HCl were added to the flask and the contents were vortex-mixed for 10 min. The flask was adjusted to volume and mixed well. The resulting solution was filtered using 0.45 μm PTFE filter into standard analytical glass vials and injected into the HPLC. Three such samples were prepared from each 20-tablet mixture according to the USP criteria and injected triplicate.

2.5. Method validation

The method was validated according to the ICH guidelines [19]. The following validation characteristics were addressed: linearity, accuracy, precision, specificity, limits of detection and quantitation and robustness.

2.5.1. System suitability testing (SST)

System suitability standard solution which contained 200 μg mL⁻¹ BH, 100 μg mL⁻¹ NH and 0.1 μg mL⁻¹ NM was prepared by appropriately diluting and mixing the corresponding stock standard solutions. System suitability was determined from six replicate injections of the system suitability standard before

sample analysis. According to the monograph, the acceptance criteria for NH were less than 2% R.S.D. and a signal-to-noise ratio of at least ten for the corresponding peak area. For NM, acceptance criteria were less than 2% R.S.D. for peak area and not less than four for the resolution between the peaks corresponding to NM and NH. Resolution was calculated as defined by the USP.

2.5.2. Linearity and range

Standard calibration curves were prepared with seven calibrators over a concentration range of 0.22–220 $\mu\text{g mL}^{-1}$ for BH and 0.1–100 $\mu\text{g mL}^{-1}$ for both NH and NM. The data of peak area versus concentration were treated by linear least square regression analysis. The standard curves were evaluated for intra-day and inter-day linearity.

2.5.3. Accuracy

To study the reliability and suitability of the developed method, recovery experiments were carried out. Placebo samples were spiked with different amount of BH and NH at 50, 100 and 150% in duplicate for each one ($n=6$) over the theoretical values, and NM at 0.1% over the NH content. Measured values were compared with the theoretical concentration. Recovery for pharmaceutical formulations should be within the range $100 \pm 5\%$. The R.S.D. percent of individual measurements was also determined. The results must be less than 5%.

2.5.4. Precision

The precision of the developed method was assessed in terms of repeatability and intermediate precision by analyzing three replicate QC standard samples at 50, 100 and 150% levels that cover the calibration ranges for BH and NH, and at a single concentration of 0.1 $\mu\text{g mL}^{-1}$ for NM. The %R.S.D. values of the results corresponding to the peak area and retention time were expressed for intra-day precision and on 3 days for intermediate (inter-day) precision.

2.5.5. Specificity

Injections of the extracted placebo were performed to demonstrate the absence of interference with the elution of the BH, NH and NM. Samples containing NH's main impurities, the NM, were also injected. For determining selectivity of the method, a powder blend of typical tablet excipients containing lactose monohydrate, mannitol, maize starch, povidone K30, citric acid anhydrous granular, sodium citrate, natural lemon and lime flavour, acesulfame potassium and magnesium stearate was prepared and analyzed. All chromatograms were examined to determine if compounds of interest co-eluted with each other or with any additional excipient peaks.

2.5.6. Limits of detection and quantitation

The limit of detection (LOD) and limit of quantitation (LOQ) for the procedure were performed on samples containing very low concentrations of analytes under the ICH guidelines. By applying the visual evaluation method, LOD was expressed by establishing the minimum level at which the analyte can be reliably detected. LOQs were considered as the lowest concentration of analytes in standards that can be reproducibly measured with acceptable accuracy and precision.

2.5.7. Robustness

The robustness of the method was evaluated by analyzing the system suitability standards and evaluating system suitability parameter data after varying, individually, the HPLC pump flow rate ($\pm 10\%$), organic solvent content ($\pm 6\%$) and column compartment temperature ($\pm 14\%$).

3. Results and discussion

3.1. Method development and optimization

NM is a major impurity of NH drug substance. The main target of the chromatographic assay method development was to separate the impurity co-eluted with naloxone. Typically, method development focuses on identifying buffer type, strength and pH, organic solvent and implementing small changes to optimize selectivity and enhance resolution. Initially, NM was found to be co-eluted with naloxone by using different stationary phases such as C-8 and C-18, with mobile phases containing buffers like phosphate, at different pH and temperature, and organic solvents like methanol and acetonitrile.

At the first stage, a C-8 column chemistry and potassium phosphate buffer, pH 3.0, were used with methanol as the organic solvent. Though the column was base deactivated for improved peak shape of basic compounds, both peak symmetry and resolution between two compounds were poor. Subsequently, an acceptable peak shape and resolution were achieved by increasing the buffer pH to 6.0, approximately 2.5 and 2.0 pH units above the pK_{a1} of BH and NH, respectively; and using ternary solvent system consisting of 10% acetonitrile and 70% methanol as organic solvent. Nevertheless, the run time was prohibitively long at approximately 14 min.

In order to better exploit the polarity differences between the desired compounds, while maintaining a short run time; two C-18 columns were evaluated. A typical silica-based monolithic column, which proves to dramatically reduce the analysis time, was examined at first. Although the retention time of buprenorphine reduced to about 6.0 min, applying the monolithic column at its best operating conditions (an organic content of 45% ACN at a flow rate of 2.0 mL min^{-1} and oven temperature of 40 °C), produced neither complete resolution between the first peak (naloxone) and contaminants co-eluted at the beginning, nor better asymmetry factor of 0.7 for studied compounds. The excessive resolution at the beginning of the chromatogram and appropriate peak shape were finally achieved by switching to a base deactivated Perfectsil target ODS3 column. For optimum resolution, peak asymmetry and analysis time, the mobile phase consisting of 10 mmol L^{-1} potassium phosphate buffer adjusted to pH 6.0 with orthophosphoric acid and acetonitrile (17:83, v/v) was used. To improve repeatability of runs, shorten analysis time and reduce back pressure, which is important to extending the column life time, the column oven temperature was set at 35 °C. In the optimized conditions, NM and the drug substances naloxone and buprenorphine were well separated with resolutions of more than 10 and 18, and asymmetry factors very close to 1.0. The optimal wavelength was established experimentally after measuring all spectra in mobile phase and testing the detector response of analytes using UV absorbance scanned over the range of 190–400 nm. Although the absorption maxima recommended by BP for BH and NH were 288 and 230 nm, respectively; it was shown that 210 nm is the optimal wavelength to maximize the sensitivity and has no interference with other components of the formulation. Under the experimental conditions investigated, the retention times for naloxone, noroxynorphine and buprenorphine were 2.40, 3.84 and 8.06 min, respectively (Fig. 2).

3.2. Method validation

When a method has been optimized it must be validated before practical use. By following the ICH guidelines for analytical method validation, Q2 (R1), the SST was performed and the validation characteristics were addressed.

Table 1
Linearity parameters for the simultaneous estimation of NH, NM and BH.

Parameter	Naloxone hydrochloride	Noroxymorphone	Buprenorphine hydrochloride
Linearity range ($\mu\text{g mL}^{-1}$)	0.10–100	0.10–100	0.22–220
Slope	67.70 ± 0.24	75.75 ± 0.55	79.80 ± 0.12
Intercept	28.90 ± 7.01	193.10 ± 0.59	-35.20 ± 6.86
Correlation coefficient (r)	0.9997 ± 0.0001	0.9961 ± 0.0005	0.9997 ± 0.0001
Residual sum of squares	0.00028	0.00378	0.00036

Values are reported as mean \pm S.D. of three calibration curves generated on three consecutive days ($n = 3$). Seven concentrations in the linearity range were evenly distributed.

Table 2
Method validation results for studied compounds.

	Naloxone hydrochloride	Noroxymorphone	Buprenorphine hydrochloride
SST			
Theoretical plates	6485	7599	8668
Asymmetry (A_s)	1.0	1.1	1.0
Resolution (R_s)	3.5	10.3	18.8
Repeatability ^a , t_R (%R.S.D.)	0.3	1.7	1.3
Repeatability ^a , A (%R.S.D.)	0.6	1.5	0.6
Validation			
Precision ^{a,b} (%R.S.D.)	3.1	2.9	4.2
Accuracy ^{a,b} (%R.S.D.)	4.1	5.0	3.3
Accuracy (%recovery)	102.8	96.2	102.3
Selectivity	No interference	No interference	No interference
LOD ($\mu\text{g mL}^{-1}$)	0.01	0.01	0.02
LOQ ($\mu\text{g mL}^{-1}$)	0.10	0.10	0.22

^a Intra-day precision (repeatability), inter-day precision and accuracy were tested by analyzing three replicate QC standard samples at 50, 100 and 150% levels for BH and NH and at a single concentration of $0.1 \mu\text{g mL}^{-1}$ for NM under the guidelines of ICH.

^b Inter-day precision and accuracy were determined with three replicates on three consecutive days.

3.2.1. System suitability

The system suitability test ensures the validity of the analytical procedure as well as confirms the resolution between different peaks of interest. All critical parameters tested met the acceptance criteria on all days. According to the monograph, however, the area of an individual secondary chromatographic peak, which appears in the test sample, should not exceed 0.5% of the naloxone peak area, and the total area of all secondary peaks, 1% naloxone peak area. In addition, the resolution between the peak corresponding to naloxone and NM in the chromatogram obtained with reference solution should not be less than 4 at S/N of at least 10 [15]. Adequate resolution of >10 between the naloxone and its impurity, NM, meets the acceptance criteria indicated in the monograph. As

shown in the chromatogram, all three analytes are eluted by forming symmetrical single peaks well separated from the solvent front (Fig. 2).

3.2.2. Linearity and range

For the construction of calibration curves, seven calibration standard solutions were prepared over the concentration range of $0.22\text{--}220 \mu\text{g mL}^{-1}$ for BH and $0.1\text{--}100 \mu\text{g mL}^{-1}$ for NH and NM. The results, summarized in Table 1, show a good correlation between analytes peak area and concentration with $r > 0.996$ ($n = 7$).

3.2.3. Accuracy and precision

Accuracy and precision were established across the analytical range for BH, NH and NM. The intra- and inter-day accuracy and precision were calculated from the QC samples (Table 2). Repeatability (intra-day precision) of the analytical method was found to be reliable based on %R.S.D. ($<2\%$) corresponding to the peak areas and retention times. Intermediate precision (inter-day accuracy) was demonstrated on different days and evaluating the peak area data at three QC standards that cover the assay method range. The %R.S.D. values were less than 5% and illustrated the good precision for the analytical method. For determining accuracy, placebo solutions spiked with reference standards were used. The recovery was $100 \pm 5\%$ for all samples with %R.S.D. less than 5%.

3.2.4. Specificity

Injections of the extracted placebo were performed to demonstrate the absence of interference with the elution of the drugs and impurity. These results demonstrate that there was no interference from other materials in the tablet formulation; therefore, confirm the specificity of the method (Fig. 2).

3.2.5. Sensitivity

The limit of detection and limit of quantitation decide about the sensitivity of the method. Tests for the procedure were performed on samples containing very low concentrations of analytes based

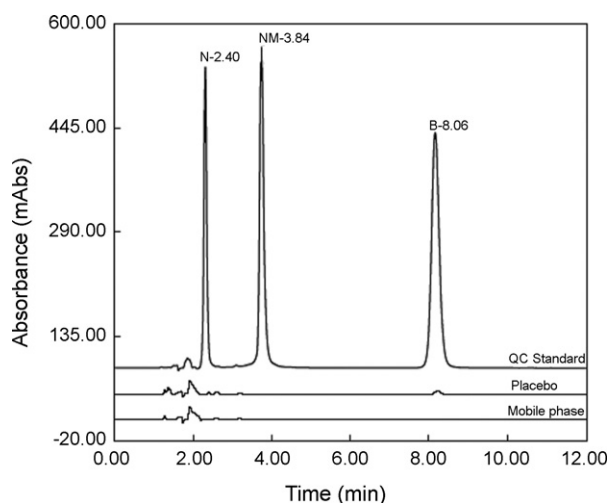


Fig. 2. Representative chromatograms obtained for the mobile phase, placebo and QC standard (corresponding to the 24, 24 and $48 \mu\text{g mL}^{-1}$ NH, NM and BH, respectively).

Table 3
Method validation data for robustness study.

Parameter altered	Retention time, t_R (min)			Resolution (R_s)			Asymmetry (A_s)		
	N	NM	B	N	NM	B	N	NM	B
Optimized chromatographic conditions ^a	2.4	3.8	8.0	3.5	10.3	18.8	1.0	1.1	1.0
Increased organic solvent (16:84)	2.3	3.7	8.0	2.5	8.75	18.1	0.9	1.0	1.0
Decreased organic solvent (18:82)	2.4	3.9	8.1	3.0	9.4	20.1	1.1	1.15	1.1
Increased flow rate (1.1 mL min ⁻¹)	2.2	3.7	7.8	1.8	8.2	17.8	1.0	1.1	1.0
Decreased flow rate (0.9 mL min ⁻¹)	2.6	3.9	8.3	4.2	9.3	18.7	1.1	1.2	1.15
Decreased column temperature (30 °C)	2.5	4.0	8.3	3.6	10.5	20.1	1.1	1.2	1.1

^a Chromatographic conditions were 10 mmol L⁻¹ potassium phosphate buffer, pH 6.0/ACN (17:83) maintained with flow rate of 1.0 mL min⁻¹, temperature at 35 °C and detection at 210 nm.

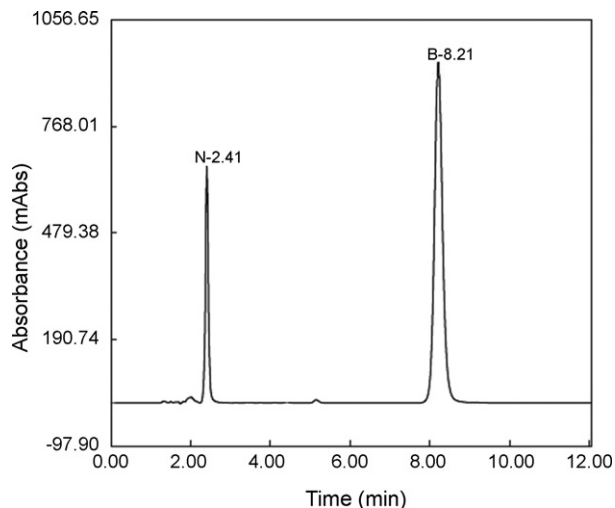


Fig. 3. Representative chromatogram obtained for a commercially available BH/NH (4:1) drug product (N: naloxone; B: buprenorphine).

on the visual evaluation method. In this method, LOD is determined by the analysis of samples with known concentration of analyte and by establishing the minimum level at which the analyte can be reliably detected. Accordingly, the LOQ is determined by the analysis of samples with known concentration of analytes and by establishing the minimum level at which the analyte can be quantified with acceptable accuracy and precision (R.S.D. <2%). The LOD and LOQ values were found to be 0.022 and 0.22 $\mu\text{g mL}^{-1}$ for BH and 0.01 and 0.1 $\mu\text{g mL}^{-1}$ for both NH and NM.

3.2.6. Robustness

To ensure the insensitivity of the developed HPLC method to minor changes in the experimental conditions, it is important to demonstrate its robustness. None of the alterations caused a significant change in resolution between naloxone and NM, peak area R.S.D., USP tailing factor and theoretical plates (Table 3). Although the changes in retention times were more significant, separation was sufficient and quantitation was still possible.

3.3. Analysis of the marketed product

The validated method was used in the analysis of a marketed product in a 70 mg tablet dosage form with dose strength of 2.0 mg BH/0.5 mg NH. Representative chromatogram is shown in Fig. 3. The results for the drugs assay and the concentration of impurity NM were in good agreement with the label claims. BH content was between 91.4 and 93.5%, and for NH between 97.2 and 104.7%. The

amount of NM was found below the detection limit (0.01 $\mu\text{g mL}^{-1}$) and, therefore, should be less than 0.1% over the NH content.

4. Conclusion

A simple isocratic reversed-phase HPLC method proposed was found to be accurate, precise, linear across the analytical range and robust. The method was specific for the simultaneous determination of BH, NH and its primary impurity NM in a tablet formulation. All the parameters for three substances met the criteria of the ICH guidelines for method validation. The method could therefore be recommended for routine quality control analysis of raw materials and various buprenorphine and naloxone dosage in tablet formulations by assaying for potency and accurately monitoring the NM impurity.

Acknowledgement

Kimia Sanat Jahan Co. is acknowledged for kindly furnishing the home edition of Autochro-2000 HPLC software.

References

- [1] S.L. Walsh, K.L. Preston, G.E. Bigelow, M.L. Stitzer, J. Pharmacol. Exp. Ther. 247 (1995) 361.
- [2] G.B. Collins, M.S. McAllister, Clev. Clin. J. Med. 74 (2007) 514.
- [3] J.W. Lewis, in: A. Cowan, J.W. Lewis (Eds.), Buprenorphine: Combating Drug Abuse with a Unique Opioid, Wiley-Liss, New York, 1995, p. 151.
- [4] R.E. Johnson, J.H. Jaffe, P.J. Fudala, J. Am. Med. Assoc. 267 (1992) 2750.
- [5] W. Ling, D.R. Wesson, C. Charuvastra, C.J. Klett, Arch. Gen. Psychiatry 53 (1996) 401.
- [6] C.N. Chiang, R.L. Hawks, Drug Alcohol Depend. 70 (2003) S39.
- [7] E.T. Everhart, P. Cheung, P. Shwonek, K. Zabel, E.C. Tisdale, P. Jacob III, J. Mendelson, R.T. Jones, Clin. Chem. 43 (1997) 2292.
- [8] A.M. Lisi, R. Kazlauskas, G.J. Trout, J. Chromatogr. Biomed. Appl. 692 (1997) 67.
- [9] L. Debrabandere, M. Van Boven, L. Laruelle, P. Daenens, Anal. Chim. Acta 275 (1993) 295.
- [10] S.Y. Liu, K.S. Liu, C.H. Kuei, J.L. Tzeng, S.T. Ho, J.J. Wang, J. Chromatogr. B 818 (2005) 233.
- [11] M.A. García-Fernández, M.T. Fernández-Abedul, A. Costa-García, Chromatographia 53 (2001) 704.
- [12] D.E. Moody, M.H. Slawson, E.C. Strain, J.D. Laycock, A.C. Spanbauer, R.L. Foltz, Anal. Biochem. 306 (2002) 31.
- [13] S. Pirnay, F. Hervé, S. Bouchonnet, B. Perrin, F.J. Baud, I. Ricordel, J. Pharm. Biomed. Anal. 41 (2006) 1135.
- [14] M.E. Rodriguez-Rosas, M.R. Lofwall, E.C. Strain, D. Siluk, I.W. Wainer, J. Chromatogr. B 850 (2007) 538.
- [15] The British Pharmacopoeia 2007, The Stationary Office (TSO), Health Ministry, London, 2006.
- [16] The United State Pharmacopoeia, 27th ed., The United States Pharmacopoeial Convection, Rockville, MD, 2004.
- [17] <http://www.usp.org/USPNF/submitMonograph/improveMon.html>.
- [18] M. Amanlou, P. Khosravian, E. Souri, O.G. Dadrass, R. Dinarvand, M.M. Alimorad, H. Akbari, Bull. Korean Chem. Soc. 28 (2007) 183.
- [19] ICH guidelines Topic Q2 (R1) Validation of Analytical Procedures: Methodology, obtained from web site: www.emea.europa.eu/hmtms/human/ich/ichquality.htm.



Trace analysis of cefotaxime at carbon paste electrode modified with novel Schiff base Zn(II) complex

Preeti Nigam^b, Swati Mohan^a, Subir Kundu^b, Rajiv Prakash^{a,*}

^a School Materials Science and Technology, Institute of Technology, Banaras Hindu University, Varanasi 221005, India

^b School of Biochemical Engineering, Institute of Technology, Banaras Hindu University, Varanasi 221005, India

ARTICLE INFO

Article history:

Received 29 July 2008

Received in revised form

12 September 2008

Accepted 16 September 2008

Available online 25 September 2008

Keywords:

Cefotaxime

Carbon paste electrode

Schiff base octahedral Zn(II) complex

Differential pulse voltammetry

Antibiotic estimation

ABSTRACT

Cefotaxime a third generation cephalosporin drug estimation in nanomolar concentration range is demonstrated for the first time in aqueous and human blood samples using novel Schiff base octahedral Zn(II) complex. The cefotaxime electrochemistry is studied over graphite paste and Zn(II) complex modified graphite paste capillary electrodes in H₂SO₄ (pH 2.3) using cyclic voltammetry and differential pulse voltammetry. Cefotaxime enrichment is observed over Zn(II) complex modified graphite paste electrode probably due to interaction of functional groups of cefotaxime with Zn(II) complex. Possible interactions between metal complex and cefotaxime drug is examined by UV–vis and electrochemical quartz crystal microbalance (EQCM) techniques and further supported by voltammetric analysis. Differential pulse voltammetry (DPV) with modified electrode is applied for the determination of cefotaxime in acidified aqueous and blood samples. Cefotaxime estimation is successfully demonstrated in the range of 1–500 nM for aqueous samples and 0.1–100 μM in human blood samples. Reproducibility, accuracy and repeatability of the method are checked by triplicate reading for large number of samples. The variation in the measurements is obtained less than 10% without any interference of electrolyte or blood constituents.

© 2008 Elsevier B.V. All rights reserved.

1. Introduction

Cephalosporins are the second major group of β-lactam class of antibiotics with broad spectrum of antimicrobial properties. Their antibacterial and pharmacokinetic properties have wide therapeutic use [1–5]. These are classified into four generations based on their resistance towards β-lactamase degradation. Cephalosporins have an added advantage that penicillin allergic patients can be treated with these antibiotics.

Cefotaxime is third generation cephalosporin having broad activity against gram positive cocci (not enterococcus) and gram negative bacteria (not Pseudomonas). The syn-configuration of the methoxyimino moiety gives stability to β-lactamase enzymes produced by many gram-negative bacteria which results into its broad antibacterial activity. Cefotaxime has wide clinical applications including treatment of infection in respiratory tract, gynecologic, skin, bone and joint, urinary tract, septicemia, and documented or suspected meningitis.

The determination of cephalosporins is important not only in the field of human health for pharmacokinetic analysis but also for quality control in food and fermentation industry to check

their illegal use as in food preservation, processing, introduction of antibiotics in dairy products and as fodder additives [6].

Till now several methods have been reported to study various cephalosporins such as spectrophotometric [7–9] and chromatographic [10–14] techniques, though these methods give good sensitivity and selectivity but are rather time consuming and have complicated analysis and sample preparation steps. Therefore, electroanalytical techniques are the method of choice for fast and rapid determination of cephalosporins. Most of these methods utilized polarographic activity involving reduction of antibiotics at hanging drop mercury electrodes by using differential pulse polarography and adsorptive stripping voltammetry [15–29]. A very few analysis incorporate electrochemical oxidation of cephalosporins, the first reference is obtained from the work of Fabre et al. [30] at solid electrodes and carbon paste electrodes to avoid the mercury hazards [31–34].

Cephalosporins are sulfur containing compounds. Electrochemical study of sulfur containing compounds have been done with gold, platinum, carbon electrodes [35–37], but severe working conditions may lead to electrode poisoning and improper current signal. To overcome this problem modified electrodes were used and reported in literature. Carbon based electrodes due to their low cost, low electrical resistance, ease of modification, and wide potential window are widely used in voltammetric analysis. Glassy carbon [38–40], carbon paste [41–43], carbon compos-

* Corresponding author. Tel.: +91 542 2307047; fax: +91 542 2368707.
E-mail address: rajivprakash12@yahoo.com (R. Prakash).

ite [44–46] are mostly used as modified electrodes for chemical analysis.

Chemically modified electrodes (CMEs) have continued to be of major concern during the past decade and much attention is paid to develop modified electrodes and applications of different types of CMEs. Recently, modified electrode with carbon nanotubes for highly sensitive and selective analysis of various analytes has been developed and applied for cephalosporins [47–50]. Modification of electrodes with suitable biocompatible materials provides a way of non-hindered electrochemistry of redox biological compounds. This phenomenon generally results in increased selectivity and sensitivity of the determinations. It is a well known fact for years that certain transition metal complexes with phthalocyanines [51,52], porphyrins [53,54] and Schiff bases [55,56] can catalyze the electro-oxidation of some chemical and biological important compounds via involvement of their central metal ions. A number of these compounds, as electron mediators in modified electrodes have been applied characterized for electrocatalysis of cysteine and its derivatives [57], glutathione [58], 2-thioglycolic acid [51], penicillamine [55], captopril [59,60], cephalosporins [56] and other sulfhydryl compounds [61,62]. Transition metal complex with Schiff base ligand shows scientific interest due to their wide implementations [55,56,60].

In the present study electrochemical estimation of cefotaxime, third generation of cephalosporin, is examined using novel Schiff base Zn complex. To the best of our knowledge for the first time an electrochemical estimation is reported involving low cost modified carbon paste electrode for nanomolar range of cefotaxime drug. The aim of this study is to demonstrate the interactions of cefotaxime drug with Schiff base Zn(II) complex and to develop a fast and rapid voltammetry method for direct detection of cefotaxime without any tedious pretreatment steps in nanomolar range.

2. Experimental

2.1. Apparatus

Electrochemical experiments were performed with Potentiostat/Galvanostat (model CHI7041C) CH-Instrument, Inc., USA, and Autolab by electrochemical quartz crystal microbalance (EQCM) instrument, The Netherlands for determination of interaction of cefotaxime with Zn(II) complex. A conventional three electrode cell assembly was used with a carbon paste as working electrode (unmodified or modified), saturated Ag/AgCl reference electrode and Pt rod as the counter electrode. A digital pH meter (cyber PH-14) was used for preparing electrolyte solution. PerkinElmer UV spectrophotometer (Obtained under DAAD Instrument grant, Germany) was also used in this study.

2.2. Reagents

The Schiff's-base (4-n-butyl) phenyl pyridoxaldimine (Hbppypr) ligand and Zn(Hbppypr)₂·2H₂O complex (Fig. 1) was synthesized in our chemistry department lab [63,64]. Graphite powder, mineral oil (Nujol) and cefotaxime sodium salt were purchased from Sigma–Aldrich. All other chemicals were of analytical grade. Fresh aqueous solutions of cefotaxime were prepared daily with double distilled deionized water. The voltammetry was carried out in H₂SO₄ (pH 2.3) and acidified human blood samples (pH 2.3).

2.3. Preparation of modified electrode

Carbon-paste capillary electrode was prepared by mixing graphite powder with (1 μm particle size) an appropriate amount of mineral oil (Nujol) and thorough hand mixing in a mortar and

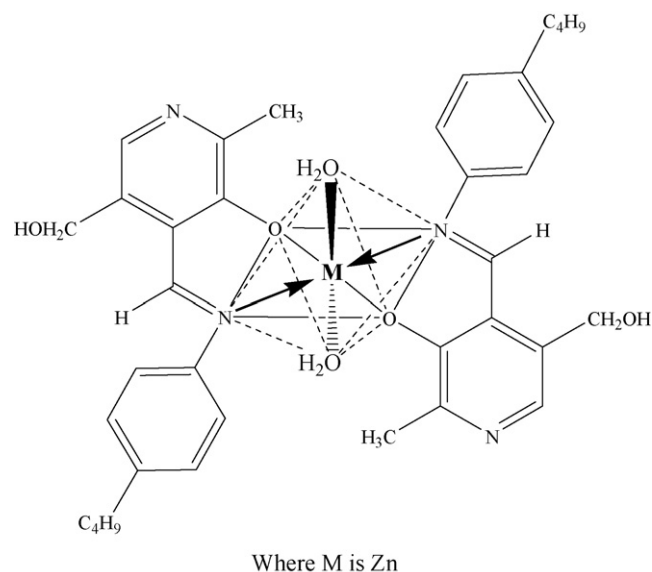


Fig. 1. Octahedral geometry of Zn(Hbppypr)₂·2H₂O complex.

pestle. A portion of the graphite paste mixture was packed into the end of a glass capillary (0.5 mm inner diameter). Electrical contact was made by forcing a copper wire down the glass capillary from back side as shown in Fig. 2. The modified electrode was prepared by mixing graphite powder with Zn(II) complex (70:30 ratio) using tetrahydrofuran (THF) solvent. The mixture was mixed in a mortar and pestle till all the solvent evaporated to give dry solid material.

2.4. Electroanalysis of cefotaxime

The electrochemical behavior of cefotaxime (a third generation cephalosporin drug as shown in Fig. 3) was studied using modified carbon paste electrode. Cyclic voltammetry (CV) and differential pulse voltammetry (DPV) were used for the estimation of drug using modified carbon paste capillary as working electrode.

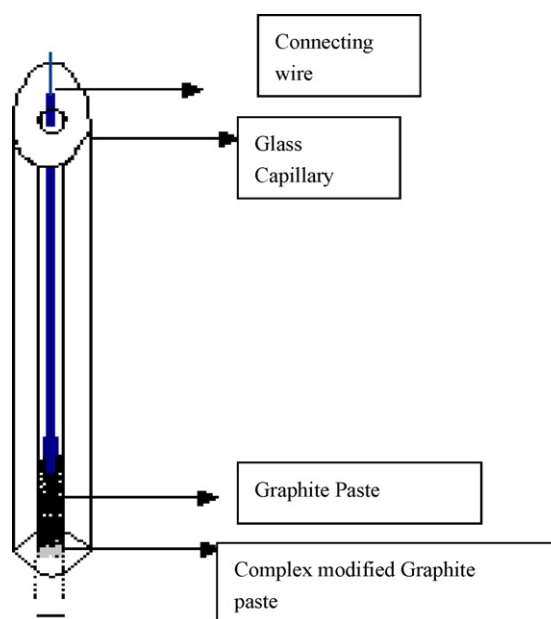


Fig. 2. Capillary graphite paste electrode used for electrochemical studies and electroanalytical applications.

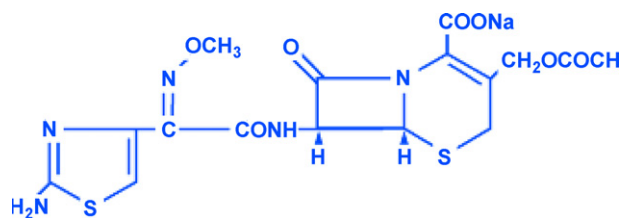


Fig. 3. Cefotaxime a third generation cephalosporin drug.

Voltammograms were recorded in a potential window -0.2 to 1.1 V vs. Ag/AgCl at various scan rates and DPV with pulse width 0.05 s. Various concentrations of cefotaxime from 0.1 mM to 1 nM were analyzed in water as well as in acidified human blood samples (pH 2.3). All measurements were performed in triplicate and average was used to plot the calibration curve.

2.5. Analysis of spiked blood serum samples

Serum samples of healthy individuals were stored in refrigerator. After gentle, thawing, an aliquot volume of serum sample was spiked with cefotaxime and left stirred for 5 min. After above procedure, the whole sample was taken carefully. The concentration of cefotaxime was varied in the range of 1×10^{-7} to 1×10^{-4} M in acidified human serum samples. These solutions were analyzed in the voltammetric cell containing dilute H_2SO_4 as supporting electrolyte (pH 2.3).

3. Results and discussion

Cefotaxime is a third generation cephalosporin drug, which is electroactive and shows well resolved redox peaks in acidic pH. Previous studies carried out on the series of cephalosporins and their decomposition products indicate that aminothiazole substituent on the side chain at position 7 of the D3-cephem ring is the electroactive group that undergoes anodic oxidation in the case of cefotaxime [31]. Cathodic reduction of cephalosporins has been widely investigated and published but there are only a few references in the literature dealing its estimation based on anodic oxidation [30–34]. Its cathodic behavior with square wave voltammetry was recently studied [65]. However, nanomolar range, anodic voltammetric analysis of cefotaxime in aqueous and biological samples is not reported till now. In this investigation the electro-oxidation of cefotaxime over modified electrode is exploited for trace estimation of drug in aqueous as well as human blood samples.

3.1. Voltammetric studies of cefotaxime

Cyclic voltammetry of cefotaxime showed two irreversible anodic peaks at 1.02 V vs. Ag/AgCl (sharp peak) and another small peak (shown by *) at 0.5 V vs. Ag/AgCl in H_2SO_4 (pH 2.3) at sweep rate 100 mVs^{-1} as shown in Fig. 4 (inset). The same was also observed with more prominent nature in DPV when carried out by mixing traces of solid cefotaxime with graphite paste as shown in Fig. 4. Our study was concentrated to the peak with large anodic peak current (at 1.02 V vs. Ag/AgCl), which was further used for the trace analysis of the drug. Using bare graphite electrode the minimum level of detection was possible up to 10^{-5} M in the solution and below this concentration no resolved peak was observed (figure not shown). Since its wide therapeutic application required micromolar and sub micromolar level detection, therefore, further electrode was modified for detection at low concentration levels.

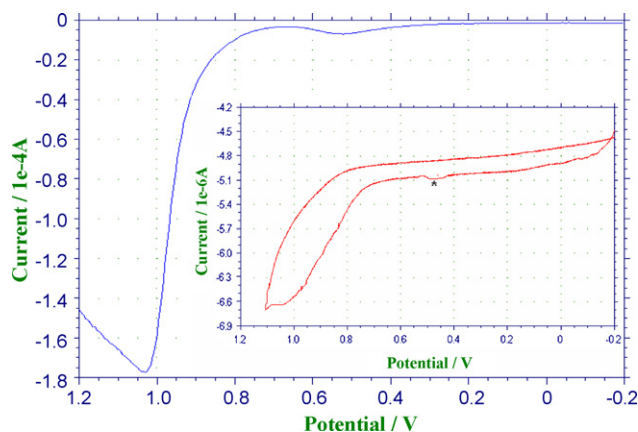


Fig. 4. DPV and CV (inset) of cefotaxime at bare graphite paste capillary electrode at pH 2.3 in H_2SO_4 .

3.2. Modification of graphite paste electrode

In order to further enhance the sensitivity graphite paste electrode was modified with our recently synthesized Zn(II) complexes of a novel Schiff base derived from pyridoxal [63,64]. Zn(II) complex is octahedral complex having two axial water molecule and uninegative bidentate ligand as shown in Fig. 1. The two water molecules present at octahedral positions may be easily replaced by other strong ligands. The criteria of this modification was adopted based on the possibility of strong interaction between cefotaxime drug functional groups with Zn(II) complex and enrichment of drug over the sensing electrode. The interaction of Schiff base Zn(II) complex with drug was studied using UV–vis, EQCM and electrochemical techniques.

3.3. UV–vis study of cefotaxime–Zn(II) complex interaction

UV–vis analysis of Zn(II) complex gives three peaks at 286, 337 and 403 nm, while cefotaxime showed three peaks at 234, 261 and 301 nm as shown in Fig. 5 curves A and B (indicated by *) respectively. Zn(II) complex peaks completely get suppressed when cefotaxime mixed with Zn(II) complex in equal molar ratio in dilute H_2SO_4 (pH 2.3). Apart from disappearance of Zn(II) complex peaks the resultant UV–vis spectrum showed significant changes. A small shift in the cefotaxime peak at 234 nm (lower shift) was observed along with appearance of two new peaks at higher wavelength at 500 and 920 nm as shown Fig. 5 (inset). Probably increase in the double bond conjugation after coupling of Zn(II) complex with the drug molecules caused the appearance of two new peaks at higher wavelength. This UV–vis spectrum itself is a clear indication of interaction between cefotaxime and Zn(II) complex. These results were further confirmed by electrochemical quartz crystal microbalance and electrochemical studies.

3.4. Electrochemical quartz crystal microbalance (EQCM) studies for interaction between cefotaxime and Zn(II) complex

Zn(II) complex spin coated quartz crystal electrode was mounted in the holder and dipped in a cell having 80 ml working volume filled with dilute H_2SO_4 (pH 2.3) as supporting electrolyte. Cefotaxime solution was added into the cell with stirring to get resultant solution of 100 μ M and responses were recorded with Maxtek EQCM software. The mass of coated EQCM crystal electrode exposed in H_2SO_4 solution was taken as zero and then change in mass and change in frequency with time were recorded after addition of cefotaxime as shown in Fig. 6. Total mass change

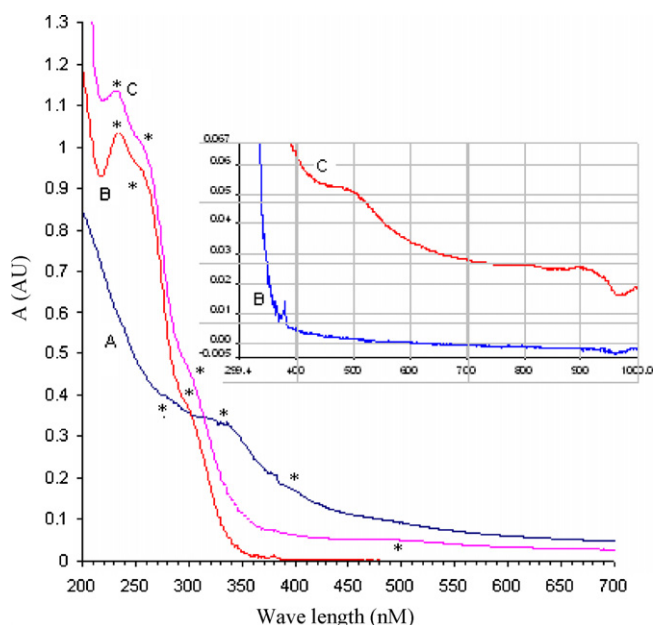


Fig. 5. UV-vis spectra of (A) Zn complex, (B) cefotaxime and (C) cefotaxime-Zn(II) complex. Two additional peaks at 500nm and 920 are shown (C) in inset for cefotaxime-Zn(II) complex.

(Δm) for the first 5 min run was $0.52 \mu\text{g}/\text{cm}^2$, which tends to constant after 5 min. The EQCM results showed an addition of $0.52 \mu\text{g}$ of cefotaxime per square cm coated Zn(II) complex electrode in 5 min. This EQCM analysis clearly showed a complexation between cefotaxime and Zn(II) complex and was in accord with the DPV results, showing time dependent interaction between cefotaxime and Zn(II) complex (effect of enrichment on electrode surface).

3.5. Electrochemical study of interaction between cefotaxime and Zn(II) complex

The evidence of interaction between cefotaxime and Zn(II) complex was also observed from DPV as shown in Fig. 7. The bare graphite electrode did not show any anodic peak in H_2SO_4 , while Zn(II) complex coated graphite paste electrode showed a sharp peak at 1.02 V vs. Ag/AgCl as shown in Fig. 7 curves A and B respectively. When the cefotaxime was added to the same solution to get the resultant concentration as $0.25 \mu\text{M}$, the anodic oxidation showed a sharp peak at 0.95 V and a broad peak at 0.51 V vs. Ag/AgCl due to presence of cefotaxime as shown in Fig. 7 curve C. When the same experiment was repeated after 3 min (without any biasing) both the peaks i.e. 0.95 V and 0.51 V vs. Ag/AgCl appeared with nearly

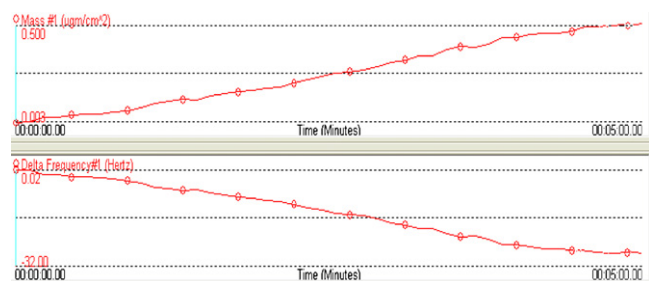


Fig. 6. EQCM data showing change in mass and frequency of the crystal (coated with Zn(II) complex) vs. time due to complex formation between cefotaxime ($100 \mu\text{M}$ solution) and Zn(II) complex.

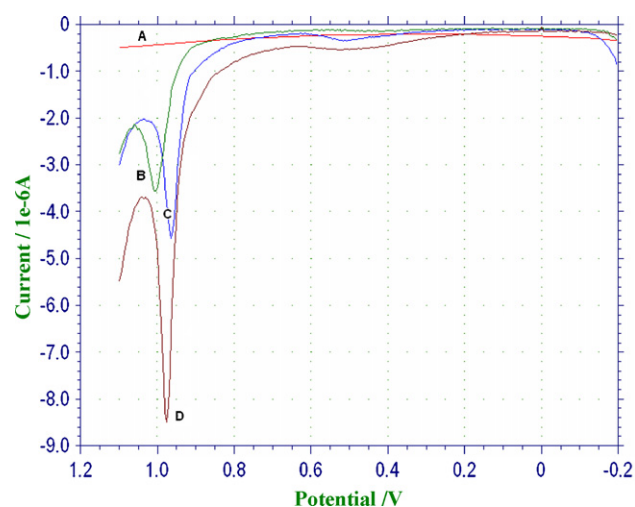


Fig. 7. DPV response in $0.25 \mu\text{M}$ cefotaxime in H_2SO_4 (2.3 pH) of (A) graphite paste electrode, (B) Zn(II) complex, (C) cefotaxime-Zn(II) complex (D) cefotaxime-Zn(II) complex after 3 min enrichment.

double peak current as shown in Fig. 7 curve D. An increase in the peak current on incubation was the clear evidence for interaction and enrichment of the cefotaxime drug over the modified electrode.

3.6. Analytical application of Zn(II) modified graphite paste capillary electrode

Above interactions between cefotaxime and Zn(II) complex and the enrichment of cefotaxime over Zn(II) complex modified electrode were utilized for sensitive detection of cefotaxime up to nanomolar concentrations. For this analysis, phosphate buffer, Tris-HCl and H_2SO_4 at various pH were examined. The best result was observed with $0.5\text{N H}_2\text{SO}_4$ ($\sim\text{pH } 2.3$). Though cefotaxime level can be determined in any of the real samples like blood, urine and milk, however we utilized the above analysis for cefotaxime level determination in water and human blood serum samples. The experiment was performed using same Zn(II) complex modified graphite paste capillary electrode by taking the cefotaxime concentration in 1–500 nM. The cefotaxime oxidations peaks were

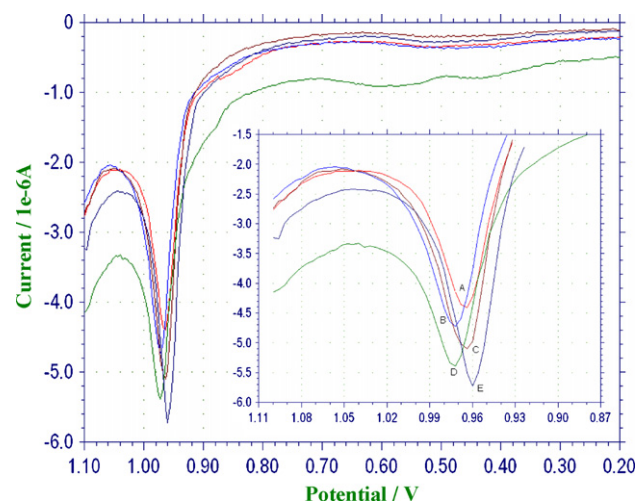


Fig. 8. DPV response for (A) 1 nM, (B) 5 nM, (C) 10 nM, (D) 25 nM and (E) 50 nM concentrations of cefotaxime in H_2SO_4 (2.3 pH) at Zn(II) complex modified graphite paste capillary electrode.

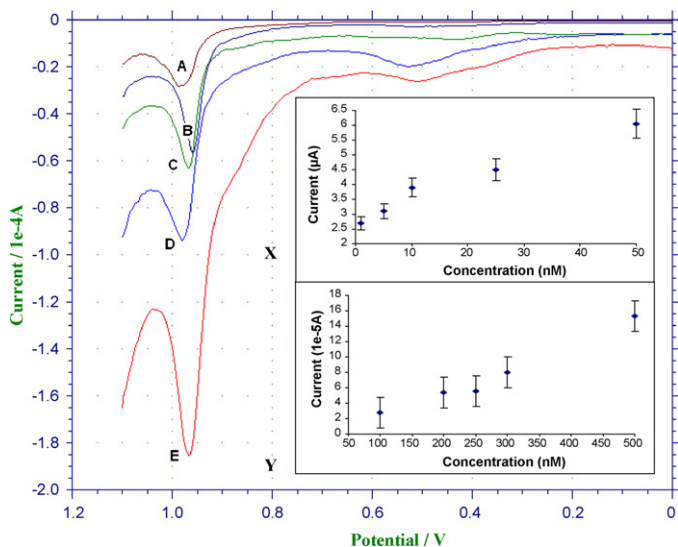


Fig. 9. DPV response for (A) 100 nM, (B) 200 nM, (C) 250 nM, (D) 300 nM and (E) 500 nM concentrations of cefotaxime in H_2SO_4 (2.3pH) at Zn(II) complex modified graphite paste capillary electrode. Inset: calibration plot for cefotaxime estimation in the range of (X) 1–50 nM and (Y) 100–500 nM.

appeared as shown in Figs. 8 and 9. The blank response was same as shown in Fig. 7 almost a straight line.

The quantitative estimation of cefotaxime was carried out by measuring the peak current vs. cefotaxime concentration. A calibration plot (Fig. 9 inset) showed linearity for the cefotaxime concentrations in the range of (X) 1 nM to 50 nM and (Y) from 100 to 500 nM. A sharp change in slope was observed between 50 and 100 nM.

Further analysis of drug in serum samples was demonstrated by spiking human blood samples without any interference. The serum samples were not subjected to any prior treatment except their 50 times dilutions with 0.5N H_2SO_4 adjusted to pH 2.3. DPV was applied and voltammograms were recorded as shown in Fig. 10. Based on the above condition cefotaxime concentrations were determined in spiked serum samples from 0.1 to 100 μM and calibration plot was obtained linear in the range of 1–100 μM with detection limit as 1 μM as shown in Fig. 10 inset. The blank gave a broad peak at 0.5 V vs. Ag/AgCl probably due to oxidation

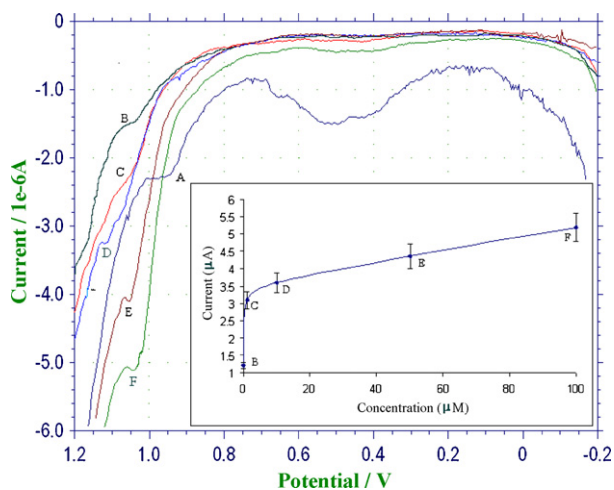


Fig. 10. DPV response for (A) Blank, (B) 0.1 μM , (C) 1 μM , (D) 10 μM , (E) 50 μM and (F) 100 μM concentrations of cefotaxime in acidified (2.3pH) human blood sample at Zn(II) complex modified graphite paste capillary electrode.

Table 1

Recovery of cefotaxime at Zn(II) complex modified graphite paste capillary electrode in acidified human serum samples.

Drug concentration (μM)	Drug recovery (μM)		
10	9.15	9.24	10.18
100	93.34	96.33	95.45

of blood constituents over complex modified graphite paste electrodes, however, it suppressed when drug was added and drug interacted with the complex modified graphite paste electrodes. The accumulation of drug over complex modified graphite paste electrode suppressed the oxidation of other constituents of blood, probably so why no interference in blood sample was observed as can be seen by absence of any extra peaks or noise present in the voltammogram (Fig. 10). Recovery of the drug in complex serum samples were also demonstrated for two concentrations 10 and 100 μM . The recovery was within the limit of 10% as shown in the Table 1.

4. Conclusions

A sensitive detection of cefotaxime, a third generation cephalosporin drug was demonstrated based on our recently synthesized Schiff base octahedral Zn(II) complex. Cefotaxime enrichment was shown over Zn(II) complex modified graphite paste electrode due to functional groups interaction of cefotaxime with Zn(II) complex. Possible interactions between metal complex and drug were explained with the help of UV–vis, Quartz Crystal Microbalance and electrochemical techniques. Cefotaxime estimation was successfully demonstrated in the nanomolar range in aqueous samples and micromolar range in human blood samples. Reproducibility, accuracy and repeatability of the method were checked by triplicate readings for large number of samples. The recovery of the drug was also checked in serum samples and found to be within the limit of 10%. The technique shows the potential to further develop this method as a quick and low cost sensor for the detection of cefotaxime like important drugs in various aqueous as well as biological samples.

Acknowledgement

The authors are thankful to Prof. T.R. Rao, Inorganic Chemistry, Department of Chemistry for synthesis of Zn(II) complex.

References

- [1] P. Garzone, J.A. Lyon, V.L. Yu, *Drug. Intell. Clin. Pharm.* 17 (1983) 507.
- [2] P. Garzone, J.A. Lyon, V.L. Yu, *Drug. Intell. Clin. Pharm.* 17 (1983) 615.
- [3] D.S. Reeves, M.J. Bywater, D.W. Bullock, H.A. Holt, *J. Antimicrob. Chemother.* 6 (1980) 647.
- [4] T. Kamimura, Y. Matsumoto, N. Okada, Y. Mine, M. Nishida, S. Goto, S. Kuwahara, *Antimicrob. Agents Chemother.* 16 (1979) 540.
- [5] K.P. Fu, H.C. Neu, *Antimicrob. Agents Chemother.* 17 (1980) 583.
- [6] N.V. Shvedene, S.V. Borovskaya, *J. Anal. Chem.* 58 (2003) 1085.
- [7] D.G. Shankar, K. Sushma, R.V. Lakshmi, Y.S. Rao, M.N. Reddy, T.K. Murthy, *Asian J. Chem.* 13 (2001) 1649.
- [8] A.F.M. El Walily, A.A.K. Gazy, S.F. Belal, E.F. Khamis, *Spectrosc. Lett.* 33 (2000) 931.
- [9] A.M. El-Walily, A.A. Gazy, S.F. Belal, E.F. Khamis, *J. Pharm. Biomed. Anal.* 22 (2000) 385.
- [10] S. Eric-Jovanovic, D. Agbaba, D.Z. Inov-Staki, S. Vladimirov, *J. Pharm. Biomed. Anal.* 18 (1998) 893.
- [11] R. Gonzalez-Hernandez, L. Nuevas-Paz, L. Soto-Mulet, M. Lopez-Lopez, J. Hoogmartens, *J. Liq. Chromatogr. Rel. Tech.* 24 (2001) 751.
- [12] I.N. Valassis, M. Parissi-poulon, P. Macheras, *J. Chromatogr.* 13 (1999) 272.
- [13] L.I. Bebawy, K. El Kelani, L.A. Fattah, *J. Pharm. Biomed. Anal.* 32 (2003) 1219.
- [14] T.M. Reddy, M. Sreedhar, S.J. Reddy, *J. Pharm. Biomed. Anal.* 31 (2003) 811.
- [15] L. Camacho, J.L. Avila, A.M. Heras, F. Garcia-Blanco, *Analyst* 109 (1984) 1507.
- [16] S. Billova, R. Kizek, F. Jelen, P. Novotna, *Anal. Bioanal. Chem.* 377 (2003) 362.
- [17] G. Bernacca, L. Nucci, F. Pergola, *Electroanalysis* 6 (1994) 327.

- [18] T. Madhusudhana Reddy, M. Sreedhar, S. Jayarama Reddy, *J. Pharm. Biomed. Anal.* 31 (2003) 811.
- [19] B. Uslu, S.A. Özkan, *Anal. Chim. Acta* 462 (2002) 49.
- [20] B. Uslu, S.A. Özkan, *Electrochim. Acta* 49 (2004) 4321.
- [21] N. Abo El-Maali, A.H. Osman, A.A.M. Aly, G.A.A. Al-Hazmi, *Bioelectrochemistry* 65 (2005) 95.
- [22] M.M. Ghaneim, W. Baumann, E. Hammam, A. Tawfik, *Talanta* 64 (2004) 857.
- [23] C.X. He, S.B. Zhang, S.M. Zhang, X.Y. Jin, X.L. Wang, 18 (1999) 15.
- [24] A.H. Al-Ghamdi, M.A. Al-Shadokhy, A.A. Al-Warthan, *J. Pharm. Biomed. Anal.* 35 (2004) 1001.
- [25] V.S. Ferreira, M.V.B. Zanoni, M. Furlan, A.G. Fogg, *Anal. Chim. Acta* 351 (1997) 105.
- [26] V.S. Ferreira, M.V.B. Zanoni, A.G. Fogg, *Anal. Chim. Acta* 384 (1999) 159.
- [27] N. Abo El-Maali, *Talanta* 51 (2000) 957.
- [28] N. Abo El-Maali, *Bioelectrochemistry* 95 (2005) 65.
- [29] E. Hammam, M.A. EL-Attar, A.M. Beltagi, *J. Pharm. Biomed. Anal.* 42 (2006) 523.
- [30] H. Fabre, M.D. Blanchin, U. Tjaden, *Analyst* 111 (1986) 1281.
- [31] N. Yilmaz, I. Biryol, *J. Pharm. Biomed. Anal.* 17 (1998) 1335.
- [32] S.A. Özkan, B. Uslu, P. Zuman, *Anal. Chim. Acta* 457 (2002) 265.
- [33] N.A. El, M.A. Maali, J.M. Ghandour, Kauffmann, *Bioelectrochem. Bioenerg.* 38 (1995) 91.
- [34] A. Golcu, B. Dogan, S.A. Ozkan, *Talanta* 67 (2005) 703.
- [35] S.A. Özkan, N. Erk, B. Uslu, N. Yilmaz, I. Biryol, *J. Pharm. Biomed. Anal.* 23 (2000) 263.
- [36] F.G. Banica, A.G. Fogg, J.C. Moreira, *Analyst* 119 (1994) 2343.
- [37] M. Heyrovsky, S. Vavricka, *J. Bioelectrochem. Bioenerg.* 48 (1999) 43.
- [38] T. Inoue, J.R. Kirchhoff, *Anal. Chem.* 72 (2000) 5755.
- [39] J.P. Hart, M.D. Norman, S. Tsang, *Analyst* 12 (1995) 1059.
- [40] J.M. Zen, A.S. Kumar, J.C. Chen, *Anal. Chem.* 73 (2001) 1169.
- [41] S. Shahrokhian, M.K. Amini, I. Mohammadpoor-Baltork, S. Tangestaninejad, *Electroanalysis* 12 (2000) 863.
- [42] M.K. Amini, S. Shahrokhian, S. Tangestaninejad, I. Mohammadpoor-Baltork, V. Mirkhani, *Anal. Biochem.* 290 (2001) 277.
- [43] M.C. Rodriguez, G.A. Rivas, *Anal. Chim. Acta* 459 (2002) 43.
- [44] N. Spătaru, B.V. Sarada, E. Popa, D.A. Tryk, A. Fujishima, *Anal. Chem.* 73 (2001) 514.
- [45] G. Favaro, M. Fiorani, *Anal. Chim. Acta* 332 (1996) 249.
- [46] L.H. Wang, Z.S. Chen, *Electroanalysis* 9 (1997) 1294.
- [47] C.R. Martin, D.T. Mitchell, *Anal. Chem.* 70 (1998) 322A.
- [48] Q. Zhao, Z. Gan, Q. Zhong, *Electroanalysis* 14 (2002) 1609.
- [49] E.D. Steinle, D.T. Mitchel, M. Writz, S.B. Lee, V.Y. Young, C.R. Martin, *Anal. Chem.* 74 (2002) 2416.
- [50] S. Majidi, A. Jabbari, H. Heli, H. Yadegari, A.A. Moosavi-Movahedi, S. Haghgoo, *J. Solid State Electrochem.* (2008) (corrected proof available on journals' web site).
- [51] S. Shahrokhian, J. Yazdani, *Electrochim. Acta* 48 (2003) 4143.
- [52] M.K. Halbert, R.P. Baldwin, *Anal. Chem.* 57 (1985) 591.
- [53] D.J. Dobson, S. Saini, *Anal. Chem.* 69 (1997) 3532.
- [54] S. Griveeau, F. Bedioui, *Electroanalysis* 13 (2001) 253.
- [55] S. Shahrokhian, A. Sourji, H. Khajehsharifi, *J. Electroanal. Chem.* 565 (2004) 95.
- [56] E.S. Jamasbi, A. Rouhollahi, S. Shahrokhian, S. Haghgoo, S. Aghajani, *Talanta* 71 (2007) 669.
- [57] M.K. Amini, J.H. Khorasani, S.S. Khaloo, S. Tangestaninejad, *Anal. Biochem.* 320 (2003) 32.
- [58] B. Nalini, S.S. Narayanan, *Electroanalysis* 10 (1998) 779.
- [59] W. Siangproh, P. Nagmukot, O. Chalapakul, *Sens. Actuators B: Chem.* 91 (2003) 60.
- [60] S. Shahrokhian, M. Karimi, H. Khajehsharifi, *Sens. Actuators B* 109 (2005) 278.
- [61] S. Shahrokhian, A. Hamzehloei, A. Tahgani, S.R. Mousavi, *Electroanalysis* 16 (2004) 15.
- [62] Y.H. Tse, P. Janda, H. Lam, A.B.P. Lever, *Anal. Chem.* 67 (1995) 981.
- [63] A.K. Singh, S. Kumari, R.K. Kumar, B. Sridhar, T.R. Rao, *Polyhedron* 27 (2008) 181.
- [64] A. Prasad, P.R. Parameswara, A.K. Singh, R. Prakash, T. Rao, *Synthesis reactivity in inorganic metal organic and nanometal chemistry*, submitted.
- [65] M.M. Aleksic, *J. Electroanal. Chem.* 593 (2006) 258.



Multisyringe flow injection system for solid-phase extraction coupled to liquid chromatography using monolithic column for screening of phenolic pollutants

Hugo M. Oliveira^a, Marcela A. Segundo^{a,*}, José L.F.C. Lima^a, Victor Cerdà^b

^a REQUIMTE, Serviço de Química-Física, Faculdade de Farmácia, Universidade do Porto, Rua Aníbal Cunha, 164, 4099-030 Porto, Portugal

^b Department of Chemistry, Faculty of Sciences, University of the Balearic Islands, Carretera de Valldemossa km 7.5, E-07122 Palma de Mallorca, Illes Balears, Spain

ARTICLE INFO

Article history:

Received 26 May 2008

Received in revised form

18 September 2008

Accepted 21 September 2008

Available online 30 September 2008

Keywords:

Phenolic pollutants

Automatic solid-phase extraction

Water analysis

On-line preconcentration

Multisyringe flow injection analysis

ABSTRACT

In this work a fast, automatic solid-phase extraction procedure hyphenated to HPLC-UV is proposed for screening of priority phenolic pollutants in waters at ng mL^{-1} levels. A flow through column, containing polystyrene-divinylbenzene sorbent, was incorporated to a multisyringe flow injection system (MSFIA), where the sample loading and analyte elution were carried out after computer control. The MSFIA system also directed the eluent to fill the injection loop of the chromatograph, coupling the sample preparation to its determination. High enrichment factors were attained for phenol and ten of its derivatives (mean value 176 for 50 mL of sample), with LOD values lower than 1 ng mL^{-1} for the maximum volume of sample used (100 mL). For all analytes, mean recoveries between 89 and 103% were obtained for different water matrices. Certified reference material and a contaminated soil (RTC-CRM 112) were also tested successfully. The determination frequency was $4\text{--}10 \text{ h}^{-1}$, providing an automatic, fast and reliable tool for water quality and environmental monitoring.

© 2008 Elsevier B.V. All rights reserved.

1. Introduction

Phenolic compounds are widespread aquatic pollutants. Considering their toxicological and organoleptic effects, the United States Environmental Protection Agency (EPA) has listed phenol and several derivatives as priority pollutants [1]. Their input into the ecosystems results directly from the human activity or indirectly from the transformation of natural or synthetic chemicals and they are often found in waters from different sources [2–5]. The screening of phenol and its derivatives in risk areas is essential for public health protection in order to spot timely illegal discharges from industry or contamination by pesticides, even at low levels.

Different strategies have been described for the quantification of phenolic compounds in water samples, including separation techniques such as liquid chromatography (LC) [6–8] or gas chromatography (GC) [9–11] coupled to different detectors. Due to the low volatility character of phenolic compounds, LC is employed more often than GC because analyte derivatization is avoided. Furthermore, with the advent of monolithic columns, fast analysis is possible [12], allowing the determination of several phenolic

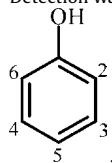
derivatives in about 3 min [13,14]. However, sample preparation is frequently required in order to attain analyte enrichment and matrix removal.

Despite the available fast chromatographic methods, the sample preconcentration/clean up step restricts the sample throughput, conditioning the number of samples that can be processed in environmental surveillance schemes. In this context, automation of the sample preparation step is relevant. In fact, some alternatives resorting to robotic systems have been described [15,16]. However, the hyphenation to the chromatograph is not easy, requiring dedicated, expensive equipment. Other alternatives using flow-systems with on-line column switching schemes have also been described for simpler hyphenation between sample treatment and determination [17,18].

Flow injection systems have been clearly underexploited for this task [19], especially the more recent, computer controlled techniques. Multisyringe flow injection analysis (MSFIA) [20] is one of them and its features (flow network design, multi-channel operation and total compatibility of the manifold with organic solvents) allow the assembling and operation of solid-phase extraction (SPE) devices [21]. Therefore, the objective of the present work is the development of a fast MSFIA-SPE procedure coupled to LC-UV determination for screening of priority phenolic pollutants in waters and environmental samples at ng mL^{-1} levels.

* Corresponding author. Tel.: +351 222078994; fax: +351 222078961.
E-mail address: msegundo@ff.up.pt (M.A. Segundo).

Table 1
Detection wavelength, log K_{ow} , pK_a and structures of EPA phenolic priority pollutants.



Phenolic compound	λ/nm	log K_{ow}^a	pK_a^a	Structure				
				C ₂	C ₃	C ₄	C ₅	C ₆
2,4-Dinitrophenol (24DNP)	360	1.53	4.09	NO ₂		NO ₂		
2-Methyl-4,6-dinitrophenol (46DNOC)	375	2.12	4.34	CH ₃		NO ₂		NO ₂
Phenol (P)	215	1.50	9.99					
4-Nitrophenol (4NP)	315	1.90	7.16			NO ₂		
2-Chlorophenol (2CP)	195	2.15	8.55	Cl				
2-Nitrophenol (2NP)	210	1.78	7.21	NO ₂				
2,4-Dimethylphenol (24DMP)	195	2.42	10.6	CH ₃		CH ₃		
4-Chloro-3-methylphenol (4C3MP)	195	3.10	9.55		CH ₃	Cl		
2,4-Dichlorophenol (24DCP)	200	2.08	7.85	Cl		Cl		
Pentachlorophenol (PCP)	220	5.01	4.93	Cl	Cl	Cl	Cl	Cl
2,4,6-Trichlorophenol (246TCP)	200	3.69	7.42	Cl		Cl		Cl

^a From references (1) Dean, J.R.; Tomlinson, W.R.; Makovskaya, V.; Cumming, R.; Hetheridge, M.; Comber, M., Solid-phase microextraction as a method for estimating the octanol–water partition coefficient. *Anal. Chem.* 1996, 68, (1), 130–133; (2) Li, N. Q.; Lee, H. K., Trace enrichment of phenolic compounds from aqueous samples by dynamic ion-exchange solid-phase extraction. *Anal. Chem.* 1997, 69, (24), 5193–5199.

2. Material and methods

2.1. Reagents and solutions

All solutions were prepared with water from MilliQ system (Millipore, Bedford, MA, USA) (resistivity $> 1.8 \times 10^5 \Omega \text{ cm}$) and chemicals of analytical-reagent grade quality. Methanolic solutions were prepared with methanol HPLC grade (Merck, Darmstadt, Germany). This organic solvent was also used as SPE eluent. The SPE sorbent Lichrolut EN (cross linked styrene-divinylbenzene) was obtained from Merck.

The phenolic compounds (Table 1) used were purchased from Sigma–Aldrich (St. Louis, MO, USA) and were the following: phenol (P), 2-nitrophenol (2NP), 4-nitrophenol (4NP), 2,4-dinitrophenol (24DNP), 2-methyl-4,6-dinitrophenol (46DNOC), 2-chlorophenol (2CP), 2,4-dichlorophenol (24DCP), 2,4,6-trichlorophenol (246TCP), pentachlorophenol (PCP), 4-chloro-3-methylphenol (4C3MP), and 2,4-dimethylphenol (24DMP). The stock solution of each phenolic compound was prepared by accurately weighing the appropriate mass and by dissolving it in methanol in order to obtain a final concentration of 1000 mg L^{-1} . The working standard solutions (containing either mixtures or individual compounds) were obtained by rigorous dilution of the stock solutions in methanol (for direct injection into HPLC system) or in 0.010 mol L^{-1} HCl (for the preconcentration step).

For accuracy assessment, recovery assays were performed using analytical grade standards of each compound obtained from Supelco (Bellefonte, PA, USA). All standards were purchased in 1 mL methanol solution with the concentration of 5000 mg L^{-1} , except for 4C3MP, whose concentration was 500 mg L^{-1} . For the preparation of working standard solutions the same procedure described for the standard solutions was adopted, except for the solvent, which was replaced by water from different sources. In this case, before spiking the water samples with the mixture of analytes, they were filtered through a $0.45 \mu\text{m}$ membrane filter and the pH was adjusted to 2 with concentrated HCl (12 mol L^{-1}). The sea water matrix was prepared after the APHA/AWWA/WEF procedure [22]. Furthermore, certified reference material from LGC-Standards (Middlesex, UK), ref. U-QCI-760 and RTC-QCI-032, was also applied for accuracy assessment.

For the HPLC methodology, HPLC grade acetonitrile was purchased from Merck. Sodium dihydrogen phosphate (Sigma, St.

Louis, MO, USA) solution was prepared by dissolving 6.8 g of the salt in 1000 mL of water, and the pH of this solution was adjusted to a final value of 5.25 using a NaOH solution (6 mol L^{-1}). All solutions were filtered through a $0.45 \mu\text{m}$ membrane filter and degassed using ultrasound before use.

2.2. Apparatus

Chromatographic determinations were conducted on a Merck/Hitachi-LaChrom 7000 series (Hitachi Ltd., Tokyo, Japan) equipped with a diode array detector (L-7455), a pump (L-7100) and a Chromolith RP-18e ($100 \text{ mm} \times 4.6 \text{ mm i.d.}$) column with pre-column ($5 \text{ mm} \times 4.6 \text{ mm i.d.}$) (Merck). The chromatographic system was controlled by an interface (D-7000) and the D-7000 software. The eluate of the preconcentrated sample was injected by using a Rheodyne 7725i manual injector (Rheodyne, Rohnert Park, CA, USA) equipped with $20 \mu\text{L}$ loop. This device was also used as interface between the chromatographic and the automatic MSFIA-SPE system.

Solutions were propelled in the preconcentration system by a multisyringe burette (Crison Instruments, Allela, Spain) and a Minipuls 3 peristaltic pump (Gilson Villiers-le-Bel, France) equipped with polyvinylchloride pumping tubes. In this work, the multisyringe module was equipped with a syringe of 10 mL in position 2 and a syringe of 5 mL in position 3. Besides the three-way commutation valve (NRResearch, Caldwell, NJ, USA) connected to the head of each syringe, four extra commutation valves were connected and controlled through the burette. For all valves, the exchange options were classified in on/off lines.

A personal computer, running lab-made software written in QuickBasic 4.5 (Microsoft, Redmond, WA, USA), controlled the multisyringe operation (number of steps and direction of piston displacement, position of all commutation valves) by a serial port. The peristaltic pump control (flow direction and rotation speed) was performed by the same software using a PCL-711 interface card (Advantech, Taipei, Taiwan).

2.3. Manifold and MSFIA procedure

The different components of the flow-system were disposed as shown schematically in Fig. 1. All connections were made with 0.8 mm i.d. polytetrafluorethylene (PTFE) tubing (Omnifit, Cam-

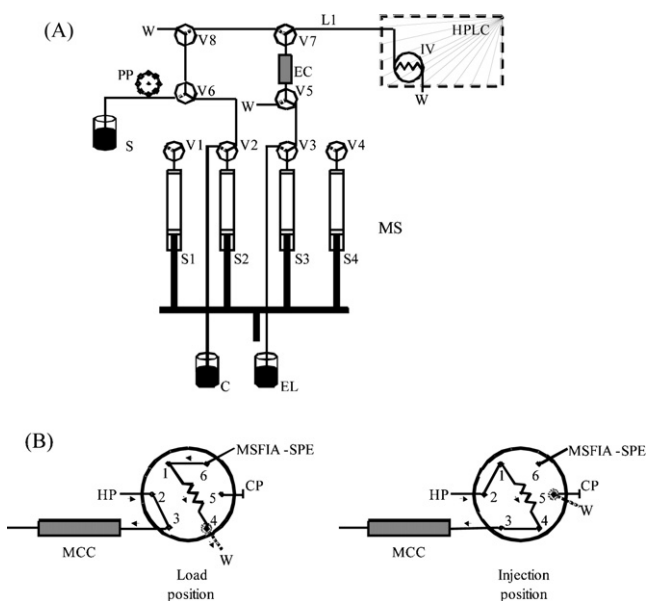


Fig. 1. (A) MSFIA-SPE manifold for the automatic preconcentration of phenolic compounds coupled to LC equipment. (B) Detailed representation of the connection between MSFIA-SPE manifold and the chromatographic system through the injection valve on “load” and “inject” positions. MS, multisyringe; S_i , syringe; V_i , commutation valves; EC, SPE column; IV, injection valve; PP, peristaltic pump; W, waste; L1, connection tubing (30 cm); S2, syringe 10 mL; S3, syringe 5 mL; C, carrier (HCl 0.010 mol L⁻¹); EL, eluent (methanol); S, sample or standard solution; HP, high-pressure pump; MCC, monolithic chromatographic column; MSFIA-SPE, preconcentration flow-system; CP, closed port. In the valves, the position “on” is represented by a solid line while the position “off” is represented by a dotted line. Needle port and connection to waste in the injection valve are also represented by dotted lines.

bridge, UK). A lab-made polyetheretherketone (PEEK) extraction column was used. This column presented a tubular configuration with 24 mm of length and 3 mm of internal diameter, containing 87 mg of sorbent. The resin was trapped inside the column by using filter disks from MoBiTec (Goettingen, Germany) with pore diameter of 10 μm (ref. #2210).

Table 2

Protocol sequence for the automatic solid-phase extraction of phenolic compounds from water.

Step	Description	MS operation	Chromatograph	Position of the commutation valves ^a								MS operation	
				1	2	3	4	5	6	7	8	Volume/ μL ^b	Time/s
1	Sorbent bed is washed with methanol	Chromatographic run (sample X-1); injection loop is washed with methanol	-	F	N	-	N	F	N	F	7000	70	
2	HCl solution is sent through the column for sorbent conditioning	Chromatographic run (sample X-1)	-	N	F	-	F	N	F	F	2500	30	
3	Syringes are refilled and sample X is loaded to the preconcentration column ^c where analytes retention take place	Chromatographic run (sample X-1) finishes	-	F	F	-	F	F	F	F	3720	14.8–750	
4	HCl solution is sent through the column for matrix removal	-	-	N	F	-	F	N	F	F	2500	30	
5	Methanol is sent through the sorbent, eluting the retained analytes	The loop of the injection valve is filled by eluent	-	F	N	-	N	F	N	F	1220	24.4	
6	-	The segment of eluate trapped in the loop is injected and the chromatographic run starts	-	-	-	-	-	-	-	-	-	-	
7	Syringes are refilled	Chromatographic run (sample X); the injection valve is returned to “load” position	-	F	F	-	F	F	F	F	9500	38	

^a N and F represent position “on” and “off”, respectively.

^b The indicated values for volume refer to syringe 2 (10 mL).

^c The peristaltic pump is activated (8 mL min⁻¹) during the time necessary for propelling the defined sample volume (up to 100 mL).

The protocol sequence adopted for the automatic solid-phase extraction of EPA phenolic compounds is described in Table 2. The complete sequence included six steps. A volume of 3500 μL of methanol was propelled through the extraction column and the chromatographic injection loop in order to clean the system (step 1). After commutation of the appropriate valves, 2500 μL of 0.010 mol L⁻¹ HCl solution were used for conditioning the sorbent (step 2). Afterwards, with all valves in “Off” position, the peristaltic pump was activated and a variable sample volume up to 100 mL was direct towards to the extraction column at flow rate of 8.0 mL min⁻¹. Simultaneously, the syringes were filled (step 3). Subsequently, the extraction column was washed with 2500 μL of HCl solution in order to remove the sample matrix (step 4). The analytes retained were eluted with 610 μL of methanol and direct to the chromatograph, filling the IV loop (step 5). Next, 20 μL of the eluate were injected into the chromatographic system by rotating the injection valve to the “inject” position (step 6), beginning the chromatographic run. Finally, the syringes were refilled and the injection valve was returned to the “load” position (step 7).

2.4. Soil sample

A certified soil sample (ref. RTC-CRM 112, LGC Standards) was analyzed. Five grams of soil were weighted and added to 100 mL of water. After 19 h of storage in the dark, the mixture was passed through a 0.22 μm filter. The filtrate was acidified to pH 2 by addition of concentrated HCl and then processed by the MSFIA system.

3. Results and discussion

3.1. Chromatographic analysis

The chromatographic method used in this work was adapted from that proposed by Cledera-Castro et al. [13]. The utilization of a monolithic column (100 mm \times 4.6 mm i.d.) allowed the separation and quantification of eleven EPA priority pollutants in approximately 5 min with an analytical performance comparable to that obtained by using conventional microparticulate reversed-phase columns. All the chromatographic conditions (mobile phase

composition, flow rate and sample volume) were maintained with exception of temperature. Room temperature (approximately 23 °C) was applied instead of 36 °C because no significant differences were observed in the performance of the method using either value.

3.2. Development of the automatic MSFIA-SPE system

The use of a MSFIA flow based manifold allowed the precise control of the flow rate and volume of the solutions used for the sorbent conditioning and respective elution. The glass syringes and PTFE valves that constitute the multisyringe burette and all remaining components of the manifold were also compatible with organic solvents. A peristaltic pump was assembled to the flow manifold in order to load sample volumes up to 100 mL. By using this device the necessity of filling a holding coil before sending the sample to the extraction column with the correspondent time-consuming repositioning movements of the piston bar [23] was avoided, allowing a drastic reduction in the time necessary to perform this step during the protocol sequence.

Some operational parameters as the carrier solution, volumes and flow rates used were fixed according to reported data [24] and our previous experience [25]. The retention of the target analytes was performed at pH 2.0, using HCl 0.010 mol L⁻¹ as carrier. Samples and standards were also acidified to this pH. Taking into account the reversed-phase interactions between the sorbent and the analytes, this pH was necessary to prevent the ionization of all priority phenolic pollutants, which pK_a is in the range 4–11 (Table 1). A volume of 3.5 mL of methanol was used for removing the analytes not injected into the HPLC system in the beginning of each protocol sequence. This procedure allowed a complete cleaning of the extraction column and the HPLC connection tubing, eliminating carryover between consecutive samples. Two portions of 2.5 mL of carrier solution (HCl 0.010 mol L⁻¹) were fed into the extraction column immediately before and after the sample loading step, performing the sorbent conditioning and the sample matrix cleanup. This volume was fixed considering the volumes of the sorbent bed, connection tubing and commutation valves, guaranteeing an operation without contamination by consecutive injections of samples. In order to prevent the formation of a liquid gap before the sorbent bed top with a consequent pressure build-up, the sample loading and the elution steps were performed in opposite ways. Therefore, the extraction column was placed between two commutation valves (Fig. 1, V5–V7). The length of the connection tubing between the exit of the extraction column and injection valve (Fig. 1, L1) was made as short as possible to prevent dispersion of the extracted analytes. The introduction of the commutation valve V8 (Fig. 1) in the flow path between the sample commutation valve (V6) and the extraction column (V7–V5) was necessary to avoid the contamination of the extraction column when the sample or standard solutions were changed.

The hyphenation between the MSFIA-SPE manifold and the chromatograph also required a precise positioning of the eluent plug in order to assure the insertion of the maximum concentration of phenolic compounds into the injection loop. Therefore, the volume of eluent is a critical aspect on attaining the highest enrichment factor and good precision in the chromatographic determination. As depicted in Fig. 2, the elution profile was assessed for eluent volumes between 550 and 750 μL. P and 246 TCP were used as model compounds because they present polarity values placed at extreme zones, considering the K_{ow} range of the target analytes (Table 1). It was observed that the maximum value for the analytical signal was obtained for 610 μL of methanol, which was chosen for further experiments. The similar elution profile obtained for both compounds (Fig. 2) indicated that methanol was a suitable

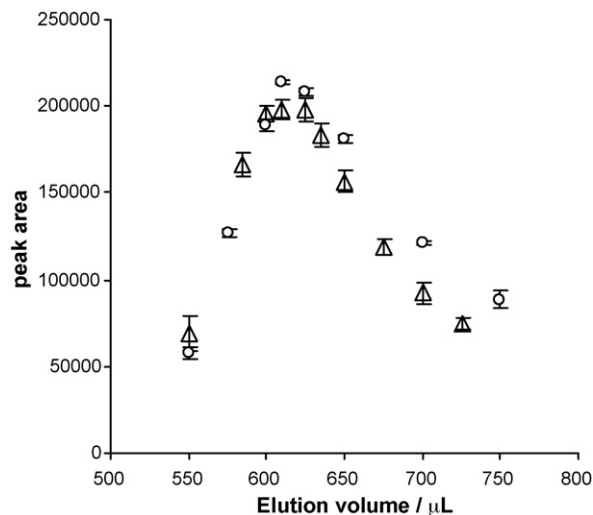


Fig. 2. Elution profile, corresponding to the peak areas obtained for different volumes of methanol used for the elution of 5 μg of P (Δ) or 246TCP (○) contained in 1 mL of HCl 0.01 mol L⁻¹.

eluent for the simultaneous desorption of all phenolic compounds from the sorbent. It was also observed that a degassing step before use and the store temperature of the eluent during the working day had a crucial role in the repeatability of the automatic SPE procedure. In the experiments, at room temperature without methanol degassing, a relative standard deviation (RSD) of 10% was obtained for 14 consecutive extractions of 10 mL of 0.5 μg mL⁻¹ of phenol. This impaired precision was caused by formation of very small gas bubbles at the surface of the sorbent bed, which appeared in the water/methanol interface when the eluent was fed into the extraction column. This source of error was minimized by degassing the eluent periodically with helium and by keeping it on ice during analysis. With these precautions, the RSD achieved for the same experimental set was lower than 3%.

The flow rate of the sample loading step is a relevant parameter due to the possibility of handling large volumes in a short period of time. Besides the determination frequency, this factor influences directly the enrichment capacity and subsequently the limit of detection and the sensitivity of the method. A study to evaluate the influence of the flow rate in the retention of the analytes was carried out by loading a volume of 50 mL of a standard mixture containing 15 ng mL⁻¹ of each phenolic compound at flow rates in the range 2–8 mL min⁻¹. Flow rates above 8 mL min⁻¹ were not used because compaction of the bed particles was observed, creating high back pressures and resulting in the clogging of the extraction column. For lower flow rates, the results showed no difference in the adsorption of all analytes into the extraction column as peak area values were similar for all flow rates tested. Therefore, the flow rate of 8 mL min⁻¹ was adopted to perform the retention of the analytes from the water sample into the sorbent bed, minimizing the time required for this step.

3.3. Analytical performance and application to water samples

The analytical performance of the MSFIA-SPE system was evaluated considering the application range, limit of detection (LOD), enrichment factor (EF), determination frequency, repeatability and accuracy.

Using the MSFIA-SPE system it was possible to obtain mass-based calibration curves, by plotting the peak area obtained for each compound against the mass of analyte loaded into the extraction column. This calibration was performed by loading different vol-

Table 3
Linear dynamic range, calibration curve parameters, values for limit of detection (LOD) and enrichment factors (EF) obtained for the proposed method.

Calibration curve ^a							
Compound	Linear range/ng	Slope/area units ng ⁻¹	Interception	r ²	LOD/ng	LOD ^b /ng mL ⁻¹	EF ^c
24DNP	350–3500	32.9 ± 0.6	1813 ± 818	0.995	207	2	n. a.
46DNOC	350–3500	31.9 ± 0.5	-830 ± 674	0.998	103	1	148 ± 5
P	300–3000	38.7 ± 0.8	424 ± 924	0.996	157	2	198 ± 5
4NP	225–2250	52 ± 1	-116 ± 949	0.997	110	1	187 ± 6
2CP	200–2000	214 ± 5	1243 ± 888	0.999	31	0.3	195 ± 4
2NP	200–2000	57 ± 1	-431 ± 891	0.994	87	0.9	189 ± 6
24DMP	200–2000	236 ± 5	1106 ± 982	0.999	30	0.3	193 ± 4
4C3MP	200–2000	147 ± 3	835 ± 286	0.996	18	0.2	215 ± 6
24DCP	150–1500	164 ± 3	644 ± 947	0.998	39	0.4	177 ± 4
PCP	200–2000	57 ± 1	-979 ± 780	0.996	66	0.7	110 ± 3
246TCP	150–1500	96 ± 2	-421 ± 1070	0.995	55	0.6	151 ± 3

^a For 25 mL of standard mixtures.

^b For sample preconcentration volume of 100 mL.

^c For sample preconcentration volume of 50 mL. n. a., not available.

umes of standard, resulting in a dynamic calibration range [25,26]. Besides using a single or a small number of standard mixtures to calibrate the system, it was also possible to adjust the loaded volume to the concentration of the target analytes for each sample.

Calibration curves (Table 3) were established by extracting 25 mL of a set of standard mixtures containing a defined amount of each compound. The linear dynamic range varied from 150–1500 ng (24DCP and 246TCP) to 350–3500 ng (24DNP and 46DNOC).

The LOD was calculated as the mass of compound corresponding to the interception plus three times $S_{y/x}$ [27]. The values obtained varied between 18 ng for 4C3MP and 207 ng for 24DNP. Considering the maximum volume of sample used in this work (100 mL) LOD values ≤ 1 ng mL⁻¹ was attained for nine of the eleven target analytes (Table 3).

The enrichment factor for each analyte was calculated by the ratio between the slope of the calibration curves obtained after SPE and the slope of the calibration curve obtained after direct injection of the analytes into the chromatographic system [28]. For the pre-concentrated volume of 50 mL the average EF was 176 and only for 24DNP and PCP the value was lower than 150 (Table 3). Higher values of EF would be easily attained by increasing the sample volume used in the extraction step.

The time required for a complete analytical cycle included the time necessary for performing the SPE protocol followed by the chromatographic run. As these two steps were performed in parallel, the total analysis time was defined by the SPE procedure when the sample volume was higher than 19.2 mL (144 s in step 3, Table 2) or by the chromatographic run (that takes about 5 min) for lower

sample volumes. For screening purposes at low $\mu\text{g L}^{-1}$ concentration levels, sample volumes between 25 and 100 mL must be applied, thus sample throughput was limited by the SPE protocol. This procedure took between 6 (for 25 mL of sample) and 15 min (for 100 mL of sample), hence the determination frequency was 4–10 h⁻¹.

Regardless of the sample volume processed, it should be emphasized that a reduced amount of reagents and solvents were necessary to perform the sample preparation. For each SPE procedure only 4.1 mL of methanol and 5 mL of HCl 0.010 mol L⁻¹ were required. Furthermore, the sorbent was reutilized up to 100 times, without loss of performance.

The accuracy and repeatability of the MSFIA-SPE method were assessed by analysing spiked water samples from different sources and certified reference material. The samples (MilliQ water, mineral water, tap water and sea water) were spiked with a mixture of certified standard solutions. An amount of 500 ng of each compound was added to 50 mL (10 ng mL⁻¹) and to 100 mL (5 ng mL⁻¹). The results provided by the MSFIA-SPE method expressed as percentage of recovery are listed in Table 4. Mean recoveries between 89 and 103% were obtained for the different samples and more than 90% of the determinations presented a recovery between 85 and 110%. The results demonstrated that the performance was not affected by the saline content or the ionic strength of the sample due to the similar results for the different matrices analyzed. Moreover, the similarity founded in the results obtained using different sample volumes indicated that no breakthrough occurred up to 100 mL. Repeatability was estimated by calculating RSD of 5 consecutive

Table 4
Values of percentage of recovery obtained for the preconcentration of 50 and 100 mL of spiked water sample containing 500 ng of each phenolic compound. The listed values correspond to a mean of five determinations \pm standard deviation.

Compound	Milli Q water		Mineral water		Tap water		Sea water	
	50 mL	100 mL	50 mL	100 mL	50 mL	100 mL	50 mL	100 mL
24DNP	90 ± 4	87 ± 5	83 ± 7	86 ± 6	n. a.	n. a.	107 ± 4	98 ± 3
46DNOC	119 ± 9	117 ± 5	93 ± 10	94 ± 6	99 ± 5	108 ± 3	124 ± 5	118 ± 5
P	96 ± 4	82 ± 3	96 ± 10	96 ± 9	88 ± 2	84 ± 5	95 ± 3	87 ± 3
4NP	98 ± 3	90 ± 5	88 ± 10	93 ± 7	85 ± 6	88 ± 4	100 ± 3	92 ± 3
2CP	91 ± 3	84 ± 3	90 ± 8	95 ± 7	86 ± 4	90 ± 5	93 ± 4	89 ± 4
2NP	112 ± 8	106 ± 5	90 ± 9	95 ± 7	88 ± 3	93 ± 1	97 ± 3	91 ± 5
24DMP	100 ± 5	93 ± 5	91 ± 10	94 ± 6	n. a.	n. a.	107 ± 4	99 ± 4
4C3MP	118 ± 8	106 ± 6	102 ± 11	114 ± 9	89 ± 6	95 ± 4	109 ± 4	105 ± 5
24DCP	112 ± 7	103 ± 4	90 ± 8	99 ± 6	89 ± 5	97 ± 4	96 ± 4	93 ± 5
PCP	86 ± 6	93 ± 2	n. a.	n. a.	n. a.	n. a.	94 ± 8	94 ± 5
246TCP	110 ± 9	126 ± 9	86 ± 10	108 ± 10	88 ± 4	103 ± 9	116 ± 10	122 ± 3
Mean recovery	103	99	91	98	89	95	103	99

n. a., not available.

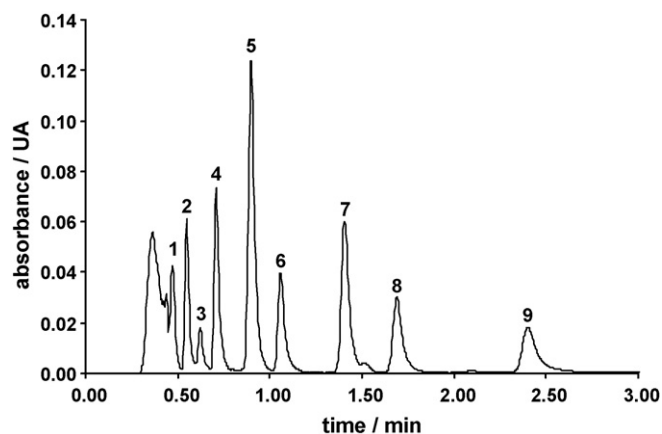


Fig. 3. Chromatogram obtained for aqueous extract of soil sample RTC-CRM 112. Sample volume = 4 mL. (1) 24DNP, (2) 46DNOC, (3) P, (4) 4NP, (5) 2CP, (6) 2NP, (7) 4C3MP, (8) 24DCP, (9) PCP.

determinations of each spiked sample. For all determined analytes a RSD $\leq 8\%$ was obtained.

Concerning the analysis of reference standard material, values of 106 ± 5 , 94 ± 4 , 45 ± 2 and 67 ± 4 ng mL^{-1} were attained for 24DNP, P, 2CP and 24DCP in sample RTC-QCI-032 (sample volume = 10 mL). The total content of phenolics was 312 ± 8 ng mL^{-1} , which is in agreement with the gravimetric certified value of 310 ng mL^{-1} . For sample U-QCI-076, values of 77 ± 3 , 54 ± 3 , 114 ± 5 and 55 ± 2 ng mL^{-1} were attained for 24DNP, P, 2CP and 24DCP (sample volume = 7 mL). The total phenolic content was 300 ± 6 ng mL^{-1} , which is also in agreement with the certified value (309 ± 3 ng mL^{-1}) and within the advisory range for this sample (138 – 340 ng mL^{-1}). Finally, an aqueous extract of a certified soil sample (RTC-CRM 112), contaminated with phenols from a wood treatment site, was also analyzed (Fig. 3). The phenolic compounds present in the soil were quantified (Table 5) and results within the certified confidence interval were obtained for 4NP, 2NP and PCP. Values lower (P, 4C3MP, 24DCP) or higher (46DNOC, 2CP) than the confidence limits were also obtained, probably due to the different extraction conditions applied here, where water was used instead of an organic solvent.

3.4. Comparison to previous techniques

Compared to previous work for fast screening of phenolics [14], the system proposed here is faster, requiring at most 15 min for sample extraction compared to the 200 min reported before. Furthermore, the automatic SPE protocol developed here was directly coupled to the LC determination, making the whole procedure less dependent of the operator when compared to other methods [29].

Table 5

Results obtained for the analysis of a certified soil sample (RTC-CRM 112), based on its aqueous extract.

Compound	Present method/ mg kg^{-1}	Reference value/ mg kg^{-1}	Confidence interval/ mg kg^{-1}
24DNP	4.62 ± 0.19	n. a.	n. a.
46DNOC	7.49 ± 0.29	4.75	2.35–7.15
P	1.25 ± 0.06	2.45	1.35–3.55
4NP	7.08 ± 0.21	5.66	2.56–8.76
2CP	4.62 ± 0.17	2.38	1.35–3.41
2NP	2.87 ± 0.13	4.33	2.40–6.27
4C3MP	2.34 ± 0.12	4.94	3.04–6.84
24DCP	1.53 ± 0.07	2.53	1.69–3.37
PCP	4.48 ± 0.12	5.05	2.12–7.98

n. a.: not available.

Other chromatographic methods hyphenated to automatic on-line SPE for the determination of EPA priority phenolic pollutants based on the “column switching” approach have also been proposed [30–34]. When compared with the present work, these methods have the inconvenient of requiring high-pressure devices and gradient elution in the chromatographic run to prevent peak broadening. Some attempts to circumvent the major drawbacks of these systems were made, using Supercritical Fluid Chromatography [31] to reduce the chromatographic run time or by performing the derivatization with an ion-pair reagent before the SPE step [30] to increase the breakthrough volume of the more polar compounds. However, the time necessary for the complete analytical procedure was about 30 min in all cases. In the present work the determination rate was enhanced up to 5 fold and this is a worthwhile aspect due to the possibility of applying this method on screening analysis. Moreover, the proposed method presents improved or similar analytical characteristics concerning the application range and limit of detection. Considering the organic solvent consumed and the effluent produced in the sample preparation step, the proposed MSFIA-SPE system is a “greener” tool, with lower values for both of them. Regarding other automatic strategies proposed for the same determination and not based on SPE hyphenated schemes, [6,35] the present method is undoubtedly more suitable for screening purposes, attaining also a higher determination frequency.

4. Conclusions

In conclusion, this is first time that a hyphenated methodology comprising the repeatable flow conditions of MSFIA systems for SPE and the high throughput offered by monolithic columns is described. Thus, a fast and reliable tool for water quality monitoring and pollutant screening is available with improved performance when compared to the conventional “off-line” and “on-line” solid-phase extraction of phenolic compounds followed by liquid chromatographic determination. This was accomplished due to the high enrichment factors attained for phenol and ten of its derivatives and the low LOD values achieved (<1 ng mL^{-1} for 100 mL of sample). Finally, the applicability of the proposed system as a screening tool was corroborated by the recovery values attained (89–103%) when different water matrices were processed. Good results were obtained for an aqueous extract from contaminated soil, indicating the suitability for determination in soil lixiviates.

Acknowledgements

Hugo M. Oliveira thanks Fundação para a Ciência e Tecnologia (FCT) and FSE (III Quadro Comunitário) for the PhD grant SFRH/BD/22494/2005. This work was partially supported by Spanish Ministry of Education (MEC) through project CTQ2007-64331 (Plan Nacional de Ciencias y Tecnologías Químicas).

References

- [1] EPA, EPA method 604, Phenols, Part VIII, 40 CFR Part 136, U.S. Environmental Protection Agency, 1984.
- [2] M.L. Barrico, C. Nabais, M.J. Martins, H. Freitas, Chemosphere 65 (2006) 482.
- [3] A.D. Dimou, T.M. Sakellarides, F.K. Vosniakos, N. Giannoulis, E. Leneti, T. Albanis, Int. J. Environ. Anal. Chem. 86 (2006) 119.
- [4] S. Lacorte, A. Latorre, D. Barcelo, A. Rigol, A. Malmqvist, T. Welander, Trac-Trends Anal. Chem. 22 (2003) 725.
- [5] J. Michalowicz, W. Duda, Pol. J. Environ. Stud. 16 (2007) 347.
- [6] J. Ruiz-Jimenez, M.D. Luque de Castro, J. Chromatogr. A 1174 (2007) 78.
- [7] M. Cledera-Castro, A. Santos-Montes, R. Izquierdo-Hornillos, R. Gonzalo-Lumbreras, J. Sep. Sci. 30 (2007) 699.
- [8] C.L. Ye, O.X. Zhou, X.M. Wang, J.P. Xiao, J. Sep. Sci. 30 (2007) 42.
- [9] N.G. Simoes, V.V. Cardoso, E. Ferreira, M.J. Benoliel, C.M.M. Almeida, Chemosphere 68 (2007) 501.

- [10] M. Kladi, M. Dassenakis, M. Scoullou, N. Psaroudakis, *Fresenius Environ. Bull.* 15 (2006) 1003.
- [11] M. Schellin, P. Popp, *J. Chromatogr. A* 1072 (2005) 37.
- [12] S. El Deeb, L. Preu, H. Watzig, *J. Sep. Sci.* 30 (2007) 1993.
- [13] M. Cledera-Castro, A. Santos-Montes, R. Izquierdo-Hornillos, *J. Chromatogr. A* 1087 (2005) 57.
- [14] M. Ali, H.Y. Aboul-Enein, *Anal. Lett.* 37 (2004) 2351.
- [15] D.T. Rossi, N. Zhang, *J. Chromatogr. A* 885 (2000) 97.
- [16] J. O'Reilly, O. Wang, L. Setkova, J.P. Hutchinson, Y. Chen, H.L. Lord, C.M. Linton, J. Pawliszyn, *J. Sep. Sci.* 28 (2005) 2010.
- [17] P. Sadilek, D. Satinsky, P. Solich, *Trac-Trends Anal. Chem.* 26 (2007) 375.
- [18] M.C. Hennion, *J. Chromatogr. A* 856 (1999) 3.
- [19] G.A. Theodoridis, C.K. Zacharis, A.N. Voulgaropoulos, *J. Biochem. Biophys. Methods* 70 (2007) 243.
- [20] V. Cerdà, J.M. Estela, R. Forteza, A. Cladera, E. Becerra, P. Altamira, P. Sitjar, *Talanta* 50 (1999) 695.
- [21] M.A. Segundo, L.M. Magalhães, *Anal. Sci.* 22 (2006) 3.
- [22] L.S. Clesceri, A.E. Greenberg, A.D. Eaton, *Standard Methods for the Examination of Water and Wastewater*, 20th ed., APHA, AWWA, WEF, Washington, 1998.
- [23] M.A. Segundo, H.M. Oliveira, J.L.F.C. Lima, M.I.G.S. Almeida, A.O.S.S. Rangel, *Anal. Chim. Acta* 537 (2005) 207.
- [24] L.A. Oliferova, M.A. Statkus, G.I. Tsisin, J. Wang, Y.A. Zolotov, *J. Anal. Chem.* 61 (2006) 416.
- [25] H.M. Oliveira, M.A. Segundo, S. Reis, J.L.F.C. Lima, *Microchim. Acta* 150 (2005) 187.
- [26] G. de Armas, M. Miró, J.M. Estela, V. Cerdà, *Anal. Chim. Acta* 467 (2002) 13.
- [27] J.N. Miller, J.C. Miller, *Statistics Chemometrics for Analytical Chemistry*, 5th ed., Pearson Education Ltd., Harlow, 2000.
- [28] Z. Fang, *Flow Injection Separation and Preconcentration*, VCH, Weinheim, 1993.
- [29] M.A. Crespín, S. Cardenas, M. Gallego, M. Valcarcel, *Rapid Commun. Mass Spectrom.* 12 (1998) 198.
- [30] E. Pocurull, G. Sanchez, F. Borrull, R.M. Marce, *J. Chromatogr. A* 696 (1995) 31.
- [31] J.L. Bernal, M.J. Nozal, L. Toribio, M.L. Serna, F. Borrull, R.M. Marce, E. Pocurull, *Chromatographia* 46 (1997) 295.
- [32] D. Puig, D. Barceló, *J. Chromatogr. A* 733 (1996) 371.
- [33] N. Masque, E. Pocurull, R.M. Marce, F. Borrull, *Chromatographia* 47 (1998) 176.
- [34] N. Masque, M. Galia, R.M. Marce, F. Borrull, *Analyst* 122 (1997) 425.
- [35] R.M. Alberici, R. Sparrapan, W.F. Jardim, M.N. Eberlin, *Environ. Sci. Technol.* 35 (2001) 2084.



Kinetic spectrofluorimetric determination of certain cephalosporins in human plasma

Mahmoud A. Omar*, Osama H. Abdelmageed, Tamer Z. Attia

Analytical Chemistry Department, Faculty of Pharmacy, Minia University, Minia, Egypt

ARTICLE INFO

Article history:

Received 9 June 2008

Received in revised form

12 September 2008

Accepted 17 September 2008

Available online 4 October 2008

Keywords:

Initial rate method

Fixed time method

Cephalosporins

Kinetic spectrofluorimetry

Plasma analysis

ABSTRACT

An accurate, reliable, specific and sensitive kinetic spectrofluorimetric method was developed for the determination of seven cephalosporin antibiotics namely cefotaxime sodium, cephapirin sodium, cephadrine dihydrate, cephalexin monohydrate, cefazoline sodium, ceftriaxone sodium and cefuroxime sodium. The method is based on their degradation under an alkaline condition producing fluorescent products. The factors affecting the degradation and the determination were studied and optimized. The reaction is followed spectrofluorimetrically by measuring the rate of change of fluorescence intensity at specified emission wavelength. The initial rate and fixed time methods were used for the construction of calibration graphs to determine the concentration of the studied drugs. The calibration graphs are linear in the concentration ranges $0.2\text{--}1.2\ \mu\text{g mL}^{-1}$ and $0.2\text{--}2.2\ \mu\text{g mL}^{-1}$ using the initial rate and fixed time methods, respectively. The results were statistically validated and checked through recovery studies. The method has been successfully applied for the determination of the studied cephalosporins in commercial dosage forms. The high sensitivity of the proposed method allows the determination of investigated cephalosporins in human plasma. The statistical comparisons of the results with the reference methods show an excellent agreement and indicate no significant difference in accuracy and precision.

© 2008 Elsevier B.V. All rights reserved.

1. Introduction

Cephalosporins consist of a fused β -lactam- Δ^3 -dihydrothiazine two-ring system, known as 7-aminocephalosporanic acids, and vary in their side chain substituents at C3 (R2), and C7 (acylamido, R1). The chemical structure of studied cephalosporins is shown in Table 1. They are used for the treatment of the infection caused by both gram-negative and gram-positive bacteria [1].

A wide variety of analytical methods have been reported for the determination of cephalosporins in pure form, in pharmaceutical preparations and in biological fluids. These methods include spectrophotometry [2–5], atomic absorptive spectrophotometry [6], fluorometry [7–12], liquid chromatography [13–20], micellar electro kinetic capillary chromatography [21,22], chemiluminescence [23–28], potentiometric [29,30] and polarographic [31–34] methods.

There are other reported methods of spectrofluorimetric determination of cephalosporins based on their alkaline degradation [35–37] and acidic hydrolysis [9]. These methods began with one concentration of cephalosporin and made serial dilution after

hydrolysis, which is not suitable for validation. But our proposed method provides some important advantages over other reported methods that can be summarized as follows:

1. The kinetic study of reaction has the advantage of avoiding the interference of coloured and/or turbidity background of samples and reduces the time required for the reaction.
2. In our method, we began the reaction with different initial concentrations on the contrary of the other reported methods. Thus ensure the right choice of our conditions studied.
3. In terms of specificity, the method we propose has proved the suitability for analyzing the investigated cephalosporins in pharmaceutical formulations, without preliminary extraction.

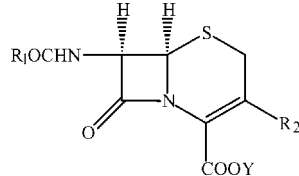
2. Experimental

2.1. Apparatus

- Perkin-Elmer UK model LS 45 Luminescence spectrometer, equipped with a 150 W Xenon arc lamp, grating excitation and emission monochromators for all measurements. Slit width for both monochromators were set at 10 mm. A 1-cm quartz cell was used, connected to an IBM PC computer loaded with the FL WINLAB™ software.
- Milwaukee SM 101 pH meter, Portugal.

* Corresponding author. Tel.: +20 2862324941; fax: +20 862369075.
E-mail address: momar71g@yahoo.com (M.A. Omar).

Table 1
Structural formula of the studied cephalosporins



Name	Generation	R1	R2	Y
Cephapirin sodium	First		-CH ₂ OCOCH ₃	Na
Cefuroxime sodium	Second		-CH ₂ OCONH ₂	Na
Cefotaxime sodium	Third		-CH ₂ OCOCH ₃	Na
Cephadrine	First		-CH ₃	H
Cefazoline sodium	First			Na
Ceftriaxone sodium	Third		H	H
Cephalexin monohydrate	First		-CH ₃	H

2.2. Materials and reagents

All the materials were of analytical reagent grade and the solutions were prepared with double distilled water. Samples of cephalosporin were generously supplied by their respective manufacturers and were used without further purification:

- Cephalexin monohydrate and cefuroxime sodium (Glaxowellcome Egypt, S.A.E., El-Salam City, Cairo, Egypt).
- Cephapirin sodium and cefazoline sodium (Bristol Myers-Squibb Pharmaceutical Co., Cairo, Egypt).
- Cefotaxime sodium, cephradine dihydrate and ceftriaxone sodium (EIPICO, Tenth of Ramadan City, Cairo, Egypt).
- Sodium hydroxide (El-Nasr Chemical Co., Egypt): 1.2 mol L⁻¹ prepared by dissolving 5.04 g in 100 mL of water. Hydrochloric acid (El-Nasr Chemical Co., Egypt): 1.0 mol L⁻¹ prepared by dissolving 9.0 mL in 100 mL of water. Boric acid, sodium hydroxide buffer solution (pH 10) and acetate buffer solution (pH 4) were prepared.

2.3. Pharmaceutical formulations

The following available commercial preparations were analyzed; Ceporex[®] tablets and vials (Glaxowellcome Egypt, S.A.E., El-Salam City, Cairo, Egypt), labeled to contain 250 mg cephalixin monohydrate per tablet or 500 mg cephalixin sodium equivalent to 500 mg cephalixin monohydrate per vial. Zinnat[®] vials (Glaxowellcome Egypt, S.A.E., El-Salam City, Cairo, Egypt), labeled to contain 250 mg cefuroxime sodium per vial. Cefatrexyl[®]

vials (Bristol Myers-Squibb Pharmaceutical Co., Cairo, Egypt), labeled to contain 500 mg cephalixin sodium per vial. Totacef[®] vials (Bristol Myers-Squibb Pharmaceutical Co., Cairo, Egypt), labeled to contain 500 mg cefazoline sodium per vial. Velosef[®] tablets (Bristol Myers-Squibb Pharmaceutical Co., Cairo, Egypt), labeled to contain 500 mg cephradine dihydrate per tablet. Velosef[®] vials (Bristol Myers-Squibb Pharmaceutical Co., Cairo, Egypt), labeled to contain 500 mg cephradine dihydrate and 166.5 mg L-arginine per vial. Cefotax[®] vials (EIPICO, Tenth of Ramadan City, Cairo, Egypt), labeled to contain 250 mg cefotaxime sodium per vial. Ceftriaxone[®] vial (Novartis Pharmaceutical S.A.E., Cairo, Egypt), labeled to contain 500 mg ceftriaxone sodium per vial.

2.4. Preparation of standard solution

Stock solution containing 1 mg mL⁻¹ of each cephalosporin was prepared in double distilled water, and working standard solutions containing 20–120 µg mL⁻¹ were prepared by suitable dilution of the stock solutions with double distilled water.

2.5. Recommended procedure

Into a series of 50 mL test tube, 5.0 mL of a standard solution of drugs was transferred over the cited concentration of 2–12 µg mL⁻¹, and 20 mL of 1.25 mol L⁻¹ sodium hydroxide was added. Then, the resulting solution was heated in a boiling-water, for about 30 min in case of cephalixin and cephradine and for about

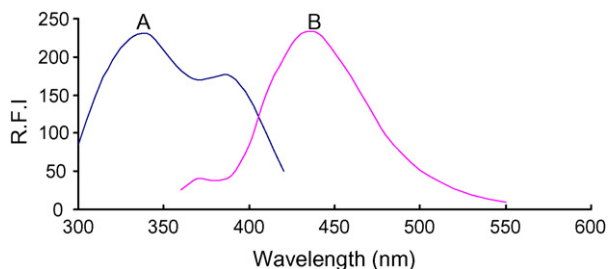


Fig. 1. Fluorescence spectrum of cefuroxime ($0.8 \mu\text{g mL}^{-1}$) where (A) excitation and (B) emission.

60 min for other investigated cephalosporins. The solutions were immediately cooled to room temperature by using an ice bath. The solutions containing the fluorescent products were adjusted to neutral pH with about 20 mL of 1 mol L^{-1} hydrochloric acid and then were transferred quantitatively to 50 mL volumetric flask and the volume was completed with double distilled water. Then,

1.0 mL of neutralized solution was transferred into 10.0 mL volumetric flask, 2.0 mL of acetate buffer was added to obtain pH 4 in case of cefotaxime, cephapirin, ceftazolin and ceftriaxone while 2 mL of phosphate buffer was added to obtain pH 10 in the final solution in case of cephradine, cefuroxime and cephalexin. Subsequently, the resulting solution was diluted to volume with double distilled water for cephalexin and cephradine or with ethanol for cefotaxime, cephapirin, ceftazolin, ceftriaxone and cefuroxime.

2.5.1. Initial rate method

The content of the mixture of each flask was mixed well and the increase in fluorescence intensity was recorded as a function of time against reagent blank treated similarly. The initial rate of the reaction (ν) at different concentrations was obtained from the slope of the tangent to fluorescence intensity time curves. The calibration graphs were constructed by plotting the logarithm of the initial rate of the reaction ($\log \nu$) versus logarithm of molar concentration of the studied drugs ($\log C$).

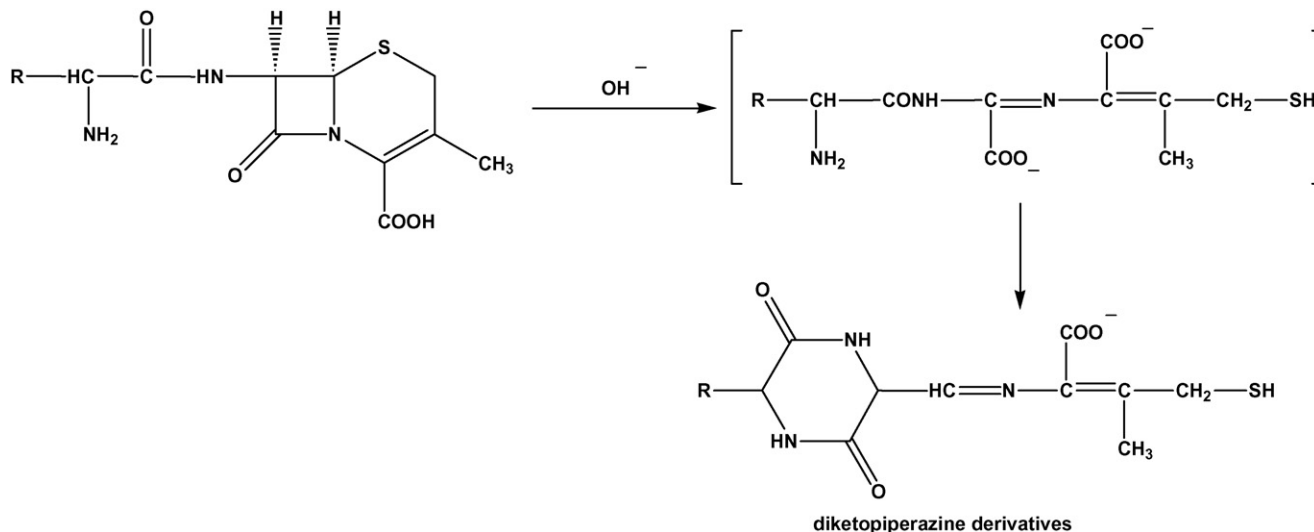


Fig. 2. Formation of diketopiperazine derivatives.

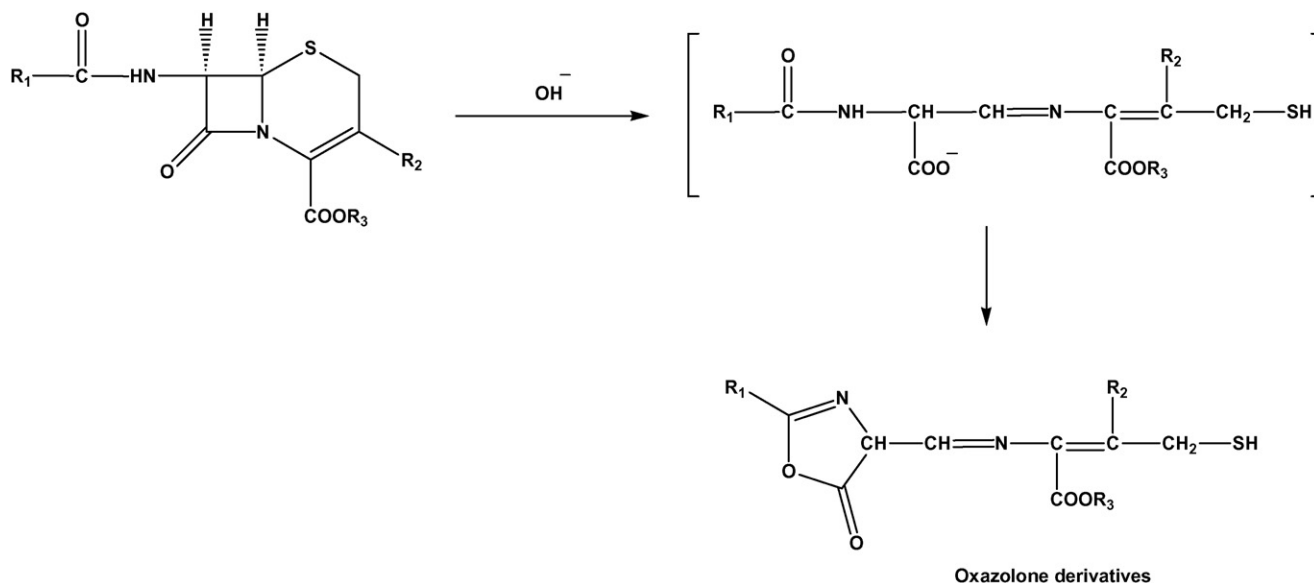


Fig. 3. Formation of oxazolone derivatives.

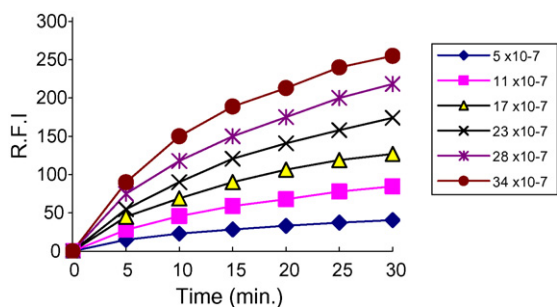


Fig. 4. Relative fluorescence intensity versus time for the reaction between cephalixin (different molar concentration) and NaOH (1.0 mol L^{-1}).

2.5.2. Fixed time method

In this method, the fluorescence intensity of each sample solution, at preselected fixed time (10 min used for cephalixin and cephradine or 20 min used for other investigated cephalosporins), was accurately measured and plotted against the final concentration of the drug.

2.6. Determination of the studied drugs in pharmaceutical formulations

2.6.1. Procedure for tablets

An accurately weighed amount equivalent to 100.0 mg of each drug from a composite of 20 powdered tablets was transferred into a 100 mL volumetric flask, dissolved and diluted to the mark with double distilled water, then sonicated for 10 min and filtered off to obtain a solution of 1.0 mg mL^{-1} ; and the first portion of filtrate was rejected. Further dilutions with double distilled water were made to obtain sample solutions $20\text{--}120 \mu\text{g mL}^{-1}$, and then the general procedure was followed.

2.6.2. Procedure for capsules or vials

The content of 20 capsules was evacuated and mixed well, an amount of vials or capsules equivalent to 100.0 mg was transferred into a 100 mL volumetric flask, dissolved and completed to the mark with double distilled water to obtain solution of 1.0 mg mL^{-1} . Further dilutions with double distilled water were made to obtain sample solutions ($20\text{--}120 \mu\text{g mL}^{-1}$), and then the general procedure was followed.

2.6.3. Procedure for spiked human plasma

A sample of 5.0 mL of drug-free human blood was taken from healthy volunteers into a heparinized tube and centrifuged at 3000 rpm for 30 min. Then, into 10 mL stoppered calibrated tube 3 mL of the supernatant was spiked with investigated cephalosporins dissolved in water. Then 1.0 mL of acetonitrile was

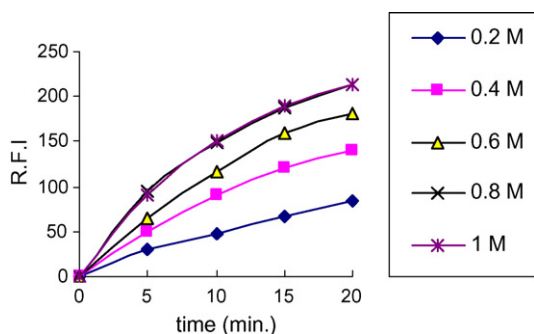


Fig. 5. Relative fluorescence intensity versus time for the reaction between cephalixin $3.4 \times 10^{-6} \text{ mol L}^{-1}$ and NaOH (different molar concentration).

Table 2

Excitation and emission wavelength of the studied cephalosporins.

Drug name	Excitation wavelength (nm)	Emission wavelength (nm)
Cephalexin	332	429
Cefotaxime	337	409
Cephapirin	338	409
Cefazolin	343	395
Ceftriaxone	339	410
Cefuroxime	339	437
Cephradine	336	431

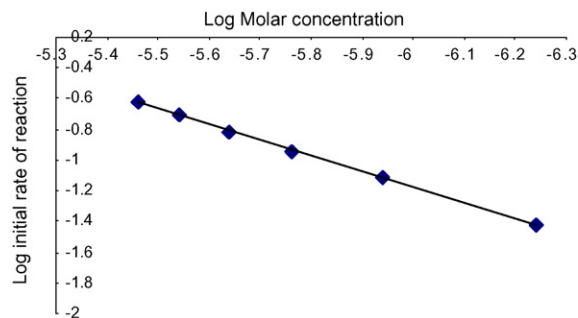


Fig. 6. Calibration plot of logarithm rate of the reaction against logarithm molar concentration of cephalixin for initial rate method.

added as a precipitating agent for protein and the resultant mixture was diluted to 10.0 mL with double distilled water to achieve the final concentration of 1.0 mg mL^{-1} . The sample was centrifuged at 3000 rpm for 10 min to remove residue. Then, 5.0 mL of protein-free supernatant was transferred carefully into 100 mL volumetric flask and diluted to volume with double distilled water in order to obtain sample solutions ($20\text{--}120 \mu\text{g mL}^{-1}$). Then, the general procedure was followed. A blank value was determined by treating the antibiotic-free blood sample in the same manner.

2.6.4. Procedure for real human plasma

As to cephalixin and cephradine, 1.0 g was orally taken by healthy human volunteers, and a 5.0 mL sample of human blood was taken by using calibrated heparinized tube after 1 h and centrifuged at 3000 rpm for 30 min. Then, into 10 mL stoppered calibrated tube 2.5 mL of obtained plasma was treated with 1.0 mL of acetonitrile, and the resultant mixture was diluted to 10.0 mL with double distilled water. The sample was centrifuged at 3000 rpm for 10 min to remove residue. Then, 5.0 mL of protein-free supernatant was taken carefully and, then, the general procedure was followed. For ceftriaxone, cefuroxime, cefazoline and cephalirin, 1.0 g was intramuscularly injected into healthy human volunteers, and a 5.0 mL sample of human blood was taken by using calibrated heparinized tube after 1/2 h, 3/4 h, 1 h and 2 h, respectively, and centrifuged at 3000 rpm for 30 min. Then, 2.5 mL of obtained plasma was treated with 1.0 mL of acetonitrile and the resultant mixture was diluted to 10.0 mL with double dis-

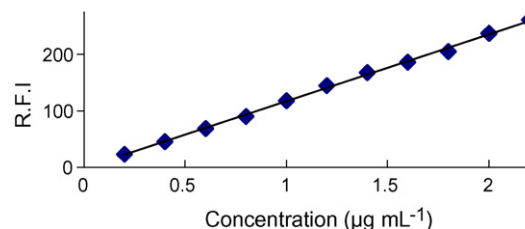


Fig. 7. Calibration plot of relative fluorescence intensity versus the concentration of cephalixin at preselected fixed time of 10 min.

Table 3
Analytical parameters for the initial rate method of kinetic spectrofluorimetric determination of investigated cephalosporins with alkaline hydrolysis.

Investigated cephalosporin	Linear range, mol L ⁻¹ ($\times 10^{-7}$ μ g mL ⁻¹)	Least square equation ($\log V = \log K' + n \log C$)		Correlation coefficient (<i>r</i>)	LOD (μ g mL ⁻¹)
		Intercept ($\log K'$)	Slope (<i>n</i>)		
Cephalexine	5–34 (0.2–1.2)	4.912	1.015	0.9995	0.2845
Cefotaxime	4–25 (0.2–1.2)	4.426	1.008	0.9995	0.2804
Cephapirin	4–28 (0.2–1.2)	4.564	1.006	0.9997	0.2317
Cefazoline	4–26 (0.2–1.2)	5.253	1.031	0.9999	0.1309
Cefotriaxone	3–21 (0.2–1.2)	5.306	1.044	0.9994	0.3003
Cefuroxime	4–28 (0.2–1.2)	5.183	1.016	0.9995	0.278
Cephradine	5–34 (0.2–1.2)	5.048	1.028	0.9997	0.2107

tilled water. The sample was centrifuged at 3000 rpm for 10 min for removing the residue. 5.0 mL of protein-free supernatant was taken carefully; and, then, the general procedure was followed. This process was repeated on the same volunteer for three times to obtain intraday assay. In addition, this process was repeated on three different volunteers in three different days to obtain interday assay. While cefotaxime [38] undergo partially hepatic metabolism into active metabolite desacetylcefotaxime (the plasma half life is about 1 h and that of active metabolite is about 1.5 h) so cannot

undergo analysis of cefotaxime in human plasma by our proposed method.

3. Results and discussion

3.1. Fluorescence spectrum

The fluorescence spectra of the degradation product of cefuroxime as a representative example for investigated cephalosporins are

Table 4
Analytical parameters for fixed time method of the kinetic spectrofluorimetric parameters for the determination of investigated cephalosporins.

Reaction time	Linear range (μ g mL ⁻¹)	Intercept (<i>a</i>)	Standard deviation of intercept (<i>S_a</i>)	Slope (<i>b</i>)	Standard deviation of slope (<i>S_b</i>)	Correlation coefficient (<i>r</i>)	LOD (μ g mL ⁻¹)
Cephalexin							
10	0.2–2.2	–1.383	2.137	118.41	2.137	0.9992	0.0541
15	0.2–1.6	0.8468	2.367	148.99	2.303	0.9993	0.0463
20	0.2–1.4	–7.787	2.804	198.35	2.804	0.9994	0.0424
25	0.2–1.4	–9.925	2.467	229.52	2.723	0.9996	0.03559
30	0.2–1.4	–14.013	1.856	264.64	1.856	0.9998	0.02103
Cefotaxime							
20	0.2–2.2	1.558	1.256	59.39	0.9259	0.9989	0.0634
30	0.2–1.6	6.608	1.198	70.82	1.198	0.9992	0.0507
40	0.2–1.4	10.831	1.018	79.47	1.138	0.9995	0.0382
50	0.2–1.4	15.176	1.269	86.011	1.418	0.9993	0.04426
60	0.2–1.4	20.429	1.067	90.893	1.193	0.9996	0.0352
Cephapirin							
20	0.2–2.2	–5.11	1.946	104.43	1.435	0.9992	0.055
30	0.2–1.6	24.665	1.436	90.586	1.436	0.9992	0.048
40	0.2–1.4	39.823	1.496	106.68	1.672	0.9994	0.042
50	0.2–1.4	54.394	1.455	124.99	1.627	0.9996	0.0349
60	0.2–1.4	71.659	1.327	130.13	1.484	0.9997	0.03059
Cefazoline							
20	0.2–2.2	–3.984	2.997	161.79	2.209	0.9992	0.05557
30	0.2–1.6	2.751	2.883	181.9	2.854	0.9993	0.04463
40	0.2–1.4	9.833	1.887	193.78	2.109	0.9997	0.02921
50	0.2–1.4	21.197	1.874	193.75	2.095	0.9997	0.02601
60	0.2–1.4	26.286	0.9897	202.14	1.107	0.9999	0.01468
Ceftriaxone							
20	0.2–2.2	–12.848	3.229	140.31	2.38	0.9987	0.069039
30	0.2–1.6	10.166	2.510	136.06	2.486	0.9990	0.05534
40	0.2–1.4	17.427	2.026	151.26	2.265	0.9994	0.04018
50	0.2–1.4	32.754	1.509	148.40	1.687	0.9997	0.030505
60	0.2–1.4	43.571	1.047	150.54	1.171	0.9998	0.02086
Cefuroxime							
20	0.2–2.2	–2.004	2.999	176.01	2.211	0.9993	0.051116
30	0.2–1.6	9.313	3.112	199.41	3.081	0.9993	0.046818
40	0.2–1.4	14.423	2.992	222.24	3.345	0.9994	0.040388
50	0.2–1.4	19.394	2.155	241.76	2.410	0.9998	0.026741
60	0.2–1.4	27.047	1.533	256.19	1.714	0.9999	0.01795
Cephradine							
10	0.2–2.2	1.038	2.324	131.41	1.713	0.9992	0.053055
15	0.2–1.6	15.580	3.127	187.58	3.096	0.9992	0.050010
20	0.2–1.4	13.421	2.778	191.29	3.106	0.9993	0.04356
25	0.2–1.4	18.184	2.432	214.61	2.719	0.9996	0.03399
30	0.2–1.4	24.591	1.863	233.65	2.082	0.9998	0.02392

Table 5
Evaluation of accuracy of the analytical procedure using initial rate method.

Drug	% Recovery ^a		
	0.2 $\mu\text{g mL}^{-1}$	0.9 $\mu\text{g mL}^{-1}$	1.2 $\mu\text{g mL}^{-1}$
Cephalexine	99.41 \pm 1.015	99.11 \pm 0.3759	100.66 \pm 0.4892
Cefotaxime	100.98 \pm 1.202	101.2 \pm 0.8232	100.05 \pm 0.6381
Cephapirin	100.15 \pm 1.112	101.47 \pm 0.8708	99.8 \pm 0.4558
Cefazoline	100.04 \pm 1.122	98.99 \pm 1.024	100.46 \pm 0.6066
Cefotriaxone	101.07 \pm 0.846	99.35 \pm 0.6819	101.35 \pm 0.7189
Cefuroxime	100.06 \pm 0.7004	99.95 \pm 0.6868	101.08 \pm 0.4855
Cephadrine	100.67 \pm 0.7493	99.24 \pm 0.6523	100.79 \pm 0.4156

^a Mean of 6 replicate \pm S.D.

shown in Fig. 1. Table 2 shows the excitation and emission peaks of investigated cephalosporins.

3.2. Optimization of variables

The effect of sodium hydroxide concentration: The fluorescence intensity increases by increasing the molar concentration of sodium hydroxide and reaches its maximum value at 0.8 mol L⁻¹, after which no further increases were observed. Thus, the adaptation of 1 mol L⁻¹ of sodium hydroxide is suitable for kinetic study.

The effect of temperature: Preliminary experiments showed that temperature affects the intensity of the fluorescence spectrum. A high RFI was obtained when the solution was heated in a boiling-water bath.

The effect of heating time: Preliminary experiments showed that the heating time affects the intensity of the fluorescence spectrum. A high RFI was obtained when the solution was heated in a boiling-water bath (100 °C) for 30 min as to cephalexin and cephadrine and for 60 min as to other investigated cephalosporins.

The effect of pH: We have examined the fluorescence intensity of the seven cephalosporins under different pH conditions. The results obtained indicate that the optimum pHs for determining cefotaxime, cephapirin, cefazolin and ceftriaxone is pH 4 and the optimum pH for the determination of cephadrine, cefuroxime and cephalexine is pH 10. Using a different type of buffer to obtain optimum pH 4, the optimum buffer to achieve this pH is acetate buffer.

Using different types of buffer to obtain optimum pH 10, the optimum buffer to achieve this pH is boric acid–sodium hydroxide buffer.

The effect of diluting solvent: Water was found to be an ideal solvent for cephalexin and cephadrine, while ethanol was found to be an ideal one for cefotaxime, cephapirin, cefazolin, ceftriaxone and cefuroxime.

3.3. Mechanism of the reaction

The presence of an α -amino benzyl group in the penicillin or cephalosporins is necessary for the formation of diketopiperazine

Table 6
Evaluation of accuracy of the analytical procedure using fixed time method.

Drug	% Recovery ^a		
	0.2 $\mu\text{g mL}^{-1}$	0.9 $\mu\text{g mL}^{-1}$	1.2 $\mu\text{g mL}^{-1}$
Cephalexine	101.08 \pm 0.9475	99.83 \pm 0.5777	100.94 \pm 0.4926
Cefotaxime	99.54 \pm 1.197	100.42 \pm 0.5068	99.98 \pm 0.5214
Cephapirin	101.53 \pm 0.9525	100.93 \pm 0.7374	99.76 \pm 0.6346
Cefazoline	100.89 \pm 1.084	99.1 \pm 0.9207	99.58 \pm 0.5601
Cefotriaxone	100.39 \pm 1.208	99.5 \pm 1.083	99.98 \pm 0.7357
Cefuroxime	100.74 \pm 1.198	100.31 \pm 0.6026	99.58 \pm 0.5347
Cephadrine	99.55 \pm 0.9175	98.71 \pm 0.7769	100.8 \pm 0.4487

^a Mean of 6 replicate \pm S.D.

product [39]. Thus, the suggested mechanism for the formation of the fluorescent product from cephadrine and cephalexin can be shown in Fig. 2.

In contrast, the formation of oxazolones as a fluorescent product of cephalosporins, which does not contain α -amino benzyl group, was also reported [40]. Thus, the suggested mechanism of other cephalosporins is shown in Fig. 3. Our study indicates that definite reaction product was obtained upon using the different initial concentration range and this is proved by reproducibility of results obtained.

3.4. Kinetics of the reaction

Under the optimum conditions, the relative fluorescence intensity time curves of the investigated cephalosporins with sodium hydroxide were constructed (Figs. 4 and 5). The initial rates of the reaction were determined from the slope of tangents of the relative fluorescence intensity time curves. The order of the reaction with respect to sodium hydroxide was determined by studying the reaction at different concentrations of sodium hydroxide with a fixed concentration of the cephalosporins under investigation. The plot of the initial rate (dA/dt) against the initial relative fluorescence intensity was linear passing the origin indicating that the initial order of the reaction with respect to sodium hydroxide was 1 (Fig. 6). The order with respect to the cephalosporins under investigation was evaluated by measuring the rate of the reaction at several concentrations of cephalosporins at a fixed concentration of sodium hydroxide. The logarithm of the initial rate of the reaction was plotted versus the logarithm of molar concentration of the investigated cephalosporins and was found to be 1 (Fig. 7).

However, under the optimized experimental conditions, the concentrations of cephalosporins were determined using a relative excess amount of sodium hydroxide solutions. Therefore, pseudo-zero-order conditions were obtained with respect to their concentrations.

Table 7
Evaluation of precision of the initial rate method and fixed time method of the proposed kinetic spectrofluorimetric method for the determination of investigated cephalosporins.

Drug	Amount taken ($\mu\text{g mL}^{-1}$)	Recovery (% \pm S.D.) ^a	
		Initial rate method	Fixed time method
Cephalexine	0.2	99.27 \pm 0.9198	101.44 \pm 0.7372
	0.6	99.18 \pm 0.3602	99.75 \pm 0.5268
	1.2	100.55 \pm 0.4186	101.02 \pm 0.4783
Cefotaxime	0.2	100.54 \pm 0.8671	98.32 \pm 0.8685
	0.6	101.17 \pm 0.7000	100.49 \pm 0.4969
	1.2	100.13 \pm 0.6086	100.02 \pm 0.5876
Cephapirin	0.2	99.92 \pm 1.056	101.56 \pm 0.8978
	0.6	101.52 \pm 0.7403	100.91 \pm 0.6261
	1.2	99.75 \pm 0.4494	99.76 \pm 0.5369
Cefazoline	0.2	100.3 \pm 1.069	101.39 \pm 0.9620
	0.6	98.85 \pm 0.9494	98.98 \pm 0.8585
	1.2	100.56 \pm 0.5831	99.55 \pm 0.4798
Cefotriaxone	0.2	101.22 \pm 0.8240	101.33 \pm 0.9419
	0.6	99.26 \pm 0.7081	99.12 \pm 0.9216
	1.2	101.54 \pm 0.7118	100.15 \pm 0.44
Cefuroxime	0.2	100.11 \pm 0.6401	101.64 \pm 0.9223
	0.6	99.94 \pm 0.5840	100.28 \pm 0.5164
	1.2	101.11 \pm 0.5874	99.42 \pm 0.6204
Cephadrine	0.2	100.91 \pm 0.7725	99.57 \pm 0.7299
	0.6	99.30 \pm 0.5891	99.35 \pm 0.9308
	1.2	100.90 \pm 0.4099	100.93 \pm 0.5277

^a Average of five determinations.

Table 8
Determination of studied drugs in their pharmaceutical dosage forms using initial rate method and fixed time method.

Drug	Pharmaceutical dosage form	Proposed methods \pm S.D. ^a (n = 5)		Reported methods \pm S.D. (n = 5)
		Initial rate	Fixed time	
Cephalexin	Ceporex [®] vials	100.79 \pm 0.8987 $t = 1.033^b$ $F = 1.073^b$	100.67 \pm 0.9559 $t = 0.8077$ $F = 1.054$	100.19 \pm 0.9310
Cephalexin	Ceporex [®] tablets	100.33 \pm 1.369 $t = 0.4311$ $F = 1.564$	99.95 \pm 0.7298 $t = 0.07138$ $F = 2.251$	99.98 \pm 1.112
Cefotaxime	Cefotax [®] vials	101.02 \pm 1.244 $t = 0.6168$ $F = 1.627$	100.38 \pm 0.8901 $t = 0.3421$ $F = 1.2$	100.58 \pm 0.9753
Cephapirin	Cefatrexyl [®] vials	100.43 \pm 0.7594 $t = 0.4011$ $F = 2.532$	100.87 \pm 1.178 $t = 0.9223$ $F = 1.053$	100.17 \pm 1.208
Cefazoline	Totacef [®] vials	100.18 \pm 1.043 $t = 1.205$ $F = 1.748$	99.74 \pm 1.06 $t = 0.6247$ $F = 1.694$	99.25 \pm 1.379
Cefotriaxone	Cefotriaxone [®] vials	99.47 \pm 1.43 $t = 0.7314$ $F = 2.154$	100.41 \pm 1.097 $t = 0.5640$ $F = 1.267$	100.04 \pm 0.9742
Cefuroxime	Zinnat [®] vials	100.45 \pm 1.019 $t = 0.2127$ $F = 1.881$	100.29 \pm 1.289 $t = 0.06312$ $F = 3.009$	100.33 \pm 0.7431
Cepharadine	Velosef [®] vials	99.86 \pm 1.02 $t = 0.04279$ $F = 1.359$	100.08 \pm 1.3 $t = 0.2411$ $F = 1.193$	99.89 \pm 1.190
Cepharadine	Velosef [®] capsuls	99.57 \pm 1.34 $t = 1.083$ $F = 2.013$	100.38 \pm 1.061 $t = 0.2155$ $F = 1.760$	100.25 \pm 0.7994
Cepharadine	Velosef [®] suspensions	100.19 \pm 1.594 $t = 0.3314$ $F = 1.756$	100.33 \pm 1.233 $t = 0.5634$ $F = 1.050$	99.9 \pm 1.203

^a Average of five determinations.

^b Tabulated value at 95% confidence limit, $t = 2.306$ and $F = 6.388$.

3.5. Quantitation methods

3.5.1. Initial rate method

The initial rate of the reaction followed a pseudo-first-order and was found to obey the following equation:

$$v = \frac{\Delta I_f}{\Delta t} = K' C^n$$

where v indicates the reaction rate, I_f the fluorescence intensity, t measuring time, K' the pseudo-first-order rate constant, C molar concentration of cephalosporins and n the order of the reaction.

The logarithmic form of the above equation is written as follows:
 $\log v = \log \Delta I_f / \Delta t = \log K' + n \log C$.

Table 9

Application of the proposed method to the determination of cephalosporins in spiked human plasma.

Drug	% Recovery ^a		
	0.2 $\mu\text{g mL}^{-1}$	0.9 $\mu\text{g mL}^{-1}$	1.2 $\mu\text{g mL}^{-1}$
Cephalexin	98.7 \pm 0.6	99.65 \pm 0.6534	98.32 \pm 1.105
Cephapirin	98.85 \pm 0.4648	99.79 \pm 1.573	97.26 \pm 1.130
Cefazoline	99.22 \pm 1.824	99.22 \pm 1.004	98.9 \pm 1.637
Cefotriaxone	99.51 \pm 0.9455	99.99 \pm 1.394	96.79 \pm 2.078
Cefuroxime	99.67 \pm 0.6881	99.98 \pm 1.912	98.09 \pm 1.073
Cephradine	96.74 \pm 1.4	97.15 \pm 1.757	97.91 \pm 1.784

^a Mean of 3 replicate \pm S.D.

Regression analysis using the method of least square was performed to evaluate the slopes, intercepts and correlation coefficients. The analytical parameters and results of regression analysis are given in Table 3. The value of n (≈ 1) in the regression equation confirmed that the alkaline hydrolysis of investigated cephalosporins was a pseudo-first-order with respect to cephalosporins concentration. The limits of detection (LOD) were calculated and the obtained results confirm good sensitivity of the proposed method; consequently, the suggested method can determine a low concentration of cephalosporins.

3.5.2. Fixed time method

In this method, the relative fluorescence intensity of the reaction solution containing varying amounts of cephalosporins was measured at a preselected fixed time. Calibration plots of relative fluorescence intensity versus the concentration of cephalosporins at a fixed time were established for each investigated cephalosporins. The regression equation, correlation coefficients and detection limits are given in Table 4. For all the investigated cephalosporins except cephalexin and cephapirin, the lowest detection limit was obtained at a fixed time of 60 min; whereas at the fixed time of 20 min, a wider concentration range for quantification was observed. As to cephalexin and cephradine, the lowest detection limit was obtained at a fixed time of 30 min; whereas at the fixed time of 10 min, a wider concentration range for quantification was observed.

Table 10

% Recoveries after application of the proposed method in real human plasma sample using initial rate method.

Drug	Delivery _{in vitro}	% Recovery _{in vitro}	Delivery _{in vivo}	% Recovery _{in vivo}
(A) Intraday assay				
Cephalexin	0.3914	97.85	0.3192 0.3332 0.3444	79.80 83.30 86.10
Mean ± S.D.				83.06 ± 3.156
Cephadrine	0.296	98.66	0.2469 0.2695 0.2613	82.36 89.83 87.09
Mean ± S.D.				86.42 ± 3.779
Cefuroxime	0.4937	98.74	0.3912 0.4008 0.3936	78.24 80.16 78.72
Mean ± S.D.				79.04 ± 0.9992
Ceftriaxone	0.9435	99.32	0.6626 0.6786 0.6728	69.75 71.43 70.82
Mean ± S.D.				70.66 ± 0.8504
Cephapirin	0.2001	100.05	0.1582 0.1624 0.1562	79.10 81.20 78.10
Mean ± S.D.				79.46 ± 1.582
Cefazoline	0.8102	101.28	0.5552 0.5394 0.5211	69.40 67.43 65.14
Mean ± S.D.				67.32 ± 2.132
(B) Interday assay				
Cephalexin	0.3926	98.15	0.3262 0.3011 0.3559	81.55 75.27 88.97
Mean ± S.D.				81.93 ± 6.858
Cephadrine	0.2943	98.10	0.2464 0.2235 0.2649	82.13 74.50 88.30
Mean ± S.D.				81.64 ± 6.913
Cefuroxime	0.4955	99.11	0.3776 0.3920 0.4168	75.53 78.41 83.37
Mean ± S.D.				79.10 ± 3.966
Ceftriaxone	0.9366	98.59	0.6741 0.6235 0.6462	70.96 65.63 68.02
Mean ± S.D.				68.2 ± 2.670
Cephapirin	0.1997	99.85	0.1578 0.1671 0.1617	78.90 83.55 80.85
Mean ± S.D.				81.10 ± 2.335
Cefazoline	0.8059	100.74	0.5177 0.5571 0.5789	64.71 69.64 72.36
Mean ± S.D.				68.9 ± 3.878

According to international conference of harmonization (ICH) guideline for validation of analytical procedures [41], the detection limit is not required to be part of the validation procedure for assay. Therefore, on the basis of the wider concentration range and less time of analysis, the fixed time of 10 min or 20 min was recommended for the determination.

3.6. Validation of the proposed method

Concentration range [41] is established by confirming that the analytical procedure provides a suitable degree of precision, accuracy and linearity when applied to the sample-containing amount

of analyte within or at the extreme of the specified range of the analytical procedure [42,43]. In this work, the concentrations ranging from $3 \times 10^{-7} \text{ molL}^{-1}$ to $34 \times 10^{-7} \text{ molL}^{-1}$ were studied for the investigated drugs in the initial rate method and the concentrations ranging from $5 \mu\text{g mL}^{-1}$ to $25 \mu\text{g mL}^{-1}$ were studied for the investigated drugs in the fixed time method (at preselected fixed time of 10 min for cephalexin, cephradine and 20 min for the other investigated cephalosporins). All the experiments were carried out through this range to ensure the validation of the proposed procedure. Linear calibration graphs were obtained for all the studied drugs by plotting the logarithm of the initial rate of the reaction versus the logarithm of molar concentration of ana-

Table 11
% Recoveries after application of the proposed method in real human plasma sample using fixed time method.

Drug	Delivery _{in vitro}	% Recovery _{in vitro}	Delivery _{in vivo}	% Recovery _{in vivo}
(A) Intraday assay				
Cephalexin	0.405	101.23	0.3235 0.3375 0.3436	80.75 84.37 85.90 83.67 ± 2.645
Mean ± S.D.				
Cephadrine	0.2983	99.43	0.2614 0.2745 0.2793	87.3 91.50 93.09 90.63 ± 2.991
Mean ± S.D.				
Cefuroxime	0.2668	98.81	0.2110 0.2162 0.2123	78.14 80.07 78.62 78.94 ± 1.005
Mean ± S.D.				
Ceftriaxone	0.9973	99.73	0.6630 0.6791 0.6733	66.3 67.91 67.33 67.18 ± 0.8154
Mean ± S.D.				
Cephapirin	0.2012	100.60	0.1559 0.1602 0.1539	77.95 80.1 76.95 78.33 ± 1.610
Mean ± S.D.				
Cefazoline	0.2952	98.40	0.2081 0.2022 0.1954	69.36 67.40 65.13 67.29 ± 2.117
Mean ± S.D.				
(B) Interday assay				
Cephalexin	0.4076	101.90	0.3260 0.3059 0.3546	81.5 76.47 88.65 82.21 ± 6.121
Mean ± S.D.				
Cephadrine	0.2949	98.30	0.2519 0.2416 0.2779	83.96 80.53 92.63 85.71 ± 6.236
Mean ± S.D.				
Cefuroxime	0.2657	98.41	0.2037 0.2114 0.2247	75.45 78.30 83.24 78.99 ± 3.941
Mean ± S.D.				
Ceftriaxone	1.013	101.30	0.6746 0.6054 0.6466	67.46 60.54 64.66 64.22 ± 3.481
Mean ± S.D.				
Cephapirin	0.1961	98.05	0.1555 0.1649 0.1595	77.75 82.45 79.75 79.98 ± 2.359
Mean ± S.D.				
Cefazoline	0.3006	100.2	0.1941 0.2088 0.2170	64.70 69.60 72.33 68.88 ± 3.866
Mean ± S.D.				

lyte in the sample (in initial rate method) within the specified range (Fig. 4):

$$\log v = \log \frac{\Delta I_f}{\Delta t} = \log K' + n \log C$$

or by plotting the relative fluorescence intensity of the studied drugs versus the drug concentration (in fixed time method) within the specified range (Fig. 5).

Linearity was studied for both initial rate and fixed time method indicated by the values of correlation coefficient (r) and determination coefficient (r^2) for both methods (Tables 3 and 4).

Accuracy [43] was checked at three concentration levels within the specified range, and six replicate measurements were recorded

at each concentration levels. The results were recorded as percent recovery ± standard deviation (Tables 5 and 6). In comparison of our results with that of other reported method, it is considered more accurate.

Precision [43] was checked at three concentration levels, and eight replicate measurements were recorded at each concentration level; the results are summarized in Table 7. The calculated relative standard deviations were all below 2.2% indicating excellent precision of the proposed procedure at both levels of repeatability and intermediate precision.

The limit of detection [41] was calculated based on the standard deviation of response and the slope of the calibration curve [42]. The limit of detection was expressed

as [43]:

$$\text{LOD} = \frac{3\sigma}{S}$$

where σ is the standard deviation of intercept and S is the slope of the calibration curve.

The results were summarized in (Tables 3 and 4) indicating a good sensitivity of the proposed method. According to USP XXV validation guidelines [43], the calculated LOD values should be further validated by laboratory experiments. In our work, good results were obtained where the calculated drug concentration by LOD equations were actually detected in these experiments.

The limit of quantitation (LOQ) was calculated based on the standard deviation of the intercept and slope of the calibration curve. In this method, the limit of quantitation is expressed as [43]:

$$\text{LOQ} = \frac{10\sigma}{S}$$

The results were summarized in (Tables 3 and 4) indicating a good sensitivity of the proposed method. According to USP XXV validation guidelines [44], the calculated LOQ values should be further validated by laboratory experiments. In our work, good results were obtained where the calculated drug concentration by LOQ equations were actually quantitated in these experiments.

Specificity and interference: It was observed that there is no interference from other additives such as the interference from L-arginine, which is commonly present in combination with cephadrine in Velosef vials. No significant difference could be detected upon comparing R.F.I. of the cited drug alone or in the presence of a ratio (3:7) drug–L-arginine, respectively. Therefore, the proposed method is suitable for the determination of cephalosporins in pharmaceutical formulations without preliminary extraction, thus saving a lot of time and eliminating the possibility of making mistakes due to extraction techniques.

3.7. Application to pharmaceutical dosage forms

The initial rate and fixed time methods have been tested for commercial pharmaceutical dosage forms. The results were statistically compared with those of reported method [2–4], in respect to accuracy and precision. The obtained mean recovery values of the obtained amount were $99.2\text{--}100.67 \pm 0.6226\text{--}1.69\%$ as shown in Table 8. According to the t - and F -tests, no significant difference was found between the calculated and theoretical value of both the proposed and the reported methods at 95% confidence level. This indicates good level of precision and accuracy.

3.8. Application to spiked human plasma

The high sensitivity of the proposed method allowed the determination of the investigated cephalosporins in spiked human plasma. Thus, it has been tested on spiked human plasma. The concentration of the investigated cephalosporins was computed from its responding regression equations. The obtained mean recovery values of the obtained amount were $96.79\text{--}99.99 \pm 0.4648\text{--}2.078\%$ as shown in Table 9. It can be seen that the proposed method is suitable for the analysis of the investigated cephalosporins in human plasma.

3.9. Analysis of cited drugs in real human plasma

% Recovery of the investigated cephalosporins in plasma was calculated by using the following equation [44]:

$$\% \text{ recovery}_{\text{in vivo}} = \frac{\text{delivery}_{\text{in vivo}}}{\text{delivery}_{\text{in vitro}}} \times \frac{\text{recovery}_{\text{in vitro}}}{\text{delivery}_{\text{in vitro}}}$$

where % recovery_{in vivo} is % recovery for drug in real human sample. Delivery_{in vivo} is concentration of the drug in real human sample. % recovery_{in vitro} is % recovery for drug in spiked human sample.

Delivery_{in vitro} is the concentration of the drug in spiked human sample. % recoveries after application of the proposed method in real human plasma sample by intra and interday assay are shown in Tables 10 and 11, respectively.

4. Conclusion

The initial rate and fixed time methods can be easily applied for the determination of investigated cephalosporin in pure and dosage forms that do not require elaborate treatment or tedious extraction of fluorophore product produced.

The proposed method is sensitive enough to enable determination of lower amounts of the studied drugs. This advantage encourages the application of the proposed method in routine-quality control of the investigated cephalosporins in industrial laboratories and in the analysis of the investigated cephalosporins in human plasma.

References

- [1] Wilson and Gisfold's Textbook of Organic Medicinal and Pharmaceutical Chemistry, 10th ed., J. B. Lippincott-Raven, 1998, p. 274.
- [2] G.A. Saleh, H. Askal, I. Darwish, A. El-Shorbagi, Anal. Sci. 19 (2003) 281.
- [3] M.M. Ayad, A.A. Shalaby, H.E. Abdellatef, H.M. Elsaid, J. Pharm. Biomed. Anal. 18 (1999) 975.
- [4] G.A. Saleh, H. Askal, M.F. Radwan, M.A. Omar, Talanta 54 (2001) 1205.
- [5] S.A. Patel, M.N. Patel, M.M. Patel, Ind. J. Pharm. Sci. 68 (2006) 278.
- [6] H. Salem, H. Askal, J. Pharm. Biomed. Anal. 29 (2002) 347.
- [7] M. Hefnawy, Y. El-Shabrawy, F. Belal, J. Pharm. Biomed. Anal. 21 (1999) 703.
- [8] P. Gutierrez Navarro, A. El Bekkouri, E. Rodriguez Reinoso, Analyst 123 (1998) 2263.
- [9] F.A. Aly, M.M. Hefnawy, F. Belal, Anal. Lett. 29 (1996) 117.
- [10] A.F.M. El-Walily, A.A. Gazy, S.F. Belal, E.F. Khamis, J. Pharm. Biomed. Anal. 20 (1999) 643.
- [11] L.L. Bebwaw, K. El Kelani, L. Abdel Fattah, J. Pharm. Biomed. Anal. 32 (2003) 1219.
- [12] Q.L. Ma, J.H. Yang, X. Wu, F. Huang, L.M. Sun, Anal. Lett. 33 (2000) 2689.
- [13] S. Shalaby, J. Liquid Chromatogr. Relat. Technol. 21 (1998) 3161.
- [14] V.F. Samanidou, A.S. Ioannou, I.N. Papadoyannis, J. Chromatogr. B 809 (2004) 175.
- [15] N.O. Can, G. Altioikka, H.Y. Aboul-Enein, Anal. Chim. Acta 576 (2006) 246.
- [16] M. Becker, E. Zittlau, M. Petz, Anal. Chim. Acta 520 (2004) 19.
- [17] M.D. Glaria, G.G. Mosciati, R.G. Ramos, J. AOAC Int. 88 (2005) 436.
- [18] I. Baranowska, P. Markowski, J. Baranowski, Anal. Chim. Acta 570 (2006) 46.
- [19] S. Al-Rawithi, R. Hussein, D.A. Raines, I. AlShoaiir, W.J. Kurdi, Pharm. Biomed. Anal. 22 (2006) 281.
- [20] R.V. Oliveira, A.C. De Pietro, Q.B. Cass, Talanta 71 (2007) 1233.
- [21] Y.M. Li, Y.X. Zhu, D. Vanderghinste, D. Schepdael, E. Roets, J. Hoogmartens, Electrophoresis 20 (1999) 127.
- [22] H.H. Yeh, Y.H. Yang, Y.W. Chou, J.Y. Ko, C.A. Chou, H.S. Chen, Electrophoresis 26 (2005) 927.
- [23] F.A. Aly, N.A. Alarfaff, A.A. Alwarthan, Talanta 47 (1998) 471.
- [24] Y. Sun, Y. Tang, H. Yao, X. Zheng, Talanta 64 (2004) 156.
- [25] C. Thongpoon, B. Liawruangrath, S. Liawruangrath, R.A. Wheatley, A. Townshend, Anal. Chim. Acta 553 (2005) 123.
- [26] Y. Li, J. Lu, Luminescence 21 (2006) 251.
- [27] C. Thongpoon, B. Liawruangrath, S. Liawruangrath, R.A. Wheatley, A. Townshend, J. Pharm. Biomed. Anal. 42 (2006) 277.
- [28] N.A. Alarfaj, S.A. Abd El-Razeq, J. Pharm. Biomed. Anal. 41 (2006) 1423.
- [29] I.F. Jones, J.E. Page, C.T. Rhodes, J. Pharm. Pharmacol. 20 (1968) 455.
- [30] M. Azza, M. Ali, Bioelectrochem. Bioenerg. 33 (1994) 201.
- [31] G.V.S. Reddy, S.J.Y. Reddy, Talanta 44 (1997) 627.
- [32] A.A. Abdel Gaber, M.A. Ghandour, H.S. El-Said, Anal. Lett. 36 (2003) 1245.
- [33] A. Hilali, J.C. Jimenez, M. Callejon, M.A. Bello, A. Guiraum, Talanta 59 (2002) 137.
- [34] M. Xu, H. Ma, J. Song, J. Pharm. Biomed. Anal. 35 (2004) 435.
- [35] J. Yang, G. Zhou, X. Cao, Q. Ma, J. Dong, Anal. Lett. 31 (1998) 1047.
- [36] J.A. Murillo, J.M. Lemus, L.F. Garcia, Talanta 41 (1993) 557.
- [37] J.A. Murillo, J.M. Lemus, L.F. Garcia, J. Pharm. Biomed. Anal. 12 (1994) 875.
- [38] K. Parfitt (Ed.), The Complete Drug Reference, 31st ed., Martindale, 1996, p. 1415.

- [39] A.B.C. Yu, C.H. Nightingale, D.R. Flangan, *J. Pharm. Sci.* 66 (1977) 213.
- [40] International Conference on Harmonization, in: *Federal Register* (Ed.), *ICH Harmonized Tripartite Guideline-Text on Validation of Analytical Procedures*, 1995, p. 11260.
- [41] Topic Q2A, in: *Text on Validation of Analytical Procedure*, International Conference on Harmonization (ICH), 1994, p. 128.
- [42] Topic Q2B, in: *Validation of Analytical Procedure, Methodology*, International Conference on Harmonization (ICH), 1996, p. 1450.
- [43] *The United States Pharmacopoeia XXV and NF XX*, American Pharmaceutical Association, Washington, DC, 2002, p. 1115.
- [44] Y. Sun, M.V. Nakashima, M. Takahashi, N. Kuroda, K. Nakashima, *Biomed. Chromatogr.* 16 (2002) 319.



Cr₂O₃-modified ZnO thick film resistors as LPG sensors

D.R. Patil, L.A. Patil*

Nano-Materials Research Lab, Pratap College, Amalner, MHS, 425 401, India

ARTICLE INFO

Article history:

Received 13 June 2008

Received in revised form

12 September 2008

Accepted 16 September 2008

Available online 1 October 2008

Keywords:

Cr₂O₃-ZnO

Thick films

Screen-printing

Gas sensors

ABSTRACT

Thick films of pure ZnO were obtained by screen-printing technique. Surface functionalized ZnO thick films by Cr₂O₃ were obtained by dipping pure ZnO thick films into 0.01 M aqueous solution of chromium trioxide (CrO₃). The dipped films were fired at 500 °C for 30 min. Upon firing, the CrO₃ would reduce to Cr₂O₃. Cr₂O₃-activated (0.47 mass%) ZnO thick films resulted in LPG sensor. Upon exposure to 100 ppm LPG, the barrier height between Cr₂O₃ and ZnO grains decreases markedly, leading to a drastic decrease in resistance. The sensor was found to sense LPG at 350 °C and no cross sensitivity was observed to other hazardous, polluting and inflammable gases. The quick response (~18 s) and fast recovery (~42 s) are the main features of this sensor. The effects of microstructures and dopant concentrations on the gas sensing performance of the sensor were studied and discussed.

© 2008 Elsevier B.V. All rights reserved.

1. Introduction

Among the various materials, ZnO is the most promising semiconductor [1] to detect the toxic and hazardous gases. It has been studied that modified Cr₂O₃ [2] was used as a gas-sensing element. In fact pure Cr₂O₃ was reported to have poor gas sensing properties and it is an insulator [3]. Cr₂O₃-activated ZnO was reported to be a humidity [4] sensor.

Liquefied petroleum gas (LPG) is utilized in almost every kitchen all over the world. It is therefore, referred as a town gas or cooking gas. Along with inevitable domestic use, it is utilized in large extent for industrial purposes and in laboratories as fuel. Cooking gas consists chiefly of butane [5], which is a colourless and odourless gas. It is usually mixed with compounds of sulphur (viz. methyl mercaptan and ethyl mercaptan) having foul smell, so that its leakage can be noticed easily. This gas is potentially hazardous because explosion accidents [6] might be caused when it leaks out by mistake. It has been reported that, at the concentration up to noticeable leakage, it is very much more than the lower explosive limit (LEL) of the gas in air. Explosion accidents destroyed many industries, laboratories, kitchens and houses, buildings, societies and what not? Many researchers are working on LPG sensor, but could not meet the challenges up to the depth of demand by society. So, there is a great demand from the society of detecting LPG for the purpose of safety applications in domestic and industrial fields. The aim

of the present work is to develop the LPG sensor by modifying ZnO thick films, which could be able to detect the trace amount of LPG.

It was studied that the gas sensing performance of the material can be improved by incorporating few additives into the base material and/or surface activation of thick films. Some well-known materials used for the fabrication of LPG sensor are SnO₂ [7], Ru-SnO₂ [8], Cu-ZnO [5], modified-SnO₂ [9], etc.

2. Experimental

2.1. Thick film preparation

AR grade (99.9% pure) zinc oxide powder was ball milled to ensure sufficiently fine particle size. The fine powder was calcined at 1100 °C for 24 h in air and re-ground. Thick films of so obtained powder were prepared by adopting the procedure explained elsewhere [10]. These films were surface functionalized by dipping them into a 0.01 M aqueous solution of CrO₃ for different intervals of time followed by firing (500 °C, 30 min). The CrO₃ dispersed on the film surface was reduced to Cr₂O₃ in firing process. Thus the sensor elements with different mass% of Cr₂O₃ were obtained. Silver contacts were made by vacuum evaporation for electrical measurements.

2.2. Characterizations

The crystalline structures of the films were analysed with X-ray diffractogram (RIGAKU DMAX 2500) using Cu K α radiation

* Corresponding author. Tel.: +91 2587 224226.

E-mail address: plalchand.phy_aml@yahoo.co.in (L.A. Patil).

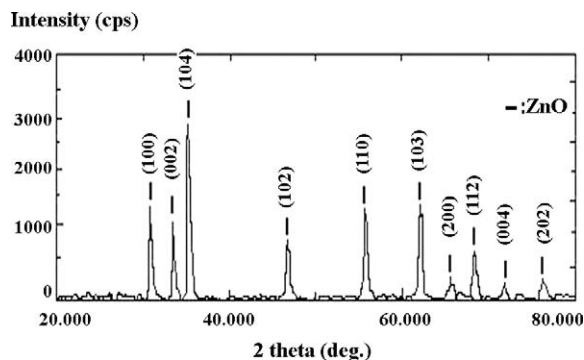


Fig. 1. X-ray diffractogram of the Cr_2O_3 -activated (5 min) ZnO.

with a wavelength 1.5418 Å. The microstructure and chemical composition of the films were analysed using a scanning electron microscope (JOEL JED 2300) coupled with an energy dispersive spectrometer (6360 LA). Thickness measurements were carried out using a Taylor-Hobson (Talystep, UK) system. Thermoelectric power measurements (TEP) were carried out in the laboratory. Electrical and gas sensing properties were measured using a static gas sensing system. The LPG sensing performance of the sensors was examined using 'static gas sensing system' reported elsewhere [11,12]. A constant D.C. voltage is provided to the sensor inside the gas chamber of static gas sensing system. The corresponding current was recorded from the pico-ammeter. Air was allowed to pass into the glass dome after every LPG exposure cycle.

3. Results and discussion

3.1. Materials characterizations

3.1.1. Structural properties (X-ray diffraction studies)

Fig. 1 shows the X-ray diffractogram of the Cr_2O_3 -activated (5 min) ZnO, most sensitive film to LPG at 350 °C. The observed peaks are matching well with JCPDS reported data of ZnO. The sharp peaks of the XRD pattern correspond to ZnO material and are observed to be polycrystalline in nature. No peaks corresponding to Cr_2O_3 may be due to its very small mass% dispersed on the surface of ZnO. The crystals show anisotropy because different directions within the repeating pattern interact differently with incident radiations. The average crystallite size determined from Scherer's formula was observed to be in the range of 150–680 nm.

3.1.2. Microstructure analysis (SEM)

Fig. 2 (a) shows randomly distributed grains with larger size and shape distribution. Fig. 2 (b) shows Cr_2O_3 grains associated with the ZnO grains. Cr_2O_3 grains may reside in the intergranular regions of ZnO. The effective surface area was thus, expected to increase largely. This may be the reason of giving maximum gas response of this film. The entire ZnO film in Fig. 2 (c) was observed to be masked as Cr_2O_3 grains fully cover the film. Thus reducing the effective surface area. The gas molecules would not reach the interstitial sites of Cr_2O_3 -ZnO grains. The surface only possesses the molecules of Cr_2O_3 .

3.1.3. Thickness measurement

The thickness of the films was observed to be in the range from 25 to 35 μm . The reproducibility of the film thickness was achieved by maintaining the proper rheology and thixotropy of the paste.

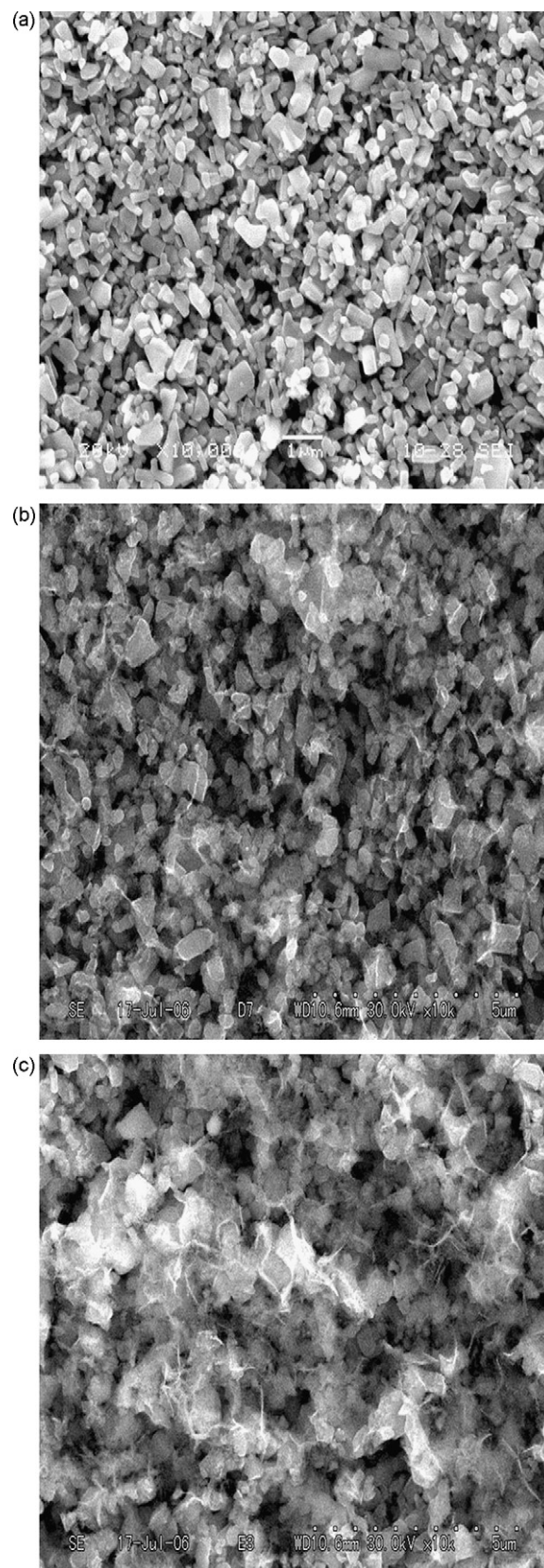


Fig. 2. Micrographs of (a) pure, (b) Cr_2O_3 -activated (5 min) and (c) Cr_2O_3 -activated (30 min) ZnO samples.

Table 1
Elemental analysis of unmodified (pure) and modified films.

Mass%	Dipping time (min)				
	0 (Pure)	2	5	15	30
Zn	91.95	95.14	94.50	94.92	94.92
O	8.05	4.83	5.17	4.72	4.68
ZnO	100	99.96	99.53	99.47	99.41
Cr	0.00	0.03	0.32	0.36	0.40
Cr ₂ O ₃	0.00	0.04	0.47	0.53	0.59
Cr ₂ O ₃ -ZnO	100	100	100	100	100

3.1.4. Thermoelectric power (TEP) measurements

The p-type semiconductivity of thick films of Cr₂O₃ and n-type semiconductivity of thick films of ZnO were confirmed by measuring thermo-electromotive force of thick film samples.

3.1.5. Quantitative elemental analysis-EDAX

The quantitative elemental composition of the pure and Cr₂O₃-activated ZnO films was analysed using an energy dispersive spectrometer and mass% of Zn, O, ZnO, Cr and Cr₂O₃ are represented in Table 1. The stoichiometric mass% of Zn and O in ZnO are 80.34 and 19.66, respectively. The mass% of Zn and O in each sample were not as per the stoichiometric proportion and all samples were observed to be oxygen deficient. Also, the films dipped in CrO₃ were observed to be most oxygen deficient than the pure ZnO film. The film dipped for 5 min was observed to be rich in oxygen than other dipped films. Excess or deficiency of the constituent material particles leads the semiconducting nature of the material. It is clear from Table 1 that the mass% of Cr₂O₃ (ZnO) goes on increasing (decreasing) with the dipping time.

3.2. Electrical properties of the sensor

3.2.1. I-V characteristics

I-V characteristics (Fig. 3) of pure and Cr₂O₃-activated ZnO samples are observed to be symmetrical in nature indicating ohmic nature of silver contacts.

3.2.2. Electrical conductivity

Fig. 4 shows the variation of log (conductivity) with reciprocal operating temperature. The conductivity values varied nonlinearly with temperature. The increase in conductivity with increasing temperature could be attributed to negative temperature coefficient of resistance and semiconducting nature of the Cr₂O₃-activated ZnO. The semiconductivity in Cr₂O₃-activated ZnO must

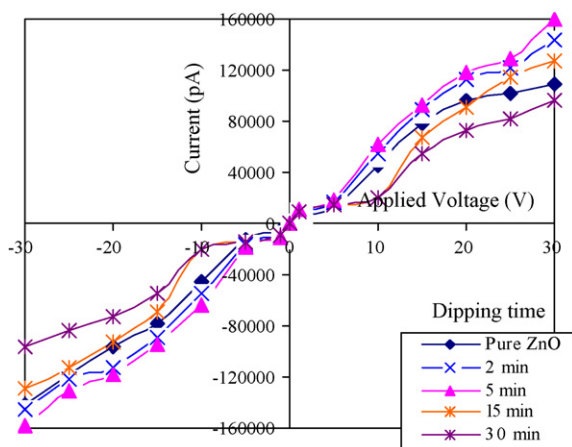


Fig. 3. I-V characteristics of the sensor.

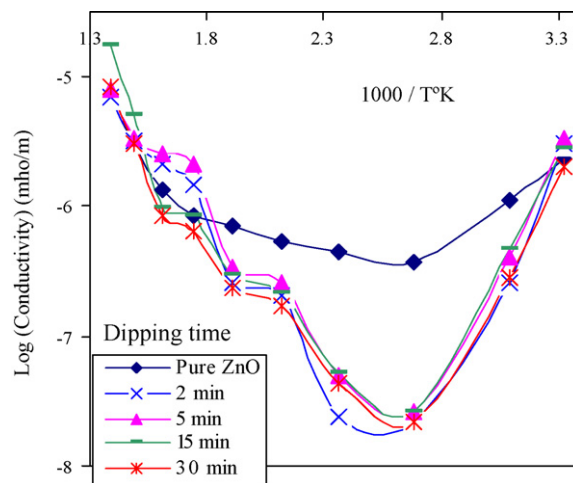


Fig. 4. Conductivity-temperature profile of pure and Cr₂O₃-ZnO samples.

be due to large oxygen deficiency in it. The material would then adsorb the oxygen species at higher operating temperatures ($O_2^- \rightarrow 2O^- \rightarrow O^{2-}$). It is observed from figure that the electrical conductivity of the pure ZnO thick film was larger than that of Cr₂O₃-activated ZnO films in air ambient. The potential barrier height is developed due to the formation of heterogeneous inter-grain boundaries of Cr₂O₃ and ZnO grains. Thus increased barrier height of the intergranular region of modified ZnO may be responsible to decrease the conductivity.

3.3. Gas sensing performance of the sensor

3.3.1. Measurement of gas response

Gas response (*S*) is defined as the ratio of change in conductance of the sensor in presence and absence of the target gas to the conductance in absence of the target gas. The relation for *S* is as:

$$S = \frac{(G_g - G_a)}{G_a}$$

where, *G_a* and *G_g* are the conductance of sensor in air and in a target gas medium, respectively.

The conductance of the sensor mounted in the static gas sensing system was measured in the absence of target gas. It is referred as (*G_a*). Then, the known volume of mixture of target gas and air was injected by a syringe through gas inlet pipe and the conductance was measured, which is referred as (*G_g*). Upon following the relation of *S*, the gas response was calculated.

3.3.2. Pure ZnO: H₂ sensor

3.3.2.1. Gas response and operating temperature. Fig. 5 depicts the variation of gas response with operating temperature of pure ZnO thick film for 1000 ppm LPG and H₂ gases. It is clear from figure that pure ZnO gives better response to H₂ at 400 °C and comparatively less response to LPG at 350 °C. In case of pure ZnO, oxygen adsorption on the surface of the film seems to be poor which may be the result of poor response to reducing gases. In addition to this, ZnO requires relatively larger operating temperature to adsorb the oxygen ions, and therefore it would respond at higher operating temperatures (~350–400 °C). To improve the sensing performance of pure ZnO thick film, it is essential to modify its surface.

3.3.2.2. Selectivity. Selectivity or specificity is defined as the ability of a sensor to respond to certain gas in the presence of other gases. It is observed from the Fig. 6 that the pure ZnO is sensitive to H₂

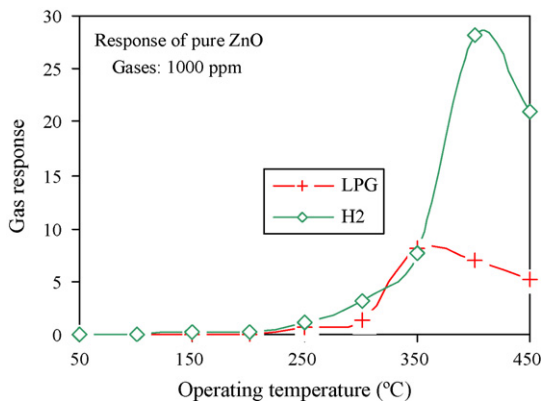


Fig. 5. Variation of gas response with operating temperature of pure ZnO film.

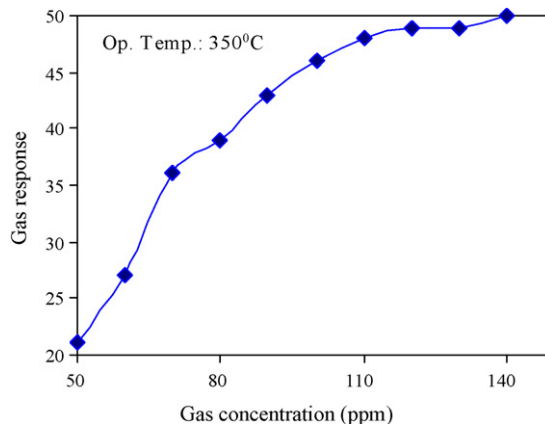


Fig. 8. Variation of gas response with gas concentration.

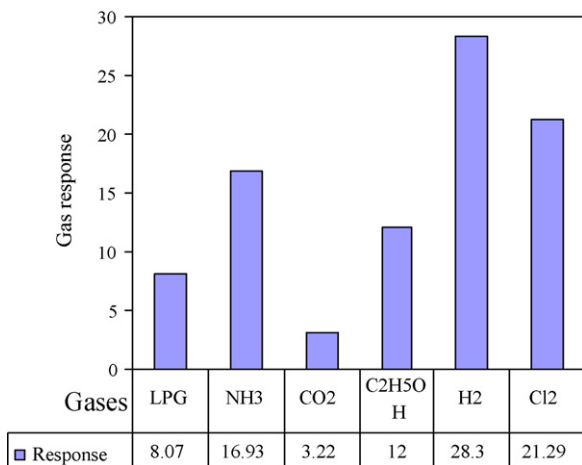


Fig. 6. Selectivity of pure ZnO to different gases.

operating temperature. At 350 °C, larger amount of oxygen would be adsorbed on the surface, which would facilitate the sensor to oxidize the LPG immediately giving larger gas response. The adsorbed oxygen may desorb from the surface at higher temperatures (>350 °C). This may be the reason of decreasing the gas response above 350 °C

3.3.3.2. *Gas response and gas concentration.* It is observed from Fig. 8 that the response of Cr₂O₃-activated ZnO film was observed to increase continuously with increasing the gas concentration up to 100 ppm, and it attains the maximum and saturates above 100 ppm. Therefore, the active region of the sensor would be up to 100 ppm, as the rate of rise of response is larger during this region. At lower gas concentrations, the unimolecular layer of gas molecules would be expected to form on the surface, which would interact with the surface more actively giving larger responses. There would be multilayers of gas molecules on the sensor surface at the higher gas concentrations (> 100 ppm) resulting in saturation in gas response.

gas. But it has least selectivity against different gases. This is the main drawback of pure ZnO thick film sensor.

3.3.3. Cr₂O₃ modified ZnO: LPG sensor

3.3.3.1. *Gas response and operating temperature.* It is clear from Fig. 7 that the gas response increases with operating temperature, reaches to maximum at 350 °C and falls with further increase in

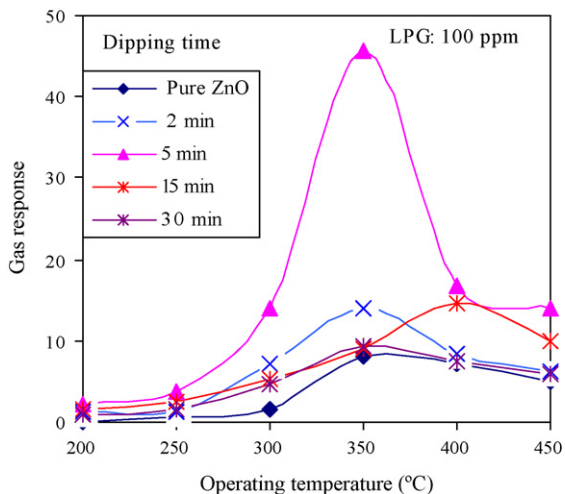


Fig. 7. Variation of gas response with operating temperature of modified ZnO film.

3.3.3.3. *Selectivity.* Fig. 9 depicts the variation of gas responses of Cr₂O₃-activated ZnO samples to LPG among the mixture of gases. It is clear from the figure that the Cr₂O₃-activated ZnO (5 min) sample shows the selective response to LPG at 350 °C among all other gases.

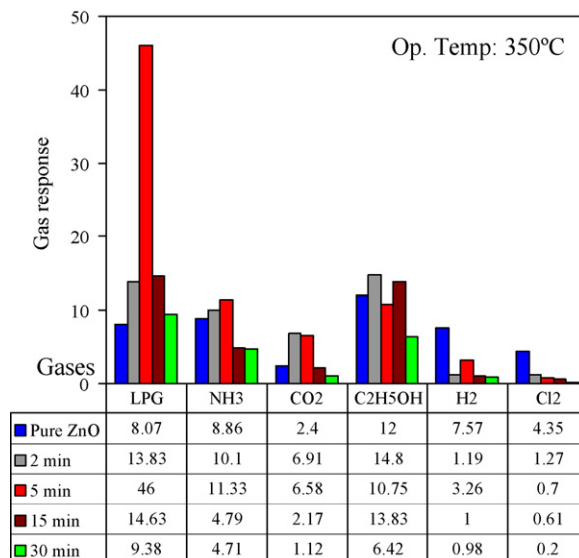


Fig. 9. Response of sensor to various gases (Selectivity).

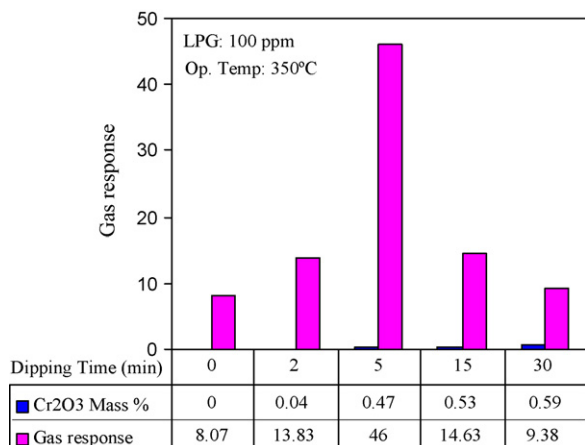


Fig. 10. Variation of gas response with dipping time and Cr-dopant.

The film surface chemistry was favourable to oxidize the LPG easily than other gases, giving response to LPG and less to others.

3.3.3.4. Gas response and dipping time. Fig. 10 depicts the variation of gas response with dipping time and Cr-dopant. The film dipped for 5 min showed larger gas response (46). At 5 min dipping time, the optimum mass% of Cr₂O₃ (0.47%) would be dispersed on the surface of the film, and mass% of oxygen was also higher than other activated films (Table 1). The larger gas response of Cr₂O₃-activated ZnO thick films can be explained as follows. The adsorption mechanism of Cr₂O₃-activated ZnO would be different from that of pure ZnO thick films. The optimum mass% of Cr₂O₃ on the surface of ZnO would form misfit regions non-uniformly on the film surface. The surface misfit regions enhance the oxygen adsorption on the surface. Thus the number of oxygen species adsorbed on the activated surface would be larger. The larger the number of oxygen species adsorbed, the faster would be the oxidation of LPG. This would increase the conductance of the film crucially, enhancing gas

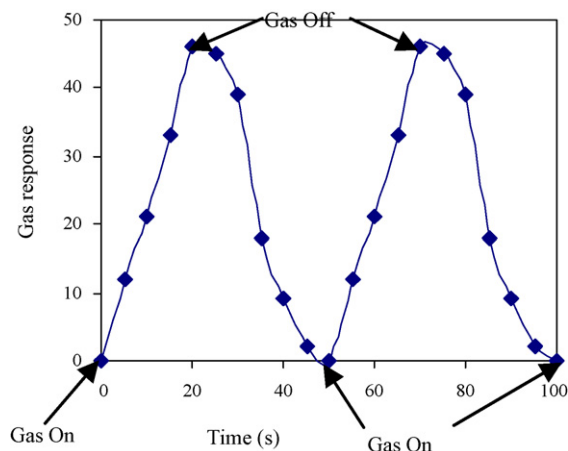


Fig. 11. Response and recovery of Cr₂O₃-activated ZnO sample.

response. It is observed from Fig. 10 that the gas response is largest at 0.47 mass% of the Cr-dopant on the surface of the film and falls down for higher and lower dopant concentrations. At lower dopant concentrations, the numbers of Cr-misfts on the film surface are less, which would adsorb less oxygen species on the film surface. However, at higher dopant concentrations, the Cr-dopant would mask the entire base material-ZnO and would resist the gas to reach up to the surface active sites, so gas response would decrease further.

3.3.3.5. Response and recovery of the sensor. The time taken for the sensor to attain 90% of the maximum increase in conductance on exposure of the target gas is known as response time. The time taken by the sensor to get back 90% of the maximum conductance when the flow of gas is switched off is known as recovery time. The response and recovery of the Cr₂O₃-activated ZnO (5 min) thick film sensor are represented in Fig. 11. The response was quick (~18 s) while the recovery was fast (~42 s). The negligible quantity

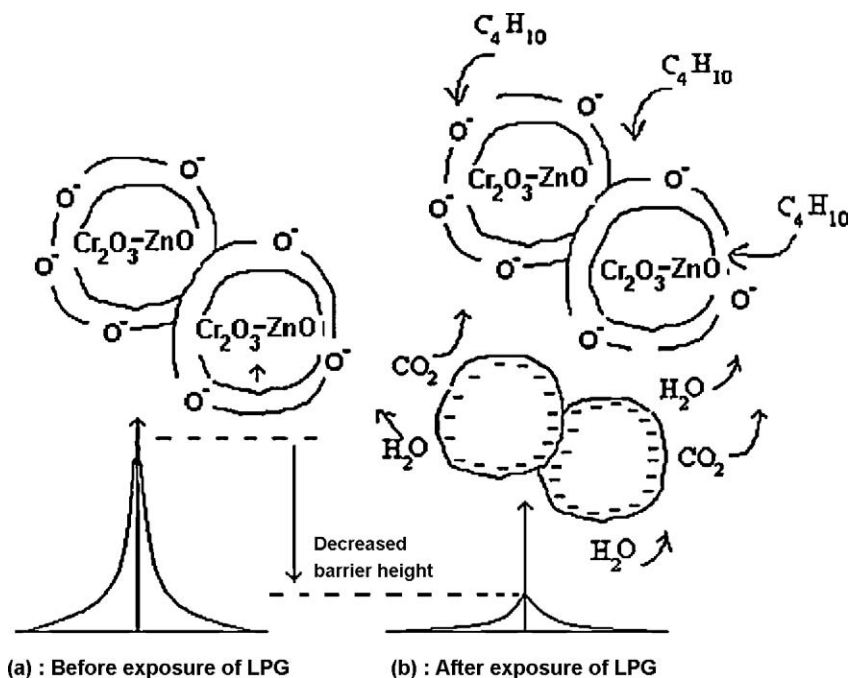
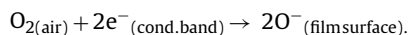


Fig. 12. LPG sensing mechanism of Cr₂O₃-ZnO thick films.

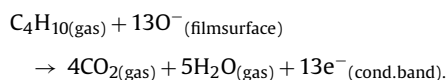
of the surface reaction products and their high volatility explain the quick response to LPG and fast recovery to its initial chemical status.

4. Discussion

Gas sensing mechanism (Fig. 12) is generally explained in terms of conductance either by adsorption of atmospheric oxygen on the surface and/or by direct reaction of lattice oxygen or interstitial oxygen with the test gases. In case of former, the atmospheric oxygen adsorbs on the surface by extracting an electron from conduction band, in the form of super-oxides or peroxides, which are mainly responsible for the detection of the test gases. At higher temperature, the adsorbed oxygen captures the electrons from conduction band as:



It would result in decreasing conductivity of the film. When LPG reacts with the adsorbed oxygen on the surface of the film, it gets oxidized to CO_2 and H_2O by following series of intermediate stages. This liberates free electrons in the conduction band. The final reaction takes place as:



This shows n-type conduction mechanism. Thus generated electrons contribute to a sudden increase in conductance of the thick film. The Cr_2O_3 misfit regions dispersed on the surface would enhance the ability of base material to adsorb more oxygen species giving high resistance in air ambient. Therefore, the higher response was obtained to 100 ppm LPG.

The mass% of Zn and O in each samples were not as per the stoichiometric proportion and all samples were observed to be the oxygen deficient (Table 1). This deficiency gets reduced (though in less extent) due to adsorption of atmospheric/molecular oxygen. This helps in decreasing electronic conductivity of the film. Upon exposure, LPG molecules got oxidized with the adsorbed oxygen ions by following the series of intermediate stages, producing CO_2 and H_2O . This results in evolving oxygen as electrically neutral atoms trapping behind the negative charges (electrons). Upon exposure, the energy released in decomposition of LPG molecules, would be sufficient for trapped electrons to jump into the conduction band of activated ZnO, resulting in increase in the conductivity of the film. The drastic increase in conductivity of the sensor could be attributed to the adsorption-desorption mechanism resulted from the electronic defects.

5. Conclusions

1. Pure zinc oxide was almost less sensitive to LPG.
2. Among various additives tested Cr_2O_3 in ZnO is outstanding in promoting the LPG sensing.
3. Surface modification by dipping process is one of the most suitable methods of modifying the surface of thick films.
4. 0.47 mass% Cr_2O_3 incorporated in pure ZnO thick film is the most sensitive element to LPG.
5. The sensor has good selectivity to LPG against NH_3 , CO_2 , Cl_2 , H_2 and $\text{C}_2\text{H}_5\text{OH}$.

Acknowledgements

Authors are grateful to the Principal and Head of P.G. Department of Physics, Pratap College, Amalner for providing laboratory facilities. Authors are grateful to UGC also for providing financial assistance for this project. D. R. Patil also acknowledges the co-operation rendered by the Principal, R. L. College, Parola.

References

- [1] P.T. Moseley, *Sens. Actuators B* 6 (1992) 149–156.
- [2] A. Gurlo, N. Barsan, U. Weimar, Y. Shimizu, *The 10th Intern. Chem. Sens.*, Tsukuba, Japan, 2004, pp. 152–153.
- [3] D.F. Shriver, P.W. Atkins, *Inorganic Chemistry*, third ed., Oxford University Press, Oxford, 2004, 627.
- [4] S. Pokhrel, B. Jeyaraj, K.S. Nagaraja, *Mater. Lett.* 4378 (2003) 1–6.
- [5] D.R. Patil, L.A. Patil, G.H. Jain, M.S. Wagh, S.A. Patil, *Sens. Transducers* 74 (2006) 874–883.
- [6] *The Hindu*, Andhra Pradesh/Hyderabad News, May 2007 and *Times of India*, Bangalore/Hyderabad, 2007.
- [7] W.Y. Chung, C.H. Shim, S.D. Choi, D.D. Lee, *Sens. Actuators B* 20 (1994) 139–143.
- [8] V.A. Chaudhary, I.S. Mulla, K. Vijayamohan, *Sens. Actuators B* 55 (1999) 127–133.
- [9] A. Srivastava, K. Jain, A.K. Rashmi, S.T. Srivastava, Laxmikumar, *Mater. Chem. Phys.* 97 (2006) 85–90.
- [10] D.R. Patil, L.A. Patil, *Sens. Actuators B* 123 (2007) 546–553.
- [11] L.A. Patil, D.R. Patil, *Sens. Actuators B* 120 (2006) 316–323.
- [12] D.R. Patil, L.A. Patil, P.P. Patil, *Sens. Actuators B* 126 (2007) 368–374.

D. R. Patil is a lecturer in physics at R. L. College, Parola, Maharashtra, India. He received his M.Sc. degree in physics from University of Pune in 1989 and PhD degree from North Maharashtra University, Jalgaon, India in 2007. He is working on gas sensing by thick film technology at Nano-Materials Research Laboratory, Pratap College Amalner, Maharashtra, India.

L. A. Patil is a reader in physics, at Pratap College, Amalner, Maharashtra, India. He received his MPhil degree in applied electronics and PhD in materials science. His topics of interest are: ceramic gas sensors, photoconducting and photo luminescent materials, art of growing crystals, dielectric properties of materials, nanomaterials, and thin and thick film physics. He established the Nano-Materials Research Laboratory at Pratap College, Amalner. He is the member of management council of North Maharashtra University, Jalgaon, Maharashtra, India.



High-speed, temperature programmable gas chromatography utilizing a microfabricated chip with an improved carbon nanotube stationary phase

Vanessa R. Reid^{a,1}, Michael Stadermann^{b,1}, Olgica Bakajin^b, Robert E. Synovec^{a,*}

^a Department of Chemistry, Box 351700, University of Washington, Seattle, WA 98195-1700, USA

^b Chemistry & Material Science, Lawrence Livermore National Laboratory, Livermore, CA 94550, USA

ARTICLE INFO

Article history:

Received 15 July 2008

Received in revised form

17 September 2008

Accepted 17 September 2008

Available online 24 September 2008

Keywords:

Gas chromatography

Carbon nanotubes

Microfabricated

High-speed

Resistively heated

ABSTRACT

A new growth recipe for producing carbon nanotubes (CNTs) combined with a new bonding technique was implemented in a microfabricated gas chromatography (micro-GC) chip. Specifically, the micro-GC chip contained a 30-cm (length) microfabricated channel with a 50 $\mu\text{m} \times 50 \mu\text{m}$ square cross-section. A CNT stationary phase “mat” was grown on the bottom of the separation channel prior to the chip bonding. Injections onto the micro-GC chip were made using a previously reported high-speed diaphragm valve technique. A FID was used for detection with a high-speed electrometer board. All together, the result was a highly efficiency, temperature programmable (via low thermal mass, rapid on-chip resistive heating) micro-GC chip. In general, the newly designed micro-GC chip can be operated at significantly lower temperature and pressure than our previously reported micro-GC chip, while producing excellent chemical separations. Scanning electron microscopy (SEM) images show a relatively thin and uniform mat of nanotubes with a thickness of ~ 800 nm inside the channel. The stationary phase was further characterized using Raman spectroscopy. The uniformity of the stationary phase resulted in better separation efficiency and peak symmetry (as compared to our previous report) in the separation of a mixture of five *n*-alkanes (*n*-hexane, *n*-octane, *n*-nonane, *n*-decane and *n*-undecane). The on-chip resistive heater employing a temperature programming rate of 26 $^{\circ}\text{C}/\text{s}$ produced a peak capacity of eight within a 1.5-s time window.

© 2008 Elsevier B.V. All rights reserved.

1. Introduction

Single and multi-wall carbon nanotube stationary phases for use in gas chromatography (GC) have been the subject of several recent reports [1–6]. The majority of these reports utilized carbon nanotubes within a silica capillary. Multi-wall carbon nanotubes (MWCNTs) utilized as a GC stationary phase have faster mass transfer properties than graphitic carbon stationary phases and result in more symmetrical peaks for both polar and non-polar compounds [3]. Carbon nanotubes utilized within open tubular capillaries have proven to be a robust stationary phase stable to high temperatures and capable of separating mixtures of compounds with good resolution [2]. Previously, we reported a microfabricated GC (micro-GC) chip implementing a single-wall carbon nanotube (SWCNT) stationary phase [1], whereby the SWCNTs were deposited through the lithographic patterning of the growth catalyst on a silicon wafer [7]. Stationary phases that can be grown within a microfabricated chan-

nel eliminate the potentially problematic coating methods that are used with polymer-based stationary phases [8,9].

While our previous report demonstrated that a SWCNT stationary phase could be readily incorporated in a on-chip resistively heated micro-GC chip, providing fast temperature programmed separations on the order of a few seconds [1], there was an observable shortcoming in the uniformity of the SWCNT phase that appeared to limit the separation efficiency, *N*, and hence limit device performance. In order to address this shortcoming, a new growth recipe for producing a highly uniform CNT phase material has been implemented. This new growth recipe has been combined with a more effective bonding technique in order to prevent damage to the nanotubes during the bonding technique and deactivate the glass surface. The channel structure is 30 cm in length, with a 50- μm by 50 μm cross-section that in principle should be able to provide rapid and efficient GC separations [10,11]. Only one of the four walls is coated with the CNT stationary phase, a coating procedure that greatly simplifies the separation channel design. However, analyte mass transfer should be extremely rapid across the narrow channel, which should minimize the potential source of band broadening due to coating only one channel wall. The CNT stationary phase was characterized via SEM and Raman

* Corresponding author. Tel.: +1 206 685 2328; fax: +1 206 685 8665.

E-mail address: synovec@chem.washington.edu (R.E. Synovec).

¹ These authors contributed equally to this work.

spectroscopy in order to verify the presence and quality of the CNTs in the channel and to determine the diameter of the nanotubes. The separations obtained with this micro-GC chip contain peaks with more Gaussian-like peak profiles, as will be demonstrated via peak symmetry measurements [12]. The on-chip resistive heater that incorporated a thin serpentine film of metal (5 nm of Ti and 100 nm of Pt) will also shown to be significantly more efficient (improved relative to our initial report [1]). In this report, we will use a simple mixture of relatively volatile hydrocarbons to test the separation performance. However, it is envisaged that the micro-GC chip can, in principle, be more widely applicable to situations in which high-speed separations are needed, e.g., field monitoring, on-line process control, and as the second dimension of comprehensive two-dimensional gas chromatography (GC \times GC).

2. Experimental

2.1. Column fabrication

In brief, the separation channel and connecting ports were etched in a silicon wafer and the nanotubes were grown in the separation channel; the channel was then sealed with SU8 2005, thus producing the GC column. The serpentine resistive heating element was fabricated on the opposite side of the wafer.

Specifically, the fabrication process began with PR4640 photoresist (Shipley Company, Marlborough, MA, USA) spun on the back side of a 500- μm thick Si wafer with native oxide. Ports 380 μm in circumference were patterned lithographically on the back of the wafer, then the photoresist was used as an etch mask for a $460 \pm 10 \mu\text{m}$ deep reactive ion etch (DRIE). After the etching process, the photoresist was removed from the back of the wafer. Next, PR4640 was again spun on the back side of the wafer and resistive heaters (metal film) were patterned onto the wafer, i.e., a 5-nm of Ti and 100 nm of Pt metal film was evaporated onto the wafer before the photoresist was removed again. Then, the front side of the wafer was coated with PR4620, and a 30-cm long and 50 μm wide channel was patterned onto the wafer. The front channel was etched with DRIE to a depth of nominally 50 μm , again using the photoresist as an etch mask. The resulting separation channel was 30 cm long with a 50 $\mu\text{m} \times 50 \mu\text{m}$ square cross-section. A rectangular cross-section keeping the 50- μm depth constant could also be used, and in principle provide essentially the same separation efficiency but a higher sample capacity. The catalyst metals (100 Å Al, 1 Å Pt, 5 Å Fe) were deposited with an electron-beam evaporator, and lift-off was performed by soaking the wafer in acetone for 10 min, followed by brief (1–5 s) sonication and rinsing with acetone, ethanol and water.

The CNTs were grown onto one of the four walls of the separation channel via chemical vapor deposition; the CNT stationary phase was grown only in the bottom of the channel to simplify the microfabrication [1]. The 2 in. diameter furnace was heated to 500 °C before the wafer was introduced. The wafer was heated at a rate of 40 °C/min to 850 °C while flowing Ar gas at 240 ml/min combined with H₂ at 160 ml/min. Once 850 °C was reached, the temperature was held constant until the end of the growth. After 10 min of heating, water was added to the reaction mixture by mixing argon that was bubbled through a water bubbler into the gas stream, maintaining the total flow of argon at 240 ml/min. The water content was regulated to be constant at 1000 ppm at the feed end. After 20 min of heating, 40 ml/min of ethylene was added for 10 min (all gases in this process were from Matheson Tri-Gas, Newark, NJ, USA). During the growth, the pressure at the exhaust was maintained at 14 psi (99,300 Pa). The CNT coverage (i.e., on

one wall of the separation channel) was analyzed with scanning electron microscopy (SEM).

After the growth of the CNT phase, the channel structure was sealed by spin-coating the glass cover slide with SU8 2005 (Micro Chem, Newton, MA, USA) at 500 rpm for 5 s, then 2000 rpm for 30 s. The glass slide was desiccated for 5 min at 200 °C then cooled by blowing nitrogen over it before the SU8 was added. The silicon column was firmly pressed on top of the coated glass slide, making sure there were no voids between the glass and the silicon. With the glass facing down, the wafer was baked in an oven by ramping to 65 °C at a rate of 5 °C/min and baking for 10 min, then ramping to 95 °C at 5 °C/min, baking for another 5 min, and finally ramping to 200 °C at 5 °C/min and baking for an additional 5 min. Bare silicon micro-GC chips were manufactured in the same manner described above, omitting the steps relating to the growth of the CNT stationary phase.

2.2. Chromatographic instrumentation

All chromatographic experiments were completed using a Agilent 6890 GC (Agilent Technologies, Santa Clara, CA, USA) modified with a single diaphragm valve (VICI Valco, Houston, TX, USA) for high-speed sample injections onto the micro-GC chip, as previously reported [13–16]. The Agilent 6890 GC serves as a platform to study the separation performance of the micro-GC chip. Briefly, a sample is injected using the standard 6890 autoinjector, and a small portion of the autoinjected pulse is subsequently injected using the high-speed diaphragm valve (set to inject a 15-ms sample pulse for this study). This 15 ms sample pulse is then separated by the micro-GC chip either with or without the CNT stationary phase (and either with or without on-chip resistive heating), followed by a high-speed FID. Note that the GC oven was used for the initial temperature setting, i.e., for isothermal separations as well. The timing and actuation of the diaphragm valve was controlled using an in-house written LabVIEW (National Instruments, Austin, TX) program [11] and the FID was modified with an in-house built electrometer for high-speed detection of the narrow chromatographic peaks (20,000 Hz sampling rate). All temperature programming was completed using the on-chip resistive heating element (discussed in more detail in Section 2.1). The timing for the resistive heating was controlled via an in-house written LabVIEW program as previously reported [1,17]. A variable autotransformer (Stace Energy Products Co., Dayton, OH, USA) supplied a variable AC voltage (0–120 V) in order to resistively heat the micro-GC chip, as previously reported [1].

2.3. Chromatographic experiments

All chromatograms were collected with the 6890 GC inlet and FID temperature of 250 °C. The inlet was set for a splitless injection with a pressure of 10 psi (69,000 Pa) of hydrogen carrier gas, resulting in a carrier gas velocity of 95 cm/s at 50 °C. The transfer line from the 6890 GC autoinjector to the diaphragm valve was a 12-cm length of methyl deactivated capillary with an internal diameter of 100 μm . The auxiliary pressure (for the hydrogen carrier gas through the chip) was also set at 10 psi (69,000 Pa). The micro-GC chip was interfaced to the diaphragm valve and FID with 13 and 16 cm lengths of methyl deactivated capillary, respectively, both with an internal diameter of 100 μm . The capillary leads were attached to the micro-GC chip with high temperature epoxy (J-B Weld, Sulfur Springs, TX, USA) as previously reported [1]. The capillary leads were isothermal during all separations; they were not resistively heated. All chromatograms were obtained using a 15-ms injection pulse from the diaphragm valve.

3. Results and discussion

3.1. Characterization of the CNT stationary phase

The CNT stationary phase on one wall of the separation channel was characterized via both SEM and Raman spectroscopy. The SEM images are shown in Fig. 1. Note that while this characterization is described first for clarity, the experiments themselves were done last, after all the chromatographic experiments were completed, since the chip needed to be carefully sliced open orthogonal to the channel to facilitate SEM and Raman characterization. Several channel locations were examined, and the results presented are representative and consistent.

The image in Fig. 1A is a SEM image and shows that the nanotubes have formed a relatively uniform mat in the microfabricated channel. This is different than the tangles (with voids) of SWCNTs that were previously reported [1]. The image in Fig. 1A shows that the CNTs are ~ 800 nm tall within the channel. A detailed SEM image of the CNT stationary phase is shown in Fig. 1B. Since only the bottom of the channel is coated with the CNT phase, there is no build up in the corners. The CNT stationary phase was further characterized

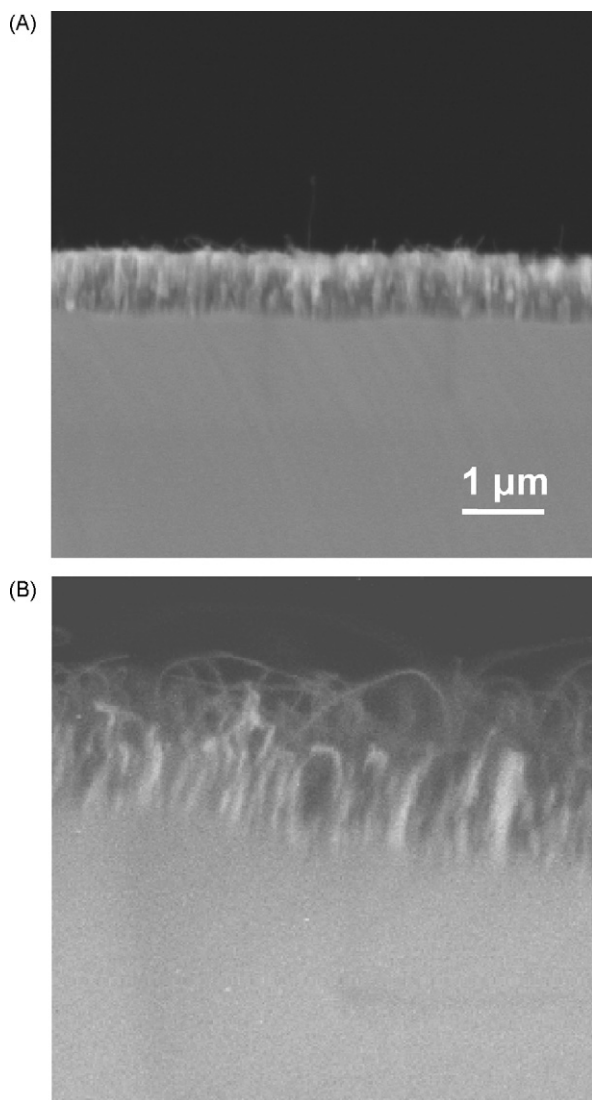


Fig. 1. (A) SEM image of the stationary phase composed of a “mat” of CNTs within a micro-GC separation channel. (B) Detailed SEM image to more readily observe individual CNTs within the separation channel.

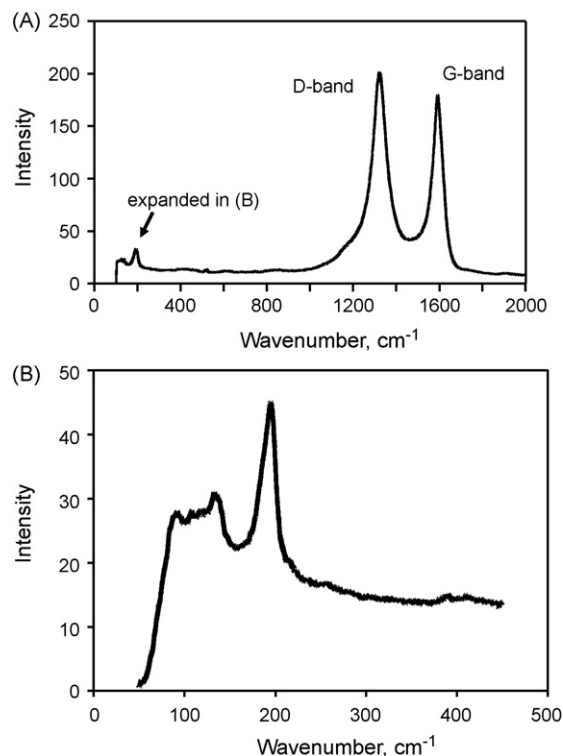


Fig. 2. Raman spectra of the CNT stationary phase grown in the separation channel. (A) Raman spectrum showing both the D-Band (~ 1350 cm^{-1}) and G-Band (~ 1600 cm^{-1}). (B) Detail of the radial breathing modes (< 500 cm^{-1}) of the spectrum shown in (A).

utilizing Raman spectroscopy (with a laser excitation wavelength of 633 nm). The full spectrum is shown in Fig. 2A; the large intensity of the broad D-band (1250 – 1400 cm^{-1}) suggests the presence of multi-wall carbon nanotubes (MWCNTs) [18]. The presence of the narrow G-band (1500 – 1700 cm^{-1}), however, also suggests the presence of SWCNTs, possibly with defects such as shortened tubes and vacancies, within the channel. The radial breathing modes (< 500 cm^{-1}), shown in Fig. 2B, suggest the presence of SWCNTs with a diameter of ~ 2 nm [18]. From high-resolution SEM images, not shown for brevity, the diameter of the MWCNTs was found to be ~ 40 nm. Overall, the CNT stationary phase appears reasonably uniform in size and distribution on the one wall within the micro-GC channel. Other channel locations analyzed provided similar results, not shown for brevity.

3.2. Evaluation of bare silicon micro-GC chips

In order to fully characterize the CNT stationary phase, chromatograms were collected utilizing bare silicon micro-GC chips. These bare silicon chips do not contain a CNT stationary phase. A five-compound *n*-alkane mixture was injected onto a representative bare micro-GC chip. Isothermal separations of the *n*-alkane mixture are shown in Fig. 3. The sample was prepared neat, so there is no solvent peak. The isothermal separation of the mixture at 50 $^{\circ}\text{C}$ is shown in Fig. 3A. The separation is complete in less than 1.5 s with minimal separation of the first four compounds. The last eluting compound, *n*-undecane, is slightly retained most likely due to the differential between the boiling point of the compound and the separation temperature. The isothermal separation of the mixture at 100 $^{\circ}\text{C}$ is shown in Fig. 3B. There is no visible separation of the five-compound mixture at this high temperature. Due to the lack of separation at both isothermal separations (relative to the micro-GC

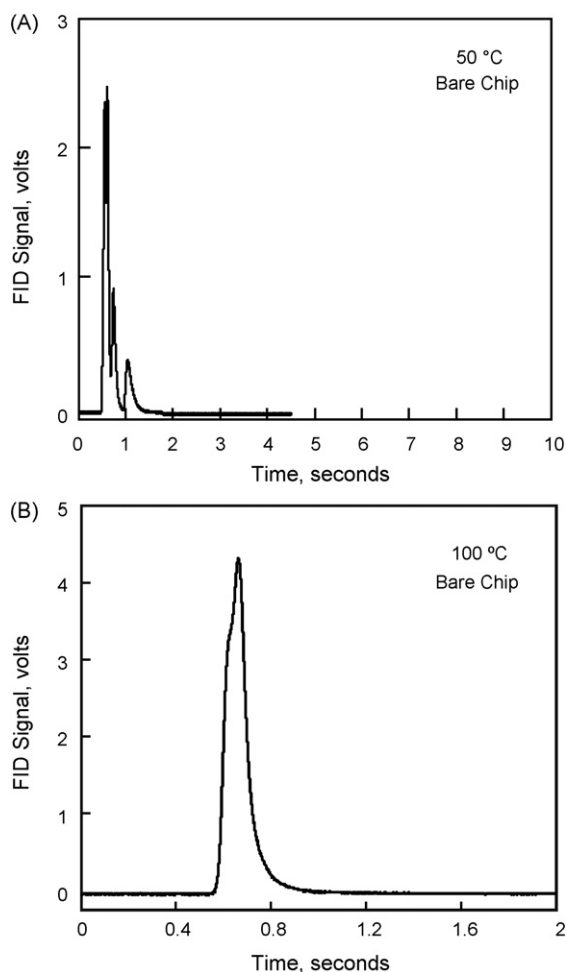


Fig. 3. Isothermal separations of a five-compound *n*-alkane mixture (retention order: *n*-hexane (C_6), *n*-octane (C_8), *n*-nonane (C_9), *n*-decane (C_{10}), *n*-undecane (C_{11})) utilizing a bare silica micro-GC chip. All data collected using H_2 carrier gas at an absolute head pressure of 10 psi (69,000 Pa). Separations were obtained using the 30 cm micro-GC chip with a $50 \mu\text{m} \times 50 \mu\text{m}$ channel cross-section. (A) Separation obtained at an isothermal temperature of 50°C . (B) Separation obtained at an isothermal temperature of 100°C .

chip separations with the CNT stationary phase shown next), the conclusion that the bare silicon chip does not contribute significantly to the separation of the compounds in the *n*-alkane mixture can be reached.

3.3. On-chip resistive heating as a means of temperature programming

The micro-GC chip with CNT stationary phase was utilized to separate a mixture of five *n*-alkanes (*n*-hexane, *n*-octane, *n*-nonane, *n*-decane and *n*-undecane). The isothermal separation of the mixture at 50°C is shown in Fig. 4A. The separation is complete in less than 10 s with the earlier peaks eluting with good signal-to-noise and adequate resolution. The later eluting peaks (*n*-decane and *n*-undecane) have significantly larger peak widths, and *n*-undecane is barely visible above the baseline. An increase of the isothermal temperature to 100°C resulted in the separation shown in Fig. 4B. The separation is complete in less than 2 s, which is fivefold faster than the isothermal separation at 50°C (Fig. 4A); however, the earlier eluting peaks are overlapped significantly. The decreased peak widths of the later eluting peaks and the increased signal-to-noise for *n*-undecane demonstrate the benefit of the higher isothermal

temperature (100°C). This is commonly referred to as the general elution problem, where for GC no single isothermal temperature provides optimal resolution with consistently narrow peaks for a mixture of compounds with a sufficiently wide boiling point range.

A common solution to the general elution problem is the use of temperature programming. To address this issue, this micro-GC chip was equipped with an on-chip resistive heating element. Applying a voltage across the heating element results in a rapid and reproducible temperature program [1]. The five-compound *n*-alkane mixture separated isothermally in Fig. 4A and B was temperature programmed by applying 36 V to the heating element, producing a temperature program of 26°C/s (with the calibration of the programming rate described below). The resulting temperature programmed separation is shown in Fig. 4C. The separation is complete in less than 2.5 s with sufficient resolution between all of the analytes and an improved signal-to-noise ratio for *n*-undecane, when compared to the separation obtained at an isothermal temperature of 50°C . A peak capacity of eight within a 1.5-s time window can be computed from the data in Fig. 4C.

The new micro-GC chip was characterized isothermally using a single analyte to determine the linearity of analyte retention as a function of temperature, and ultimately to calibrate the temperature programming rate as a function of applied voltage. The test analyte, *n*-decane, was injected neat at four isothermal temperatures in order to create a van't Hoff plot (a plot of $\ln k$ vs. $1/T$), where k is the analyte retention factor and T is the separation temperature in Kelvin. This plot along with the best fit line and equation are shown in Fig. 4D. The equation of the line shown was used, as previously reported [1,17], to determine the rate of temperature programming in Fig. 4C. The rates of temperature programming resulting from several different voltages are tabulated in Table 1. The linearity of the van't Hoff plot suggests that the low temperatures do not adversely affect the retention of the analyte; the retention of *n*-decane is linear over the temperature range reported. Also, the on-chip resistive heater employed appears to be slightly more efficient than the previously reported model [1]. The previously reported temperature program of 60°C/s was produced by applying 96 V to the heating element. The new micro-GC chip would require one third less voltage (63 V as extrapolated from the data in Table 1) to produce the same temperature programming rate.

3.4. Comparison of the new CNT micro-GC chip to previous study

The CNT micro-GC chip reported herein is a redesign and improvement over our previous report [1] (see p. 5642, Figs. 3B and 4C and p. 5643, Table 1 of that reference), consequently a comparison of the two chips is presented. The new growth recipe for the CNT stationary phase results in a very uniform stationary phase (see Fig. 1 in the report herein). The old growth recipe resulted in a stationary phase consisting of nanotube “tangles” with spaces up to 500 nm between them (see p. 5642, Fig. 3B). The spaces between the nanotube “tangles” contributed to significant band broadening, and a uniform mat of stationary phase is preferred.

Table 1

Temperature programming rates for the on-chip resistive heater ($T_i = 50^\circ\text{C}$) for various applied voltages.

Voltage applied (V)	Temperature programming rate ($^\circ\text{C/s}$)
24	10
30	18
36	26
42	33

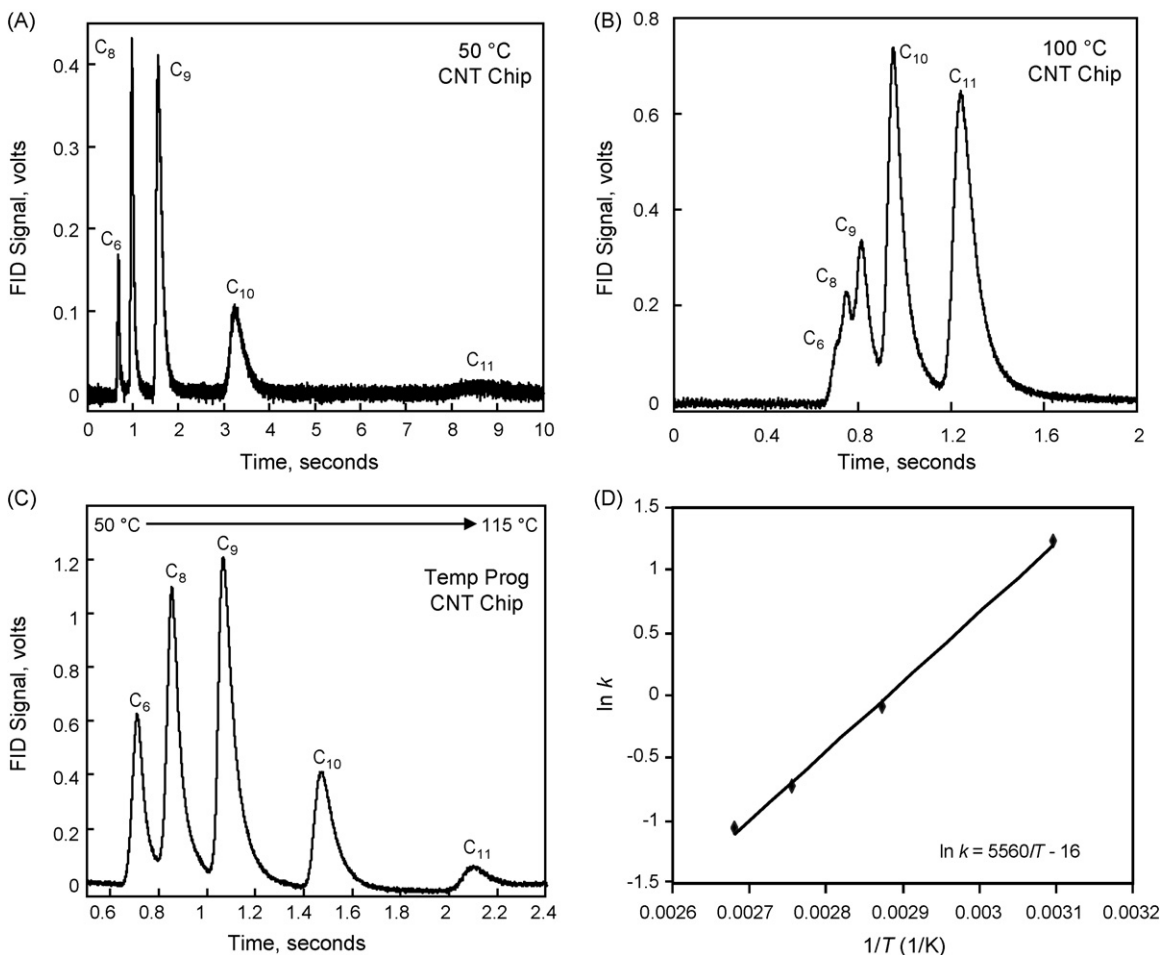


Fig. 4. Isothermal and temperature programmed separations of a five-compound *n*-alkane mixture (retention order: *n*-hexane (C_6), *n*-octane (C_8), *n*-nonane (C_9), *n*-decane (C_{10}), *n*-undecane (C_{11})) utilizing a silica micro-GC chip with CNT stationary phase. All data collected using H_2 carrier gas at an absolute head pressure of 10 psi (69,000 Pa). Separations were obtained using the 30-cm micro-GC chip with a $50 \mu\text{m} \times 50 \mu\text{m}$ channel cross-section. (A) Separation obtained at an isothermal temperature of 50°C . (B) Separation obtained at an isothermal temperature of 100°C . (C) Temperature programmed separation obtained by applying 36 V across the on-chip resistive heating element resulting in a temperature programming rate of 26°C/s (initial column temperature was 50°C). (D) van't Hoff plot ($\ln k$ vs. $1/T$) of *n*-decane for the micro-GC chip with the CNT stationary phase used for the calibration of the temperature programming rates. The best fit line and equation are displayed on the graph. All data obtained using H_2 carrier gas at an absolute head pressure of 10 psi (69,000 Pa). Methane was used as a dead time marker for k calculations, $t_M = 632$ ms.

The previously reported chips resulted in chromatograms with highly tailed peaks, even when temperature programmed (see p. 5642, Fig. 4C). Chromatograms obtained with the chips reported herein contain peaks that are significantly more Gaussian-like in nature. The peak tailing, even in the isothermal chromatogram at 50°C , is minimal when compared to the previously reported chips. The separations using the new chips resulted in a 66% reduction in the skew of the isothermal *n*-hexane peaks. For *n*-octane, which was slightly more retained, a reduction in the skew of 98% was observed. Since there was minimal retention for the bare chips (Fig. 3A and B), adsorption to the bare walls was not a significant contributor to peak tailing. More likely, the observed peak tailing in the present study was due to the difficulty in minimizing sources of extra-column band broadening such as dead volumes.

A plot of the peak width-at-half-height, w_h , as a function of the adjusted retention time, $t_R - t_M$ (the retention time minus the dead time), for both the isothermal (at 50°C) and temperature programmed separations is shown in Fig. 5A (data from separations shown in Fig. 4A and C). For isothermal GC, band broadening is essentially linear with adjusted retention time (as well as k) [11]. Temperature programming significantly reduces the width and retention time of the more retained compounds, which leads to a larger S/N ratio. For example, at a common adjusted retention

time of ~ 0.9 s, the temperature programmed peak width is approximately two thirds of the isothermal peak width. A detailed view of the temperature programmed data from the plot in Fig. 5A is shown in Fig. 5B. Since the w_h values increase only moderately as a function of $t_R - t_M$ suggests that the temperature programming rate has been nearly optimized in the context of the slow velocity utilized for the separation in Fig. 4C. The same statement cannot be applied to the previously reported devices, where the w_h values increase dramatically as a function of $t_R - t_M$ (see p. 5642 Fig. 4C).

Moreover, the analyte *n*-hexane, with the smallest adjusted retention time on the previously reported micro-GC chip, has a peak width that is actually fourfold narrower than obtained with the new chip, ~ 12 ms versus ~ 50 ms. This is predominately due to the difference in the carrier gas velocities for the two chips. The previous micro-GC chip was operated at an average linear flow velocity, \bar{u} , of ~ 1100 cm/s while the new micro-GC chip was operated at a \bar{u} of ~ 95 cm/s. Meanwhile, as for the more retained analytes, the peak widths on the new chip are significantly narrower, suggesting that the temperature programming rate for the new chip was essentially optimized.

The new micro-GC chip also results in a higher peak capacity for a temperature programmed separation. The peak capacity for the new micro-GC device is approximately 8 for a time window of 1.5 s

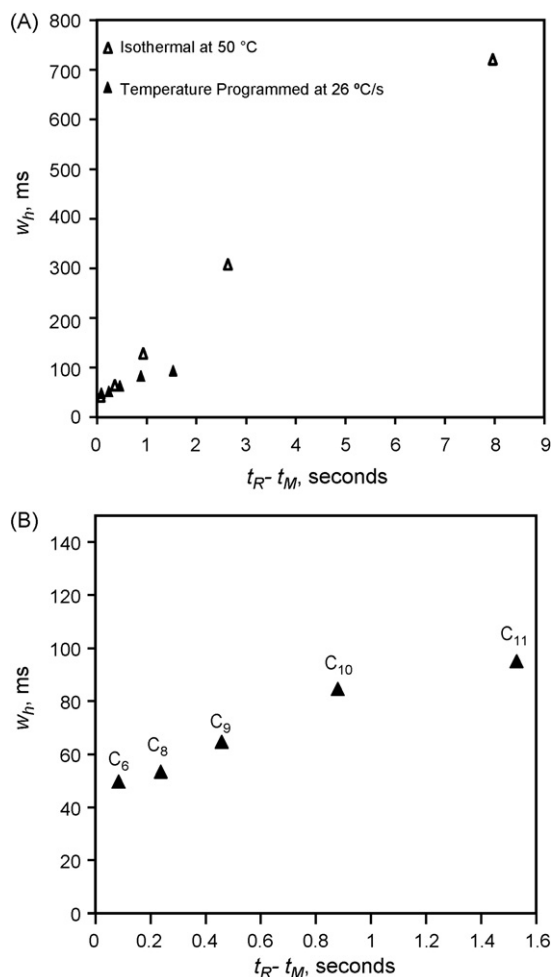


Fig. 5. Plots of width-at-half-height, w_h , as a function of adjusted retention time, $t_R - t_M$ for the five compound *n*-alkane mixture separations shown in Fig. 4. (A) Isothermal data at 50 °C (Δ) (data from Fig. 4A) and temperature programmed data at 26 °C/s (\blacktriangle) (data from Fig. 4C). (B) Detail of the plot in (A) containing only the temperature programmed data at 26 °C/s. Methane was the dead time marker, $t_M = 632$ ms.

(for the separation shown in Fig. 4C). The previously reported device has a peak capacity of approximately 6 for the same 1.5 s time frame (see p. 5642, Fig. 4C). The fact that the average linear flow velocity for the previously reported micro-GC chip is approximately 12-fold higher than the average linear flow velocity of the new micro-GC chip should be an advantage. In most cases the faster the velocity, the higher the peak capacity of the resulting separation. For this particular case, the new device has a higher peak capacity even though it was operated at a much lower velocity.

The new micro-GC chip has a separation channel that is 30 cm with a $50 \mu\text{m} \times 50 \mu\text{m}$ cross-section. The previously reported micro-GC chip had a separation channel 50 cm in length with

a $100 \mu\text{m} \times 100 \mu\text{m}$ cross-section. The dependence on channel dimensions for the anticipated peak width, in the absence of any extra-column band broadening, can be estimated from Golay theory [11]. The improvement in the new micro-GC chip is a combination of factors. These factors include, but are not limited to, the new nanotube growth recipe that led to a uniform thickness of the nanotube “mat” in the channel (as per Fig. 1), the uniform size of the nanotubes (length and diameter), and the different chip bonding technique. The major improvements in peak shape suggest that the presented micro-GC chip utilizing CNTs as the stationary phase is a significant enhancement of the previously reported chips.

4. Conclusions

The micro-GC chip reported herein utilized a carbon nanotube (CNT) stationary phase grown utilizing a new growth recipe, which resulted in a more uniform stationary phase morphology and an improvement in peak symmetry, peak capacity, and overall separation performance. Micro-GC chips can be fabricated in a batch format because multiple columns can be etched onto one wafer. The lower energy and carrier gas consumption make these chips more appealing and likely more applicable for field portable applications of micro-GC.

Acknowledgements

A portion of this work was supported by DARPA MTO MGA program and performed at Lawrence Livermore National Laboratory. Lawrence Livermore National Laboratory is operated by Lawrence Livermore National Security, LLC, for the U.S. Department of Energy, National Nuclear Security Administration under Contract DE-AC52-07NA27344. We thank Ulrich Bonne for his interest in, and support of, this research project.

References

- [1] M. Stadermann, A.D. McBrady, B. Dick, V.R. Reid, A. Noy, R.E. Synovec, O. Bakajin, *Anal. Chem.* 78 (2006) 5639.
- [2] C. Saridara, S. Mitra, *Anal. Chem.* 77 (2005) 7094.
- [3] Q. Li, D. Yuan, *J. Chromatogr. A* 1003 (2003) 203.
- [4] L.A. Kartsova, A.A. Makarov, *J. Anal. Chem.* 59 (2004) 724.
- [5] L. Yuan, C. Ren, L. Li, P. Ai, Z. Yan, M. Zi, Z. Li, *Anal. Chem.* 78 (2006) 6384.
- [6] L.A. Kartsova, A.A. Markov, *Russ. J. Appl. Chem.* 75 (2002) 1725.
- [7] J. Kong, H.T. Soh, A.M. Cassell, C.F. Quate, H. Dai, *Nature* 395 (1998) 878.
- [8] K. Grob, *Making and Manipulating Capillary Columns for Gas Chromatography*, Verlag, Heidelberg, 1986.
- [9] G.M. Gross, J.W. Grate, R.E. Synovec, *J. Chromatogr. A* 1029 (2004) 185.
- [10] V.R. Reid, R.E. Synovec, *Talanta* 76 (2008) 703.
- [11] G.M. Gross, B.J. Prazen, J.W. Grate, R.E. Synovec, *Anal. Chem.* 76 (2004) 3517.
- [12] J.P. Foley, J.G. Dorsey, *Anal. Chem.* 55 (1983) 730.
- [13] J.L. Hope, K.J. Johnson, M.A. Cavelti, B.J. Prazen, J.W. Grate, R.E. Synovec, *Anal. Chim. Acta* 490 (2003) 223.
- [14] C.A. Bruckner, B.J. Prazen, R.E. Synovec, *Anal. Chem.* 70 (1998) 2796.
- [15] C.G. Fraga, B.J. Prazen, R.E. Synovec, *Anal. Chem.* 72 (2000) 4154.
- [16] A.E. Sinha, K.J. Johnson, B.J. Prazen, S.B. Lucas, C.G. Fraga, R.E. Synovec, *J. Chromatogr. A* 983 (2003) 195.
- [17] V.R. Reid, A.D. McBrady, R.E. Synovec, *J. Chromatogr. A* 1148 (2007) 236.
- [18] A.C. Dillion, M. Yudasaka, M.S. Dresselhaus, *J. Nanosci. Nanotechnol.* 4 (2004) 691.



Comparison of MTBSTFA and BSTFA in derivatization reactions of polar compounds prior to GC/MS analysis

Claude Schummer^{a,b,*}, Olivier Delhomme^a, Brice M.R. Appenzeller^b, Robert Wennig^b, Maurice Millet^a

^a Centre de Géochimie de la Surface, UMR 7517 (CNRS–Université Louis Pasteur), Laboratoire de Physico-Chimie de l'Atmosphère, 1, rue Blessig, 67084 Strasbourg Cedex, France

^b Laboratoire de Toxicologie, Centre de Recherche Public–Santé/Laboratoire National de Santé; Université du Luxembourg, Campus Limpertsberg, 162A, avenue de la Faïencerie 1511 Luxembourg, Luxembourg

ARTICLE INFO

Article history:

Received 9 June 2008

Received in revised form 8 September 2008

Accepted 21 September 2008

Available online 5 October 2008

Keywords:

MTBSTFA

BSTFA

Derivatization

Silylation

ABSTRACT

In this study, MTBSTFA and BSTFA, which are among the preferred derivatization reagents for silylation were both tested on derivatization of six different groups of polar chemicals to get information about usefulness in terms of sensitivity and specificity of both reagents. Tested compound groups were nitrophenols and methoxyphenols, sterols and sugars, dicarboxylic acids and hydroxylated polycyclic aromatic hydrocarbons.

It was found that MTBSTFA-derivates produce characteristic fragmentation patterns presenting mainly the fragments $[M]^+$, $[M-57]^+$ and $[M-131]^+$, of which $[M-57]^+$ is generally dominant on the mass spectrogram. BSTFA-derivates mainly show the fragments $[M]^+$, $[M-15]^+$ and $[M-89]^+$ whereof the molecular ion $[M]^+$ is generally dominant. It was also found that steric hindrance and molecular mass play a very important role in the choice of the best suited derivatization reagent: compounds with sterically hindered sites derivatized with MTBSTFA produce very small analytical responses or no signal at all, and compounds with high molecular mass produce no characteristic fragmentation pattern when derivatization is performed with BSTFA.

It was also found that MTBSTFA-derivatization facilitates separation of isomer analytes, suggesting its choice in combination to semi-polar columns, whilst BSTFA seems better for sterically hindered compounds.

Findings were confirmed with applications of both reagents to biological and environmental matrices (urine and atmospheric aerosols).

© 2008 Elsevier B.V. All rights reserved.

1. Introduction

Derivatization is a chemical process for modifying compounds in order to generate new products with better chromatographic properties. Several reasons may necessitate a derivatization step, namely improving the thermal stability of some compounds—basically compounds containing polar functional groups ameliorating the volatility, and introducing a detector-oriented marker on the molecule [1–3]. For gas chromatographic (GC) analysis, molecules containing functional groups such as $-COOH$, $-OH$, $-NH$, and $-SH$ (i.e. sugars, steroids, cholesterol) are of major concern due to their ability to form hydrogen bonds in-between compounds. This leads to weak volatility, to insufficient

thermal stability, or may induce interactions of the compounds with the solid column packing [3,4] resulting in low detectability. Sometimes, non-derivatized molecules (i.e. amphetamines and its metabolites) [5] also produce inoperative chromatograms due to multiple peaks or bad separations of stereoisomers. Derivatization with a selective reagent improves detectability in complex matrix samples, and derivatization with chiral reagents improves separation of the peaks [5]. Thus, derivatization is a very useful tool for detecting compounds in complex samples, and is used widely in forensic, medical and environmental chemistry [4].

Derivatization is usually done by substitutions on the polar function, where the most common reactions are alkylation, acylation and silylation [3,6,7]. Alkylation reagents reduce the polarity of the compounds by substituting labile hydrogens for an aliphatic or aliphatic–aromatic (e.g., benzyl) group. This technique is often used to modify compounds containing acidic hydrogens, such as

* Corresponding author. Tel.: +352 46 66 44 6488; fax: +352 22 13 31.
E-mail address: claudio.schummer@ins.etat.lu (C. Schummer).

carboxylic acids and phenols, which are converted either into esters or ethers [3].

In acylation reactions, compounds containing a labile hydrogen are transformed into esters, thioesters and amides through the action of carboxylic acid and/or their derivatives [3]. Because of the presence of residual acid, the products cannot be directly injected into the GC, but a purification step is required before injection [8]. Acylation is commonly used to add fluorinated groups to molecules for analysis by electron capture detectors [4,8].

In silylation reactions, a labile hydrogen from acids, alcohols, thiols, amines, amides or enolizable ketones and aldehydes is replaced by a trimethylsilyl group [3]. Reaction occurs through nucleophilic attack (S_N2) [4,9], and the presence of a strong leaving group often improves the reaction yield. The products are generally more volatile and thermally stable. In opposition to acylation, silylation normally does not require a purification step, and the derivatives can be injected directly into the GC [6,9].

Silylation is the most prevalent derivatization technique [4,10–13], and common reagents are trimethylchlorosilane (TMCS), trimethylsilylimidazole (TMSI), N-methyl-trimethylsilyltrifluoroacetamide (MSTFA), N,O-bis-(trimethylsilyl)trifluoroacetamide (BSTFA) and N-(t-butyltrimethylsilyl)-N-methyltrifluoroacetamide (MTBSTFA) [4,14], whereof the two last ones are most frequently used, particularly when analyzing phenolic compounds, sterols and sugars [6,9,15]. Both reagents have already been used with success in analyses performed in biological matrices on hypnotics like benzodiazepines [16], anti-inflammatory drugs like naproxen [17], hydroxylated polycyclic aromatic hydrocarbons [18], personal-care products and pharmaceuticals [19], contaminants like hydroxylated polycyclic biphenyls [20] and flavonoids [21], and in analyses performed in environmental matrices on organic acids and peroxides in water [22], and chlorophenols and nitrophenols in atmosphere [9,23].

The aim of this study is to compare BSTFA and MTBSTFA in derivatization reactions of different hydroxylated compound groups. This study is intended for increasing knowledge about behavior and interest of both reagents. Studied compounds are nitrophenols (NPh) and methoxyphenols (MPh), sterols and sugars, dicarboxylic acids (DA), and hydroxylated polycyclic aromatic hydrocarbons (OH-PAHs). Both reagents are applied to OH-PAHs in urine samples and methoxyphenols in atmospheric aerosols to verify that the findings and conclusions remain true when applied to selected biological and environmental matrices.

2. Materials and methods

2.1. Reagents and equipments

All compounds were purchased from Fluka (l'Isle d'Abeau, France), Sigma-Aldrich (l'Isle d'Abeau, France), Dr. Ehrenstorfer (Augsburg, Germany), Acros Organics (Noisy le Grand, France) or Chiron AS (Trondheim, Norway). All compounds are listed in Table 1.

Stock solutions at 1 g L⁻¹ and working solutions of all compounds except sugars were prepared in acetonitrile.

Stock solutions at 1 g L⁻¹ and all dilutions of sugars were prepared in dimethylformamide.

MTBSTFA and BSTFA were purchased from Sigma-Aldrich (St. Quentin Fallavier, France), acetonitrile, dichloromethane, n-hexane, methanol and toluene of HPLC grade were purchased from Lab-Scan (Dublin, Ireland). Dimethylformamide of HPLC grade was purchased from Prolabo (Fontenay sous bois, France).

β-Glucuronidase/arylsulfatase and sodium acetate were purchased from Sigma-Aldrich (l'Isle d'Abeau, France) and Focus

Table 1

List of analyzed chemical compounds.

Compounds
Methoxyphenols
Guaiacol ^a
2,6-Dimethoxyphenol ^a
4-Hydroxybenzaldehyde ^a
Vanillin ^a
Homovanillic alcohol ^a
4-Hydroxybenzoic acid ^a
Coumaric acid ^a
Syringaldehyde ^a
3,5-Dimethoxy-4-hydroxyacétophenone ^a
Vanillic acid ^b
Homovanillic acid ^b
Coniferyl alcohol ^a
Syringic acid ^d
Succinic acid-d ⁴ (ISTD ⁺) ^a
Nitrophenols
Phenol ^a
3-Methyl-4-nitrophenol ^a
2,6-Dinitrophenol ^a
2,5-Dinitrophenol ^a
2,6-Dinitro-p-cresol ^a
2,4-Dinitrophenol ^a
4,6-Dinitro-o-cresol ^a
3,4-Dinitrophenol ^a
4-Nitrophenol-d ⁴ (ISTD ⁺) ^a
Sugars
l(+)-Rhamnose ^c
l(+)-Arabinose ^a
D(+)-Xylose ^d
D(+)-Mannose ^d
D(+)-Glucose ^a
Levoglucofan ^a
Erythritol ^d
Xylitol ^a
D(+)-Arabitol ^c
D(+)-Mannitol ^a
Inositol ^d
D(+)-Sucrose ^a
D(+)-Maltose ^d
Lactose ^a
D(+)-Melezitose ^a
Sterols
Cholesterol ^a
Campesterol ^a
Stigmasterol ^a
β-Sitosterol ^a
Phtalic acid-d ⁴ (ISTD ⁺) ^a
Dicarboxylic acids
Oxalic acid ^a
Methylmalonic acid ^a
Malonic acid ^a
Maleic acid ^b
Methylsuccinic acid ^a
Succinic acid ^a
Fumaric acid ^b
Glutaric acid ^a
Adipic acid ^a
Pimelic acid ^a
Phtalic acid ^b
Suberic acid ^a
Oleic acid ^a
Linoleic acid ^a
Azelaic acid ^b
Sebacic acid ^a
Decanoic acid-d ¹⁹ (ISTD ⁺) ^a
OH-PAHs
1-Hydroxynaphthalene (1-OHNAPH) ^a
2-Hydroxynaphthalene (2-OHNAPH) ^a
2-Hydroxyfluorene (2-OHFLU) ^a
9-Hydroxyfluorene (9-OHFLU) ^a
1-Hydroxyphenanthrene (1-OHPHEN) ^c

Table 1 (Continued).

2-Hydroxyphenanthrene (2-OHPHEN) ^c
3-Hydroxyphenanthrene (3-OHPHEN) ^c
4-Hydroxyphenanthrene (4-OHPHEN) ^c
9-hydroxyphenanthrene (9-OHPHEN) ^c
1-Hydroxypyrene (1-OHPyr) ^a
2-Hydroxy-benzo(c)phenanthrene ^a
6-Hydroxychrysene (6-OHCHRYS) ^c
1-Hydroxypyrene-d ⁹ (ISTD*) ^c
Benzo(a)pyrene ^a

Compounds were purchased from ^aSigma–Aldrich, ^bFluka, ^cDr. Ehrenstorfer, ^dAcros Organics or ^eChiron AS.

* ISTD = internal standard.

60 mg spe cartridges were purchased from Varian (Mechelen, Belgium).

2.2. Derivatization method

For derivatization of OH-PAHs, 20 μL of a working solution at 1 mg L^{-1} were transferred to a sampling vial with aluminium-lined screw caps containing 100 μL acetonitrile, 20 μL toluene and 20 μL benzo(a)pyrene at 1 mg L^{-1} as internal standard. The solution was concentrated to approximately 20 μL under a gentle stream of nitrogen, and 30 μL of derivatization reagent were added. The derivatization conditions were determined after the investigation of various experimental parameters including the reaction time and the temperature on the analytical responses of the compounds. Details are given in Section 3.1. 1 μL of the derivatized solution was subjected to GC analysis.

All other compounds were derivatized as follows: 500 μL solution containing the internal standard (succinic acid-d⁴ for MPh, decanoic acid-d¹⁹ for DA, 4-nitrophenol-d⁴ for NPh, and phthalic acid-d⁴ for sterols; at 20 mg L^{-1} for full scan mode or 1 mg L^{-1} for SIM mode, except for sugars where external calibration was done) were transferred into sampling vials with PTFE-lined screw caps and 100 μL derivatization reagent were added. The solution was heated at 80 °C for one hour, under stirring with a magnetic stirrer bar. 1 μL of the derivatized solution was injected for GC analysis [14,24].

2.3. Instrumentation

An Agilent GC/MS instrument equipped with a 7673A automatic sampler, a 6890 series II gas chromatograph with a split/splitless injector and a 5973 mass selective detector was used for the analysis of OH-PAHs. The gas chromatograph was equipped with a Hewlett-Packard HP-ULTRA 2 column (crosslinked 5% phenyldimethylsiloxane) capillary column (12 m \times 0.20 mm \times 0.33 μm film thickness). The injector temperature and the GC/MS interface were kept at 260 °C and 280 °C respectively. The helium carrier gas flow rate was kept at 1 mL min^{-1} .

All other measurements were performed with an autosampler AS3000, a Thermo Quest GC 2000 with a split/splitless injector and coupled to a Thermo Finnigan Trace MS detector. For the gas chromatographic separation, an OPTIMA-210 Macherey-Nagel column was used (30 m \times 0.32 mm \times 0.25 μm film thickness). The injector temperature and the GC/MS interface temperature were both kept at 250 °C. The helium carrier gas flow rate was kept at 1.9 mL min^{-1} .

All temperature programs are given in Table 2.

When quantification of compounds was done, peak areas were normalized with the respective internal standard.

In all cases, the mass spectrometer was operated in the electron ionization mode (EI) at 70 eV. The retention times and the characteristic fragments of the EI mass spectra were determined by total ion monitoring (SCAN). The most abundant ions and/or ions with-

Table 2

GC temperature programs.

	Start temperature	Ramp	End temperature	Hold time
Methoxyphenols	50 °C	–	50 °C	5 min
	50 °C	10 °C min ⁻¹	270 °C	5 min
Total time				32.0 min
Nitrophenols	80 °C	–	80 °C	1 min
	80 °C	5 °C min ⁻¹	150 °C	1 min
	150 °C	20 °C min ⁻¹	230 °C	1 min
	230 °C	5 °C min ⁻¹	280 °C	5 min
Total time				36.0 min
Sterols	100 °C	–	100 °C	2 min
	100 °C	20 °C min ⁻¹	230 °C	5 min
	230 °C	5 °C min ⁻¹	270 °C	5 min
Total time				26.5 min
Sugars	50 °C	–	50 °C	2 min
	50 °C	5 °C min ⁻¹	250 °C	5 min
Total time				47.0 min
Dicarboxylic acids	60 °C	–	60 °C	4 min
	60 °C	15 °C min ⁻¹	155 °C	6 min
	155 °C	5 °C min ⁻¹	190 °C	4 min
	190 °C	5 °C min ⁻¹	210 °C	0 min
	210 °C	20 °C min ⁻¹	270 °C	5 min
Total time				39.3 min
OH-PAHs	70 °C	–	70 °C	2 min
	70 °C	10 °C min ⁻¹	150 °C	0.5 min
	150 °C	5 °C min ⁻¹	280 °C	5 min
Total time				41.5 min

out apparent cross-contribution and interferences were chosen as target ions for the quantification (SIM mode).

2.4. Application to selected matrices

In order to confirm that the findings obtained upon standard solutions still fit when derivatizations are done on the same compounds in environmental and biological matrices, urine samples and atmospheric aerosols containing OH-PAHs and methoxyphenols respectively, were analyzed as described above after sample treatment.

Two urine samples (one supplemented with standards and one left unchanged) collected from a volunteer (non-smoker) from the laboratory staff were prepared according to a previously described method [25]. Briefly, 3 mL were transferred into a 10 mL glass tube, and the pH was adjusted by adding 5 mL acetate buffer (0.1 M; pH 5.5) to reach optimal conditions for enzymatic deconjugation. 20 μL of deuterated 1-hydroxypyrene (1-OHPYR-d⁹) at 20 mg L^{-1} were added as internal standard. For supplemented samples, 20 μL of a solution containing the targeted OH-PAHs at 1 mg L^{-1} were added to the solution. Conjugates were hydrolyzed by adding 10 μL β -glucuronidase/arylsulfatase to the sample, followed by incubation (37 °C) for 17–18 h (overnight). Samples were vortexed and extracted with solid-phase extraction using Focus 60 mg cartridges. The sample extract was supplemented with 20 μL toluene and the solvents were evaporated to approximately 20 μL . Derivatization was done as described above (Section 2.2.).

Atmospheric aerosols were collected in Strasbourg (France) at the Botanical Institute of Strasbourg University at 25 m above ground level using a high-volume air sampler (Digitel, Hegnau, Switzerland). In accordance with previous studies [26] particulate matter (PM₁₀) sample was collected onto quartz fiber filter (QM-A, Whatman, Florham Park, NJ, USA). After sampling, the filter was

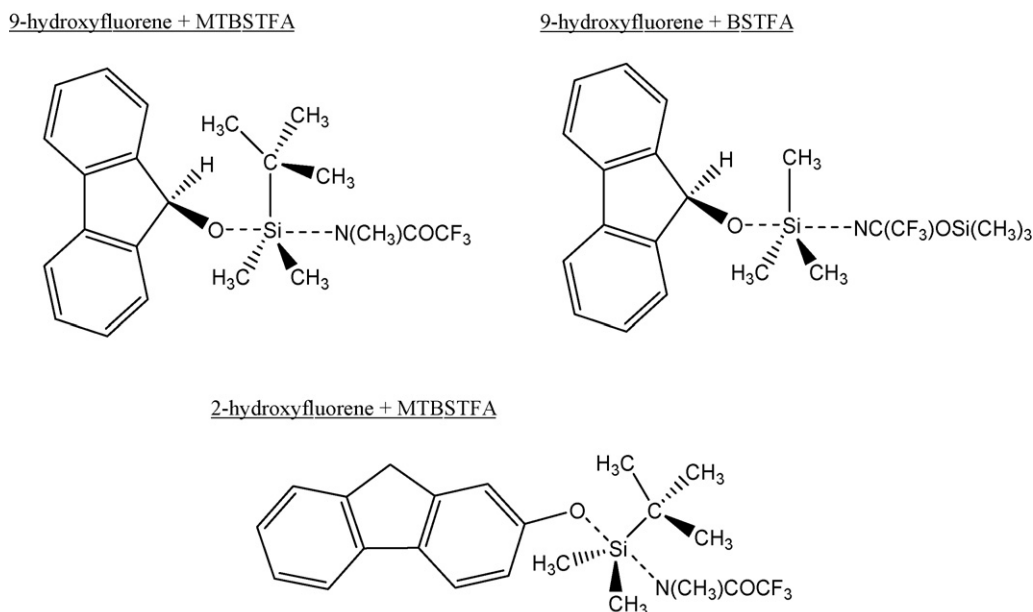


Fig. 1. Transition states of hydroxyfluorene-isomeres derivatized with MTBSTFA and 9-hydroxyfluorene derivatized with BSTFA.

stored at -18°C until analyses and extracted, concentrated and derivatized as previously described [14,24].

3. Results and discussion

3.1. Optimization of the derivatization conditions of OH-PAHs with MTBSTFA and BSTFA

Derivatization conditions of all compounds except OH-PAHs have been previously tested for both reagents [24], and it was found that neither time nor temperature have a great influence on the analytical responses. It was not known if OH-PAHs show similar behavior towards MTBSTFA and BSTFA, so this was checked in the present work.

The derivatization conditions mainly depend on reaction temperature and time. These two parameters were studied separately for each compound and with both reagents. Derivatizations were performed as described in Section 2.2. Analytical responses were normalized towards the analytical response of benzo(a)pyrene, as it is not affected by derivatization.

Influence of reaction time was tested at both 60°C and 80°C for each 10, 20, 30, 40, 50 and 60 min, and with both derivatization reagents.

It was found that both temperature and time only have limited effects on the analytical responses. However, slight differences were observed, and it was concluded that derivatization of OH-PAHs should be performed at a reaction temperature of 60°C , and reaction time should be 20 min when MTBSTFA is used and 40 min when BSTFA is used.

3.2. Chromatographic separation and analytical responses

OH-PAHs were generally separated using standard non-polar capillary columns [27,28]. The ULTRA-2 column also produced very good separations of all OH-PAHs, except for 1-hydroxyphenanthrene and 3-hydroxyphenanthrene when derivatization was performed with BSTFA. This problem was also reported for derivatization performed with MSTFA [28]. So, only when derivatization is performed with MTBSTFA, a perfect resolution

of the studied hydroxylated phenanthrenes can be achieved. It was also observed that 9-hydroxyfluorene produces quite a weak response in comparison with its isomer 2-hydroxyfluorene for derivatization performed with MTBSTFA, although derivatization with BSTFA produces responses of similar intensity for both isomers. This might be explained by steric hindrance: As silylation is a bimolecular nucleophilic substitution ($\text{S}_{\text{N}}2$) [6], the nucleophile (hydroxyfluorene) attacks the silicon of the derivatization reagent (MTBSTFA or BSTFA) at 180° to the leaving group, since this provides the best overlap between the nucleophile's lone pair and the Si-O σ^* antibonding orbital. Both compounds form a transition state before the leaving group is ejected the opposite side and the final product is formed [29]. In this kind of reactions, steric hindrance sometimes is a problem, as an important amount of space is needed to form the transition state (Fig. 1). Or, due to the sp^2 -carbon in the alpha-position, silicon in MTBSTFA is less accessible than in BSTFA, and reaction yields of MTBSTFA with the also hindered hydroxyl group of 9-hydroxyfluorene are lower than with BSTFA. Derivatization reactions of all other studied OH-PAHs, including 2-hydroxyfluorene, with MTBSTFA are not concerned by this problem as their hydroxyl-bonded carbon is sp^2 -hybridised and less hindered. Steric hindrance was also observed to be a problem for derivatizations of sugars and sterols. No signal could be observed for all sugars when derivatization was performed with MTBSTFA. In opposition, analyzed sterols were detected but a loss of sensitivity of about a factor four was observed for derivatizations performed with MTBSTFA compared to derivatizations performed with BSTFA. This loss of sensitivity may occur due to the low accessibility of the hydroxyl group of sterols, as described above for 9-hydroxyfluorene. So, for these two families, derivatization with BSTFA should be preferred in terms of analytical responses. However, even when derivatization of sterols is performed with BSTFA, analytical responses remain rather small.

In terms of analytical responses, it was found that those of tbdms-derivatives generally are slightly higher than those of tms-derivatives. For example, glutaric acid, adipic acid and suberic acid show MTBSTFA/BSTFA ratios of 1.6, 1.8 and 1.3 respectively, and 1-hydroxynaphthalene, 2-hydroxynaphthalene, 2-hydroxyfluorene

Table 3
Fragmentation pattern obtained for MTBSTFA and BSTFA.

<i>m/z</i>	Fragmentation	Observed for
MTBSTFA		
[M] ⁺	Molecular ion	OH-PAHs except 9-OHFLU; nitrophenols with no substitutions on the ortho-position
[M–57] ⁺	Cleavage of the t-butyl moiety (–C(CH ₃) ₃)	All compounds except sugars, sterols, some DA (glutaric, adipic, suberic, and azelaric acid).
[M–131] ⁺	Cleavage of the t-butyl-dimethyl silyl moiety including the phenolic oxygen (OSi(CH ₂)C(CH ₃) ₃)	9-OHFLU, cresols, methoxyphenols containing a COOH function or a second OH-function
[M–73] ⁺	Cleavage of a t-butylsilyl fragment and a molecular oxygen or cyclization involving the silyl group	Nitrophenols, methoxyphenols containing an aldehyde function and for some OH-PAHs (see cyclization in paragraphe 3.3.1)
[M–15] ⁺ [M–118] ⁺ [M–103] ⁺ [M–133] ⁺	Cleavage of a methyl from the molecular ion [M–118] ⁺ results from the cleavage of NO ₂ and CH ₃ of the fragment [M–57] ⁺ , [M–103] ⁺ from the cleavage of the neutral fragment NO ₂ and the major fragment [M–C(CH ₃) ₃] ⁺ and [M–133] ⁺ results from the successive cleavage of NO ₂ and NO of the major fragment [M–57] ⁺ .	Glutaric, adipic, suberic, and azelaric acid Nitrophenols
[M–101] ⁺	Mac Lafferty rearrangement causing the cleavage of (HSi(CH ₃) ₂ –C(CH ₃) ₂), [M–72] ⁺ from the cleavage of CH ₃ from the ketone function of the fragment [M–57] ⁺	Methoxyphenols containing an acetone function or containing no other function than methoxy
BSTFA		
[M] ⁺	Molecular ion	All compounds
[M–89] ⁺	Cleavage of the trimethylsilyl ether moiety (OSi(CH ₃) ₃)	9-Hydroxyfluorene; sterols
[M–104] ⁺	Cleavage of the trimethylsilyl ether moiety plus one methyl group	Sterols
[M–31] ⁺	The cleavage of the trimethylsilyl ether moiety followed by cyclization involving the silyl group. (see cyclization-paragraphe)	Some OH-PAHs (1-OHNAPH, 1-OHPHEN, 4-OHPHEN, 9-OHPHEN, 1-OHPYR and 6-OHCHRY)
[M–15] ⁺	Cleavage of a methyl from the molecular ion	OH-PAHs, methoxyphenols, nitrophenols and sterols

and 6-hydroxychrysene show MTBSTFA/BSTFA ratios of 1.8, 1.5, 1.4 and 1.8 respectively.

3.3. Derivatization and mass spectral characteristics of derivatized compounds

During the silylation reaction, all the hydroxyl groups are converted into their corresponding trimethylsilyl (tms) ethers (for derivatizations with BSTFA) or t-butyl dimethylsilyl (tbdms) ethers (for derivatizations with MTBSTFA) via an SN₂ substitution reaction, yielding a single derivative for each compound [6,9]. Derivatized standards were analyzed by electron impact (EI) in the full scan mode in order to obtain the fragmentation pattern of each compound. Both derivatization reactions produce different fragmentation pattern (Table 3). Examples of mass spectrograms are given in Fig. 2 (MTBSTFA) and Fig. 3 (BSTFA).

For derivatization with MTBSTFA, [M]⁺, [M–57]⁺ and [M–131]⁺ were the most abundant fragments all over the different chemical groups of OH-PAHs, methoxyphenols and nitrophenols. Each of these groups also presented some other characteristic fragments for the analyzed compounds, what makes identification very reliable. For these three groups, relative abundances of the fragments are very high, especially for [M–57]⁺ what generates good detection limits. For these groups, MTBSTFA-derivatization produces very good results.

For dicarboxylic acids, important fragments were observed at *m/z* = 73, 75, 147 and 189, but these are not characteristic for the analyzed compound and cannot be used for quantification. Dicarboxylic acids only showed one characteristic fragment ([M–15]⁺ or [M–57]⁺), so identification of peaks is limited, but relative abundances are still high so good detection limits can be achieved with the observed fragment.

Sterols and sugars could not be derivatized with MTBSTFA.

Mass spectrograms of sugars derivatized with BSTFA showed that derivatized products are quite unstable and produce a lot of fragments. This makes interpretation of mass spectrograms quite difficult. However, fragments with *m/z* = 204, 217 and 191 (for monosaccharides), 204, 217 and 333 (for anhydrosaccharides), 217, 319, 307 and 205 and 204, 361, 191 and 417 (for disaccharides) allow quantification of sugars in SIM mode (Fig. 3).

The same phenomenon of unstable derivatives and strong fragmentation was also observed for dicarboxylic acids. A lot of non-characteristic fragments were observed in low *m/z* ranges, but unfortunately no characteristic fragments could be identified for dicarboxylic acids. So BSTFA is not suitable for derivatization of these compounds.

Results show that for compounds with small molecular mass like methoxyphenols, nitrophenols and OH-PAHs with a maximum of three rings, derivatization can be performed with both reagents. For compounds with high molecular mass like OH-PAHs with more than three rings, MTBSTFA should be preferred as fragmentation pattern become more specific for the analyzed compounds, unless the derivatized compound has sterically hindered sites. In this case, BSTFA should be preferred because steric hindrance lowers analytical responses of MTBSTFA derivatized compounds or inhibits derivatization.

3.3.1. Cyclization

Some spectrograms showed the fragment [M–73]⁺ (for MTBSTFA-derivatizations) or [M–31]⁺ (for BSTFA-derivatizations). Calculations indicate that these fragments could result from the cleavage of the t-butyl moiety and one hydrogen (mass count = 73) respectively two methyl groups and one hydrogen (mass count = 31). A similar fragmentation pattern was observed before

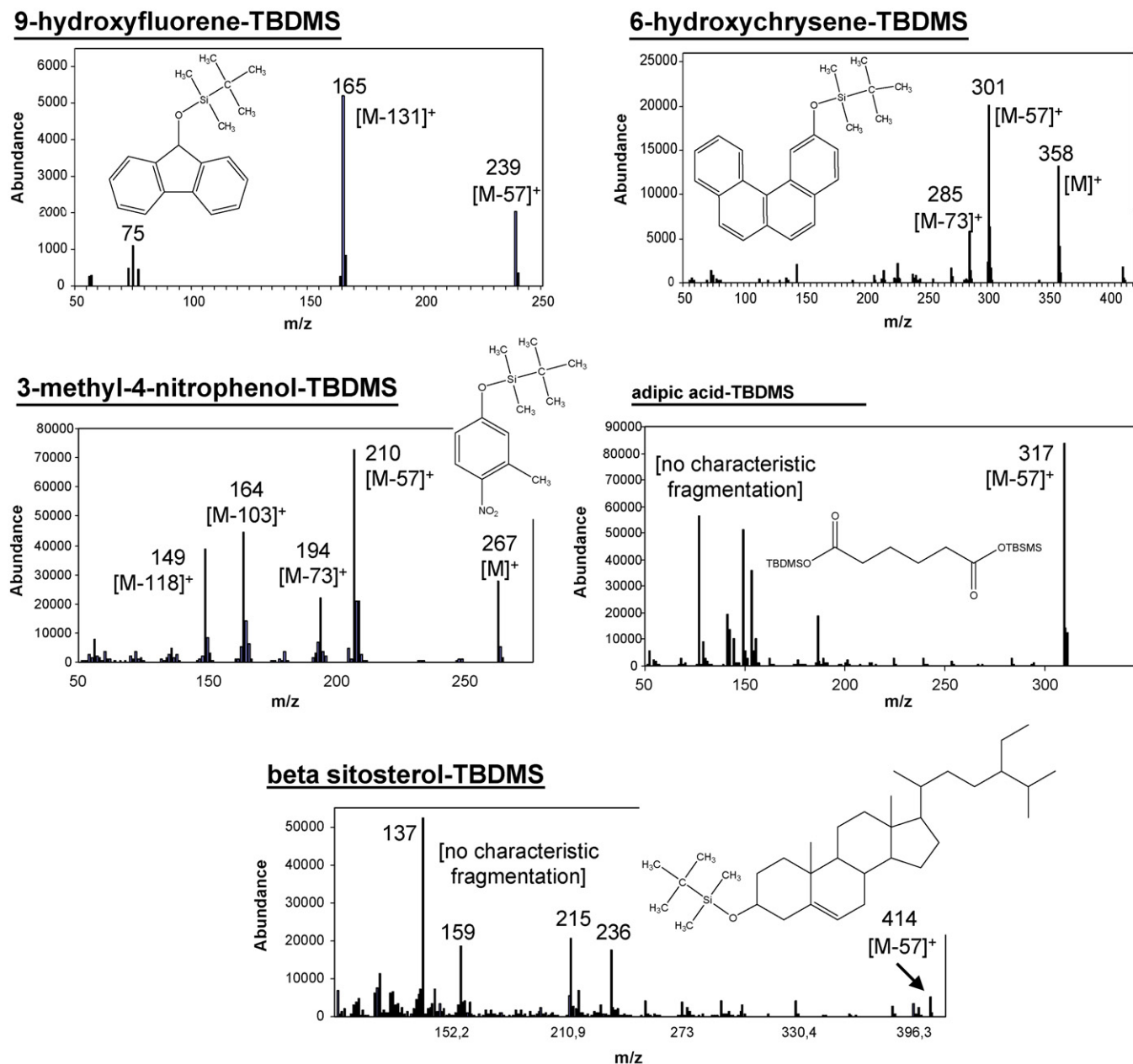


Fig. 2. EI full SCAN mass spectra of some MTBSTFA-derivatized compounds with the corresponding structure.

by Gmeiner et al. [29] and Jacob et al. [30] for silylated hydroxyphenanthrenes and hydroxyfluorenes, and the authors supposed cyclization involving the silyl group and generating a five-atom ring respective a six-atom-ring, but unfortunately this was not demonstrated.

If cyclization occurs, the hydrogen mentioned above must be cleaved from the aromatic part of the molecule, and not from the silyl group. So, 1-hydroxypyrene- d^9 , where all hydrogens on the aromatic rings have been replaced by deuteriums, was derivatized with both MTBSTFA and BSTFA and analyzed (Figs. 4 and 5). The expected fragments $[M]^+$ and $[M-57]^+$ (for MTBSTFA-derivatization) or $[M]^+$ and $[M-15]^+$ (for BSTFA-derivatization) were identified on the spectrograms, however change occurred for the fragments $[M-73]^+$ (became $[M-74]^+$) and $[M-31]^+$ (became $[M-32]^+$). So, the hydrogen must be cleaved from the aromatic part, as 1-hydroxypyrene- d^9 released a deuterium,

and a cyclization involving the silyl group and resulting in a five-atom-ring took place, as shown in Fig. 4.

Interestingly, cyclization only happened for 1-hydroxynaphthalene, 1-hydroxyphenanthrene, 4-hydroxyphenanthrene, 9-hydroxyphenanthrene, 1-hydroxypyrene and 6-hydroxychrysene, so for all compounds having another aromatic ring in the alpha position of the carbon carrying the hydroxyl-group. This suggests that cyclization should also be possible for silylated sterols, however this was not observed.

3.4. Application to selected matrices

3.4.1. OH-PAHs in urine

The comparison of chromatograms obtained from supplemented sample analyses (Fig. 6-2A and 6-2B) with those obtained for standard solutions (Fig. 6-1A and 6-1B) demonstrates that sepa-

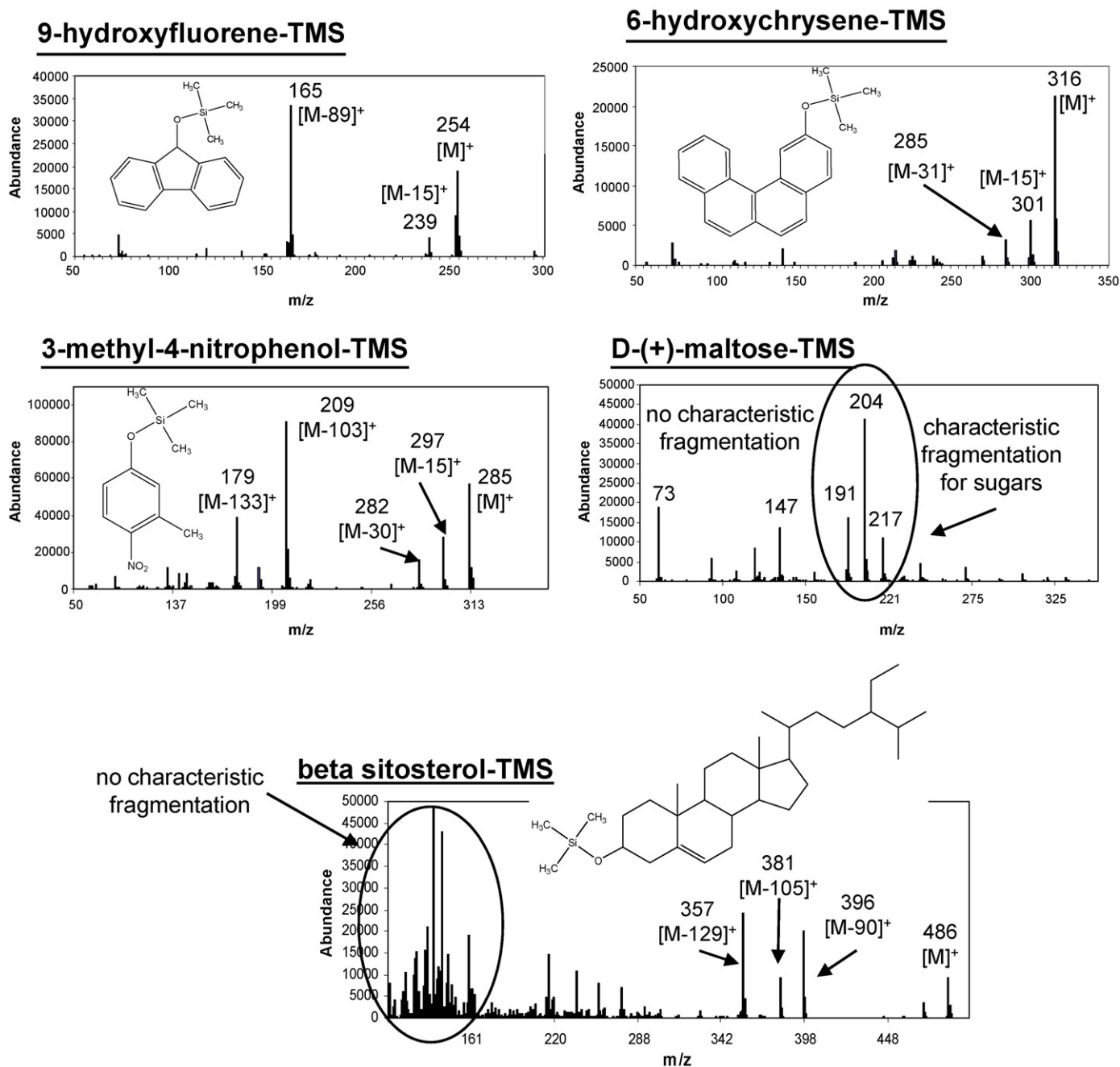


Fig. 3. EI full SCAN mass spectra of some BSTFA-derivatized compounds with the corresponding structure.

ration and fragmentation pattern were not affected by matrix effect. In the non-supplemented urine sample derivatized with MTBSTFA (Fig. 6-3A), only 1-OHNAPH, 2-OHNAPH, 1-OHPHEN, 2-OHPHEN and 3-OHPHEN were detected, while in the sample derivatized with BSTFA (Fig. 6-3B), also 9-OHFLU was found. This is due to the very low analytical response produced by 9-OHFLU when derivatization is performed with MTBSTFA (see Section 3.2.), and that is too low to be distinguished from the background noise.

1-OHPHEN and 3-OHPHEN were clearly identified when derivatization was performed with MTBSTFA, while they were not separated when derivatization was performed with BSTFA. With the latter it is not possible to know that two isomers were present or just one of them, as fragmentation pattern are identical and relative abundances of the selected masses very similar.

Even though 9-OHFLU will not be detected in urine samples due to high detection limits, MTBSTFA should be preferred in these analyses as it provides better separations for the other metabolites and higher analytical responses resulting in lower detection limits what improves the quality of the analytical method.

3.4.2. Methoxyphenols in atmospheric aerosols

The comparison of chromatograms obtained from sample analyses with those obtained for standard solutions (Fig. 6-4A and 6-4B) demonstrates that separation and fragmentation pattern were not affected by matrix effect.

In the non-supplemented atmospheric aerosols derivatized with MTBSTFA (Fig. 6-5A), 4-hydroxybenzaldehyde, vanillin, syringaldehyde, 3,5-dimethoxy-4-hydroxyacetophenone, vanillic

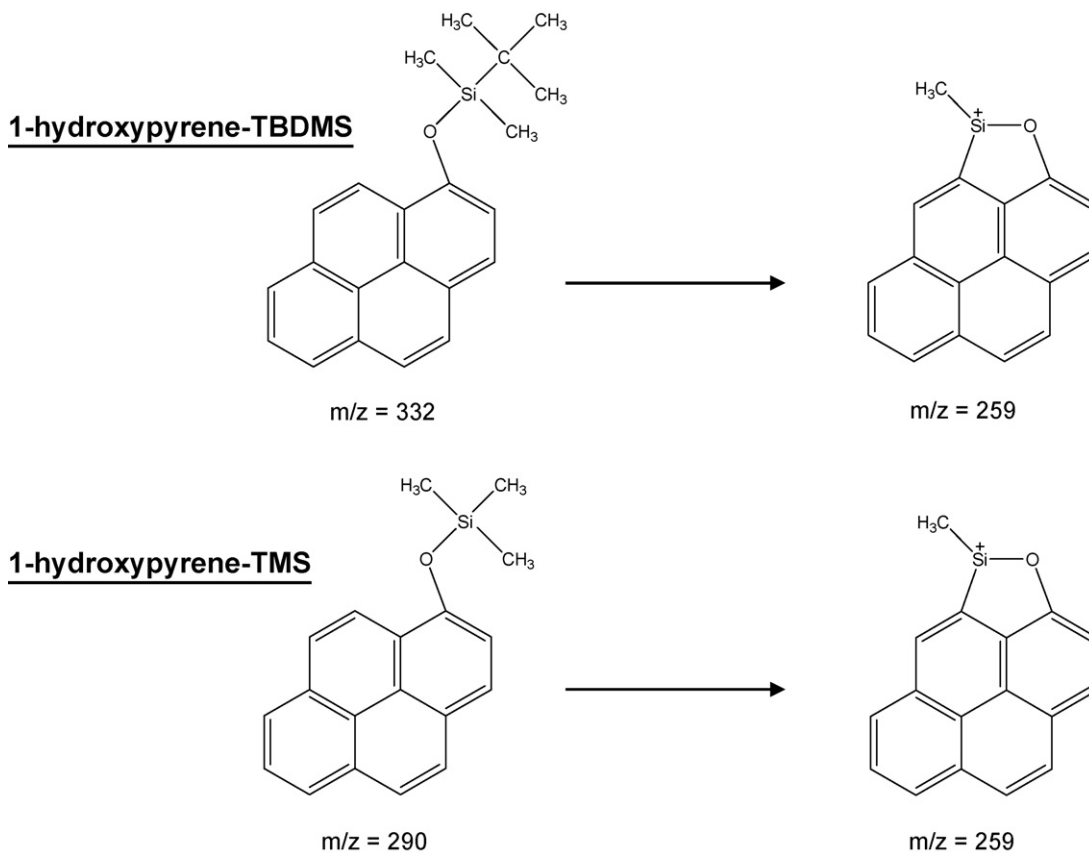
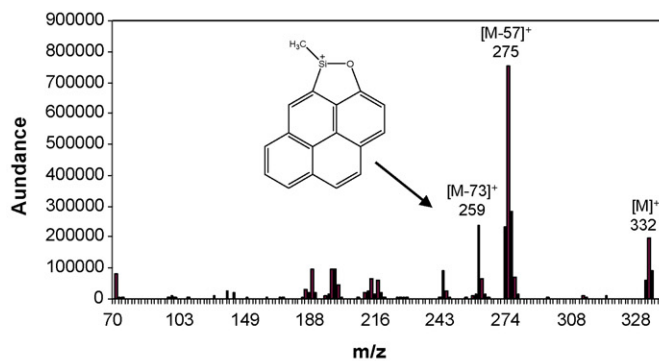
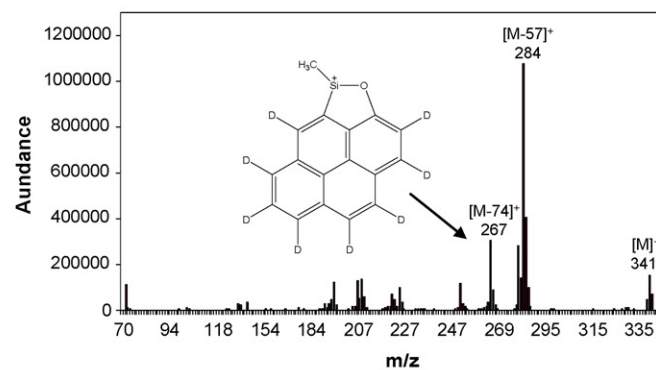
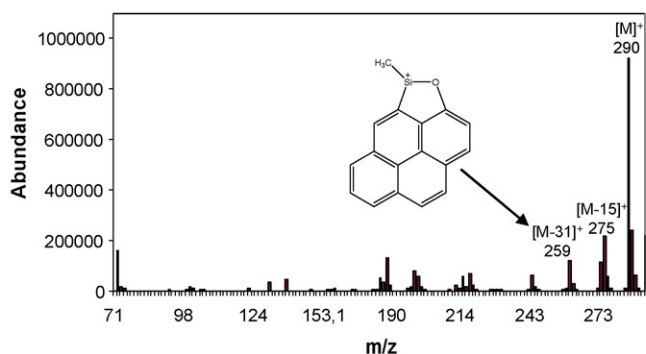
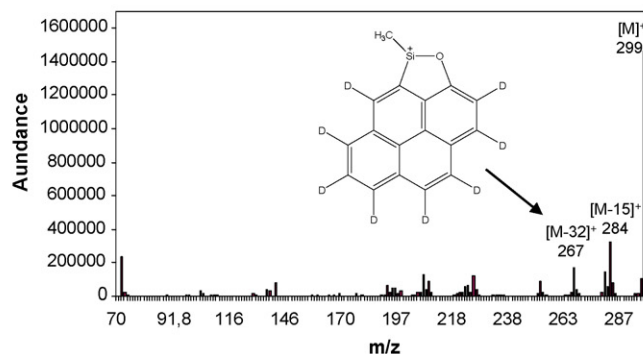


Fig. 4. Cyclization of silylated 1-hydroxypyrene.

1-hydroxypyrene + MTBSTFA**1-hydroxypyrene-d⁹ + MTBSTFA****1-hydroxypyrene + BSTFA****1-hydroxypyrene-d⁹ + BSTFA**Fig. 5. Mass spectrograms of 1-OHPYR and 1-OHPYR-d⁹ derivatized with MTBSTFA resp. BSTFA, with the cyclic fragments [M-73]⁺ and [M-74]⁺ resp. [M-31]⁺ and [M-32]⁺.

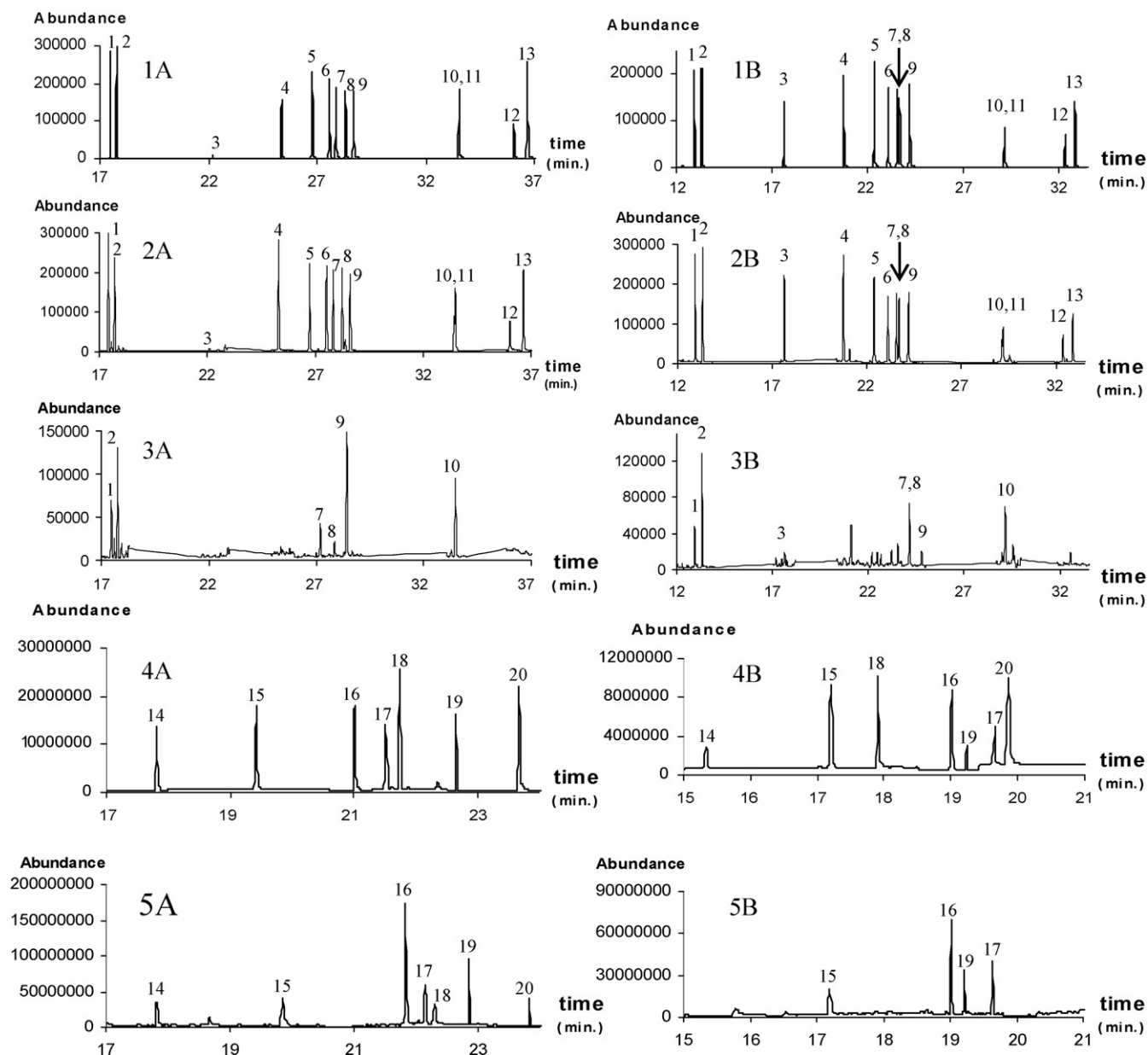


Fig. 6. Chromatograms of OH-PAHs (1–3) and methoxyphenols (4 and 5) derivatized with MTBSTFA (A) and BSTFA (B) from standard solutions (1 and 4), supplemented urine extract (2), non-supplemented urine extract (3) and non-supplemented atmospheric aerosols extract (5). OH-PAHs: (1) 1-hydroxynaphthalene, (2) 2-hydroxynaphthalene, (3) 9-hydroxyfluorene, (4) 2-hydroxyfluorene, (5) 4-hydroxyphenanthrene, (6) 9-hydroxyphenanthrene, (7) 3-hydroxyphenanthrene, (8) 1-hydroxyphenanthrene, (9) 2-hydroxyphenanthrene, (10) 1-hydroxypyrene-*d*⁹ (internal standard), (11) 1-hydroxypyrene, (12) 2-benzo(c)phenanthrene, (13) 6-hydroxychrysene. Methoxyphenols: (14) 4-hydroxybenzaldehyde, (15) vanillin, (16) syringaldehyde, (17) 3,5-dimethoxy-4-hydroxyacetophenone, (18) vanillic acid, (19) syringic acid, (20) coumaric acid.

acid, syringic acid and coumaric acid were detected, while in the sample derivatized with BSTFA (Fig. 6-5B), only vanillin, syringaldehyde, syringic acid and 3,5-dimethoxy-4-hydroxyacetophenone could be identified.

The analytical responses of the detected compounds derivatized with MTBSTFA are better than the responses of the compounds derivatized with BSTFA. This is due to the fact that tms-derivates produce much more fragments than tbdms-derivates, what results in lower analytical responses in SIM mode and thus in higher detection limits. This also explains why only four methoxyphenols were identified on the chromatogram resulting from the derivatization with BSTFA.

MTBSTFA should be preferred for analyses of methoxyphenols in atmospheric aerosols as it provides better analytical responses

and thus lower detection limits what improves the quality of the analytical method.

4. Conclusions

Analyses of tertibutyldimethylsilyl-derivates (tbdms) and trimethylsilyl-derivates (tms) of six groups of polar compounds were compared in this study to conclude about the use of MTBSTFA and BSTFA as a derivatization reagent prior to GC/MS analyses.

It was found that the molecular mass of the analyzed compounds plays a major role in derivatizations: small compounds do not show important differences in specificity of fragmentation pattern whereas big molecules as four-ring OH-PAHs, dicarboxylic acids or sterols only produce characteristic fragmentation pattern

when derivatization is performed with MTBSTFA. However, rather than BSTFA-derivatization, MTBSTFA-derivatization is not always possible, especially when the target compound presents sterically hindered sites. In this case, analytical responses decrease dramatically (e.g. 9-hydroxyfluorene, sugars), resulting in higher detection limits and loss of sensitivity.

In terms of chromatographic responses, it was found that separation of isomers (e.g. hydroxyphenanthrenes) is more easily when derivatization is performed with MTBSTFA, and analytical responses of non sterically hindered tbdms-derivatized molecules generally are higher. This was confirmed through authentic applications on urine samples and atmospheric aerosols.

The results suggest that, if the choice of the derivatization reagent is not imposed by the structure of the target compound, MTBSTFA should be preferred due to generally higher analytical responses.

References

- [1] J.M. Halket, Handbook of Derivatives for Chromatography, 2nd ed., Wiley, 1993, p. 297.
- [2] C.F. Poole, Handbook of Derivatives for Chromatography, Heyden, 1997, p. 152.
- [3] A.E. Pierce, Silylation of Organic Compounds, Pierce Chemical Co., 1968, p. 21.
- [4] J.M. Halket, V.G. Zaikin, Eur. Mass Spectrom. 9 (2003) 1.
- [5] L. Martins Ferreira, M. Yegles, H. Chung, R. Wennig, J. Chromatogr. B 825 (2005) 57.
- [6] D.C. Harris, Quantitative Chemical Analysis, fourth ed., Freeman, 1995, p. 74.
- [7] J.A. Dean, Analytical Chemistry Handbook, 4, McGraw-Hill, Inc., 1995, p. 16.
- [8] H.J. Hübschmann, Handbuch der GC/MS, VCH, 1996, p. 437.
- [9] C. Schummer, M. Sadiki, Ph. Mirabel, M. Millet, Chromatographia 63 (2006) 189.
- [10] M. Yegles, A. Labarthe, V. Auwärter, S. Hartwig, H. Vater, R. Wennig, F. Pragst, Forensic Sci. Int. 145 (2004) 167.
- [11] J. Segura, R. Ventura, C. Jurado, J. Chromatogr. B 713 (1999) 61.
- [12] J.M. Halket, D. Waterman, A.M. Przyborowska, R.K. Patel, P.D. Fraser, P.M. Bramley, J. Exp. Bot. 56 (2004) 219.
- [13] Regis 1998–99 Chromatography Catalog.
- [14] S. Morville, A. Scheyer, Ph. Mirabel, M. Millet, J. Environ. Monit. 6 (2004) 963.
- [15] A. Lottmann, Ph.D. thesis, University of Strasbourg I, 2006.
- [16] T. Gunnar, K. Ariniemi, P. Lillsunde, J. Chromatogr. B 818 (2005) 175.
- [17] Á. Sebök, A. Vasánits-Zsigrai, G. Palkó, G. Záray, I. Molnár-Perl, Talanta 76 (2008) 642.
- [18] J. Horn, J.W. Flesher, A.F. Lehner, Chem. Biol. Interact. 145 (2003) 17–32.
- [19] C. Hao, X. Zhao, P. Yang, Trends Anal. Chem. 26 (2007) 569.
- [20] J.E. Hong, H. Pyo, S.J. Park, W. Lee, Anal. Chim. Acta 531 (2005) 249.
- [21] I. Molnár-Perl, Z. Füzfa, J. Chromatogr. A 1073 (2005) 201.
- [22] H.S. Weinberg, W.H. Glaze, Water Res. 31 (1997) 1555.
- [23] A. Cecinato, V. Di Palo, D. Pomata, M.C. Tomasi Scianò, M. Possanzini, Chemosphere 59 (2005) 679.
- [24] S. Morville, Ph.D. thesis, University of Strasbourg I, 2005.
- [25] L.C. Romanoff, Z. Li, K.J. Young, N.C. Blakely III, D.G. Patterson Jr., C.D. Sandau, J. Chromatogr. B 835 (2006) 47.
- [26] O. Delhomme, P. Herckes, M. Millet, Anal. Bioanal. Chem. 389 (2007) 1953.
- [27] C.J. Smith, W. Huang, C.J. Walcott, W. Turner, J. Grainger, D.G. Patterson Jr., Anal. Bioanal. Chem. 372 (2002) 216.
- [28] N. Grova, F. Monteau, B. Le Bizec, C. Feidt, F. Andre, G. Rychen, J. Anal. Toxicol. 29 (2005) 175.
- [29] G. Gmeiner, P. Gärtner, C. Krassnig, H. Tausch, J. Chromatogr. B 766 (2002) 209.
- [30] J. Jacob, A. Schmoltdt, G. Grimmer, Toxicology 25 (1982) 333.



Creation and application of psychoactive designer drugs data library using liquid chromatography with photodiode array spectrophotometry detector and gas chromatography–mass spectrometry

Misako Takahashi^{a,*}, Machiko Nagashima^a, Jin Suzuki^a, Takako Seto^a,
Ichirou Yasuda^a, Takemi Yoshida^b

^a Tokyo Metropolitan Institute of Public Health, 3-24-1 Hyakunin-cho, Shinjyuku-ku, Tokyo 169-0073, Japan

^b Showa University, 1-5-8 Hatanodai, Shinagawa-ku, Tokyo 142-8555, Japan

ARTICLE INFO

Article history:

Received 4 June 2008

Received in revised form 27 July 2008

Accepted 28 July 2008

Available online 13 August 2008

Keywords:

Tryptamine

Phenylethylamine

Piperazine

LC/PDA

GC/MS

Psychoactive designer drug

ABSTRACT

In order to quickly confirm a potentially hazardous psychoactive designer drug (a compound in which part of the molecular structure of a stimulant or narcotic has been modified), we created a psychoactive drugs data library by performing analysis using liquid chromatography with photodiode array spectrophotometry (LC/PDA) and gas chromatography–mass spectrometry (GC/MS). The data in this library consist of the LC capacity factor (k') ratios in relation to the internal standard, the ultraviolet (UV) spectra and the MS spectra of 104 compounds. By performing a comparative study of the data in this report with the analytical data for commercial and illegal drug products, it is possible to quickly identify the psychoactive designer drugs in 205 purchased products by using the library. Further, it is possible to analogize the structure of drugs for which there is no matching data in the library using similar data.

Furthermore, when structural isomers of controlled substances have detected from the presented library, similarity of their biological effects on human will be predicted, thus leading to regulate their public circulation. Examples of these types of isomers include, for instance, the narcotic 3,4,5-trimethoxyamphetamine (TMA) and its positional isomers 2,4,5-trimethoxyamphetamine (TMA-2) and 2,4,6-trimethoxyamphetamine (TMA-6), or the narcotic 1-(3-chlorophenyl)piperazine (3CPP) and its isomers 1-(*o*-chlorophenyl)piperazine (2CPP) and 1-(*p*-chlorophenyl)piperazine (4CPP). Differentiation of these compounds is necessary in regulating them, and we report here the results of a study of a method to confirm these compounds using the present library.

© 2008 Elsevier B.V. All rights reserved.

1. Introduction

In recent years, the popularity of synthetic drugs, sometimes referred to as psychoactive designer or rave drugs, has been increasing among young people. This is due to their reputation as being safe, having stimulating and hallucinogenic effects, and also causing unusual perceptions and experiences after ingestion. These synthetic drugs can be easily obtained on the street or on the Internet. Among the drugs commonly seen in cases of drug abuse, there have emerged drugs for which the sale or possession of these materials is regulated by the “Stimulant Drugs Control Act”, the “Narcotic and Psychotropic Drug Control Law”, the “Poisonous and Deleterious Substances Control Law” and the “Pharmaceutical

Affairs Law”, in Japan. And some compounds referred to as psychoactive designer drugs that may show similar efficacy to other controlled substances but which are only implicitly regulated. As shown in Fig. 1, these psychoactive designer drugs have I, II and III basic skeletons. Type I structure is phenylethylamine (PEA)-related compounds with structural similarities to both amphetamine and the psychedelic PEA, mescaline. Type II structure is tryptamines (T)-related compounds with structural similarities to hallucinogenic psilocin. Type III structure is phenylpiperazine (PP)-related compounds with structural similarities to stimulus effects 1-(3-trifluoromethylphenyl)piperazine (TFMPP). But the types of morphine/heroin-like narcotics are excluded in this study.

In order to prevent damage resulting from drug abuse, it is necessary to analyze the active ingredients, publicize the risks of these compounds, and, if illegal, to quickly act to regulate them. For that, the library required for the screening of these compounds, while there were a few of data for gas chromatography–mass spectrom-

* Corresponding author. Tel.: +81 333633231; fax: +81 333684060.

E-mail address: [Misako.Takahashi@member.metro.tokyo.jp](mailto: Misako.Takahashi@member.metro.tokyo.jp) (M. Takahashi).

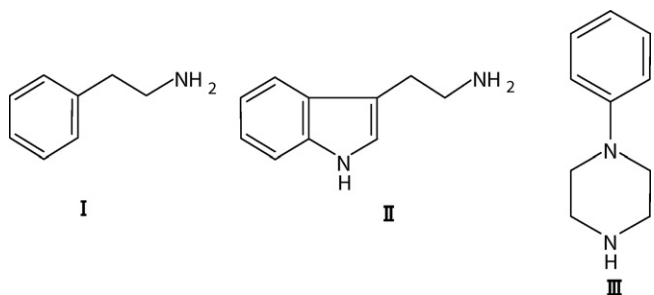


Fig. 1. Structures of basic skeletons. I: phenylethylamine; II: tryptamine; III: phenylpiperazine.

etry (GC/MS) [1–6], liquid chromatography–mass spectrometry (LC/MS) [7,8], there was little data on psychoactive designer drugs. Also, there were few library systems for the liquid chromatography with photodiode array spectrophotometry (LC/PDA) [9,10]. Furthermore, it is difficult to obtain reference products for these drugs. Therefore, for those drugs for which it is not possible to obtain reference standards, the compounds are synthesized or commercial products are separated and purified, and the compounds for which a structural determination is made using high mass spectrometry (HR/MS) and nuclear magnetic resonance (NMR) spectra measurements are used as the reference standards. As shown in Fig. 1, 104 types of psychoactive designer drugs are analyzed (the chemical names and abbreviations are shown in Tables 1–3), where these drugs have I, II and III basic skeletons. There are 51 types of PEA compounds with a type I structure, where these have a PEA skeleton such as 3,4,5-trimethoxyamphetamine (TMA), 2,5-dimethoxy-4-ethylthiophenethylamine (2C-T-2), 2,5-dimethoxy-4-propylthiophenethylamine (2C-T-7), and 4-bromo-2,5-dimethoxyphenethylamine (2C-B). There are 32 types of T compounds with a type II structure, where these have a T skeleton such as bis(methylethyl)[2-(5-methoxyindol-3-yl)ethyl]amine (5-MeO-DIPT) and 1-indol-3-ylprop-2-ylamine (AMT) [11], and there are 21 types of PP compounds with a type III structure, where these have a piperazine skeleton such as 1-(3-chlorophenyl)piperazine (3CPP), 1-(4-methoxyphenyl)piperazine (4MPP) and TFMPP. These are tested using LC/PDA and GC/electron ionization (EI)/MS, and a library is created based on the analysis data obtained. The data registered into the library consisted of the capacity factor (k') ratio of each drug with the internal standard (IS), the ultraviolet (UV) spectrum and the MS data. It is possible to quickly confirm the psychoactive designer drugs from the results of screening of 205 purchased products containing psychoactive designer drugs [12] using the library. Also, we have studied whether or not it is possible to differentiate positional isomers using this library.

2. Experimental

2.1. Apparatus

The HPLC apparatus consisted of a JASCO Model 880-PU pump (Japan Spectroscopic, Tokyo, Japan), a Rheodyne injector Model 7125 equipped with a 100- μ L loop (Rheodyne, Berkeley, CA, USA), a JASCO Model 860-CO column oven, a JASCO Model 821-PDA photo diode array detector (PDA). Data were collected using the JASCO ChromNAV software. The HPLC-I system: column used was a L-column ODS, 4.6 i.d. \times 150 mm, 5 μ m (CERI, Saitama, Japan) or a SymmetryShield RP₁₈, 4.6 i.d. \times 150 mm, 5 μ m. (Waters, MA, USA). The gradient system was used with a mobile phase A (10 mM/L sodium dodecyl sulfate (SDS) in acetonitrile/water/phosphoric

acid (300:700:1)) and mobile phase B (10 mM/L SDS in acetonitrile/water/phosphoric acid (700:300:1)), the SDS was dissolved in the water before mixing with other solvents. The gradient program was utilized with an initial for 10 min held 75:25 A/B. This was followed by a 20-min ramp from 75:25 A/B to 90:10 A/B. This was held for 5 min. The flow rate was 1.0 mL/min; the HPLC-II system: column used was an Atlantis-dC18 ODS, 4.6 i.d. \times 150 mm, 5 μ m, (Waters, MA, USA). The gradient system was used with a mobile phase A (acetonitrile) and mobile phase B (5 mM/L heptafluorobutyric acid (PFFA-4) water solution). A:B 18:82 (0 min)–18:82 (10 min)–28:72 (15 min)–30:70 (25 min). The flow rate was 1.0 mL/min; LC/PDA conditions: column temp was 40 °C; for the detection system of PDA, 199–360 nm. The injection volume was 10 μ L.

The GC/MS system used was an Agilent N3520 (Agilent Technologies Japan Ltd., Tokyo, Japan). GC conditions: DB-5MS capillary column (30 m \times 0.25 mm i.d., 0.25 μ m film thickness, Agilent Technologies, USA). Carrier gas, helium; flow-rate, 1.1 mL/min; oven temperature from 100 °C (5 min) to 290 °C at 10 °C/min, 20 min isotherm; injector temperature, 250 °C; splitless; transfer line, 290 °C; MS conditions; electron impact ionization, full scan at m/z 30–350, electron energy was 70 eV, ion source temperature was 200 °C; the injection volume was 1 μ L; data were collected using the Agilent Technologies ChemStation software.

2.2. Chemicals and reagents

Phosphoric acid, SDS, chloroform, acetonitrile and methanol (all of analytical grade) were purchased from Wako (Osaka, Japan). PFFA-4 was purchased from Tokyo Kasei (Tokyo, Japan). Water was purified using a Milli-Q water purification unit (Nihon Millipore, Tokyo, Japan). The origins of other reagents were shown in Tables 1–3. The compounds which were shown “Synthesis” in Tables 1–3 were synthesized. The procedures for their synthesis have been described previously by the published books titled TiHKAL and PiHKAL, respectively [13,14]. And the compounds which were shown “Extraction” in Tables 1–3 were separated and given clean-up from “purchased products” on the market. These synthesized compounds and purified compounds were identified by LC/TOF/MS, GC/MS and NMR [15,16].

Methods of separation and clean-up: each of these purchased products was dissolved in 20 mM/L hydrochloric acid. Extractions were then performed with chloroform from the ammonia alkaline solutions and the chloroform layer was filtered. The filtrate was evaporated to remove the solvent, purified and then used for analysis.

Test solutions: these were prepared according to the General Tests and General Notices of the Japanese Pharmacopoeia [17].

2.3. Preparation of sample solutions

2.3.1. Products

Powdered samples of the products, contents of capsules and tablets were extracted with the respective solvent by ultrasonication for 10 min. LC/PDA: approximately 10.0 mg of each sample was dissolved in 20 mM/L hydrochloric acid/methanol (1:1). Subsequently, 1.0 mL of each solution was diluted with methanol to the total volume of 10.0 mL. The solution was then filtered with a 0.45- μ m membrane filter for the analytical use. GC/MS: approximately 10.0 mg of each sample was dissolved in 10 mL of methanol. The solution was diluted ten times with methanol.

As described below, test solutions were prepared by the use of synthetic and commercial powdered samples and 0.1 mL of the samples was distilled to prepare sample solutions for the commercial liquid products.

Table 1
Data of phenylethylamines

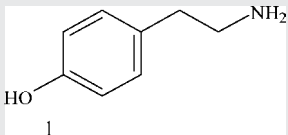
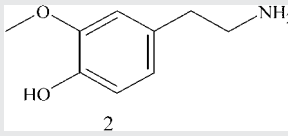
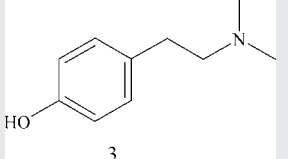
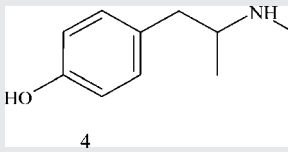
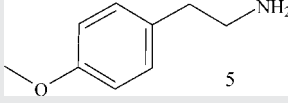
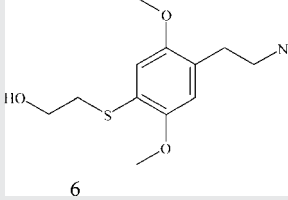
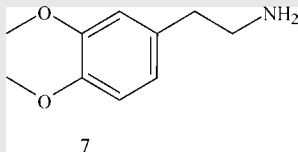
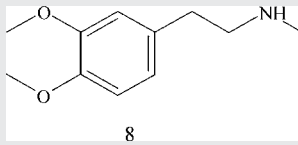
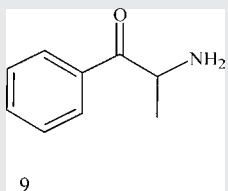
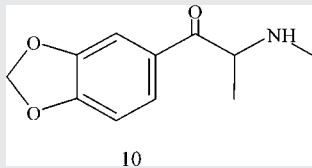
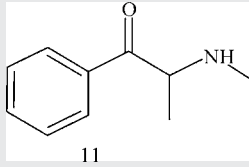
No.	Chemical name (abbreviated name)	Formula: molecular weight	Origin	HPLC-I (k') ^a	HPLC-I k'/k' (IS)	HPLC-II k'	HPLC k'/k' (IS)	GC (t_R , min)	EI-MS (m/z , %)	Structures
1	4-(2-Aminoethyl)phenol (Tyramine)	C ₈ H ₁₁ NO: 137	TCI (Tokyo, Japan)	3.72	0.36	0.91	0.32	12.18	137 (M ⁺ , 14), 108 (100), 77 (23), 30 (69)	
2	3-Methoxy-tyramine (3-MT)	C ₉ H ₁₃ NO ₂ : 167	Sigma-Aldrich (St. Louis, MO, USA)	4.00	0.39	0.76	0.27	13.95	167 (M ⁺ , 11), 138 (100), 123 (20), 58 (21), 30 (41)	
3	<i>N,N</i> -Dimethylaminotyramine (Hordenine)	C ₁₀ H ₁₅ N ₁ O ₁ : 165	TCI (Tokyo, Japan)	4.54	0.44	1.35	0.48	12.70	165 (M ⁺ , 1), 107 (3), 77 (5), 58 (100), 42 (5)	
4	<i>p</i> -Hydroxy-methamphetamine (4HO-MA)	C ₁₀ H ₁₅ NO: 165	Extraction ^b	5.16	0.50	1.41	0.50	11.23	150 (1), 107 (7), 77(6), 58 (100), 30(4)	
5	<i>p</i> -Methoxyphen ethylamine (PMP)	C ₉ H ₁₃ NO: 151	Sigma-Aldrich (St. Louis, MO, USA)	5.49	0.53	2.19	0.78	10.91	151 (M ⁺ , 5), 122 (100), 77 (12), 30 (26)	
6	2-(4-(2-Aminoethyl)-2,5-dimethoxy phenylthio)ethanol (2C-T-2-OH)	C ₁₂ H ₁₉ NO ₃ S: 257	Extraction	5.78	0.56	14.39	5.10	18.57	257 (M ⁺ , 25), 228 (100), 183 (30), 153 (47), 30 (36)	

Table 1 (Continued)

No.	Chemical name (abbreviated name)	Formula: molecular weight	Origin	HPLC-I (k') ^a	HPLC-I $k'/k'(IS)$	HPLC-II k'	HPLC $k'/k'(IS)$	GC (t_R , min)	EI-MS (m/z , %)	Structures
7	2-(3,4-Dimethoxyphenyl)ethylamine (DMPEA)	C ₁₀ H ₁₅ NO ₂ : 181	TCI (Tokyo, Japan)	6.09	0.59	1.96	0.70	13.89	181 (M ⁺ , 12), 152 (100), 137 (22), 107 (12), 30 (17)	
8	2-(3,4-Dimethoxyphenyl)- <i>N</i> -methylethylamine (<i>N</i> -Me-DMPEA)	C ₁₁ H ₁₇ NO ₂ : 195	TCI (Tokyo, Japan)	7.08	0.69	2.36	0.84	14.38	195 (M ⁺ , 1), 152 (100), 137 (9), 44 (93)	
9	2-Aminopropiophenone (Cathinone)	C ₉ H ₁₁ NO: 149	Synthesis	7.56	0.74	2.05	0.73	10.56	134 (1), 105 (9), 77 (20), 51 (12), 44 (100)	
10	2-Methylamino-1-(3,4-methylene dioxypyphenyl)propan-1-one (Mlone)	C ₁₁ H ₁₃ NO ₃ : 207	Extraction	8.01	0.78	3.66	1.30	15.63	207 (M ⁺ , 1), 149 (7), 58 (100)	
11	2-(Methylamino)-1-phenylpropan-1-one (Methcathinone)	C ₁₀ H ₁₂ NO: 162	Extraction	8.68	0.85	2.56	0.91	11.06	105 (4), 77 (101), 58 (100), 30 (7)	

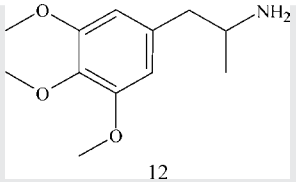
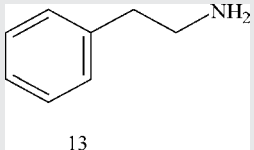
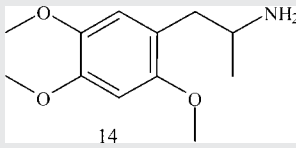
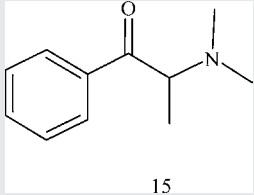
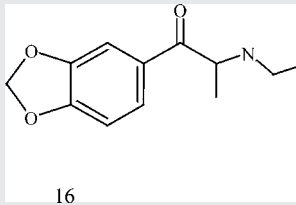
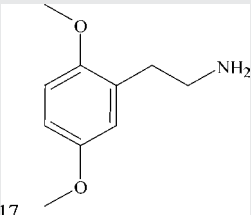
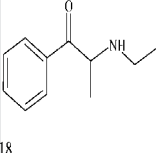
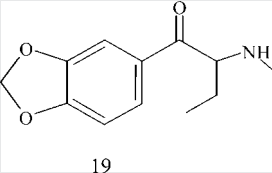
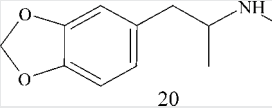
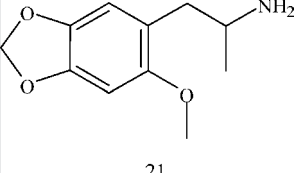
12	3,4,5-Trimethoxyamphetamine (TMA)	C ₁₂ H ₁₉ NO ₃ : 225	Extraction	8.91	0.87	3.38	1.20	15.76	225 (M ⁺ , 1), 182 (91), 167 (25), 44 (100)	
13	2-Phenylethylamine (PEA)	C ₈ H ₁₁ N: 121	Wako (Osaka, Japan)	9.12	0.89	2.11	0.75	7.63	121 (M ⁺ , 7), 91 (32), 77(4), 30 (100)	
14	2,4,5-Trimethoxyamphetamine (TMA-2)	C ₁₂ H ₁₉ NO ₃ : 225	Extraction	9.13	0.89	3.93	1.39	15.89	225 (M ⁺ , 2), 182 (100), 167 (33), 151 (12), 44 (54)	
15	2-Dimethylamino-1-phenylpropan-1-one (Dimethylcathinone)	C ₁₁ H ₁₅ NO: 177	Extraction	9.20	0.90	3.13	1.11	11.59	177 (M ⁺ , 1), 77 (8), 72 (100), 56 (4), 44 (4), 42 (5)	
16	2-Ethylamino-1-(3,4-methylenedioxyphenyl)propan-1-one (bk-MDEA)	C ₁₂ H ₁₅ NO ₃ : 221	Extraction	9.78	0.95	3.85	1.37	16.01	149 (11), 121 (10), 72 (100), 65 (13), 44 (28)	

Table 1 (Continued)

No.	Chemical name (abbreviated name)	Formula: molecular weight	Origin	HPLC-I (k') ^a	HPLC-I k'/k' (IS)	HPLC-II k'	HPLC k'/k' (IS)	GC (t_R , min)	EI-MS (m/z , %)	Structures
17	2,5-Dimethoxyphenethylamine (2C-H) ^c	C ₁₀ H ₁₅ NO ₂ : 181	Sigma–Aldrich (St. Louis, MO, USA)	10.27	1.00	2.82	1.00	13.79	181 (M ⁺ , 21), 152 (100), 137 (50), 121 (15), 30 (21)	
18	2-Ethylamino-1-phenyl-propan-1-one (Ethcathinone)	C ₁₁ H ₁₅ NO: 177	Sigma–Aldrich (St. Louis, MO, USA)	10.52	1.02	3.20	1.13	11.80	176 (1), 105 (6), 77 (13), 72 (100), 44 (29)	
19	2-Methylamino-1-(3,4-methylenedioxyphenyl)butan-1-one (bk-MBDB)	C ₁₂ H ₁₅ NO ₃ : 221	Extraction	10.70	1.04	4.50	1.60	16.11	149 (11), 121 (10), 72 (100), 65 (11), 42 (8)	
20	N-Methyl-3,4-methylenedioxy-amphetamine (MDMA)	C ₁₁ H ₁₅ NO ₂ : 193	Extraction	11.25	1.10	4.28	1.52	13.56	193 (M ⁺ , 1), 178 (1), 135 (8), 77 (7), 58 (100)	
21	1-(6-Methoxy-2H-benzo[d]1,3-dioxolan-5-yl)prop-2-ylamine (MMDA-2)	C ₁₁ H ₁₅ NO ₃ : 209	Extraction	11.53	1.12	5.00	1.77	15.22	209 (M ⁺ , 3), 167 (10), 166 (100), 165 (14), 151 (28)	

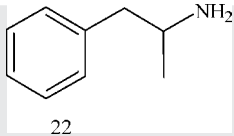
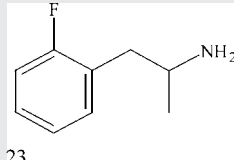
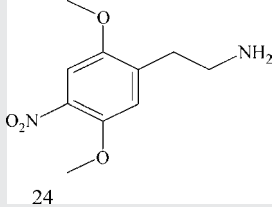
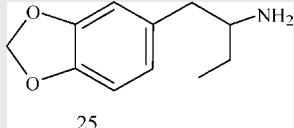
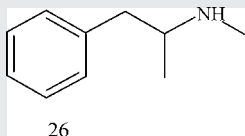
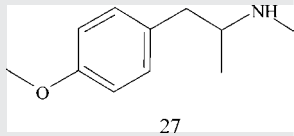
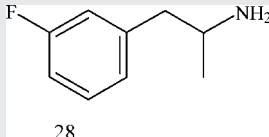
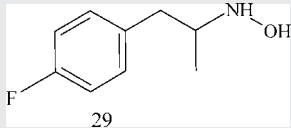
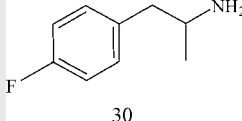
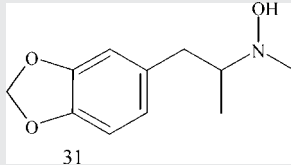
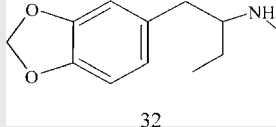
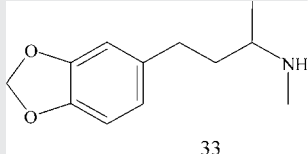
22	1-Phenylprop-2-ylamine, Amphetamine (AM)	C ₉ H ₁₃ N: 135	Extraction	11.65	1.13	3.05	1.08	8.03	134 (1), 120 (44), 91 (17), 65 (80), 44 (100)	
23	1-(2-Fluorophenyl)prop-2-ylamine (2FMP)	C ₉ H ₁₂ FN: 153	Synthesis	11.69	1.14	3.36	1.19	8.11	152 (2), 109 (30), 44 (100)	
24	2,5-Dimethoxy-4- nitrophenethylamine (2C-N)	C ₁₀ H ₁₄ N ₂ O ₄ : 226	Extraction	12.49	1.22	5.08	1.80	18.35	226 (M ⁺ , 53), 197 (100), 180 (19), 167 (31), 30 (51)	
25	2-Amino-1-(3,4-methylenedioxy phenyl)butane (BDB)	C ₁₁ H ₁₅ NO ₂ : 193	Extraction	13.25	1.29	5.11	1.81	14.22	193 (M ⁺ , 3), 136 (18), 82 (9), 77 (11), 58 (100)	
26	Methyl(1-methyl-2- phenylethyl)amine, Methamphetamine (MA)	C ₁₀ H ₁₅ N: 149	Extraction	13.27	1.29	3.90	1.38	8.87	148 (1), 134 (4), 91 (12), 65 (5), 58 (100), 30 (4)	
27	[2-(4-Methoxyphenyl)- isopropyl]methylamine (PMMA)	C ₁₁ H ₁₇ NO: 179	Extraction	13.33	1.30	1.91	0.68	12.37	179 (M ⁺ , 1), 164 (1), 121 (9), 78 (5), 58 (100)	

Table 1 (Continued)

No.	Chemical name (abbreviated name)	Formula: molecular weight	Origin	HPLC-I (<i>k'</i>) ^a	HPLC-I <i>k'/k'</i> (IS)	HPLC-II <i>k'</i>	HPLC <i>k'/k'</i> (IS)	GC (<i>t_R</i> , min)	EI-MS (<i>m/z</i> , %)	Structures
28	1-(3-Fluorophenyl)prop-2-ylamine (3FMP)	C ₉ H ₁₂ FN: 153	Synthesis	13.47	1.31	3.90	1.38	8.09	152 (2), 109 (30), 44 (100)	 28
29	4-Fluoro- <i>N</i> -hydroxyamphetamine (<i>N</i> -HO-4FMP)	C ₉ H ₁₂ FNO: 169	Extraction	13.59	1.32	3.83	1.36	8.39	152 (2), 109 (30), 44 (100)	 29
30	1-(4-Fluorophenyl)prop-2-ylamine, 4-Fluoromethamphetamine (4FMP)	C ₉ H ₁₂ FN: 153	Synthesis	13.79	1.34	3.97	1.41	8.10	152 (2), 109 (30), 44 (100)	 30
31	4-(2 <i>H</i> -Benzo[<i>d</i>]1,3-dioxolan-5-yl)- 3-methylbutan-2-ol (FLEA)	C ₁₁ H ₁₅ NO ₃ : 209	Extraction	14.17	1.38	6.34	2.25	13.52	193 (1), 135 (7), 77 (6), 58 (100),	 31
32	<i>N</i> -Methyl-1-(1,3-benzodioxol-5-yl)- 2-butanamine (MBDB)	C ₁₂ H ₁₇ NO ₂ : 207	Extraction	14.75	1.44	6.26	2.22	14.65	206 (1), 178 (4), 135 (8), 72 (100)	 32
33	3-(2 <i>H</i> -Benzo[<i>d</i>] 1,3-dioxolan-5-yl)-1- methylpropyl)methylamine (HMDMA)	C ₁₂ H ₁₇ NO ₂ : 207	Synthesis	14.88	1.45	6.93	2.46	14.93	207 (M ⁺ , 13), 176 (8), 135 (31), 77 (10), 58 (100)	 33

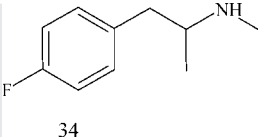
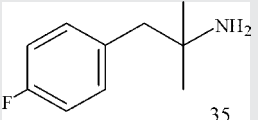
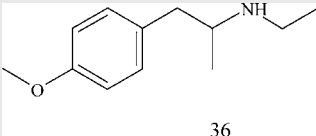
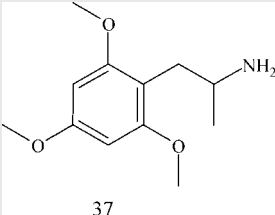
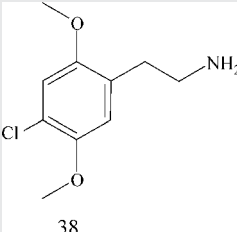
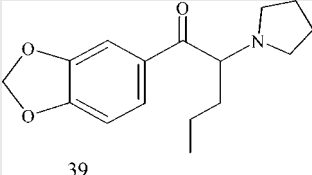
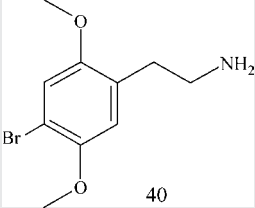
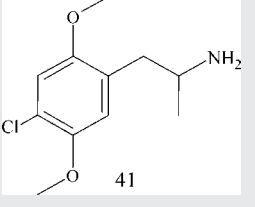
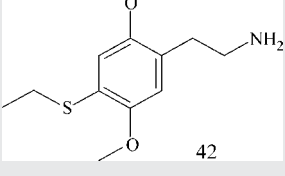
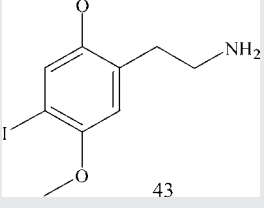
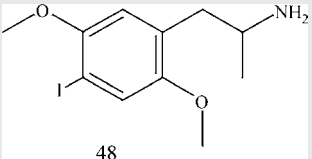
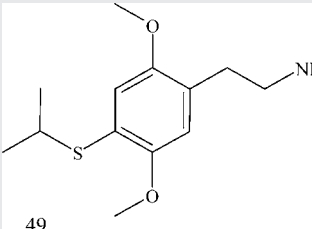
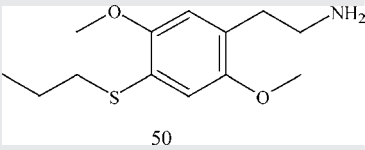
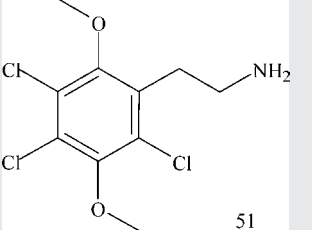
34	[2-(4-Fluorophenyl)-isopropyl]methylamine (N-Me-4FMP)	C ₁₀ H ₁₄ FN: 167	Extraction	15.17	1.48	4.31	1.53	9.09	166 (1), 109 (16), 83 (6), 58 (100), 30 (5)	
35	1-(4-Fluorophenyl)-2-methyl-2-propylamine (4F-Phentermine)	C ₁₀ H ₁₄ FN: 167	Alfa Aesar (Lancs, USA)	15.76	1.54	4.76	1.69	8.76	152 (11), 109 (20), 83 (79), 58 (100), 42(7)	
36	2-Ethylamino-1-(4-methoxyphenyl)propane (PMEA)	C ₁₂ H ₁₉ NO: 193	TCI (Tokyo, Japan)	15.83	1.54	5.78	2.05	12.97	192 (1), 178 (1), 121 (9), 72 (100), 44 (13)	
37	2,4,6-Trimethoxyamphetamine (TMA-6)	C ₁₂ H ₁₉ NO ₃ : 225	Extraction	16.52	1.61	9.41	3.34	16.28	224 (1), 182 (100), 136 (10), 121 (13), 44 (22)	
38	4-Chloro-2,5-dimethoxyphenethylamine (2C-C)	C ₁₀ H ₁₄ ClNO ₂ : 215	Extraction	16.93	1.65	1.02	0.36	15.87	215 (M ⁺ , 15), 186 (100), 171 (36)	

Table 1 (Continued)

No.	Chemical name (abbreviated name)	Formula: molecular weight	Origin	HPLC-I (k') ^a	HPLC-I $k'/k'(IS)$	HPLC-II k'	HPLC $k'/k'(IS)$	GC (t_R , min)	EI-MS (m/z , %)	Structures
39	1-(2 <i>H</i> -Benzo[d]1,3-dioxolan-5-yl)-2-pyrrolidinylpentan-1-one (MDPV)	C ₁₆ H ₂₁ NO ₃ : 275	Extraction	17.77	1.73	12.41	4.40	20.06	274 (1), 149 (3), 126 (100), 103 (1), 96 (2)	
40	4-Bromo-2,5-dimethoxyphenethylamine (2C-B)	C ₁₀ H ₁₄ BrNO ₂ : 260	Extraction ^a	17.79	1.73	0.75	0.27	16.86	260 (M ⁺ , 14), 259 (13), 232 (95), 230 (100)	
41	1-(4-Chloro-2,5-dimethoxyphenyl)prop-2-ylamine (DOC)	C ₁₁ H ₁₆ ClNO ₂ : 230	Extraction	18.77	1.83	11.91	4.22	15.98	229 (2), 186 (33), 171 (3), 44 (100)	
42	2,5-Dimethoxy-4-ethylthiophenethylamine (2C-T-2)	C ₁₂ H ₁₉ NO ₂ S: 241	Extraction	19.18	1.87	14.38	5.10	18.12	241 (M ⁺ , 34), 212 (100), 211 (51), 183 (37), 197 (18)	
43	4-Iodo-2,5-dimethoxyphenethylamine (2C-I)	C ₁₀ H ₁₄ INO ₂ : 307	Extraction	19.53	1.90	14.81	5.25	17.94	307 (M ⁺ , 14), 278 (100), 263 (18), 30(36)	

44	2-[(<i>tert</i> -Butyl)amino]-1-(3-chlorophenyl)propan-1-one (Bupropion)	C ₁₃ H ₁₈ ClNO: 239	Sigma-Aldrich (St. Louis, MO, USA)	20.29	1.98	14.29	5.07	14.45	224 (6), 111 (11), 100 (77), 57 (13), 44(100)	
45	3,4-Trimethyleneamphetamine (3,4-TMA)	C ₁₂ H ₁₇ N: 175	Extraction	20.49	2.00	14.46	5.13	12.24	131 (7), 117 (11), 115 (10), 91 (7), 44 (100)	
46	2,5-Dimethoxy-4-ethylphenethylamine (2C-E)	C ₁₂ H ₁₉ NO ₂ : 209	Extraction	20.61	2.01	15.32	5.43	15.17	209 (M ⁺ , 19), 180 (100), 165 (50)	
47	2,5-Dimethoxy-4-ethylthioamphetamine (ALEPH-2)	C ₁₃ H ₂₁ NO ₂ S: 255	Extraction	20.95	2.04	16.22	5.75	18.75	255 (M ⁺ , 3), 212 (100), 197 (14), 183 (9), 44(36)	

Table 1 (Continued)

No.	Chemical name (abbreviated name)	Formula: molecular weight	Origin	HPLC-I (k') ^a	HPLC-I $k'/k'(IS)$	HPLC-II k'	HPLC $k'/k'(IS)$	GC (t_R , min)	EI-MS (m/z , %)	Structures
48	2-(4-Iodo-2,5-dimethoxyphenyl)ethylamine (DOI)	C ₁₁ H ₁₆ INO ₂ : 321	Extraction	21.27	2.07	16.53	5.86	17.92	320 (M ⁺ , 16), 278 (56), 263 (58), 77 (68), 44 (100)	
49	2,5-Dimethoxy-4-isopropylthio phenethylamine (2C-T-4)	C ₁₃ H ₂₁ NO ₂ S: 255	Extraction	22.04	2.15	17.26	6.12	18.14	255 (M ⁺ , 41), 226 (83), 183 (100), 153 (22), 169 (20)	
50	2,5-Dimethoxy-4-propylthiophenethylamine (2C-T-7)	C ₁₃ H ₂₁ NO ₂ S: 255	Extraction	22.79	2.22	18.52	6.57	18.94	255 (M ⁺ , 33), 226 (100), 183 (50), 153 (22), 169 (21)	
51	2-(2,4,5-Trichloro-3,6-dimethoxy phenyl)ethylamine (2C-C-3)	C ₁₀ H ₁₂ Cl ₃ NO ₂ : 283	Extraction	22.85	2.23	18.08	6.41	18.39	256 (7), 254 (11), 249 (18), 247 (27), 30 (100)	

^a Capacity factor ($k' = (t_R - t_M)/t_M$), retention time (t_R), mobile phase to pass through the column (t_M), t_M of HPLC-I = 2.00 min, t_M of HPLC-II = 197 min.

^b Extraction from the products.

^c Internal standard (IS).

Table 2

Data of tryptamines

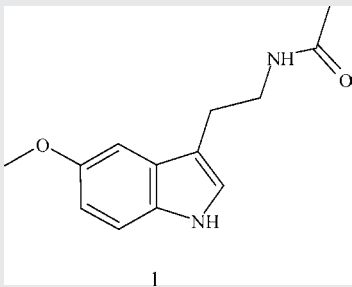
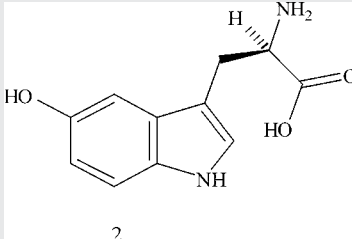
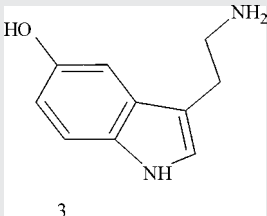
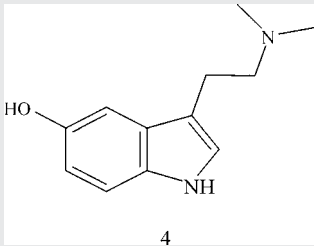
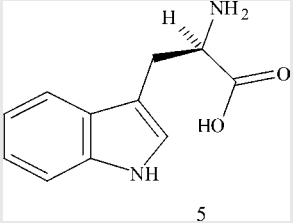
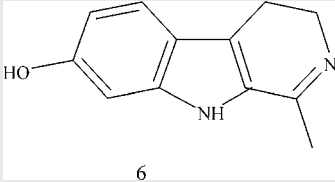
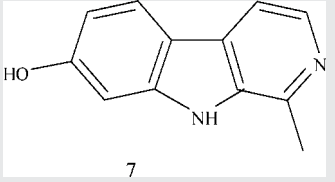
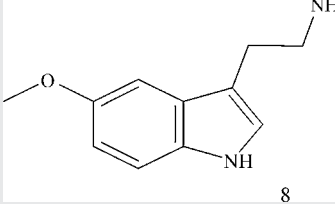
No.	Chemical name (abbreviated name)	Formula: molecular weight	Origin	HPLC-I (<i>k'</i>) ^a	HPLC-I <i>k'/k'</i> (IS)	HPLC-II (<i>k'</i>)	HPLC-II <i>k'/k'</i> (IS)	GC (<i>t_R</i> , min)	EI-MS (<i>m/z</i> , %)	Structures
1	<i>N</i> -[2-(5-Methoxyindol-3-yl)ethyl]acetamide (Melatonin)	C ₁₃ H ₁₆ N ₂ O ₂ : 232	Nacalai (Kyoto, Japan)	0.81	0.09	4.31	1.47	22.32	232 (M ⁺ , 26), 173 (100), 160 (99), 145 (23)	
2	2-Amino-3-(5-hydroxyindolin-3-yl)propanoic acid, 5-hydroxy-tryptophan (5-HO-TP)	C ₁₁ H ₁₂ N ₂ O ₃ : 220	Wako (Osaka, Japan)	2.79	0.31	0.69	0.23	-	-	
3	3-(2-Aminoethyl)indol-5-ol (5-HO-T)	C ₁₀ H ₁₂ N ₂ O: 176	Wako (Osaka, Japan)	4.12	0.46	1.06	0.36	19.29	176 (M ⁺ , 20), 146 (100), 117 (8), 91 (7)	
4	3-(2-Dimethylaminoethyl)- 1 <i>H</i> -indol-5-ol (Bufotenin)	C ₁₂ H ₁₆ N ₂ O: 204	CER (TX, USA)	4.52	0.50	2.03	0.69	17.20	204 (M ⁺ , 10), 160 (4), 146 (11), 58 (100)	

Table 2 (Continued)

No.	Chemical name (abbreviated name)	Formula: molecular weight	Origin	HPLC-I (k') ^a	HPLC-I k'/k' (IS)	HPLC-II (k')	HPLC-II k'/k' (IS)	GC (t_R , min)	EI-MS (m/z , %)	Structures
5	(2 <i>R</i>)-2-Amino-3-indol-3-ylpropanoic acid (TP)	C ₁₁ H ₁₂ N ₂ O ₂ : 204	Wako (Osaka, Japan)	5.44	0.60	1.90	0.65	–	–	
6	1-Methyl-3,4-dihydro-beta-carboline-7-ol (Hannalol)	C ₁₂ H ₁₂ N ₂ O: 200	Wako (Osaka, Japan)	6.16	0.68	3.12	1.06	21.80	200 (M ⁺ , 85), 199 (100), 172 (13), 159 (8), 91 (6)	
7	1-Methyl-beta-carboline-7-ol (Harmol)	C ₁₂ H ₁₀ N ₂ O: 198	Wako (Osaka, Japan)	6.36	0.71	3.77	1.28	22.11	198 (M ⁺ , 100), 170 (13), 115 (3), 99 (7)	
8	2-(5-Methoxyindol-3-yl)ethylamine (5MeO-T)	C ₁₁ H ₁₄ N ₂ O: 190	Wako (Osaka, Japan)	8.25	0.92	3.07	1.04	18.52	190 (M ⁺ , 27), 160 (100), 146 (12), 145 (26), 117 (15)	

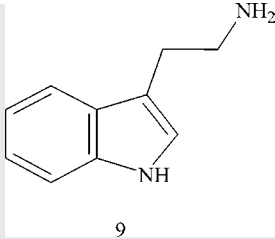
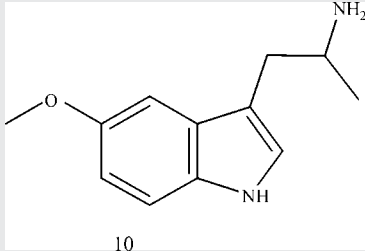
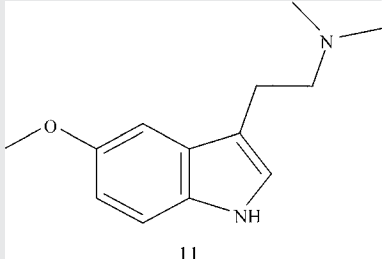
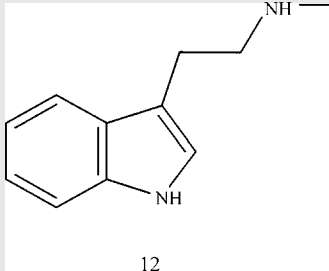
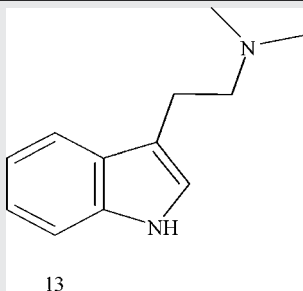
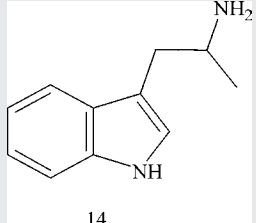
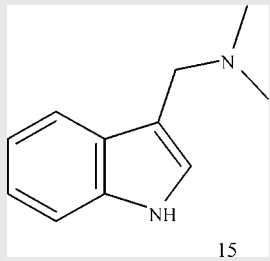
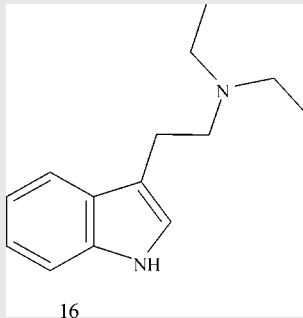
9	2-Indol-3-ylethylamine, tryptamine (T) ^c	C ₁₀ H ₁₂ N ₂ : 160	Wako (Osaka, Japan)	9.00	1.00	2.94	1.00	15.98	160 (M ⁺ , 15), 130 (100), 131 (55), 77 (11)	
10	1-(5-Methoxyindol-3-yl)prop-2-ylamine (5-MeO-AMT)	C ₁₂ H ₁₆ N ₂ O: 204	Extraction ^b	10.15	1.13	4.01	1.36	18.62	204 (M ⁺ , 4), 161 (100), 160 (44), 146 (21), 44 (34)	
11	[2-(5-Methoxyindol-3-yl)ethyl]dimethylamine (5-MeO-DMT)	C ₁₃ H ₁₈ N ₂ O: 218	Sigma-Aldrich (St. Louis, MO, USA)	10.20	1.13	4.31	1.47	18.91	218 (M ⁺ , 15), 160 (8), 145 (5), 117 (5), 58 (100)	
12	(2-Indol-3-ylethyl)methylamine (NMT)	C ₁₁ H ₁₄ N ₂ : 174	Wako (Osaka, Japan)	10.52	1.17	3.57	1.21	16.44	174 (M ⁺ , 3), 131 (100), 77 (12), 44 (54)	

Table 2 (Continued)

No.	Chemical name (abbreviated name)	Formula: molecular weight	Origin	HPLC-I (k') ^a	HPLC-I k'/k' (IS)	HPLC-II (k')	HPLC-II k'/k' (IS)	GC (t_R , min)	EI-MS (m/z , %)	Structures
13	(2-Indol-3-ylethyl)dimethylamine, dimethyltryptamine (DMT)	C ₁₂ H ₁₆ N ₂ : 188	Extraction	11.05	1.23	4.51	1.53	16.51	188 (M ⁺ , 8), 130 (9), 115 (4), 77 (4), 58 (100)	 13
14	1-Indol-3-ylprop-2-ylamine (AMT)	C ₁₁ H ₁₄ N ₂ : 174	Sigma-Aldrich (St. Louis, MO, USA)	11.28	1.25	4.10	1.39	16.26	174 (M ⁺ , 4), 131 (100), 130 (80), 77 (13), 44 (43)	 14
15	(Indol-3-ylmethyl)dimethylamine (Gramine)	C ₁₁ H ₁₄ N ₂ : 174	Wako (Osaka, Japan)	11.36	1.26	3.53	1.20	15.00	174 (M ⁺ , 22), 130 (100), 103 (7), 77 (9)	 15
16	<i>N,N</i> -Diethyltryptamine (DET)	C ₁₄ H ₂₀ N ₂ : 216	Synthesis	12.16	1.35	8.24	2.80	18.40	216 (M ⁺ , 2), 144 (6), 130 (16), 86 (100)	 16

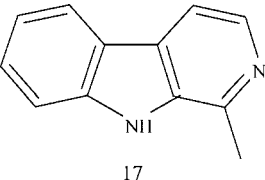
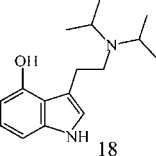
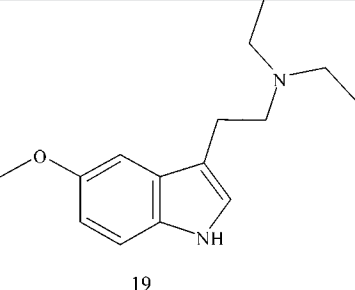
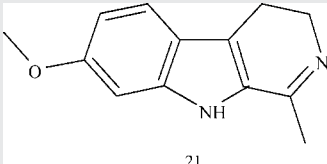
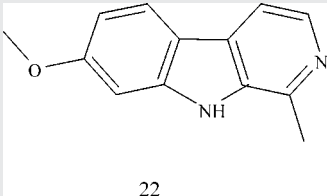
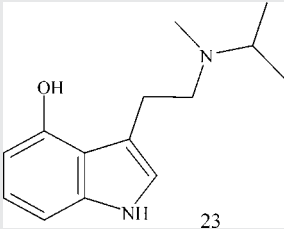
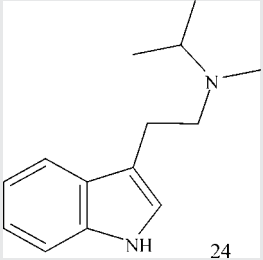
17	Methylbeta-carboline (Harman)	C ₁₂ H ₁₀ N ₂ : 182	Wako (Osaka, Japan)	12.28	1.36	6.97	2.37	18.33	182 (M ⁺ , 100), 154 (20), 127 (7), 91 (7), 77 (5)	
18	3-{2- [Bis(methylethyl)amino]ethyl} indol-4-ol (4-HO-DIPT)	C ₁₆ H ₂₄ N ₂ O: 260	Extraction	13.76	1.53	6.87	2.34	21.58	260 (M ⁺ , 11), 146 (10), 114 (100), 72 (20)	
19	Diethyl [2-(5-methoxyindol-3- yl)ethyl]amine (5-MeO-DET)	C ₁₅ H ₂₂ N ₂ O: 246	Synthesis	14.43	1.60	7.73	2.63	20.16	246 (M ⁺ , 3), 160 (4), 86 (100), 58 (5)	
20	[2-(5-Methoxyindol-3- yl)ethyl]methyl (methylethyl)amine (5-MeO-MIPT)	C ₁₅ H ₂₂ N ₂ O: 246	Extraction	14.79	1.64	7.38	2.51	20.23	246 (M ⁺ , 3), 160 (5), 117 (4), 86 (100), 44 (27)	

Table 2 (Continued)

No.	Chemical name (abbreviated name)	Formula: molecular weight	Origin	HPLC-I (k') ^a	HPLC-I k'/k' (IS)	HPLC-II (k')	HPLC-II k'/k' (IS)	GC (t_R , min)	El-MS (m/z , %)	Structures
21	7-Methoxy-1-methyl-3,4-dihydrobeta-carboline (Harmaline)	C ₁₃ H ₁₄ N ₂ O: 214	Wako (Osaka, Japan)	14.99	1.67	10.03	3.41	20.80	214 (M ⁺ , 100), 198 (24), 170 (18), 143 (7), 115 (6)	 21
22	7-Methoxy-1-methylbeta-carboline (Harmine)	C ₁₃ H ₁₂ N ₂ O: 212	Wako (Osaka, Japan)	15.01	1.67	11.69	3.98	21.06	212 (M ⁺ , 100), 197 (22), 183 (5), 169 (55), 140 (5)	 22
23	3-{2-[Methyl(methylethyl)amino]ethyl}indol-4-ol (4HO-MIPT)	C ₁₄ H ₂₀ N ₂ O: 232	Extraction	15.52	1.72	10.55	3.59	20.42	232 (M ⁺ , 21), 146 (8), 86 (100), 44 (33)	 23
24	(2-Indol-3-ylethyl)methyl(methylethyl)amine (MIPT)	C ₁₄ H ₂₀ N ₂ : 216	Synthesis	15.73	1.75	7.96	2.71	18.25	216 (M ⁺ , 26), 144 (7), 130 (9), 86 (100), 44 (24)	 24

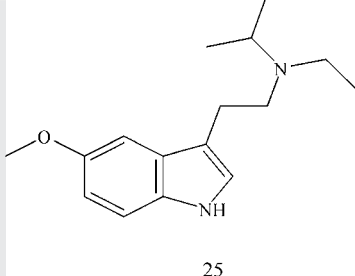
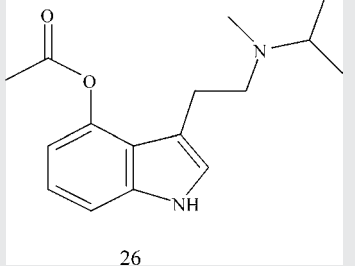
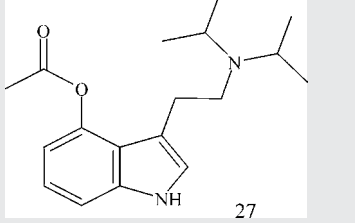
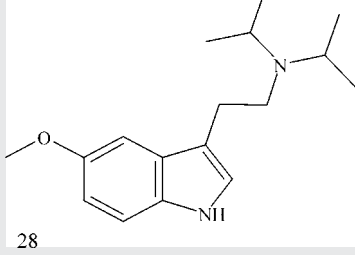
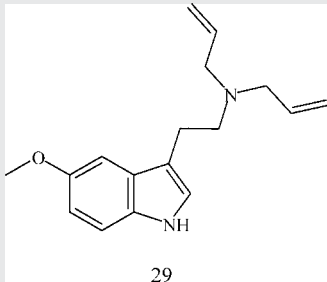
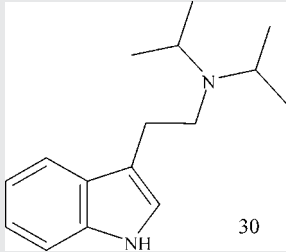
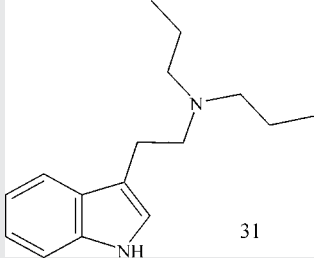
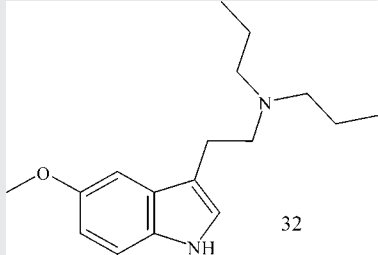
25	N-Ethyl-N-(2-(5-methoxy-1 <i>H</i> -indol-3-yl)ethyl)propan-2-amine (5-MeO-EIPT)	C ₁₆ H ₂₄ N ₂ O: 260	Extraction	16.32	1.81	9.65	3.28	20.55	260 (M ⁺ , 1), 160 (9), 117 (6), 100 (100), 58 (31)	
26	3-(2-[Methyl(methylethyl)-amino]ethyl)indo-4-yl acetate (4-AcO-MIPT)	C ₁₆ H ₂₂ N ₂ O ₂ : 274	Extraction	17.27	1.92	12.86	4.37	21.57	274 (M ⁺ , 2), 146 (5), 86 (100), 44 (23)	
27	3-(2-[Bis(methylethyl)-amino]ethyl)indol-4-yl acetate (4-AcO-DIPT)	C ₁₈ H ₂₆ N ₂ O ₂ : 302	Extraction	17.51	1.95	13.86	4.71	22.40	302 (M ⁺ , 1), 114 (100), 72 (15), 43 (5), 30 (9)	
28	Bis(methylethyl)[2-(5-methoxyindol-3-yl)ethyl]amine (5-MeO-DIPT)	C ₁₇ H ₂₆ N ₂ O: 274	Extraction	17.71	1.97	13.02	4.43	21.30	274 (M ⁺ , 1), 174 (4), 159 (22), 114 (100)	

Table 2 (Continued)

No.	Chemical name (abbreviated name)	Formula: molecular weight	Origin	HPLC-I (k') ^a	HPLC-I k'/k' (IS)	HPLC-II (k')	HPLC-II k'/k' (IS)	GC (t_R , min)	EI-MS (m/z , %)	Structures
29	[2-(5-Methoxyindol-3-yl)ethyl]diprop-2-enylamine (5-MeO-DALT)	C ₁₇ H ₂₂ N ₂ O: 270	Extraction	18.55	2.06	13.07	4.45	21.48	270 (M ⁺ , 2), 160 (8), 174 (3), 110 (100)	 29
30	Bis(methylethyl)(2-indol-3-ylethyl)amine (DIPT)	C ₁₆ H ₂₄ N ₂ : 244	Extraction	18.69	2.08	13.57	4.62	19.27	244 (M ⁺ , 1), 130 (11), 114 (100), 72 (18), 30 (7)	 30
31	(2-Indol-3-ylethyl)dipropylamine (DPT)	C ₁₆ H ₂₄ N ₂ : 244	Extraction	21.33	2.37	15.92	5.41	19.50	244 (M ⁺ , 2), 144 (7), 130 (9), 114 (100), 86 (6)	 31
32	[2-(5-Methoxyindol-3-yl)ethyl]dipropylamine (5-MeO-DPT)	C ₁₇ H ₂₆ N ₂ O: 274	Extraction	22.08	2.45	15.48	5.27	21.39	274 (M ⁺ , 1), 160 (7), 114 (100), 86 (5), 72 (4)	 32

^a Capacity factor ($k' = (t_R - t_M)/t_M$), retention time (t_R), mobile phase to pass through the column (t_M), t_M of HPLC-I = 2.00 min, t_M of HPLC-II = 1–97 min.

^b Extraction from the products.

^c Internal standard (IS).

Table 3
Data of piperazines

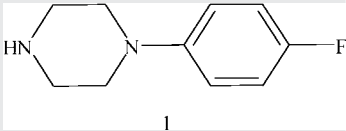
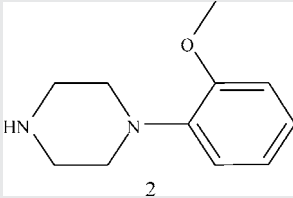
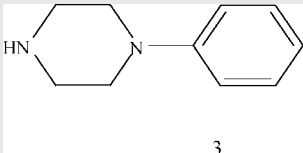
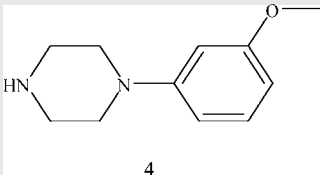
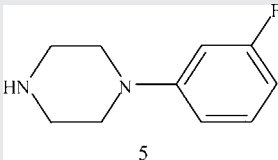
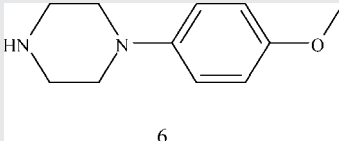
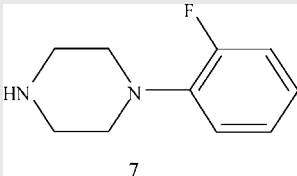
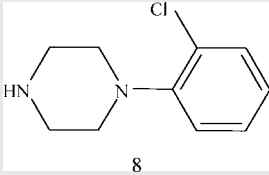
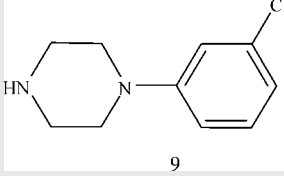
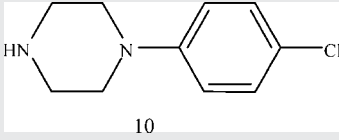
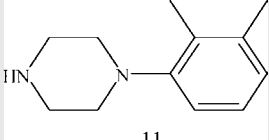
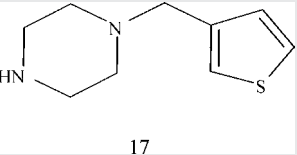
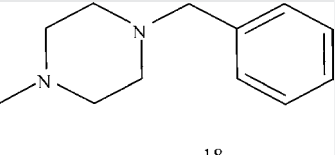
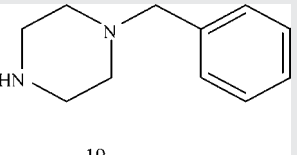
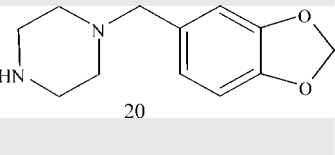
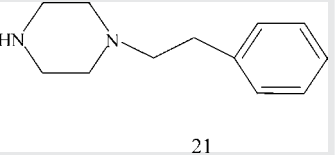
No.	Chemical name (abbreviated name)	Formula: molecular weight	Origin	HPLC-I (<i>k'</i>) ^a	HPLC-I <i>k'/k'</i> (IS)	HPLC-II (<i>k'</i>)	HPLC-II <i>k'/k'</i> (IS)	GC (<i>t_R</i> , min)	EI-MS (<i>m/z</i> , %)	Structures
1	1-(<i>p</i> -Fluorophenyl)piperazine (4FPP)	C ₁₀ H ₁₃ FN ₂ : 180	Wako (Osaka, Japan)	9.28	0.87	1.13	0.53	13.37	180 (M ⁺ , 33), 138 (100), 123 (14), 122 (17), 95 (12)	
2	1-(2-Methoxyphenyl)piperazine (2MPP)	C ₁₁ H ₁₆ N ₂ O: 192	Sigma-Aldrich (St. Louis, MO, USA)	10.69	0.98	3.07	1.22	14.85	192 (M ⁺ , 43), 150 (100), 135 (23), 134 (16), 120 (14)	
3	1-Phenylpiperazine (PP) ^b	C ₁₀ H ₁₄ N ₂ : 162	TIC (Tokyo, Japan)	11.00	1.00	2.15	1.00	13.75	162 (M ⁺ , 32), 120 (100), 104 (15), 77 (18), 56 (8)	
4	1-(3-Methoxyphenyl)piperazine (3MPP)	C ₁₁ H ₁₆ N ₂ O: 192	Sigma-Aldrich (St. Louis, MO, USA)	11.11	1.01	3.82	1.41	16.47	192 (M ⁺ , 35), 151 (10), 150 (100), 136 (59), 135 (11)	
5	1-(3-Fluorophenyl)piperazine (3FPP)	C ₁₀ H ₁₃ FN ₂ : 180	FLC (Derbyshire, UK)	11.38	1.03	4.49	1.57	13.71	180 (M ⁺ , 35), 138 (100), 123 (11), 122 (14), 95 (12)	

Table 3 (Continued)

No.	Chemical name (abbreviated name)	Formula: molecular weight	Origin	HPLC-I (k') ^a	HPLC-I k'/k' (IS)	HPLC-II (k')	HPLC-II k'/k' (IS)	GC (t_R , min)	EI-MS (m/z , %)	Structures
6	1-(4-Methoxyphenyl)piperazine (4MPP)	C ₁₁ H ₁₆ N ₂ O: 192	Sigma–Aldrich (St. Louis, MO, USA)	11.47	1.04	3.07	1.22	16.15	192 (M ⁺ , 40), 151 (10), 150 (100), 135 (14), 120 (15)	 6
7	1-(2-Fluorophenyl)piperazine (2FPP)	C ₁₀ H ₁₃ FN ₂ : 180	Wako (Osaka, Japan)	11.97	1.07	3.78	1.40	12.77	180 (M ⁺ , 34), 138 (100), 123 (11), 122 (17)	 7
8	1-(o-Chlorophenyl)piperazine (2CPP)	C ₁₀ H ₁₃ ClN ₂ : 196	Wako (Osaka, Japan)	16.81	1.45	7.20	2.23	14.64	196 (M ⁺ , 6), 161 (13), 156 (32), 154 (100), 138 (14)	 8
9	1-(3-Chlorophenyl)piperazine (3CPP)	C ₁₀ H ₁₃ ClN ₂ : 196	Wako (Osaka, Japan)	17.35	1.49	8.66	2.58	15.99	196 (M ⁺ , 29), 156 (32), 154 (100), 138 (10)	 9
10	1-(p-Chlorophenyl)piperazine (4CPP)	C ₁₀ H ₁₃ ClN ₂ : 196	Wako (Osaka, Japan)	17.45	1.50	8.84	2.62	16.04	196 (M ⁺ , 28), 156 (32), 154 (100)	 10
11	1-(2,3-Dimethylphenyl)piperazine (2 3-XP)	C ₁₂ H ₁₈ N ₂ : 190	Sigma–Aldrich (St. Louis, MO, USA)	18.64	1.59	12.52	3.52	15.26	190 (M ⁺ , 41), 148 (100), 132 (16), 117 (6)	 11

12	1-(3,4-Dimethylphenyl)piperazine (3,4-XP)	C ₁₂ H ₁₈ N ₂ : 190	Acros (New Jersey, USA)	18.68	1.59	10.30	2.98	16.25	190 (M ⁺ , 31), 148 (100), 132 (6), 105 (10)	
13	1-(3-Trifluoromethylphenyl)piperazine (4-TFMPP)	C ₁₁ H ₁₃ F ₃ N ₂ : 230	Fluka (Steinheim, BLD)	19.19	1.63	15.07	4.14	14.65	230 (M ⁺ , 25), 188 (100), 172 (13), 145 (14)	
14	1-(2,5-Dimethylphenyl)piperazine (2,5-XP)	C ₁₂ H ₁₈ N ₂ : 190	Acros (New Jersey, USA)	19.98	1.69	13.93	3.86	14.81	190 (M ⁺ , 33), 148 (100), 132 (18), 117 (8), 105 (4)	
15	1-(2,4-Dimethylphenyl)piperazine (2,4-XP)	C ₁₂ H ₁₈ N ₂ : 190	Acros (New Jersey, USA)	20.19	1.71	14.65	4.03	14.87	190 (M ⁺ , 33), 148 (100), 132 (20), 117 (6), 105 (4)	
16	1-(5-Trifluoromethylphenyl)piperazine (TFMPP)	C ₁₁ H ₁₃ F ₃ N ₂ : 230	Extraction ^c	20.37	1.72	14.26	3.94	13.53	230 (M ⁺ , 25), 189 (10), 188 (100), 172 (12), 145 (11)	

Table 3 (Continued)

No.	Chemical name (abbreviated name)	Formula: molecular weight	Origin	HPLC-I (k') ^a	HPLC-I k'/k' (IS)	HPLC-II (k')	HPLC-II k'/k' (IS)	GC (t_R , min)	EI-MS (m/z , %)	Structures
17	1-(3-Thienylmethyl)piperazine (3TMP)	C ₉ H ₁₄ N ₂ S: 182	Synthesis	22.61	1.89	1.91	0.94	13.32	182 (M ⁺ , 42), 140 (46), 97 (96), 85 (35), 56(100)	 17
18	1-Benzylmethylpiperazine (MBZP)	C ₁₂ H ₁₈ N ₂ : 190	Alfa Aesar (Lancs, UK)	24.44	2.03	2.45	1.07	13.05	190 (M ⁺ , 60), 119 (46), 99 (34), 91 (100), 56 (28)	 18
19	1-Benzylpiperazine (BZP)	C ₁₁ H ₁₆ N ₂ : 176	Sigma-Aldrich (St. Louis, MO, USA)	24.80	2.06	2.35	1.05	13.10	176 (M ⁺ , 25), 134 (80), 91 (100), 65 (11), 56 (17)	 19
20	Piperonylpiperazine (MDBZP)	C ₁₂ H ₁₆ N ₂ O ₂ : 220	Extraction	25.08	2.08	2.58	1.10	17.32	220 (M ⁺ , 24), 135 (100), 85 (15), 77 (13), 56(14)	 20
21	1-(2-Phenylethyl)piperazine (2PEP)	C ₁₂ H ₁₈ N ₂ : 190	Alfa Aesar (Lancs, UK)	26.42	2.19	3.12	1.24	15.00	190 (M ⁺ , 2), 105 (12), 99 (100), 91 (14), 70 (21), 56 (31)	 21

^a Capacity factor ($k' = (t_R - t_M)/t_M$), retention time (t_R), mobile phase to pass through the column (t_M), t_M of HPLC-I = 2.00 min, t_M of HPLC-II = 1.97 min.

^b Extraction from the products.

^c Internal standard (IS).

2.3.2. Standards

Solutions for each of the analogues were prepared by dissolving the appropriate amount in methanol to obtain a final concentration. These solutions were freshly prepared for each analysis. The analytical solution (0.05 mg/mL methanol) was used in the LC/PDA for analysis. For the IS, 2,5-dimethoxyphenethylamine (2-C-H) was used for the PEA compounds, T was used for the T compounds, and PP was used for the PP compounds. Preparation of analysis for GC/MS was same as described above.

3. Results and discussion

3.1. LC/PDA

The calculated k' ratios to the IS for each drug are shown in Tables 1–3. While PEA was chosen as the IS for the PEA compounds, however the solution was unstable at ambient temperature, thus we decided to use the commercially available 2-C-H to be the more stable IS.

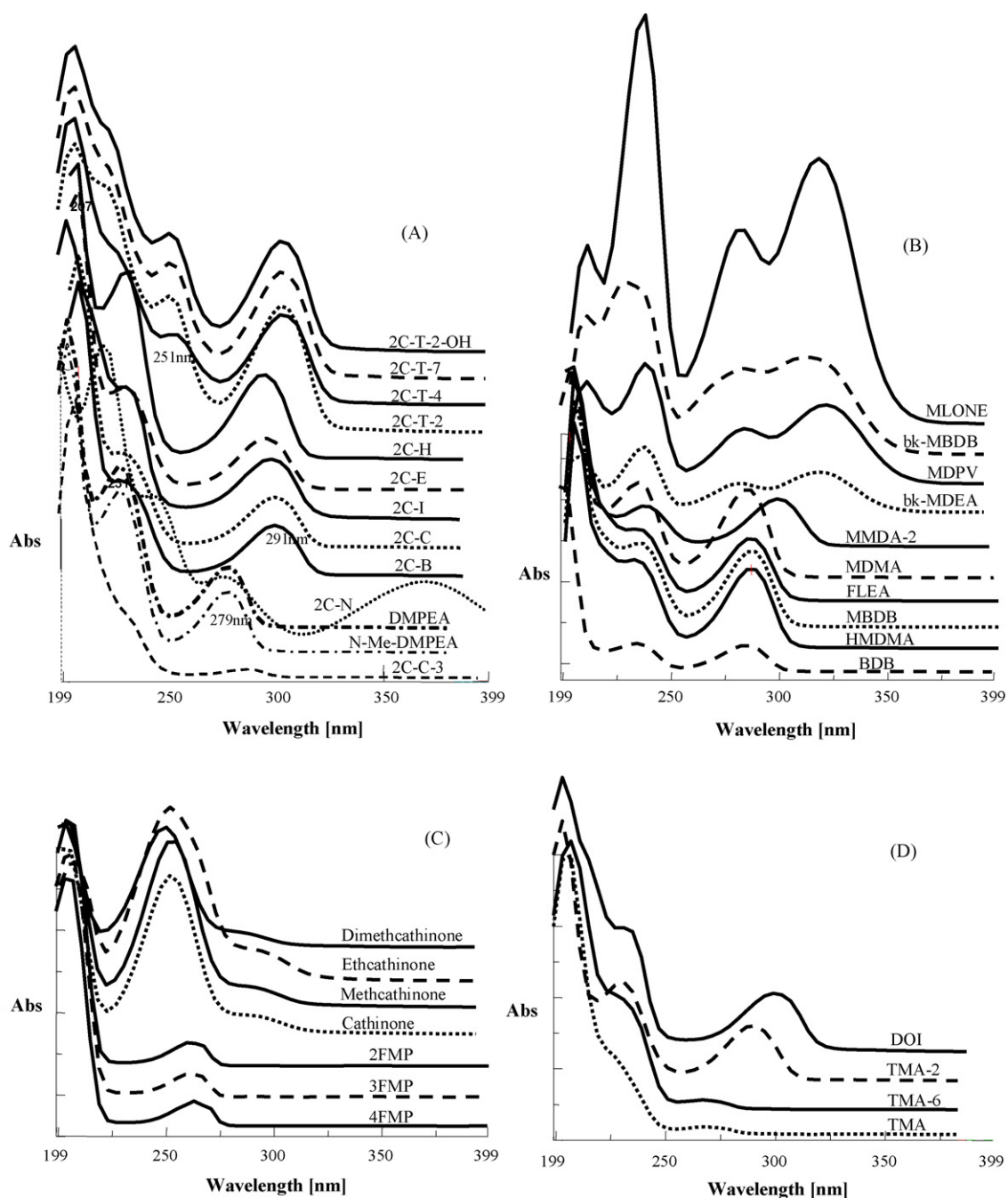


Fig. 2. UV spectra of phenylethylamines.

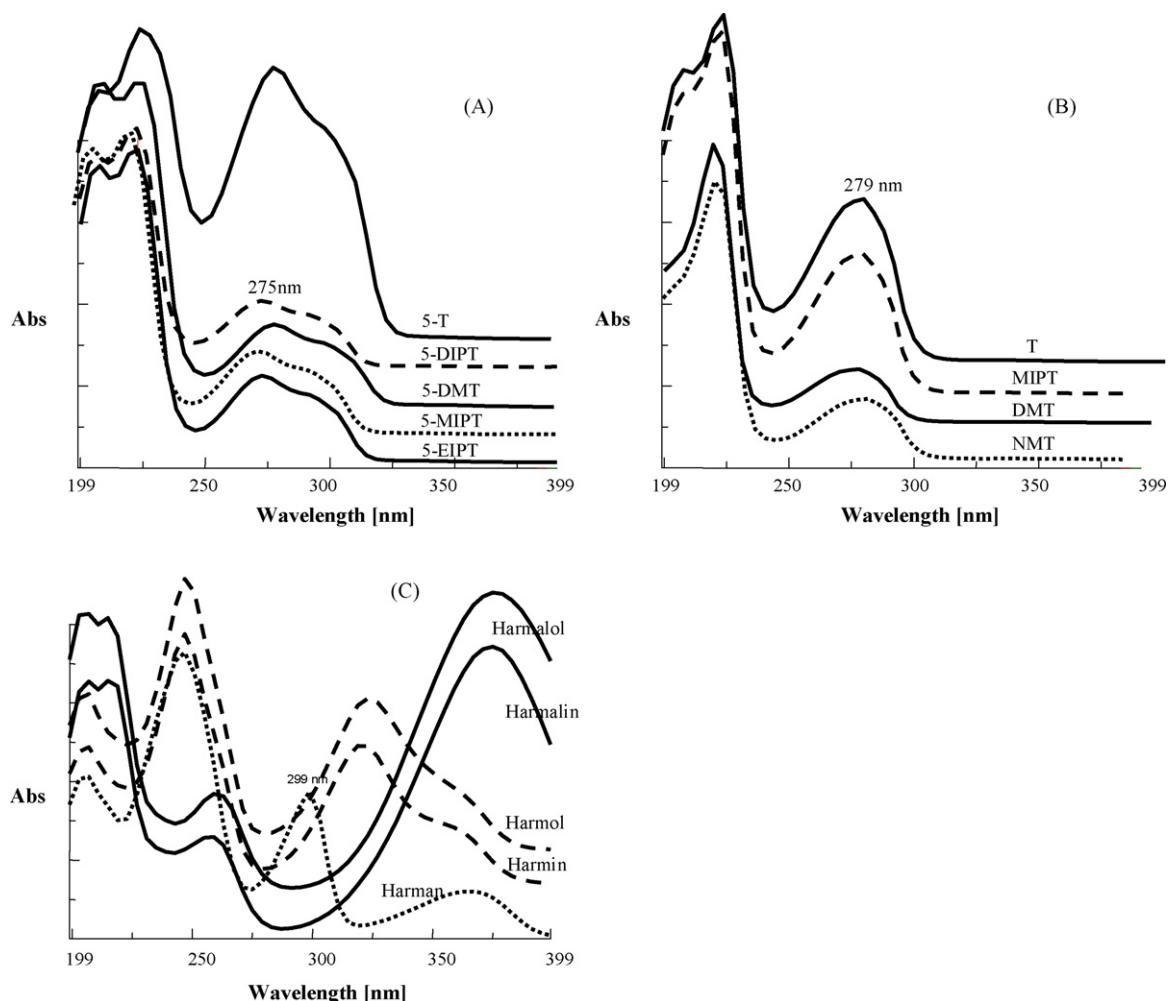


Fig. 3. UV spectra of tryptamines.

Though there were no particular characteristics of the types of compounds in terms of the k' , under these conditions, k' of the PP compounds showed 9.2 or more, respectively.

Under the HPLC conditions, sulfonic acid-based ion pair reagent was used in the mobile phase. However, this reagent was unsuitable for use in the analysis with LC/MS during performing a study; we therefore used an easily volatilized PFFA-4 ion pair reagent. Favorable results were obtained when using the gradient separation method with a 5-mM/L PFFA-4 water solution/acetonitrile mixture. Table 1 shows the results as well as the k' obtained by both LC conditions. Tables 2 and 3 also show results for both LC conditions.

The reproducibility of the peak separation was better for the SDS mixture than it was for the PFFA-4 mixture. In addition, since about more 15 min were required for the column equilibration in the latter condition after the completion of one cycle of analysis and moving to the next analysis, the entire analysis period was longer than 50 min.

3.2. UV spectra (Figs. 2–4)

PEA compounds were further classified into four types as shown, respectively, in Fig. 2A–D. Fig. 2A shows compounds in which the 4th position of the 2,5-dimethoxy-PEA was substituted with an ethyl group (2,5-dimethoxy-4-ethylphenethylamine (2C-E)), a thioethyl group (2C-T-2), or a chlorine group (4-chloro-2,5-dimethoxyphenethylamine (2C-C)), and the characteristic

spectra for these compounds showed absorption maxima near 205, 250 and 300 nm, respectively. However, when the substitution group for the 4th position was Cl, Br or I, the absorption maxima shifted to a shorter wavelength by 10–20 nm. 2-(2,4,5-Trichloro-3,6-dimethoxy phenyl)ethylamine (2C-C-3) and 2,5-dimethoxy-4-nitrophenethylamine (2C-N) showed specific absorption spectra, as shown in Fig. 2A. Fig. 2B shows *N*-methyl-3,4-methylenedioxy-amphetamine (MDMA)-analogous drugs such as PEA and phenylpropylamine, where they have a 3,4-methylenedioxy group, and these compounds characteristically showed absorption maxima near 207, 235, and 280 nm, respectively. Further, 2-methylamino-1-(3,4-methylene dioxypheyl)propan-1-one (Mlone), 1-(2*H*-benzo[*d*]1,3-dioxolan-5-yl)-2-pyrrolidinylpentan-1-one (MDPV), 2-methylamino-1-(3,4-methylenedioxy phenyl)butan-1-one (bk-MBDB) and 2-ethylamino-1-(3,4-methylenedioxy phenyl)propan-1-one (bk-MDEA), which also have a ketone group, showed another absorption maximum at 320 nm. Fig. 2C shows compounds in which the α position has been substituted to a methyl group, such as the case of stimulant amphetamine (AM) and the narcotic cathinone, where these compounds showed absorption maxima near 204 and 250 nm, respectively. However, as shown in Fig. 2C, the UV spectra for 1-(2-fluorophenyl)prop-2-ylamine (2FMP), 1-(3-fluorophenyl)prop-2-ylamine (3FMP) and 1-(4-fluorophenyl)prop-2-ylamine (4FMP), in which the phenyl group has been substituted by fluorine (F), were shifted to longer

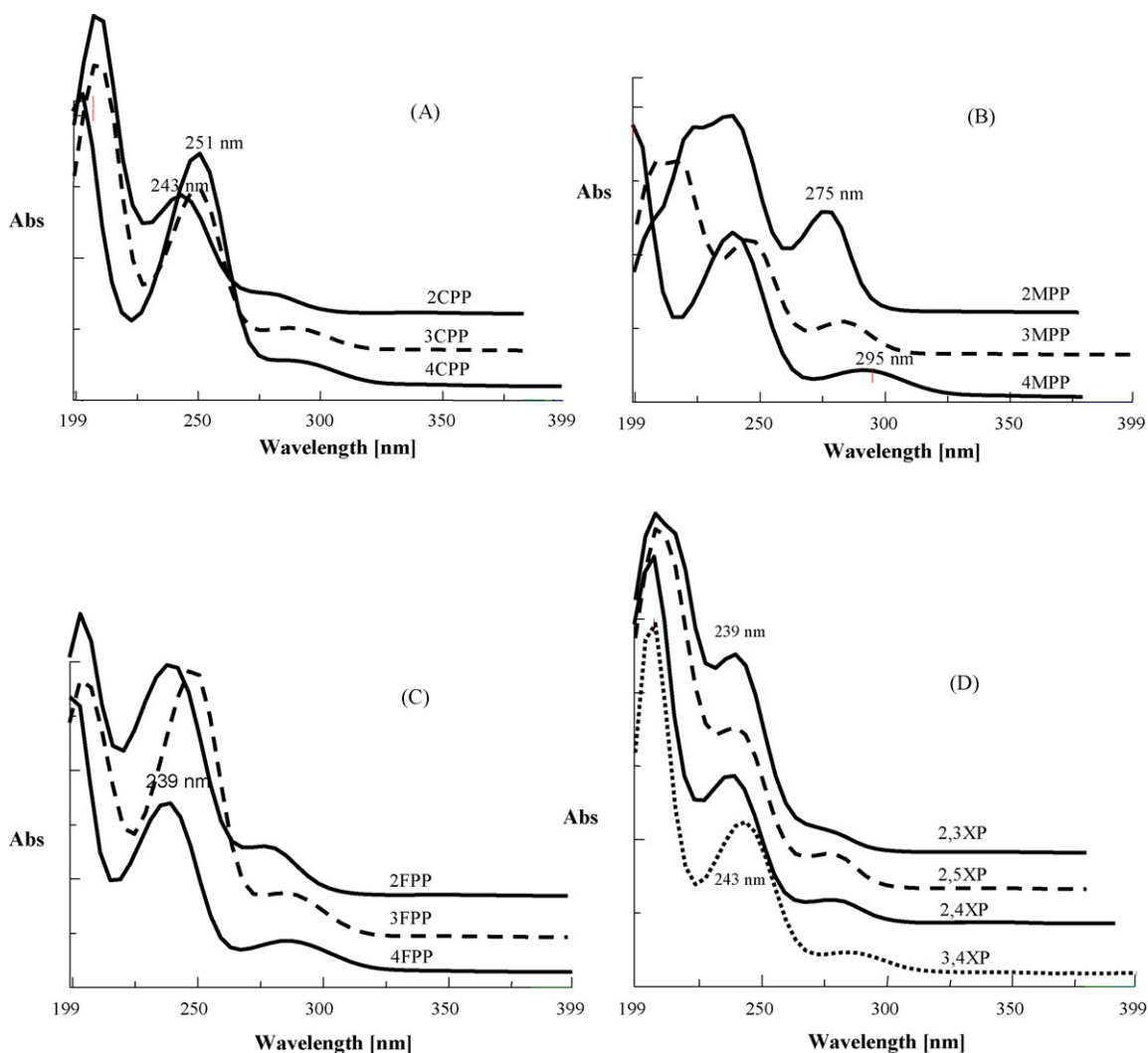


Fig. 4. UV spectra of piperazines.

wavelength, with absorption maxima near 207 and 263 nm, respectively. Furthermore, Fig. 2D shows compounds such as TMA or 2-(4-iodo-2,5-dimethoxyphenyl)ethylamine (DOI), in which there have been substitutions at three positions of the phenyl group in AM. These compounds showed absorption maxima near 203, 231 and 291 nm, respectively. When compared the obtained UV spectra for TMA, TMA-2 and TMA-6, where they are positional isomers with the different substituted methoxyl group, both TMA and TMA-6 showed no absorption near 290 nm, while TMA-2 showed similar spectra to DOI. Differentiation between the isomers is possible due to their different k' .

Tryptamine compounds (Fig. 3A–C), 5-methoxytryptamine compounds (Fig. 3A) in which a methoxyl group has been added to the 5th position of the indole skeleton showed absorption maxima near 207, 223 and 275 nm. Fig. 3B shows the spectra for the compounds in which no methoxyl group has been added. These were similar spectra, in which the absorption maxima have been shifted approximately 4 nm to the longer wavelength side. The five components contained in *Harmala* showed spectra that were different from those of the other tryptamine compounds (Fig. 3C). Though harmaline and harmalol, which have a single benzene ring, showed the same spectra, while the k' were different to be 14.99 and 6.16, respectively.

Piperazine compounds (Fig. 4A–D) showed absorption maxima at three locations: 207, 251 and 295 nm.

3CPP and 4CPP showed absorption maxima near 207 and 251 nm, respectively, while 2CPP showed maxima at the 10 nm shift to the lower wavelength side. The k' of these compounds were 17.35, 17.45, and 16.81, respectively, indicating that the differentiation between 3CPP and 4CPP would be difficult. 1-(2-Methoxyphenyl)piperazine (2MPP), 1-(3-methoxyphenyl)piperazine (3MPP) and 4MPP, which they are positional isomers showed different spectra (Fig. 4B). 1-(2-Fluorophenyl)piperazine (2FPP) and 1-(*p*-fluorophenyl)piperazine (4FPP) showed the same spectra (Fig. 4C), while the k' were different to be 11.97 and 9.28, respectively. 1-(2,3-Dimethylphenyl)piperazine (2,3XP), 1-(2,5-dimethylphenyl)piperazine (2,5XP) and 1-(2,4-dimethylphenyl)piperazine (2,4XP) showed absorption maxima near 207 and 239 nm (Fig. 4D), respectively, while the k' of these compounds were 18.64, 19.98, and 20.19, respectively, indicating that the differentiation between 2,5XP and 2,4XP would be difficult.

3.3. GC analysis

Using the experimental conditions noted in the section of the analysis methods, it was possible to detect peaks between 8 and 20 min for the PEA compounds, between 16 and 23 min for the T compounds, and between 13 and 17 min for the PP compounds.

In terms of the EI/MS spectra, the fragment ion due to N- β cleavage of both PEA and T compounds having amino groups on the side branches, were the base ions [1]. Each Table shows the other fragment ions used as indicators. As there was mostly no molecular ion peak (M^+) for the drugs that contained a hydroxyl group, it will be necessary to study further by derivatizing these compounds using trifluoroacetyl (TFA) or trimethylsilyl (TMS) as reported in the literatures [18–20].

4. Analysis of commercial products

From April 2005 to March 2008, 205 commercial products were purchased at adult shops located in Tokyo or via the Internet and were subsequently examined their components by the present methods. In the purchased products, we were able to detect 26 PEA-related compounds, 12 T-related compounds and 4 PP-related compounds, as listed in Table 4.

Table 4
The compounds detected in the 205 samples

Compound number	Detected compounds	Number of detection
Number of phenylethylamines in Table 1		
6	2C-T-2-OH	1
10	Mlone	25
13	PEA	2
14	TMA-2	4
16	bk-MDEA	1
18	Ethcathinone	1
20	MDMA	1
21	MMDA-2	2
25	BDB	4
27	PMMA	3
29	N-HO-4FMP	1
30	4FMP	8
31	FLEA	3
32	MBDB	2
34	N-Me-4FMP	3
37	TMA-6	4
38	2C-C	3
39	MDPV	1
41	DOC	1
42	2C-T-2	2
43	2C-I	4
46	2C-E	1
47	ALEPH-2	1
49	2C-T-4	3
50	2C-T-7	2
51	2C-C-3	2
Number of tryptamines in Table 2		
3	5-HO-T	1
10	5-MeO-AMT	7
11	5-MeO-DMT	7
18	4-HO-DIPT	9
20	5-MeO-MIPT	22
25	5-MeO-EIPT	2
26	4-AcO-MIPT	1
27	4-AcO-DIPT	9
28	5-MeO-DIPT	5
29	5-MeO-DALT	5
31	DPT	2
32	5-MeO-DPT	2
Number of piperazines in Table 3		
6	4MPP	2
9	CPP	4
18	MBZP	4
20	MDBZP	1
	Total	168

5. Conclusions

In order to quickly confirm a potentially hazardous psychoactive designer drug, we created a library by performing simultaneous analysis using LC/PDA and GC/EI/MS and then analyzed the obtained data. The data shown in this library consist of the UV spectra, the HPLC k' in relation to the IS, and the MS spectra for 104 types of drugs. We were able to quickly confirm psychoactive designer drugs by applying this data library to the analysis of purchased products. Even in the case of positional isomers, it is possible to perform a comparative study and differentiate the compounds by combining information such as the UV, k' , MS spectra and the GC retention times. Furthermore, it is possible to analogize the structure of drugs even when there is no reference standard available by targeting the range for the k' and MS spectra, and then performing a high-precision search of the library. The ability to perform quick confirmation of compounds using this library will be useful in publicizing dangers of psychoactive designer drugs.

Acknowledgment

This work was partly supported by a “High-Tech Research Center” Project for Private Universities: matching fund subsidy from MEXT (Ministry of Education, Culture, Sports, Science and Technology) 2006(7)–2008(9).

References

- [1] B.-H. Chen, J.-T. Liu, W.-X. Chen, H.-M. Chen, C.-H. Lin, *Talanta* 74 (2008) 512.
- [2] T. Ishida, K. Kudo, A. Kiyoshima, H. Inoue, A. Tsuji, N. Ikeda, *J. Chromatogr. B* 823 (2005) 47.
- [3] D.S. Theobald, S. Fehn, H.H. Maurer, *J. Mass Spectrom.* 40 (2005) 105.
- [4] L.F. Martins, M. Yagles, H. Chung, R. Wennig, *J. Chromatogr. B* 842 (2006) 98.
- [5] R. Kikura-Hanajiri, M. Hayashi, K. Saisho, Y. Goda, *J. Chromatogr. B* 825 (2005) 29.
- [6] S.D. Brandt, S. Freeman, I.A. Fleet, P. McGagh, J.F. Alder, *Analyst* 130 (2005) 330.
- [7] R. Gottardo, F. Bortolotti, G. de Paoil, J.P. Pascali, *J. Chromatogr. A* 1159 (2007) 185.
- [8] T. Matsumoto, R. Kikura-Hanajiri, H. Kamakura, N. Kawahara, Y. Goda, *J. Health Sci.* 52 (2006) 805.
- [9] T.K. Spratley, P.A. Hays, L.C. Geer, S.D. Cooper, T.D. McKibben, *Microgram J.* 3 (2005) 54.
- [10] K. Doi, M. Miyazawa, H. Fujii, T. Kojima, *Yakugaku Zasshi* 126 (2006) 815.
- [11] M.M. Zimmerman, *Microgram J.* 1 (2003) 158.
- [12] D. de Boer, I. Bosman, *Pharm. World Sci.* 26 (2004) 110.
- [13] A.T. Shulgin, A. Shulgin, *TiHKAL The Continuation*, Transform Press, Berkeley, CA, 1997.
- [14] A.T. Shulgin, A. Shulgin, *PiHKAL A Chemical Love Story*, Transform Press, Berkeley, CA, 1991.
- [15] M. Takahashi, M. Nagashima, J. Suzuki, T. Seto, I. Yasuda, T. Yoshida, *J. Health Sci.* 54 (2008) 1.
- [16] T. Seto, M. Takahashi, M. Nagashima, J. Suzuki, I. Yasuda, *Ann. Rep. Tokyo Metr. Inst. P.H.* 56 (2005), 75.
- [17] *Japan Pharmacopoeia with commentary*, 15th Ed., Hirokawa Publishing Co., Inc., Tokyo, 2006, B-15.
- [18] G. Frison, L. Tedeschi, D. Favretto, A. Rehemann, S.D. Ferrara, *Rapid Commun. Mass Spectrom.* 19 (2005) 919.
- [19] S. Lee, Y. Park, W. Yang, E. Han, S. Choe, S. In, M. Lim, H. Chung, *J. Chromatogr. B* 865 (2008) 33.
- [20] K. Zaitso, M. Katagi, H. Kamata, T. Kamata, N. Shima, A. Miki, T. Iwamura, H. Tsuchihashi, *J. Mass Spectrom.* 43 (2008) 528.



Ultra-sensitive hydrazine chemical sensor based on high-aspect-ratio ZnO nanowires

Ahmad Umar, M.M. Rahman, Yoon-Bong Hahn*

School of Semiconductor and Chemical Engineering, BK21 Centre for Future Energy Materials and Devices and Nanomaterials Processing Research Centre, Chonbuk National University, Jeonju 561-756, South Korea

ARTICLE INFO

Article history:

Received 6 August 2008

Received in revised form 8 September 2008

Accepted 10 September 2008

Available online 19 September 2008

PACS:

62.23.Hj

82.45.Yz

87.85.Rs

81.05.Dz

81.07.-b

81.10.Bk

Keywords:

ZnO nanowires

Hydrazine sensors

Amperometric sensors

ABSTRACT

High-aspect-ratio ZnO nanowires based ultra-sensitive hydrazine amperometric sensor has been fabricated which showed a high and reproducible sensitivity of $12.76 \mu\text{A cm}^{-2} \text{nM}^{-1}$, detection limit, based on S/N ratio, 84.7 nM, response time less than 5 s, linear range from 500 to 1200 nM and correlation coefficient of $R=0.9989$. This is the first report in which such a very high-sensitivity and low detection limit has been achieved for the hydrazine sensors by using ZnO nanostructures modified electrodes. Therefore, this work opens a way to utilize simply grown ZnO nanostructures as an efficient electron mediator to fabricate efficient hydrazine sensors.

© 2008 Elsevier B.V. All rights reserved.

1. Introduction

Due to high industrial, pharmacological, military and aerospace applications, the detection of hydrazine has attracted considerable analytical interests. Hydrazine is widely used as catalyst, emulsifier, corrosion inhibitor, reducing agent, antioxidant, photographic developer, pesticide and insecticide, plants growth regulator, etc. [1,2]. Hydrazine is a neurotoxin, therefore it produces carcinogenic and mutagenic effects which causes the damages to lungs, liver, kidneys, respiratory tract infection and long-term effects on the central nervous system [3]. Moreover, it is widely used in high-energy propellants in rockets and spacecrafts by military and aerospace industries, missile systems, weapons for mass destruction and fuel cells [4]. It is therefore obvious that reliable and sensitive analytical methods for the determination of hydrazine are needed. Among various detection methods, the electrochem-

ical method offers a portable, cheap and rapid method for the determination of hydrazine. Hitherto, various modified electrodes have been developed and used for the detection of hydrazine by using electrochemical method [5–11]. Due to extraordinary properties of ZnO such as biocompatibility, non-toxicity, chemical and photochemical stability, higher-specific-surface area, high-electron communication features, electrochemical activities, and so on, we have recently reported the ZnO nanostructures based electrochemical sensors [11,12]. Recently, we fabricated, for the first time, the hydrazine sensor based on ZnO nanonails grown by thermal evaporation process. However, the sensitivity and detection limit of the previously fabricated sensor was as low as of $8.56 \mu\text{A cm}^{-2} \mu\text{M}^{-1}$ and $0.2 \mu\text{M}$, respectively.

In this paper, we are reporting an ultra-sensitive hydrazine amperometric sensor based on high-aspect-ratio ZnO nanowires. The fabricated sensor showed a very high and reproducible sensitivity of $12.76 \mu\text{A cm}^{-2} \text{nM}^{-1}$ with the detection limit of 84.7 nM. Moreover, to the best of our knowledge, this is the first time such a very high-sensitivity and low-detection limit has been achieved for the hydrazine sensors by using ZnO nanostructured modified electrodes.

* Corresponding author. Fax: +82 63 270 2306.

E-mail addresses: ahmadumar@chonbuk.ac.kr (A. Umar), ybhahn@chonbuk.ac.kr (Y.-B. Hahn).

2. Experimental details

The growth of high-aspect-ratio ZnO nanowires assembled in urchin-like morphologies was performed in a horizontal quartz tube furnace [13,14]. High-purity metallic zinc powder (99.999%) and oxygen was used as source materials for zinc and oxygen, respectively. Commercially available steel alloy was used as a substrate. In a typical reaction process, metallic zinc powder was put into a quartz boat and placed at the left hand side of centre of furnace. The substrate was placed adjacent to the source material. Before starting the reaction, the substrate was pre-treated by the mixture of H₂ and N₂ gases (1:1 ratio) for 20 min at 450 °C. After pre-treatment, the furnace was heated to 550 °C with continuous introduction of high-purity oxygen (300 sccm) and nitrogen (200 sccm) gases to facilitate the growth of high-aspect-ratio ZnO nanowires assembled in urchin-like morphologies. The reaction lasted for 60 min. After terminating the reaction, the furnace was cooled to room-temperature under the continuous flow of high-purity argon gas (100 sccm) and finally gray colored products were deposited onto the steel alloy substrate.

To fabricate the hydrazine amperometric sensor, the as-grown high-aspect-ratio ZnO nanowires were coated onto the surface of a gold (Au) electrode with the area of 2.0 mm². Prior to the modification, the gold electrode was polished with the 0.05 μm alumina slurry and then sonicated in de-ionized water. The prepared ZnO nanowires/Au electrode was wetted by phosphate buffer solution (PBS) with pH 7.4 and dried gently by the high purity nitrogen gas. After drying the modified ZnO/Au electrode, a 5 wt% (5 μl) Nafion solution was dropped onto the electrode and dried for 24 h at 4 °C to form a net-like film which is important to tightly attach the ZnO nanowires on the surface of the electrode. For the amperometric experiments, aliquots of hydrazine (from 500 nM to 1.4 μM) were injected into the stirred electrolyte solution and each addition of hydrazine resulted in a rapid increase in the current. When not in use, the ZnO-modified gold electrodes (i.e., Nafion/ZnO/Au electrodes) were stored in PBS (pH 7.4) at 4 °C. The electrochemical experiments were carried out at room-temperature using an electrochemical analyzer (SHIn 2000, EQCM, Korea) with a conventional three-electrode configuration: a working electrode (ZnO-modified Au electrode with the diameter of 2 mm), a Pt wire as a counter electrode and Ag/AgCl (sat. KCl) as a reference electrode.

3. Results and discussion

Fig. 1(a–c) shows the general morphologies of the as-grown ZnO nanowires on steel alloys substrate. It is clearly seen from the low-magnification images that the urchin-like ZnO morphologies containing high-aspect-ratio ZnO nanowires are grown in very high density over the whole substrate surface (Fig. 1(a and b)). The average diameter of a single urchin-like structure is in the range of 15–20 μm. The high-resolution FESEM image exhibit more clear features of urchin-like morphologies which clearly confirmed that these structures are made by the accumulation of numerous high-aspect-ratio ZnO nanowires (Fig. 1(c)). The high-aspect-ratio ZnO nanowires of urchin-like morphologies are radially originated from the centre in such a special manner that they form spherical like morphologies. The typical diameters of the nanowires are in the range of 80–100 nm at the head and 40–50 nm in the roots. The typical lengths of the grown ZnO nanowires are in the range of 10–12 μm, which confirms the high-aspect-ratio of the as-grown products. Fig. 1(d) exhibits the typical X-ray diffraction pattern for the as-grown high-aspect-ratio ZnO nanowires. All the observed peaks in the pattern are well matched with the reported

values of wurtzite hexagonal phase pure bulk ZnO (JCPDS Card No. 75-1526). A strongest peak at 34.2° attributed as ZnO (0002) in the pattern confirming that the as-grown nanowires are grown along the [0001] direction in preference. The inset of Fig. 1(d) exhibits the typical growth behaviour of ZnO nanowires grown in urchin-like morphologies. Even though not shown here, the EDS analysis confirms that the grown ZnO nanowires are made in a proper stoichiometric ratio of Zn and oxygen. The detailed structural characterizations was done with transmission electron microscopy (TEM) and shown in Fig. 2.

Fig. 2(a) demonstrates the low-resolution TEM image of as-grown high-aspect-ratio ZnO nanowires, which revealed the full consistency with the FESEM observations shown in Fig. 1, in terms of density and dimensionality, i.e. diameters at the top and bottom of the nanowires. The high-resolution TEM image taken from the circled portion in (a) clearly delineates the fringes of ZnO (0001) planes with the interplanar spacing of about 0.52 nm and confirms the single crystallinity with the preferential growth in the [0001] direction (Fig. 2(b)) [13,14]. The inverse Fast Fourier transformation (FFT) analysis also confirms that the synthesized nanowires are single crystalline with the wurtzite hexagonal phase and grown along the [0001] direction (Fig. 2(c)). Moreover, the corresponding SAED pattern of the grown nanowire (circled portion in Fig. 2(a)) is also consistent with the HRTEM and FFT results (Fig. 2(d)).

The cyclic voltammograms (CV) of the hydrazine sensor using high-aspect-ratio ZnO nanowires-modified gold (Nafion/ZnO/Au) electrode in a 0.01 M phosphate buffer solution (PBS) (pH 7.4) with 1 mM hydrazine (dotted line) and without hydrazine (solid line), at the scan rate of 100 mV/s, are shown in Fig. 3(a). The modified (Nafion/ZnO/Au) electrode does not show any redox peak in the potential range of –0.5 to 1.0 V. However, interestingly, it was observed that compare to Nafion/ZnO/Au electrode without hydrazine (solid line); a substantial enhancement of the anodic peak current was observed in 0.01 M PBS (dotted line) with the addition of 1 mM hydrazine.

The observed peak potential (E_{pa}) and current (I_{pa}) for the oxidation peak was 0.08 V and 0.39 μA, respectively. Moreover, the oxidation process starts around –0.45 V and the anodic peak was appeared at 0.08 V. The electrochemical response is irreversible as no cathodic current is observed during the reverse sweep. Hence, one can conclude that the ZnO is an effective mediator for the oxidation of hydrazine. Moreover, as the faster electron transfer leads to a sharper and well-defined peak, therefore substantial increase in the peak height reflects a faster electron-transfer reaction by Nafion/ZnO-modified gold electrodes.

As the amperometry under stirred conditions has a much higher current sensitivity than the cyclic voltammetry, hence the amperometric experiments have been performed under continuous stirring. A typical amperometric response of the Nafion/ZnO/Au electrode on a successive addition of hydrazine (from 500 nM to 1.4 μM) into continuously stirred 0.01 M PBS solution (pH 7.4) at an applied potential in the range of –0.5 to 0.4 V is shown in Fig. 3(c). A rapid increase in the current was noticed in the amperometric measurements after each addition of the hydrazine into the electrolyte solution.

The 95% steady state response was achieved in less than 5 s from the modified electrode, which confirms a good electrocatalytic oxidative and fast electron exchange behaviour of ZnO nanowires modified electrode. Inset of Fig. 3(c) demonstrates the relation between the response current and hydrazine concentration for the fabricated amperometric hydrazine sensor. The response current increases as the concentration of hydrazine increases, and shows linear range up to the value of 1.0 μM. Moreover, under the optimized condition, the steady-state current showed a linear relationship with the hydrazine concentration in the

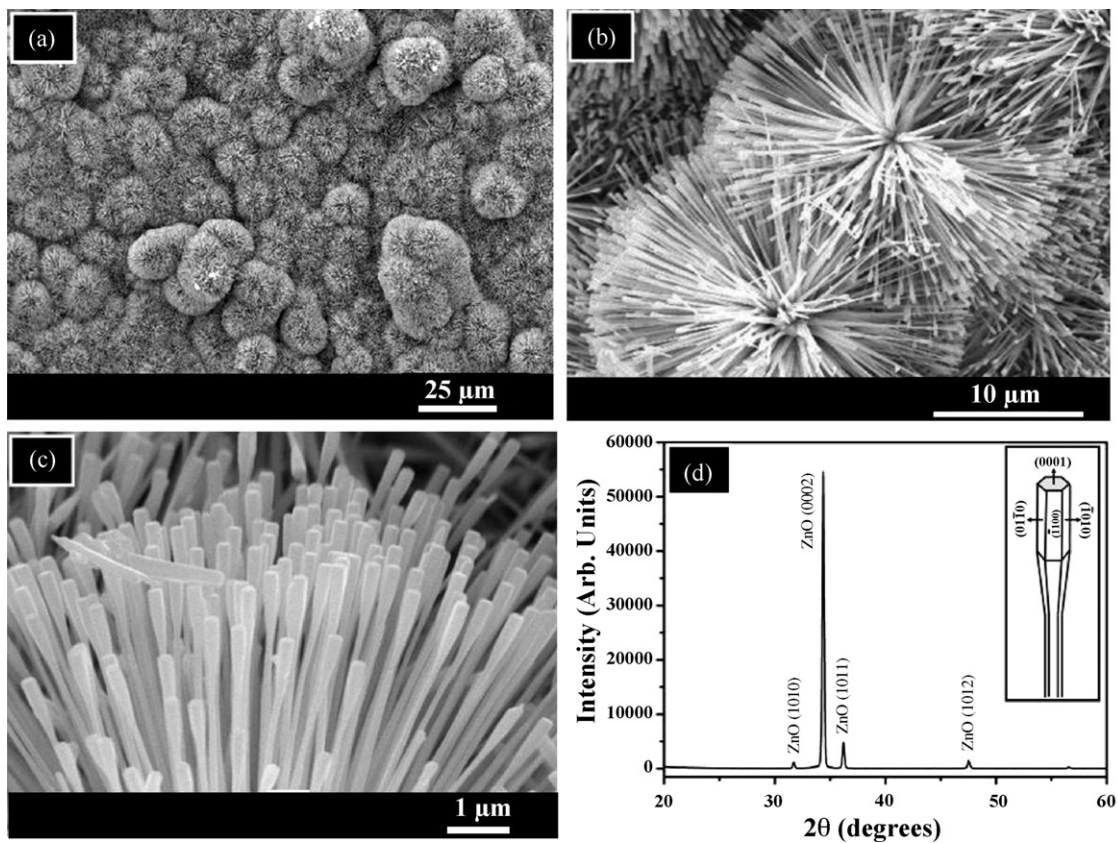


Fig. 1. (a–c) Typical FESEM images and (d) X-ray diffraction pattern of the as-grown high-aspect-ratio ZnO nanowires assembled in urchin-like structures. Inset of (d) exhibits the schematic growth habit of as-synthesized ZnO nanowires.

range of 500–1200 nM (Fig. 3(d)). The correlation coefficient (R) was estimated to be $R=0.9989$. The sensitivity of the fabricated hydrazine sensor, from the slope of calibration curve, was found to be $12.76 \mu\text{A cm}^{-2} \text{nM}^{-1}$. Moreover, the detection limit, estimated

based on signal to noise ratio (S/N), was found to be 84.7 nM ($0.0847 \mu\text{M}$). To the best of our knowledge, this is the first time such a very high-sensitivity and low detection limit has been achieved for hydrazine sensors by using ZnO nanostructures modified elec-

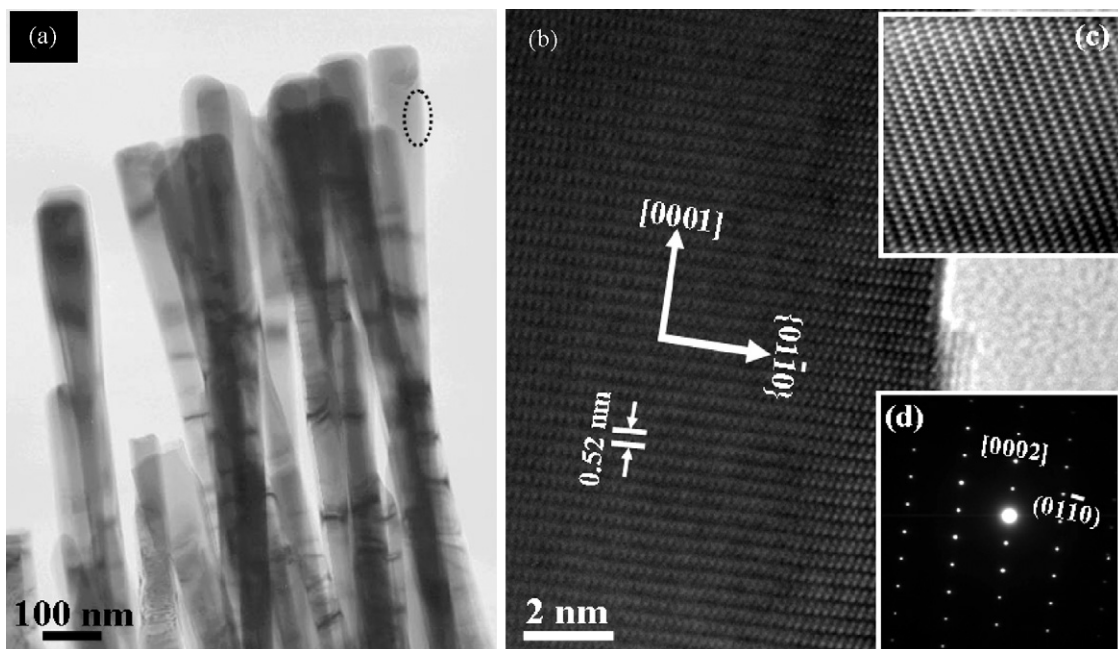


Fig. 2. Typical (a) low-magnification and (b) high-resolution, (c) inverse Fast Fourier transformation (FFT) and (d) corresponding SAED pattern of as-grown high-aspect-ratio ZnO nanowires assembled in urchin-like structures.

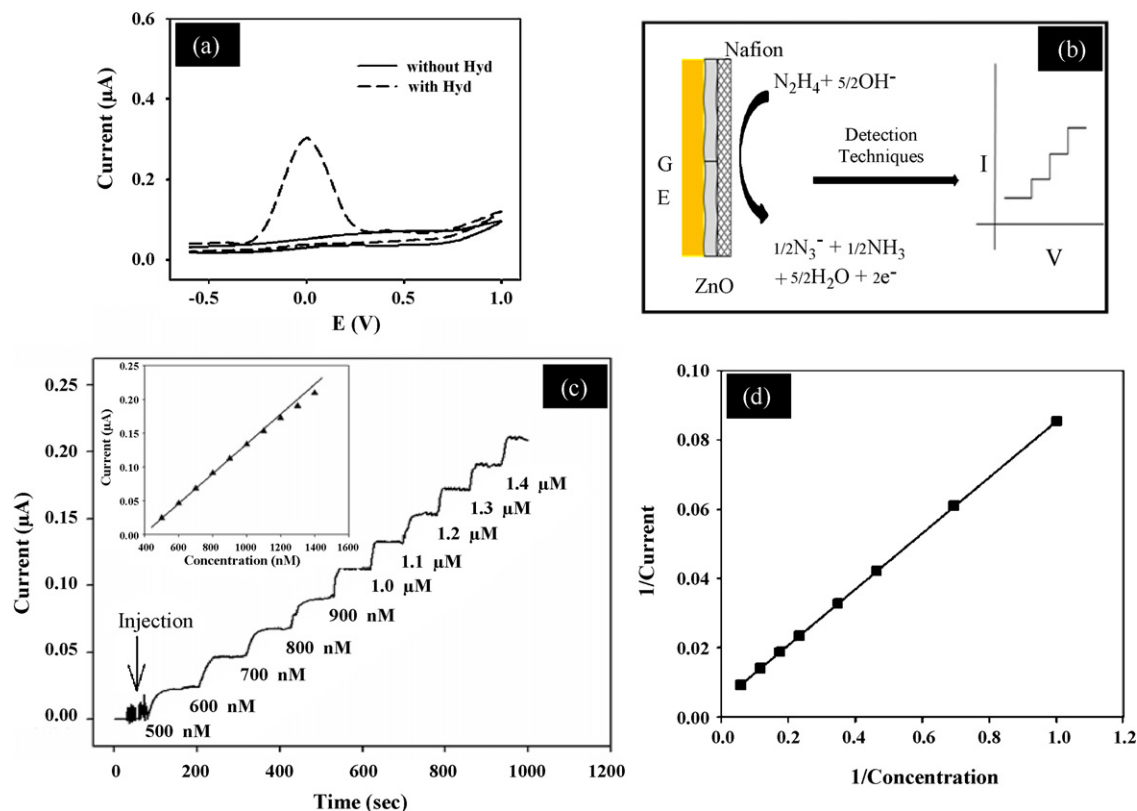


Fig. 3. (a) Cyclic voltammogram sweep curve for the Nafion/ZnO/Au electrode without hydrazine (solid line) and with 1 mM hydrazine (dotted line) in 0.01 M PBS (pH 7.4). The scan rate was 100 mV/s; (b) schematic of hydrazine detection by electrochemical method using ZnO nanowires modified gold electrode; (c) amperometric response of the Nafion/ZnO/Au electrode with successive addition of hydrazine into 0.01 M PBS buffer solution (pH 7.4). (d) The plot of 1/current vs. 1/concentration exhibiting a linear relationship with the steady state current and hydrazine concentration.

trodes. In addition to this, for comparing the characteristics and performances of the fabricated high-aspect-ratio ZnO nanowire-based hydrazine sensors, the properties of the previously reported hydrazine sensors based on the utilization of different materials as the working electrode are summarized in Table 1 which confirms that the fabricated hydrazine sensor exhibited an excellent performance. Moreover, it is also seen that the performance of the ZnO nanostructures based hydrazine sensor is also depend upon the morphologies and surface area of the nanostructures. As the high-aspect-ratio ZnO nanowires have high-surface area than the previously reported ZnO nanonails [11], hence the nanowires are exhibiting higher sensitivity and detection limit (Table 1).

The fabricated ZnO nanowires modified electrodes exhibited a good sensitivity and reproducibility and it was found that the fabricated sensors did not show any significant decrease in the sensitivity for more than 35 days, while storing in an appropriate form when not in use. The Nafion/ZnO/Au sensor was evaluated amperometrically in the presence of common electro-active compounds, such as ascorbic acid (AA), glucose (GL), uric acid (UA),

and acetaminophen (AP) and it was seen that no amperometric response was observed when 0.2 mM ascorbic acid, glucose, uric acid, and acetaminophen introduced in 0.01 M PBS (Fig. 4). Thus, the selectivity of Nafion/ZnO/Au sensor is good for hydrazine detection in the presence of common interfering compounds in normal biological systems compared to previously reported literature [15].

The proposed hydrazine sensor was tested to detect the hydrazine concentration in direct real commercial compound. The real sample was diluted 10 times with 0.01 M PBS before performing experiments. The standard addition method was followed and the hydrazine concentration in sample was determined from standard addition curves. The hydrazine concentration in the commercial sample was found to be $0.73 \pm 0.05 \mu\text{M}$. A series of five successive measurements of 0.5 μM hydrazine in 0.01 M PBS yielded a good reproducible signal at Nafion/ZnO/Au sensor with relative standard deviation (R.S.D.) of 3.87%. The intra and inter assay reproducibility of fabricated sensor for 0.5 μM hydrazine detection were found to be 1.39 and 1.26%, respectively. To examine the long-term storage stabilities, the response for the Nafion/ZnO/Au sensor was exam-

Table 1

Comparison of the responses of some amperometric hydrazine sensors constructed based on different modified electrode materials.

Electrode materials	Sensitivity ($\mu\text{A}/\text{cm}^2 \mu\text{M}$)	Detection limit (μM)	Response time (s)	Linear range (μM)	Ref.
MWCNT and chlorogenic acids	0.0041	8	–	2.5–5000	[6]
SWCNT and catechin hydrate	0.183	2.0	–	0.5–1000	[6]
Caffeic acid modified GCE	3.16	0.4	–	2.5–1000	[7]
Nickel hexacyanoferrate modified carbon ceramic electrode	0.26	2.28	<3	2–5000	[8]
Hematoxylin multi-wall carbon nanotubes	0.0208	0.68	<2	2.0–122.8	[9]
Carbon nanotubes powder microelectrode	0.9944	–	<3	–	[10]
ZnO nanonails	8.56	0.2	<5	0.1–1.2	[11]
High-aspect-ratio ZnO nanowires	$12.7 \mu\text{A}/\text{cm}^2 \mu\text{M}$	0.0847	<5	0.5–1.2	This work

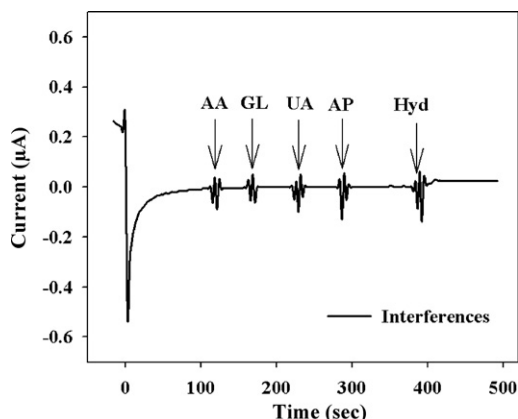


Fig. 4. The chronoamperometric responses for the common interfering compounds with hydrazine. Interfering agents (ascorbic acid (AA), glucose (GL), uric acid (UA), and acetaminophen (AP)) concentration was used (0.2 mM into 0.01 M PBS).

ined with respect to the storage time. After each experiment, the sensor washed with the buffer solution and stored in a 0.01 M PBS at 4 °C. The long-term storage stability of the sensor was tested for 35 days. The sensitivity retained 93.8% of initial sensitivity up to 35 days. After 35 days, the response gradually decreased, which might have been due to the loss of the catalytic activity. The above results clearly suggested that the sensor can be used for more than 1 month without any significant loss in sensitivity.

4. Conclusions

In conclusion, an ultra-sensitive hydrazine sensor has been fabricated by modifying the gold electrode with the high-aspect-ratio ZnO nanowires grown by simple thermal evaporation process at low temperature. A high reproducible sensitivity of $12.76 \mu\text{A cm}^{-2} \text{ nM}^{-1}$, response time less than 5 s and detection

limit of 84.7 nM was found from the fabricated sensor. To the best of our knowledge, this is the first time such a very high-sensitivity and low detection limit has been achieved for hydrazine sensors by using ZnO nanostructures modified electrodes. Thus, one can conclude that because of very easy synthesis and electrode fabrication, ultra-sensitivity, low detection limit, fast response and high-surface area, the ZnO nanowires are the promising nanostructures for the fabrication of amperometric sensors for the efficient detection of hydrazine.

Acknowledgements

This work was supported by the Korea Science and Engineering Foundation grant funded by the Korean Government (MEST) (R01-2006-000-11306-0). Authors wish to thanks Mr. T. S. Bae and J. C. Lim, KBSI, Jeonju branch, and Mr. Jong-Gyun Kang, Centre for University Research Facility (CURF) for taking good quality FESEM and TEM images, respectively.

References

- [1] S. Amlathe, V.K. Gupta, *Analyst* 113 (1998) 1481.
- [2] E.H. Vernot, J.D. MacEwen, R.H. Bruner, C.C. Haus, E.R. Kinkead, *Fundam. Appl. Toxicol.* 5 (1985) 1050.
- [3] S.M. Golabi, H.R. Zare, *J. Electroanal. Chem.* 465 (1999) 168.
- [4] S.D. Zelnick, D.R. Mattie, P.C. Stepaniak, *Aviat. Space Environ. Med.* 74 (2003) 1285.
- [5] J. Xu, M.C. Granger, J. Wang, *Electrochem. Soc. Proc.* 99 (1999) 403.
- [6] A. Salimi, L. Miranzadeh, R. Hallaj, *Talanta* 75 (2008) 147.
- [7] S.M. Golabi, H.R. Zare, *Electroanalysis* 11 (1999) 1293.
- [8] A. Salimi, K. Abdi, *Talanta* 63 (2004) 475.
- [9] H.R. Zare, N. Nasirrizadeh, *Electrochim. Acta* 52 (2007) 4153.
- [10] Y.D. Zhao, W.D. Zhang, H. Chen, Q.M. Luo, *Talanta* 58 (2002) 529.
- [11] A. Umar, M.M. Rahman, S.H. Kim, Y.B. Hahn, *Chem. Commun.* 2 (2008) 166.
- [12] A. Umar, M.M. Rahman, S.H. Kim, Y.B. Hahn, *J. Nanosci. Nanotechnol.* 8 (2008) 3216.
- [13] A. Umar, Y.B. Hahn, *Appl. Phys. Lett.* 88 (2006) 173120.
- [14] A. Umar, B. Karunagaran, S.H. Kim, E.K. Suh, Y.B. Hahn, *Inorg. Chem.* 47 (2008) 4088.
- [15] G.G. Gerhardt, J.J. Burmeister, in: R.A. Meyers (Ed.), *Encyclopedia of Analytical Chemistry*, Wiley & Sons, Chichester, 2000, p. 710.



Direct electrochemistry and electrocatalysis of heme proteins on SWCNTs-CTAB modified electrodes

Shengfu Wang^{a,*}, Fen Xie^a, Guodong Liu^{b,*}

^a College of Chemistry and Chemical Engineering, Hubei University, Wuhan 430062, PR China

^b Department of Chemistry and Molecular Biology, North Dakota State University, Fargo, ND 58105-5516, USA

ARTICLE INFO

Article history:

Received 29 June 2008

Received in revised form 5 September 2008

Accepted 10 September 2008

Available online 19 September 2008

Keywords:

Single wall carbon nanotubes

Heme proteins

Cetyltrimethylammonium bromide

Direct electron transfer

Electrocatalysis

ABSTRACT

Direct electrochemistry and electrocatalysis of heme proteins including hemoglobin (Hb), myoglobin (Mb) and horseradish peroxidase (HRP) were studied with the protein incorporated single walled carbon nanotubes (SWCNTs)-cetyltrimethylammonium bromide (CTAB) nanocomposite film modified glassy carbon electrodes (GCEs). The incorporated heme proteins were characterized with Fourier transform infrared spectroscopy (FTIR), ultraviolet visible (UV) spectroscopy, atomic force microscopy (AFM) and electrochemistry, indicating the heme proteins in SWCNTs-CTAB nanocomposite films keep their secondary structure similar to their native states. The direct electron transfer between the heme proteins in SWCNTs-CTAB films and GCE was investigated. The electrochemical parameters such as formal potentials and apparent heterogeneous electrontransfer rate constants (k_s) were estimated by square wave voltammetry with nonlinear regression analysis. The heme protein-SWCNT-CTAB electrodes show excellent electrocatalytic activities for the reduction of H_2O_2 and NO_2^- , which have been utilized to determine the concentrations of H_2O_2 and NO_2^- .

© 2008 Elsevier B.V. All rights reserved.

1. Introduction

Recently, the direct electron transfer (DET) between the redox proteins and the electrode surface has received more and more attentions. The DET between proteins and electrodes provide an ideal model for mechanistic studies of electron transfer in real biological systems, and play an important role for fabricating protein based biosensors, biomedical devices, and enzymatic bioreactors [1,2]. However, there are three main blocks to study the DET of protein with an electrode: (i) the redox centers tend to be buried inside the proteins and are far away from the electrode surface; (ii) the diffusion coefficients of the proteins are small; (iii) the proteins adsorb strongly at the metallic electrode surface and then denaturation. Thus, the studies are focusing on finding ideal electrode materials and suitable protein immobilization methods to obtain their direct electrochemical reactions and retain their bioactivities [3,4]. Since Rusling and co-workers developed a technique of surfactant-films to incorporate proteins on the electrode surface [5–7], various materials and methods have been used to immobilize proteins, such as sol-gel films [8], hydrogel polymers [9] or

biopolymers [10], room temperature ion liquid films [11], layer-by-layer assembly films [12] and inorganic mesoporous materials [13,14].

Carbon nanotubes (CNTs) have attracted a great deal of interest because of their unique physical and chemical properties since CNTs were discovered by Iijima in 1991 [15]. CNTs show electrical properties as metal or semiconductors, depending on their size and lattice helicity [16]. The subtle electronic properties suggest that CNTs, when used as an electrode material in electrochemical reactions, have the ability to promote electron transfer reactions, which represents a new application of CNTs [17,18]. Recently, CNTs also have been used to immobilize proteins and accelerate the DET of proteins, such as glucose oxidase, bilirubin oxidase and cytochrome c [19]. Yang and co-worker [20] immobilized the horseradish peroxidase (HRP) on glassy carbon electrode (GCE) based on cross-linking HRP by glutaraldehyde with multi-wall CNTs/chitosan composite film. Cai and Chen [21] dispersed the CNTs into surfactant and mixed with hemoglobin (Hb), then immobilized hemoglobin on electrode by Nafion.

In the present work, CNTs were used to directly immobilize redox heme proteins including myoglobin (Mb), Hb and HRP on the surface of the GCE in the presence of cetyltrimethylammonium bromide (CTAB). The use of CTAB would offer a quick and effective method to disperse single walled carbon nanotubes (SWCNTs) and facilitate the immobilization of proteins on the

* Corresponding authors. Tel.: +1 701 231 8697; fax: +1 701 231 8831.

E-mail addresses: wangsf@hubei.edu.cn (S. Wang), guodong.liu@ndsu.edu (G. Liu).

SWCNTs. The biocompatible characteristics of CTAB would provide a favorable microenvironment to keep the activities of the immobilized proteins [21]. We expect that the biocompatible CTAB-SWCNTs nanocomposite film would enhance the direct electron transfer capabilities of the redox proteins on the electrode surfaces. We have also discussed the electrocatalytic reactions of various substrates with biological or environmental significance at the protein-SWCNTs-CTAB nanocomposite film electrodes. The protein-SWCNTs-CTAB films have been characterized by different technologies. The properties of electrocatalytic reduction of NO_2^- and H_2O_2 and its analytical applications were also studied.

2. Experimental

2.1. Chemicals and reagents

Horse heart myoglobin and horseradish peroxidase were obtained from Sigma. Bovine hemoglobin was purchased from Fluka. SWCNTs were obtained from Chengdu Organic Chemicals Co. (Shiquan, China) and were purified before using. CTAB (10 mg mL^{-1}) was obtained from Sigma. Phosphate buffer solution (PBS) was prepared with potassium dihydrogen phosphate and sodium dihydrogen phosphate. All other reagents were of analytical grade. All solutions were prepared with double-distilled water.

2.2. Apparatus

Electrochemical measurements were carried out with a CHI 660 electrochemical analyzer (CH Instrumental Co., U.S.A) controlled by a personal computer. A three-electrode system was used in the measurements, with a bare GCE (3 mm diameter) or protein-SWCNTs-CTAB/GCE as the working electrode, a saturated calomel electrode (SCE) as the reference electrode and a platinum wire as the auxiliary electrode. ultraviolet (UV) visible spectroscopy was carried out with a Cintra 10e UV-visible spectrophotometer (GBC PerkinElmer 17). Sample films for the spectroscopy were prepared by depositing protein-SWCNTs-CTAB films onto quartz slides, which were then being dried in air. Fourier transform infrared spectroscopy (FTIR) spectra were recorded using a PerkinElmer Spectrum One FTIR spectrometer. All the spectra were obtained with an average of 100 scans and 4 cm^{-1} resolution. Transmission electron microscopy (TEM) was performed with a TEM-100CX11, JEOL) operating at 200 kV. Atomic force microscopy (AFM) images were obtained from a Nanoscope III atomic force microscopy (Digital Instruments, USA) using tapping mode, with commercially ultrasharpened Si_3N_4 tips.

2.3. Preparation of protein-SWCNTs-CTAB/GCE

Prior to use, the bare GCE was polished to a mirror-like surface with $0.5 \mu\text{m}$ and $0.05 \mu\text{m}$ $\alpha\text{-Al}_2\text{O}_3$ powder, respectively, then rinsed ultrasonically with water and absolute ethanol and sonicated in twice-distilled water. SWCNTs (1.0 mg) were dispersed in 1.0 mL CTAB (10 mg mL^{-1}) and the mixture was agitated in an ultrasonic bath for 1 h to achieve a well-dispersed suspension. The suspension was sonicated again for 15 min just before preparing the films. To get the best CV responses of protein-SWCNTs-CTAB films, the experimental conditions of film casting, such as the concentration of proteins, the ratio of protein to SWCNTs-CTAB composite and the total volume of protein-SWCNTs-CTAB suspension, were optimized. Typically, $20 \mu\text{L}$ of the suspension containing 5 mg mL^{-1} protein (Mb, Hb or HRP) and 1.0 mg mL^{-1} SWCNTs-CTAB was spread evenly onto GCE electrodes for preparing Mb, Hb or HRP-SWCNTs-CTAB films. A small bottle was fitted tightly over the electrode to serve as a closed evaporation chamber so that the water evaporated slowly

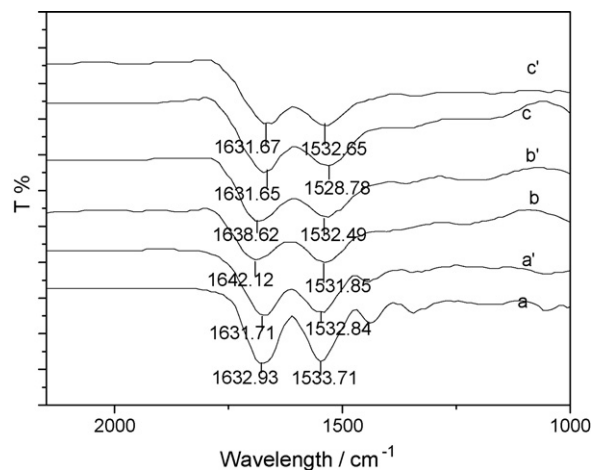


Fig. 1. FTIR spectra for (a) Hb film, (a') Hb-SWCNTs-CTAB film, (b) HRP film, (b') HRP-SWCNTs-CTAB film and (c) Mb film, (c') Mb-SWCNTs-CTAB film.

and more uniform films were formed. The films were then dried in air overnight.

3. Results and discussion

3.1. Characterization of the protein-SWCNTs-CTAB film

3.1.1. FTIR Spectra

FTIR spectroscopy is a sensitive tool for studying the secondary structure of proteins. The characteristic amide I ($1700\text{--}1600 \text{ cm}^{-1}$) and amide II ($1620\text{--}1500 \text{ cm}^{-1}$) bands of proteins provide detailed information on the secondary structure of polypeptidechain [22]. Fig. 1 presents the typical FTIR spectrum of the Hb and Hb-SWCNT-CTAB films. The amide I and amide II bands of Hb in Hb-SWCNTs-CTAB film (curve a', 1631.71 and 1532.84 cm^{-1}) are very similar to those obtained with the Hb film (curve a, 1632.93 and 1533.71 cm^{-1}), indicating that Hb retains the essential features of its original structure in the SWCNTs-CTAB film. Similar bands are also observed with HRP (curve b) and HRP-SWCNTs-CTAB films (curve b'), Mb film (curve c) and Mb-SWCNTs-CTAB film (curve c'). The above results indicate the incorporated heme proteins in the SWCNT-CTAB films may keep their secondary structure.

The secondary structure of heme proteins in the SWCNT-CTAB films was further confirmed with UV-vis spectroscopy. It is

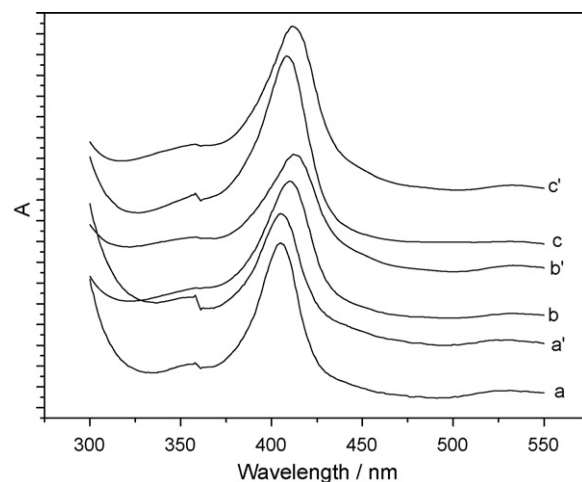


Fig. 2. UV-vis spectra for (a) HRP film, (a') HRP-SWCNTs-CTAB film; (b) Hb film, (b') Hb-SWCNTs-CTAB film and (c) Mb film, (c') Mb-SWCNTs-CTAB film.

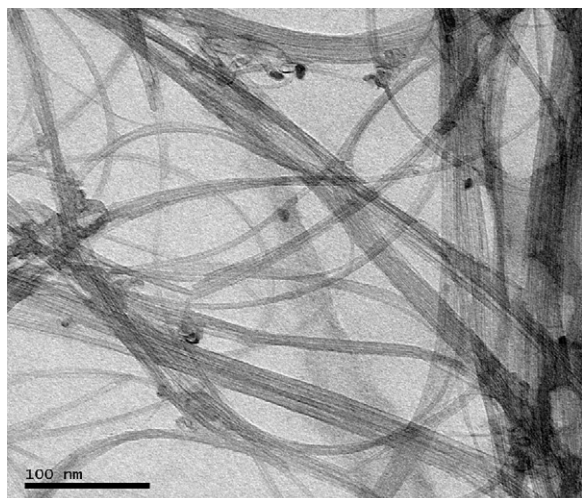


Fig. 3. TEM image of the SWCNTs in the presence of CTAB.

well-known the position of the Soret absorption band of heme in the UV–vis spectroscopy provides information about possible denaturation of proteins, especially conformational change in the heme group region. Fig. 2 presents the typical UV–vis spectroscopy of the films. It can be seen that the HRP cast films gave a heme band at 413 nm (curve a). The Soret band was also found at 413 nm with the HRP-SWCNTs-CTAB film (curve a'). The Soret bands at the same wavelength were obtained with Hb film (curve b), Hb-SWCNT-CTAB film (curve b'), Mb film (curve c) and Mb-SWCNT-CTAB (curve c'). These suggest that the proteins in SWCNTs-CTAB films have an unchanged secondary structure.

3.1.2. TEM and AFM images

The microstructure of SWCNT in the presence of CTAB and the morphologies of protein films were characterized by transmission electron microscopy (TEM) and AFM, respectively. Fig. 3 presents the typical TEM image of SWCNT in the presence of CTAB. The fiber-like SWCNTs were distributed evenly on the grids, although few bundles were observed. A large number of aggregates were observed in the absence of CTAB (not shown). It indicated that the use of CTAB would help the SWCNTs to disperse in the solution, resulting an even and stable SWCNT film. Fig. 4 presents the AFM images of Mb film (Fig. 4(A)), SWCNTs-CTAB film (Fig. 4(B)) and Mb-SWCNTs-CTAB film (Fig. 4(C)). One can see that the image of the Mb on the HOPG surface looked loose and uneven. The fiber-like SWCNTs were observed clearly in the SWCNTs-CTAB film and the globular-like CTAB close to the SWCNTs tightly. However a uniform,

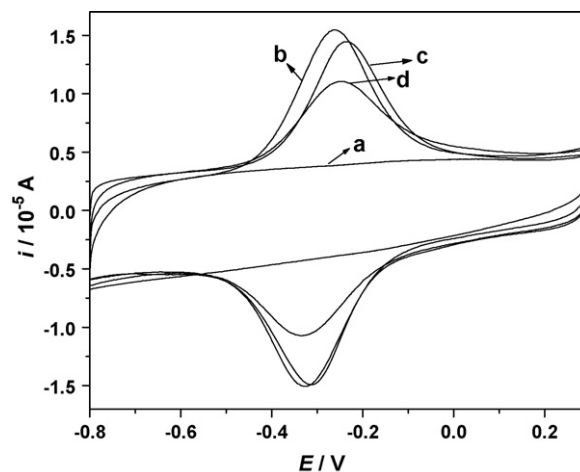


Fig. 5. Cyclic voltammograms at scan rate 0.2 V s^{-1} in pH 7.0 PBS (a) SWCNTs-CTAB films; (b) Mb-SWCNTs-CTAB films; (c) Hb-SWCNTs-CTAB films and (d) HRP-SWCNTs-CTAB films.

stable, and regularly patterned compact structure was observed on Mb-SWCNTs-CTAB film. The film may weaken the congregation of protein on bare GC electrodes and expose the heme crevice to a more hydrophobic environment, thus lowering the reorganization energy for electron transfer [23].

3.2. Direct electrochemistry of protein-SWCNTs-CTAB films

Fig. 5 presents the cyclic voltammograms of SWCNTs-CTAB (curve a), Mb-SWCNTs-CTAB (curve b), Hb-SWCNTs-CTAB (curve c) and HRP-SWCNTs-CTAB (curve d) film electrodes in pH 7.0 PBS. No voltammetric peak was observed at SWCNTs-CTAB film electrode (curve a) in the selected potential range. A pair of well-defined, quasi-reversible redox peaks were observed for the heme protein incorporated film electrodes at potentials -0.293 V (Mb), -0.274 V (Hb) and -0.291 V (HRP). The redox peaks were located at the potentials characteristic of the heme Fe (III)/Fe (II) redox couples of the proteins. For these protein-SWCNTs-CTAB films, the peak currents reached the steady-state after several CV cycles in the PBS. Thus, all voltammetric experiments with protein-SWCNTs-CTAB film electrodes were conducted at their steady-states. CVs of protein-SWCNTs-CTAB films had roughly symmetrical peak shapes and approximately equal heights of reduction and oxidation peaks. In order to investigate the promote effect of SWCNTs; the CVs of Mb/GCE, Mb-SWCNT/GCE, Mb-CTAB/GCE and Mb-SWCNTs-CTAB/GCE were studied. As can be seen in Fig. 6, running at the same

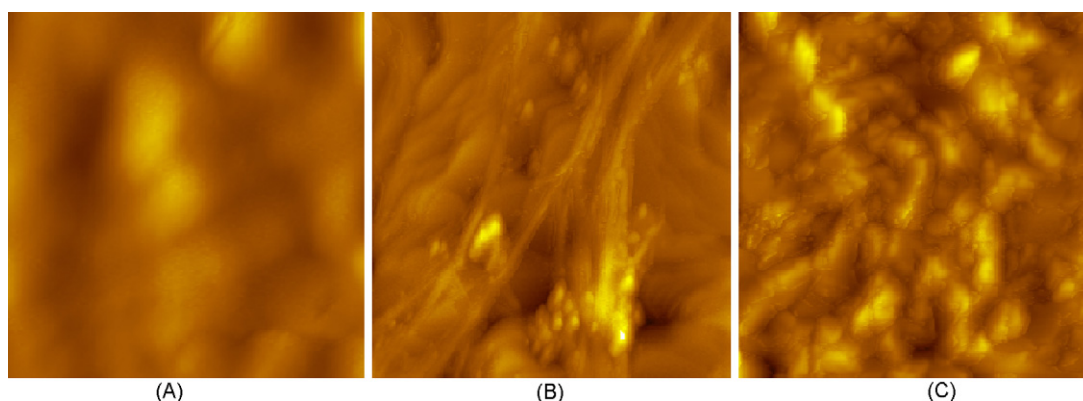


Fig. 4. AFM images of (A) Mb; (B) SWCNTs-CTAB and (C) Mb-SWCNTs-CTAB on HOPG surface. Scan size = $1 \times 1 \mu\text{m}^2$, data scale = 100 nm.

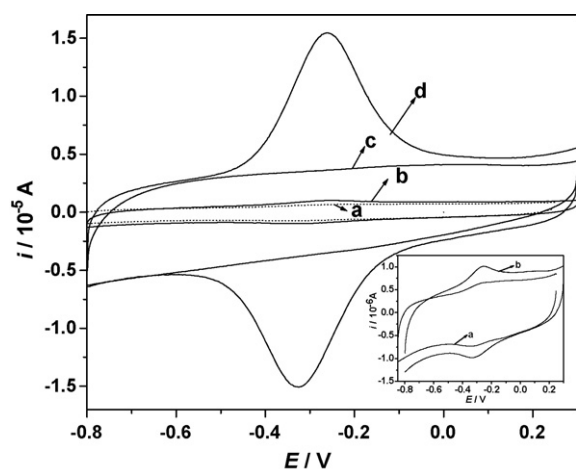


Fig. 6. Cyclic voltammograms of Mb/GCE (a); Mb-CTAB/GCE (b); SWCNTs-CTAB/GCE (c) and Mb-SWCNTs-CTAB/GCE (d) at scan rate 0.2 V s^{-1} in pH 7.0 PBS. Inset: Close-up of curve a and b.

potential window, the redox peak currents of Mb (curve d) with the Mb-SWCNTs-CTAB film electrode is significant higher than that with the Mb/GCE (curve a) or Mb-CTAB/GCE (curve b). An ill-defined CV (not shown) was obtained with the Mb-SWCNT/GCE because of the heavy aggregations of SWCNTs in Mb solution. The reason for the better performance of the CTAB-SWCNTs-modified GCE may be due to the nanometer dimensions of the CNTs, the electronic structure and the topological defects present on the CNTs surfaces [24]. Meanwhile the CNTs increased the effective area of the electrode; the portion of the electroactive proteins is greatly improved compared with those on bare GCE and CTAB film [25].

The reduction peak currents increased linearly with scan rates in the range $0.05\text{--}0.5 \text{ V/s}$ (Fig. 7). The peak-to-peak separation also increased with scan rates. The logarithm plot peak current ($\log i_p$) vs. logarithm of scan rates $\log \nu$ of HRP gives linear relationship, with a slope of 0.91 ($\log i_{pc}$ vs. $\log \nu$, $R=0.998$) and 0.84 ($\log i_{pa}$ vs. $\log \nu$, $R=0.999$). These values are very close to the value of 1. It is the characteristic of surface-confined thin-layer electrochemical process. Using the integrals of the reduction peaks and Faraday's laws, $\Gamma = Q/(nFA)$, where Q is the charge involved in the reaction, n is the number of electrons transferred, F is Faraday's constant, and A is the electrode area, the amount of electroactive protein molecules was estimated to be $8.83 \times 10^{-10} \text{ mol cm}^{-2}$ for HRP, assuming a one-electron reaction. This value is 10.74% of the total amount of HRP deposited on the electrode surface. This may suggest that only those proteins in the inner layers of the films close to the electrode and

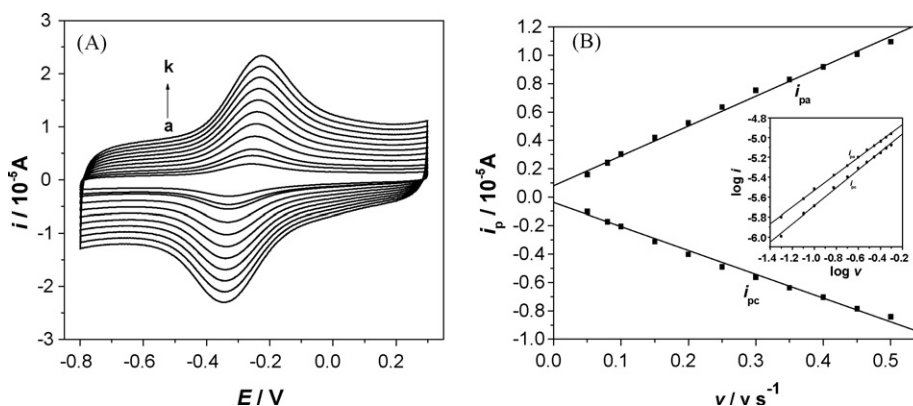


Fig. 7. (A) Cyclic voltammograms of HRP-SWCNTs-CTAB film at different scan rates (curves a \rightarrow k) 0.05, 0.08, 0.1, 0.15, 0.2, 0.25, 0.3, 0.35, 0.4, 0.45, 0.5 V s^{-1} in pH 7.0 PBS. (B) Plot of peak current vs. scan rate, inset: linear logarithm plot of peak current vs. scan rate.

Table 1
Ratio of electroactive protein to total protein.

Film	Γ_{ads} (mol cm^{-2})	Γ_{active} (mol cm^{-2})	$\Gamma_{\text{active}}/\Gamma_{\text{ads}}$ (%)
HRP	8.22×10^{-9}	1.51×10^{-11}	0.18
HRP-CTAB	8.22×10^{-9}	2.61×10^{-11}	0.32
HRP-SWCNTs-CTAB	8.22×10^{-9}	8.83×10^{-10}	10.74

with a suitable orientation can exchange electrons with the electrode surface. However, compared with those on bare GCE and CTAB film, the portion of the electroactive proteins is greatly improved (Table 1).

The pH effect of supporting electrolyte on the redox peak current and potential of the heme protein was investigated. Fig. 8 (A) shows the typical cyclic voltammograms of Hb-SWCNTs-CTAB film electrode in pH 2.5–9.0 PBS. An increase in pH of the solution leads to a negative shift in potential for both cathodic and anodic peaks for Hb-SWCNTs-CTAB films. Nearly reversible voltammograms with stable and well-defined redox peaks were obtained for three proteins in the pH range of 2.5–9.0. The E_{pa} , E_{pc} and E^0 (formal potential) had a linear relationship with the pH value of PBS (Fig. 8(B)) with the slope values of 28.6, 30.6 and 32.6 mV pH^{-1} , respectively. All these slope values are smaller than the theoretical value of 57.6 mV pH^{-1} at 18°C for a single-proton coupled, reversible one-electron transfer [26,27]. The reason might be the influence of the protonation states of trans ligands to the heme iron and amino acids around the heme, or the protonation of the water molecule coordinated to the central iron [28].

The average formal potentials (E^0) and apparent heterogeneous electron transfer rate constants (k_s) were estimated by employing nonlinear regression analysis of SWV forward and reverse curves [29,30]. Fig. 9 presents the typical SWV forward and reverse current voltammograms for Mb-SWCNTs-CTAB films in pH 7.0 PBS at different frequencies. The results calculated were listed in the Table 2. E^0 values estimated as a midpoint of CV reduction and oxidation peak potential for the films are also listed, which are in good agreement with those obtained by SWV. From Table 2, we found that the k_s value obtained in this study was higher than that of the previous studies by using MWCNT [31] and other materials [5]. It can be concluded that the use of the SWCNTs-CTAB film obviously increase the DET of heme proteins.

3.3. Catalytic reactivity

We studied the catalytic reactivities of the proteins (Mb, Hb and HRP) in SWCNTs-CTAB films toward various substrates with

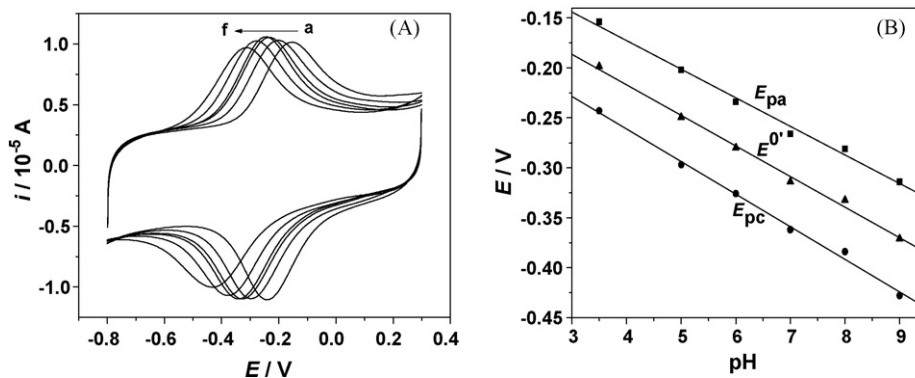


Fig. 8. (A) Cyclic voltammograms of Hb-SWCNTs-CTAB film at different pH (curves a → f) 3.5, 5.0, 6.0, 7.0, 8.0, 9.0. Scan rate: 0.2 V s^{-1} . (B) Plots of E_p vs. pH.

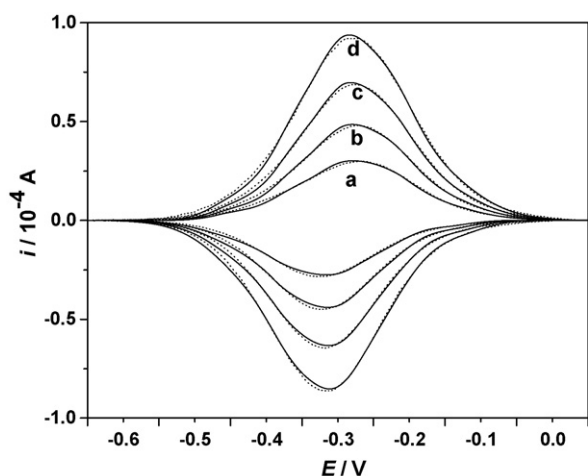


Fig. 9. SWV forward and reverse current voltammograms for Mb-SWCNTs-CTAB films in pH 7.0 PBS at different frequencies. The solid lines represent the experimental SWV from which background has been subtracted. Points are the best fit by nonlinear regression onto the $5 - E^0$ dispersion model. SWV conditions: pulse height 60 mV and frequencies (Hz): (a) 132; (b) 152; (c) 172 and (d) 185.

biological or environmental significance, such as nitrite and hydrogen peroxide. Electrocatalytic reduction of these substrates at the three protein-SWCNTs-CTAB film electrodes was examined by CV. The HRP-SWCNTs-CTAB film is cited as an example. When H_2O_2 was added to pH 7.0 PBS, an increasing reduction peak at about -0.3 V was observed with the disappearance of the oxidation peak for HRP-Fe(II). The reduction peak current increased with the increase of the concentration of H_2O_2 in solution (Fig. 10(A)). However, no direct reduction peak was observed on SWCNTs-CTAB films in the presence of H_2O_2 in the selected potential range.

The catalytic reduction of H_2O_2 at protein-SWCNTs-CTAB film electrodes could be used to determine H_2O_2 concentration in the solution by CV. The linear relationship of the electrocatalytic reduction peak current and H_2O_2 concentration was observed between 1.07×10^{-6} and $4.84 \times 10^{-5} \text{ M}$. The linear regression equation is $i(\text{A}) = 3.639 \times 10^{-6} + 0.198c(\text{M})$ with a correlation coefficient of 0.9995 (Fig. 10(B) (inset)). The calibration curve tended to level

off when the concentration of H_2O_2 became larger. The relationship between catalytic current and the concentration of H_2O_2 showed a typical characteristic of Michaelis–Menten curve. For a thin film of immobilized proteins, the maximum current measured under saturated substrate conditions (I_{max}) and the apparent Michaelis–Menten constant (K_m^{app}), which give an indication of the enzyme-substrate kinetics can be obtained from the Lineweaver–Burk equation [32]:

$$\frac{1}{I_{\text{ss}}} = \frac{1}{I_{\text{max}}} + \frac{K_m^{\text{app}}}{I_{\text{max}}c}$$

K_m^{app} and I_{max} can be obtained by the analysis of the slope and the intercept of the plot of the steady-state current versus H_2O_2 concentration. Accordingly, the I_{max} value was estimated to be $1.22 \times 10^{-5} \text{ A}$ and the K_m^{app} value was $1.02 \times 10^{-5} \text{ M}$ for the enzymatic activity of the HRP-SWCNTs-CTAB film to H_2O_2 , which implied that the HRP-SWCNTs-CTAB film electrode exhibited a high affinity for H_2O_2 . The other two heme protein-SWCNTs-CTAB films showed similar catalytic behavior and calibration curve, and the same analysis was also carried out for them. The results were summarized in Table 3.

The protein-SWCNTs-CTAB film electrodes were also used to catalyze the reduction of nitrite. For example, with HRP-SWCNTs-CTAB films, when NO_2^- was added in pH 7.0 buffer, a new reduction peak appeared at about -0.9 V and the peak increased with a further addition of NO_2^- (Fig. 11(A)). Direct reduction of NO_2^- on SWCNTs-CTAB films free of HRP was found at the potential more negative than -1.3 V , showing that HRP-SWCNTs-CTAB films decreased the reduction overpotential for NO_2^- by at least 0.4 V . The mechanism of nitrite reduction at HRP-SWCNTs-CTAB film electrodes is not yet clear. However, since a similar catalytic reduction of NO_2^- was observed previously with HRP-DDAB (didodecyldimethylammonium bromide) film electrodes by Farmer and co-workers [33,34], we speculate that the mechanism of catalytic reduction of NO_2^- on both protein films would be similar. The catalytic CV reduction peak of NO_2^- had a linear relationship with the concentration of NO_2^- in the range of 6.67×10^{-6} to $1.03 \times 10^{-4} \text{ M}$ with a detection limit of $2.22 \times 10^{-6} \text{ M}$ and a correlation coefficient of 0.9988 (Fig. 11(B)).

Table 2
Electrochemical parameters of protein-SWCNTs-CTAB films.

Films	CV			SWV			
	E^0 (V)	ΔE (mV)	$\Gamma \times 10^{10}$ (mol cm $^{-2}$)	E^0 (V)	$\Gamma \times 10^{10}$ (mol cm $^{-2}$)	α	k_s (s $^{-1}$)
Mb-SWCNTs-CTAB	-0.292	59	10.78	-0.290	9.36	0.52	85.6 ± 0.2
Hb-SWCNTs-CTAB	-0.274	79	9.86	-0.260	9.21	0.52	86.1 ± 0.1
HRP-SWCNTs-CTAB	-0.291	87	8.83	-0.286	8.14	0.50	89.1 ± 0.2

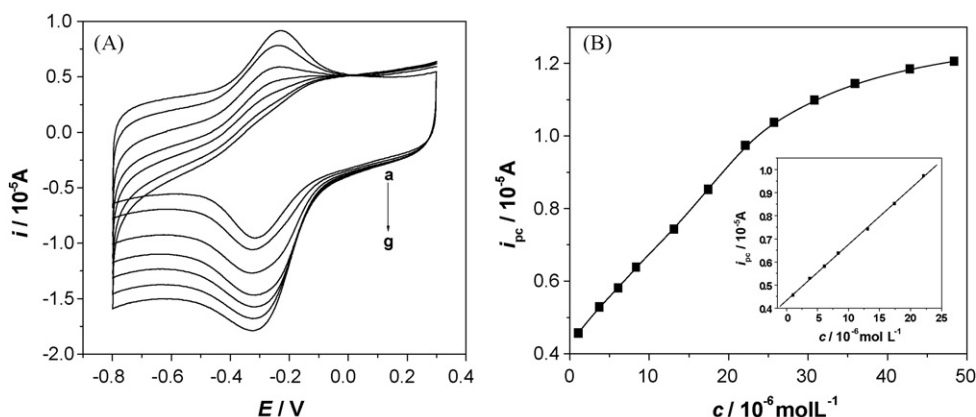


Fig. 10. (A) Typical cyclic voltammograms of HRP-SWCNTs-CTAB film electrode in pH 7.0 PBS containing different concentration of H_2O_2 , the concentrations of the added H_2O_2 : from a to g: 1.07×10^{-6} , 1.31×10^{-5} , 1.74×10^{-5} , 2.21×10^{-5} , 2.59×10^{-5} , 3.59×10^{-5} , 4.84×10^{-5} M. (B) Plot of catalytic peak current vs. concentration of H_2O_2 . Inset: line relationship between peak current and the concentration of H_2O_2 .

Table 3

Electrocatalytic parameters and relationship between catalytic current and H_2O_2 concentrations.

Modified electrodes	K_M^{app} (10^{-5} M)	$I_{\text{max}}/10^{-5}$ (A)	Linear range (M)	Detection limit (M)	Sensitivity ($\mu\text{A } \mu\text{M}^{-1}$)
HRP-SWCNTs-CTAB	1.02	1.22	1.07×10^{-6} to 4.84×10^{-5}	3.57×10^{-7}	0.20
Hb-SWCNTs-CTAB	1.20	2.04	2.36×10^{-5} to 1.34×10^{-4}	7.87×10^{-6}	0.13
Mb-SWCNTs-CTAB	1.21	2.15	2.42×10^{-5} to 1.67×10^{-4}	8.07×10^{-6}	0.11

Mb- and Hb-SWCNTs-CTAB films demonstrated similar catalytic CV behavior and a similar calibration curve for determining nitrite. For Mb-SWCNTs-CTAB films, the linear range was 6.61×10^{-6} to 3.88×10^{-4} M with a detection limit of 2.20×10^{-6} M, while for Hb-SWCNTs-CTAB films the linear range was 6.46×10^{-6} to 1.82×10^{-4} M with detection limit of 2.15×10^{-6} M.

3.4. Amperometric determination of H_2O_2 and NO_2^-

The electrocatalytic reduction of hydrogen peroxide at protein-SWCNTs-CTAB film electrodes was also studied by amperometry. The potential dependence of amperometric signal was tested in the range from -0.05 to -0.60 V. The steady-state reduction current increased as the applied potential decreased from -0.05 to -0.50 V, which was due to the increased driving force for the fast reduction of H_2O_2 at low potential. The response approached maximum at -0.40 V, so we selected this value as the working potential. Fig. 12(A) illustrates a typical amperometric response of the HRP-SWCNTs-CTAB film electrode at -0.40 V on successive step changes of H_2O_2 concentration under stirring. When an aliquot of H_2O_2 was

added, the reductive current rose steeply to reach a stable value. The electrode achieved 95% of steady-state current within 4 s. The current had a linear relationship with the concentration of H_2O_2 for the protein-SWCNTs-CTAB films. The linear ranges were 1.23×10^{-5} to 1.45×10^{-4} M with the slope of $0.133 \mu\text{A } \mu\text{M}^{-1}$ and the detection limit of 3.69×10^{-6} M for HRP-SWCNTs-CTAB films (Fig. 12(B)), 2.46×10^{-5} to 1.69×10^{-4} M with the slope of $0.112 \mu\text{A } \mu\text{M}^{-1}$ and the detection limit of 7.38×10^{-6} M for Hb-SWCNTs-CTAB films, and 2.76×10^{-5} to 2.44×10^{-4} M with the slope of $0.094 \mu\text{A } \mu\text{M}^{-1}$ and the detection limit of 8.28×10^{-6} M for Mb-SWCNTs-CTAB films. Apparently, HRP-SWCNTs-CTAB film is the most sensitive for detecting H_2O_2 with the largest slope and the lowest detection limit, which is qualitatively consistent with the CV results.

The amperometry was also used to determine the concentration of nitrite. In our experiment, the potential was set at -1.0 V versus SCE for the protein-SWCNTs-CTAB films, and the catalytic reduction currents were followed when aliquots of NO_2^- were added (Fig. 13(A)). The current had a linear relationship with the concentration of NO_2^- for the protein-SWCNTs-CTAB films. The linear ranges were 1.67×10^{-4} to 1.64×10^{-3} M with the slope of

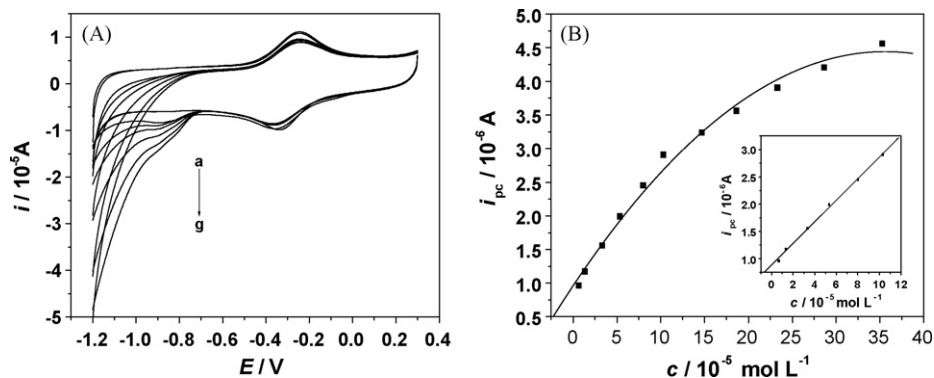


Fig. 11. (A) CVs of HRP-SWCNTs-CTAB film electrode in pH 7.0 PBS containing different concentration of NO_2^- , the concentrations of the added NO_2^- : from a to g, 6.66×10^{-6} , 1.03×10^{-5} , 4.52×10^{-4} , 7.50×10^{-4} , 1.40×10^{-3} , 2.68×10^{-3} , 3.93×10^{-3} M. (B) Plot of catalytic peak current vs. concentration of NO_2^- . Inset: line relationship between peak current and the concentration of NO_2^- .

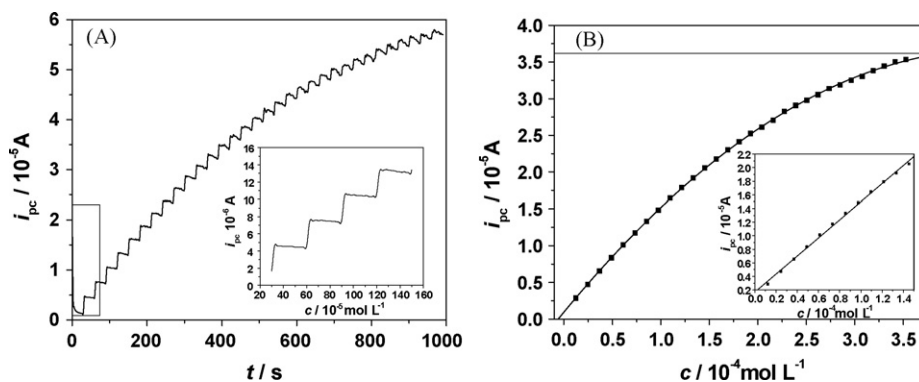


Fig. 12. (A) Amperometric response of the HRP-SWCNTs-CTAB film electrode upon successive additions of 7.41×10^{-3} M H_2O_2 to 6 ml of PBS at -0.50 V. Also shown (inset) is the magnification of the first four steps. (B) Relationship between response current and the concentration of H_2O_2 , inset: calibration curve for H_2O_2 .

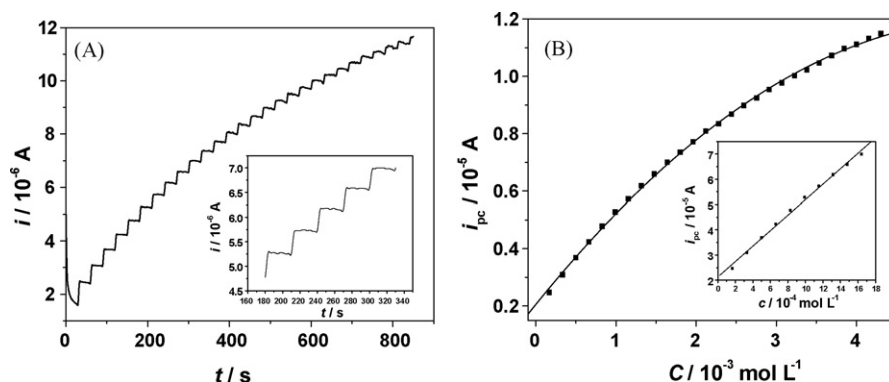


Fig. 13. (A) Amperometric response of the HRP-SWCNTs-CTAB film electrode upon successive additions of 0.2 M NO_2^- to 6 ml PBS at -1.0 V. Also shown (inset) is the magnification of the first five steps. (B) Relationship between current and the concentration of NO_2^- , inset: calibration curve for NO_2^- .

$3.06 \mu\text{A mM}^{-1}$ and the detection limit of 5.01×10^{-5} M for HRP-SWCNTs-CTAB films (Fig. 13(B)), 3.33×10^{-4} to 1.61×10^{-3} M with the slope of $2.33 \mu\text{A mM}^{-1}$ and the detection limit of 9.99×10^{-5} M for Hb-SWCNTs-CTAB films, and 3.33×10^{-4} to 1.84×10^{-3} M with the slope of $2.14 \mu\text{A mM}^{-1}$ and the detection limit of 9.99×10^{-5} M for Mb-SWCNTs-CTAB films. Similarly, HRP-SWCNTs-CTAB film is the most sensitive for detecting NO_2^- with the largest slope and the lowest detection limit, which is qualitatively consistent with the CV results.

These analytical parameters such as the linear ranges and the detection limits are comparable to or improvements in measurements reported by others for the electroanalytical determination of hydrogen peroxide [20,35] and nitrite [36,37] with the carbon nanotube modified electrodes. In addition, the biosensors exhibited good sensitivities and rapid response for H_2O_2 and NO_2^- in the absence of mediator. And the preparation method of modified electrode is comparable easy. It is suitable for the fabrication of the third generation biosensors.

3.5. Stability and reproducibility of the modified electrodes

The stability and reproducibility of the protein-SWCNTs-CTAB film electrodes were also studied. All the three protein modified electrodes can retain constant current values upon continuous cyclic sweep over the potential rang from -0.8 to 0.3 V. The peak current decreased with the increase of storage time, when the electrode was stored in air for about 2 weeks, the electrode can still retain about 78% of initial response. These may be attributed to the aspect that the SWCNTs were stable in the CTAB and the CTAB can retain the biological activity of heme proteins. The fabrication

of 7 Mb-SWCNTs-CTAB electrodes, made independently, showed an acceptable reproducibility with a R.S.D. of 2.67% for the current determined at a H_2O_2 concentration of 5.0×10^{-5} M and 3.12% at a NaNO_2 concentration of 1.0×10^{-4} M.

4. Conclusions

In this paper, different protein-SWCNTs-CTAB film modified electrodes were constructed by casting the mixture of heme protein solutions and SWCNTs-CTAB suspensions onto the surface of GCE. The protein-SWCNTs-CTAB films have been characterized by different technologies. The proteins immobilized in SWCNTs-CTAB films showed direct cyclic voltammetric responses. The experiment results indicate that effective electron transfer rate involving the heme Fe(III)/Fe(II) redox couples on the SWCNTs-CTAB film modified electrode is much faster than those for proteins on bare GCE electrodes. The protein-SWCNTs-CTAB films were quite stable, and the proteins retained their native states in the SWCNTs-CTAB films. Good electrocatalytic properties of the protein-SWCNTs-CTAB films towards hydrogen peroxide and nitrite showed that the films have a promising potential in fabricating the third generation biosensor based on the direct electrochemistry of enzymes.

Acknowledgements

The authors wish to thank Prof. J.F. Rusling and Prof. D.W. Pang for providing the software for nonlinear regression analysis of SWV data. S. Wang acknowledges the financial support from the National Natural Science Foundation of China (no. 20575017). G. Liu acknowledges the financial support from North Dakota

Experimental Program to Stimulate Competitive Research (EPSCoR) and new faculty startup funds of North Dakota State University.

References

- [1] M.F. Chaplin, C. Bucke, *Enzyme Technology*, Cambridge University Press, Cambridge, UK, 1990.
- [2] F.A. Armstrong, H.A.O. Hill, N.J. Walton, *Acc. Chem. Res.* 21 (1988) 407.
- [3] D.M. Sun, C.X. Cai, X.G. Li, W. Xing, T.H. Lu, *J. Electroanal. Chem.* 566 (2004) 415.
- [4] X.J. Han, W.M. Huang, J.B. Jia, S.J. Dong, E.K. Wang, *Biosens. Bioelectron.* 17 (2002) 741.
- [5] Q. Huang, Z.Q. Lu, J.F. Rusling, *Langmuir* 12 (1996) 5472.
- [6] J.F. Rusling, A.E.F. Nassar, *J. Am. Chem. Soc.* 115 (1993) 11891.
- [7] Z. Zhang, S. Chouchane, R.S. Magliozzo, J.F. Rusling, *Anal. Chem.* 74 (2002) 163.
- [8] H. Chen, S. Dong, *Biosens. Bioelectron.* 22 (2007) 1811.
- [9] Y.X. Sun, J.T. Zhang, S.W. Huang, S.F. Wang, *Sens. Actuators B: Chem.* 124 (2007) 494.
- [10] L. Shen, R. Huang, N.F. Hu, *Talanta* 56 (2002) 1131.
- [11] H. Chen, Y. Wang, Y. Liu, Y. Wang, L. Qi, S. Dong, *Electrochem. Commun.* 9 (2007) 469.
- [12] J.J. Feng, J.J. Xu, H.Y. Chen, *Biosens. Bioelectron.* 22 (2007) 1618.
- [13] L. Zhang, Q. Zhang, J. Li, *Electrochem. Commun.* 9 (2007) 1530.
- [14] D. Cao, P. He, N. Hu, *Analyst* 128 (2003) 268.
- [15] S. Iijima, *Nature* 354 (1991) 56.
- [16] P.J. Britto, K.S.V. Santhanam, P.M. Ajayan, *Bioelectrochem. Bioenerg.* 41 (1996) 121.
- [17] F. Valentini, S. Orlanducci, M.L. Terranova, A. Amine, G. Palleschi, *Sens. Actuators B* 100 (2004) 117.
- [18] P.F. Liu, J.H. Hu, *Sens. Actuators B* 84 (2002) 94.
- [19] J.X. Wang, M.X. Li, Z.J. Shi, N.Q. Li, Z.N. Gu, *Anal. Chem.* 74 (2002) 1993.
- [20] L. Qian, X. Yang, *Talanta* 68 (2006) 721.
- [21] C. Cai, J. Chen, *Anal. Biochem.* 325 (2004) 285.
- [22] T.G. Spiro, T.C. Streckas, *J. Am. Chem. Soc.* 96 (1974) 338.
- [23] B.R. Van Dyke, P. Saltman, F.A. Armstrong, *J. Am. Chem. Soc.* 118 (1996) 3490.
- [24] P.J. Britto, K.S.V. Santhanam, A. Rubio, J.A. Alonso, P.M. Ajayan, *Adv. Mater.* 11 (1999) 154.
- [25] Y. Yan, W. Zheng, M. Zhang, L. Wang, L. Su, L. Mao, *Langmuir* 21 (2005) 6560.
- [26] A.M. Bond, *Modern Polarographic Methods In Analytical Chemistry*, Marcel Dekker, New York, 1980, pp. 29–30.
- [27] L. Meites, *Polarographic Techniques*, 2nd ed., Wiley, New York, 1965, pp. 282–284.
- [28] I. Yamazaki, T. Araiso, Y. Hayashi, H. Yamada, R. Makino, *Adv. Biophys.* 11 (1978) 249.
- [29] J.J. O'Dea, J.G. Osteryoung, *Anal. Chem.* 65 (1993) 3090.
- [30] A.E.F. Nassar, Z. Zhang, N. Hu, J.F. Rusling, T.F. Kumosinski, *Phys. Chem. B* 101 (1997) 2224.
- [31] L. Zhao, H. Liu, N. Hu, *J. Colloid Interface Sci.* 296 (2006) 204.
- [32] F.D. Munteanu, Y. Okamoto, L. Gorton, *Anal. Chim. Acta* 476 (2003) 43.
- [33] R. Lin, M. Bayachou, J. Greaves, P.J. Farmer, *J. Am. Chem. Soc.* 119 (1997) 12689.
- [34] M. Bayachou, R. Lin, W. Cho, P.J. Farmer, *J. Am. Chem. Soc.* 120 (1998) 9888.
- [35] V.S. Tripathi, V.B. Kandimalla, H. Ju, *Biosens. Bioelectron.* 21 (2006) 1529.
- [36] G.L. Turdean, I.C. Popescu, A. Curulli, G. Palleschi, *Electrochim. Acta* 51 (2006) 6435.
- [37] H.J. Jiang, H. Yang, D.L. Akins, *J. Electroanal. Chem.* 623 (2008) 181–186.



Electrodeposition of gold nanoparticles on indium/tin oxide electrode for fabrication of a disposable hydrogen peroxide biosensor

Jianwen Wang, Liping Wang, Junwei Di*, Yifeng Tu

Department of Chemistry, Suzhou University, Suzhou, Jiangsu 215123, PR China

ARTICLE INFO

Article history:

Received 3 May 2008

Received in revised form

13 September 2008

Accepted 19 September 2008

Available online 30 September 2008

Keywords:

Gold nanoparticles

Indium tin oxide

Direct electron transfer

Horseradish peroxidase

Disposable biosensor

ABSTRACT

A novel disposable third-generation hydrogen peroxide (H_2O_2) biosensor based on horseradish peroxidase (HRP) immobilized on the gold nanoparticles (AuNPs) electrodeposited indium tin oxide (ITO) electrode is investigated. The AuNPs deposited on ITO electrode were characterized by UV–vis, SEM, and electrochemical methods. The AuNPs attached on the ITO electrode surface with quasi-spherical shape and the average size of diameters was about 25 nm with a quite symmetric distribution. The direct electron chemistry of HRP was realized, and the biosensor exhibited excellent performances for the reduction of H_2O_2 . The amperometric response to H_2O_2 shows a linear relation in the range from $8.0 \mu\text{mol L}^{-1}$ to 3.0mmol L^{-1} and a detection limit of $2 \mu\text{mol L}^{-1}$ ($S/N=3$). The K_M^{app} value of HRP immobilized on the electrode surface was found to be 0.4mmol L^{-1} . The biosensor indicates excellent reproducibility, high selectivity and long-term stability.

© 2008 Elsevier B.V. All rights reserved.

1. Introduction

Hydrogen peroxide (H_2O_2) is not only a by-product of several highly selective oxidases, but also an essential mediator in food, biology, medicine, industry and environmental analysis [1]. The sensitive and accurate determination of H_2O_2 is becoming of practical importance. Many techniques have been developed for the determination of H_2O_2 . Among these procedures, electrochemical technique based on enzyme biosensors has been extensively employed for determination of H_2O_2 with simplicity, intrinsic selectivity and sensitivity [2,3]. As a result of the easy availability in high purity and low cost, horseradish peroxidase (HRP) has been the most widely studied in the development of enzyme-based amperometric biosensors [4–6].

However, the utility of an enzyme-based electrode may be limited by the gradual fouling of its surface and/or loss of enzyme activity. Such a problem can be minimized with the use of disposable electrodes. The most commonly amperometric disposable electrodes based on HRP enzyme for the analysis of H_2O_2 were mainly constructed by screen-printed carbon electrodes. Unfortunately, redox enzymes usually exhibit sluggish electron transfer at conventional electrode surfaces due to their three-dimensional structure, the shielding of redox active centers by their insulated

protein shells and unfavorable orientation on the electrode surface [7]. The disposable amperometric HRP biosensors were usually based on mediators. Gao et al. [8] constructed the disposable biosensor using multilayer HRP enzymes which covalently immobilized onto the surface of amino groups modified screen-printed carbon electrode. Morrin presented an effective, facile method for biosensor fabrication by drop-coating conducting non-diffusion PANI/DBSA mediator and enzyme simultaneously onto disposable screen-printed carbon electrodes [9]. Such mediated peroxide biosensors could facilitate the electron transfer and provide low-detection limit, but it is inconvenient to add a mediator in the fabrication process and reduce the reaction selectivity due to mediators [10].

Gold nanoparticles (AuNPs) are used increasingly in many electrochemical applications since they have the ability to enhance the electrode conductivity and facilitate the electron transfer, thus, improving the analytical selectivity and sensitivity. Especially the small size and biocompatible ability of AuNPs allows them utilized widely as a base in modification of various biosensors to promote the direct electron transfer (DET) of some proteins, such as HRP [1,11,12], hemoglobin [13], myoglobin [2], glucose oxidase [14,15] and superoxide dismutase [16,17]. AuNPs can assist in constructing an interface for DET of redox-active proteins while retaining their bioactivity, operating simplicity without mediator and low expense of fabrication. The incorporation of the HRP with AuNPs in the matrix produces very satisfying results with enhanced sensitivity, high reproducibility, wide linearity and a low-detection limit.

* Corresponding author. Tel.: +86 512 65880354.
E-mail address: djw@suda.edu.cn (J. Di).

However, there is less report of screen-printed electrode design based on HRP and AuNPs. Tangkuaram developed a highly stable H_2O_2 biosensor on screen-printed carbon electrode based on HRP bound with AuNPs in the matrix of chitosan [18].

Another attractive approach for fabricating the disposable biosensors is to use indium tin oxide (ITO) electrode as the substrate due to their prominent electrochemical and physical characteristics, as well as low cost [19–21]. Zhang has reported the disposable H_2O_2 biosensors based on ITO electrode. One method is to immobilize HRP enzyme in colloidal AuNPs modified chitosan membrane to modify ITO electrode [22]. Another method is based on co-entrapment of enzyme and mediator by gold nanoparticles on ITO electrode [23]. Although this served an effective method for fabrication disposable biosensors, the mediators cannot be avoided even though using AuNPs.

As usually, the approaches for AuNPs grown onto ITO coated glass were assembling with polymer [24] and seed-mediated growth method [25]. Electrochemical deposition could provide an easy and rapid alternative for the preparation of gold nanoparticles electrodes in a short time. However, the size of the AuNPs is very large (114–217 nm) [26], which are not very suitable to immobilize enzyme for fabrication biosensors. In the present paper, we develop the method for direct electrochemical deposition of AuNPs on the low-cost ITO substrate to fabricate AuNPs modified ITO electrode. The AuNPs formed on the electrode surface were characterized by UV–vis, SEM, and electrochemical methods. HRP enzyme was chemically adsorbed on the self-assembled monolayers by L-Cysteine (Cys) on the AuNPs/ITO electrode. The optimized conditions for the fabrication and electrochemical behaviors of the enzyme electrode were studied. As far as we know, there is no report about disposable H_2O_2 biosensor based on the DET of HRP on ITO electrode facilitated by AuNPs.

2. Experimental

2.1. Reagents

Potassium aurous cyanide ($\text{KAu}(\text{CN})_2$) was obtained from Soochow university special Chemical Reagent Co. Ltd. 2.0 mmol L^{-1} $\text{KAu}(\text{CN})_2$ solution was prepared by dissolving 0.0576 g $\text{KAu}(\text{CN})_2$ in 100 mL of deionized water. HRP (EC 1.11.1.7, 250 units mg^{-1}) was purchased from Shanghai Chemical Reagent Factory (Shanghai, People's Republic of China). A 3.5 mg mL^{-1} HRP stock solution was stored at 4°C . 0.05 M phosphate buffer solutions (PBS, pH 6.85), which were prepared from Na_2HPO_4 and KH_2PO_4 , were always employed as supporting electrolyte. L-Cysteine was obtained from Guoyao Chemical Regent Co. Ltd. (Shanghai, China). The Cys aqueous solution was freshly prepared and deoxygenated by bubbling pure N_2 gas for about 10 min prior to use. H_2O_2 (30% w/v solution) was purchased from Shanghai Chemical Reagent Company (Shanghai, People's Republic of China), and the fresh solutions of H_2O_2 were prepared daily. All other chemicals employed were of analytical grade and used without further purification. All solutions were made up with doubly distilled deionized water throughout this study.

2.2. Apparatus

Indium tin oxide (ITO) glass (1.1 mm thickness, less than 100 Ω resistance) was purchased from Conduc Optics and Electronics Technology Company. All electrochemical experiments were performed with a CHI830 electrochemical workstation (Shanghai Chenhua Apparatus Inc., China). A homemade three-electrode cell was used with the enzyme electrode ($0.6 \text{ cm} \times 0.6 \text{ cm}$) as a working electrode, a platinum foil as the counter electrode and a satu-

rated calomel electrode (SCE) as the reference. All potentials were reported with respect to the reference electrode. All electrochemical experiments were carried out in 10 mL 0.1 mol L^{-1} phosphate buffer solutions (PBS, pH 6.85) at room temperature. A magnetic stirrer was used to stir the testing solution during the amperometric experiments. All experimental solutions were deaerated by nitrogen gas for at least 15 min, and a nitrogen atmosphere was kept over the solutions in the cell to protect the solution from oxygen during the measurements.

Scanning electron microscopy (SEM) was run with an S-4700 scanning electron microanalyzer (Hitachi, Japan). The samples were coated with thin Au film to well characterize the film. Optical spectra were acquired on a TU-1810 spectrophotometer (Beijing purkinje General Instrument Co. Ltd).

2.3. Preparation of gold-nanoparticle electrode

A sheet of ITO ($3 \text{ cm} \times 0.6 \text{ cm}$) was firstly pretreated according to the method described in our previous work [16]. It was sonicated with dilute ammonia, deionized water, absolute ethanol and deionized water for about 5 min, respectively. Then the certain part of ITO glass sheet was immersed into the solution: 0.3 mL 2.0 mmol L^{-1} $\text{KAu}(\text{CN})_2$ solution, 0.5 mL phosphate buffer solutions (PBS, pH 8.0) and deionized water in a total of 5.0 mL . The mixed solution was deaerated by nitrogen gas for about 5 min. The upper part of the ITO electrode was directly connected with electrochemical workstation. The electrodeposition experiment was carried out in the electric-heated thermostatic water bath at 50°C . The gold-nanoparticle electrode was prepared in the potential range of -0.4 to -1.3 V for 20 circles at a scan rate of 50 mV s^{-1} .

2.4. Fabrication of HRP/Cys/AuNPs/ITO electrode

The prepared AuNPs modified ITO electrode was firstly immersed in a 10 mmol L^{-1} aqueous solution of Cys for 4 h in the fridge at 4°C to self-assemble a monolayer of thiols on the AuNPs/ITO electrode. A Cys monolayer was chemisorbed onto the AuNPs. Then the electrode was thoroughly rinsed with water to remove physically adsorbed Cys. Finally, the Cys/AuNPs/ITO electrode was incubated in 3.5 mg mL^{-1} HRP for 8 h in the fridge at 4°C to fabricate the HRP/Cys/AuNPs/ITO electrode. After rinsed clearly with twice-distilled deionized water, the enzyme electrodes were stored at 4°C in a refrigerator when not in use.

3. Results and discussion

3.1. Characteristics of AuNPs electrodeposited on ITO electrode

SEMs were used to evaluate the physical appearance and surface characteristics of AuNPs on electrode surfaces. Fig. 1 illustrates the typical SEM images of AuNPs/ITO (a) and Cys/AuNPs/ITO (b) electrode surfaces at high magnification. As can be seen, many spherical gold nanoparticles are electrodeposited on the ITO film coated glass surface (Fig. 1a). The AuNPs prepared by this method are similar to that made by seed-mediated growth [2,25]. The average diameter of these spherical nanoparticles is about 25 nm with a quite symmetric distribution. It is much smaller than that of the report [26], which also used the electrodeposition method. The AuNPs size is a very important factor for the performance of enzyme electrode. It is reported that the small size AuNPs (20 and 24 nm, respectively) results in a higher catalytic capability of HRP based biosensors than larger-sized AuNPs [27,28]. The size of AuNPs has not shown marked difference after soaking in Cys aqueous solution (Fig. 1b). These indicate clearly that the moderate size AuNPs can be effectively formed on the ITO electrode surface through electrodeposition.

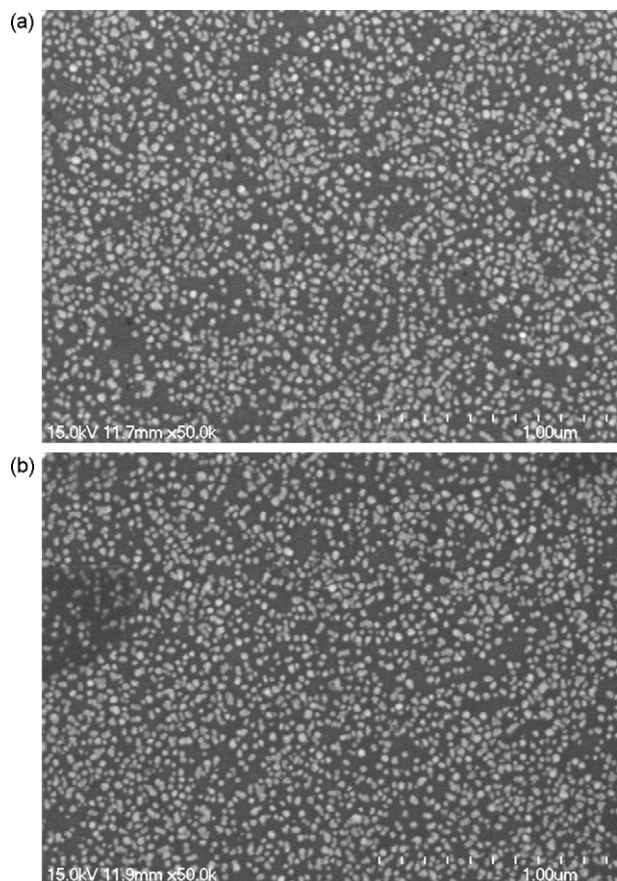


Fig. 1. SEM images of AuNPs/ITO (a) and Cys/AuNPs/ITO (b) electrodes.

UV–vis spectra of the electrodeposited AuNPs are shown in Fig. 2. The AuNPs on the ITO coated glass shows a strong surface plasmon band at 540 nm (Fig. 2a). The absorbance maximum was a little red shift compared with that of the similar size AuNPs made by colloidal methods [29–31]. This was consistent with Zhao's result [32] that the plasmon resonance was shifting to the red for 8 nm when AuNPs immobilized onto glass slide surfaces. The optical properties of metal nanoparticles have much to do with the nanoparticle size, shape, and dielectric environment [33]. After self-assembled with Cys monolayer (Fig. 2b), the strong surface plasmon

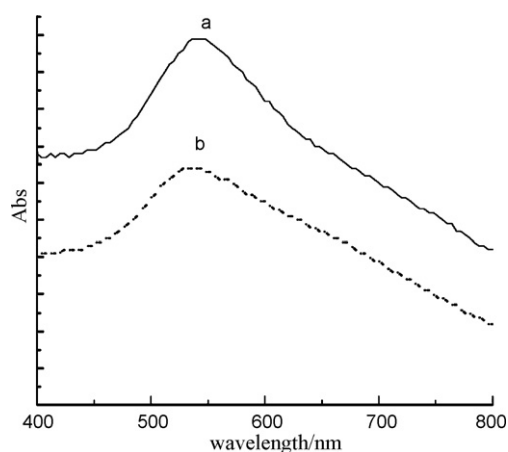


Fig. 2. UV–vis absorption spectra corresponding to: AuNPs/ITO (a) and Cys/AuNPs/ITO (b) electrodes.

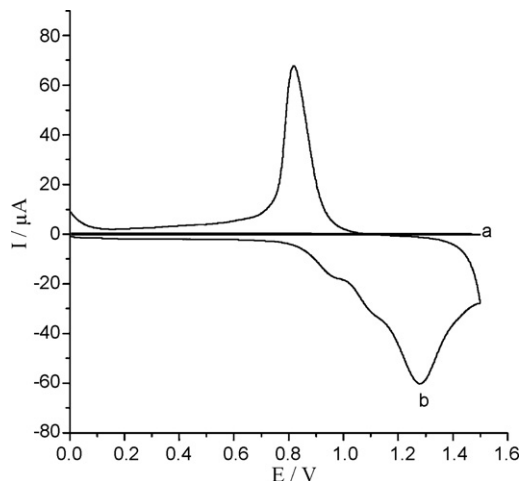


Fig. 3. Cyclic voltammograms of bare ITO (a) and AuNP/ITO (b) electrodes in N_2 -saturated $0.05 \text{ mol L}^{-1} \text{ H}_2\text{SO}_4$ solution. Scan rate: 20 mV s^{-1} .

band was located at 533 nm, which shifted to the purple for 7 nm. Considering the results of the SEM images, this may attribute to the interaction between AuNPs and its ligands, which produce changes in the nanoparticle's local dielectric environment [34]. The stability of the AuNPs modified ITO electrode was also investigated through the comparison of the spectra. After sonicated for 3 min, the UV–vis spectrum of the AuNPs electrodeposited on the ITO electrode has nearly no change. It is obvious that the AuNPs can be electrodeposited onto the ITO electrode in high stability.

The characteristic CV responses were measured in N_2 -saturated $0.05 \text{ M H}_2\text{SO}_4$ at the scan rate of 100 mV s^{-1} for getting the real surface information of the AuNPs electrodeposited on the ITO electrode. Fig. 3 shows the corresponding CV curves of the bare ITO (a) and AuNPs/ITO (b) electrodes. There is no observable Faradaic current on the bare ITO electrode. The CV of an AuNPs/ITO electrode (Fig. 3b) shows a single oxidation peak at +1.3 V along with the reduction peak at +0.80 V, which attributes to the reduction of gold surface oxide. The AuNPs/ITO electrode exhibits the typical characteristic cyclic voltammetric curves of the bulk Au. This is similar to other gold nanoparticles modified ITO electrodes [11,19,35]. This gives another confirmation that the AuNPs are formed on ITO electrode surfaces.

$\text{Fe}(\text{CN})_6^{3-}$ which undergoes a reversible electrochemical reaction at various electrode, is widely used as an electrochemical probe to investigate the characteristics of films on electrode surfaces [36,37]. Fig. 4 shows the CVs of different electrodes in $5 \text{ mmol L}^{-1} \text{ K}_3\text{Fe}(\text{CN})_6$ aqueous solution containing 0.1 M KCl at a scan rate of 20 mV s^{-1} . At bare ITO electrode, a reversible electrochemical response for $\text{Fe}(\text{CN})_6^{4-}/3-$ with a bigish peak potential separation was observed (Fig. 4a). However, there is a drastic decrease in the peak potential separation when AuNPs electrodeposited on the ITO electrode (Fig. 4b). The peak potential separation, which is inversely proportional to the electron transfer rate [38], is used for electrochemical evaluation of the conductivity of the electrode. Obviously, the AuNPs electrodeposited on the ITO surface largely enhanced the conductivity of the electrode.

3.2. Direct electrochemistry of HRP at HRP/Cys/AuNPs/ITO electrode

The typical CVs of bare ITO, AuNPs/ITO and HRP/Cys/AuNPs/ITO electrode in $0.05 \text{ mol L}^{-1} \text{ PBS}$ solution (pH 6.85) at 100 mV s^{-1} are shown in Fig. 5. A pair of well-behaved and nearly symmetric redox peaks was observed at the HRP/Cys/AuNPs/ITO electrode (Fig. 5c).

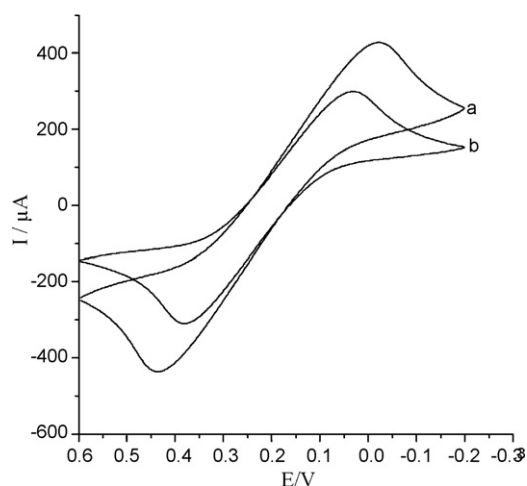


Fig. 4. CVs of 5 mmol L⁻¹ K₃Fe(CN)₆ in 0.1 mol L⁻¹ KCl at bare ITO (a) and AuNP/ITO (b) electrodes. Scan rate: 20 mV s⁻¹.

In contrast, there was no cathodic or anodic peak on both bare ITO (Fig. 5a) and AuNPs modified ITO (Fig. 5b) electrodes. In addition the presence of AuNPs resulted in an obvious increase in the background current due to the increased active electrode area. It confirms clearly that the redox peaks of the HRP/Cys/AuNPs/ITO electrode are attributed to the direct electron transfer of HRP. The formal potential E° of the enzyme electrode, estimated as $(E_{pa} + E_{pc})/2$, is 0.080 V versus SCE. The peak-to-peak separation is 0.167 V at a scan rate of 100 mV s⁻¹. After successive scanning, no noticeable change in CVs of this enzyme electrode was observed. It indicates that AuNPs in biosensors can provide a biocompatibility environment for enzyme and the smaller particles can benefit the electron transfer between HRP and the electrode surface. Furthermore the special nano-structure of AuNPs may acts as “molecular wire”, which leads electrons to the redox centers of HRP.

Fig. 6 depicts the typical CVs of the enzyme electrode in 0.05 mol L⁻¹ PBS (pH 6.85) at different scan rates. With the increasing potential scan rate, the separation of the anodic and cathodic peak potential increased. The anodic (I_{pa}) and cathodic (I_{pc}) peak currents are both linearly proportional to the scan rate (ν) from 10 to 800 mV s⁻¹, as displayed in the inset of Fig. 6. The peak-to-peak separation of HRP also increased with the increase of scan rate

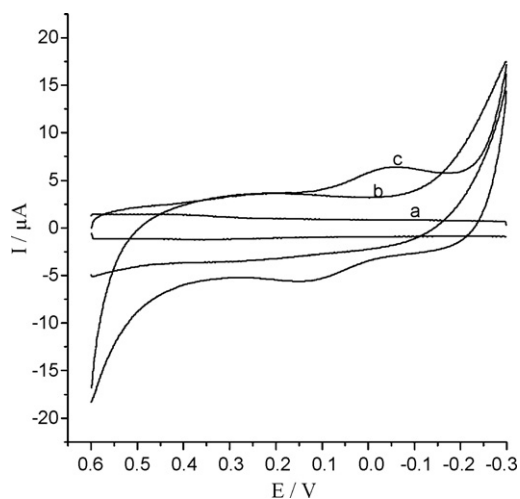


Fig. 5. CVs of bare ITO (a), AuNPs/ITO (b) and HRP/Cys/AuNPs/ITO (c) electrodes in 0.05 mol L⁻¹ PBS solution (pH 6.85) at 100 mV s⁻¹.

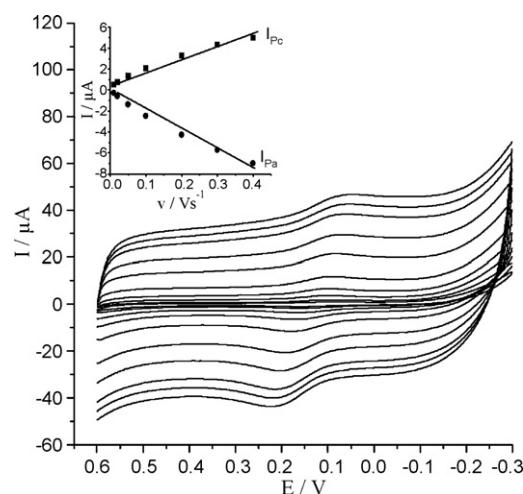


Fig. 6. CVs of the biosensor in 0.05 mol L⁻¹ PBS (pH 6.85) at various scan rates. The scan rate (from inner to outer) is 10, 20, 50, 100, 200, 400, 600, 800 mV s⁻¹, respectively. (Inset) Plot of currents vs. scan rate.

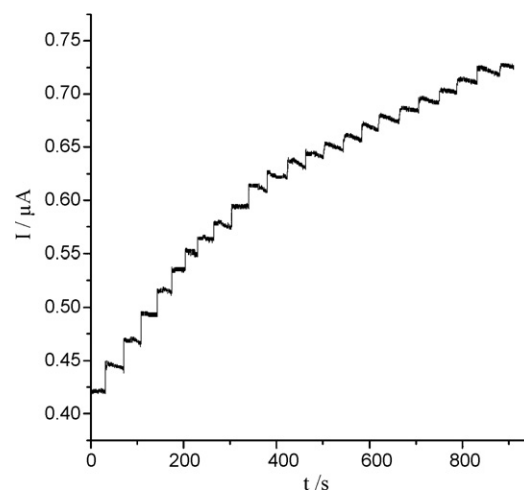


Fig. 7. Typical steady-state response of HRP/Cys/AuNP/ITO electrode on successive injection of aliquot H₂O₂ into 10 mL of stirring PBS (pH 6.85).

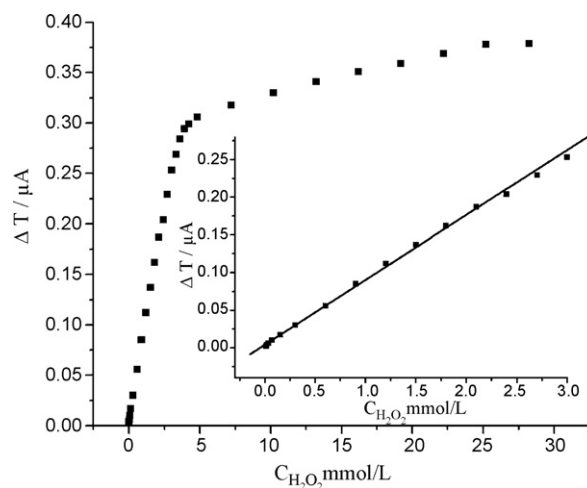


Fig. 8. Calibration curve of the response of the biosensor to concentration. (Inset) The linear part of the calibration curve.

Table 1
Determination of H₂O₂ in plant leaves (n = 3).

Samples	Found (mmol L ⁻¹)	Added (mmol L ⁻¹)	Total found (mmol L ⁻¹)	Recovery (%)	Spectrophotometry [44] (mmol L ⁻¹)
1	0.0532 ± 0.0024	0.050	0.101 ± 0.003	95.6	0.0514
		0.100	0.147 ± 0.007	93.8	
2	0.0613 ± 0.0031	0.050	0.109 ± 0.004	95.4	0.0573
		0.100	0.158 ± 0.005	96.7	

higher than 1.0 V s⁻¹. All these results are in accordance with the typical surface-controlled or thin-layer electrochemical behavior, as expected for immobilized systems.

3.3. Steady-state amperometric response to H₂O₂ and calibration

The dependence of the enzyme electrode on the applied potential for amperometric signal to 0.1 mmol H₂O₂ was investigated initially. In the range between 0.1 and -0.25 V, the response increased first and then reached a pseudo-plateau for lower than -0.15 V. Thus -0.15 V was selected as applied potential in subsequent experiments. Under the optimized experimental conditions, the typical current-time plot of the enzyme electrode resulted from successive injections of H₂O₂ was observed in the stirred buffer solution as shown in Fig. 7. When an aliquot of H₂O₂ was added into the stirring buffer solution, the reduction current rose sharply to reach a steady-state value. The response time (reaching 90% of the maximum response) was less than 5 s, which indicates a fast process and the immobilized HRP could well catalyze the reduction of H₂O₂. It is faster than the reported results of HRP that immobilized on gold colloid/cysteine/nafion-modified platinum disk electrode (10 s) [39] and similar to that of HRP in silica sol-gel network on gold modified electrode [11]. The faster response was mainly attributed to the follows: first, H₂O₂ can freely diffuse to the HRP molecules which are exposed to the surface of AuNPs. Second, the AuNPs are favorable to the orientation of the HRP molecule and provide a necessary conductive pathway to transfer electrons.

Fig. 8 corresponded to the calibration plot of the biosensor. The currents had a good linear relationship with the concentration of H₂O₂ in the range of 8.0 μmol L⁻¹ to 3.0 mmol L⁻¹ with a correlation coefficient of 0.999. The biosensor has a detection limit of 2.0 μmol L⁻¹ estimated at a signal to noise ratio of 3. Tangkuaram reported the H₂O₂ biosensors fabricated by modified HRP on disposable screen-printed carbon electrodes with AuNPs and the linear range of concentration was 10 μmol L⁻¹ to 11.3 mmol L⁻¹ [18]. By comparison this result, the proposed biosensor shows similar low limit and narrow wide of the linear range. This maybe attribute to lower load of enzyme in the proposed biosensor than that in the screen-printed carbon electrode.

The plot shows a Michaelis-Menten type response when the concentration of H₂O₂ is at a higher level. The apparent Michaelis-Menten constant (K_M^{app}), a reflection of both the enzymatic affinity and the ratio of microscopic kinetic constants, can be obtained from electrochemical version of the Line weaver-Burk equation [40]. The K_M^{app} was determined by analysis of the slope and intercept for the plot of the reciprocals of the steady-state current versus H₂O₂ concentration. The K_M^{app} value for the HRP/Cys/AuNPs/ITO electrode was found to be 0.4 mmol L⁻¹, which is smaller than those of 4.51 mmol L⁻¹ for HRP bound with AuNPs in the matrix of chitosan on screen-printed carbon electrodes [18], 2.3 mmol L⁻¹ for HRP/Au colloid self-assembly monolayer electrode [41] and 2.2 mmol L⁻¹ for HRP on TMB/AuNPs modified ITO electrode [22], and close to 0.57 mmol L⁻¹ of HRP based on chitosan-gold nanoparticle nanocomposite [7]. These results further show that the biosensor exhibits higher biological affinity to

H₂O₂ and the HRP enzyme on the electrode kept its activity with a low-diffusion barrier.

3.4. Reproducibility and stability

The repeatability of the biosensor was valued at a H₂O₂ concentration of 0.05 mmol L⁻¹ in 50 mmol L⁻¹ PBS with the same enzyme electrode. The relative standard deviation (R.S.D.) was 3.2% for nine successive assays. The electrode-to-electrode reproducibility was determined in the presence of the same concentration H₂O₂ with six different enzyme electrodes, prepared independently. It shows an acceptable reproducibility with a R.S.D. of 4.6%.

The stability of the enzyme electrode was also examined during storage in a drying state at 4 °C. It was found that the current response remained nearly 83% of its initial value over 12 weeks. The stability of the biosensor is much better than HRP bound with AuNPs in the matrix of chitosan on screen-printed carbon electrodes [18] or immobilized on AuNPs modified ITO electrode with mediator [22]. The long-term stability can be attributed to good biocompatibility of AuNPs and strongly interaction between enzyme and AuNPs.

3.5. Selectivity and real sample analysis

The effect of substances that might interfere with the response of the biosensor was studied. The selectivity of the biosensor was examined in the presence of 0.2 mmol L⁻¹ H₂O₂. The addition of the same concentration uric acid, acetaminophen and glucose did not cause observable interference. While in the presence of 0.2 mmol L⁻¹ ascorbic acid the response of the biosensor increased about 8%, which interfered slightly. Only 0.05 mmol L⁻¹ sulfide decreased the response 21% and has a significant interference. This result was similar to previous report [42].

In order to illustrate feasibility of the composite modified electrode in practical analysis, the HRP/Cys/AuNPs/ITO electrode was used to detect the H₂O₂ concentration in the extraction solution of the plant leaves. The extraction solution of the plant leaves was prepared as follows [43], the fresh plant leaves were first clear, then triturated the clear leaves, and finally centrifuged. The determination was developed by standard addition method. Table 1 shows the determined values and the recovery values. The results obtained by proposed HRP biosensor were also compared to those determined by spectrophotometric method [44]. The aliquot of sample solution was added in the mixture solution which contained 3,3',5,5'-tetramethylbenzidine and HRP in acetate buffer (pH 5.0). The absorbance of the resulting solution at 652 nm was recorded by spectrophotometer. Analytical recoveries were in the range 93–97% and the results are satisfactory by comparison with the reference method.

4. Conclusions

The method for direct electrochemical deposition of AuNPs onto ITO electrode surface has been developed. The average size of the deposited AuNPs is about 25 nm with a quite symmetric distribution. A disposable electrochemical H₂O₂ biosensor was fabricated

by immobilizing HRP on AuNPs/ITO electrode surface in the presence of Cys. AuNPs is very efficient for retaining the enzyme activity and promoting the electron transfer. The direct electron transfer of HRP in the enzyme electrode was realized and the biosensor could catalyze the direct reduction of H₂O₂. The enzyme electrode exhibits several good electrochemical characteristics such as short response time, high sensitivity, selectively and long-term stability. Based on the AuNPs and low-cost ITO substrate, this proposed method presented here is rapid, easy, and simple. Practically, the promising platform presented here not only can be used for fabrication of disposable biosensors based on HRP, but also can be extended to other proteins.

Acknowledgements

This work was supported by the National Natural Science Foundation of China (no. 20675055), the Science Foundations of the Education Bureau (07KJB150101) and Key Academic Discipline of Organic Chemistry of Jiangsu Province.

References

- [1] L. Wang, E. Wang, *Electrochem. Commun.* 6 (2004) 225.
- [2] J. Zhang, M. Oyama, *J. Electroanal. Chem.* 577 (2005) 273.
- [3] E. Ferapontova, K. Schmengler, T. Borchers, T. Ruzgas, L. Gorton, *Biosens. Bioelectron.* 17 (2002) 953.
- [4] G. Maduraiveeran, R. Ramaraj, *Electrochem. Commun.* 9 (2007) 2051.
- [5] J. Xu, J. Zhu, Q. Wu, Z. Hu, H. Chen, *Electroanalysis* 15 (2003) 219.
- [6] L. Qian, X. Yang, *Talanta* 68 (2006) 721.
- [7] Q. Xu, C. Mao, N. Liu, J. Zhu, J. Sheng, *Biosens. Bioelectron.* 22 (2006) 768.
- [8] Q. Gao, F. Yang, Y. Ma, X. Yang, *Electroanalysis* 16 (9) (2004) 730.
- [9] A. Morrin, F. Wilbeer, O. Ngamna, S.E. Moulton, A.J. Killard, G.G. Wallace, M.R. Smyth, *Electrochem. Commun.* 7 (2005) 317.
- [10] A. Heller, *Acc. Chem. Res.* 23 (1990) 128.
- [11] J. Di, C. Sheng, S. Peng, Y. Tu, S. Li, *Anal. Chim. Acta* 553 (2005) 196.
- [12] C. Lei, S. Hu, G. Shen, R. Yu, *Talanta* 59 (2003) 981.
- [13] Y. Wang, W. Qian, Y. Tan, S. Ding, H. Zhang, *Talanta* 72 (2007) 1134.
- [14] S. Zhang, N. Wang, Y. Niu, C. Sun, *Sens. Actuat. B: Chem.* 109 (2005) 367.
- [15] J. Li, J. Yu, F. Zhao, B. Zeng, *Anal. Acta Chim.* 587 (2007) 33.
- [16] L. Wang, W. Mao, D. Ni, J. Di, Y. Wu, Y. Tu, *Electrochem. Commun.* 10 (2008) 673.
- [17] J. Di, S. Peng, C. Shen, Y. Gao, Y. Tu, *Biosens. Bioelectron.* 23 (2007) 88.
- [18] T. Tangkuaram, C. Ponchio, T. Kangkasomboon, P. Katikawong, W. Veerasai, *Biosens. Bioelectron.* 22 (2007) 2071.
- [19] J. Zhang, M. Kambayashi, M. Oyama, *Electroanalysis* 17 (2005) 408.
- [20] K. Hayashi, Y. Iwasaki, T. Horiuchi, K. Sunagawa, A. Tate, *Anal. Chem.* 77 (2005) 5236.
- [21] X. Sun, K.D. Gillis, *Anal. Chem.* 78 (2006) 2521.
- [22] J. Lin, L. Zhang, S. Zhang, *Anal. Biochem.* 370 (2007) 180.
- [23] J. Lin, W. Qu, S. Zhang, *Anal. Biochem.* 360 (2007) 288.
- [24] W. Cheng, E. Wang, S. Dong, *Langmuir* 18 (2002) 9947.
- [25] J. Zhang, M. Oyama, *Anal. Chim. Acta* 540 (2005) 299.
- [26] X. Dai, R.G. Compton, *Anal. Sci.* 22 (2006) 567.
- [27] J. Jia, B. Wang, A. Wu, G. Cheng, Z. Li, S. Dong, *Anal. Chem.* 74 (2002) 2217.
- [28] Y. Xiao, H. Ju, H. Chen, *Anal. Chim. Acta* 391 (1999) 73.
- [29] Y. Zhuang, J.W. Zheng, Q. Zhou, *Rare Met. Mater. Eng.* 36 (2007) 431.
- [30] I. Hussain, Z. Wang, A.I. Cooper, M. Brust, *Langmuir* 22 (2006) 2938.
- [31] H. Cui, W. Wang, C. Duan, Y. Dong, J. Guo, *Chem. Eur. J.* 13 (2007) 6975.
- [32] H. Zhao, F. Yin, X. Xu, D. Wang, Z. Xu, W. Zhang, J. Zheng, *Precious Met.* 28 (3) (2007) 29.
- [33] K.L. Kelly, E. Coronado, L.L. Zhao, G.C. Schatz, *J. Phys. Chem. B* 107 (2003) 668.
- [34] S.K. Ghosh, S. Nath, S. Kundu, K. Esumi, T. Pal, *J. Phys. Chem. B* 108 (2004) 13963.
- [35] A.N. Shipway, E. Katz, I. Willner, *ChemPhysChem* 1 (2000) 18.
- [36] G. Decher, J.D. Hong, *Macromol. Symp.* 46 (1991) 321.
- [37] G. Decher, *Science* 277 (1997) 1232.
- [38] J.J. Harris, M.L. Bruening, *Langmuir* 16 (2000) 2006.
- [39] Y. Zhao, W. Zhang, H. Chen, Q. Luo, S. Fong, Y. Li, *Sens. Actuat. B: Chem.* 87 (2002) 168.
- [40] R.A. Kamin, G.S. Willson, *Anal. Chem.* 52 (1980) 1198.
- [41] E.E. Ferapontova, *Electroanalysis* 16 (2004) 225.
- [42] B. Wang, B. Li, Z. Wang, G. Xu, Q. Wang, S. Dong, *Anal. Chem.* 71 (1999) 1935.
- [43] S. Cao, R. Yuan, Y. Chai, L. Zhang, X. Li, F. Gao, *Bioprocess Biosyst. Eng.* 30 (2007) 71.
- [44] P.D. Josephy, T. Eling, R.P. Mason, *J. Biol. Chem.* 257 (1982) 3669.



Synthesis of aqueous CdTe quantum dots embedded silica nanoparticles and their applications as fluorescence probes

Chao Wang, Qiang Ma, Wenchao Dou, Shamsa Kanwal, Guannan Wang, Pingfan Yuan, Xingguang Su*

Department of Analytical Chemistry, College of Chemistry, Jilin University, 10 Qianwei Road, Changchun 130012, China

ARTICLE INFO

Article history:

Received 2 July 2008

Received in revised form 4 September 2008

Accepted 10 September 2008

Available online 19 September 2008

Keywords:

Quantum dots

Silica nanoparticles

Reverse microemulsion method

Bioassay

ABSTRACT

This paper presents the synthesis of aqueous CdTe QDs embedded silica nanoparticles by reverse microemulsion method and their applications as fluorescence probes in bioassay and cell imaging. With the aim of embedding more CdTe QDs in silica spheres, we use poly(dimethyldiallyl ammonium chloride) to balance the electrostatic repulsion between CdTe QDs and silica intermediates. By modifying the surface of CdTe/SiO₂ composite nanoparticles with amino and methylphosphonate groups, biologically functionalized and monodisperse CdTe/SiO₂ composite nanoparticles can be obtained. In this work, CdTe/SiO₂ composite nanoparticles are conjugated with biotin-labeled mouse IgG via covalent binding. The biotin-labeled mouse IgG on the CdTe/SiO₂ composite nanoparticles surface can recognize FITC-labeled avidin and avidin on the surface of polystyrene microspheres by protein–protein binding. Finally, the CdTe/SiO₂ composite nanoparticles with secondary antibody are used to label the MG63 osteosarcoma cell with primary antibody successfully, which demonstrates that the application of CdTe/SiO₂ composite nanoparticles as fluorescent probes in bioassay and fluorescence imaging is feasible.

© 2008 Elsevier B.V. All rights reserved.

1. Introduction

Quantum dots (QDs), also named semiconductor nanocrystals, show great potentials as a new type of labeling and imaging material in biological and biomedical applications for their unique optical properties such as size tunable fluorescence and narrow and symmetric emission profile with a broad excitation range [1–3]. However, QDs are still facing some unsolved problems as follows: ultra-sensitivity of their fluorescence to the surface states, cytotoxicity of heavy metal ions used in the process of synthesis which are released upon photo-oxidation, and chemical and colloidal instabilities in harsh chemical environments [2]. So depositing a layer with the capability of impeding surface ruin of QDs and inhibiting release of heavy metal ions are effective ways to solve the problems. Silica is one of the most popular inert materials for surface coating, which has several particular advantages compared with other materials. Firstly, silica is a non-toxic substance and can be easily modified with functionalized groups which can conjugate with biomolecules. Secondly, because of the resistance of silica to both aqueous (except extremely high-pH solution) and non-aqueous solvents, leakage can be avoided [4]. Finally, silica nanoparticles are easy to be separated by centrifugation during preparation, func-

tionalization, and other solution treatment processes due to high density of silica [5].

Up to the present time, there are mainly two kinds of routes for preparing silica spheres. One is Stöber process-based approaches, the other is reverse microemulsion method. Stöber process is difficult to apply when nanoparticles are insoluble in the alcohol–water solution. So for QDs synthesized by organometallic method, ligand exchange is usually required prior to the Stöber process [6–9], which is commonly associated with a decrease of fluorescent efficiency of QDs. For aqueous QDs, the Stöber process can be directly utilized to synthesize both QDs@SiO₂ core–shell structure [10] and “raisin-bun”-type submicrometer-size composite spheres [11]. Previous investigations revealed that the size of QDs/SiO₂ particles synthesized by Stöber method can be controlled by the thickness of the silica shell over the range from a few nanometers to several micrometers, but multi-step procedures were required [2], and the size distribution of the QDs/SiO₂ particles is not fairly narrow.

As an alternative method, reverse microemulsion method utilizes water-in-oil microemulsions where the silica spheres are synthesized by the hydrolysis of tetraethoxysilane (TEOS), followed by its condensation in the water nanodroplets [12]. Nanoparticles [2], chelates [13], and organic dye molecules [14] can be encapsulated by silica spheres as long as they are soluble in water. Recently, Ying and his co-workers [3,15] reported a reverse micelle-based approach for synthesizing silica-coating hydrophobic QDs

* Corresponding author. Tel.: +86 431 85168352.
E-mail address: suxg@mail.jlu.edu.cn (X. Su).

and varieties of hydrophobic nanoparticles. So both aqueous and non-aqueous nanoparticles can be introduced into silica spheres by reverse microemulsion method. Using this method, more uniform spheres in the size range of 30–150 nm (particle in this size range can penetrate the cells) can be obtained comparing with the Stöber process. Simultaneously, the reaction condition of the reverse microemulsion method is relatively robust, and the resulting silica spheres have smoother surfaces [16]. So the study on the synthesis of CdTe/SiO₂ composite nanoparticles with high fluorescence emission by reverse microemulsion method is expected to be quite significant, and few reports [18–20] are available on the applications of CdTe/SiO₂ composite nanoparticles as fluorescent probes.

In this work, we embedded aqueous CdTe QDs in silica spheres by reverse microemulsion method and functionalized the silica spheres as photostable fluorescent probes were applied to biological labels. High-quality CdTe QDs were synthesized with mercaptosuccinic acid (MSA) as stabilizer which can accelerate the growth of CdTe QDs [21]. As the intermediate silica species can carry negative charges at pH 11, the same pH as CdTe QDs stabilized by MSA, only one QD can be coated by silica sphere [1], which may weaken the fluorescence intensity of CdTe@SiO₂ core-shell nanoparticles and limit their applications. With the aim of embedding more CdTe QDs in silica spheres, we used poly(dimethyldiallyl ammonium chloride) (PDDA) to balance the electrostatic repulsion between CdTe QDs and silica intermediates, which enhanced the fluorescence intensity of CdTe/SiO₂ composite nanoparticles effectively. Subsequently, we modified the surface of silica spheres with 3-aminopropyltrimethoxysilane (APS) and 3-(trihydroxysilyl)-propylmethylphosphonate (THPMP). The modified surface of silica nanoparticles has amino groups as functional groups which combine with biomolecules and methylphosphonate groups as stabilizing groups which reduce aggregation of silica nanoparticles [17]. The CdTe/SiO₂ composite nanoparticles were linked with biotin-labeled mouse IgG via covalent binding. Furthermore, they can recognize FITC-labeled avidin and avidin on the surface of polystyrene microspheres successfully through the high affinity between avidin and biotin. Finally, the CdTe/SiO₂ composite nanoparticles were used to label the MG63 osteosarcoma cell, which demonstrates the application of CdTe/SiO₂ composite nanoparticles as fluorescent probes in bioassay and fluorescence imaging is feasible.

2. Experimental

2.1. Materials

All chemicals used are of analytical reagent grade without further purification. Mercaptosuccinic acid (MSA) (99%) and poly(dimethyldiallyl ammonium chloride) (PDPA, Mw = 70,000 g/mol) were purchased from J&K Chemical Co. Tellurium powder (~200 mesh, 99.8%), CdCl₂ (99%), NaBH₄ (99%), cyclohexane, Triton X-100, *n*-hexanol, tetraethoxysilane (TEOS), 3-aminopropyltrimethoxysilane (APS), 3-(trihydroxysilyl)-propylmethylphosphonate (THPMP), fluorescamine, biotin-labeled mouse IgG, FITC-labeled avidin, avidin, poly(sodium 4-styrene sulfonate) (PSS, Mw = 70,000 g/mol), and negatively charged sulfate-stabilized polystyrene (PS) microsphere of average diameter 3 μm, were purchased from Sigma-Aldrich Chemical Co. The primary antibody (β-actin raised against gizzard actin of chicken origin) was purchased from Santa Cruz Biotechnology Inc. The secondary antibody (rabbit anti-chicken IgG) was purchased from Beijing Ding Guo Biotech. Co. Ltd. The MG63 osteosarcoma cells in the cell culture medium were obtained from the key laboratory of pathobiology ministry of education, Jilin University.

The water used in all experiments has a resistivity higher than 18 MΩ/cm.

2.2. Instrument

Fluorescence measurements were performed on a ShimadzuRF-5301 PC spectro fluorophotometer. UV-vis absorption spectra were obtained using a Varian GBC Cintra10e UV-visible spectrometer. In both experiments, a 1-cm path-length quartz cuvette was used. Transmission electron microscopy (TEM) and high-resolution transmission electron microscopy (HRTEM) images were obtained with a JEOL-3010 electron microscope operating at 300 kV. TEM samples were prepared by dropping the CdTe/SiO₂ composite nanoparticles dispersed in absolute ethanol solution onto carbon-coated copper grids, while the excess solvent evaporated. A dynamic light scattering technique (Nano ZS model, ZEN 3600, Malvern Instruments) was used to determine the hydrodynamic radius and zeta potential of CdTe/SiO₂ composite nanoparticles. The particle size and zeta potential were analyzed using a dilute suspension of particles in water with resistivity higher than 18 MΩ/cm. Fluorescence microscopy was carried out using an inverted optical microscope (Leica DM IRB, Germany) equipped with a charge-coupled device camera (TOTA 500 II, Japan) and a 100-W Hg excitation lamp. All optical measurements were carried out at room temperature under ambient conditions.

In this experiment, the fluorescence intensities are reported in arbitrary units, the experimental parameters within a given experiment are the same and the fluorescence intensities are comparable within a given experiment.

2.3. Preparation of CdTe QDs

CdTe QDs were synthesized by refluxing routes as described in detail in Ref. [21]. Briefly, the precursor solution of CdTe QDs was formed in water by adding fresh NaHTe solution to 10-mM N₂-saturated CdCl₂ solution at pH 11.2 in the presence of MSA as stabilizing agent. The molar ratio of Cd²⁺/MSA/HTe⁻ was charged at 1:1.5:0.2. The CdTe precursor solution was subjected to reflux at 100 °C under open-air conditions with condenser attached, and different sizes of CdTe QDs were obtained at different refluxing times. The synthesis of CdTe QDs with MSA as stabilizer was less-time consuming and the obtained QDs had high quantum yield [21]. The photoluminescence (PL) emission wavelengths of CdTe QDs used in this study are 591 nm and 633 nm, respectively. The mean diameters of QDs with PL emission wavelength at 591 nm and 633 nm are 3.3 nm and 3.8 nm, respectively [21].

2.4. Synthesis of CdTe/SiO₂ composite nanoparticles

The CdTe/SiO₂ composite nanoparticles were prepared by reverse microemulsion method at room temperature. In this method, cyclohexane was used as a continuous phase, and Triton X-100 and *n*-hexanol were regarded as surfactant and co-surfactant respectively. Briefly, we mixed 7.5 mL cyclohexane, 1.77 mL Triton X-100, 1.8 mL *n*-hexanol, 400 μL aqueous solution of as-prepared CdTe QDs, certain amount of PDPA solution (0.075%, v/v) and 60 μL NH₄OH to form microemulsion. Then adding 100 μL TEOS to the microemulsion system to initiate the hydrolysis, the reaction progressed in the dark for 24 h of stirring. The microemulsion was broken by adding 20 mL of acetone to the reaction system and the resultant precipitate was CdTe/SiO₂ composite nanoparticles which were washed in sequence with iso-propyl alcohol, ethanol and water. During each washing procedure, the silica composite nanoparticle dispersion was first subjected to high-velocity centrifugation (8000 rpm, 10 min), followed by decantation of the

supernatant and re-dispersion of the precipitate in the next solvent with the aid of supersonication. Ultimately, aqueous dispersed CdTe/SiO₂ composite nanoparticles were obtained for further characterization.

2.5. Surface functionalization of CdTe/SiO₂ composite nanoparticles

Surface functionalization of CdTe/SiO₂ composite nanoparticles is important for further application as fluorescent biomarkers. Initially, we added 50 μL TEOS to the reaction system after the hydrolysis of TEOS for 24 h. After stirring for 30 min, 10 μL APS and 40 μL THPMP were injected into the reaction system. The reaction system was then kept under stirring for one more day. The resultant amine-functionalized CdTe/SiO₂ composite nanoparticles were washed by the same purification procedures as those mentioned above. The presence of surface amino groups of the composite nanoparticles was proved by fluorescamine.

2.6. Covalent binding of the biotin-labeled mouse IgG with CdTe/SiO₂ composite nanoparticles

The biotin-labeled mouse IgG was connected with the amino groups on the surface of the CdTe/SiO₂ composite nanoparticles by glutaraldehyde [13,22]. Amino-modified CdTe/SiO₂ composite nanoparticles were suspended in phosphate buffer (2 mM PBS, pH 7.4). We added 100 μL 1% glutaraldehyde to the 100 μL CdTe/SiO₂ composite nanoparticles solution vibrating for 1 h. Then 200 μL biotin-labeled mouse IgG (1%, v/v) was incubated with amine-activated silica composite nanoparticles for 12 h at 4 °C. After that, 2 mg of NaBH₄ was added, and the mixture was vibrated at room temperature for 2 h. Here, biotin-labeled mouse IgG was covalently bonded to the CdTe/SiO₂ composite nanoparticles. At last, the nanoparticles were centrifuged and washed with the PBS several times to remove the excess biotin-labeled mouse IgG, and kept in the dark at 4 °C.

2.7. Protein–protein binding between biotin-labeled mouse IgG on the surface of CdTe/SiO₂ composite nanoparticles and FITC-labeled avidin

The biotin-labeled mouse IgG-modified CdTe/SiO₂ composite nanoparticles (biotin-silica NPs) were blocked with 100 μL PBS and BSA (1%, w/v). Then different volumes of FITC-labeled avidin solution (1 μg/mL) were added to the 100 μL solution. The mixture was diluted with PBS to 1 mL and incubated for 12 h at 4 °C. Finally, the mixture was centrifuged to remove the excess FITC-labeled avidin, and re-dispersed with 1 mL PBS to measure the PL emission of FITC.

2.8. Bioassay

Layer-by-layer method was utilized for immobilizing avidin on PS microspheres (PS-avidin microspheres). The first step is the deposition of 200 μL 2 mg/mL PDDA and PSS onto the PS microspheres alternately [23]. Then four-layer (PDDA/PSS/PDDA/PSS, PE₄) polyelectrolyte film provided both a smooth and uniform negatively charged outer surface to facilitate the adsorption of the positively charged avidin by electrostatic attraction. By using avidin solution (0.1 mg/mL), tri-layer (avidin/PSS/avidin) film was deposited on the surface of PS microspheres in the same way. During each deposition process, the microspheres were washed twice with 1 mL PBS by centrifugation (3000 rpm, 10 min). At last, the PS-avidin microspheres were dispersed with 1 mL PBS and BSA (1%, w/v) for the next bioassay.

We took 100 μL biofunctional biotin-silica NPs solution, adding different amounts of PS-avidin microspheres to the solution, which were vibrated overnight at 4 °C. By high-binding activity between avidin and biotin, the PS-avidin microspheres can be combined with biotin-silica NPs. After supersonic dispersion of mixture, centrifugation (2000 rpm, 10 min) was used to separate the PS-avidin microspheres/biotin-silica NPs (PS-silica spheres) from the excess biotin-silica NPs. The PS-silica spheres were resuspended in 1 mL PBS and sonicated before detection.

2.9. Cell labeling experiment

The MG63 osteosarcoma cells were cultured (5% CO₂ at 37 °C) on glass coverslips in 24-well plate in cell culture medium. When the cultured cells reached about 50–60% confluence, 2 μL primary antibodies (β-actin) were added to the well with 200 μL cell culture medium. After 12 h, 10 μL CdTe/SiO₂ composite nanoparticles conjugated with secondary antibody (rabbit anti-chicken IgG) solution were added into the same well, and incubated for 6 h. After washing with PBS for three times, the cells were fixed with 2.5% glutaraldehyde for 10 min at room temperature. After washing with PBS for three times, the coverslips with cells were mounted onto glass slides and allowed to dry overnight prior to investigation by fluorescence microscopy.

3. Results and discussion

3.1. Photoluminescence properties of CdTe/SiO₂ composite nanoparticles

The UV–vis and PL emission spectra of CdTe/SiO₂ composite nanoparticles and CdTe QDs were shown in Figs. 1 and 2, respectively. It can be seen that the position of the PL emission peak of CdTe/SiO₂ composite nanoparticles was nearly invariant, though the PL emission intensity of the composite nanoparticles was much weaker than that of CdTe QDs. The possible explanation to this phenomenon may be that the interaction between the silica networks and QDs exists in the composite nanoparticles, which is unfavorable for the fluorescence emission of the QDs.

The quantity of CdTe QDs embedded in the CdTe/SiO₂ composite nanoparticles is determined in the hydrolysis process of TEOS. The electrostatic forces of repulsion between the negatively charged silica intermediates and negatively charged CdTe QDs during the hydrolysis step of TEOS were not negligible [1,2]. Before TEOS was introduced into the reaction system, the electrostatic forces of repulsion between the negatively charged CdTe QDs were

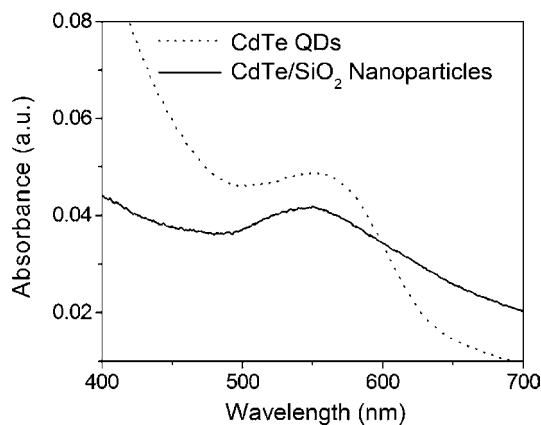


Fig. 1. The UV absorption spectra of CdTe QDs and CdTe/SiO₂ composite nanoparticles.

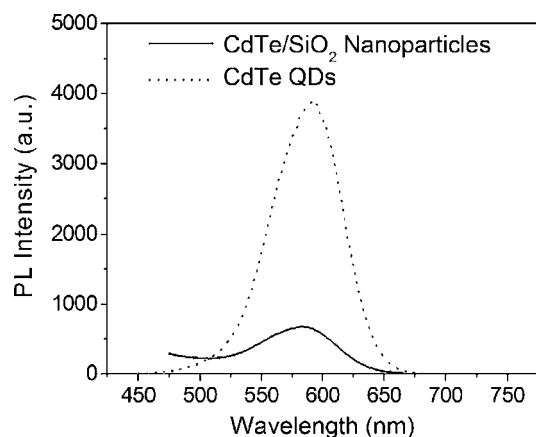


Fig. 2. The PL emission spectra of CdTe QDs and CdTe/SiO₂ composite nanoparticles.

screened by the positive charge from the background cations, NH₄⁺, and Na⁺, making the whole system in the condition of electrostatic equilibrium, which was consistent with the aqueous solution of CdTe QDs that can exist stably for over years. However, after addition of TEOS into the reaction system, TEOS can cross the oil–water interface by diffusion and start to hydrolyze upon the catalysis of ammonia. And the partly hydrolyzed TEOS molecules are strong hydrophilic which will enter the aqueous phase completely. The succeeding condensation between hydrolyzed species in reverse micro-micelles results in silica oligomers, which are regarded as negatively charged polyelectrolyte as the pK_a of the silanol groups were reported to be 7 approximately. Therefore, the former condition of electrostatic equilibrium was disturbed. With the process of condensation, the silica oligomers evenly distributed throughout the whole micro-micelle, and the local negatively charged background would reduce the screen between different CdTe QDs. So most of the CdTe QDs will be driven to the boundary of the aqueous microdroplet, and the washing processes can remove the QDs from the surface of composite nanoparticles.

Therefore, we wanted to introduce a kind of polycation, which will not affect the PL emission of CdTe QDs, and can keep the electrostatic balance during the process of condensation. PDDA is the appropriate one that we needed, because many quaternary ammonium cations exist in its solution which can balance the electrostatic interactions between the silica oligomers and CdTe QDs. We introduced different amounts of PDDA to optimize the PL emission intensity of CdTe/SiO₂ composite nanoparticles and the results are

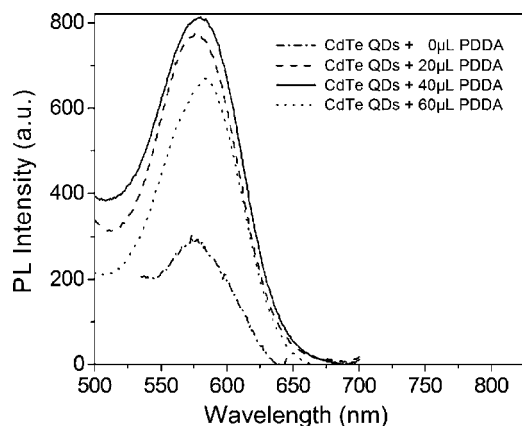


Fig. 3. The change of PL emission spectra with different amounts of PDDA added to the reverse microemulsion system.

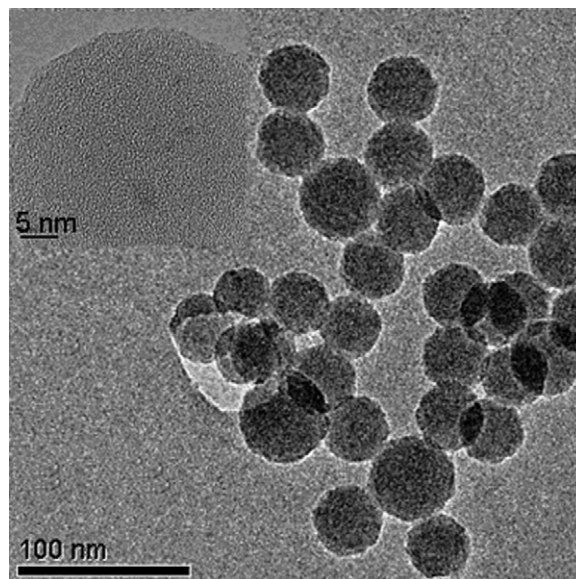


Fig. 4. The TEM image of CdTe/SiO₂ composite nanoparticles. The insert is the HRTEM image of a part of CdTe/SiO₂ composite nanoparticles.

indicated in Fig. 3. From Fig. 3, it can be seen that suitable amount of PDDA can screen the electrostatic repulsion effectively during the process of hydrolysis, thus the PL emission property of CdTe/SiO₂ composite nanoparticles is improved. Without PDDA, only one CdTe QD can be coated by the silica sphere [1], which may weaken the fluorescence intensity of CdTe@SiO₂ core–shell nanoparticles and limit their applications. Oppositely, excess amount of PDDA can make CdTe QDs precipitate so as to lower the PL emission intensity of CdTe/SiO₂ composite nanoparticles. Thus by introducing 40 μL PDDA (0.075%, v/v) into the reverse microemulsion system, we obtained the optimal PL emission intensity of CdTe/SiO₂ composite nanoparticles. Furthermore, through images of HRTEM and TEM of CdTe/SiO₂ composite nanoparticles shown in Fig. 4, we proved the CdTe QDs were indeed embedded in silica spheres. From the HRTEM image (Fig. 4 insert), the black spot can be seen in the silica composite nanoparticles and the size of the black spot is the same as the size of CdTe QDs used (3.3 nm). So we can conclude that CdTe QDs have been embedded in silica nanoparticles successfully by reverse microemulsion method.

3.2. Surface modification of CdTe/SiO₂ composite nanoparticles

Proper surface modification of silica composite nanoparticles is important for further biological applications. Various silane-coupling agents can be connected with the silica composite nanoparticles to functionalize the surface of nanoparticles. In our study, APS was grafted on the surface of CdTe/SiO₂ composite nanoparticles to introduce amino groups as the active functional groups.

In neutral solution, the amino groups have positive charges, and silica groups have negative charges. The amine-modified silica nanoparticles can back bond to the surface silanol groups, which conduces the very low total charges on the silica nanoparticle surface and no driving force on the nanoparticle surface to keep them separated, so the nanoparticles tend to aggregate [17]. To avoid agglomeration of nanoparticles, the inert stabilizing groups – methylphosphonate – were introduced onto the surface of silica composite nanoparticles. The majority of amino groups electrostatic interact with methylphosphonate groups, which blocks the aggregation of nanoparticles effectively.

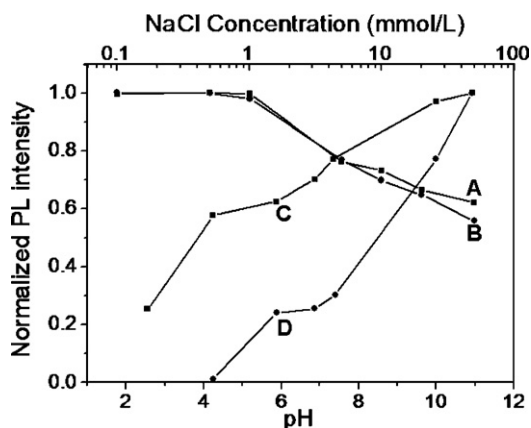


Fig. 5. The influence of ionic strength on the PL emission of CdTe/SiO₂ composite nanoparticles (A) and CdTe QDs (B). The influence of pH on the PL emission of CdTe/SiO₂ composite nanoparticles (C) and CdTe QDs (D).

We measured the overall surface charges by the zeta potential and the average hydrodynamic particle size by dynamic light scattering (DLS) to investigate the dispersion of CdTe/SiO₂ composite nanoparticles in solution. From the results, the zeta potential of CdTe/SiO₂ composite nanoparticles is -36.9 mV, which can prevent the aggregation of composite nanoparticles effectively by electrostatic repulsion [24]. At the same time, by the DLS measurement, the average hydrodynamic particle size of CdTe/SiO₂ composite nanoparticles is 72 nm, which is more representative actual size of the composite nanoparticles in solution (the average diameter of CdTe/SiO₂ composite nanoparticles is 40 nm, as determined by TEM measurements in Fig. 4) [17]. The size distribution of CdTe/SiO₂ composite nanoparticles is quite narrow (Pd I: 0.132), which proves that the composite nanoparticles really appear in the form of monodisperse species in solution. That was also verified by the TEM image of the silica composite nanoparticles, from which it can be seen that the silica composite nanoparticles were kept apart from each other.

After surface modification of CdTe/SiO₂ composite nanoparticles, the presence of amino groups on the surface of CdTe/SiO₂ composite nanoparticle was detected by fluorescamine. Fluorescamine is not a fluorescent chemical essentially, and it has not any fluorescent emission in acetone. Only when fluorescamine reacts with primary amines, the fluorescence peak at 480 nm can appear in the fluorescent spectra. In this study, when fluorescamine was added into the CdTe/SiO₂ composite nanoparticles solution, besides the PL emission peak of CdTe/SiO₂ composite nanoparticles, a new high-PL emission peak at 480 nm can also be seen (not shown). The appearance of a new PL emission peak at about 480 nm suggests that amino groups were successfully grafted on the surface of the CdTe/SiO₂ composite nanoparticles.

3.3. Stability property of the CdTe/SiO₂ composite nanoparticles

Under physiological condition, ionic strength and pH are the important parameters of the buffer solution. So the influences of ionic strength and pH on the PL properties of CdTe/SiO₂ composite nanoparticles and CdTe QDs were investigated in this study. It is known to all, high ionic strength and high acidity will affect the PL emission intensity of CdTe QDs. Especially, when the $\text{pH} \leq 4$, the PL emission intensity of naked CdTe QDs was quenched totally [22]. Fig. 5 shows the influence of both ionic strength and pH on the PL emission of CdTe/SiO₂ composite nanoparticles and CdTe QDs. In different ionic strength solution, CdTe/SiO₂ composite nanoparticles are more insusceptible than naked CdTe QDs. When the concentration of NaCl is up to 50 mM, there is still not any precipitation in the CdTe/SiO₂ composite nanoparticles solution. As to the effect of pH, the CdTe/SiO₂ composite nanoparticles exhibit good stability obviously. When the pH is 4.24, the PL emission intensity of the silica composite nanoparticles is 60% as compared to that in alkaline solution. However, at the same pH, the PL emission intensity of CdTe QDs almost decreased to zero. So when the CdTe QDs were coated by silica, the stability of PL emission of the CdTe QDs could be enhanced. For higher ionic strength and acidity, H⁺ and salt ion in the aqueous solution can slowly permeate through

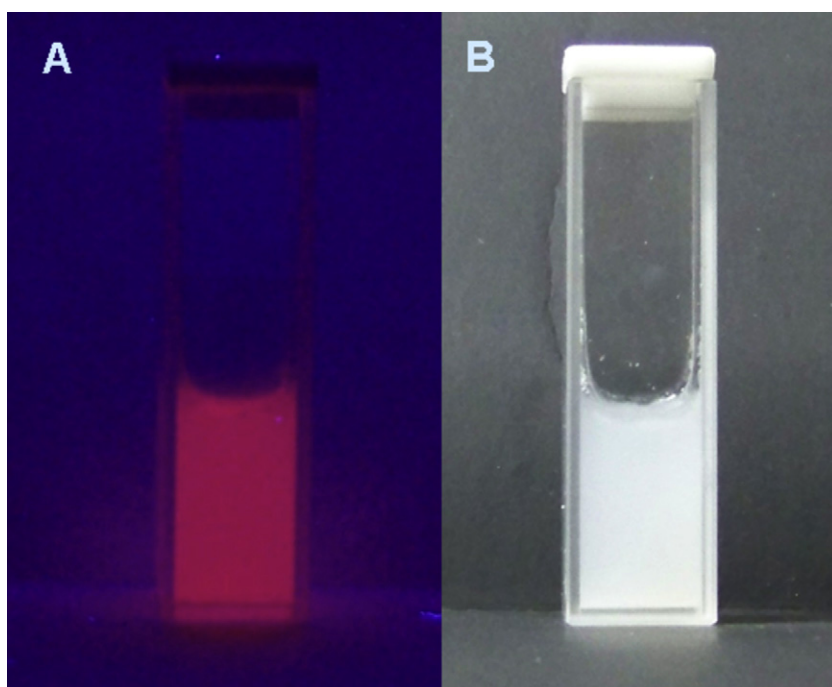


Fig. 6. The photographs of CdTe/SiO₂ composite nanoparticles with amino groups under UV light (A) and daylight (B).

the silica coatings to affect the PL emission intensity of the CdTe QDs due to the hydrophilic essence and porous structure of the silica. The above-mentioned results indicate that the PL emission of CdTe QDs can be well protected by the silica network structure when CdTe QDs embedded in silica nanoparticles.

The photographs of CdTe/SiO₂ composite nanoparticles with amino groups on their surface under UV light and daylight were shown in Fig. 6. The bright red fluorescence emitted from CdTe/SiO₂ composite nanoparticles (the emission wavelength is at 630 nm) can be seen under UV light. The stable, monodisperse and highly fluorescent silica composite nanoparticles as fluorescent probes applied in bioassay were studied as follows.

3.4. Bioapplicable property of CdTe/SiO₂ composite nanoparticles

As mentioned in Section 2, the CdTe/SiO₂ composite nanoparticles were combined with biotin-labeled mouse IgG by glutaraldehyde. After centrifuging and supersonic washing, biotin-silica NPs can be directly applied to the bioassays. For this purpose, a series of different volumes of FITC-labeled avidin were added to 100 μ L biotin-silica NPs. The FITC-labeled avidin can be captured by the biotin-silica NPs through the sensitive protein–protein binding between biotin and avidin. After reaction, the mixture was centrifuged to remove the excess FITC-labeled avidin, and re-dispersed with 1 mL PBS for fluorescence detection, thus the amount of biotin-silica NPs is fixed. It can be seen that the fluorescence of FITC and CdTe QDs can be detected simultaneously in the solution as indicated in Fig. 7. The PL emission intensity of FITC increases with the increase of the concentration of FITC-labeled avidin, while the PL emission intensity of biotin-silica NPs keeps constant. It indicates that the amount of FITC-labeled avidin captured by biotin-silica NPs increases with the increase of the concentration of FITC-labeled avidin, which proved that the biotin-labeled mouse IgG had been immobilized on the surface of CdTe/SiO₂ composite nanoparticles and the protein–protein binding between avidin and biotin on the surface of CdTe/SiO₂ composite nanoparticles occurred. So the CdTe/SiO₂ composite nanoparticles can be considered as fluorescence probes labeled with biomolecules which can recognize the corresponding target biomolecules by means of protein–protein binding.

Accordingly, we designed the composite structures of PS-avidin, which was produced by immobilizing avidin on the surface of PS microspheres. Then CdTe/SiO₂ composite nanoparticles were used as fluorescence probes to detect the biomolecules (avidin) on the PS microspheres. As the affinity between avidin and biotin is

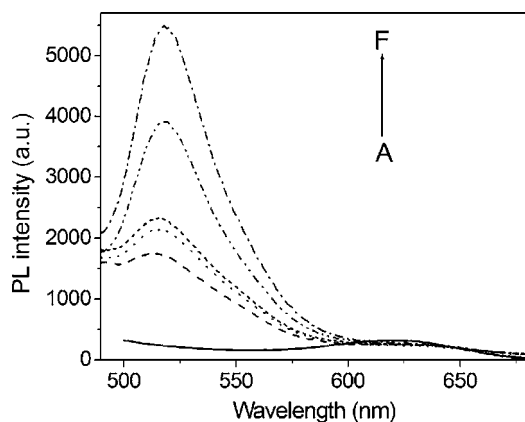


Fig. 7. The PL emission of biotin-silica NPs reacting with FITC-labeled avidin. The concentration of FITC-labeled avidin is 0 μ g/mL (A), 0.05 μ g/mL (B), 0.09 μ g/mL (C), 0.105 μ g/mL (D), 0.2 μ g/mL (E), and 0.3 μ g/mL (F), respectively.

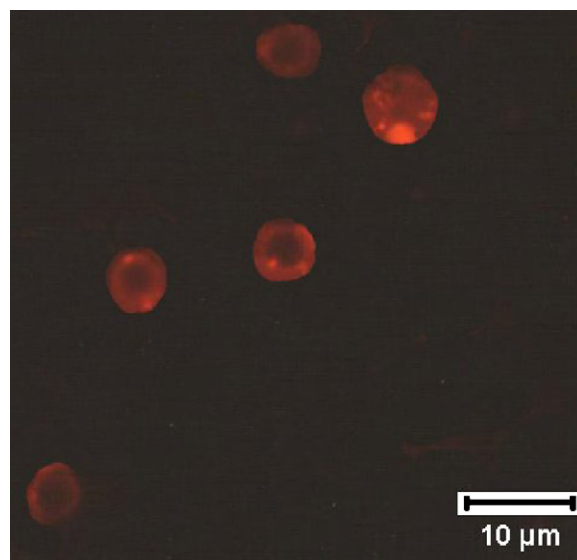


Fig. 8. The fluorescence microscopy image of PS-silica spheres.

very strong (binding constant, ca. 10^{15} M⁻¹) [23], PS microspheres can combine with CdTe/SiO₂ composite nanoparticles (PS-silica spheres) through avidin and biotin. In this way, the PS microspheres can be observed by the fluorescence microscope (Fig. 8) and the fluorescence can be detected by the fluorophotometer (Fig. 9). The fluorescent image (Fig. 8) shows the red fluorescence of CdTe/SiO₂ composite nanoparticles, which proves that the avidin has been recognized by the biotin on the silica composite nanoparticles. From Fig. 9, we can see that the more PS-avidin added to the biotin-silica NPs solution, the stronger PL emission intensity of PS-silica spheres is detected, demonstrating the feasibility of CdTe/SiO₂ composite nanoparticles as fluorescence probes in biomedical analysis.

In this study, the CdTe/SiO₂ composite nanoparticles were used to label the MG63 osteosarcoma cells. For this purpose, β -actin which was expressed by all eukaryotic cells and existed in cytoplasm was used as recognition molecule for the receptors in the MG63 osteosarcoma cells. β -Actin raised against gizzard actin of chicken origin was used as primary antibody. Rabbit anti-chicken IgG was used as secondary antibody, which was conjugated with CdTe/SiO₂ composite nanoparticles. First, β -actin was incubated with MG63 osteosarcoma cells for it to be recognized by the cells. Then CdTe/SiO₂ composite nanoparticles with secondary antibody

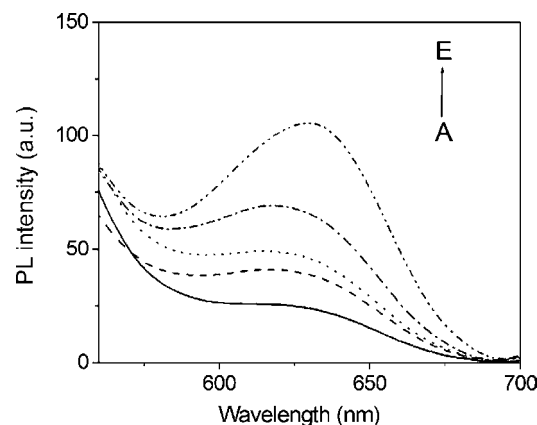


Fig. 9. The PL emission spectra of biotin-silica NPs reacting with PS-avidin. The adding amount of PS-avidin is 20 μ L (A), 50 μ L (B), 80 μ L (C), 100 μ L (D), and 180 μ L (E), respectively.

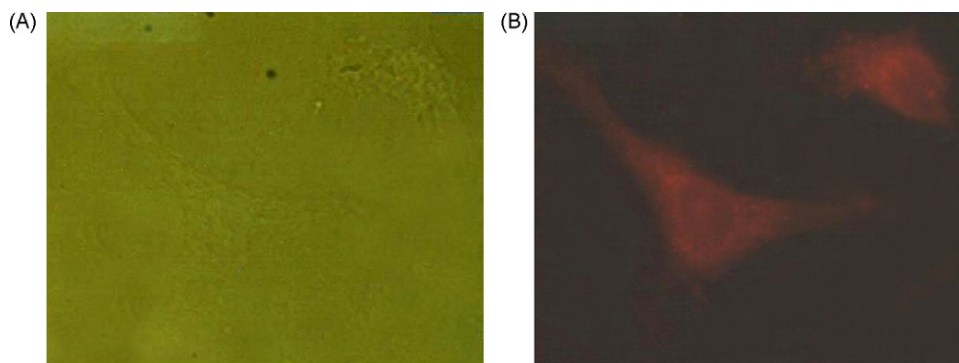


Fig. 10. The bright field (A) and fluorescence microscopy (B) images of MG63 osteosarcoma cells labeled with CdTe/SiO₂ composite nanoparticles.

were incubated with the MG63 osteosarcoma cells. As shown by the cell fluorescent image in Fig. 10, the cells in the field of view of the microscope were labeled by the CdTe/SiO₂ composite nanoparticles, which indicate that CdTe/SiO₂ composite nanoparticles can enter the MG63 osteosarcoma cells via the primary antibody and secondary antibody binding. The bright field image (Fig. 10A) correlated well with the fluorescence image (Fig. 10B). The results show that the CdTe/SiO₂ composite nanoparticles are able to perform as biomarkers for cancer cells fluorescence imaging which is under further investigations.

4. Conclusions

In this work, CdTe/SiO₂ composite nanoparticles have been successfully prepared by inverse microemulsion method. By modifying the surface of CdTe/SiO₂ composite nanoparticles with amino groups and methylphosphonate groups, biologically functionalized and monodisperse silica composite nanoparticles can be obtained. Comparing with naked CdTe QDs, the resultant CdTe/SiO₂ composite nanoparticles are relatively stable. Simultaneously, biotin-labeled mouse IgG immobilized on the surface of CdTe/SiO₂ composite nanoparticles can recognize FITC-labeled avidin and PS-avidin by protein–protein binding. Finally, we label the MG63 osteosarcoma cells by CdTe/SiO₂ composite nanoparticles successfully, which demonstrate that the application of CdTe/SiO₂ composite nanoparticles as fluorescent probes in bioassay and fluorescence imaging is feasible. As the fluorescence-labeling agent, CdTe/SiO₂ composite nanoparticles will promote the design of homogeneous assays such as antibody–antigen binding, DNA hybridization, enzyme–substrate interaction, etc. Based on the work above, our further researches will focus on the applications of multi-color CdTe-encoded SiO₂ composite nanoparticles on immunofluorescence and cell imaging aspects.

Acknowledgements

This work was financially supported by the National Natural Science Foundation of China (Nos. 20475020 and 20075009). The authors thank Prof. Shuming Nie (Wallace H. Coulter Department of Biomedical Engineering, Emory University and Georgia Institute of Technology, USA) for the helpful suggestions.

References

- [1] Y. Yang, M. Gao, *Adv. Mater.* 17 (2005) 2354.
- [2] Y. Yang, L. Jing, X. Yu, D. Yan, M. Gao, *Chem. Mater.* 19 (2007) 4123.
- [3] N.R. Jana, C. Earhart, J.Y. Ying, *Chem. Mater.* 19 (2007) 5074.
- [4] S. Santra, P. Zhang, K. Wang, R. Tapeç, W. Tan, *Anal. Chem.* 73 (2001) 4988.
- [5] L. Wang, W. Tan, *Nano Lett.* 6 (2006) 84.
- [6] A. Wolcott, D. Gerion, M. Visconte, J. Sun, A. Schwartzberg, S. Chen, J.Z. Zhang, *J. Phys. Chem. B* 110 (2006) 5779.
- [7] M. Bruchez Jr., P. Moronne, P. Gin, J.S. Weiss, A.P. Alivisatos, *Science* 281 (1998) 2013.
- [8] T. Nann, P. Mulvaney, *Angew. Chem. Int. Ed.* 43 (2004) 5393.
- [9] Y. Chan, J.P. Zimmer, M. Stroh, J.S. Stechel, R.K. Jain, M.G. Bawendi, *Adv. Mater.* 16 (2004) 23.
- [10] M.A. Correa-Duarte, M. Giersig, L.M. Lia-Marzán, *Chem. Phys. Lett.* 286 (1998) 497.
- [11] A.L. Rogach, D. Nagesha, J.W. Ostrander, M. Giersig, N.A. Kotov, *Chem. Mater.* 12 (2000) 2676.
- [12] Song-yuan, L. Liu, S.A. Asher, *J. Am. Chem. Soc.* 116 (1994) 6739.
- [13] Z. Ye, M. Tan, G. Wang, J. Yuan, *Anal. Chem.* 76 (2004) 513.
- [14] X. Zhao, R.P. Bagwe, W. Tan, *Adv. Mater.* 16 (2004) 173.
- [15] T. Selvan, T.T. Tan, J.Y. Ying, *Adv. Mater.* 17 (2005) 1620.
- [16] M. Darbandi, R. Thomann, T. Nann, *Chem. Mater.* 17 (2005) 5720.
- [17] R.P. Bagwe, L.R. Hilliard, W. Tan, *Langmuir* 22 (2006) 4357.
- [18] T.R. Sathe, A. Agrawal, S. Nie, *Anal. Chem.* 78 (2006) 5627.
- [19] S.T. Selvan, P.K. Patra, C.Y. Ang, J.Y. Ying, *Angew. Chem. Int. Ed.* 46 (2007) 2448.
- [20] L. Jin, D. Yu, Y. Liu, X. Zhao, J. Zhou, *Talanta* 76 (2008) 1053–1057.
- [21] C. Wang, Q. Ma, X. Su, *J. Nanosci. Nanotechnol.* 8 (2008) 4408–4414.
- [22] H. Yang, H. Qu, P. Lin, S. Li, M. Ding, J. Xu, *Analyst* 128 (2003) 462.
- [23] J. Anzai, T. Hoshi, N. Nakamura, *Langmuir* 16 (2000) 6306.
- [24] S. Liu, H. Zhang, T. Liu, B. Liu, Y. Cao, Z. Huang, Y. Zhao, *J. Biomed. Mater. Res. Part A* 80A (2006) 752.



Modified iron oxide nanoparticles as solid phase extractor for spectrophotometric determination and separation of basic fuchsin

B. Zargar*, H. Parham, A. Hatamie

Chemistry Department, College of Science, Shahid Chamran University, Ahvaz, Iran

ARTICLE INFO

Article history:

Received 23 July 2008

Received in revised form 3 September 2008

Accepted 4 September 2008

Available online 18 September 2008

Keywords:

Iron oxide nanoparticles

Sodium dodecyl sulfate

Preconcentration

Basic fuchsin

Determination

Spectrophotometry

ABSTRACT

This study presents a novel separation, preconcentration and determination of basic fuchsin (BF) in an aqueous solution by sodium dodecyl sulfate (SDS)-bounded iron oxide nanoparticles (S-IONPs). It is shown that the novel magnetic nano-adsorbent is quite efficient for the adsorption and desorption of BF at 25 °C. Different parameters such as pH, temperature, ionic strength and composition of desorbent solvent were optimized. The effect of some co-existing ions on the determination was investigated. The nanoparticles were analyzed by transmission electron microscopy (TEM) and the sizes of S-IONPs were in the range of 20–100 nm. The method showed good linearity for the determination of BF in the range of 10–300 ng mL⁻¹ with a regression coefficient of 0.9989. The limit of detection (LOD) (signal-to-noise ratio of 3:1) was 0.0073 µg L⁻¹ and the relative standard deviation (RSD) for 0.03 µg mL⁻¹ and 0.2 µg mL⁻¹ of BF were 4.53% and 4.73%, respectively. The BF was determined successfully in spiked samples of Karoon River water.

© 2008 Elsevier B.V. All rights reserved.

1. Introduction

The treatment of industrial effluents is a challenging topic in environmental sciences, since control of water pollution has become of increasing importance in recent years [1]. Effluents from the textile industries are important sources of water pollutions, because wastewater dyes undergoes chemical as well as biological changes, consume dissolved oxygen, and destroy aquatic life. Moreover, some dyes and their degradation products may be carcinogenic and/or toxic. Therefore, it is necessary to treat textile effluents prior to their discharge into receiving water [2]. Basic fuchsin (BF) (Fig. 1) is a triphenylmethane dye with molecular formula of C₂₀H₂₀ClN₃ and is one of those rare dyes that are inflammable in nature. It is widely used as coloring agent in textile and leather industries and also is used to stain collagen, muscle, mitochondria, and tubercle bacillus. BF possesses anesthetic, bactericidal (Gram positive), and fungicidal properties. The physical contact with the dye may cause severe eye and skin irritation. Its ingestion may cause gastrointestinal irritation with nausea, vomiting, and diarrhea and the inhalation of the dye causes irritation to the respiratory tract [3].

Keeping the toxicity of the dye in mind, there is a need to develop effective methods for its removal, recovery and determination in

wastewater. Several methods have been tried to remove various dyes with different adsorbents [2]. Recently magnetic nanoparticles as a new adsorbent with large surface area and small diffusion resistance have been recognized [4]. Ferrofluids are colloidal dispersions of small single domain magnetic particles suspended in a carrier fluid. Ferrofluids characteristically have both magnetic and fluid properties [5]. Nanosized magnetic iron oxide particles have been studied extensively due to their wide range of applications in ferrofluids, high-density information storage, magnetic resonance imaging (MRI), biological cell labeling and sorting, separation of biochemicals, targeting, and drug delivery. For many of these applications, surface modification of nanosized magnetic particles is a key of challenge [6–10]. In general, surface modification can be accomplished by physical and/or chemical adsorption of the desired molecules to coat the surface, depending on the specific applications [11]. Several methods for the separation and removal of chemical species such as metals [12–16], dyes [2,17–19] and gases [20] have been reported. The stability of dispersed particles and magnetic properties are of most importance. The nanoparticles which have a large ratio of surface area to volume, tends to agglomerate in order to reduce their surface energy by strong magnetic dipole–dipole and London–van der Waals attractions between particles.

These nanoparticles can be coated with surfactants and as a result prevent their aggregation in liquids and improve their chemical stability. The repulsive interactions between particles can be created by coating a surfactant layer on particle surfaces [21].

* Corresponding author. Tel.: +98 611 3331094 fax: +98 611 3331098.
E-mail address: zargar_b@scu.ac.ir (B. Zargar).

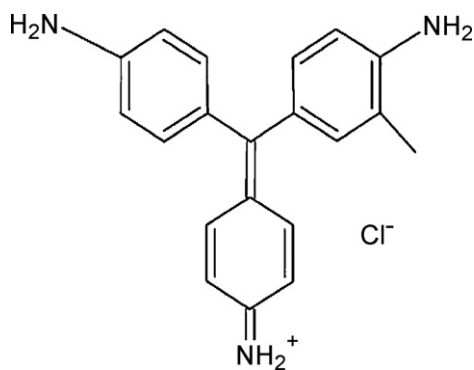


Fig. 1. Chemical structure of basic fuchsin.

Diluted ferrofluid dispersions are not stable. Therefore anionic and cationic surfactants are used as stabilizer. In this study, we used sodium dodecyl sulfate (SDS) which is an anionic surfactant and tends to interact with surface of nanoparticles and coated them. Iron oxide magnetic nanoparticles as cores and SDS as ionic exchange groups were used for recovery and determination of BF dye.

2. Experimental

2.1. Chemicals and reagents

All chemicals and reagents were of analytical grade. Basic fuchsin, phosphoric acid (85% m/m), methanol (99.9% m/m), ammonia solution (25% m/m), hydrochloric acid (37% m/m), acetic acid (99.9% m/m), FeCl₃ (96% m/m), FeCl₂·4H₂O (99.9% m/m), and sodium dodecyl sulfate were purchased from Merck (Darmstadt, Germany). Phosphate buffer solutions (pH 7) were prepared by adding appropriate amounts of 0.1 M sodium hydroxide solution into a mixture of 0.1 M of phosphoric acid.

2.2. Apparatus

The spectrophotometric measurements were carried out with a Cintra 101 spectrophotometer (GBC SCIENTIFIC EQUIPMENT, Australia). A transmission electron microscope (906E, LEO, Germany), pH-meter (632 Metrohm, Herisau, Switzerland) and a super magnet (1.2 T, 10 cm × 5 cm × 2 cm) were used.

2.3. Preparation of SDS-bounded iron oxide nanoparticles (S-IONPs)

Iron oxide nanoparticles were prepared according to a previous work [22]. In order to coat the particles, 5 mL of SDS solution (5% m/v) was added to about 5 g of damped nanoparticles in a beaker. The solution was stirred for 1 min by a glassy rod and the beaker was then placed on the magnet. After complete precipitation of S-IONPs occurred the solution was decanted and ferrofluid was washed with distilled water for several times (3 times on average) to eliminate extra amount of surfactant from nanoparticles.

2.4. Adsorption and desorption of BF

About 0.6 g of damped S-IONPs (equivalent to 0.06 g dry S-IONPs) were added to the 50 mL of BF solution (0.01–1 μg mL⁻¹) in a beaker. The pH of the solution was adjusted to 7 by addition of 2 mL of 0.03 M of phosphate buffer pH 7. The mixture was stirred by a glassy rod for about 100 s and the beaker was then placed on the magnet. The S-IONPs which adsorbed BF (BF-S-IONPs) were

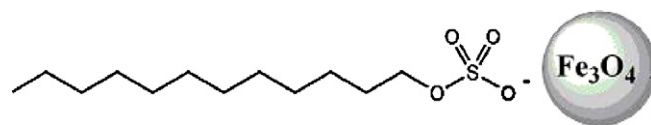
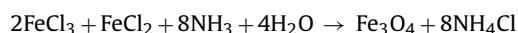


Fig. 2. Suggested mechanism for the adsorption of sodium dodecyl sulfate on the surface of IONP.

separated magnetically and the initial red colored solution became colorless. The mixture was decanted and the solution above the nanoparticles was removed completely. Finally 2.5 mL of desorbent solution (a mixture of methanol and acetic acid with a ratio of 80:20, v/v) was added to the BF-S-IONPs in a beaker. The beaker was placed on the magnet and the mixture was decanted. The absorption of the solution which has been separated from IONPs by magnet was measured spectrophotometrically at 547 nm.

3. Results and discussion

The synthesis of nanoparticles is based on the reaction of ferric and ferrous ions in an aqueous ammonia solution to form magnetite (Fe₃O₄). Suggested reaction for the formation of nanoparticles is as follow [20]:



Experimental conditions such as temperature, rate of ammonia addition and rate of solution stirring have critical effect on the size of nanoparticles.

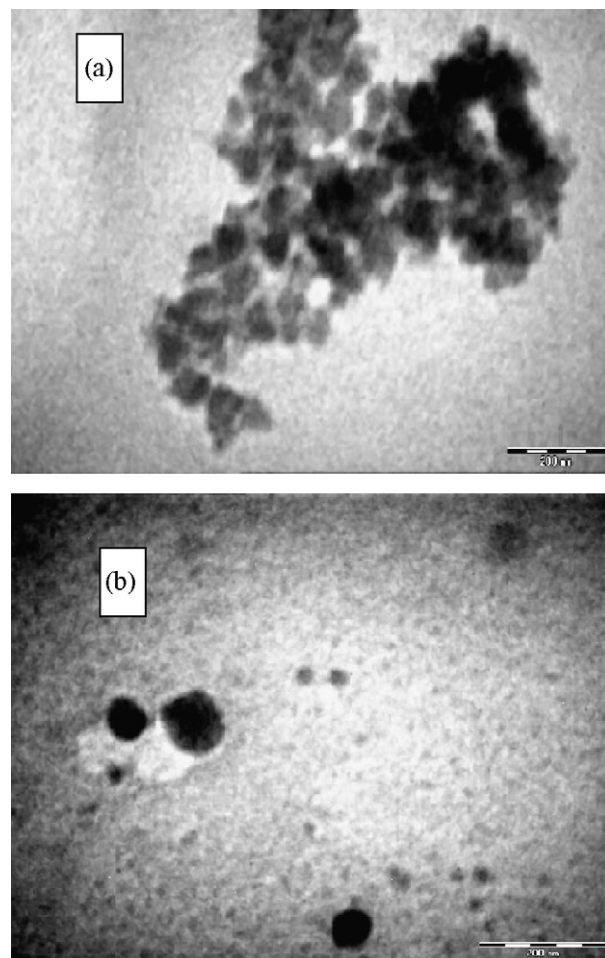


Fig. 3. Transmission electron microscope images of (a) IONPs and (b) S-IONPs.

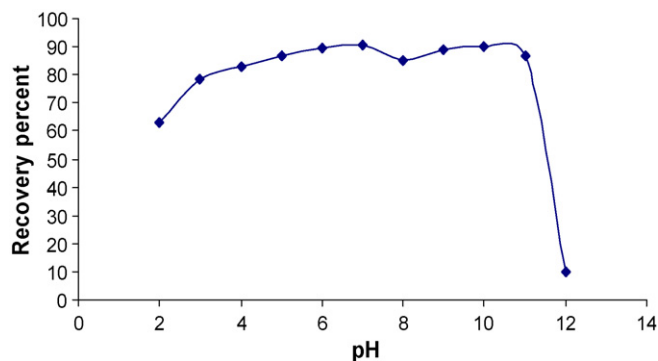


Fig. 4. Effect of different pH values on the BF separation [conditions: 50 mL of $1 \mu\text{g mL}^{-1}$ solution of BF; 1 g of damped IONPs; 2.5 mL of desorbent solution (methanol/acetic acid 80:20, v/v)].

The suggested mechanism for the coating of IONP with sodium dodecyl sulfate is shown in Fig. 2. The S-IONPs have bigger sizes compared to the initial IONPs as can be seen by TEM pictures (Fig. 3). IONPs without coating did not adsorb BF but S-IONPs adsorbed BF and separated it from the bulk of solution.

The presence of trace amount of IONPs in the spectrophotometer cell could affect the absorption of the solution. It could be eliminated by holding the cell on the magnet for a few second before measuring.

Absorption of the desorbed solution was measured at 547 nm instead of 542 nm (as a result of solvent changing from water to a mixture of methanol and acetic acid the λ_{max} was shifted to higher wavelengths).

The pH of the solutions was adjusted by NaOH and HCl to find the optimum pH value. Separation and Determination of BF was performed in the pH range from 2 to 12. The obtained results are shown in Fig. 4. In low pH values, the solution was darkly because iron oxide nanoparticles had begun to dissolve; on the other hand, at high pH values the IONPs were converted to colloidal particles and did not respond to the magnetic field (adsorption of hydroxide ions on the particles surfaces produce a dark colloid suspension). The amount of separation and desorption of BF in the pH range from 5 to 8 was constant and therefore this range was chosen as optimum range for pH. However pH 7 was selected for all other experiments and phosphate buffer was used to obtain this value. The amount of added buffer was investigated and it was demonstrated that with the amount of buffer volume exceeding 2 mL of 0.03 M solution in the 50 mL test sample solution; the amount of separation and adsorption of BF decreases.

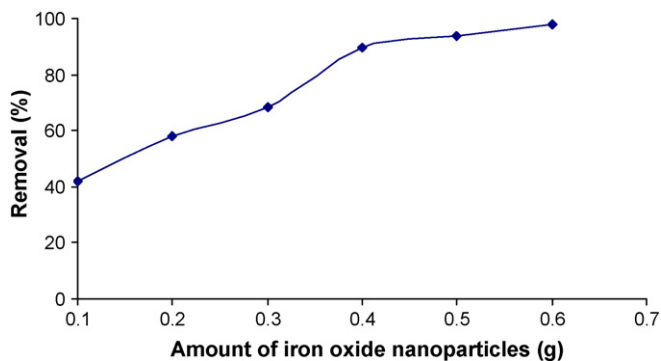


Fig. 5. Effect of different amounts of IONPs on the BF separation [conditions: 50 mL of $1 \mu\text{g mL}^{-1}$ solution of BF; pH 7; 2.5 mL of desorbent solution (methanol/acetic acid 80:20, v/v)].

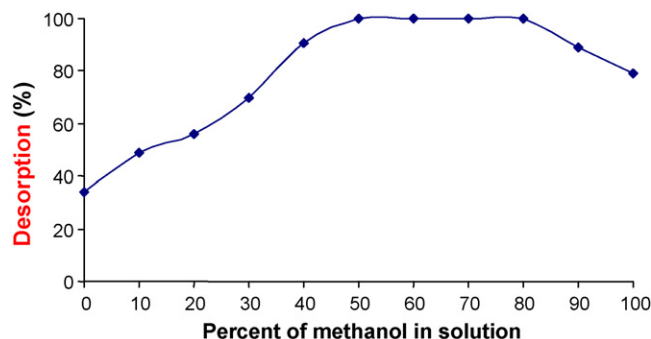


Fig. 6. Effect of different compositions of desorbent solution on the desorption of BF from IONPs (conditions: 50 mL of $0.2 \mu\text{g mL}^{-1}$ solution of BF; pH 7; 0.6 g of damped IONPs; 2.5 mL of desorbent solution).

The required amount of iron nanoparticles for the complete separation of BF in 50 mL solution (containing $1 \mu\text{g mL}^{-1}$ of BF) at pH 7 was investigated. To this end, different amounts of damped iron nanoparticles were added to the solution following mixing and separation of IONPs with magnet. The adsorption of solution was then measured at 542 nm. The results are shown in Fig. 5. Addition of 0.6 g of damped iron nanoparticles (equivalent to 0.06 g dry IONPs) separated the BF from this solution completely.

In order to find the best composition for desorbent solution, we used solutions with different ratios of methanol and acetic acid reported in references to be suitable for this purposes [2]. The obtained results are shown in the Fig. 6. Adsorption of BF by IONPs and its desorption by different compositions of desorbent solutions were studied in a constant volume of desorbent solution. Pure methanol and acetic acid (1 M) were used as stock solutions. The obtained results are showed that with 50–70% methanol in the final desorbent solution, the BF can be completely desorbed from nanoparticles surfaces. Addition of desorbent solution in multiple steps (3 steps) can improved the desorption process.

The effect of ionic strength on the system was examined in different concentrations of KCl as an electrolyte. The adsorption of BF decreases with increasing the ionic strength of the solution. This implied that electrostatic attraction between the negatively charged SDS ions on the IONPs and positively charged of BF ions was affected by the KCl under the examination conditions.

The adsorption of BF was studied in four different temperatures. The recovery of BF was slightly increased with increasing the temperature.

The optimum experimental conditions which have been described were used to study the effect of some ions and two red dyes (Rodamin B, Allura red) on the determination process. To this end separation and determination of BF was performed in the presence of co-existing ions. The maximum acceptable error was $\pm 5\%$. The obtained results are shown in Table 1. The table shows that Ca^{2+} , Mg^{2+} and Rodamin B strongly interfered even in the same

Table 1

Effect of co-existing ions (conditions: 100 mL BF $0.2 \mu\text{g mL}^{-1}$; pH 7. IONPs: 0.6 g; volume of desorbent solution: 2.5 mL (methanol/acetic acid 60:40, v/v)).

Ions ^a	Tolerance ratio (w/w)
K^+ , Na^+ , Cl^- , Br^- , Pb^{2+} , NO_3^-	200
I^- , F^-	100
CO_3^{2-}	60
Ni^{2+}	40
Co^{2+}	10
Ca^{2+} , Mg^{2+} , Rodamin B, Allura red	1

^a All cations were prepared from nitrate salts and anions were prepared from sodium and potassium salts.

Table 2
Determination of BF in spiked Karoon River water samples.

Added BF ($\mu\text{g mL}^{-1}$)	Found BF ($\mu\text{g mL}^{-1}$)	Recovery (%)
0.100	0.096 ^a	96.0%
0.150	0.147 ^a	98.0%

^a Average of three determinations.

concentration with BF. A solution of EDTA was used to eliminate the interference affect of Ca^{2+} and Mg^{2+} .

4. Analytical characteristics

The calibration curve was linear in the range of $0.01 \mu\text{g mL}^{-1}$ to $0.3 \mu\text{g mL}^{-1}$ of BF with an equation of $y = 4.2113x + 0.1222$ ($R = 0.9989$) in which y is absorbance and x is concentration of BF ($\mu\text{g mL}^{-1}$). The relative standard deviation ($n = 8$) for $0.2 \mu\text{g mL}^{-1}$ and $0.03 \mu\text{g mL}^{-1}$ of BF were 4.53% and 4.73%, respectively and the LOD of the method was $0.0073 \mu\text{g mL}^{-1}$. The enrichment factor of the method was calculated to be 40.

5. Analysis of Karoon River water sample

To determine the ability of the proposed method for the analysis of BF in a real sample, Karoon River water was spiked. The spiked levels were 100 ng mL^{-1} and 150 ng mL^{-1} of BF. The spiked solutions were successfully determined in two different river waters samples. The results are summarized in Table 2. Excellent recoveries indicated that the complex matrix of river water samples does not interfere with the analysis of BF.

6. Conclusion

Basic fuchsin could be removed from an aqueous solution by the SDS-bounded iron oxide nanoparticles. The nanoparticles can rapidly adsorbed BF and desorbed it in a suitable solution in less

than 5 min. The proposed method is recommended for removal and/or determination of BF in different water samples.

Acknowledgement

The authors wish to thank Shahid Chamran University Research Council for financial support of this work (Grant 1386).

References

- [1] V. Rocher, J.M. Siaugue, V. Cabuil, A. Bee, *Water Res.* 42 (2008) 1290.
- [2] S.Y. Mak, D.H. Chen, *Dyes Pigments* 61 (2004) 93.
- [3] V.K. Gupta, A. Mittal, V. Gajbe, J. Mittal, *J. Colloid Interface Sci.* 319 (2008) 30.
- [4] M.H. Liao, D.H. Chen, *Biotechnol. Lett.* 24 (2002) 1913.
- [5] C.L. Lin, C.F. Lee, W.Y. Chiu, *J. Colloid Interface Sci.* 291 (2005) 411.
- [6] H.Y. Shen, Y. Zhu, X. Wen, Y. Zhuang, *Anal. Bioanal. Chem.* 387 (2007) 2227.
- [7] S.S. Banerjee, D.H. Chen, *J. Hazard. Mater.* 147 (2007) 792.
- [8] I. Safarik, L.F.T. Rego, M. Borovska, E.M. Szablewskae, F. Weyda, M. Safarikova, *Enzyme Microb. Technol.* 40 (2007) 1551.
- [9] J. Li, X. Zhao, Y. Shi, Y. Cai, S. Mou, G. Jiang, *J. Chromatogr. A* 1180 (2008) 24.
- [10] Y.C. Chang, D.H. Chen, *J. Colloid Interface Sci.* 283 (2005) 446.
- [11] M. Takafuji, S. Ide, H. Ihara, Z. Xu, *Chem. Mater.* 16 (2004) 1977.
- [12] L. Wang, Z. Yang, J. Gao, K. Xu, H. Gu, B. Zhang, X. Zhang, B. Xu, *J. Am. Chem. Soc.* 128 (2006) 13358.
- [13] J.T. Mayo, C. Yavuz, S. Yean, L. Cong, H. Shipley, W. Yu, J. Falkner, A. Kan, M. Tomson, *V.L. Colvin, Sci. Technol. Adv. Mater.* 8 (2007) 71.
- [14] A. Uheida, G. Salazar-Alvarez, E. Björkman, Z. Yu, M. Muhammed, *J. Colloid Interface Sci.* 298 (2006) 501.
- [15] C. Huang, B. Hu, *Spectrochim. Acta Part B* 63 (2008) 437.
- [16] J.E. Macdonald, J.A. Kelly, J.G.C. Veinot, *Iron/Iron Oxide Nanoparticle Sequestration of Catalytic Metal Impurities from Aqueous Media and Organic Reaction Products*, *Langmuir* 23 (2007) 9543.
- [17] N. Yang, S. Zhu, D. Zhang, S. Xu, *Mater. Lett.* 62 (2008) 645.
- [18] Y.C. Chang, D.H. Chen, *Macromol. Biosci.* 5 (2005) 254.
- [19] M.H. Liao, K.Y. Wu, D.H. Chen, *Chem. Lett.* 6 (2003) 488.
- [20] P. Li, D.E. Miser, S. Rabiei, R.T. Yadav, M.R. Hajaligol, *Appl. Catal. B: Environ.* 43 (2003) 151.
- [21] G. Gnanaprakash, J. Philip, T. Jayakumar, B. Raj, *J. Phys. Chem. B* 111 (2007) 7978.
- [22] P. Berge, N.B. Adelman, K.J. Beckman, D.J. Campbell, A.B. Ellis, G.C. Isensky, *J. Chem. Educ.* 7 (1999) 943.



Rapid and direct speciation of methyltins in seawater by an on-line coupled high performance liquid chromatography–hydride generation–ICP/MS system

Guangshu Zhai, Jingfu Liu, Lu Li, Lin Cui, Bin He, Qunfang Zhou, Guibin Jiang*

State Key Laboratory of Environmental Chemistry and Ecotoxicology, Research Center for Eco-Environmental Sciences, Chinese Academy of Sciences, P.O. Box 2871, Shuangqing Road 18, Beijing 100085, China

ARTICLE INFO

Article history:

Received 26 June 2008

Received in revised form 29 August 2008

Accepted 30 August 2008

Available online 9 September 2008

Keywords:

Speciation

Methyltin

Seawater

High performance liquid chromatography

Hydride generation

ICP/MS

ABSTRACT

A novel on-line coupled HPLC–hydride generation (HG)–ICP/MS system was developed for rapid, direct and sensitive speciation of methyltins in seawater without any pretreatment step. Methyltin compounds were separated by reversed phase HPLC, and then on-line reacted with potassium borohydride and acetic acid to generate volatile hydride products. The volatile derivatization products were separated in the spray chamber of ICP/MS and then introduced into ICP/MS by argon gas for detection. Monomethyltin (MMT), dimethyltin (DMT) and trimethyltin (TMT) were baseline separated in less than 15 min by reversed phase HPLC. The influence of KBH_4 concentration and type of acid on the system performance was investigated and optimized. Calibration curves, based on peak heights against concentration, were linear in the range of 0.5–50 ng (Sn) mL^{-1} of methyltins with correlation coefficients of 0.9990, 0.9990 and 0.9996 for MMT, DMT and TMT, respectively. The relative standard deviations measured at 10 ng (Sn) mL^{-1} for these three methyltins were in the range of 0.6–1.4% ($n = 5$), and the calculated detection limits ($S/N = 3$) for MMT, DMT and TMT were 0.266, 0.095 and 0.039 ng (Sn) mL^{-1} , respectively. This method was successfully applied to the speciation of methyltins in seawater with spiked recovery in the range of 95.4–106.9%. MMT and DMT were detected in all the seawater samples with concentrations in the range of 1.0–1.5 and 0.30–0.57 ng (Sn) mL^{-1} for MMT and DMT, respectively.

© 2008 Elsevier B.V. All rights reserved.

1. Introduction

Extensive applications of methyltin compounds as biocides, antifouling agents and polyvinyl chloride heater stabilizers have caused serious pollution to the environment because of their high toxicity to organisms [1,2]. Up to date the occurrence of methyltin compounds have been found in many different environmental media such as seawater [3,4], river water [5,6], lake water [6,7], sediments [8] and biological samples [3]. In addition to the anthropogenic sources [1], methyltins can be produced by the biotic and abiotic methylation [9–11].

Although some methods are available for analyzing organotin compounds, there is lack of technique for rapid, direct and sensitive detection for organotins, especially for methyltins. Methyltins are more difficult to be detected than butyltin and phenyltin compounds because of their minor structural difference and higher solubility in water and thus their low extraction efficiencies from aqueous medium. The shortage in rapid, direct and sensitive meth-

ods is often the bottleneck of research on the mechanisms of methyltin biogeochemical cycling in the environment and their toxicity to organisms.

The speciation methods for methyltin compounds mainly focus on hyphenated systems based on gas chromatography (GC) and liquid chromatography (LC). Methods based on coupling GC with different detectors such as atomic absorption spectrometry (AAS) [7], quartz surface-induced luminescence flame photometric detector (QSIL-FPD) [12] and mass spectrometry (MS) [13] are commonly used. However, the major limitation of these methods is that methyltins have to be off-line derivatized with sodium borohydride, sodium tetraethylborate or Grignard reagents [14]. The existence of methyltins as methyltin salts in the environment leads to the utilization of time-consuming steps involving complexation, extraction and derivatization, and is the main sources of errors. When sodium borohydride method is utilized, the hydrides of methyltin compounds have to be trapped using cryogenic purge and trap method [12] or hydride trap method [3] due to the lower boiling points of the hydride generation products of methyltin compounds (CH_3SnH_3 1.4 °C, $(\text{CH}_3)_2\text{SnH}_2$ ca. 35 °C, $(\text{CH}_3)_3\text{SnH}$ ca. 60 °C) [3]. It is more complicated to use Grignard reagent method because this reaction must be conducted under anhydrous condition. Typ-

* Corresponding author. Tel.: +86 10 62849129; fax: +86 10 62849179.
E-mail address: gjjiang@rcees.ac.cn (G. Jiang).

ically, organotins in water are complexed with a chelating agent, such as sodium diethyldithiocarbamate (DDTC, 0.2 g) in the presence of sodium chloride [13]. The chelated organotins are then extracted with toluene. After the phase separation, the organic phase collected through a column of anhydrous sodium sulfate was evaporated to ca. 1 mL under reduced pressure. Grignard reagent, such as pentylmagnesium bromide is added to the organic phase and then allowed to stand at 40 °C for 60 min. As can be seen it is a very time-consuming process.

HPLC coupled with different detectors, such as AAS [15], MS [16] and inductively coupled plasma mass spectrometry (ICP/MS) [17], are widely used for the speciation of methyltins because they avoid the complex extraction and derivatization step. Some reviews on the speciation of organotins using HPLC coupled with different detectors are available in the literatures [18,19]. One of the major problems for organotin determination is that the shortage of conventional high sensitive detectors limits the application of HPLC-base hyphenated method. ICP/MS is a powerful tool for analyzing organotins due to its high sensitivity and selectivity and has been hyphenated with several modes of LC, such as ion-exchange, reversed phase and ion-pairing. An important issue in the hyphenation of reversed phase LC with ICP/MS is the compatibility of mobile phase and plasma source. The presence of high percent organic solvent in the mobile phase can result in poor plasma stability and may even extinguish the plasma. In addition, carbon deposits may form on the sampler and the skimmer cones within the ICP/MS interface region, and could contribute to higher noise and reduced signals. As a result, it is necessary to add oxygen to the nebulizer argon-gas flow to allow complete combustion of the organic solvent in the plasma. However, many ICP/MS systems are not configured for the oxygen addition, which seriously restricts the applications of reversed phase HPLC-ICP/MS. Furthermore, the traditional nebulizer mode normally has low efficiency, with only 5–10% being delivered to the ICP plasma. For example, the organotins compounds, focused on butyltin and phenyltin compounds, were detected by HPLC-ICP/MS system using traditional mode [20–23]. Sample introduction using hydride generation has proved to be a powerful tool to increase the sensitivity of ICP/MS [24]. For example, a 16-fold sensitivity enhancement is obtained for cadmium determination by using HPLC-HG-ICP/MS rather than the conventional nebulization [24]. So far the HPLC-HG-ICP/MS technique has been applied for the speciation of elements such as cadmium [24] and arsenic [25,26]. Anion exchange chromatographic separation mode was used in these hyphenated systems. However, it is unable to completely separate methyltins with ion-exchange mode. A reversed phase separation mode seems to be a good choice. To our best knowledge, this is the first report on the direct determination of methyltins in water without preconcentration.

In this paper, a reversed phase HPLC-HG-ICP/MS hyphenated system was developed to directly and rapidly determine methyltins without any preconcentration step. This method successfully avoided the extinguishing of plasma resulted from the high percentage of methanol without oxygen addition system or other equipment modification. This technique was applied to the speciation of methyltins in seawaters. Analysis of one seawater sample can be completed within 15 min.

2. Experimental

2.1. Reagents

All reagents were used as purchased without further purification. Three methyltin compounds, including trimethyltin chloride

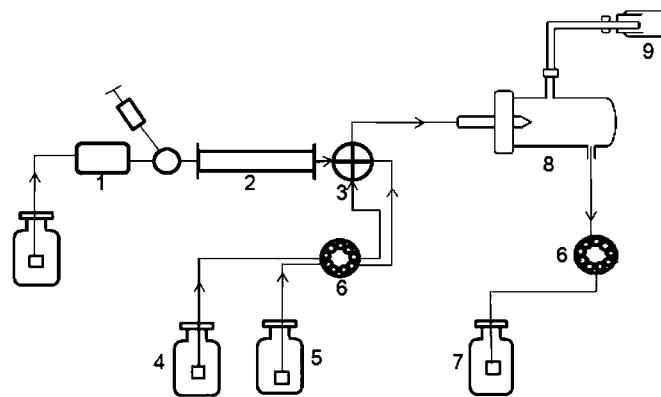


Fig. 1. Schematic diagram of the HPLC-HG-ICP/MS system. (1) HPLC pump; (2) C₁₈ column; (3) four-way connector; (4) HAc; (5) KBH₄; (6) peristaltic pump; (7) waste; (8) spray chamber; (9) ICP/MS.

(TMT, 98%), dimethyltin dichloride (DMT, 97%) and monomethyltin trichloride (MMT, 97%), were obtained from Aldrich Chemical Co. (USA). Standard stock solutions were prepared by dissolving methyltin compounds in deionized water and stored at 4 °C. The working solutions were prepared daily by appropriately diluting the stock solutions with deionized water. Methanol was HPLC grade solvent (J. T. Baker, Phillipsburg, NJ, USA). Tropolone (98%) was from Acros Organics (NJ, USA). Nitric acid (GR, 65%) was purchased from Merck, Germany. Acetic acid (AR, 99.5%), hydrochloric acid (GR, 36–38%), and potassium hydroxide (GR) were obtained from Beijing Chemical Factory (Beijing, China). Potassium borohydride (95%) was purchased from Institute of Geophysical and Geochemical Exploration (Langfang, China). Deionized water (18.3 MΩ cm) was produced from an ultrapure water system (Barnstead International, Dubuque, IA, USA).

2.2. Apparatus

Fig. 1 shows the schematic diagram of hyphenated HPLC-HG-ICP/MS system, which mainly consists of three parts. Methyltin compounds were first separated by the HPLC system which consists of a DGU-12A degasser, a LC-10A pump (Shimadzu, Japan), an injector valve (Rheodyne 7725i with a 200 μL sample loop), and a C₁₈ separation column (Agilent Zorbax Eclipse XDB-C18, 5 μm particle size, 4.6 mm × 150 mm). In the hydride generation (HG) component, the analytes from the HPLC column reacted with the derivatization reagents, introduced by a peristaltic pump, in a four-way-cross connector to form volatile methyltin hydride. These volatile methyltin hydrides were then introduced into ICP/MS (Agilent 7500ce with Babington nebulizer, USA) for detection. In the third part, the spray chamber of the ICP/MS was used as a gas-liquid separator and the mode of nebulization was changed to make organic mobile phase adapt ICP/MS which would be discussed later in detail. The operating conditions of this hyphenated system are listed in Table 1.

2.3. Preparation of seawater sample

Seawater samples from Yantai (Bohai Sea, China) were stored at –20 °C in the refrigerator. The samples were analyzed without any pretreatment except being filtered with a 0.4 μm filter membrane before injected into the HPLC system.

Table 1
Optimum operating conditions for the HPLC–HG–ICP/MS system

Parameter	Optimized value
HPLC	
Column	Agilent Zorbax Eclipse XDB-C ₁₈ , 5 μm, 4.6 mm × 150 mm
Mobile phase	70% (v/v) methanol, 3% (v/v) HAc, 27% (v/v) water, 0.1% (m/v) tropolone; pH 3.5
Flow rate of mobile phase	0.3 mL min ⁻¹
Sample injection	200 μL
Derivatization reagent	
HAc	1% (v/v), flow rate: 0.36 mL min ⁻¹
KBH ₄	0.5% (m/v), (containing 0.2% KOH), flow rate: 0.36 mL min ⁻¹
ICP/MS	
S/C Temperature	2 °C
Makeup gas (Ar)	0.72 L min ⁻¹
Carrier gas (Ar)	0.22 L min ⁻¹
RF power	1550 W
Isotope monitored	¹¹⁸ Sn, ¹²⁰ Sn

3. Results and discussion

3.1. Optimization of HPLC–HG–ICP/MS

HPLC separation of methyltin compounds was conducted as described in our previous paper [23] and the adopted parameters are listed in Table 1. In these liquid chromatographic conditions, three methyltins were baseline separated in less than 15 min and the eluent sequence of these three methyltins is TMT, MMT and DMT because of the function of tropolone as complexant in the mobile phase. As for the operational parameters of ICP/MS, the isotope ¹²⁰Sn signal intensity was selected to optimize the instrumental performance. HAc (2% v/v, containing 3.0 ng (Sn) mL⁻¹ MMT) and KBH₄ (0.5% (m/v) containing 0.2% (m/v) KOH), introduced via the peristaltic pump of ICP/MS, were mixed in a four-way-cross connector, and the produced volatile MMT hydride was introduced into the spray chamber (2 °C) of ICP/MS. The instrumental parameters were adjusted until the ¹²⁰Sn signal intensity reaches maximum value. The signal intensity was strongly dependent on flow rate of the carrier gas and makeup gas of the HPLC–HG–ICP/MS system. Generally, the flow rate of carrier gas was higher than that of makeup gas in order to improve the nebulization efficiency and sensitivity. However, the carrier gas flow rate used in this HPLC–HG–ICP/MS system was lower than that of makeup gas for the following two purposes: (1) the Babington nebulizer with bigger spray pore than concentric nebulizer used in this system can easily decrease the nebulization efficiency by changing the flow rate of carrier gas to reduce the influence of methanol in mobile phase to the plasma and (2) increasing the flow rate of makeup gas can efficiently carry the volatile hydride to the plasma and thus greatly increases the sensitivity. As a result, the optimum flow rates of the carrier gas and the makeup gas in this hyphenated system were 0.22 and 0.72 L min⁻¹, respectively. Furthermore, there is no interference of other elements to the methyltin determination because only the isotope of ¹¹⁸Sn and ¹²⁰Sn were selected to be detected. Overall, it is very easy to set up this HPLC–HG–ICP/MS system as no special auxiliary equipment was needed, and the only difference of using ICP/MS procedure with the conventional mode is to adjust the flow rate ratio of the carrier and makeup gases.

Generally, the commonly used temperature of spray chamber, precisely controlled by Peltier cooling device, is 2 °C. Peltier cooling spray chamber can remove some of the water from the sample, delivering only the smallest droplets to the plasma. Consequently, this Peltier cooling device can provide the plasma with a very stable ion signal and produce low levels of polyatomic

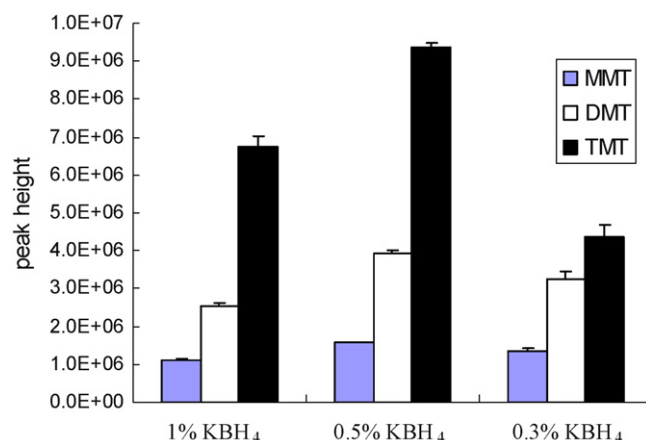


Fig. 2. Effects of KBH₄ concentrations on signal intensities of methyltins. Analyte concentrations (as Sn): 10 ng mL⁻¹ of MMT, DMT, and TMT. Derivatization reagents: 2% (v/v) HCl and different concentration of KBH₄ (containing 0.2% (m/v) KOH).

oxide species, which in turn reduces the interferences on certain analytes. Considering the boiling points of (CH₃)₂SnH₂ (35 °C) and (CH₃)₃SnH (60 °C), we initially speculated that the low spray chamber temperature at 2 °C would liquefy the methyltin hydrides and lead to low transfer efficiency to the plasma. Therefore, the effect of spray chamber temperature on the signal intensities of the three methyltins was investigated at 10 ng (Sn) mL⁻¹ of methyltins. The signal intensities of methyltins varied slightly with the spray chamber temperature increased from 2 to 15 °C, which is because the total flow rates of carrier gas and makeup gas is about 1 L min⁻¹, which can carry the methyltin hydrides to pass through the spray chamber rapidly and give almost no chance to liquefy these hydrides. As the reflected power of ICP/MS, normally at 1 W, increases from 1 to 25 W and becomes very unstable by increasing the temperature of spray chamber from 2 to 15 °C, the selected temperature of spray chamber was 2 °C in the following experiments.

3.2. Optimization of derivatization reagents

The concentrations of derivatization reagents have a great influence on the hydride generation of methyltins and thus on the detection limit of ICP/MS. Low KBH₄ concentration results in low hydride reaction efficiency, whereas too high KBH₄ produces too much hydrogen that could affect the stability of plasma, even extinguish the plasma. Fig. 2 displays the effect of KBH₄ concentrations on the peak height of methyltins when the flow rate of KBH₄ was set at 0.36 mL min⁻¹. As can be seen, the best signal intensities for these three methyltins were obtained at 0.5% (m/v) KBH₄, which was adopted in the following studies.

With a constant flow rate of 0.36 mL min⁻¹ for both the acid and 0.5% (m/v) KBH₄, the influence of acid type and concentration were studied (Fig. 3). Similar signal responses were observed for hydrochloric acid, nitric acid and acetic acid at their optimum concentrations. Relatively lower acid concentrations in this experiment seem to have higher signals. For example, the signals of methyltins obtained at 1% (v/v) HCl were higher than those at 2% and 3% HCl. However, too lower acidic concentrations may lead to incomplete hydride reaction, which produces lower signal intensity. Overall, relatively higher signal were obtained using 0.6% (v/v) nitric acid or 1.0% (v/v) acetic acid. Considering acetic acid is a weak acid and is used in the mobile phase, 1.0% (v/v) acetic acid was adopted in the following experiments. The final operating conditions were shown in Table 1.

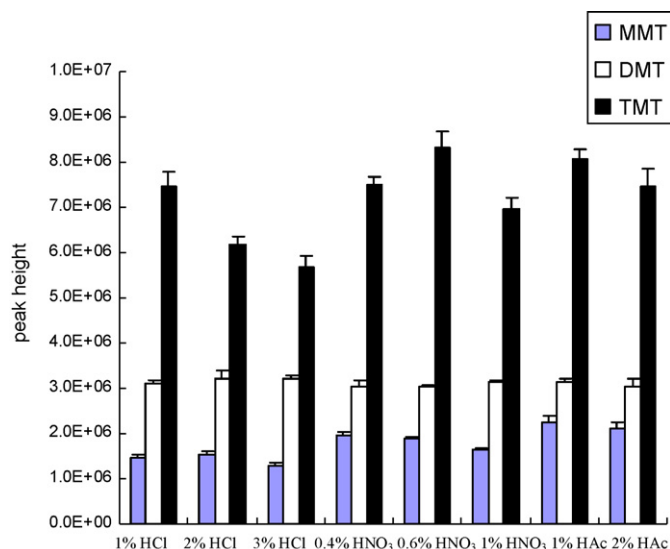


Fig. 3. Effects of the types and concentrations of acids used for derivatization on the signal intensities of methyltins. Analyte concentrations (as Sn): 10 ng mL^{-1} of MMT, DMT and TMT. Derivatization reagents: 0.5% (m/v) KBH_4 (containing 0.2% (m/v) KOH) and various acids.

3.3. Analytical performance

The three methyltins were baseline separated in less than 15 min. Table 2 shows the analytical performance data of this developed HPLC–HG–ICP/MS system. Linear calibration curves, based on peak heights to concentrations, were obtained in the range of $0.5\text{--}50 \text{ ng (Sn) mL}^{-1}$ of methyltins with correlation coefficients of 0.9990, 0.9990 and 0.9996 for MMT, DMT and TMT, respectively. The relative standard deviations measured at $10 \text{ ng (Sn) mL}^{-1}$ level were in the range of 0.6–1.4% ($n = 5$). Based on the relative standard deviations measured at $2.0 \text{ ng (Sn) mL}^{-1}$, the calculated detection limits ($S/N = 3$) for MMT, DMT and TMT were 0.266, 0.095 and $0.039 \text{ ng (Sn) mL}^{-1}$, respectively.

3.4. Determination of methyltins in seawater samples

The proposed method was successfully applied to directly measure methyltins in seawater samples collected from Bohai Sea at

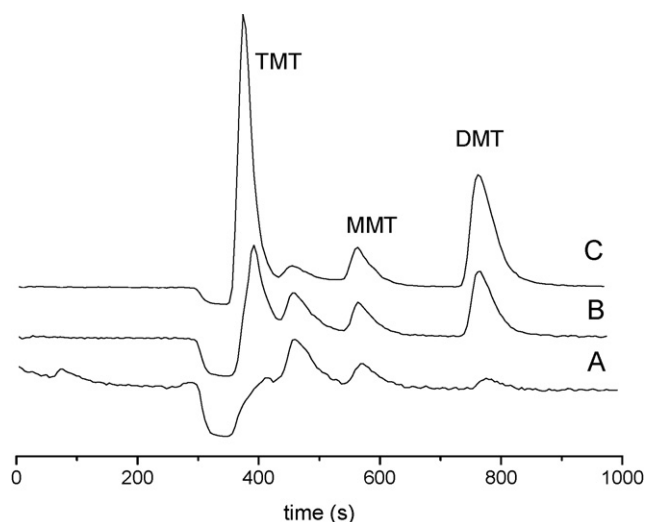


Fig. 4. Typical chromatograms for methyltin analysis in water. (A) Seawater sample; (B) seawater sample spiked with standards ($2.0 \text{ ng (Sn) mL}^{-1}$); (C) methyltin standards.

Yantai city (Shandong Province, China). The chromatograms of seawater sample analyses with and without addition of standards, as well as standard of methyltins are shown in Fig. 4. Three methyltins can be well separated. The results of seawater samples were shown in Table 3. Good spiked recoveries (%) of 5 samples, 95.8–108 for MMT, 95.4–106.9 for DMT, and 97.0–103.7 for TMT, were obtained at $2.0 \text{ ng (Sn) mL}^{-1}$ spiking level. MMT and DMT were detected in all seawater samples and the concentration of MMT ($1.0\text{--}1.5 \text{ ng (Sn) mL}^{-1}$) is higher than that of DMT ($0.30\text{--}0.57 \text{ ng (Sn) mL}^{-1}$). TMT was not detected in any of these seawater samples, even though the proposed method has the highest sensitivity for TMT. This could be due to the fact that TMT is less stable than MMT and DMT in the environment. TMT can be degraded to DMT and MMT by biotic and abiotic demethylation [28]. In addition, biotic and abiotic methylation of inorganic tin in seawater could also lead to the formation of MMT.

The concentrations of methyltins in our results are consistent with the previous work conducted in Ontario Lake water [7], which contains $0.53\text{--}1.22 \text{ ng (Sn) mL}^{-1}$ MMT, $0.10\text{--}0.40 \text{ ng (Sn) mL}^{-1}$ DMT, and below detection limit of TMT. Furthermore, the omnipresent

Table 2
Some analytical performance data of the proposed method

Compound	Calibration curve ^a	Correlation coefficient	Detection limit (ng mL^{-1})	RSD (% , $n = 5$) ^b
MMT	$Y = 1.56 \times 10^5 X + 7.87 \times 10^4$	0.9990	0.266	1.4
DMT	$Y = 5.08 \times 10^5 X - 3.63 \times 10^5$	0.9990	0.095	0.6
TMT	$Y = 1.00 \times 10^6 X - 2.54 \times 10^5$	0.9996	0.039	0.6

^a The methyltins concentration range was $0.5\text{--}50 \text{ ng (Sn) mL}^{-1}$.

^b Obtained at concentration of $10 \text{ ng (Sn) mL}^{-1}$ for each tin species.

Table 3
Recoveries and concentrations of methyltin compounds in seawater samples collected in Bohai Sea (Yantai) ($n = 3$) by HPLC–HG–ICP/MS

Sampling site	Recovery (%) ^a			Concentration found (ng mL^{-1}) ^b		
	MMT	DMT	TMT	MMT	DMT	TMT
Huangzhuang	104.0 ± 4.0	95.4 ± 2.0	97.0 ± 2.5	1.44 ± 0.06	0.57 ± 0.02	ND
Jiulaojumatou	95.8 ± 0.6	104.9 ± 1.0	98.0 ± 2.0	1.06 ± 0.05	0.31 ± 0.02	ND
Yueliangwan	108.0 ± 4.3	106.9 ± 1.5	103.7 ± 3.2	1.16 ± 0.08	0.33 ± 0.03	ND
Haishuiyuchang	106.0 ± 1.1	104.0 ± 0.7	101.7 ± 1.8	1.25 ± 0.05	0.35 ± 0.04	ND
Yugangmatou	96.0 ± 1.8	101.0 ± 1.6	96.7 ± 2.6	1.14 ± 0.06	0.33 ± 0.02	ND

^a Standards were spiked at $2 \text{ ng (Sn) mL}^{-1}$ for each tin species.

^b Values are means of three measurements \pm standard deviation. ND = not detectable.

Table 4

Comparisons of the pretreatment procedures for methyltin analysis in water using AAS, GC and HPLC-based methods

Method	Sample	Pretreatment method	Reference
AAS	100 mL seawater or lake water	Volatile hydrides were generated using NaBH ₄ and then trapped in liquid nitrogen followed by sequential elution with increasing temperature and detection using AAS	[3]
GC-AAS	4–5 L water, Ontario Lakes and Rivers	Saturation with NaCl, extraction of 4–5 L water with 100 mL of benzene/0.5% tropolone. Extracts were evaporated to a small volume, butylated with butylmagnesium bromide. Then samples were cleaned up and concentrated	[6]
GC-AAS	Lake water (5–10 L)	Extraction with benzene containing tropolone from water saturated with sodium chloride, butylation to form tetramethylbutyltins. Then samples were cleaned up and concentrated	[7]
GC-FPD	SnCl ₂ reaction solution (1–2 mL)	Samples were placed in a centrifugation tube together with citric acid–NaH ₂ PO ₄ buffer solution (pH 5.0). The internal standard (MeSnPr ₃) and 0.1% tropolone–cyclohexane were added. The mixture was extracted in an ultrasonic bath and centrifuged twice at 3000 r min ⁻¹ . Then, the organic phases were dried using anhydrous Na ₂ SO ₄ and reacted with <i>n</i> -PeMgBr (Grignard reagent) in an ultrasonic bath. Excess Grignard reagent was eliminated by the addition of 5% (v/v) H ₂ SO ₄ solution, and the organic phase was purified by anhydrous Na ₂ SO ₄ and Florisil. Finally, the eluted organic phase was concentrated to 2 mL under a stream of nitrogen	[11]
HPLC–HG–ICP/MS	200 µl water	Without any other pretreatment except being filtered with 0.4 µm filter membrane	This work

Table 5

Comparisons of the detection limits for methyltin analysis using HPLC coupled with different detectors

Method of detection	Detection limits (ng(Sn) mL ⁻¹)	Reference
HPLC–HG–QSIL–FPD	MMT: 1.69; DMT: 0.51; TMT: 0.36	[27]
HPLC–Flame AAS	MMT: 380; DMT: 340; TMT: 320	[30]
HPLC–ICP/MS (with DIN)	MMT: 20; DMT: 16; TMT: 18	[31]
HPLC–ICP/MS	MMT: 0.46; DMT: 0.26; TMT: 1.26	[32]
MLC–ICP/MS	DMT: 1.02; TMT: 0.70	[33]
HPLC–HG–ICP/MS	MMT: 0.266; DMT: 0.095; TMT: 0.039	This work

existence of the methyltin compounds in different seas has been reviewed in previous literature [29].

Comparison of the pretreatment methods listed in Table 4 suggests that direct AAS method and GC-based methods need the more volume of natural waters and the solvent- and time-consuming pretreatment procedures. Compared with these methods, HPLC-based method reported in this paper has a great advantage due to no pretreatment step involved. The detection limits of methyltins for methods reported in literature using HPLC coupled with various detectors are listed in Table 5. The detection limits obtained with the present technique are markedly lower than HPLC–Flame AAS and HPLC–ICP/MS with direct injection nebulizer (DIN), and are about 5–20 times better than HPLC–HG–QSIL–FPD, micellar liquid chromatography (MLC)–ICP/MS and conventional HPLC–ICP/MS. This is the reason why this HPLC–HG–ICP/MS technique, rather than other techniques, can direct detect the methyltins in seawater.

4. Conclusions

HPLC was on-line coupled with hydride generation and ICP/MS for the speciation of methyltins in water samples. Speciation of methyltins in seawater samples can be rapidly and directly performed with high sensitivity and without interferences. Sample pretreatment steps can be avoided and the use of time and toxic

organic solvents can be greatly reduced. This hyphenated system also broadens the application of reversed phase HPLC and ICP/MS without the oxygen addition system for ICP/MS. This technique could also speciate methyltins in beverage, wine and other natural waters, such as tap water, lake water and river water. It is expected that this system could also be used for direct speciation of butyltins and phenyltins with appropriate modification of the interface (e.g. maintaining the temperature of the transfer line).

Acknowledgments

This work was supported by the National Natural Science Foundation of PR China (20577057 and 40503014) and by the State High Tech Development Plan (2006AA06Z424).

References

- [1] K. Fent, Crit. Rev. Toxicol. 26 (1996) 1.
- [2] G.W. Pettibone, J.J. Cooney, J. Industr. Microbiol. Biotechnol. 2 (1998) 373.
- [3] V.F. Hodge, S.L. Seidel, E.D. Goldberg, Anal. Chem. 51 (1979) 1256.
- [4] S. Turul, T.I. Balkas, E.D. Goldberg, Mar. Pollut. Bull. 14 (1983) 297.
- [5] L. Schebek, M.O. Andreae, H.J. Tobschall, Environ. Sci. Technol. 25 (1991) 871.
- [6] R.J. Magulre, Y.K. Chau, G.A. Bengert, E.J. Hale, P.T.S. Wong, O. Kramar, Environ. Sci. Technol. 16 (1982) 698.
- [7] Y.K. Chau, P.T.S. Wong, G.A. Bengert, Anal. Chem. 54 (1982) 246.
- [8] C.C. Gilmour, J.H. Tuttle, J.C. Means, Anal. Chem. 58 (1986) 1848.
- [9] J.R. Ashby, P.J. Craig, Sci. Total Environ. 73 (1988) 127.
- [10] S. Rapsomanikis, J.H. Weber, Environ. Sci. Technol. 19 (1985) 352.
- [11] B. Chen, Q. Zhou, J. Liu, D. Cao, T. Wang, G. Jiang, Chemosphere 68 (2007) 414.
- [12] J. Liu, G. Jiang, Q. Zhou, Z. Yao, Anal. Sci. 17 (2001) 1279.
- [13] S. Tsunoi, T. Matoba, H. Shioji, L.T.H. Giang, H. Harino, M. Tanaka, J. Chromatogr. A 962 (2001) 197.
- [14] R. Morabito, P. Massanisso, Trends Anal. Chem. 19 (2000) 113.
- [15] K. Kadokami, T. Uehiro, M. Morita, K. Fuwa, J. Anal. At. Spectrom. 3 (1998) 187.
- [16] J. Wu, Z. Mester, J. Pawliszyn, J. Anal. At. Spectrom. 16 (2001) 159.
- [17] B. Fairman, R. Wahlen, Spectrosc. Eur. 13 (2001) 16.
- [18] E. Gonzalez-Toledo, R. Compano, M. Granados, M.D. Prat, Trends Anal. Chem. 22 (2003) 26.
- [19] C.F. Harrington, G.K. Eigendorf, W.R. Cullen, Appl. Organomet. Chem. 10 (1996) 339.
- [20] S. Chiron, S. Roy, R. Cottier, R. Jeannot, J. Chromatogr. A 879 (2000) 137.

- [21] C. Rivas, L. Ebdon, E. Hywei Evans, S.J. Hill, *Appl. Organomet. Chem.* 10 (1996) 61.
- [22] R. Wahlen, T. Catterick, *J. Chromatogr. B* 783 (2003) 221.
- [23] L. Yang, J.W.H. Lam, *J. Anal. At. Spectrom.* 16 (2001) 724.
- [24] H.G. Infante, M.L.F. Sanchez, A. Sanz-Medel, *J. Anal. At. Spectrom.* 14 (1999) 1343.
- [25] J.L. Gomez-Ariza, D. Sanchez-Rodas, I. Giraldez, E. Morales, *Analyst* 125 (2000) 401.
- [26] R.T. Gettar, R.N. Garavaglia, E.A. Gautier, D.A. Batistoni, *J. Chromatogr. A* 884 (2000) 211.
- [27] G. Zhai, J. Liu, G. Jiang, B. He, Q. Zhou, *J. Anal. At. Spectrom.* 22 (2007) 1420.
- [28] J. Huang, E. Matzner, *J. Plant Nutr. Soil Sci.* 167 (2004) 33.
- [29] S. Yemencioğlu, S. Tugrul, N. Kubilay, I. Salihoglu, *Mari. Pollut. Bull.* 34 (1997) 739.
- [30] D.T. Burns, F. Gloeking, M. Harriott, *Analyst* 106 (1981) 921.
- [31] S.C.K. Shum, R. Neddersen, R.S. Houk, *Analyst* 117 (1992) 577.
- [32] H. Suyani, D. Heitkemper, J. Creed, J. Caruso, *Appl. Spectrosc.* 43 (1989) 962.
- [33] Y. Inoue, K. Kawabata, Y. Suzuki, *J. Anal. At. Spectrom.* 10 (1995) 363.